

Design Manual for

ORTHOTROPIC STEEL PLATE
DECK BRIDGES

AMERICAN INSTITUTE OF STEEL CONSTRUCTION
101 PARK AVENUE, NEW YORK 17, NEW YORK



Copyright, 1963

by

American Institute of Steel Construction, Inc.

*All rights reserved. This book or any part thereof
must not be reproduced in any form without the
written permission of the publisher.*

PRINTED IN THE UNITED STATES OF AMERICA

Foreword

The successful development in Europe of steel deck bridge construction, commonly known as "orthotropic plate" construction, and the increasing awareness of American engineers of its advantages in the design of long span highway bridges, has created a need for a comprehensive presentation of the theory and practice of this modern system. Until now such information could only be found scattered in various foreign publications. To meet the American need, the American Institute of Steel Construction retained Roman Wolchuk, consulting engineer, to prepare the manuscript for this Manual.

The development of a technical publication of such scope must of necessity be largely the work of a single individual. For his skillful handling of the assignment the Institute gratefully acknowledges its indebtedness to Mr. Wolchuk.

The "Design Manual for Orthotropic Steel Plate Deck Bridges" is an attempt to summarize experiences with this new type of steel bridge and to provide bridge engineers with criteria and methods for the design of such structures.

The material contained in this Manual is presented in three parts:

Chapters 1 through 6 present a general review of bridges with steel decks, describe their structural behavior, outline general theory and present a practical method for the design of steel bridge decks.

Chapters 7 and 8 discuss the construction of steel decks and wearing surfaces.

Chapters 9, 10 and 11 and Appendices I and II give design criteria and outline in detail practical design procedure which is illustrated by numerical examples. Appendix I contains charts for the design of steel bridge decks in accordance with AASHO specifications; Appendix II gives formulas for checking the elastic stability of the steel decks.

The method of designing steel plate bridge decks given in Chapter 3, 4 and 5, was developed by Prof. Dr.-Ing. Walter Pelikan and Dr.-Ing. Maria Esslinger and published in *Forschungsheft No. 7*, Maschinenfabrik Augsburg-Nuernberg, 1957. Permission of M.A.N. in Gustavsburg, Germany, to use the material is much appreciated.

In the adaptation of this material for the purposes of the Manual, the design procedure has occasionally been expanded and implemented by Mr. Wolchuk by adding new formulas to cover more fully the practical needs of the design of steel decks. Thus the following formulas and procedures have been added: computation of the effects of the deck flexibility in the design of the open ribs, shortcut formulas facilitating the numerical computations of the closed ribs, computations of the shears in the elastic floor beams, computation of the effects of the heavier floor beams in a rather common case of the deck supported by floor beams of non-uniform rigidity, etc.

A design may be made either by means of the formulas given in Chapters 3, 4, 5 and 6 of the Manual for the general case of the deck loading, or, by means of charts, for the standard loading of the AASHO specifications. While computation by the general formulas may require a rather large amount of numerical work, especially in the design of a deck with closed ribs, the design by means of the charts is relatively simple and should present no difficulties in general application.

The recommendations contained in this Manual regarding the design and the details of steel bridge decks are, of necessity, tentative. It may be expected that further rules and recommendations for more advantageous utilization of steel deck bridge construction in this country will evolve from actual practice.

The American Institute of Steel Construction wishes to express its appreciation to all those whose review of the manuscript and whose extensive comments and valuable information have enhanced the usefulness of the Manual. In particular, it wishes to thank Prof. Dr.-Ing. W. Pelikan, Prof. Dr.-Ing. K. Kloepffel, Dr.-Ing. M. Esslinger and Prof. J. G. Fouwkamp for their study of the manuscript and Mr. R. M. Mayrbaur for his assistance to Mr. Wolchuk in its preparation and editing.

Table of Contents

	PAGE
<i>Foreword</i>	v
<i>Nomenclature</i>	xiv
Chapter 1—General Description, Structural Behavior, Economy of Steel Plate Deck Bridges	
1.1 General Description; Applications	1
1.1.1 Introduction	
1.1.2 Evolution of Steel Plate Deck Construction	
1.1.3 Applications	
1.1.3.1 Girder Bridges	
1.1.3.2 Cable-Stiffened Girder Bridges	
1.1.3.3 Suspension Bridges	
1.1.3.4 Arch Bridges	
1.1.3.5 Truss Bridges	
1.1.3.6 Movable Bridges	
1.1.3.7 Railroad Bridges	
1.2 Structural Behavior of Steel Plate Deck Bridges	15
1.2.1 Comparison with Conventional Bridges	
1.2.2 Component Structural Systems of Steel Plate Deck Bridges	
1.2.3 System I—The Deck as Part of the Main Carrying Members	
1.2.4 System II—The Deck as the Bridge Floor	
1.2.4.1 Structural Behavior under Design Loads	
1.2.4.2 Structural Behavior under Higher Loads	
1.2.5 System III—The Deck Plate Acting between Longitudinal Ribs	
1.2.6 Stress Superposition	
1.3 Economic Considerations	26
1.3.1 Factors Contributing to the Economy of Steel Plate Deck Construction	
1.3.1.1 Steel Weight Saving	
1.3.1.2 Erection Efficiency	
1.3.1.3 Cost Differential between a Concrete Deck and a Wearing Surface on Steel Plate Deck	
1.3.1.4 Savings Due to Reduction of the Depth of Structure	
1.3.1.5 Substructure Savings	
1.3.2 AISC Cost Studies	
Chapter 2—Theoretical Background of the Deck Design	
2.1 Introduction	30
2.2 Properties of an Ideal Orthotropic Plate	30
2.2.1 Basic Assumptions	
2.2.2 Rigidity Coefficients	
2.2.3 Comparison with an Isotropic Plate	
2.3 Differential Equation of an Orthotropic Plate and Its Solutions	32
2.4 Design Analysis of Steel Plate Decks Based on the Orthotropic Plate Theory	35
2.4.1 Applicability of the Orthotropic Plate Theory to Steel Plate Decks	
2.4.1.1 General	
2.4.1.2 Properties of Steel Plate Decks at Variance with the Assumptions of the Orthotropic Plate Theory	
2.4.1.3 Effects of Discontinuity in Computation of Stresses	
2.4.2 Evolution of the Design Methods Based on the Orthotropic Plate Theory	
2.4.3 Attempts at a Rigorous Treatment of Steel Plate Decks	

Chapter 3—Outline of the Design Method, Rigidity Coefficients, Loading

3.1 Introduction	40
3.2 Outline of the Method	40
3.2.1 General Description of the Design Procedure	
3.2.2 Simplifying Assumptions Used in the Design	
3.2.2.1 General	
3.2.2.2 Decks with Closed Ribs	
3.2.2.3 Decks with Open Ribs	
3.3 Rigidity Coefficients	43
3.3.1 Introduction	
3.3.2 Flexural Rigidity	
3.3.2.1 Effective Width of Deck Plate	
3.3.2.2 Section Properties of Ribs and Floor Beams	
3.3.3 Torsional Rigidity	
3.3.3.1 Theoretical Background	
3.3.3.2 Formulas for Effective Torsional Rigidity	
3.4 Loading	51
3.4.1 General	
3.4.1.1 Dead Load	
3.4.1.2 Live Load	
3.4.2 Application of the AASHO Loads in the Design of Steel Plate Bridge Decks	
3.4.2.1 Wheel Loads	
3.4.2.2 Loaded Area Dimensions	
3.4.2.3 Impact Factors and Load Reduction Coefficients	
3.5 Fourier Analysis of Loading	54
3.5.1 Introduction	
3.5.2 Application of the Fourier Analysis to the Deck Design	
3.5.3 Fourier Coefficients Q_{nx}/Q_0 Used in Computation of Moments in the Orthotropic Plate on Rigid Supports	
3.5.3.1 One Wheel in Center of the Plate Strip Considered	
3.5.3.2 One Axle Symmetrically Placed	
3.5.3.3 Axles Symmetrically Placed	
3.5.4 Fourier Coefficients Q_{1x}/Q_0 (Coefficients for $n = 1$) Used in Computation of the Effects of Floor Beam Flexibility	
3.5.4.1 One Axle in Any Position	
3.5.4.2 Two Axles in Any Position	
3.5.4.3 Many Axles in Any Position	

Chapter 4—Formulas for Steel Plate Decks on Rigid Supports

4.1 Introduction	57
4.2 Deck with Open Ribs	57
4.2.1 General	
4.2.1.1 Differential Equation	
4.2.1.2 Carry-over Factor	
4.2.1.3 Influence Lines	
4.2.1.4 Computation of the Bending Moments in the Ribs	
4.2.2 Bending Moment at the Support of Ribs	
4.2.2.1 Concentrated Load at any Point	
4.2.2.2 Distributed Load	
4.2.3 Bending Moment at the Midspan of Ribs	
4.2.3.1 Concentrated Load at Any Point	
4.2.3.2 Distributed Load	
4.2.4 Reactions	
4.2.4.1 Floor Beam Reactions on Ribs	
4.2.4.2 Rib Reactions on the Deck Plate	
4.2.5 Influence Line Ordinates	

4.2.6 Charts for the Design of Decks with Open Ribs on Rigid Supports

4.2.7 Design of the Open Ribs on Rigid Supports with Consideration of the Effects of the Deck Plate Rigidity, D_P

 4.2.7.1 General

 4.2.7.2 Formulas for the Moment Relief, ΔM_R

 4.2.7.3 Criteria for Determination of the Error Due to the Simplified Computation of the Moments in Ribs

4.3 Deck with Closed Ribs 64

 4.3.1 General

 4.3.1.1 Differential Equation and Its Solution

 4.3.1.2 Sinusoidal Affinity between the Loads and the Deformations, Shears and Moments

 4.3.1.3 Carry-over Factor

 4.3.2 General Expressions for the Bending Moments

 4.3.2.1 Bending Moments M_B in a Continuous Plate Due to Sinusoidal Loading

 4.3.2.2 Bending Moments in the Deck Due to Actual Loads

 4.3.3 Bending Moment at the Support, M_S

 4.3.4 Bending Moment at the Midspan, M_C

 4.3.4.1 Influence Line

 4.3.4.2 Bending Moment Due to a Distributed Load

 4.3.5 Shortcut Formulas for Numerical Computations

 4.3.5.1 General

 4.3.5.2 Constants

 4.3.5.3 Moment Formulas

 4.3.6 Charts for the Design of the Decks with Closed Ribs on Rigid Supports for AASHO Loads

 4.3.6.1 Range of Charts

 4.3.6.2 Loading

 4.3.6.3 Computation of the Charts

Chapter 5—Effects of Floor Beam Flexibility

5.1 Introduction 73

5.2 Bending Moments and Reactions of a Continuous Beam on Elastic Supports 73

5.3 Application of the Formulas for a Beam on Elastic Supports to the Analysis of Steel Plate Decks Continuous over Floor Beams of Uniform Rigidity 74

 5.3.1 Basic Concepts

 5.3.2 Relative Rigidity Coefficient, γ

 5.3.3 Bending Moment Corrections Due to Floor Beam Flexibility

 5.3.3.1 Moment Increase, ΔM_R , in the Ribs

 5.3.3.2 Moment Relief, ΔM_F , in the Floor Beams

 5.3.4 Shear Corrections Due to Floor Beam Flexibility

 5.3.4.1 Shears in the Ribs

 5.3.4.2 Shears in the Floor Beams

 5.3.5 Charts for the Determination of the Effects of Floor Beam Flexibility Due to AASHO Loads

5.4 Bridge Decks with Floor Beams of Non-Uniform Rigidity 80

 5.4.1 General

 5.4.2 Designations

 5.4.3 Formulas for the Effect of One Heavier Floor Beam

 5.4.3.1 Derivation for Beam on Elastic Supports

 5.4.3.2 Change of the Bending Moments in Ribs

 5.4.3.3 Change of the Bending Moments in Floor Beams

5.5 Bridge Decks with Floor Beams Elastically Restrained at the Main Girders or Continuous over More than Two Main Girders 83

Chapter 6—Design of the Deck Plate

6.1 Design Criteria 84

6.2 Structural Behavior of the Deck Plate Acting as an Independent Structural Element (System III) 85

 6.2.1 Deck Plate Subjected to Small Loads

 6.2.1.1 Tests on Decks Subjected to Design Loads

 6.2.1.2 Analytical Determination of the Local Stresses in the Deck Plate Under the Design Loads

 6.2.1.3 Numerical Examples of the Deck Plate Analysis

- 6.2.2 Deck Plate Subjected to Large Loads
 - 6.2.2.1 General
 - 6.2.2.2 Ultimate Load Test on a Deck Plate
 - 6.2.2.3 Effects of Axial Prestress and Initial Dishing of the Plate
- 6.2.3 Fatigue Strength of the Deck Plate
 - 6.2.3.1 Fatigue Tests
 - 6.2.3.2 Discussion of the Factors Affecting the Fatigue Strength of the Deck Plate
 - 6.2.3.3 Conclusion
- 6.3 Empirical Formulas for the Design of Steel Deck Plates 97**
 - 6.3.1 AISC Formulas for the Deck Plate of Battledack Bridge Floors
 - 6.3.2 Formula for the Plate Thickness Based on Allowable Deflection
 - 6.3.3 Formula for Ultimate Capacity of the Plate
- 6.4 Summary and Conclusions. 99**

Chapter 7—Construction Details

- 7.1 Construction Elements. 100**
 - 7.1.1 Open Ribs
 - 7.1.1.1 General
 - 7.1.1.2 Evaluation of the Open Rib System
 - 7.1.1.3 Optimum Spacing and Span
 - 7.1.2 Closed Ribs
 - 7.1.2.1 Types of Closed Ribs
 - 7.1.2.2 Evaluation of the Closed Rib System
 - 7.1.3 Floor Beams
 - 7.1.4 Main Bridge Members
 - 7.1.5 Miscellaneous Details
- 7.2 Fabrication. 106**
 - 7.2.1 General Comments on Welding of Steel Plate Decks
 - 7.2.2 Fabrication of the Deck Plating Panels
 - 7.2.3 Thoughts on the Economy of Fabrication of Steel Plate Decks
- 7.3 Erection 109**
 - 7.3.1 Field Splice Details
 - 7.3.1.1 Riveted and Bolted Splices
 - 7.3.1.2 Welded Splices
 - 7.3.2 Erection Procedures
 - 7.3.3 Effects of the Erection Procedure on the Final Stresses in the Bridge System
- 7.4 Protection Against Corrosion. 118**
 - 7.4.1 Steel Deck Plate
 - 7.4.2 Insides of Closed Ribs and Other Inaccessible Closed Hollow Sections
 - 7.4.3 Box Girder Sections

Chapter 8—Wearing Surfaces

- 8.1 General Requirements 120**
- 8.2 Bituminous-Mix Wearing Surfaces 121**
 - 8.2.1 General
 - 8.2.2 Materials for Bituminous Wearing Surfaces
 - 8.2.2.1 Asphalt
 - 8.2.2.2 Aggregate
 - 8.2.3 Corrosion Protection and Bonding
 - 8.2.3.1 Purpose, Desirable Properties
 - 8.2.3.2 Protective Materials
 - 8.2.3.3 Mechanical Anchorage Devices
 - 8.2.4 Binder and Surface Courses
 - 8.2.4.1 Composition and Properties of Bituminous-Mix Pavements on Steel Plate Decks
 - 8.2.4.2 Typical Wearing Surfaces on Existing Steel Deck Bridges

8.2.5	Construction and Maintenance	
8.2.5.1	Preparation of the Steel Surface	
8.2.5.2	Placing of the Wearing Surface	
8.2.5.3	Joints	
8.2.5.4	Maintenance	
8.2.6	Conclusions	
8.3	Asphalt Plank Wearing Surfaces	134
8.3.1	General	
8.3.2	Composition and Physical Properties	
8.3.3	Laying the Planks	
8.3.4	Performance	
8.3.5	Conclusions	
8.4	Epoxy Resins	136
8.4.1	General	
8.4.2	Material Properties	
8.4.3	Spray Applications	
8.4.3.1	Existing Installations	
8.4.3.2	Application Methods	
8.4.3.3	Conclusions	
8.4.4	Epoxy Concrete	
8.5	Other Materials	140
8.6	Summary and Conclusions	140

Chapter 9—Design Criteria and Specifications

9.1	Main Structural Members of the Bridge (System I)	141
9.1.1	General	
9.1.2	Dead Load and Live Load Stresses	
9.1.3	Dynamic Effects	
9.1.4	Deflections under Live Load	
9.1.5	Fatigue Strength	
9.2	Bridge Deck Structure (System II)	142
9.2.1	General	
9.2.2	Static Strength	
9.2.3	Deflections	
9.2.4	Dynamic Effects	
9.2.5	Fatigue Strength	
9.3	Superposition of System I and System II Stresses	143
9.3.1	General	
9.3.2	Reduction of System II Stresses	
9.3.3	Increase of the Allowable Stresses for Superposition of the System I and System II Effects	
9.3.4	Second-Order Effects in the Superposition of Stresses	
9.4	Deck Plate (System III)	146
9.5	Design Specifications	146
9.5.1	Proposed Tentative Design Provisions	
9.5.2	Commentary on the Proposed Design Provisions for Steel Deck Bridges	
9.5.3	Thoughts on Future Design Specifications for Steel Deck Bridges	

Chapter 10—Computation Procedure for Practical Design

10.1	Introduction	149
10.2	Bending Moments in the Deck with Open Ribs	149
10.2.1	General	
10.2.2	Section Properties and Relative Rigidities	
10.2.2.1	Longitudinal Ribs	
10.2.2.2	Floor Beams	
10.2.2.3	Relative Rigidity Coefficients, γ	
10.2.3	Computation of the Bending Moments by General Formulas	
10.2.3.1	Bending Moments in a System with Rigid Floor Beams	
10.2.3.2	Bending Moment Corrections Due to Floor Beam Flexibility	

10.2.4	Computation of the Bending Moments by Charts for AASHO Loads	
10.2.4.1	Bending Moments in a System with Rigid Floor Beams	
10.2.4.2	Bending Moment Corrections Due to Floor Beam Flexibility	
10.3	Bending Moments in the Deck with Closed Ribs	153
10.3.1	General	
10.3.2	Section Properties and Relative Rigidities	
10.3.2.1	Flexural Rigidity of the Ribs	
10.3.2.2	Torsional Rigidity of the Ribs	
10.3.2.3	Flexural Rigidity of the Floor Beams	
10.3.2.4	Relative Rigidities	
10.3.3	Computation of the Bending Moments by General Formulas	
10.3.3.1	Bending Moments in the Ribs in a System with Rigid Floor Beams	
10.3.3.2	Bending Moments in Rigid Floor Beams	
10.3.3.3	Additional Bending Moments Due to Floor Beam Flexibility	
10.3.4	Computation of the Bending Moments by Charts for AASHO Loads	
10.3.4.1	Bending Moments in a System with Rigid Floor Beams	
10.3.4.2	Additional Bending Moments Due to Floor Beam Flexibility	
10.4	Computation of Stresses	158
10.4.1	Stresses in System II	
10.4.1.1	Flexural Stresses in the Ribs	
10.4.1.2	Flexural Stresses in the Floor Beams	
10.4.2	Stress Superposition, System I + II	
10.4.3	Shearing Stresses	
10.4.4	Alternating and Pulsating Stresses	

Chapter 11—Numerical Examples

11.1	Introduction	159
11.2	Deck with Open Ribs	159
11.2.1	General	
11.2.1.1	Dimensions and Details	
11.2.1.2	Choice of Deck Plate Thickness	
11.2.1.3	Section Properties	
11.2.1.4	Relative Rigidity Coefficients	
11.2.1.5	Elastic Stability of Ribs	
11.2.1.6	Stresses in the Deck as the Flange of the Main Girders	
11.2.2	Design by General Formulas	
11.2.2.1	Bending Moments in a System with Rigid Floor Beams	
11.2.2.2	Effects of Floor Beam Flexibility, All Floor Beams Uniform	
11.2.2.3	Effects of Heavy Floor Beams	
11.2.2.4	Summary of Moments and Stresses	
11.2.3	Design by Charts for AASHO Loads	
11.2.3.1	Bending Moments in a System with Rigid Floor Beams	
11.2.3.2	Effects of Floor Beam Flexibility, All Floor Beams Uniform	
11.2.3.3	Effects of Heavy Floor Beams	
11.2.3.4	Summary of Moments and Stresses	
11.3	Deck with Closed Ribs	173
11.3.1	General	
11.3.1.1	Dimensions and Details	
11.3.1.2	Section Properties	
11.3.1.3	Relative Rigidity Coefficients	
11.3.2	Design by General Formulas	
11.3.2.1	Bending Moments in a System with Rigid Floor Beams	
11.3.2.2	Effects of Floor Beam Flexibility	
11.3.2.3	Summary of Moments and Stresses	
11.3.3	Design by Charts for AASHO Loads	
11.3.3.1	Bending Moments in a System with Rigid Floor Beams	
11.3.3.2	Effects of Floor Beam Flexibility	
11.3.3.3	Summary of Moments and Stresses	

References	185
-------------------	------------

Appendix I—Design Charts

Chart 1.	Effective width of deck plate acting with one rib or floor beam	A3
Chart 2.	Load on rib under wheel and effective spacing of open ribs, general case	A3
Chart 3.	Load on open rib under wheel, AASHO loading	A4
Chart 4.	Effective spacing of open ribs, AASHO loading	A4
Chart 5.	Influence lines of a beam on an infinite number of rigid supports	A5
Chart 6.	Total maximum moment at midspan of ribs on rigid supports	A6
Chart 7.	Total maximum moment at support of ribs on rigid supports	A7
Chart 8.	Total maximum moments for computing alternating stresses in ribs on rigid supports	A8
Chart 9.	Maximum moment at midspan of the deck with closed ribs on rigid supports, loading a and b	A9
Chart 10.	Maximum moment at midspan of the deck with closed ribs on rigid supports, loading c.	A10
Chart 11.	Maximum moment at midspan of the deck with closed ribs on rigid supports, loading a_1	A11
Chart 12.	Maximum moment at midspan of the deck with closed ribs on rigid supports, loading c_1	A12
Chart 13.	Maximum moment at support of the deck with closed ribs on rigid supports.	A13
Chart 14.	Maximum moments for computing alternating stresses in the deck with closed ribs.	A14
Chart 15.	Maximum load, F_0 , on a rigid floor beam due to one AASHO vehicle	A15
Chart 16.	Maximum live load moment in a rigid floor beam.	A16
Chart 17.	Influence ordinates for moment at midspan of a continuous beam on elastic supports.	A17
Chart 18.	Influence ordinates for moment at support of a continuous beam on elastic supports	A18
Chart 19.	Influence ordinates for reaction at point 0 of a continuous beam on elastic supports	A19
Chart 20.	Computation of additional moment at midspan of ribs due to floor beam flexibility. Values of $\Sigma(F/P)(\bar{\eta}_c/s)$, loading a and a_1	A20
Chart 21.	Computation of additional moment at midspan of ribs due to floor beam flexibility. Values of $\Sigma(F/P)(\bar{\eta}_c/s)$, loading b and b_1	A21
Chart 22.	Computation of additional moment at midspan of ribs due to floor beam flexibility. Values of $\Sigma(F/P)(\bar{\eta}_c/s)$, loading c and c_1	A22
Chart 23.	Computation of additional moment at midspan of ribs due to floor beam flexibility. Values of $\Sigma(F/P)(\bar{\eta}_c/s)$, other than critical lanes loaded	A23
Chart 24.	Computation of moment relief at the support of ribs due to floor beam flexibility. Values of $\Sigma(F/P)(\bar{\eta}_s/s)$, loading d.	A24
Chart 25.	Computation of moment relief at the support of ribs due to floor beam flexibility. Values of $\Sigma(F/P)(\bar{\eta}_s/s)$, loading e	A25
Chart 26.	Computation of moment relief at the support of ribs due to floor beam flexibility. Values of $\Sigma(F/P)(\bar{\eta}_s/s)$, loading f	A26
Chart 27.	Computation of moment relief at the support of ribs due to floor beam flexibility. Values of $\Sigma(F/P)(\bar{\eta}_s/s)$, loading g	A27
Chart 28.	Computation of additional moment in ribs due to floor beam flexibility. Values of Q_{1z}/Q_0 at critical rib, lane over critical rib loaded.	A28
Chart 29.	Computation of additional moment in ribs due to floor beam flexibility. Values of Q_{1z}/Q_0 at critical rib, lane over critical rib loaded.	A29
Chart 30.	Computation of moment relief in a floor beam due to floor beam flexibility. Values of $(F_0/P) - \Sigma(F/P)\bar{\nu}_0$ for $s = 4'$ to $12'$	A30
Chart 31.	Computation of moment relief in a floor beam due to floor beam flexibility. Values of $(F_0/P) - \Sigma(F/P)\bar{\nu}_0$ for $s = 12'$ to $25'$	A31
Chart 32.	Computation of moment relief in a floor beam due to floor beam flexibility. Values of Q_{1z}/Q_0 at critical point of a floor beam.	A32

Appendix II—Buckling Formulas for Steel Decks

II.1	Local Buckling of Rib Plate	A33
II.1.1	Elastic Buckling	
II.1.2	Inelastic Buckling	
II.1.3	Computation of Critical Buckling Stress	
II.1.3.1	Choice of k	
II.1.3.2	Determination of f_{cr}	
II.2.	Overall Buckling of the Deck	A35
II.2.1	Elastic Buckling	
II.2.2	Inelastic Buckling	

Nomenclature

Lengths

a	spacing of open ribs; top width of closed ribs
a_0	effective width of plate acting with one open rib, computed under an assumption of equal loading of all ribs
a_0'	effective width of plate acting with the directly loaded open rib in a case of unequal loads on ribs
a^*	effective spacing of unequally loaded open ribs
$a_0 + e_0$	effective width of plate acting with one closed rib, computed under an assumption of equal loading of all ribs
$a_0' + e_0'$	effective width of plate acting with the directly loaded closed rib in a case of unequal loads on ribs
b	substitute span length of the orthotropic plate in the x -direction, used in the computation of the bending moments in the closed ribs
$2c$	length along the rib of a uniformly distributed wheel load
d	distance in the x -direction from the support to the center line of a load
e	width of deck plate between two closed ribs
e^*	effective distance between the unequally loaded closed ribs
$2g$	width in the direction perpendicular to ribs of a uniformly distributed wheel load
h	depth of open ribs; depth of closed ribs as defined in Figure 3.9
h'	length of side wall of a closed rib
j	bottom width of a trapezoidal closed rib
l	floor beam span
r	radius of curvature of the rib plate at the bottom of closed ribs
s	spacing of floor beams
s_0	effective width of plate acting with one floor beam
s_1	$= 0.7s =$ effective span of longitudinal ribs, used in computation of a_0
s_2	$= 0.81s =$ effective span of longitudinal ribs, used in computation of H

Lengths

s^*	effective spacing of unequally loaded floor beams
t_P, t_R	thickness of deck plate or rib plate, respectively
u	developed width of one rib plate, see Figure 3.9
w	vertical deflection
x	ordinate in the transverse direction of bridge
y	ordinate in the longitudinal direction of bridge; distance along the rib to the nearest support with a smaller number m
z	vertical ordinate; one-half of the wheel spacing in an axle

Section Properties, Rigidities

A	area enclosed by one closed rib
C	torsional rigidity coefficient, as defined in Figure 2.2
D_P	$= \frac{Et_P^3}{12(1 - \gamma)^2} =$ flexural rigidity of the deck plate
D_x, D_y	flexural rigidity of the orthotropic plate in the x - or y -direction, respectively
H	torsional rigidity; effective torsional rigidity of the orthotropic plate representing the actual steel deck
I_F, I_R	moment of inertia of a floor beam, or a rib, respectively, computed with the appropriate effective width of the deck plate
K	section property characterizing torsional resistance, defined by equation (3.14)
k	spring constant (k/in.)
S	section modulus
γ	coefficient characterizing the relative flexural rigidity of the ribs and the floor beams
γ'	coefficient characterizing the relative flexural rigidity of the deck plate and the open ribs
μ	reduction coefficient, used in determination of the effective torsional rigidity, H

Forces, Moments

F_m	reaction at support m of a continuous beam on rigid supports
\bar{F}_m	reaction at support m of a continuous beam on elastic supports
F_0	reaction at support $m = 0$ of a continuous beam on rigid supports; load on floor beam $m = 0$ due to one lane loaded, computed under an assumption of rigid floor beams
M	bending moment (k-in. or k-ft); bending moment in the orthotropic plate per unit width (k-in./in.)
M_C, M_S	bending moment at midspan or at support, respectively, of a continuous beam (k-in. or k-ft); bending moment at midspan or at support, respectively, of a continuous orthotropic plate per unit width (k-in./in.)
M_R, M_F	bending moment acting on one rib, or one floor beam, respectively
$\Delta M_R, \Delta M_F$	bending moment correction in a rib or a floor beam, respectively, due to floor beam flexibility
$\bar{\Delta} M_R, \bar{\Delta} M_F$	bending moment correction in a rib or a floor beam, respectively, due to the effect of a heavy floor beam in a system with non-uniform floor beams
$\Delta' M_R$	bending moment correction in an open rib due to deck plate rigidity
M_n	the n th component moment in the orthotropic plate acting around a line perpendicular to the y -axis due to the n th component load, Q_{nx} , per unit width
M_x, M_y	bending moment in the orthotropic plate acting around a line perpendicular to the x - or y -axes, respectively, per unit width
M_{xy}	twisting moment in the orthotropic plate
P	load; wheel load
p	uniformly distributed load (k/in. ²)
Q_0	$= P/2g =$ load on deck per unit length in the x -direction of bridge (k/in.)
Q_n	maximum value (amplitude) of the n th component load of the Fourier series representing the actual deck load, Q_0 (k/in.)

Forces, Moments

Q_{nx}	$= Q_n \sin \frac{n\pi x}{l} =$ loading intensity at the location x of the n th component of the Fourier series (k/in.)
R	load on one open rib
V_F	shear in a rigid floor beam
ΔV_F	shear correction in a floor beam due to floor beam flexibility
\bar{V}_F	shear in a flexible floor beam
η_C, η_S	influence ordinate for bending moment at midspan or at support, respectively, of a continuous beam on rigid supports
η_{Cn}, η_{Sn}	n th component influence ordinate for bending moment at midspan or at support, respectively, of a continuous orthotropic plate, used in conjunction with the n th component load, Q_{nx}
$\bar{\eta}_{Cm}, \bar{\eta}_{Sm}; \bar{\eta}_C, \bar{\eta}_S$	influence ordinate at support m for the bending moment at midspan or at support, respectively, of a continuous beam on elastic supports
ϑ_0	influence ordinate for reaction F_0 at support $m = 0$ of a continuous beam on rigid supports
$\bar{\vartheta}_{0m}, \bar{\vartheta}_0$	influence ordinate at support m for reaction F_0 at support $m = 0$ of a continuous beam on elastic supports

General Designations

C, C'	integration constants
E	$= 29 \times 10^3$ k/in. ² = modulus of elasticity of steel in tension or compression
G	$= \frac{E}{2(1 + \nu)} = 11.2 \times 10^3$ k/in. ² = modulus of elasticity of steel in shear
f	axial stress
v	shearing stress
m	designation of support
n	1, 2, 3, 4, 5 . . .
α	$= \frac{n\pi}{b} \sqrt{\frac{2H}{D_y}} =$ parameter used in computation of moments in orthotropic plate
κ, κ_n	carry-over factor
ν	$= 0.3 =$ Poisson's ratio for steel

Additional symbols used are explained in the text.

CHAPTER 1

General Description, Structural Behavior, Economy of Steel Plate Deck Bridges

1.1 GENERAL DESCRIPTION; APPLICATIONS

1.1.1 Introduction

The two essential conditions for economy in steel bridge design are: (a) an efficient utilization of steel, and (b) a maximum reduction of the dead weight of the structure.

(a) The *design efficiency*, which may be expressed as a strength to weight ratio of a structural member, has been considerably enhanced during recent years by the application of the high strength structural steels and by the use of welding. Advances in structural theory have further contributed to a more rational utilization of steel, leading to the increased application of statically indeterminate structures, having generally a better overload capacity than statically determinate structures, and to a two-dimensional approach to the design of structures supporting moving loads, permitting an advantageous load distribution. An example is the design of a bridge deck as a grid consisting of intersecting and mutually supporting floor beams and stringers.

Further improvements of efficiency in steel design can be achieved by a judicious re-evaluation of the safety factors currently used, on the basis of a more precise evaluation of the ultimate behavior of the various types of structures, and by a preferred use of the structural elements having inherently large carrying capacity reserves. This points toward an increased use of the steel *plate* as a load-carrying element having considerably larger reserves of safety than one-dimensional beam members.

(b) The overall *dead weight saving*, which is always desirable, becomes especially important in the design of long span bridges where, in some conventional girder bridges, the dead weight may account for up to 80% of the total design moment.

Thus it is obvious that, if bridges of long spans are to be built economically, the dead weight of the superstructure must be kept to a minimum.

This may be achieved, in addition to the weight saving obtained by an efficient design of steel, by avoid-

ing heavy bridge decks, which contribute to the weight but not to the overall strength of the bridge.

The two most notable developments resulting from the requirements of design efficiency and maximum possible saving in dead weight are composite construction and steel plate deck construction.

In *composite construction* bridges, well suited for short and medium-range spans, the concrete deck participates in the stresses of the main girders to which it is bonded

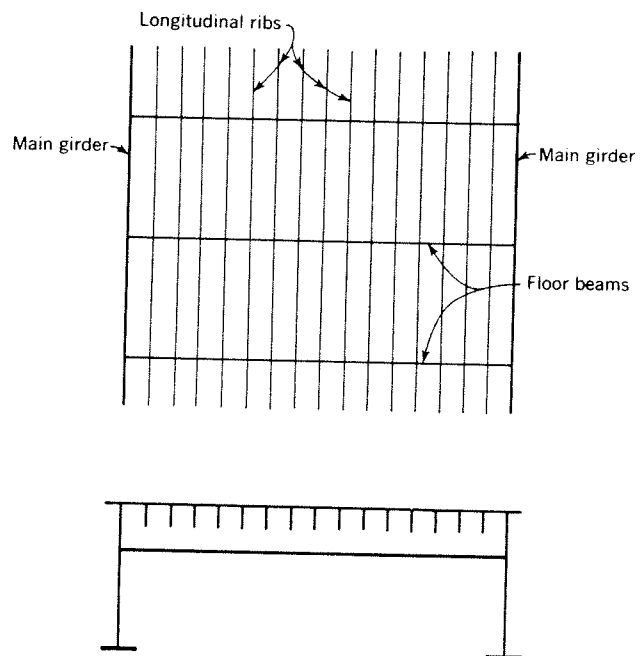


Fig. 1.1. Scheme of a bridge with a steel plate deck

by means of shear connectors. Composite design, the discussion of which is beyond the scope of this Manual, is being used for both simple and continuous girder bridges.

Steel plate deck construction, which is economically advantageous for bridges of longer spans, eliminates the concrete deck altogether and replaces it by a steel deck plate, stiffened in two mutually perpendicular directions by a system of longitudinal and transverse ribs welded to it. The steel deck is considered as an integral

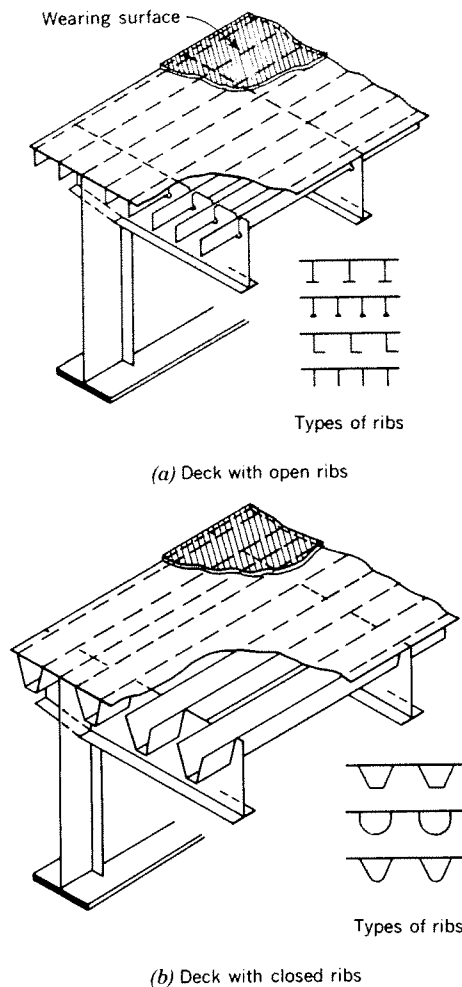


Fig. 1.2. Two basic types of steel plate bridge decks

part of the main carrying members of the bridge and acts as their flange.

Since the behavior of a cross-stiffened steel plate deck may be likened to that of a plate having dissimilar elastic properties in the two mutually perpendicular directions, known as an *orthogonal-anisotropic* plate, or, in an

abbreviated form, "orthotropic plate", the steel plate deck bridges of this type are often referred to as *orthotropic steel plate deck bridges*.

A general scheme of a bridge with an orthotropic steel plate deck is shown in Figure 1.1.

Two basic types of longitudinal ribs are used: *open* ribs (flat bars, bulb sections, angles, inverted T-sections) spaced approximately 1 ft o.c., and *closed* ribs of a trapezoidal or rounded cross section (Fig. 1.2). The characteristic difference between the open and the closed ribs is in their resistance to torsion; the torsional rigidity of the closed ribs is considerable, while that of the open ribs is very small.

The floor beams, which utilize the deck plate as their top flange, may be spaced from 4 to 15 ft and more, depending on design conditions, material vs. fabrication costs and other factors.

The deck is surfaced, in most cases, with a $1\frac{1}{2}$ to $2\frac{1}{2}$ -in. thick layer of asphalt concrete.

Due to its outstanding structural properties and light weight, the steel plate deck system, which has only recently come into existence, has gained a quick acceptance, becoming one of the most important elements of modern steel bridge construction.

1.1.2 Evolution of Steel Plate Deck Construction

In the 1930's, a steel plate deck bridge system, known as the "battledeck floor", was introduced by the American Institute of Steel Construction in an attempt to reduce the dead weight of highway bridges. In this system, which was used mostly on movable bridges and for replacement of floors in old bridge structures, steel deck plate $\frac{3}{8}$ to $\frac{3}{4}$ in. thick was welded to the longitudinal I-beam stringers spaced 10 to 33 in. o.c., supported by or framed into transverse floor beams (Fig. 1.3). The function of the deck plate was to transmit the local wheel loads transversely to the stringers and to participate in the stresses of the individual stringers as a part of their top flanges, with an assigned effective width. However, the deck plate did not participate in the floor beam stresses, nor did it contribute to the

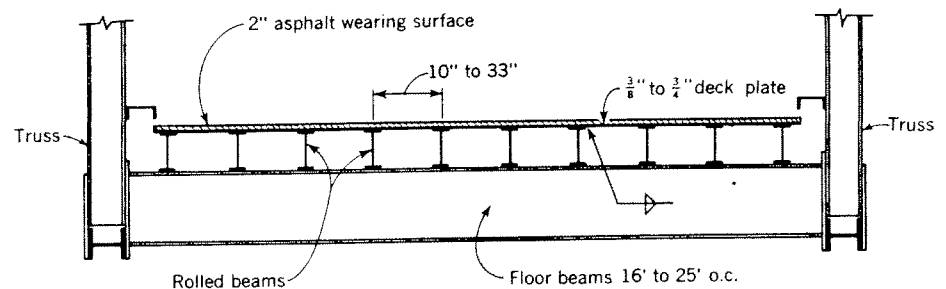


Fig. 1.3. Typical "battledeck floor" bridge cross section

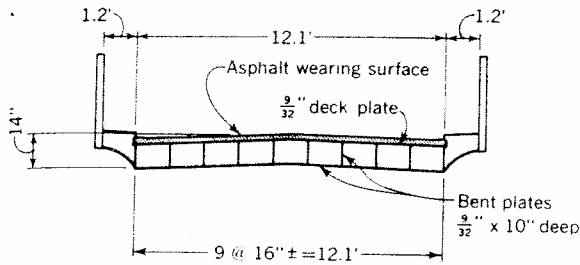


Fig. 1.4. Autobahn overpass at Jungingen, Germany (1934)
(spans 26-37-37-26 ft)

rigidity and strength of the main carrying members of the bridge. For these reasons the battledeck floor construction failed to show the hoped for economy.

However, an important insight into the structural behavior of steel plate bridge decks was gained through the tests conducted on battledeck floors, showing that the strength of a flat steel plate loaded by a wheel is much greater than predicted by ordinary flexural theory. This has been recognized in the semi-empirical formulas proposed by AISC for the design of battledeck bridge floors, recommending a 40% increase of the allowable stress in the steel plate [2].†

At the same time, German engineers experimented with lightweight steel bridge decks of cellular construction [43]. These decks consisted of a thin steel plate

† Numbers in brackets refer to the list of references, page 185.

stiffened in both directions by a relatively shallow gridwork of welded ribs spaced 1 to 2 ft o.c., the entire system acting as a plate (Fig. 1.4).

The great amount of welding in this type of structure, which had to be done manually, later caused the designers to increase the spacing of the stiffeners, creating larger panels of the floor plate. While the strength of the steel plate was still ample, the deck was subject to large local deflections which, in turn, caused cracking in the 2-in. asphaltic wearing surface.

The chief distinction of the system was its shallow depth, giving a slender appearance to the bridges and reducing the amount of earthwork in the bridge approaches (Fig. 1.5). However, as in this country, it was soon realized that true economy may be achieved with the steel deck system only if the spans are sufficiently long and if the deck fully participates in the stresses of the main carrying members of the bridge.

Practical realization of these principles came only after World War II, when an economic stimulus was provided by the necessity of rebuilding the long span bridges in Germany, with steel being in short supply.

The first bridge using the steel plate deck as the top flange of the main girders was the 184-246-184 ft span Kurpfalz Bridge over the Neckar River in Mannheim, opened to traffic in 1950 (Fig. 1.6). This bridge, with a depth of structure at midspan of only 5 ft, to provide the required clearance for navigation, has an average steel weight of 80 lbs per sq ft, as compared with 120 lbs per sq ft of the destroyed bridge, built in 1940 [75].

A further milestone in the development was the com-

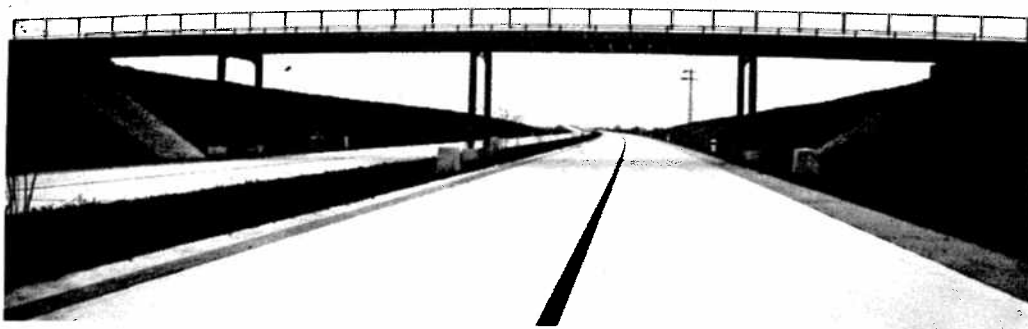


Fig. 1.5. Autobahn overpass at Jungingen

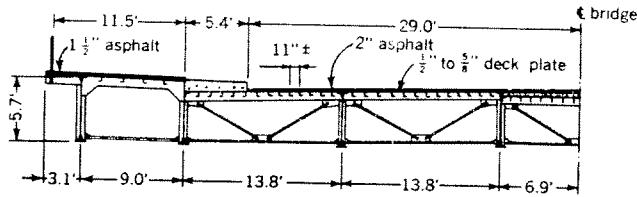


Fig. 1.6. Kurpfalz Bridge in Mannheim, Germany (1950)
(spans 184-246-184 ft)

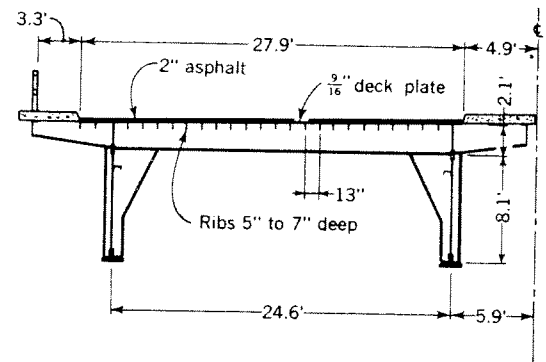


Fig. 1.7. Eddersheim Bridge, Germany (1953)
(spans 164-180-246-180-164-131 ft)

pletion in 1951 of the Cologne-Muelheim Bridge over the Rhine (Figs. 1.21, 1.22), demonstrating the economic superiority of the steel plate deck system applied to suspension bridge design [74, 80]. Other important bridge structures, several of them breaking the previously established span length records, followed in quick succession.

At the same time significant advances in the theory of steel plate deck bridges have brought better and simpler design methods, and experimental research, indicating a high ultimate strength of the steel plate decks, has provided a new insight into the problems of the structural behavior of this system. These developments are still in progress.

In 1954, the first bridges employing closed, torsionally stiff longitudinal ribs were built (Figs. 1.12, 1.23).

The year 1956 brought the completion of the 246-856-246 ft span Save River Bridge in Belgrade, Yugoslavia, which is now the longest plate girder span in the world (Figs. 1.8, 1.9). The design of the steel plate deck of this bridge was based, for the first time (if only to a moderate degree), on ultimate strength considerations, rather than on the conventional "allowable stress" criteria [42].

By 1960, at least 40 orthotropic steel plate bridges had been built in Germany, and several more in other countries.

In the spring of 1960, construction was started on foundations for the tied stiffened arch Port Mann Bridge

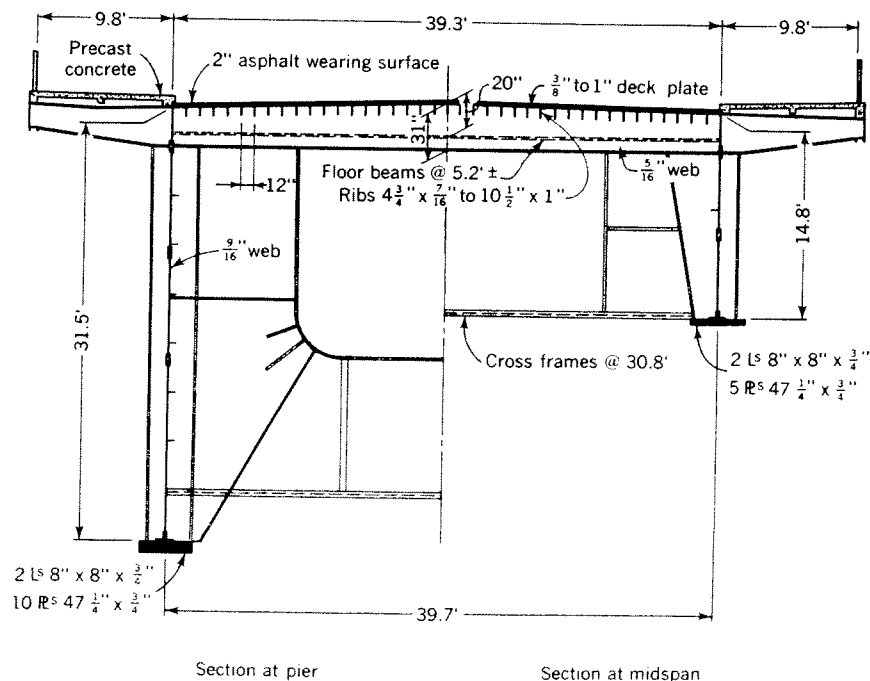


Fig. 1.8. Save River Bridge in Belgrade, Yugoslavia (1956) (spans 246-856-246 ft)

in Vancouver, Canada, with a main arch span of 1200 ft, using a steel plate as a part of the stiffening system (Figs. 1.24, 1.25). This is the first bridge employing orthotropic steel plate deck construction this side of the Atlantic [62].

There are many indications that the steel plate deck system will soon find its due application in American bridge construction practice.

1.1.3 Applications

As a rule, steel plate decks are used in conjunction with plate girders. However, there are no objections to the use of the steel decks in conjunction with bridge trusses, and this construction has been used in several cases.

The following typical examples illustrate the use of the steel plate decks with the various structural bridge systems. Some of the construction details of the bridges listed below are discussed in Chapter 7. More comprehensive information on the design and construction of these structures may be found in the references given.

1.1.3.1 Girder Bridges

1.1.3.1.1 Single-Web Girders

(a) *Eddersheim Bridge*, Germany, 1953 (Fig. 1.7) [71].

This is a 6-span continuous bridge with span lengths of 164-180-246-180-164-131 ft. The deck plate thick-

ness is $\frac{9}{16}$ in. The flat bar ribs, spaced 13 in. o.c., vary in size transversely across the bridge. The webs and the lower flanges of the 10.2-ft deep girders are riveted.

(b) *Save River Bridge*, Belgrade, Yugoslavia, 1956 (Figs. 1.8, 1.9) [42, 76].

In contrast with the above bridge of moderate span lengths, this is one of the most spectacular plate girder bridges built in recent years, having span lengths of 246-856-246 ft.

The deck plate thickness varies from $\frac{3}{8}$ to 1 in., depending on the required cross-sectional area of the deck to act as the top flange of the girders. The rib sizes vary in the longitudinal and the transverse direction of the bridge. The light intermediate floor beams are 20 in. deep at the middle of the bridge cross section and are spaced approximately 5 ft-2 in. o.c. Heavier floor beams 31 in. deep at the cross frames are spaced 30.8 ft o.c.

The webs of the main girders, in spite of their maximum depth of 31 ft - 6 in. at the supports, are only $\frac{9}{16}$ in. thick, and are stiffened by up to 7 rows of longitudinal stiffeners. The webs and the lower flanges of the main girders are of riveted construction, with a maximum cross-sectional area of one flange of approximately 390 sq in.

The material for the steel deck and the main structural members was the German St 52 steel, approximately corresponding in its yield point and ultimate strength to American low-alloy structural steels.

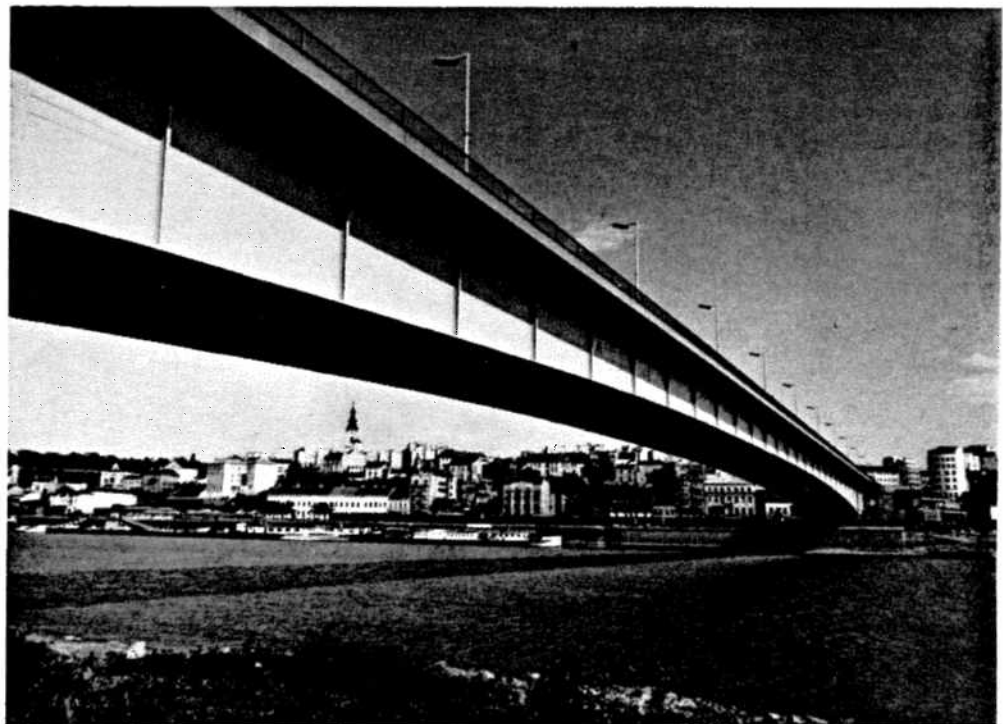


Fig. 1.9. View of Save River Bridge in Belgrade

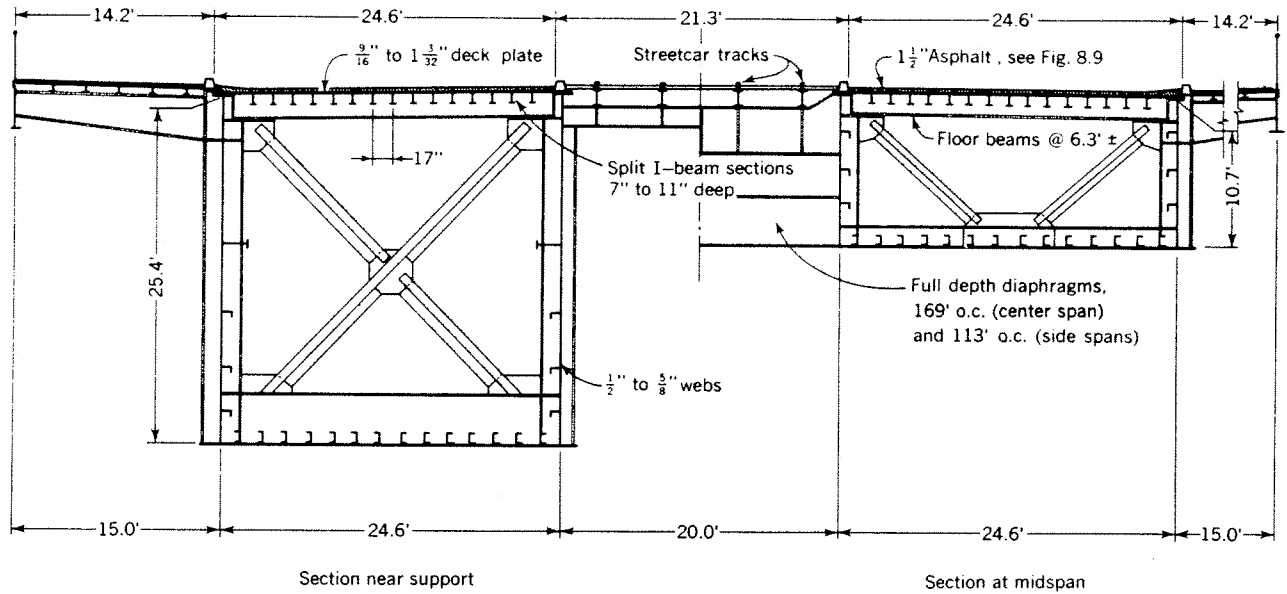


Fig. 1.10. Duesseldorf-Neuss Bridge, Germany (1951). (spans 338-676-338 ft)

1.1.3.1.2 Box-Girders

(a) *Duesseldorf-Neuss Bridge*, Germany, 1951 (Figs. 1.10, 1.11) [68, 78].

The cross section of this 3-span continuous structure, with span lengths of 338-676-338 ft, consists of two box-girders 24.6 ft wide, carrying 4 automobile traffic lanes, 2 street car tracks and 2 sidewalks. The center span is unusually slender, with a depth of structure at midspan of only 11 ft, resulting in a depth-to-span ratio of 1/62.

The deck plate thickness, governed primarily by the required cross section area of the deck acting as the top flange of the girders, varies from $\frac{9}{16}$ to $1\frac{3}{32}$ in. The longitudinal ribs, spaced 17 in. o.c., consist of split rolled sections running continuously through slots in the transverse floor beams spaced 6.3 ft o.c.

The deck plate panels were shop-welded in units 38 ft \times 26 ft, and transported to the erection site by platform trucks.

All field splices of the deck plate, the ribs and the main girders are riveted.

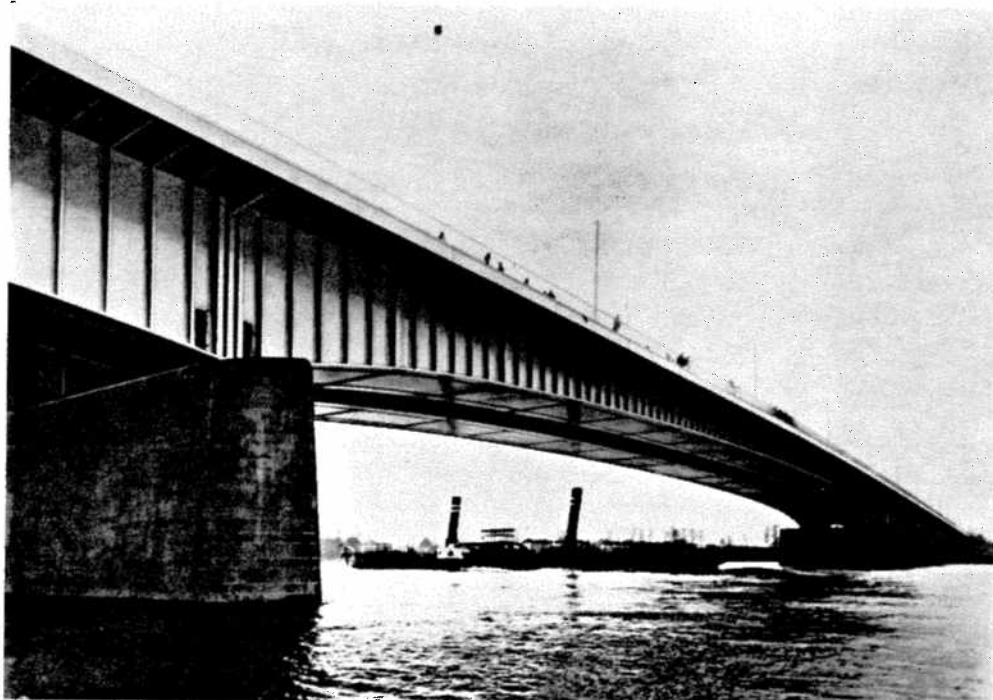


Fig. 1.11. View of Duesseldorf-Neuss Bridge

(b) *Weser Bridge Porta*, Germany, 1954 (Figs. 1.12, 1.13) [60].

The spans of this bridge are 209-255-348 ft. The cross section is a torsionally stiff box-girder with a 19.4 ft width and an 11.5 ft uniform depth. The top flange, serving as a deck, and the bottom flange, as well as the

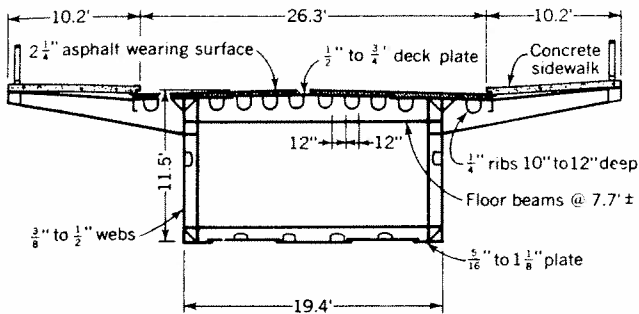


Fig. 1.12. *Weser Bridge Porta*, Germany (1954)
(spans 209-255-348 ft)

vertical webs, are stiffened longitudinally by means of U-shaped ribs $\frac{1}{4}$ in. thick. The deck plate thickness is $\frac{1}{2}$ in. in the shorter spans, and varies up to $\frac{3}{4}$ in. in the 348 ft span.

All field splices of this bridge are welded.

(c) *Saint-Christophe Bridge*, Lorient, France, 1960 (Fig. 1.14) [57].

This three-span continuous girder bridge with 207-305-207 ft spans has two box-girders 16.4 ft wide and varying in depth from 8.2 to 12.1 ft.

The steel deck plate has a $2\frac{3}{8}$ -in. reinforced concrete wearing surface, rather than the usual asphalt surfacing. The concrete, bonded to the steel deck by means of

welded shear connectors, participates in the steel deck stresses. Thus the wearing surface contributes to the strength of the main girders and of the deck plate, making a 3.3-ft rib spacing possible.

1.1.3.2 Cable-Stiffened Girder Bridges

Cable-stiffened bridges occupy a middle position between unstiffened girder bridges and suspension bridges.

Bridges of this system, including various possible types, may be advantageously used for spans exceeding the capacity of unstiffened girders. One of the advantages of this system, compared with a suspension bridge, is its greater rigidity.

(a) *Duesseldorf-North Bridge*, Germany, 1957 (Figs. 1.15, 1.16) [59, 73].

This is a continuous girder bridge stiffened by a parallel-cable system, sometimes referred to as a "harp" system or a "bridle-chord" system. The span lengths are 354-853-354 ft. The bridge cross section consists of two box-girders 10.7 ft deep and 5.3 ft wide, and a steel plate deck $\frac{9}{16}$ in. thick, acting in conjunction with the girders. The longitudinal ribs, spaced 16 in. o.c., are made of $8 \times 4 \times \frac{7}{16}$ -in. angles running continuously through rectangular cutouts in the floor beams spaced 6.1 ft apart.

The field splices are riveted.

(b) *Severin Bridge*, Cologne, Germany, 1959 (Figs. 1.17, 1.18, 1.19, 1.20) [63, 69].

The Severin Bridge consists of six continuous spans with lengths of 161-292-157-990-494-172 ft. The two largest spans are stiffened by a system of 12 cables intersecting at the top of an A-shaped tower. This cable

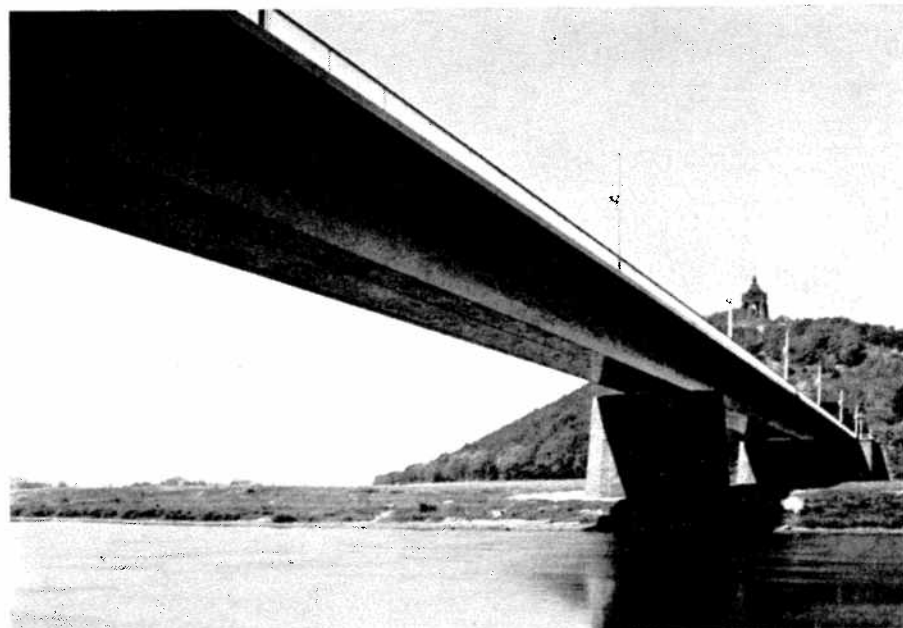


Fig. 1.13. View of
Weser Bridge Porta

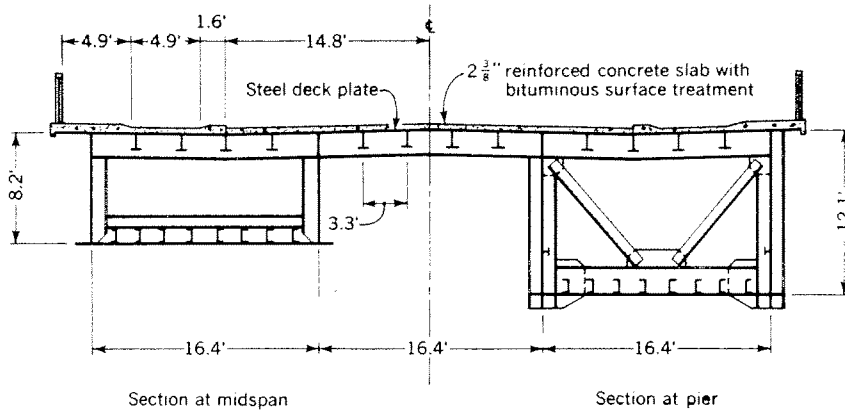


Fig. 1.14. Saint-Christophe Bridge, Lorient, France (1960) (spans 207-305-207 ft)

arrangement, in addition to providing a very good torsional rigidity to the bridge, has the advantage of avoiding an unpleasant intersection of cables when viewed from any point. The asymmetry of the bridge, with a single tower located near the right bank of the Rhine, as required by the local navigation conditions, also provides a logical counterbalance to the city picture on the left bank, and avoids any obstruction of the view of the revered Cologne Cathedral situated nearby.

The cross section of the bridge consists of two box-girders 10.5 ft wide, with a depth varying from approximately 10 ft at the end abutments to 15 ft at the middle of the bridge, acting together with the steel deck plate,

which is 62.3 ft wide and 3/8 in. thick. The deck plate is stiffened by flat bar longitudinal ribs spaced 12 in. o.c. and transverse floor beams with a maximum depth of about 3 ft, spaced approximately 6.6 ft o.c. In order to stiffen the deck system near the center of the bridge cross section and to relieve the bending moments in the floor beams, an additional longitudinal rib, with a cross section similar to that of the floor beams, has been arranged at the bridge center line.

Cross diaphragms of considerable rigidity connecting the two main girders are spaced from 130 to 230 ft o.c.

Field splices of the deck plate and the ribs are welded; floor beam and main girder splices are riveted.

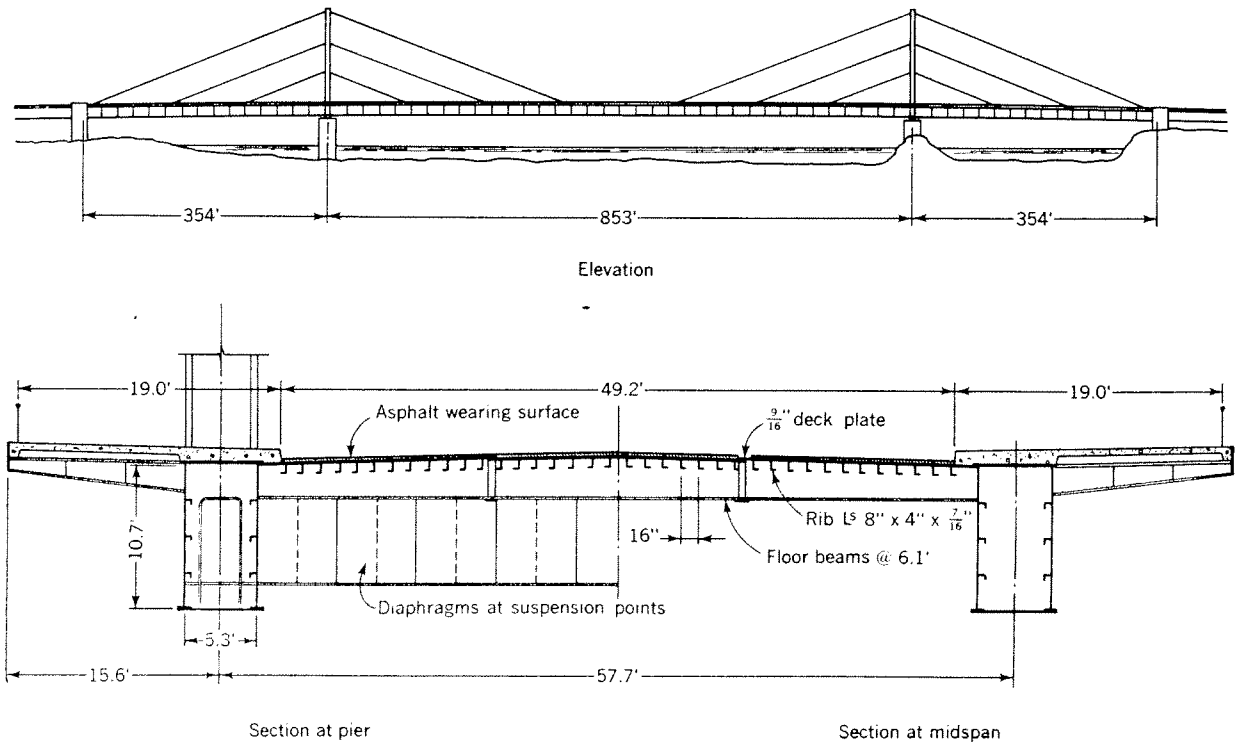


Fig. 1.15. Duesseldorf-North Bridge, Germany (1957)



Fig. 1.16. View of Duesseldorf-North Bridge

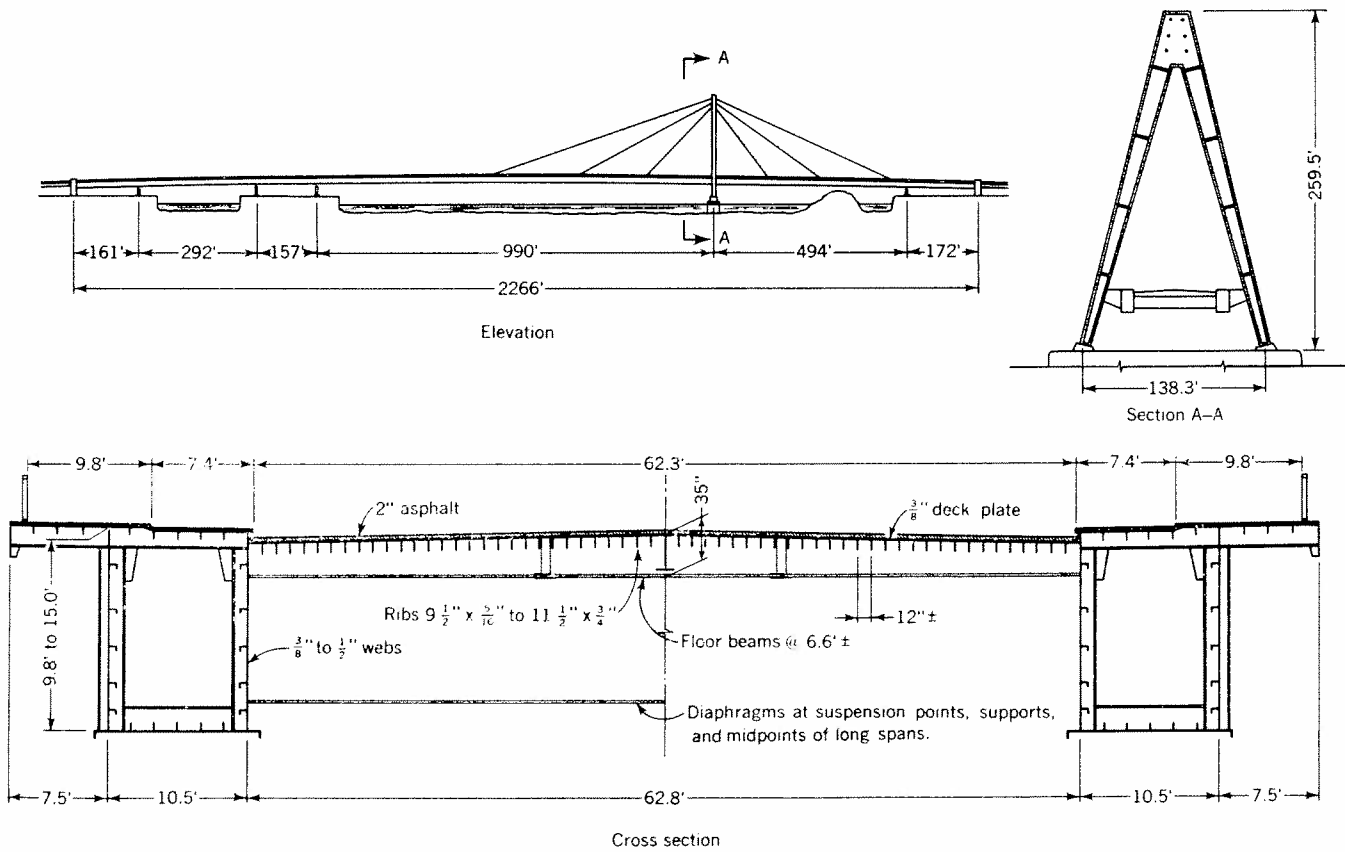


Fig. 1.17. Severin Bridge, Cologne, Germany (1959)



Fig. 1.18. General view of Severin Bridge, Cologne

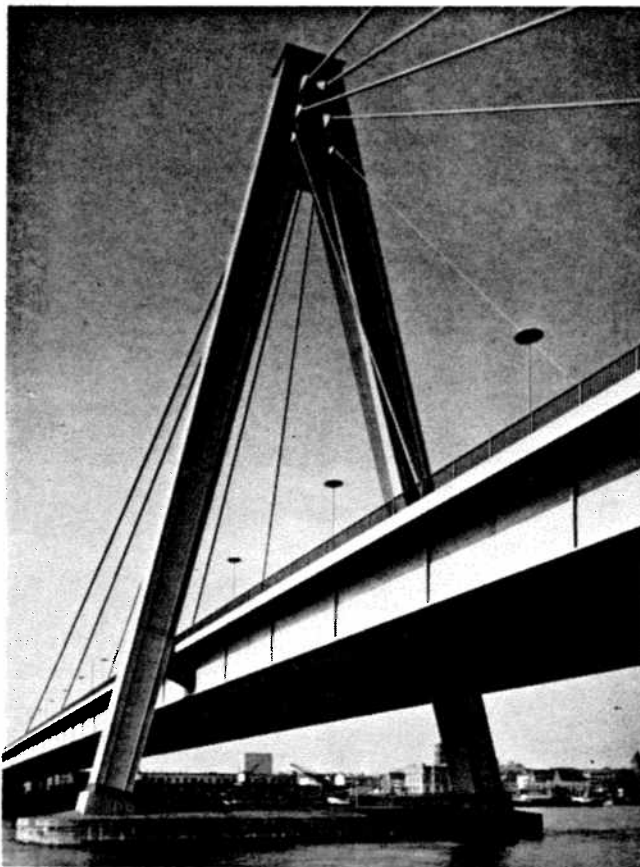


Fig. 1.19. View of Tower of Severin Bridge

1.1.3.3 Suspension Bridges

The stability of a suspension bridge depends generally on two major factors: the dead weight of the superstructure and the rigidity of the stiffening girders or trusses.

By the use of a steel plate deck, the dead weight is likely to be reduced, even as compared with an open grating or other conventional lightweight flooring



Fig. 1.20. Underside view of Severin Bridge

systems. However, the effect of the dead weight reduction on the stability may be more than offset by the increase of the flexural and torsional rigidity of the bridge stiffening system, due to the participation of the deck plate in sharing the stiffening system stresses.

Until now, the use of orthotropic steel plate decks with suspension bridges has been confined to structures having plate girders as stiffening members. However, the use of a steel plate deck is entirely feasible in conjunction with the stiffening trusses of suspension bridges and has been proposed in several long-span bridge projects.

If "air slots" are required in the deck near the stiffening trusses for increased aerodynamic stability, they may be provided by introducing a horizontal truss between the top chord of the stiffening truss and the steel plate deck.

Application of the steel plate deck to suspension bridges is illustrated by the following examples:

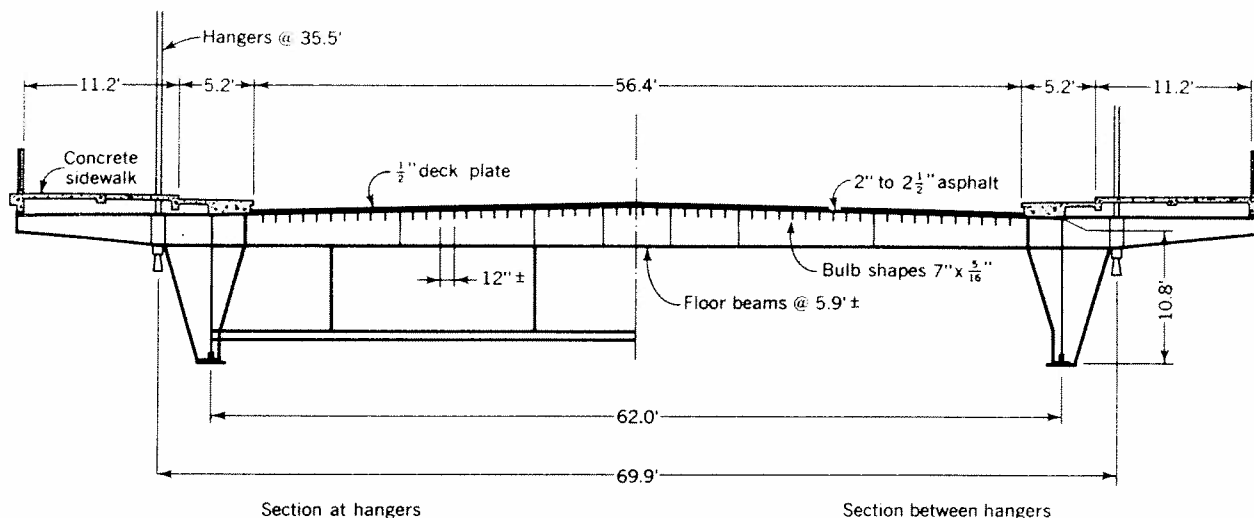


Fig. 1.21. Cologne-Muelheim Suspension Bridge, Germany (1951) (spans 279-1033-279 ft)

(a) *Cologne-Muelheim Bridge*, Germany, 1951 (Figs. 1.21, 1.22) [74, 80].

This structure was built to replace a self-anchored suspension bridge destroyed during the war. The span lengths are 279-1033-279 ft.

The $\frac{1}{2}$ -in. thick deck plate is made of carbon structural steel, except near the pylons where a $\frac{5}{8}$ -in. low-alloy steel plate has been used. The longitudinal stiffeners spaced 12 in. o.c. are $7 \times \frac{5}{16}$ -in. bulb shapes. The 62 ft long floor beams spaced 5.9 ft o.c., are 2.4 ft deep at the center.

The webs and the bottom flanges of the 10.8 ft deep main girders made of low-alloy steel are of riveted construction.

All field splices are riveted.

A comparison of the principal features and the weights of the old and the new bridges is given in Section 1.3.1.1.

(b) *Duisburg-Homberg Bridge*, Germany, 1954 (Fig. 1.23) [65, 81].

The structural system of this bridge resembles that of a self-anchored suspension bridge, except that in the

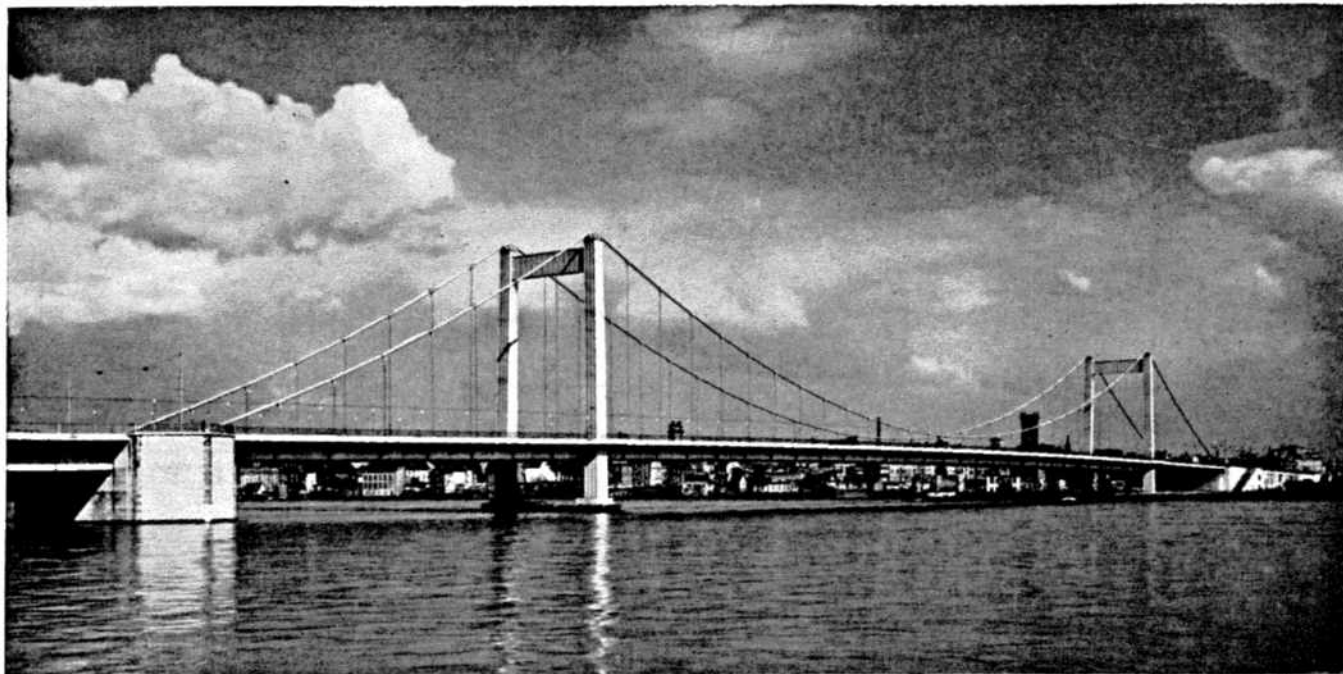


Fig. 1.22. View of Cologne-Muelheim Bridge

ORTHOTROPIC STEEL DECK BRIDGES

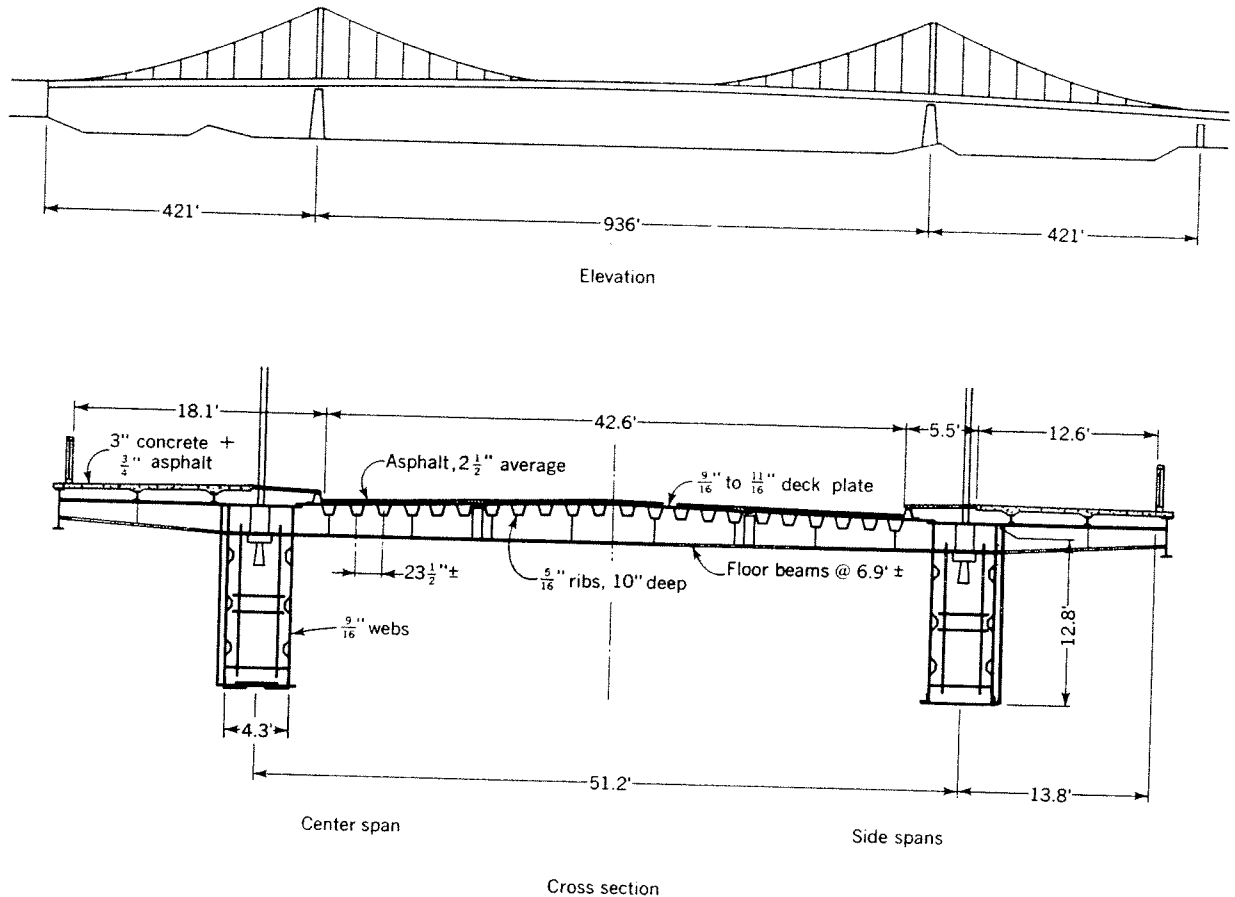


Fig. 1.23. Duisburg-Homberg Bridge, Germany (1954)

center span the main cables are discontinuous and are anchored in the stiffening girders.

In this structure torsionally stiff trapezoidal closed ribs were used for the first time.

These ribs, stiffening the $\frac{9}{16}$ -in. thick deck plate, have a span of 6.9 ft between the floor beams, are 10 in. deep and $\frac{5}{16}$ in. thick and are spaced approximately 2 ft o.c.

The box-shaped main girders with a constant depth of 13.5 ft are welded in the center span and riveted in the side spans of the bridge.

The field splices of the girders and the deck plate are riveted. The ribs are high-strength bolted. For handling the bolts, special hand holes have been provided in the bottoms of the ribs at splices (see Fig. 7.12).

1.1.3.4 Arch Bridges

In a stiffened-arch system, the steel plate deck, acting in conjunction with the stiffening girders, will contribute significantly to their flexural rigidity and thus increase their participation in carrying the loads. For a given stiffness desired, the deck contribution to the rigidity of the bridge cross section may permit making the stiffening girders shallower than they would have to

be without the deck participation. Thus a slender appearance may be obtained without sacrificing rigidity.

In a stiffened tied arch bridge the deck, in addition to being a part of the stiffening girders, will also participate in the tensile stresses of the girders acting as ties.

An example of such a structure is the *Port Mann Bridge*, Vancouver, Canada (Figs. 1.24, 1.25) [22, 62].

The span lengths of this three-span tied arch bridge are 360-1200-360 ft. The box-shaped arch ribs with a maximum depth of only 4.5 ft give the structure a very slender appearance.

The two main girders, together with the steel plate deck floor functioning as their upper flange, act as a tie of the arch system and provide the necessary stiffness.

The deck consists of a $\frac{7}{16}$ -in. thick plate stiffened by closed ribs 11 in. deep and $\frac{5}{16}$ in. thick, spaced 2 ft o.c., spanning the distance of approximately 6 ft-3 in. between the floor beams. The ribs and their splices are similar to those used in the Duisburg-Homberg Bridge (see Section 1.1.3.3b), except that the bottoms of the ribs are rounded.

The floor beams are 3 ft-6 in. deep at the center line of the bridge.

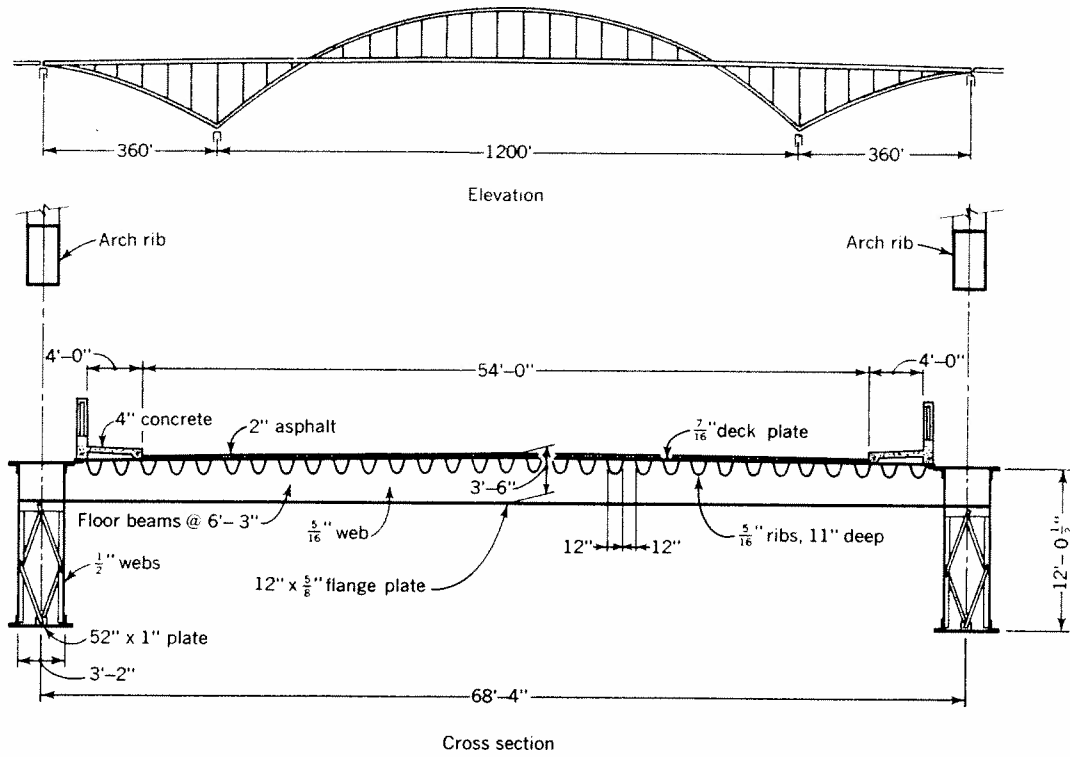


Fig. 1.24. Port Mann Bridge in Vancouver, B. C., Canada (under construction)

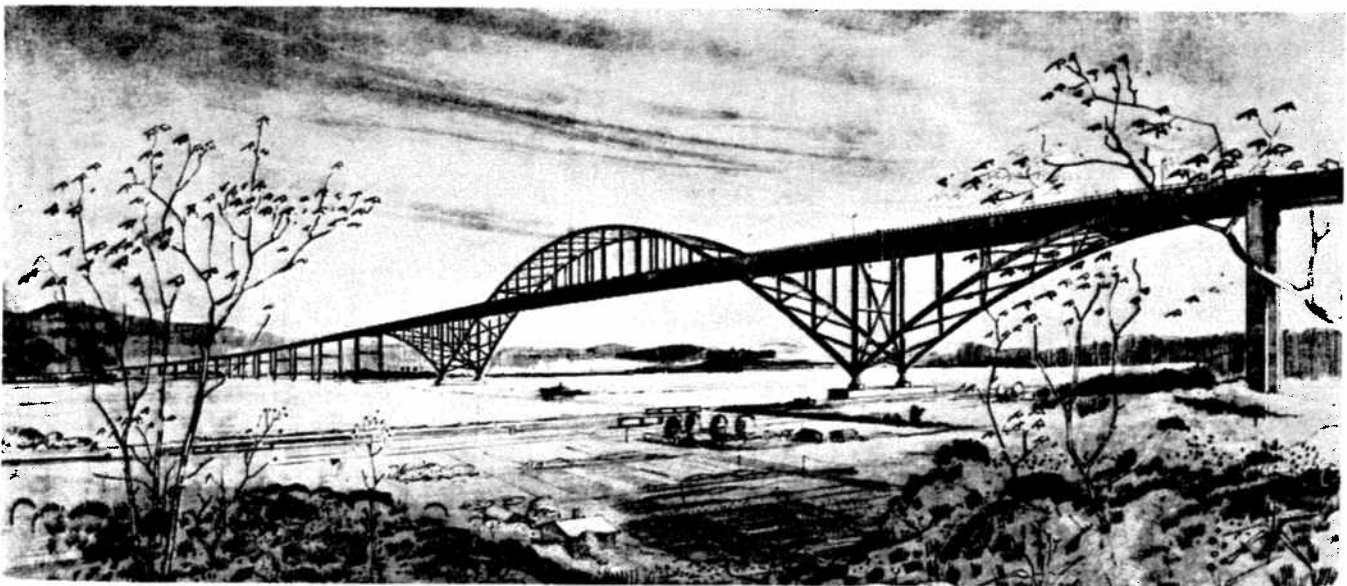


Fig. 1.25. Rendering of Port Mann Bridge in Vancouver

The main girders are box sections 3 ft - 2 in. wide and 12 ft deep.

The deck plate, deck stiffeners, arch ribs and the portions of the girders in tension are designed in low-alloy steel. The floor beams, the girder portions in compression and the remaining parts are of carbon steel. Because of the wide main girder spacing of 68 ft - 4 in., the use of low-alloy steel for the floor beams would have resulted in floor beam deflections that were considered too large.

The steel deck is shop-welded. The girders and the arches are of riveted construction; the field splices of all bridge members are high-strength bolted.

1.1.3.5 Truss Bridges

As an example of a truss bridge using a steel plate deck the *Fulda River Bridge* in Bergshausen, Germany, is shown in Figure 1.26 [72].

In this 7-span continuous truss bridge the deck plate and the longitudinal ribs participate in the upper chord stresses.

The detail of the ribs of this bridge is shown in Figure 7.3e.

Another example of a truss bridge with steel deck is shown in Figure 7.5.

1.1.3.6 Movable Bridges

In the design of movable bridges of all types, dead weight saving is one of the most important considerations.

The steel plate deck system, with a light-weight wearing surface (see Chapter 8) may provide a lighter unit weight of the bridge than any of the conventional systems, including the open grating floor. The additional advantages are: a solid riding surface, a considerable rigidity of the bridge and a shallow depth of structure.

An example of a bascule bridge with a steel plate deck is the *Bascule Bridge in Krakeroy*, Norway, 1957 (Fig. 1.27) [66].

The span length of this modified Scherzer type double-leaf bascule bridge is $2 \times 79 = 158$ ft.

The steel deck plate is stiffened by longitudinal flat bar ribs spaced 12 in. o.c. and transverse floor beams spaced approximately 4.9 ft o.c. The depth of structure at the midspan is only 2.4 ft.

The $1\frac{1}{2}$ -in. thick asphalt wearing surface is secured

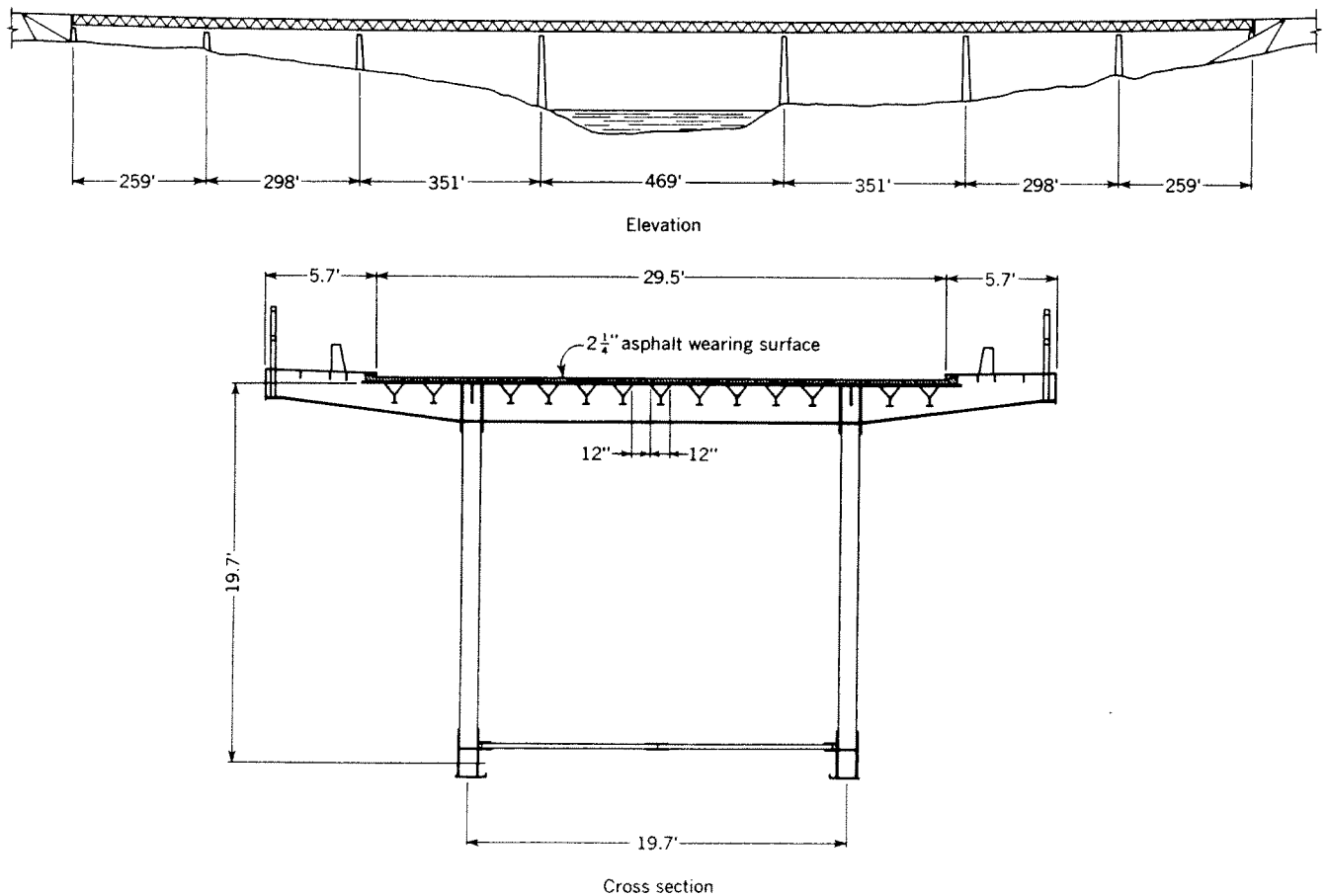


Fig. 1.26. Fulda River Bridge, Bergshausen, Germany (1961)

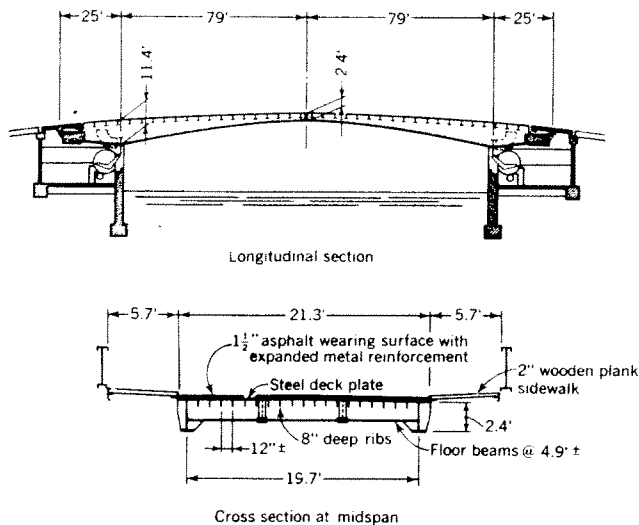


Fig. 1.27. Bascule Bridge in Krakeroy, Norway (1957)

against sliding in the open position of the bridge by expanded metal reinforcement welded to the deck.

The total average dead weight of the bridge (not including the two counterweights) is approximately 62 lbs per sq ft.

1.1.3.7 Railroad Bridges

A steel plate deck participating in the main girder stresses may be used to retain the ballast of a railroad bridge. This is exemplified by the *Railroad Bridge over the Autobahn in Wuppertal, Germany, 1959* (Fig. 1.28) [83].

The principal requirement specified for this structure by the railroad was speed of erection, needed to limit detouring operations to the shortest possible period of time. Another condition was to provide a structure with a slender appearance, desired for aesthetic reasons.

Both requirements were satisfied by a steel plate deck bridge, completely prefabricated in the shop, consisting of two flexurally and torsionally stiff box sections 7.3 ft deep and approximately 125 ft long, to span the 120-ft opening. Torsional rigidity was important because of the skew of the structure.

The upper flanges of the box-girders consist of a $\frac{3}{8}$ -in. thick deck plate stiffened by three triangular

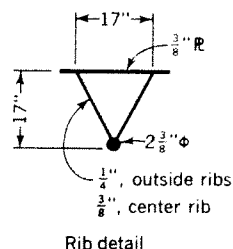


Fig. 1.28. Railroad Bridge in Wuppertal, Germany (1959) 120-ft span

stiffening ribs 17 in. deep, spaced 2.9 ft o.c. The middle rib is open at the top and serves also as the drainage trough of the roadbed. The ribs are continuous through the cross diaphragms spaced approximately 11.9 ft o.c.

The deck, the lower flanges and the lower portions of the main girder webs are made of carbon steel; the upper portions of the main girders consist of low-alloy steel.

The structure is all-welded.

1.2 STRUCTURAL BEHAVIOR OF STEEL PLATE DECK BRIDGES

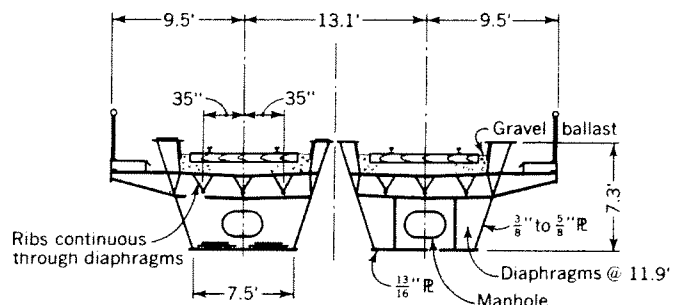
1.2.1 Comparison with Conventional Bridges

In contrast with the conventionally designed bridge, where the individual structural elements (decks, stringers, floor beams, main girders, etc.) are assumed to perform separate, clearly defined functions, the steel plate deck bridge is a complex structural system in which the component members are closely inter-related.

The basic difference between the two design approaches is illustrated in Figure 1.29, giving a comparison between the old and the new design of a highway bridge near Hedemuenden, Germany [45].

The old design (Fig. 1.29a) shows the usual piling up of the structural members. The concrete deck carries the wheel loads to the longitudinal stringers which, in turn, react on the transverse floor beams, delivering their load to the two bridge trusses. The floor system does not contribute to the strength or rigidity of the trusses, nor is it counted upon to secure the transverse stability of the bridge, which is provided by the upper and the lower wind bracing.

In the new design (Fig. 1.29b) the deck slab, the stringers and the floor beams have been integrated into one structural element—the stiffened steel plate deck with relatively closely spaced longitudinal and transverse stiffening ribs using the steel plate deck as a common top flange. The sharp distinction between the floor system and the main carrying members has disappeared, with the deck, including the longitudinal ribs, becoming a part of the main girders as their upper flange. The



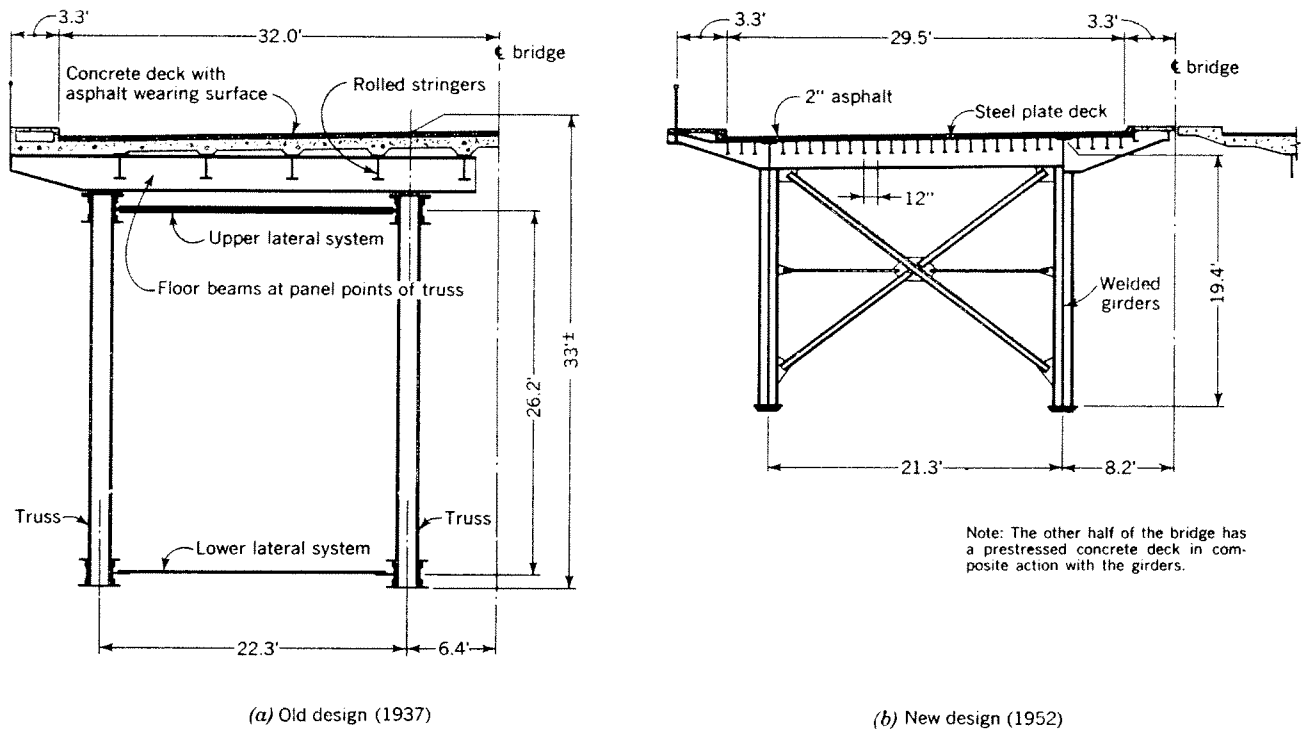


Fig. 1.29. Comparison of the old and the new design of the Autobahn Bridge near Hedemuenden, Germany (spans 210-263-314-314-263 ft)

steel plate deck also provides the bridge with ample transverse rigidity, thus obviating the need for a separate lateral system required in the original design.

The closely spaced grid structure of the stiffened steel plate deck, with the ribs continuous and rigidly connected to each other at intersections, is highly statically indeterminate and has a good load distributing capacity for concentrated wheel loads governing the deck design.

The safety of such a system against failure due to a concentrated load is considerably greater than that of a conventional bridge floor, since a local overload on a steel plate deck causes an elastic and, eventually, plastic stress redistribution to the adjoining elements rather than an immediate failure of the member. Should the local load be further increased beyond the critical limits, the eventual failure would be, necessarily, a local one, affecting only one out of the many ribs in the deck, without destroying the overall usefulness of the deck. A comparison may be made with a steel rope, where a failure of one wire does not significantly reduce the carrying capacity of the rope.

Additional safety reserves of steel plate decks are due to the membrane behavior of the deck plating at higher loads. This is discussed in Section 1.2.4.

1.2.2 Component Structural Systems of Steel Plate Deck Bridges

Stress in any member of a loaded steel plate bridge deck, and especially in the deck plate, is due to the com-

bined effects of the various functions performed by the deck in the bridge structure. Although these functions and the resulting stresses are inter-related, it is necessary, for clarity and design convenience, to treat separately the following structural component systems:

System I. The main bridge system, with the steel plate deck and the longitudinal ribs acting as a part of the main carrying members of the bridge.

System II. The stiffened steel plate deck consisting of the longitudinal ribs, transverse floor beams and the deck plate as their common upper flange, acting as a bridge floor.

System III. The deck plate, acting locally as a continuous member directly supporting the concentrated wheel loads placed between the ribs and transmitting the reactions to the ribs.

It is seen that the function of the steel deck plate, participating in all three structural systems, is especially significant.

1.2.3 System I—The Deck as Part of the Main Carrying Members

In the usual case of a girder bridge, the steel deck plate, together with the longitudinal stiffeners rigidly connected to it, functions as the top flange of the main girders. This requires an adequate shear connection between the deck plate and the webs of the girders.

The determination of the *effective width* of the deck

Fig. 1.30. Test measurements of stresses in the deck plate acting as the flange of the main girders of the Save River Bridge at the supports

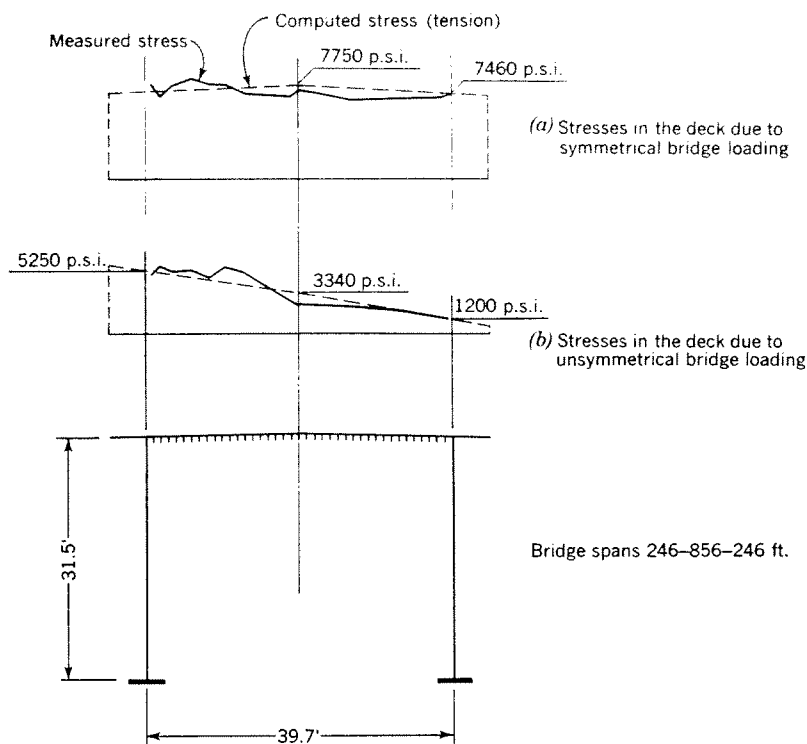


plate acting with a girder web is based on theoretical investigations by Chwalla [7] and others. Generally, the effective width depends on the girder span and the type of loading and is independent of the plate thickness. For a uniform loading of the girder, it amounts to about one-third of the girder span and is approximately the same in the midspan and over the supports of a continuous girder.

For design purposes, it may be assumed that the entire cross-sectional area of the steel deck participates as the top flange of the main girders, provided the girder spacing is smaller than one-third of the girder span.

The full participation of the deck in the main girder stresses has been confirmed by stress measurements on existing steel plate deck bridges. An example showing the stress distribution across the entire width of the deck at the support of the Save River Bridge in Belgrade is given in Figure 1.30a. Figure 1.30b shows that, in the case of an unsymmetrical loading of the bridge girders, the stress in the deck varies linearly between the girders.

In the vertical direction, the stress in the deck varies with the distance from the neutral axis of the bridge cross section. Thus, the stress in the bottoms of the stiffening ribs is somewhat lower than in the deck plate (Fig. 1.37).

The cross-sectional area of the deck plate and its longitudinal stiffeners is, as a rule, considerably larger than the bottom flange area of the girders. This results in an *unsymmetrical girder cross section*, with the neutral

axis shifted toward the deck, and the stresses in the deck lower than in the bottom flanges (Fig. 1.37). Such unsymmetrical distribution of the main girder stresses (System I) is very advantageous in the design, since it provides the necessary stress reserves for the local bending in the deck (System II).

The bending moments, shears and stresses of System I are computed by the usual methods.

The *live load distribution* to the individual main girders depends on the type of bridge cross section and the transverse connections between the girders. In the case of two single-web main girders, the steel plate deck may be assumed to transmit the loads to the girders as a simple beam. With box-shaped girders, proper consideration should be given to the torsional rigidity of the bridge cross section. If more than two main girders are present, the load distributing action of the transverse diaphragms or cross frames should be taken into account.

Participation of the deck in the main girder stresses will cause *tension* in the deck in the areas of the negative moments of the main girders and *compression* in the areas of the positive moments.

The factor of safety against *overall buckling* of the deck in compressive stress areas is usually high because of the ample longitudinal and transverse stiffening of the deck plate by the ribs and floor beams and the generally low intensity of the System I compressive stresses in the deck. Therefore, in the usual cases, an investigation of the elastic stability of the deck is not needed.

However, the safety against *local buckling* of the flat bar ribs may have to be investigated, especially if such ribs are made deep and slender to increase their effectiveness as flexural members in System II. It should be noted that a ratio of depth to thickness of open ribs between 20 and 30 to 1 is not uncommon in existing bridges.

Formulas for the computation of the safety factor against local buckling are given in Appendix II.

Box-shaped longitudinal stiffening ribs of usual proportions may be considered safe against local buckling.

1.2.4 System II—The Deck as the Bridge Floor

1.2.4.1 Structural Behavior under Design Loads

The floor system, consisting of the longitudinal ribs and the transverse floor beams, both using the steel deck plate as their common top flange, may be treated as an independent structural member of the bridge by assuming all horizontal shear connections between the deck and the main girders to be severed. According to this assumption, the floor system rests on the main girders; however, no longitudinal forces can be transmitted from the girders into the deck, which is subject only to the local effects of the external loads applied to the deck.

A concentrated load applied to the steel deck between the ribs is first transmitted to the nearest longitudinal ribs through the deck plate acting in bending and tension. As has been noted above, these local plate stresses are treated separately in System III.

The longitudinal ribs, acting as continuous members,

react on the floor beams, which carry their load to the main girders.

The transverse floor beams deflect proportionately to the loads they carry and thus provide elastic supports for the longitudinal ribs. This is illustrated in Figure 1.31a. It is seen that, due to the floor beam flexibility and the continuity of the steel deck plate forming the common top flange of all stiffeners, the ribs cannot act independently of each other, and the ribs over which there is no load also must deflect and become stressed.

Figure 1.31b shows schematically the deflection line and the corresponding bending moment diagram of a longitudinal rib directly loaded by a wheel. It is seen that the rib behaves in a manner similar to a *continuous beam on elastic supports*. However, near the main girders the effect of the floor beam flexibility is small and the ribs act more nearly as continuous members on rigid supports (Fig. 1.31c).

The floor beams framed into single-web girders may be regarded as simply supported. However, with box-shaped girders, the end restraint of the floor beams must be considered. If there are more than two main girders, the floor beams are usually treated as continuous beams on unyielding supports. This presumes that the bridge cross section preserves its geometric shape under all loading conditions, which must be secured by strong diaphragms connecting the main girders.

In accordance with present design practice, the ribs and the floor beams carrying locally applied loads (System II) are assumed to act as purely flexural structural members (i.e., free from axial forces), conforming

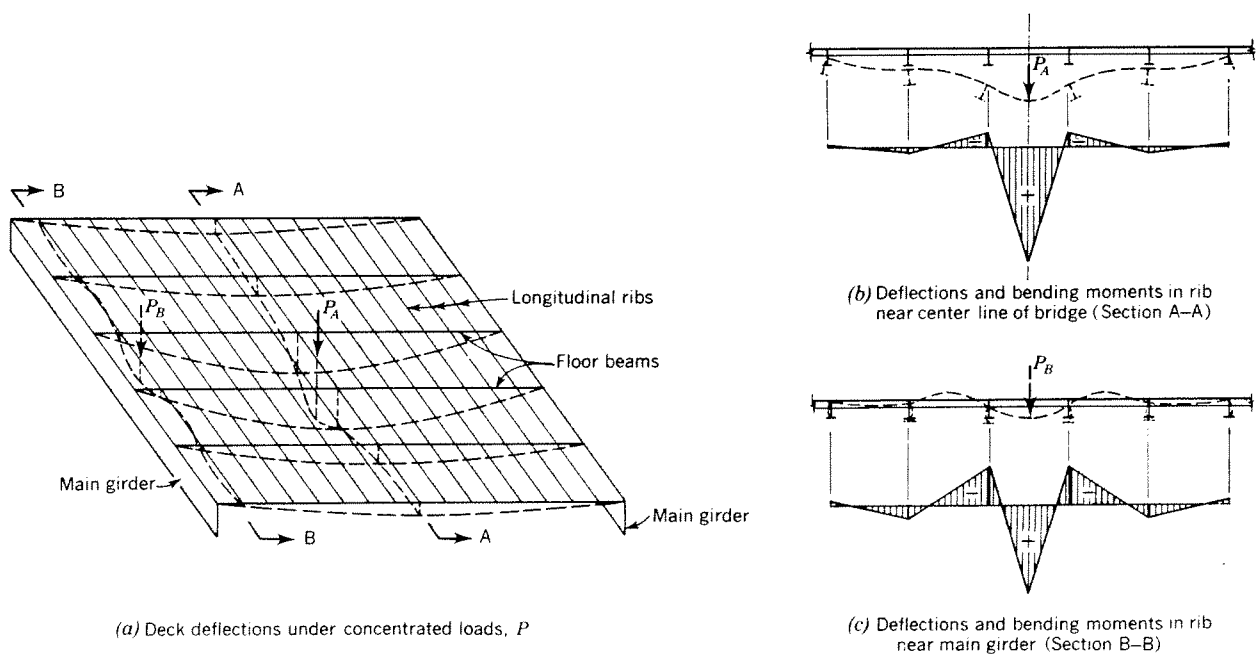


Fig. 1.31. Deflections of a steel plate deck and bending moments in longitudinal ribs (System II)

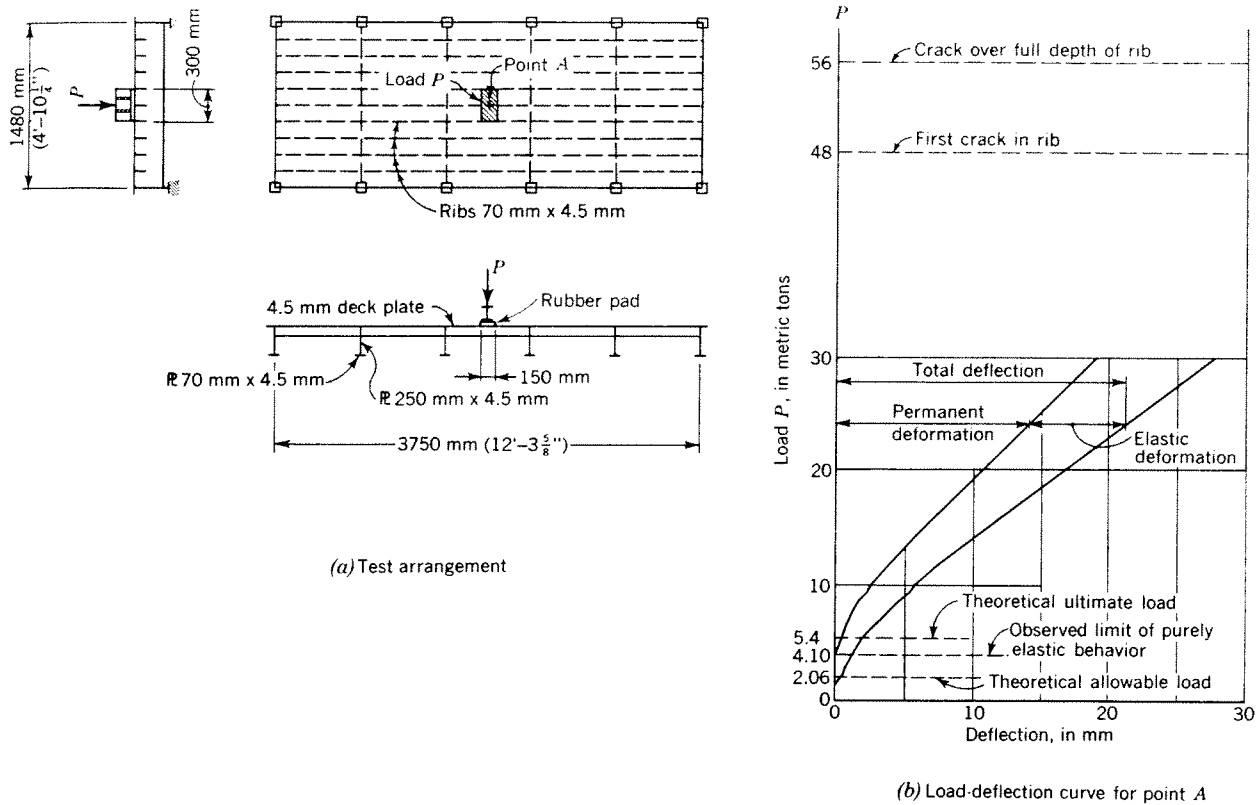


Fig. 1.32. Load test on a half scale model of Save River Bridge deck plating

to the usual first-order theory of bending, disregarding the effects of the deflections on the stresses.

Within the range of the usual working loads and geometric proportions of the steel plate bridge decks this assumption, underlying all theoretical methods available today for the design of such decks, is confirmed by the test measurements of the stresses in ribs, which are generally found to be in reasonable agreement with the computed values [42]. However, analytical methods based on the first-order flexural theory fail to describe correctly the steel plate deck behavior under large loads and deflections and cannot be used for evaluation of its actual carrying capacity. This is discussed in Section 1.2.4.2.

1.2.4.2 Structural Behavior under Higher Loads

(a) General

Tests on steel plate bridge decks have shown that, if a load on the deck is increased beyond the usual wheel load limits, or if the ratio of the deflection to the span of a rib is relatively large, internal axial stresses begin to appear in the loaded ribs, in addition to the purely flexural stresses. An additional tension, due to a *membrane action* of the deck plate, occurs in the directly loaded rib, and has to be balanced by an equally large compression in the adjoining ribs.

As the loads and the corresponding deflections increase, a complete redistribution of the stresses takes place in the system, and the membrane stresses almost entirely replace the flexural stresses which are predominant under working loads.

Thus, with sufficiently large deflections, the steel plate deck behaves in a manner radically different from that predicted by the usual flexural theory which disregards the effect of the deformations of a system on its stresses. Most importantly, its strength has been found to be many times greater than predicted by the ordinary flexural theory.

This is illustrated by the tests on steel plate decks described below.

(b) Tests on the Model of the Save River Bridge Deck Plating with Open Ribs

Tests for the purpose of determining the deflections and the ultimate strength of a steel plate deck with open ribs under a concentrated wheel load were conducted at the Technological University in Darmstadt (Germany), to provide the design criteria for the deck of the Save River Bridge in Belgrade [30].

The 5-span continuous test panel, made of structural carbon steel, was a half-scale model of the deck plating intended for this bridge. The model dimensions and the

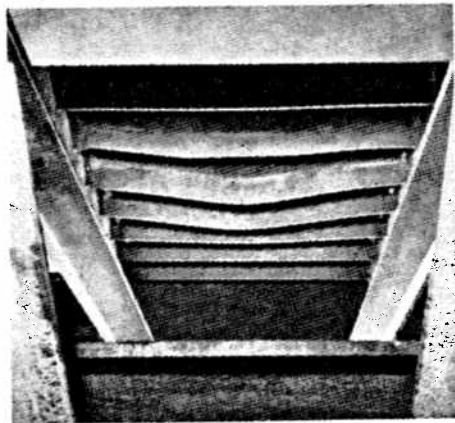
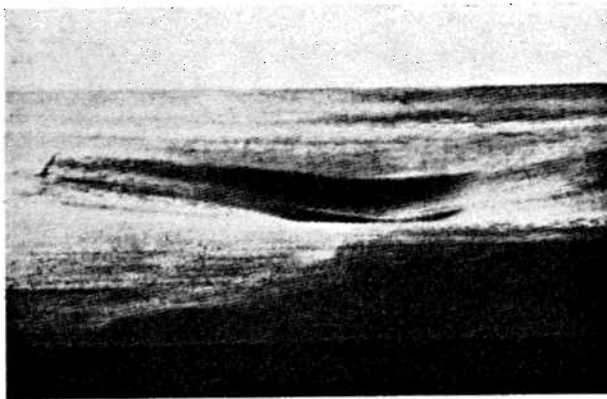
(a) Crack in rib at $P=48$ tons(b) Deformation at $P=56$ tons

Fig. 1.33. Load test on model of Save River Bridge deck plating (Fig. 1.32)

arrangement of one of the two tests made are shown in Figure 1.32a.

The computation based on ordinary flexural theory indicated that the following conditions should occur at the bottom fiber of the rib directly under the load, P :

Allowable stress of 1.4 t/cm^2 (19.8 ksi)†	at $P = 2.06 \text{ t}$
Yield stress	at $P = 3.52 \text{ t}$
Ultimate strength	at $P = 5.42 \text{ t}$

However, the behavior and ultimate strength observed in the test were strikingly different from the predicted values. Under repeated loading, a purely elastic behavior was observed up to a load $P = 4.1 \text{ t}$, at which the first permanent deflection of 0.01 mm was measured, indicating yield stress in the rib. Beyond this point, unlike an ordinary flexural member, there was no unrestrained increase of deflection followed by collapse, but the deflections increased, at a somewhat faster rate, still in linear proportion to the load. Deflections were recorded up to the load $P = 30.5 \text{ t}$, as shown in Figure 1.32b.

† $\text{t} = \text{metric tons}$.

The first crack in the bottom fiber of the rib occurred at a load $P = 48 \text{ t}$; the crack spread through the entire depth of the rib at $P = 56 \text{ t}$. However, the capacity of the test panel was not yet exhausted, since the remaining ribs were still intact. The underside view of the panel at a load of 48 t is shown in Figure 1.33a, the view of the deck after test is shown in Figure 1.33b.

With $P = 56 \text{ t}$ considered the ultimate load, we obtain a ratio of the actual to computed ultimate load of $56/5.42 = 10.3$.

The excess load carrying capacity of the deck plating was partially utilized in the final design of the bridge as discussed in Section 9.3.2.

(c) Tests on a Deck Plating Panel with Closed Ribs

Tests on deck plating panels with closed (torsionally rigid) longitudinal stiffening ribs were made at the Technological University in Stuttgart [42, 44].

The dimensions of the test panel with trapezoidal ribs, which may be regarded as a half scale model of an actual bridge panel, are shown in Figure 1.34a. Since one of the purposes of the tests was to determine the effect of the torsional rigidity of the ribs, which becomes more pronounced with longer rib spans, a relatively long span of the ribs was chosen, with a low rib depth-to-span ratio of $1/44$. The material was structural carbon steel.

The characteristic values for a concentrated wheel load, P , were computed in accordance with the first-order flexural theory as follows:

Allowable stress of 1.4 t/cm^2 (19.8 ksi) at the bottom of the loaded rib	at $P = 1.45 \text{ t}$
Yield stress in rib	at $P = 2.56 \text{ t}$
Ultimate strength	at $P = 3.8 \text{ t}$

The stress and deflection measurements made on the panel loaded by the theoretical allowable load of 1.45 t were in good to fair agreement with the results obtained by the formulas given in Chapter 5 of this Manual, with the exception of points directly under the load, where, because of an unusually small depth-to-span ratio, the flexural stresses in the loaded rib were found to have a superimposed tensile stress of the order of 2.5 ksi , indicating a partial membrane condition. This is also evidenced by the shape of the deflection line of the loaded rib No. I (Fig. 1.34a), which is an almost straight line, rather than a parabolic curve characterizing deflected structural members acting in pure bending.

It should be noted that, in this rather exceptional case, a measurable membrane condition occurred well within the elastic range, before reaching the plastic limit at any point, and with the deflection under load of only $1/500$ of the rib span.

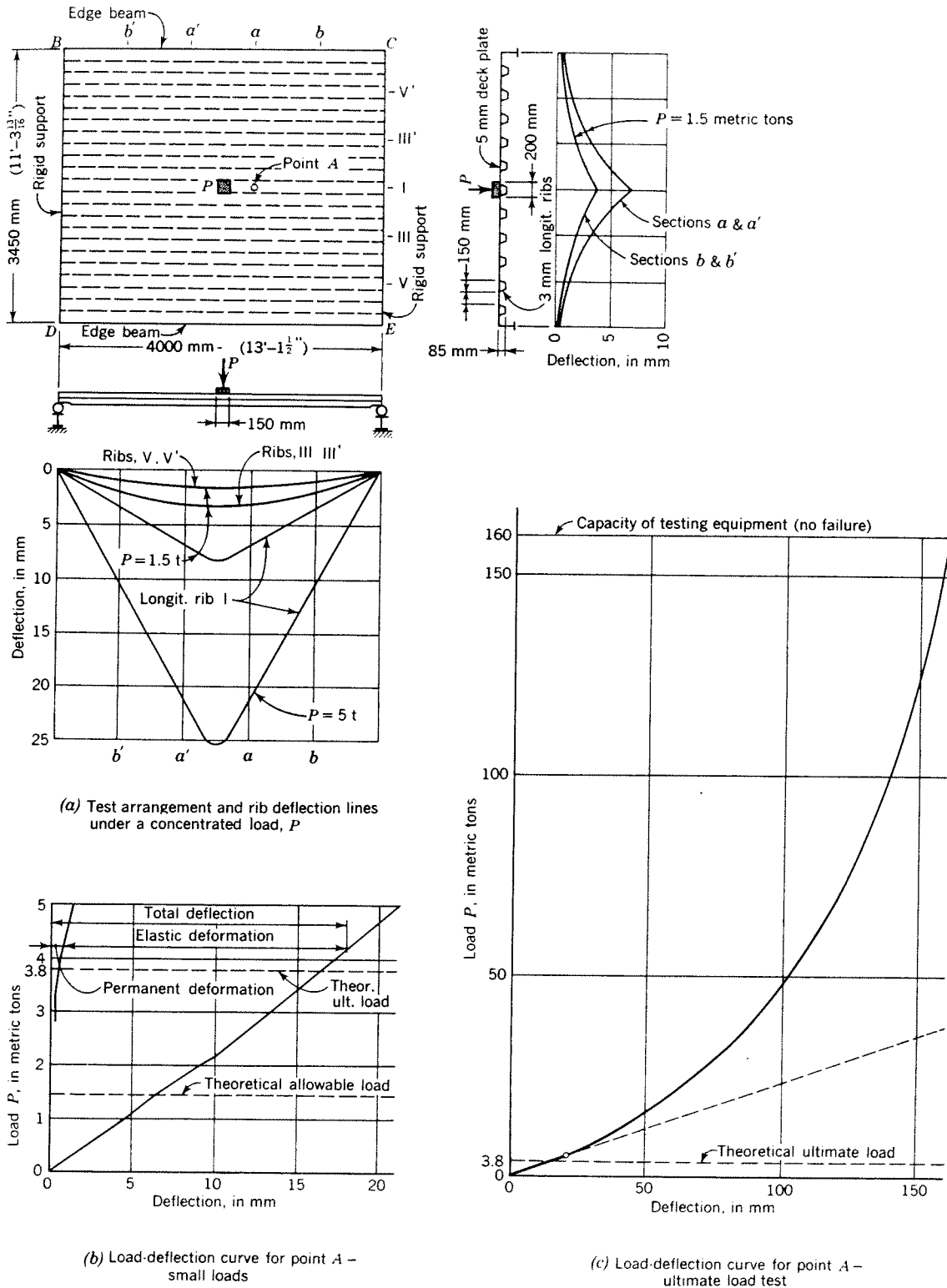
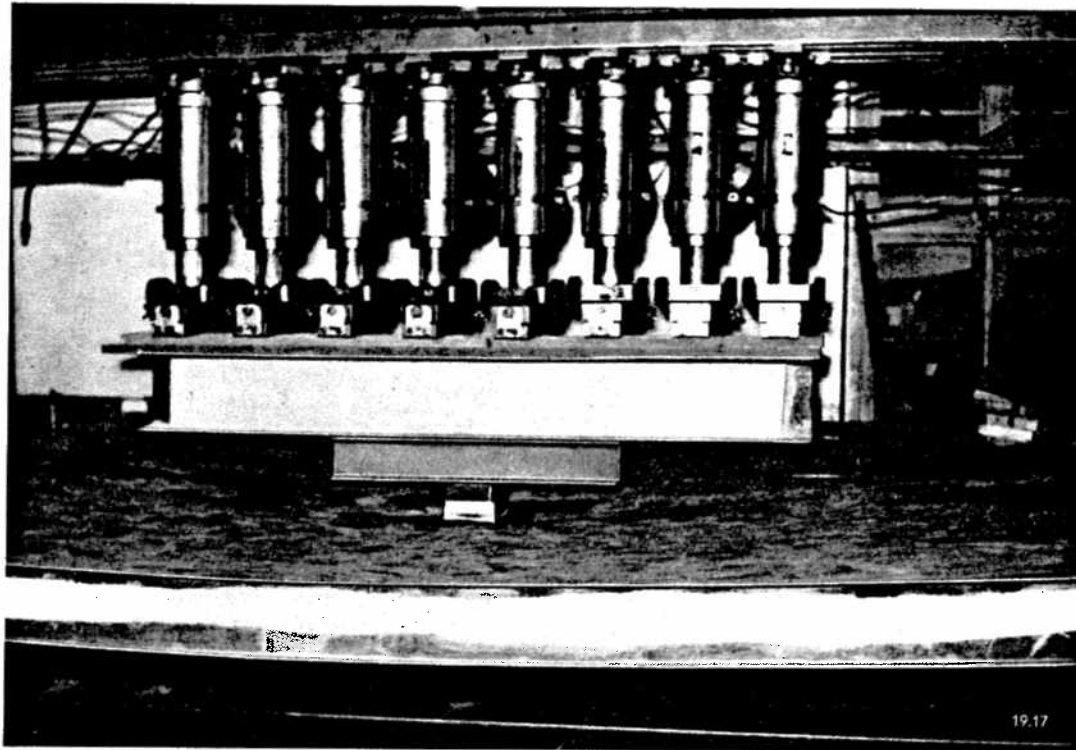


Fig. 1.34. Load test on a steel deck panel with closed ribs

(a) Test panel under maximum load, $P = 160$ tons

(b) Side view of the central portion of the test panel cut out after test



(c) Cross section through the central portion of the test panel after test

Fig. 1.35. Load test on a steel deck panel with closed ribs (Fig. 1.34)

As the load was further increased, an almost linear relationship between the load and the deflection was observed up to the value of $P = 5$ metric tons, beyond the theoretically computed ultimate load. At this loading a permanent set of 1.3 mm ($\frac{1}{3000}$ of the rib span) was measured (Fig. 1.34b).

The deflections under loads greater than 5 tons were no longer proportional to the loads, but grew at a *slower* rate relative to the loads (Fig. 1.34c), unlike in the test on the Save River Bridge plating (Fig. 1.32). Such behavior may be explained by a particularly effective membrane action in this case, made possible by the large deflections of the slender plating panel and the presence of sufficiently rigid closed ribs and the edge beams BC and DE, capable of developing the compressive and flexural reactions necessary to balance the tensile membrane stresses in the loaded portion of the panel. It should be noted that no horizontal external reactions could de-

velop at the rigid supports BD and CE of the panel.

In an attempt to cause failure of the panel, the load was increased up to 160 metric tons, at which point the full capacity of the test equipment was reached (Fig. 1.35). However, even at this load, no crack in the rib or in the welds could be observed. Thus the ultimate load in this case was greater than 42 times the computed critical load of 3.8 metric tons.

The importance of sufficient compressive strength of the plating adjoining the directly loaded rib was demonstrated in a test with a deck plating panel made of a 3-mm thick plate and closed rectangular stiffening ribs of the same wall thickness [44]. The capacity of the panel was found limited by the buckling strength of the deck plate which failed before any considerable membrane action could develop. Still, even in this case, the actual ultimate load was greater than the computed value.

(d) *Conclusions*

In all static load tests on steel plate deck panels the actual ultimate capacity of the longitudinal ribs was found to be considerably greater than the computed values.

The tests have also shown that the limit of a purely elastic behavior of a loaded rib is higher than predicted by ordinary flexural theory. This could be an indication of a non-linear relationship between the stresses in ribs and the loads in the elastic range above the working load level, with stresses increasing at a slower rate than the loads (Fig. 1.36). Thus the actual safety against

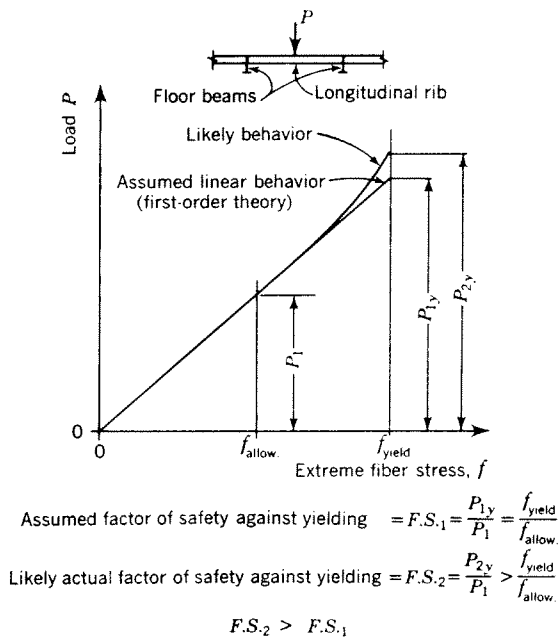


Fig. 1.36. Schematic load-stress diagram of a longitudinal rib of a steel plate deck

reaching the yield point stress may be higher than that computed on the basis of a straight line load-stress relationship. It should also be noted that, unlike in a tensile member or a beam, reaching plasticity at one location of the steel plate deck does not seem to be a characteristic point at which the structural behavior is changed in any significant way.

No load tests have been made on floor beams of steel plate decks: however, a similar excess of carrying capacity of the floor beams may be expected.

The observed structural behavior and the surprisingly high load carrying capacity of the steel plate deck under a static concentrated load are explained by a favorable combination of the *membrane action* of the steel plate and the *plastic strength* reserves of the highly statically indeterminate system of the deck. However, a more precise understanding of the extremely complex structural

mechanism of a steel plate deck under large loads is still lacking, and some aspects of its structural behavior have not yet been sufficiently clarified.

It should be noted that practical utilization of the high static strength of the steel plate deck may be limited by two factors: undesirable deck deformations and the fatigue strength, defined as the ability of the deck to withstand a very large number of pulsating stress cycles caused by moving vehicle loads.

While the design limitations based on undesirable deflections or deformations of the members may be defined with relative ease, the question of the theoretical fatigue strength of the deck plate and the ribs and its practical significance in the deck design has not yet been adequately explored.

Dynamic load tests made at the Technological University in Darmstadt [31] on a flat deck plate acting between the ribs (System III) have shown that the fatigue strength of the deck plate subject to a pulsating load is high and reaches the order of the yield point of the material (see Chapter 6). No reports on dynamic tests on the longitudinal ribs of a steel plate deck have as yet been published; however, it appears that the fatigue strength of the ribs ought to be less critical than that of the flat plate, since the System II stresses subject to pulsation under passing wheel loads, to be superimposed on the System I stresses in the ribs, are usually lower than the System III stresses in the flat deck plate, and the likelihood of developing the full design values of the System I live load stresses is small.

The observed discrepancies between the predicted and the actual behavior of steel plate decks make it obvious that the design methods based on the assumed linear proportionality of the loads, deflections and stresses and using the traditional "allowable stress" concept, while useful for computation of the stresses under working loads, are not appropriate for determination of the deformations of a steel plate deck under higher loads and its actual safety. Since an accurate computation of stresses under working loads is of little value in the design if a proper evaluation of the actual safety of the structure against failure or undesirable deformations is lacking, any undue analytical refinements of the design methods based on the ordinary flexural theory should be considered unwarranted.

The ultimate behavior of a steel plate deck under the effect of wheel loads could be adequately described only by a second order theory, taking into account both the effects of the deflections on the stresses and the plasticity of steel. While a rigorous analytical solution of this problem, if it could be achieved at all, would be much too complex for engineering purposes, simplified design methods based on the observed behavior under static as well as dynamic loading are certainly desirable for

a more realistic design of steel plate bridge decks. Research work along these lines is in progress.

Until such improved methods are developed, the presently available first-order flexural theory will serve for design purpose.

Discussion of the theory and the design method of the steel plate deck as an independent element (System II) is the subject of the Chapters 2 to 5 of this Manual.

The shortcomings of the first order design theory may be partly compensated by an appropriate choice of stresses to be used in the design, as discussed in Chapter 9.

1.2.5 System III—The Deck Plate Acting between Longitudinal Ribs

A wheel load placed on the steel deck plate between the stiffening ribs is transmitted to the ribs by the deck plate

acting as a continuous isotropic plate (System III).

In addition to the stresses due to transmitting the directly applied load to the ribs, additional flexural stresses occur in the deck plate due to the shear transfer in the transverse direction of the bridge in a system with torsionally stiff ribs.

The above local stresses in the deck plate are not included in the System II stresses discussed in Section 1.2.4.

If a concentrated load on a flat steel plate supported on ribs is increased, the flexural stresses in the plate are gradually replaced by membrane stresses and a load-carrying capacity much higher than that computed by the first-order theory is observed, as in System II.

In view of the proved high strength of a flat steel

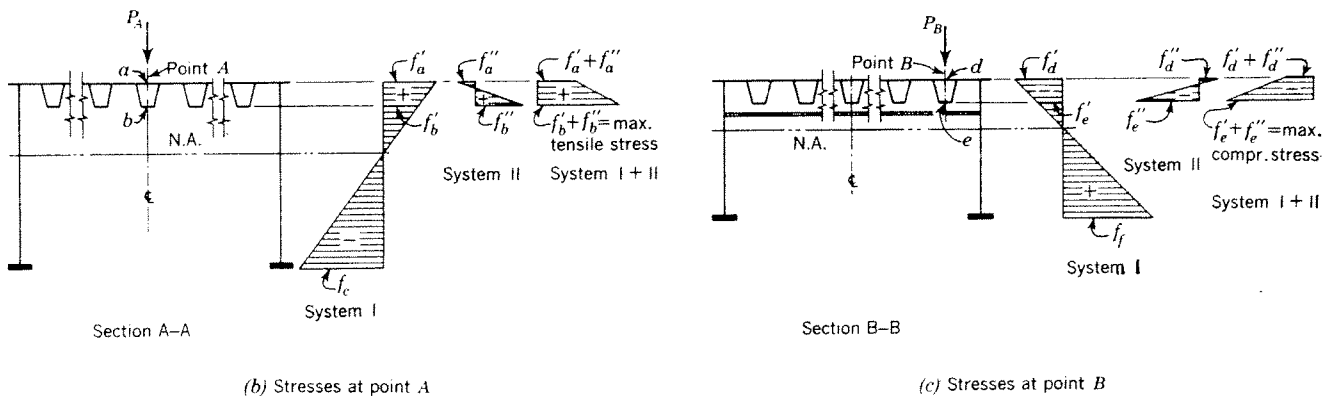
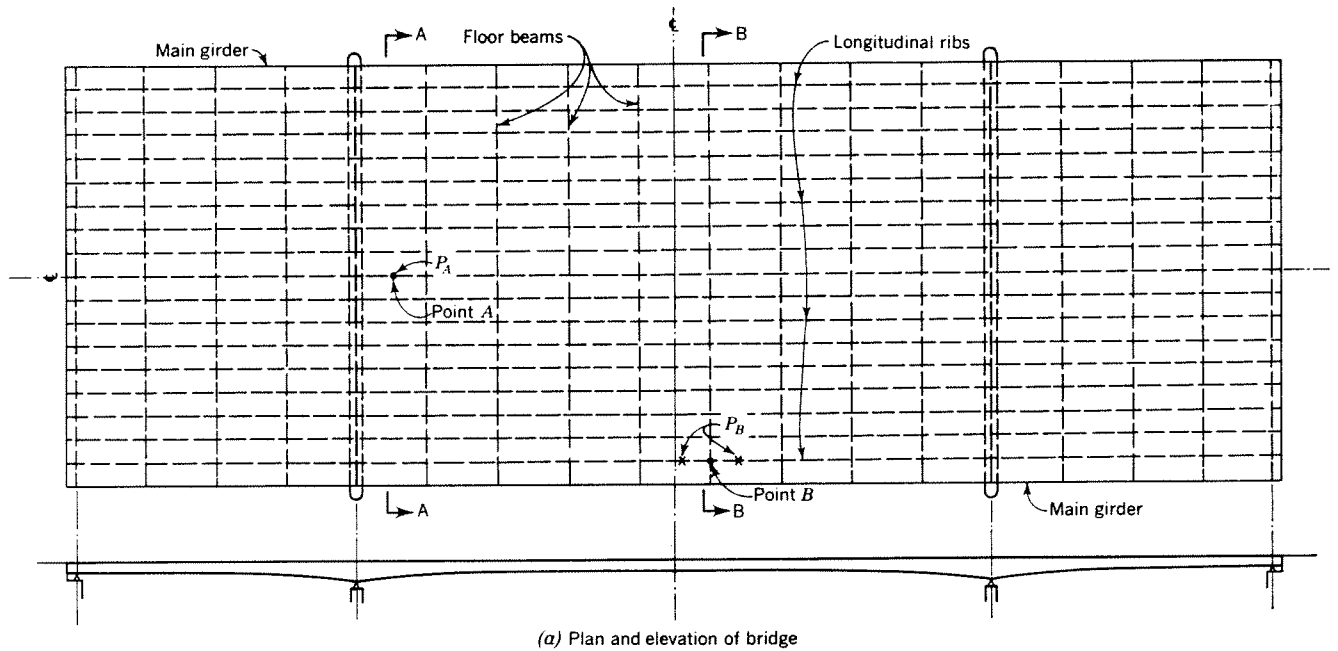


Fig. 1.37. Stress superposition in a steel plate deck bridge

plate under concentrated loads, the local System III stresses are, as a rule, disregarded in the design.

This is discussed in more detail in Chapter 6.

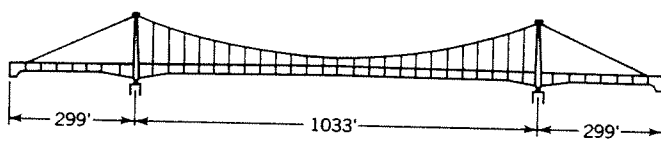
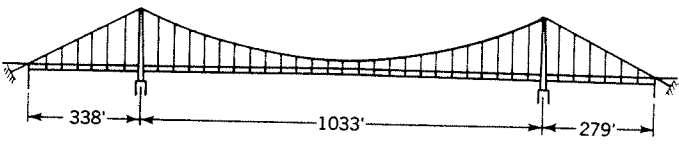
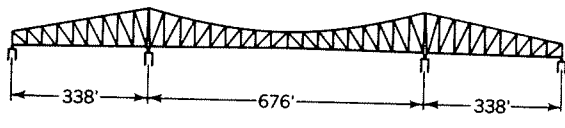
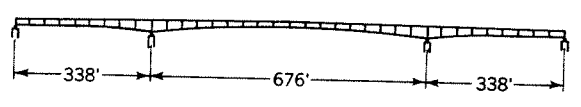
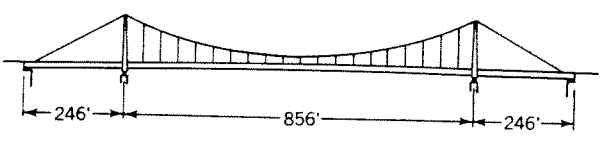
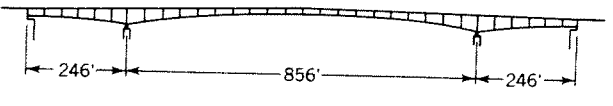
1.2.6 Stress Superposition

The maximum stress in any member of a steel plate deck under working loads is obtained by an appropriate superposition of the stress components due to the mem-

ber's participation in the basic structural systems discussed in the foregoing sections.

It should be noted that such superposition is based on an assumption that the linear relationship between the loads and the stresses is not affected by the interaction of the individual systems. For a discussion of this assumption see Section 9.3.4.

In a deck girder bridge, the System I action of the deck will cause compression in the areas of positive

BRIDGE	ELEVATION	YEAR	WEIGHT, TONS OF 2000 LBS.	
			STEEL*	TOTAL
COLOGNE- MUELHEIM		1929	14,150	20,000
		1951	6,400	9,500
DUESSELDORF- NEUSS		1930	9,300	22,000
		1951	6,970	8,400
SAVE RIVER, BELGRADE		1934	7,500	13,000
		1956	4,200	5,200

*Note: Weights of suspension bridges include towers and cables.

Fig. 1.38. Steel weight and total dead weight of the old and the new designs of three bridges

moments and tension in the areas of negative moments of the main girders.

To the axial stresses of System I, the flexural stresses of System II in the longitudinal direction of the bridge have to be added. Due to the asymmetrical rib cross sections, these stresses will reach their maximum values at the lower fibers of the directly loaded longitudinal ribs, with maximum tension occurring directly under a wheel load located at the midspan of the rib between the floor beams, and maximum compression at the intersection with the floor beam.

The contribution of the local System III stresses in the deck plate, acting primarily in the transverse direction of the bridge, to the longitudinal stresses of Systems I and II is generally disregarded in the stress superposition.

An example of a stress superposition in the bridge deck is given in Figure 1.37. Points *A* and *B* indicate the locations where the maximum stresses in Systems I and II are of the same signs, producing local stress peaks.

The stress components of Systems I and II to be added have to be caused by the same loading. It should be noted that the loads and their positions producing maximum stresses at a certain location are not necessarily the same in both systems.

It is important to note that, for any loading on the bridge, the critical peak stresses obtained through superposition occur only in a few isolated points, surrounded by material subject to a substantially lower stress intensity.

It is obvious that the values of stresses obtained through superposition of the stress components of structural systems having basically different characteristics and inherent safety factors should not be interpreted in the same manner as the stresses in a homogeneous

system, if these values are to be used to evaluate the safety of the structure. This is discussed in Chapter 9.

1.3 ECONOMIC CONSIDERATIONS

1.3.1 Factors Contributing to the Economy of Steel Plate Deck Construction

1.3.1.1 Steel Weight Saving

The weight per sq ft of structural steel in orthotropic steel plate deck bridges with spans exceeding about 150 to 200 ft is, as a rule, less than that of similar steel bridges of conventional design. The steel weight saving becomes remarkable as the bridge spans increase.

This is illustrated in Figure 1.38, giving a weight comparison of three structures: (a) the Cologne-Muelheim Bridge (Fig. 1.21), (b) the Duesseldorf-Neuss Bridge (Fig. 1.10) and (c) the Save River Bridge (Fig. 1.8). In the above cases the old, conventionally designed bridges, destroyed during the war, have been replaced by the new structures using steel plate decks.

It is seen that the respective steel weight savings are: (a) 55%, (b) 25%, (c) 44%.

In case (a), the original self-anchored suspension bridge design has been changed to the more efficient earth-anchored system; however, the major part of the steel saving is due to a lighter deck construction and the deck participation in the stiffening system stresses [43].

The steel weight saving in case (b) is remarkable, since in this case a deep truss has been replaced by an unusually shallow girder structure.

It should be noted that the total dead weight savings in the above structures are: (a) 52%, (b) 62%, (c) 60%.

The steel weights and the dead weights per square foot of bridge deck of the representative steel plate deck bridges in the various span ranges are given in Table 1.3.1.1.

TABLE 1.3.1.1
STEEL WEIGHT AND DEAD WEIGHT OF REPRESENTATIVE EXISTING STEEL PLATE DECK BRIDGES

Structure	Year	Spans (ft)	Weight of Steel (lbs per sq ft of deck)	Total Dead Weight (lbs per sq ft of deck)
(a) Plate Girder Bridges				
1. Weser Bridge, Porta, Germany	1954	209-256-348	55	100
2. St. Alban Bridge, Basle, Switzerland	1955	189-443-189	73	100
3. Duesseldorf-Neuss Bridge, Germany	1951	338-676-338	104	126
4. Save Bridge, Belgrade, Yugoslavia	1956	246-856-246	105	138
(b) Cable-Stiffened Girder Bridges				
5. Duesseldorf-North Bridge, Germany	1957	354-853-354	75	133
6. Severin Bridge, Cologne, Germany	1959	161-292-157-990-494-172	86	110
(c) Suspension Bridges				
7. Duisburg-Homberg Bridge, Germany	1954	421-936-421	98	130
8. Cologne-Muelheim Bridge, Germany	1951	279-1033-279	90	135

NOTE: The weights for the cable-stiffened and suspension bridges include the towers and the cables.

An analysis of the weight data of the steel plate deck bridges given in Table 1.3.1.1 indicates considerable steel weight and dead weight savings, as compared with the conventional bridges of similar types, designed under the same specifications.

A discussion of the steel weights of bridges designed in accordance with the AASHTO specifications is given in Section 1.3.2.

The savings in cost are smaller than the savings in weight, since the cost per pound of erected steel is higher for steel plate deck bridges, which require more fabrication work, than for conventional girder bridges. Also, the ratio of the more expensive low-alloy structural steel to carbon structural steel is generally higher in a steel plate deck bridge.

European experiences indicate that, on the average, 15% to 20% more man-hours per ton of fabricated and erected steel are needed for a steel plate deck bridge than for a girder bridge of conventional construction.

Assuming that labor costs constitute approximately one-half to two-thirds of the unit price of erected steel, the additional man-hour requirement ought to result in a cost differential between conventional and steel deck bridge construction of roughly 10% to 15%. Thus, a steel weight saving exceeding this percentage indicates a likely cost saving in the steel superstructure.

These estimates are in agreement with the results of recent economic studies conducted by the AISC with participation by several steel fabricating firms (see Section 1.3.2).

An incidental verification of these figures is provided by the recent Port Mann Bridge construction (see Section 1.1.3.4), where the differential between the bid price for the steel plate deck bridge and the estimated unit price for an alternative conventional design was 10%.

It should be noted that in European bridge construction the ratio of material to labor cost is much higher than in this country, and, in most cases, the material saving alone decides the choice of the design.

1.3.1.2 Erection Efficiency

Another cost saving factor is increased efficiency in the erection of steel plate deck bridges.

Main girder sections are generally lighter, which is an important factor in the cantilever method of erection.

Concrete construction is confined to one operation—the erection of the substructure in the first phase of the construction job. In this respect the construction schedule of a steel plate deck bridge differs from that of a conventional bridge requiring that concreting equipment be brought to the construction site twice—for foundation work and for pouring of the deck after completion of the steel framework.

Elimination of one concrete operation tends to shorten the erection period, which may be further cut by shop-prefabrication of large bridge units (see Section 1.1.3.7).

1.3.1.3 Cost Differential between a Concrete Deck and a Wearing Surface on Steel Plate Deck

In addition to the direct savings in the cost of structural steel, further benefit is gained by replacement of a reinforced concrete deck by a less expensive wearing surface.

The cost of the usual 7½-in. reinforced concrete deck slab is approximately \$2 per sq ft, and more if lightweight concrete is used. In many cases an additional wearing surface is required, which further increases the cost.

The cost of a 2-in. bituminous wearing surface, as discussed in Chapter 8, may be expected to be less than 50¢ per sq ft, including the preparation of the steel surface. The cost of the more expensive thin wearing surfaces ought not to exceed \$1 per sq ft.

1.3.1.4 Savings Due to Reduction of the Depth of Structure

Steel plate deck bridges are often characterized by a slenderness impossible to achieve economically by conventional designs. This is illustrated by several examples given in Section 1.1.3 of this Chapter.

The depth-of-structure reduction, in addition to enhancing the aesthetic appearance of the structure, reduces the cost of the approaches to high-level bridges and allows flatter approach grades.

1.3.1.5 Substructure Savings

The dead weight reduction of the superstructure, which may be of the order of one-half to two-thirds of the weight of conventional bridge superstructures (see Section 1.3.1.1), may have a considerable effect on the substructure design.

Substructure cost saving may result either from reducing the footing dimensions, or the number of piles, corresponding to the decreased load, or from reducing the number of supports and locating them at more convenient locations, longer superstructure spans being economically feasible with steel plate deck design.

Substructure savings may be considerable where foundation conditions are difficult and require deep pile driving.

Comparative substructure cost estimates based on the actual foundation conditions of several existing long-span girder bridges of conventional design indicate that foundation cost savings of the order of 5% to 15%

would be possible if lightweight steel plate deck construction were used.

1.3.2 AISC Cost Studies

In order to evaluate the economic merits of steel plate deck design application in this country, the American Institute of Steel Construction has conducted a series of design and cost studies.

In the first phase of these studies, the typical design details of steel plate decks were reviewed by a number of structural steel fabricators and suggestions were made for the most advantageous adaptation of these details to the American fabrication and erection practice.

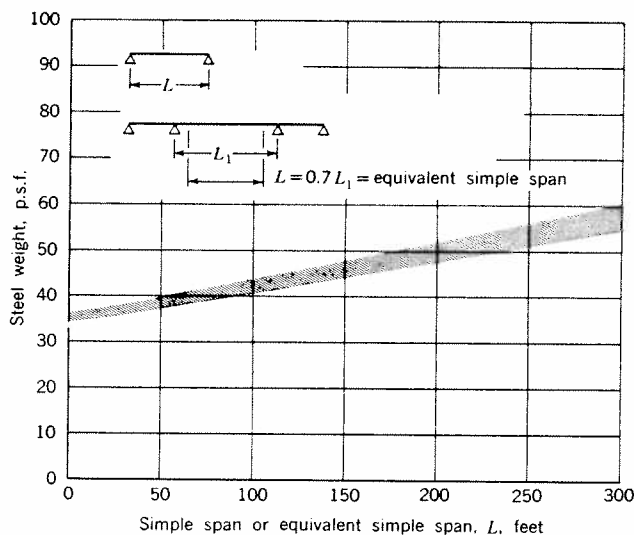


Fig. 1.39. Approximate weight of structural steel in steel plate deck girder bridges designed in accordance with the AASHO specifications

As one of the tentative findings, it appeared that the closed-rib type of deck would not be more expensive than the open-rib type, especially if the floor beam spacing were increased beyond the limits customary in European construction.

Approximate weights of steel per sq ft of steel plate deck girder bridges (two main girders), designed in accordance with the AASHO specifications, as determined in the course of the studies, are given in Figure 1.39. Weight data on the deck stiffeners alone (longitudinal ribs and floor beams) are given in Figure 7.2.

A general comparison of steel deck bridges with conventional girder bridges using concrete decks is not feasible, because the steel weight of the existing struc-

tures varies widely, depending on such factors as the type of design (riveted or welded), width of bridge, type of steel, unit weight of the concrete deck and wearing surface, degree of utilization of composite action, etc.

However, it may be noted that the steel weight of simple span rolled-beam composite action stringer bridges in spans of 50 to 100 ft ranges between 20 and 55 lbs per sq ft, while the unit steel weight of the existing three-span continuous riveted girder bridges with center spans of 200 to 400 ft ranges generally between 55 and 95 lbs per sq ft, depending on the design and the span.

The simple span length at which both concrete and steel plate deck designs require approximately equal weights of steel seems to be in the neighborhood of 150 ft.

Following the preliminary investigations, a three-span continuous four-lane bridge with span lengths of 275-375-275 ft was selected for a complete study. Several bridges of a similar description with concrete decks have been constructed in the past decade providing a ready basis for cost comparisons.

Two alternate designs have been prepared—one with a steel plate deck (Alternate A) and one with a concrete deck (Alternate B).

The basic features of the deck of Alternate A were essentially those of Numerical Example No. 2, given in Chapter 7 of this Manual, except that the closed deck ribs were $\frac{5}{16}$ in. rather than $\frac{1}{4}$ in. thick, to satisfy the minimum thickness requirements of the present AASHO specifications, which governed all design details of both Alternates A and B.

Alternate B was a conventional scheme designed in accordance with the best current practice of welded bridge construction, with two welded main girders, floor beams and stringers, and a $6\frac{3}{4}$ -in. thick reinforced concrete deck, without additional wearing surface.

The use of composite design for Alternate B did not appear to offer economic advantages over the scheme chosen.

The result of a cost comparison of the two alternates, taking into consideration the fabrication and erection costs of both schemes, is given in Table 1.3.2.

This cost comparison, based on conservative calculations, indicates a cost saving in Alternate A of the order of 10%. This does not include the cost savings in the substructure due to a substantially lighter superstructure of the steel plate deck alternate.

It should be noted that the reduction of the rib thickness to $\frac{1}{4}$ in. which is entirely adequate from the design point of view, would have reduced the steel weight of Alternate A from 57 to 55 lbs per sq ft, thus raising the overall cost saving to approximately 15%. Furthermore, the girder webs, proportioned in accordance with the current AASHO limitations of

TABLE 1.3.2
COST COMPARISON: 275-375-275 FT SPAN CONTINUOUS GIRDER, FOUR-LANE BRIDGE

Item	Quantity	Unit Price	Cost
Alternate A (Steel Plate Deck Bridge, conforming to 1957 AASHO Code)			
Structural low-alloy steel			
Deck	1,592,000 lbs	\$ 0.34	\$ 541,300
Other	1,665,000 lbs	0.28	466,200
Structural carbon steel	336,000 lbs	0.26	87,400
Reinforcing steel	49,200 lbs	0.13	6,400
Lightweight concrete (mall, curbs)	292 cu yd	90.00	26,300
Asphalt wearing surface	660 tons	20.00	13,200
			<hr/>
			\$1,140,800
Total weight of steel	57 lbs per sq ft		
Total dead weight	91 lbs per sq ft		
Alternate B (Welded Girder Bridge with Concrete Deck)			
Structural low-alloy steel	2,641,000 lbs	\$ 0.28	\$ 739,500
Structural carbon steel	1,498,000 lbs	0.26	389,500
Reinforcing steel	295,000 lbs	0.13	38,400
Concrete (standard)	1,490 cu yd	60.00	89,400
			<hr/>
			\$1,256,800
Total weight of steel	66 lbs per sq ft		
Total dead weight	166 lbs per sq ft		

the web slenderness, could be made considerably thinner in Alternate A, due to smaller shears in this design, thus further decreasing its cost.

Additional weight savings could be obtained by application of the suggested special design provisions based on the specific structural characteristics of orthotropic steel plate decks, as discussed in Chapter 9 of this Manual.

Cost comparisons of Alternate A and existing riveted girder bridges of identical or similar proportions, made by several steel fabricating firms, indicated superstructure cost savings due to the steel plate deck design of the order of 25% and more.

Based on the above investigations, it appears that for deck girder highway bridges, steel plate deck construction may be economically advantageous for

simple spans above the 150 to 180 ft span range or continuous spans above 200 to 250 ft center span length. In this range a comparison with composite design may be advisable to determine the relative economy.

However, special conditions, requiring a light weight, low structural depth and erection efficiency may indicate the use of steel plate deck design even for shorter spans.

With increasing span lengths, the cost saving due to steel plate deck construction increases considerably. This is confirmed by the example of the Port Mann Bridge in Vancouver, Canada (see Section 1.1.3.4), where the cost saving obtained by the use of steel plate deck design has been estimated to be of the order of one million dollars.

CHAPTER 2

Theoretical Background of the Deck Design

2.1 INTRODUCTION

This chapter deals only with the analysis of the bridge deck as an independent structural element (System II). The stresses in the deck as a part of the main carrying members of the bridge (System I) are not considered.

The steel plate bridge deck, consisting of a flat deck plate and the mutually perpendicular longitudinal ribs and transverse floor beams using the deck plate as their common top flange, is a highly statically indeterminate structural system. For design purposes it may be treated either as a grid or as an orthogonal-anisotropic ("orthotropic") plate, both approaches being permissible idealizations of the actual system.

In the treatment of a steel plate deck as a *grid* the deck plate is assumed slit between the longitudinal ribs, which are treated as individual beams between the panel points of the grid system, with the deck plate strips acting as upper flanges of the ribs. If the rib spacing is smaller than or equal to the effective width of the deck plate, the entire deck plate area is utilized; however, the effect of the deck plate rigidity in the direction perpendicular to the ribs is disregarded and must be considered separately [13, 25].

In the design approach treating the deck as a *plate* it is assumed that the rigidities of both the floor beams and the longitudinal ribs, or of the longitudinal ribs only, are uniformly distributed throughout the deck in the directions perpendicular to the respective members. Thus, the actual discontinuous structure of the steel plate deck is represented by an idealized substitute orthotropic plate, reflecting the characteristic properties of the actual system.

Of the two possible approaches, the orthotropic plate concept is essentially simpler and possesses important practical advantages.

This approach underlies the design method presented in this Manual.

The deck with closed ribs is analyzed as a continuous orthotropic plate.

In the design of decks with open ribs a simplification of the orthotropic plate equation leads to a treatment of the open ribs as continuous beams. This is discussed in Chapters 3 and 4.

For a clearer understanding of the design method presented in this Manual, its theoretical background is briefly outlined in this chapter.

Sections 2.2 and 2.3 contain basic information on the general theory of orthotropic plates.

In Section 2.4 of this chapter application of the orthotropic plate theory to the analysis of steel plate decks is discussed and a brief review of the design methods based on the orthotropic plate theory is given.

2.2 PROPERTIES OF AN IDEAL ORTHOTROPIC PLATE

2.2.1 Basic Assumptions

An orthogonal-anisotropic plate is defined as a plate which has different elastic properties in two mutually perpendicular directions in the plane of the plate, designated x and y (Fig. 2.1). Since the plate thickness is constant and the plate material is continuous, as required by the general conditions outlined below, the different elastic properties in the two principal directions must be due to different moduli of elasticity, $E_x \neq E_y$, and different Poisson's ratios, $\nu_x \neq \nu_y$, of the material, as is evident from the rigidity formulas, equation (2.1). Thus, the orthotropic plate theory assumes an *anisotropic material* of the plate.

A good example of such material is a wooden plank, having markedly different moduli of elasticity in the direction of the grain and transversely to it.

Except for the added condition of anisotropy, computation of deformations and stresses of an orthotropic plate by means of the ordinary theory of elastic plates is based on the same assumptions as are used in analysis of an isotropic plate.

These assumptions are:

1. The material of the plate is *homogeneous*, i.e., the physical properties of the material are identical at each point of the plate. Further, the material is *continuous* between the outer surfaces of the plate. This precludes the existence of voids, slits or other geometric irregularities within the plate.

2. The plate *thickness*, t , is *uniform* and *small*, compared with other dimensions of the plate. Thus, the stresses normal to the middle plane of symmetry

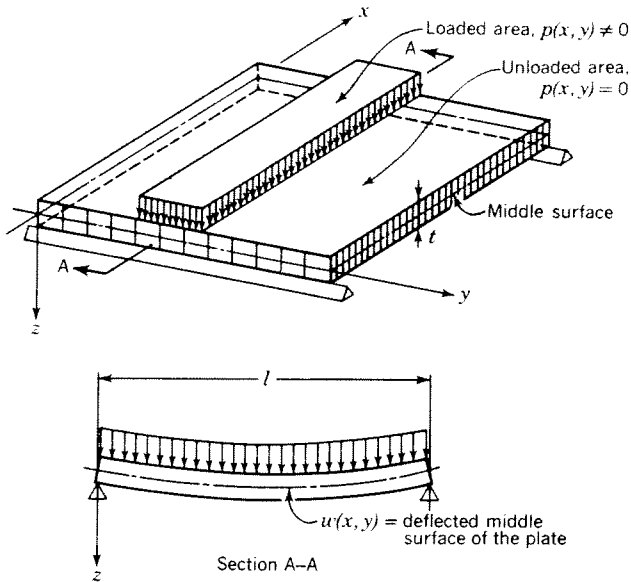


Fig. 2.1. Basic designations

of the plate (x, y) , and the effects of the shearing stresses on the plate deformations may be disregarded.

3. The deformations of a loaded plate are purely elastic and are in accordance with Hooke's law. The straight lines normal to the middle surface of the plate remain straight and normal to the deformed middle surface of the loaded plate (Bernoulli's hypothesis).

4. The deflections of the loaded plate are small compared with the plate thickness. This assumption precludes the occurrence of the membrane stresses in the plate.

2.2.2 Rigidity Coefficients

The elastic properties of an orthotropic plate are defined by three rigidity coefficients:

D_x = the flexural rigidity of the plate in the x -direction

D_y = the flexural rigidity of the plate in the y -direction

H = the effective torsional rigidity

The rigidities D_x and D_y , expressed in units of $k\text{-in.}^2/\text{in.}$, characterize the resistance to flexure of a plate strip having a unit width and a thickness t , in the x - or y -direction, respectively, and are defined by the formulas

$$D_x = \frac{E_x t^3}{12(1 - \nu_x \nu_y)}; \quad D_y = \frac{E_y t^3}{12(1 - \nu_x \nu_y)} \quad (2.1)$$

The effective torsional rigidity, H , characterizing the resistance of a plate element to twisting, is defined by the formula

$$2H = 4C + \nu_y D_x + \nu_x D_y \quad (2.2)$$

The value of $2C$, known as the torsional rigidity coefficient, is defined as the reciprocal value of the angle of twist of a plate element with the side lengths $dx = dy = 1$ due to the action of twisting moments $M_{xy} = M_{yx} = 1$ (Fig. 2.2)

$$2C = \frac{1}{\vartheta} \quad (2.3)$$

While the determination of the flexural rigidities D_x and D_y presents no difficulties, the determination of the value of $2C$ of an orthotropic plate by either theoretical or experimental methods is not easily possible.

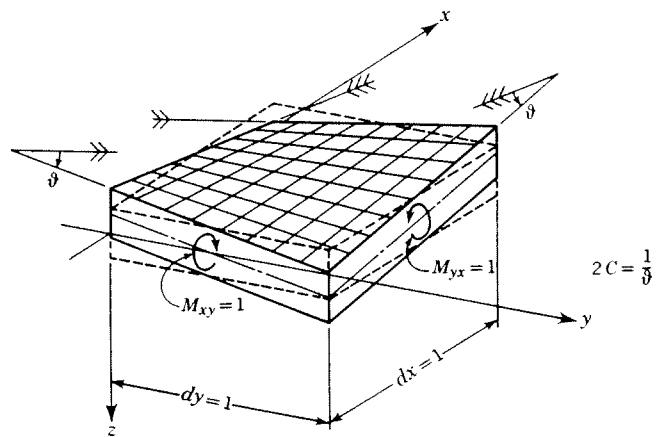


Fig. 2.2. Plate element subject to twisting

For an ideal orthotropic plate an approximate value of the torsional rigidity coefficient, $2C$, determined by Huber [28], is

$$2C = (1 - \sqrt{\nu_x \nu_y}) \sqrt{D_x D_y} \quad (2.4)$$

Considering that, in accordance with Betti's law of reciprocity,

$$\frac{D_x}{D_y} = \frac{\nu_x}{\nu_y} \quad (2.5)$$

an approximate expression for the effective torsional rigidity of an orthotropic plate is obtained from equations (2.2) and (2.4)

$$H = \sqrt{D_x D_y} \quad (2.6)$$

This value was recommended by Huber for computation of reinforced concrete plates with different reinforcement ratios in two perpendicular directions.

It must be emphasized that equations (2.4) and (2.6) are applicable only to special cases and cannot be used in the computations of stiffened steel plate decks treated as orthotropic plates.

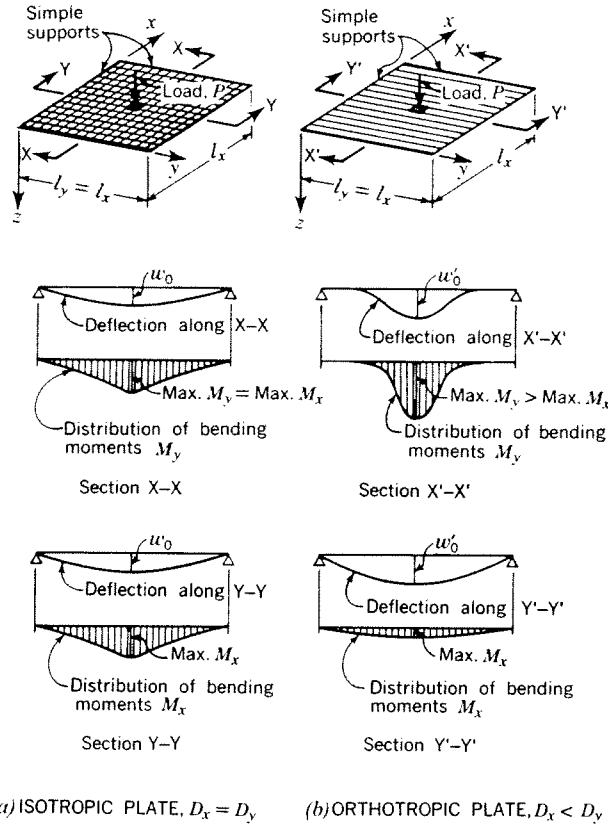


Fig. 2.3. Comparison of deflections and bending moments in a square isotropic and a square orthotropic plate

2.2.3 Comparison with an Isotropic Plate

It should be noted that the more commonly used isotropic plate may be regarded as a special case of an orthotropic plate. With $E_x = E_y$ and $\nu_x = \nu_y$, equation (2.1) becomes

$$D_x = D_y = D = \frac{Et^3}{12(1 - \nu^2)} \quad (2.7)$$

which is the familiar expression for plate rigidity.

The torsional rigidity coefficient of an isotropic plate is computed by the formula

$$2C = \frac{Et^3}{12(1 + \nu)} \quad (2.8)$$

By substituting equations (2.7) and (2.8) into equation (2.2) the expression for H is obtained:

$$2H = \frac{Et^3}{6(1 - \nu^2)} = 2D, \quad \text{or } H = D \quad (2.9)$$

It is seen that for an isotropic plate the effective torsional rigidity, H , is equal to the flexural rigidity.

A comparison of the structural behavior of an isotropic plate (e.g., a steel plate or a concrete slab of

constant thickness) with that of an orthotropic plate is given in Figure 2.3.

Figure 2.3a shows a square isotropic plate supported on four sides and loaded with a load, P , distributed over a small area in the center of the plate. Because of the symmetry, the load is carried equally in both directions of the plate and the deflections and the bending moments, M_x and M_y , acting in the x - and y -directions of the plate, are identical.

Figure 2.3b shows the deflections and the bending moment diagrams of a square orthotropic plate having the same dimensions and support conditions as the isotropic plate in Figure 2.3a, however with the flexural rigidity in the y -direction, D_y , greater than the rigidity in the x -direction, D_x .

It is seen that, under the same load P , the deflection lines along the sections $X'-X'$ and $Y'-Y'$ are dissimilar, except for the common ordinate under the load. The load is carried predominantly in the direction of the greater rigidity, y , which is evidenced by the larger values of the bending moments M_y acting in the stiffer direction than the moments M_x in the weaker direction of the plate, as shown in sections $X'-X'$ and $Y'-Y'$.

It is also seen that the maximum values of the bending moments M_y of the orthotropic plate are greater than the corresponding values of the moments of the isotropic plate and that in the orthotropic plate the bending moments do not extend over the entire span length, l_x , but are confined to a plate strip near the load (see section $X'-X'$).

Thus, a square orthotropic plate, which is stiffer in the y - than in the x -direction, may be compared with an elongated isotropic plate, having the span l_x greater than the span l_y . A load applied in the center of such a plate will be carried mainly in the y -direction, and, if the ratio l_x/l_y is large, the effects of the load will not extend to the edges $x = 0$ and $x = l_x$, similarly as in the case of the orthotropic plate, Figure 2.3b.

If, in an extreme case, the rigidity values D_x and H of an orthotropic plate are very small compared with the rigidity D_y , the bending moments M_y in the plate due to an applied load may be assumed to act only within the plate strip corresponding to the width of the load. In such a case the plate may be visualized as a series of beams lying side by side, as represented in Figure 2.7b.

2.3 DIFFERENTIAL EQUATION OF AN ORTHOTROPIC PLATE AND ITS SOLUTIONS

The problem of an anisotropic plate was first studied by F. Gehring (1860) and F. Boussinesq (1879). A comprehensive treatment of an orthotropic plate, including a systematic solution of its differential equa-

tion was first presented by M. T. Huber (1914) [27, 28].

The differential equation giving the relationship between the deflection and the loading of an orthotropic plate, often referred to as *Huber's equation*, is

$$D_x \frac{\partial^4 w}{\partial x^4} + 2H \frac{\partial^4 w}{\partial x^2 \partial y^2} + D_y \frac{\partial^4 w}{\partial y^4} = p(x, y) \quad (2.10)$$

where w is the deflection of the middle surface of the plate at any point (x, y) (Fig. 2.1).

D_x , D_y and H are the rigidity coefficients defined by equations (2.1) and (2.2), and $p(x, y)$ is the loading intensity at any point, expressed as a function of the co-ordinates x and y .

Equation (2.10) is a *non-homogeneous* differential equation, since the function $p(x, y)$ does not contain the deflection, w .

A function $w(x, y)$ satisfying equation (2.10) is known as a *solution* of the differential equation.

Over the areas of the plate where no direct vertical load is applied (see Fig. 2.1) the load function, $p(x, y)$, is equal to zero, and the deflection, w , of the unloaded portion of the plate is expressed by the equation

$$D_x \frac{\partial^4 w}{\partial x^4} + 2H \frac{\partial^4 w}{\partial x^2 \partial y^2} + D_y \frac{\partial^4 w}{\partial y^4} = 0 \quad (2.11)$$

This equation is called *homogeneous*, because the unknown function w is contained in each of its terms.

Generally, the homogeneous equation (2.11) represents a plate loaded by bending moments and line loads applied only along the edges of the plate.

The methods used in solving equations (2.10) and (2.11) of an orthotropic plate are essentially the same as used for the similar equations of an isotropic plate, except that, in this case, the integration constants and the arguments of the functions used in the solution must include the characteristic rigidities of the orthotropic plate, D_x , D_y and H .

Equations (2.10) and (2.11) may be satisfied by many functions. However, only that solution, w , is of value for engineering purposes which also satisfies the *boundary conditions* of the given plate. These are the required specific values of the deflections, w , slopes, $\partial w / \partial x$, $\partial w / \partial y$, and curvatures, $\partial^2 w / \partial x^2$, $\partial^2 w / \partial y^2$, $\partial^2 w / \partial x \partial y$, corresponding to the geometric conditions and the values of the shears, the bending moments and the twisting moments along the edges of the plate. These boundary conditions provide the equations necessary for the determination of the integration constants of the differential equations.

A general solution of the non-homogeneous differential equation (2.10) is obtained by adding a *general solution* of the corresponding homogeneous equation

(2.11) (containing the arbitrary constants) and a *particular solution* of the non-homogeneous equation (2.10) (any specific function, containing no arbitrary constants, satisfying equation (2.10))

$$w = w_h + w_p \quad (2.12)$$

Geometrically, equation (2.12) represents a superposition of two deflection surfaces, w_p being the deflection surface of a plate under the given loading $p(x, y)$, possibly satisfying some, but not all, boundary conditions of the actual plate, and w_h , representing the deflection of the plate with no load over its surface ($p(x, y) = 0$), under the effects of such deflections, rotations, line loads or bending moments applied along the edges as are necessary to compensate for the departures of the particular solution, w_p , from the required shape of the actual plate. Thus, by adding the two surfaces, w_h and w_p , a deflection surface of the actual loaded plate is obtained which satisfies all boundary conditions.

While a particular solution, w_p , may always be easily found, the determination of a general solution, w_h , of the homogeneous equation (2.11) which, combined with w_p , satisfies both equation (2.10) and the *boundary conditions* at the edges of the plate, is most difficult and often impossible. Generally, such solution of the homogeneous equation (2.11) can be only given as an *infinite series*.

For the technically important case of a plate simply supported along the edges $x = 0$ and $x = l$ and subject to *any* boundary conditions along the edges $y = \text{constant}$ (e.g., free edge, simple support, elastically restrained edge, etc.), a solution of the homogeneous equation can be given by a *simple series* (involving only one summation). This solution, first applied by Levy to the computation of an isotropic plate, may be represented in the general form

$$w_h = \sum_{n=1}^{\infty} Y_n \sin \frac{n\pi x}{l} \quad (2.13)$$

where Y_n is a function of the variable y only and contains four integration constants, corresponding to the fourth order of the differential equation.

If Levy's solution is applied to equation (2.11) of an orthotropic plate, the function Y_n also contains the rigidity coefficients D_x , D_y and H . Depending on the relationship between the rigidity coefficients, three different expressions for Y_n are obtained for the three basic cases: H greater than, equal to or less than $\sqrt{D_x D_y}$. These expressions involve trigonometric and hyperbolic functions of the variable y and of the rigidity coefficients.

For example, for the case of $H < \sqrt{D_x D_y}$ the expression for Y_n is [42]:

$$Y_n = C_{1n} \sinh \alpha_n y \sin \beta_n y + C_{2n} \cosh \alpha_n y \cos \beta_n y \\ + C_{3n} \sinh \alpha_n y \cos \beta_n y + C_{4n} \cosh \alpha_n y \sin \beta_n y \quad (2.14)$$

where

$$\alpha_n = \frac{n\pi}{l} \sqrt{\frac{1}{2D_y} (\sqrt{D_x D_y} + H)} \\ \beta_n = \frac{n\pi}{l} \sqrt{\frac{1}{2D_y} (\sqrt{D_x D_y} - H)} \quad (2.15)$$

C_{1n} , C_{2n} , C_{3n} and C_{4n} are the constants to be determined by the boundary conditions of the plate under consideration.

By inserting expression (2.14) into equation (2.13) the solution of the homogeneous equation (2.11) is obtained for the special case $H < \sqrt{D_x D_y}$ considered, as can be verified by substituting the expression so obtained into equation (2.11).

For a loaded plate, simply supported along the edges, $x = 0$ and $x = l$, the particular solution, w_p , of equation (2.10) may be given by the equation of the deflection line of a simply supported plate strip with the span l (Fig. 2.1). However, since the particular and the homogeneous solutions have to be added in accordance with equation (2.12), in order to obtain the general solution and to determine the constants, the particular solution, involving the loading, p , must also be represented by a series. Thus, in this case, the particular solution may be expressed [23]

$$w_p = \frac{1}{D_x} \sum_{n=1}^{\infty} \left(\frac{l}{n\pi} \right)^4 p(x) \quad (2.16)$$

where

- D_x = the plate rigidity in the x -direction
- l = the span in the x -direction
- $p(x)$ = the loading, represented by a Fourier series (see Section 3.5).

It should be noted that in equation (2.16) the load, p , is a function of x only, this being one of the conditions for application of Levy's solution. This is equivalent to the requirement of a load extending in the y -direction over the entire length of the plate.

If the loading is discontinuous in the y -direction, the above solution may be applied by cutting the plate into loaded and unloaded portions and treating them separately. The continuity of the plate is then restored by application of the appropriate boundary conditions along the cut edges [20, 35].

In the case of a line load extending in the x -direction of the plate, it is possible to obtain the deflection surface, w , of the plate by using the homogeneous equation (2.11) only. This is done by cutting the plate along the line load and thus having the load acting on the free edge of the plate. This treatment may also be further extended to a load having a certain width in the y -direction [20].

When the deflection surface, w , of the orthotropic plate and the values of the constants have been determined, the bending and the torsional moments, shears and reactions of the plate may be determined at any point from the expressions for slopes and curvatures of the deflection surface. The formulas for moments, shears, etc. of an orthotropic plate are similar to those used for an isotropic plate, except that all three rigidity values, D_x , D_y and H occur in these expressions, rather than the single plate rigidity coefficient of an isotropic plate. These formulas may be found in reference [20].

For example, the expressions for moments in an orthotropic plate are:

$$M_x = -D_x \left(\frac{\partial^2 w}{\partial x^2} + \nu_y \frac{\partial^2 w}{\partial y^2} \right) \\ M_y = -D_y \left(\frac{\partial^2 w}{\partial y^2} + \nu_x \frac{\partial^2 w}{\partial x^2} \right) \quad (2.17) \\ M_{xy} = M_{yx} = -2C \frac{\partial^2 w}{\partial x \partial y}$$

The bending moments in an orthotropic plate may also be determined indirectly, through evaluation of the influence surfaces obtained by application of unit deformations or loads to the plate.

It should be noted that the formulas for moments, equation (2.17), obtained by differentiating the series (2.13) and (2.16), or the formulas for influence surfaces, are also expressed as infinite series.

From the above discussion of the differential equation of the orthotropic plate it is seen that its direct application to the engineering problems presents mathematical difficulties even in the simplest cases. Also tedious and time consuming is the computation of the many constants from long expressions involving hyperbolic functions, and the numerical evaluation of the slowly converging series.

Application of the orthotropic plate theory to the analysis of steel plate bridge decks has been facilitated by systematic presentation of the formulas for the values needed in design, tables of integration constants, influence ordinates, and other data, presented by several authors. In these publications attempts

have also been made to simplify the rigorous theory and to adapt it to the specific geometric properties of the steel plate decks. These problems are discussed in Section 2.4.

2.4 DESIGN ANALYSIS OF STEEL PLATE DECKS BASED ON THE ORTHOTROPIC PLATE THEORY

2.4.1 Applicability of the Orthotropic Plate Theory to Steel Plate Decks

2.4.1.1 General

Systems consisting of a flat plate stiffened by ribs in one or two perpendicular directions may be treated as orthotropic plates under the general condition that the spacing of the stiffening ribs is sufficiently smaller than their span to insure full participation of the flat plate in the flexural action of the ribs. In stiffened steel plate bridge decks this condition is usually fulfilled.

Thus, the highly complex structural system of the actual deck can be represented by an essentially simpler substitute plate system, much more convenient for design analysis.

Generally, a steel plate deck consisting of the deck plate, longitudinal ribs and transverse floor beams may be idealized as a plate in two ways:

Approach A. The rigidities of both longitudinal ribs and transverse floor beams are assumed to be continuously distributed throughout the deck. Thus an *orthotropic plate strip* supported on the main girders is obtained (Fig. 2.5). This approach, justifiable in a case of closely spaced floor beams, has been used in earlier designs.

Approach B. The rigidity of the longitudinal ribs only is assumed to be uniformly distributed, while the floor beams are retained as individual members. In this manner the deck is treated as a *continuous orthotropic plate*, supported on the main girders and the floor beams (Fig. 2.9).

In both cases the bending moments are computed for the substitute orthotropic plate, and from these values the bending moments and stresses in the individual members of the actual deck system are obtained.

2.4.1.2 Properties of Steel Plate Decks at Variance with the Assumptions of the Orthotropic Plate Theory

In application of the orthotropic plate theory to the design of steel plate decks, proper consideration must be given to the fact that a steel plate deck differs

in several respects from an ideal orthotropic plate, described in Section 2.2.1. The most important properties of the actual system at variance with the assumptions of the general orthotropic plate theory are the *discontinuity* and the *asymmetry* of the steel plate decks.

A stiffened steel plate deck is *discontinuous* in the sense of the requirements of plate theory since its material does not fill the space between the two outer parallel planes enclosing the deck plate structure in a continuous manner, as seen in Figure 2.4a. Thus, unlike in the case of an ideal orthotropic plate, the different rigidities in the two perpendicular directions result from different geometric properties rather than from different moduli of elasticity of the material which, in this case (steel), is isotropic rather than anisotropic.

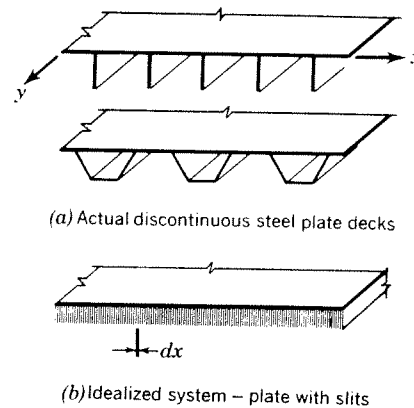


Fig. 2.4. Actual steel decks and their idealized representation as an orthotropic plate

Because of the location of the stiffening ribs on one side of the deck plate only, the system is also *asymmetrical* about the middle surface of the flat deck plate (x, y). Due to the eccentric arrangement of the stiffeners, the neutral surfaces of the deck for bending in the x - and y -directions do not coincide, unlike the case of an ideal homogeneous plate of a constant thickness, as stipulated by the theory. This is of consequence in rigorous determination of the stresses, especially in the deck plate.

The non-coincidence of the neutral surfaces in the two perpendicular directions also has an effect on the effective torsional rigidity, H , of the stiffened steel plate deck, which is difficult to determine.

Poisson's ratio, ν , for an idealized plate representing the actual steel plate deck may be assumed to be negligible.

$$\nu_x \cong \nu_y \cong 0 \quad (2.18)$$

This may be visualized by contemplating bending of the actual deck (Fig. 2.4a) or its idealized model,

which may be thought of as a plate with closely spaced deep slits in it (Fig. 2.4b), rather than a homogeneous orthotropic plate. It may be seen that bending of the system in the direction of the ribs, y , does not cause any appreciable stresses in the direction normal to the ribs, since the actual or the idealized ribs separated by the slits may freely expand or contract in the transverse direction. It may also be seen that if the system is bent in the transverse direction, x , the effect on the stresses in the y -direction is likewise negligible because of the geometric conditions.

The assumption expressed by equation (2.18) simplifies the expressions for the moments and stresses in the deck, as can be seen from equations (2.17).

It should be noted, however, that this assumption is used only in the computation of the bending moments in the idealized orthotropic plate (System II) and does not apply in the determination of the rigidity values of the ribs (Section 3.3), or in the computation of the local stresses in the deck plate acting as a continuous isotropic plate (Chapter 6). In these cases the usual value of Poisson's constant for steel, $\nu_x = \nu_y = 0.3$, is used.

2.4.1.3 Effects of Discontinuity in Computation of Stresses

The discontinuity of the steel plate deck system is of consequence in determination of the bending moments and stresses in the individual members from the moments computed for the substitute orthotropic plate if the spacing of the members, the rigidity of which is assumed to be continuously distributed, is of the same order or larger than the dimensions of the applied loads. This is usually the case in bridge deck design using concentrated wheel loads.

In design treating the deck as an *orthotropic plate strip* (approach *A*, as defined in Section 2.4.1.1), only the floor beam moments can be obtained from the orthotropic plate computation. Additional steps are needed to evaluate the moments and stresses in the longitudinal ribs under wheel loads placed between the panel points of the deck, as shown in Figures 1.31 and 2.6. This is discussed in Section 2.4.2.

In the design method treating the deck as a *continuous orthotropic plate* (approach *B*, see Section 2.4.1.1), the effects of the actual discontinuity of the system on the computation of stresses are as follows:

In the *open rib system*, with both the transverse rigidity, D_x , and the torsional rigidity, H , much smaller than the longitudinal rigidity, D_y , the effective width obtained in the idealized orthotropic plate representing the rigidity values of the actual system is hardly larger than the width of the applied load itself. Thus, for

the loading width nearly equal to the rib spacing, the effective width in the idealized system may be smaller than the width over which the effect of the load extends in the actual deck as a result of the action of the deck plate as a continuous member between the ribs (see Fig. 2.7). In such a case the moment in the directly loaded rib obtained from an orthotropic plate computation would be larger than the actual bending moment in the rib, as may be seen by comparison of Figures 2.7a and 2.7c.†

It should be noted that, in some loading cases, conditions may be reversed and a moment smaller than the correct value may be obtained from the substitute system. Thus, a deck with open ribs may not always be adequately represented by an idealized orthotropic plate.

In a *deck with closed ribs*, having a better load distributing capacity in the transverse direction than the open rib system, the load distribution obtained from a computation of an equivalent orthotropic plate is generally in good agreement with the actual conditions, as determined experimentally. The inaccuracy in the computation of the bending moments and the stresses in the ribs stems here from the fact that the total rib moment is usually obtained by multiplying the moment per unit width, M_y , computed in the substitute orthotropic plate system at the center of the loaded rib by the width, $a + e$, of the rib. The total rib moment thus obtained is larger than the actual average moment over the width of the rib, as is shown in Figure 2.8b. With a constant width of loading, this discrepancy tends to decrease as the relative transverse rigidity of the system is increased. The correct average value of the rib moment could be obtained by integration of the moment curve under the rib; however, in the interest of simplification this is usually not done. It should also be noted that the discrepancy between the correct and the somewhat too high stress value computed in this manner for the bottom of the rib will be partly compensated by the additional effects of the System III stresses in the rib bottom (see Section 6.2.1.3c).

2.4.2 Evolution of the Design Methods Based on the Orthotropic Plate Theory

Huber's equation (2.10) was first applied to the problem of computing stresses in a steel plate deck by Cornelius in conjunction with the design of the Cologne-Muelheim Bridge [9].

The deck, consisting of the deck plate, bulb bar longitudinal ribs and floor beams was treated as an

† A numerical example for such a case is given on pg. 148 of reference [42].

orthotropic plate strip simply supported on the two main girders with the rigidities of the ribs and the floor beams assumed to be distributed continuously. For the torsional rigidity of the substitute system the value of $H = 0.3\sqrt{D_x D_y}$ was used, determined empirically to make the deflections measured on a test model agree with the results obtained from Huber's equation. However the propriety of such a procedure and the correctness of the value obtained has been questioned.

In his subsequent publication [10] Cornelius gave general expressions for the integration constants and for the various coefficients occurring in the formulas for the deflections, moments, shears, etc. of an orthotropic plate, using $\nu_x = \nu_y = 0$ and $H < \sqrt{D_x D_y}$, the latter assumption corresponding to the properties of steel plate decks with open ribs.

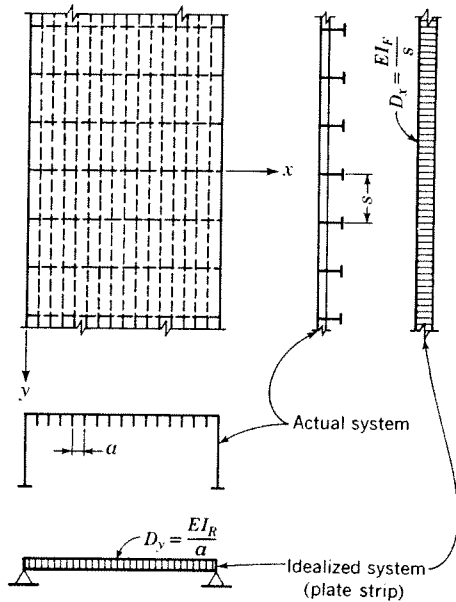


Fig. 2.5. Bridge deck treated as an orthotropic plate strip

Numerical evaluation of the expressions for the bending moments for the various specific cases has been presented by several authors [25, 26, 41, 48].

A simpler, but less accurate method, based on the application of orthotropic plate theory to open grids has been given by Guyon and Massonet [21, 37]. Numerical tables, facilitating its application, may be found in [38]. However, like other methods mentioned above, this method is useful only if the loads are applied at the floor beams, and not between them.

In order to obtain the stresses in the longitudinal

ribs under loads between the floor beams (which cannot be determined from the deck computation as an orthotropic plate strip with floor beam rigidity assumed to be uniformly distributed, see Section 2.4.1.1), the original approach (Fig. 2.5) was refined by Cornelius and Mader [36]. The rigidity of the floor beams was assumed to be continuously distributed only in areas outside of the loaded panel and the panel under load was treated as a secondary orthotropic plate, elastically supported by the two adjoining floor beams and continuous with the primary orthotropic plate of the rest of the deck (Fig. 2.6).

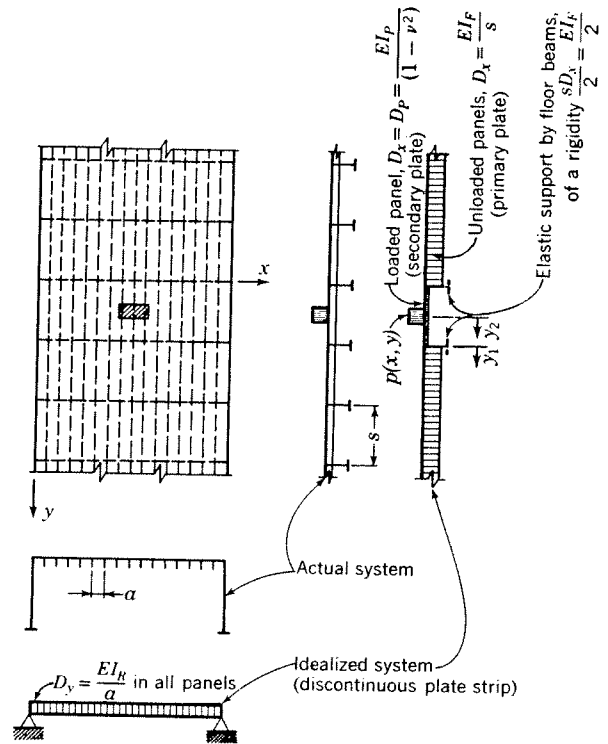


Fig. 2.6. Bridge deck treated as an orthotropic plate strip, with consideration of the discontinuity in the loaded panel

This approach was used in the design of the deck of the Save River Bridge (see Section 1.1.3.1) and several other structures with open ribs. The disadvantage of this method of design was in its complexity, requiring considerable mathematical skills, and a great amount of numerical work.

Bridge decks with torsionally rigid closed ribs were designed in a similar manner. In these designs the reduction of the torsional rigidity, H , due to deck plate bending has been recognized, and the first formulas for the reduced deck rigidity have been proposed [81].

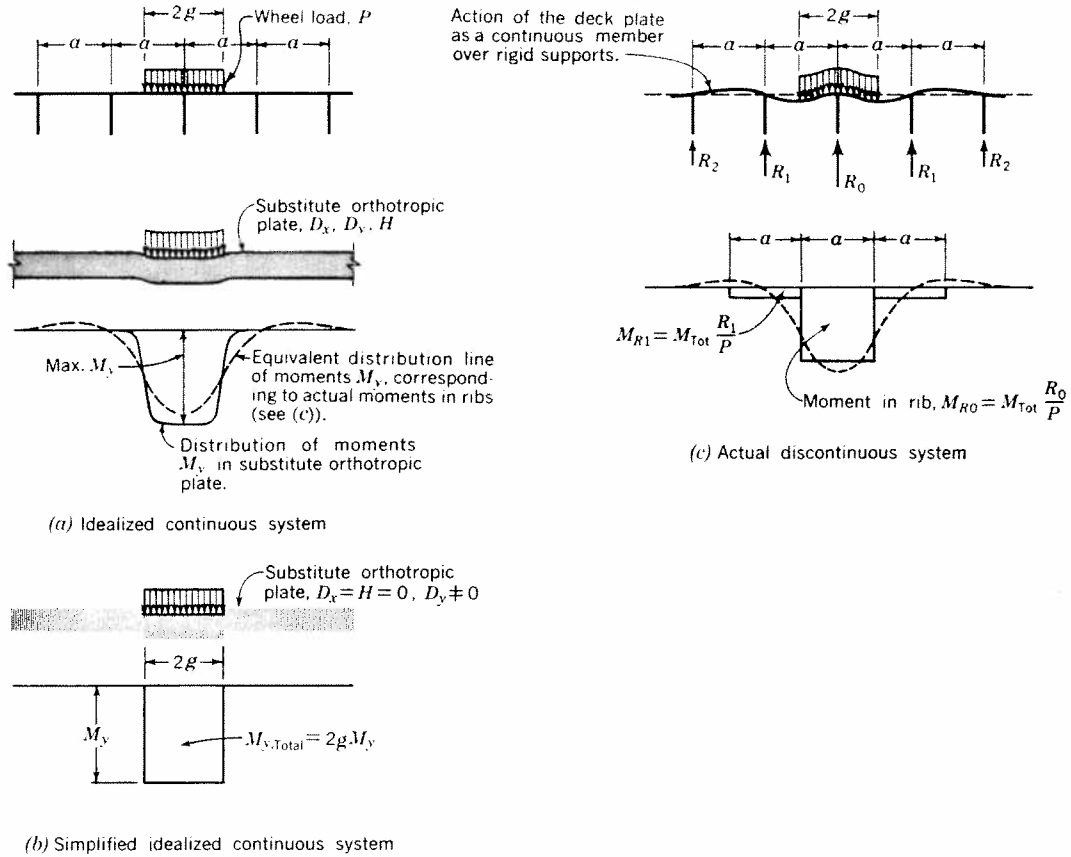


Fig. 2.7. Determination of the bending moments in the open ribs

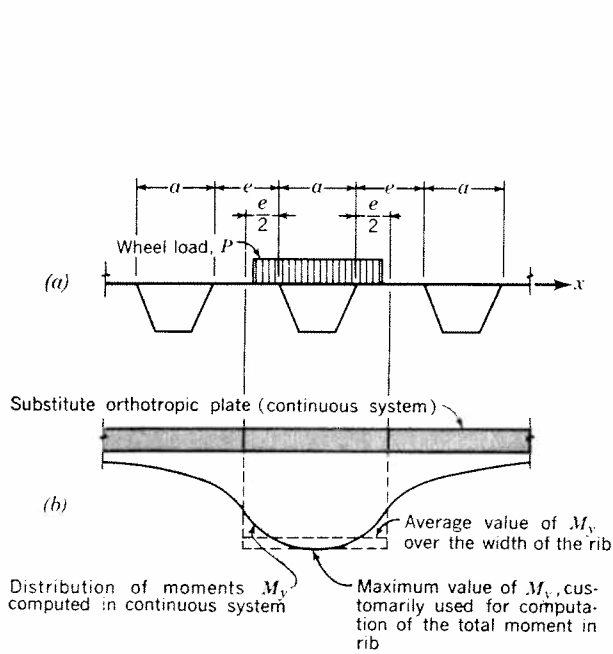


Fig. 2.8. Determination of the bending moments in the closed ribs

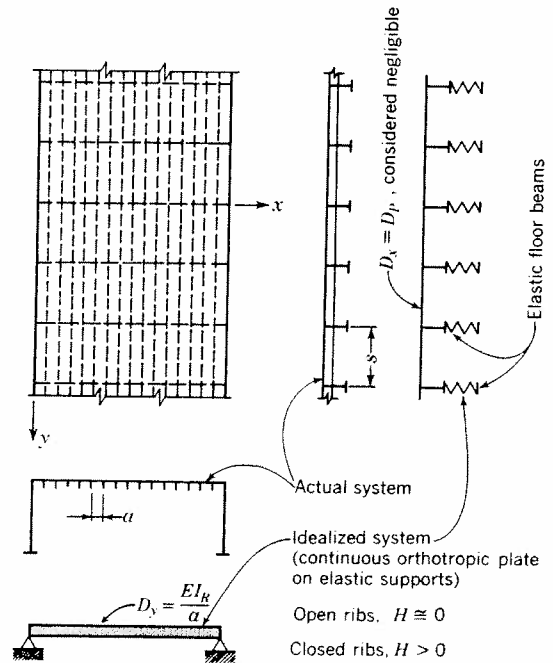


Fig. 2.9. Bridge deck treated as an orthotropic plate on elastic supports

Influence surfaces for orthotropic plates have also been developed and may be found in references [23, 26, 33, 53].

The moments in a steel plate deck can be obtained by utilizing the influence surfaces in two ways:

(a) The longitudinal and transverse bending moments in a steel deck consisting of the deck plate, longitudinal ribs and transverse floor beams are determined by means of influence surfaces for moments in an orthotropic plate strip. The local bending moments in the longitudinal ribs acting as continuous beams in rigid supports have then to be superimposed on the overall moments to obtain final moments in the ribs [23].

(b) The longitudinal bending moments are determined by means of an influence surface for an orthotropic plate panel, consisting of the deck plate and the longitudinal ribs only, and supported on the main girders and the floor beams. The effects of the deck continuity and the floor beam elasticity and the final bending moments in the floor beams are then computed in the second step.

It is seen that in both cases the influence surfaces provide only a part of the needed answer, with the remaining part left to be computed by other methods. Practical usefulness of this approach is further limited by the fact that the available influence surfaces, determined by the characteristic plate rigidity values D_x , D_y and H , necessarily cover only certain of the many possible combinations of these values.

A simplified, yet sufficiently accurate method for the design of steel plate bridge decks has been developed by Pelikan and Esslinger [42]. This method is based on an abbreviated rather than full form of Huber's equation, obtained by elimination of the parameters of little importance in the design. The deck plate with longitudinal ribs is treated as a continuous orthotropic plate supported on rigid main girders and elastic floor beams (Fig. 2.9). The design computation is made in two steps: in the first step the floor beams are considered rigid and the moments in the deck are computed in accordance with this assumption. In the second step the effects of the actual elastic flexibility of the floor beams are determined.

The design procedure may be further simplified by charts, prepared for a specified loading.

The outline of the Pelikan-Esslinger design method, selected for use in this Manual, and its application to the bridge design in accordance with the AASHTO specifications, is presented in Chapters 3, 4, 5, 10 and 11.

The design charts based on the AASHTO loads are given in Appendix I.

2.4.3 Attempts at a Rigorous Treatment of Steel Plate Decks

Some of the more rigorous analytical studies based on the actual geometric properties of steel plate decks, at variance with the assumptions of the orthotropic plate theory (see Section 2.4.1), shall be briefly mentioned here.

The effects of the *asymmetry* of the deck plate stiffeners, placed on one side of the deck plate only and causing deformations and stresses in the deck plate, have been studied by several authors.

Trenks has shown that the elastic behavior of a steel plate deck with open ribs may be rigorously described by three simultaneous differential equations, expressing the three deformation components of the deck plate, which may be transformed into one differential equation of the eighth order [55].

The problem of a plate eccentrically stiffened by flat bar ribs has also been treated by Giencke [14, 15].

Schumann has analyzed the stresses in the deck with open ribs with consideration of the *discontinuity* of the rib arrangement [50].

The deck plate with closed stiffening ribs has been studied by Pflueger [46] and Giencke [16], who have attempted to determine rigorously the effective torsional rigidity of this system.

The effect of *shear deformation* of the ribs on bending moments has been investigated by Girkmann and Beer [19] and Giencke [18].

The computation procedures presented in the above studies are far too complicated to be considered for practical engineering purposes. The stresses in the stiffening ribs obtained through these methods are generally somewhat lower than those obtained from Huber's equation; however, the results obtained by the individual authors are often at variance with each other and a precise experimental verification of the computed stresses is still lacking.

It should be kept in mind that the refined analytical investigations of the steel plate decks mentioned above are all based on the structural *theory of first order* and may be considered "rigorous" only as long as the basic premise of this theory is satisfied, requiring that the deflections of the system be small and have no secondary effects on the stresses.

However, as has been shown in Chapter 1, these assumptions are satisfied only in steel plate decks of usual proportions under the working loads, while under higher loads the structural behavior of the decks departs entirely from the pattern predicted by the first order theory.

CHAPTER 3

Outline of the Design Method, Rigidity Coefficients, Loading

3.1 INTRODUCTION

The procedure for the design of steel plate bridge decks presented in this Manual is based on the method developed by Pelikan and Esslinger [42].

A general description of the design procedure and a discussion of the simplifying assumptions used is given in Section 3.2. More basic information on the theory underlying this method has been presented in Chapter 2.

The bending moments and stresses in a steel plate bridge deck depend on its dimensions and characteristic rigidity values and on the loads applied. It is appropriate to discuss these factors first.

The characteristic rigidity coefficients are discussed and formulas for their computation are given in Section 3.3.

Section 3.4 contains a discussion of the wheel and axle loads to be used in the design.

In order to evaluate the formulas for bending moments, presented in Chapters 4 and 5, it is necessary to represent the actual truck wheels acting on the deck by substitute loads obtained through a Fourier analysis of loading. The formulas needed for these computations are given in Section 3.5.

3.2 OUTLINE OF THE METHOD

3.2.1 General Description of the Design Procedure

The design method presented in Chapters 3, 4, 5 and 10 of this Manual deals with the bridge deck as an independent structure (System II), transmitting the loads to the main carrying members of the bridge (girders or trusses).

The stresses in the deck due to its action as a flange of the main members (System I) are not considered. These stresses are computed separately by the usual methods and superimposed on the System II stresses, as discussed in Section 1.2.6.

The bridge deck, consisting of a flat deck plate and longitudinal stiffening ribs, is treated as a continuous orthotropic plate supported on infinitely rigid main girders and on uniformly spaced elastic floor beams (Fig. 3.1).

The bending moments in the deck with *closed* (tor-

sionally stiff) ribs (Fig. 1.2b) are determined by *orthotropic plate* formulas.

Simplifying assumptions applicable to the deck with *open* (torsionally soft) ribs (Fig. 1.2a) lead, in effect, to the computation of the bending moments in the open ribs by *continuous beam* formulas. For the open-rib decks of usual proportions this approach is both much simpler and more appropriate than computation by orthotropic plate formulas.

The design of steel plate decks with open or closed ribs is made in two computation steps.

In the *first step* the maximum values of the bending moments in the longitudinal ribs and in the floor beams are computed under the assumption that the floor beams are infinitely rigid.

In the *second step* the effects of the elastic flexibility of the floor beams are determined and the values of the bending moments obtained in the first step are adjusted.

The reader is reminded again that the design method presented in this Manual, like all other methods currently available, is based on the flexural theory of first order, assuming a purely elastic behavior of the steel plate deck in accordance with Hooke's law, small deflections and no membrane stresses in the system. These assumptions are generally valid for steel plate bridge decks of the usual types under working loads; however, they are too conservative for decks subject to very large concentrated loads. Therefore the formulas presented, valid for computation of stresses under the design conditions, cannot be used to evaluate the behavior of the deck under large loads or the actual safety of the structure, which is, generally, much higher than predicted by the ordinary first order theory.

3.2.2 Simplifying Assumptions Used in the Design

3.2.2.1 General

The bending moments in a steel plate deck treated as an orthotropic plate theoretically depend on the following factors:

- a. Loading
- b. Floor beam spacing, s
- c. Main girder spacing, l

d. The magnitudes and the ratio of the three characteristic rigidities of the substitute orthotropic plate used to represent the actual system: the flexural rigidities in the x - and y -directions, D_x and D_y , and the effective torsional rigidity, H . (See Chapter 2.)

As a practical matter, some of the above factors are of little importance and may be eliminated from the computations.

The main girder spacing, l , has no effect on the bending moments in the longitudinal ribs under concentrated wheel loads in Step 1 of the computation (floor beams assumed rigid), since the effective width of the deck loaded by a wheel is small compared with the main girder spacing. Therefore, in the design

of *closed ribs*, the actual deck width, l , may be replaced in the computations by a shorter substitute width, b (see Fig. 4.20). This simplifies the numerical work considerably, as will be shown in Chapter 4.

In Step 1 of the design of *open ribs* the length l does not enter the computations at all.

However, in determination of the effects of floor beam elasticity (Step 2 of the computation) the true span length of the floor beams, l , must be used in both cases.

The effect of the rigidity factor D_x on the bending moments in the deck with closed ribs is small in structures of usual proportions, as is the effect of the rigidity factors D_x and H on the bending moments in the deck with open ribs. This is realized by comparing the

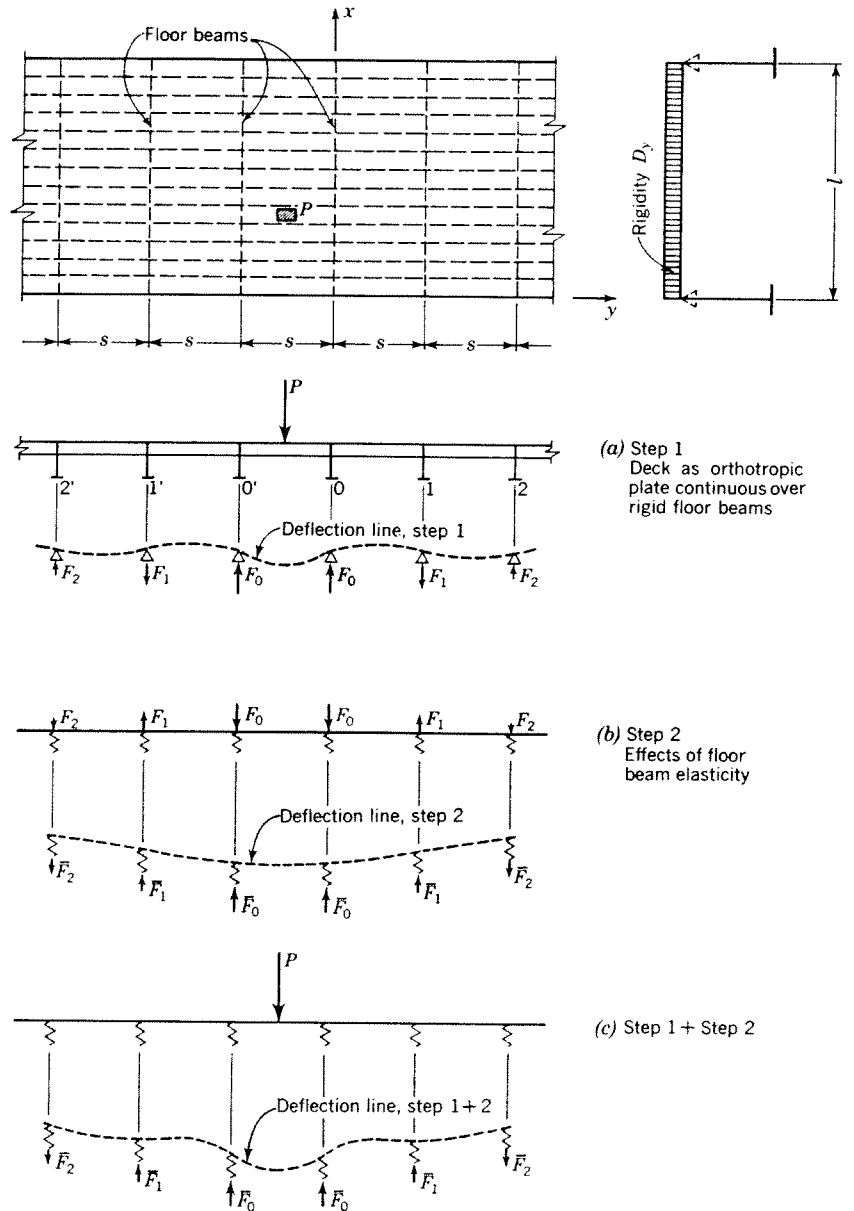


Fig. 3.1. The two-step computation procedure, Pelikan-Esslinger design method

magnitudes of the three rigidity coefficients, D_x , D_y and H , of a steel bridge deck consisting of a flat deck plate and longitudinal ribs.

In this case the characteristic rigidities have the following meaning:

- D_x is the transverse rigidity of the system, equal to the rigidity of the flat deck plate, D_P .
- D_y is the longitudinal rigidity, obtained by dividing the rigidity of one rib, acting in conjunction with the deck plate, by the rib spacing.
- H is the effective torsional rigidity of the system which is determined, practically, by the torsional rigidity of the ribs alone.

In steel plate bridge decks of usual design the longitudinal rib rigidity, D_y , is always considerably larger than the deck plate rigidity, $D_x = D_P$, and the ratio D_y/D_x usually ranges between 500 and 2000.

The torsional rigidity, H , of the decks with open (torsionally soft) ribs is generally of the same order as the deck plate rigidity, D_x . Thus, for this type of bridge deck, the ratio D_y/H is also large.

Therefore, in the design of the deck on rigid supports (Step 1 of the computation) the following simplifying assumptions may be made:

- For decks with closed ribs: $D_x = 0$
- For decks with open ribs: $D_x = 0$, $H = 0$

The validity of the above assumptions is discussed in Sections 3.2.2.2 and 3.2.2.3.

In Step 2 of the computation procedure (effects of floor beam elasticity) the transverse and the torsional rigidity of the deck, D_x and H , may be disregarded in both types of decks. This is discussed in Chapter 5.

3.2.2.2 Decks with Closed Ribs

With the assumption $D_x = 0$, the differential equation of the orthotropic plate (2.10) is reduced to:

$$2H \frac{\partial^4 w}{\partial x^2 \partial y^2} + D_y \frac{\partial^4 w}{\partial y^4} = p(x, y) \quad (3.1)$$

The solution of the abbreviated equation (3.1) and the resulting formulas for the bending moments are considerably simpler than those of the full original equation (2.10), and the amount of computation work required in the design is reduced to tolerable limits.

It should be noted that although the transverse rigidity, D_x , equal to the rigidity of the deck plate, D_P , does not enter equation (3.1) directly, its effect is not entirely disregarded, since the rigidity of the deck plate is a factor in determination of the effective torsional rigidity, H , as will be shown in Section 3.3.3.1.

Comparison of the bending moments in a deck with

closed ribs computed by formulas derived from the full differential equation (2.10) with the values obtained from the abbreviated equation (3.1) indicates that the error due to the assumption $D_x = 0$ is small [42].

In steel plate decks of usual proportions, with a deck plate $\frac{3}{8}$ in. to $\frac{1}{2}$ in. thick, and a span of closed ribs of 10–15 ft, the error may range from less than 1% to 3%. In cases of rib spans up to 20–25 ft, or with a greater plate thickness, the error may be of the order of 4% to 5%.

In all cases the moments computed with the assumption $D_x = 0$ are greater than those determined from the full equation. Thus the results obtained by the simplified method are always on the safe side.

3.2.2.3 Decks with Open Ribs

The assumptions $D_x = 0$ and $H = 0$ reflect the fact that a steel bridge deck with open ribs of usual proportions, i.e., with a relatively thin deck plate and comparatively short rib spans, has very small load distributing capacity in the transverse direction.

With $D_x = 0$ and $H = 0$, equation (2.10) becomes:

$$D_y \frac{\partial^4 w}{\partial y^4} = p(x, y) \quad (3.2)$$

Equation (3.2) defines an idealized structural system representing the actual steel plate deck with open ribs. This idealized system may be visualized as a series of infinitely narrow plate strips placed side by side and running continuously in the y -direction (Fig. 2.7b). It is seen that in such a system the effective width is equal to the width of loading applied, $2g$.

If it is further assumed that the loading, p , varies in the y -direction only, and is constant in the x -direction, $p = p(y)$, differential equation (3.2) represents the deflection line of a beam. The bending moment expressions derived from this equation are the familiar continuous beam formulas.

Comparative computations of bending moments per unit width made with the plate formulas based on the full equation (2.10) and with the beam formulas corresponding to equation (3.2) have shown that, for the usual span lengths and sizes of the members, the results obtained by the two methods differ by less than 3%. This justifies the use of beam formulas for the design of steel plate decks with open ribs.

As has been pointed out in Section 2.4.1.3, if the load dimension is of the same order as the rib spacing, the load per rib, M_R , in an open rib system cannot be obtained directly from the value of moment per unit width at the center of the rib. The correct value must be computed from the value of the total moment

multiplied by the factor R_0/P , which reflects the load distributing action in the transverse direction of the deck plate acting as a continuous plate over the ribs (Fig. 2.7c). Therefore, the computation by the beam formulas, giving directly the magnitude of the total moment, is more appropriate than the computation by the plate formulas, giving only the maximum moment ordinate under the load (Fig. 2.7a).

Thus it is seen that the use of the beam formulas rather than the plate formulas in the design of decks with open ribs is not only much simpler, it is also more correct.

As has been stated above, such simplified computation of the deck with open ribs is appropriate with decks having a small load distribution capacity in the transverse direction.

If the deck plate is unusually thick, or if the span of the open ribs exceeds 6 ft, the effect of the rigidity of the deck plate, D_P , may become more pronounced. In such cases a correction, based on the relative deck plate and rib rigidity, may be applied to the original simplified computation. This is discussed in Chapter 4.

However, for economic reasons, open flat bar ribs with spans exceeding 6 ft and thick deck plates will be used only in exceptional cases. Therefore a need for the more refined design computation of the open ribs will seldom arise.

3.3 RIGIDITY COEFFICIENTS

3.3.1 Introduction

In the computation of bending moments in a deck with closed ribs, treated as an orthotropic plate on rigid supports (Step 1 of the computation), the following rigidity coefficients of the substitute orthotropic plate are needed:

- D_y , flexural rigidity in the y -direction
- H , effective torsional rigidity

The transverse flexural rigidity, D_x , does not enter into the moment computations. However, it is used in the determination of the effective torsional rigidity, H .

The bending moments in a deck with open ribs on rigid supports, computed by the beam formulas, are independent of the rigidity of the deck. Therefore no rigidity coefficients need be computed for this system.

The rigidity coefficient D_y denotes the flexural rigidity per unit width of the deck of the longitudinal ribs acting together with the deck plate.

In order to determine the rigidity of the individual ribs and the section moduli of the ribs, needed for the computation of the stresses, the effective width of the deck plate acting with one rib must be known.

The effective width of the deck plate acting with one longitudinal rib may be smaller, equal to, or larger than the spacing of the ribs. The effective width depends on the loading and the ratio of the rib spacing to its effective span and is independent of the deck plate thickness. Thus, depending on the conditions, the rigidity and the section modulus of a rib may vary. This is discussed and the necessary formulas given in Section 3.3.2.

The effective torsional rigidity, H , of a deck with closed ribs depends on the dimensions, the spacing and the span of the ribs and the thickness of the ribs and the deck plate.

A discussion and formulas for determination of the effective torsional rigidity, H , are given in Section 3.3.3.

3.3.2 Flexural Rigidity

3.3.2.1 Effective Width of Deck Plate

(a) General

In order to define the effective width of the deck plate acting with a rib, let us consider an elementary case of an infinitely wide plate strip of a span s_1 stiffened by one longitudinal rib and subjected to flexure (Fig. 3.2). The plate strip is axially loaded by shearing forces, V , introduced into the plate along the junction with the rib.

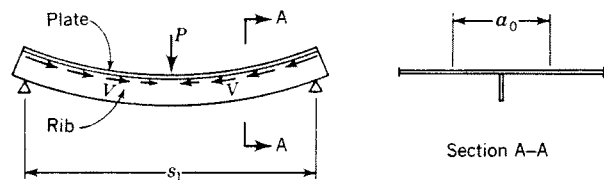


Fig. 3.2

The rib and the plate acting together have the same unit elongation or contraction at each point along the junction.† Based on this condition, the effective width of plate, a_0 , acting with one rib is defined as the width of a plate strip that will have the same contraction when uniformly compressed by the forces V as the actual plate at the junction with the rib.

Generally, the effective width, a_0 , depends on the span of the rib, s_1 , and the load distribution.

If the plate is stiffened by one rib only (Fig. 3.3a), the effective width of plate acting with the rib is approximately equal to one-third of its span, s_1 , and is

† The assumption of equal elongation is not equivalent to that of equal axial stress in the rib and the plate at the junction, since the effect of the lateral contraction in the plate has to be considered.

independent of loading. Additional ribs spaced far apart do not affect the effective width of the rib under consideration, which remains the same as in the previous case (Fig. 3.3b).

If ribs are closely spaced and only one rib is loaded, the system is essentially similar to that in the first case and the effective width may still be assumed to be approximately one-third of the span (Fig. 3.3c), as before. If, however, the closely spaced ribs are all uniformly loaded, the effective widths are of the order of the actual spacing of the ribs (Fig. 3.3d).

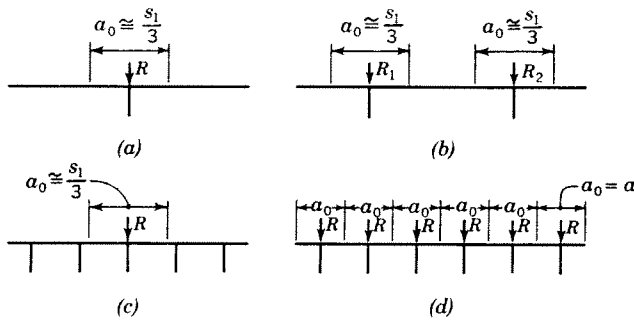


Fig. 3.3

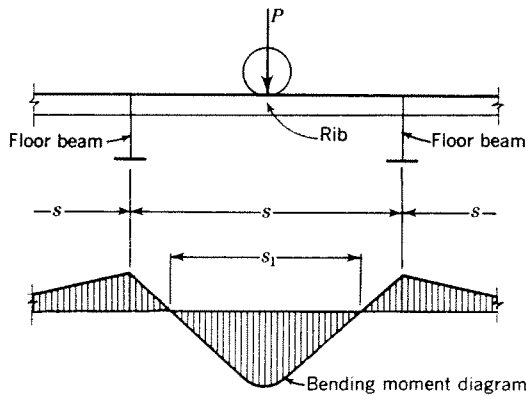


Fig. 3.4

If the ribs are closely spaced and the loading of the adjoining ribs differs considerably, as is the case in a bridge deck, the exact computation of the effective width becomes rather involved. However, for practical purposes it is sufficient to use the approximate formulas presented in Sections 3.3.2.1b, c and d.

The use of the approximate formulas for the determination of the effective width is permissible, since the effect of small variations of the effective width, a_0 , on the magnitude of the bending moments obtained from the orthotropic plate computation and the stresses in the bottom fiber of the ribs is insignificant.

Similar considerations are valid for the effective width, s_0 , of the deck plating acting as the upper flange of a floor beam.

(b) *Effective span*

The effective span of the rib, s_1 , used in the computations of the effective width of plate, is defined as the average length of the positive moment area of the rib (Fig. 3.4).

In Step 1 of the design procedure (ribs continuous over rigid floor beams) the average value of

$$s_1 = 0.7s \tag{3.3}$$

may be used.

For computation of the effects of the floor beam flexibility, the effective span of the ribs is always large, so that an approximation may be used:

$$s_1' = \infty \tag{3.4}$$

The effective span of floor beams supported on two single-web main girders may be assumed to be equal to the main girder spacing, l .

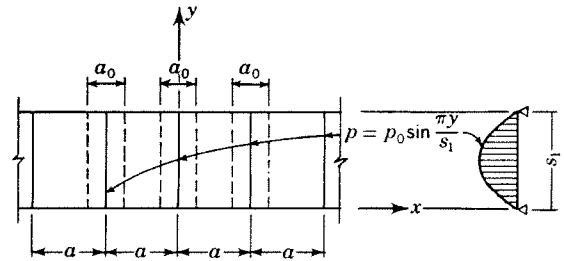


Fig. 3.5

The effective span of floor beams framed into torsionally rigid box-girders or continuous over more than two main girders must be determined in each case (see Section 5.5).

(c) *Effective width of plate in the case of equal loading of all ribs*

In the case of a plate stiffened by uniformly spaced ribs, the effective width of plate, a_0 , as defined in Section 3.3.2.1a, is easiest to determine in the case of equal sinusoidal line loads applied to all ribs, as shown in Figure 3.5 [42].

The effective width ratios obtained from this case are given in Table 3.3.2.1.

For practical purposes, it may be assumed that the effective width is essentially the same for other types of loads equally applied to all ribs.

It is seen that the ratio of the effective width to span, a_0/s_1 , increases with the ratio of the rib spacing to span, a/s_1 .

The same considerations apply to the ratios of the effective width of the deck plate, s_0 , acting with one floor beam, to the floor beam span, l .

The fact that, with all ribs equally loaded, the effective width may be greater than the actual rib spacing

TABLE 3.3.2.1
EFFECTIVE WIDTH OF PLATE RATIOS FOR ALL RIBS
EQUALLY LOADED

a/s_1	a_0/a	a_0/s_1
0.0	1.099	0.000
0.2	1.005	0.201
0.4	0.808	0.323
0.6	0.620	0.372
0.8	0.480	0.384
1.0	0.383	0.383
∞	0.000	0.363

a = rib spacing, a_0 = effective width of plate acting with one rib, s_1 = effective rib span.

(as is the case if the rib spacing is smaller than one-fifth of their span), is explained by the effect of transverse contraction in the plate due to a bi-axial stress condition.

The effective width ratios given in Table 3.3.2.1 are also represented graphically in Chart 1 (Appendix). In this chart the effective spacing of the ribs and the floor beams, a^* , e^* and s^* , is used rather than the actual spacing, a , e and s , as explained in Section 3.3.2.1d.

(d) *Effective width of plate in the case of unequal loading of ribs*

The loads on the individual ribs due to a wheel load on the deck are not equal. The rib directly under the wheel receives a load R_0 , the adjoining rib is loaded with R_1 , etc. (Fig. 3.6a). Thus, the effective width ratios given in Table 3.3.2.1, computed under an assumption of equal loading of all ribs, do not apply in this case.

However, these ratios are approximately correct if an *effective spacing*, a^* , rather than the actual spacing, a , is used. The idealized effective spacing is determined from the condition that the effective distances of the ribs be proportional to the actual loads (or moments) in the individual ribs. Hence, the effective spacings, a_0^* , a_1^* , a_2^* . . . , of ribs No. 0, 1, 2 . . . etc., are determined by the following formulas:

$$a_0^* = \frac{2R_0}{R_0 + R_1} a = \frac{2M_0}{M_0 + M_1} a$$

$$a_1^* = \left(\frac{R_1}{R_0 + R_1} + \frac{R_1}{R_1 + R_2} \right) a \quad (3.5)$$

$$= \left(\frac{M_1}{M_0 + M_1} + \frac{M_1}{M_1 + M_2} \right) a, \quad \text{etc.}$$

It is seen that the effective spacing of ribs, a^* , can be computed only if the final values of loads or moments in the ribs are known.

With the values of a^* determined, the corresponding effective widths of plate, a_0' , may be obtained from

Table 3.3.2.1 or Chart 1, similarly as for the case of equal loading on all ribs.

3.3.2.2 **Section Properties of Ribs and Floor Beams**

(a) *General*

The section properties of the ribs and the floor beams depend on the effective width of the deck plate, discussed above. The assumptions and procedures used in the computations of the section properties needed in the design are summarized below.

The following designations are used:

Under an assumption of *equal loading* on all ribs or floor beams,

a_0 = effective width of plate acting with one open rib

s_0 = effective width of plate acting with one floor beam

I = moment of inertia of ribs or floor beams

S = section modulus of ribs or floor beams

Under an assumption of *unequal loading* on the ribs or floor beams,

a_0' = effective width of plate acting with one open rib

s_0' = effective width of plate acting with one floor beam

I' = moment of inertia of ribs or floor beams

S' = section modulus of ribs or floor beams

For *all* assumptions of loading,

s_1 = effective span of ribs

(b) *Open ribs*

In Step 1 of the computation (continuous ribs on rigid floor beams) the stresses in the ribs are due to the truck wheel loads, which cause unequal loads on the individual ribs. Therefore, the effective spacing, a^* , computed by equation (3.5) must be used in determination of the effective plate width, a_0' , of the loaded rib.

In the design of the deck with open ribs it is assumed that the deck plate acts as a continuous plate on rigid supports and distributes the wheel load to the individual ribs accordingly, as discussed in Section 3.2.2.3. Thus the rib reactions $R_0, R_1, R_2 \dots$ needed in formulas (3.5) may be obtained by means of the influence line of a continuous beam on rigid supports (Chart 5c).

For the various ratios of the wheel width to rib spacing, the values of the load on the directly loaded rib No. 0, R_0/P (Fig. 3.6a) and the effective rib spacing ratios, a_0^*/a , have been obtained in this manner and are given in Chart 2.

For the specific case of AASHO wheel loads, the load per rib, R_0 , and the effective spacing, a_0^* , are given directly in Charts 3 and 4.

With the value of a_0^* obtained from Chart 2 or 4 and with an effective rib span $s_1 = 0.7s$, in accordance with equation (3.3), the effective width, a_0' , is determined from Chart 1. The value of a_0' is then used in the computation of the section properties, I_R' and S_R' of the rib.

In Step 2 of the computation (effects of floor beam elasticity) all ribs may be considered equally loaded, as will be explained in Chapter 5.

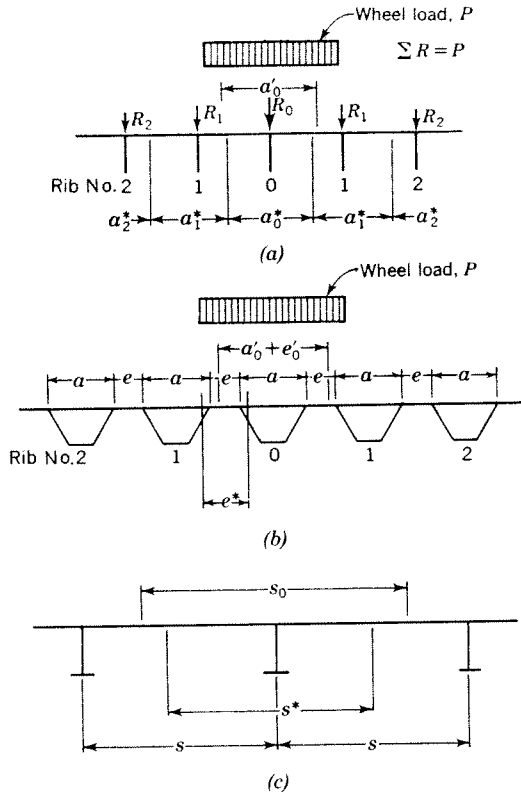


Fig. 3.6

Therefore, in this case, the effective rib spacing is assumed to be equal to the actual rib spacing, $a^* = a$. In accordance with equation (3.4) the effective rib span, s_1 , is assumed to be infinitely large.

With these values the effective width, a_0 , is computed similarly as for Step 1, and the section properties I_R and S_R are determined.

(c) Closed ribs

In a deck with closed ribs the top width of the rib, a , and the width of deck plate between ribs, e , are generally different (Fig. 3.6b). Therefore, the contributions of these plate widths to the effective width of plate acting with the rib are determined separately.

Assuming that all ribs are equally loaded, their effective spacing equals the actual spacing, and the

effective width, $a_0 + e_0$, may be computed by the formula

$$a_0 + e_0 = \frac{a_0}{a} a + \frac{e_0}{e} e \tag{3.6}$$

where, as before, a_0/a and e_0/e are coefficients which may be obtained from Chart 1.

The wheel loads on individual ribs on rigid supports (Step 1 of the computation) are not equal. However, in the computation of the flexural rigidity, D_y , of the substitute orthotropic plate, needed for determination of the bending moments in closed ribs, the effective width, $a_0 + e_0$, computed by equation (3.6) is used, since this value represents a fair average effective width of plate acting with the ribs affected by the wheel load. In this case, the effective span, $s_1 = 0.7s$, is used, in accordance with equation (3.3).

Thus, the flexural rigidity coefficient, D_y , is computed by the formula:

$$D_y = \frac{EI_R}{a + e} \tag{3.7}$$

where I_R is the moment of inertia of one rib, based on the effective width, $a_0 + e_0$, computed by equation (3.6).

For the determination of stresses in the rib directly under the load in Step 1 of the computation, the value of the effective width, $a_0' + e_0'$, may be obtained with consideration of the effective rib spacing, similarly as in the case of open ribs. For this purpose the bending moment, M_0 , in the rib directly under load, as well as the moment, M_1 , in the adjoining rib must be computed.

With the values of the bending moments, M_0 and M_1 , known, the effective width of plate acting with the directly loaded rib No. 0 (Fig. 3.6b) is computed by the formula:

$$a_0' + e_0' = \frac{a_0}{a} a + \frac{e_0}{e^*} e^* \tag{3.8}$$

where

$$e^* = \frac{2M_0}{M_0 + M_1} e \tag{3.8a}$$

It should be noted that a variation of the top flange width, $a_0' + e_0'$, of a rib has only a small effect on the bottom section modulus of a rib. Therefore, if a more exact determination of the stresses in the deck plate, acting as the upper flange of the ribs, is not required, the computation of the adjusted effective width, $a_0' + e_0'$, by equation (3.8) may be omitted entirely, and the critical stresses at the bottom fiber of the ribs may be computed with sufficient accuracy with

the section moduli based on the effective width obtained by equation (3.6).

For determination of moments and stresses in the ribs in Step 2 of the computation (effects of floor beam elasticity), the I_R and S_R values, based on the effective width, $a_0 + e_0$, computed by equation (3.6) should be used, with $s_1 = \infty$, in accordance with equation (3.4). Practically, however, it is sufficient to use the values of I_R and S_R already determined in the computation of the bending moments in Step 1.

(d) Floor beams

For computation of the dead load stresses and of the ratio of the floor beam rigidity to rib rigidity the values of I_F and S_F are used, based on the effective width of the deck plate (Fig. 3.7c),

$$s_0 = s \frac{s_0}{s} \tag{3.9}$$

where s is the actual floor beam spacing and s_0/s is a coefficient obtained from Chart 1, using the actual floor beam span, l , as the effective floor beam span. This assumes that the floor beams are simply supported at the main girders. If the floor beams are continuous or elastically restrained at the ends, an appropriate value of the effective span, l_1 , must be used.

For computation of the live load stresses in the floor beams the section modulus S_F' should be used, based on the effective width, s_0' , computed with consideration of the unequal loading of the floor beams

$$s_0' = s^* \frac{s_0}{s^*} \tag{3.10}$$

with

$$s^* = \frac{2F_0}{F_0 + F_1} s \tag{3.10a}$$

where F_0 is the load on the floor beam under consideration and F_1 is the load on the adjoining floor beam.

However, for practical purposes, it is sufficient in most cases to use the value S_F , computed under the assumption of all floor beams equally loaded.

(e) Summary

The section properties of the ribs and floor beams are computed with an appropriate value of the effective width of the deck plate, depending on the loading case.

For convenience, the assumptions and the formulas used in the computations are summarized in Table 3.3.2.2.

TABLE 3.3.2.2
FLEXURAL RIGIDITY COMPUTATIONS—SUMMARY OF ASSUMPTIONS AND FORMULAS

	Line No.	Computation	Effective Span	Effective Spacing	Effective Width of Plate (From Chart 1)	Values Needed	Remarks
Open Ribs	1	Stresses—ribs on rigid supports	$s_1 = 0.7s$	$a_0^* = \frac{2R_0}{R_0 + R_1} a$ (from Chart 2)	$a_0' = a_0^* \frac{a_0}{a^*}$	I_R', S_R'	
	2	Stresses—effects of floor beam elasticity	$s_1 = \infty$	$a^* = a$	$a_0 = 1.1 a$	I_R, S_R	
Closed Ribs	3	Moments—ribs on rigid supports	$s_1 = 0.7s$	$a^* = a$ $e^* = e$	$a_0 + e_0 = a \frac{a_0}{a} + e \frac{e_0}{e}$	$I_R, D_v = \frac{EI_R}{a + e}$	
	4	Stresses—ribs on rigid supports	$s_1 = 0.7s$	$a^* = a$ $e^* = \frac{2M_0}{M_0 + M_1} e$	$a_0' + e_0' = a \frac{a_0}{a} + e^* \frac{e_0}{e^*}$	I_R', S_R'	Values in line 3 may be used instead of lines 4 and 5
	5	Stresses—effects of floor beam elasticity	$s_1 = \infty$	$a^* = a$ $e^* = e$	$a_0 + e_0 = 1.1(a + e)$	I_R, S_R	
Floor Beams	6	Relative rigidity stresses—dead load	l —see Note	$s^* = s$	$s_0 = s \frac{s_0}{s}$	I_F, S_F	
	7	Stresses—live load	l —see Note	$s^* = \frac{2F_0}{F_0 + F_1} s$	$s_0' = s^* \frac{s_0}{s^*}$	I_F', S_F'	Values in line 6 may be used instead of line 7

Note: Floor beams are assumed to be simply supported at main girders. If this is not the case, the appropriate effective span, l_1 , of floor beams is to be used.

3.3.3 Torsional Rigidity

3.3.3.1 Theoretical Background

(a) Introduction

The torsional rigidity of a deck with open (torsionally soft) ribs is small and is disregarded, as explained in Section 3.2.2.1.

The torsional rigidity of a deck with closed (torsionally stiff) ribs may be considerable. Its value enters the design computations through the effective torsional rigidity, H , of a substitute orthotropic plate representing the actual system.

The general expression for the effective torsional rigidity of an orthotropic plate is given by equation (2.2). Considering that the Poisson's ratio of orthotropic plates representing steel plate bridge decks of the usual types may be assumed to be zero, $\nu_x = \nu_y = 0$, as discussed in Section 2.4.1.2, equation (2.2) reduces to

$$H = 2C \quad (3.11)$$

The meaning of the torsional rigidity coefficient, $2C$, has been explained in Section 2.2.1. It should be noted that in an ideal orthotropic plate the value of $2C$, represented by the twisting angle, ϑ , results from two equal contributions to the torsional rigidity of the plate element in the two perpendicular directions (Fig. 2.2). However, in a steel plate deck with closed ribs the torsional rigidity of the system is supplied, practically, in one direction only by the resistance of the ribs to the twisting moments M_{yx} , acting in the planes perpendicular to the ribs, while the resistance of the system to the twisting moments M_{xy} , acting in the planes parallel to the ribs is negligible, as may be visualized by contemplating a small element of the deck, Figure 2.4a. Therefore, if the actual deck system is to be represented by an idealized orthotropic plate, the effective torsional rigidity of the idealized system must be assumed to be equal to one-half of the torsional rigidity of the ribs per unit width.

(b) Torsional deformation of the ribs

Formulas for the effective torsional rigidity, H , presented in Section 3.3.3.2, are based on the assumption that the deck consists of the hollow ribs and the deck plate only, as shown in Figure 3.6b, and is not additionally stiffened between the floor beams by diaphragms or other members built in to improve the effective torsional rigidity and the transverse load distributing capacity resulting from it (Fig. 7.4). It should also be noted that, in accordance with the AASHO specifications, the design loads are distributed in the transverse direction of the bridge by placing several trucks side-by-side, and, therefore, the additional benefits obtained from a better load distribution capacity of the deck are smaller than in the case where a single truck load is used in the design.

The theoretical torsional rigidity of the ribs, corresponding to their shape and plate thickness, does not enter the computation of the effective torsional rigidity, H , of the deck in full amount. It must be reduced, due to the elastic flexibility of the deck plate between and above the ribs.

This is explained in Figure 3.7 which shows, in an exaggerated manner, a cross section between the floor beams of a steel plate deck with closed ribs deflected by a load.

If the deck plate were sufficiently rigid, the deflection line would be smooth, as shown by the dashed line. In this case the ribs participate in the load distributing action of the deck to the full extent of their torsional rigidity.

If, at the other extreme, the deck plate were absolutely soft, there would be no torsional deformation of the ribs due to load and the torsional rigidity of the ribs would have no effect on the load distribution and the stress flow in the deck. In an actual case, the deck plate has a certain flexural rigidity and, consequently, the ribs are forced to twist. However, the relatively thin deck plate deforms due to shear transfer from one rib to the next, and a wavy rather than smooth

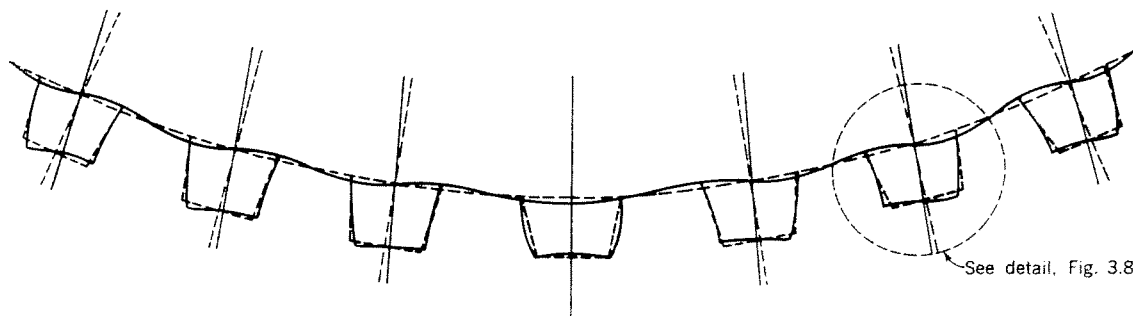


Fig. 3.7

deflection curve results, as shown by the solid line in Figure 3.7. Consequently, the torsional rotation of the ribs is *smaller* than it would be in a system with a very rigid deck plate, as shown by the dashed line. This means that in an actual deck structure the torsional rigidity of the ribs, corresponding to their geometric properties, is not fully utilized because of the flexural deformations of the deck plate.

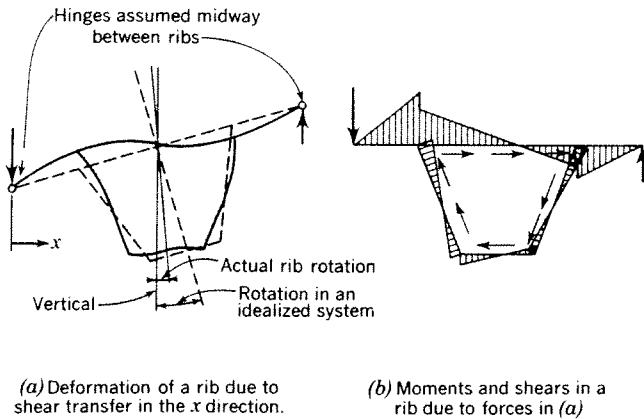


Fig. 3.8

The flexural deformations and stresses in the deck plate are also imparted to the side walls and the bottoms of the ribs (Fig. 3.8), since the rib walls are rigidly connected to the deck plate by welds. These flexural stresses in the direction transverse to the ribs (System III stresses, see Chapter 1) are generally disregarded in the design, as explained in Chapter 6.

However, the flexural stresses and deformations of the deck plate and the rib walls are of importance in determination of the effective torsional rigidity, H , of the deck. Thus, the flexural rigidity of the system in the transverse direction, $D_x = D_P$, disregarded in the simplified equation (3.1) of the substitute orthotropic plate, enters the computations indirectly, through the reduced effective torsional rigidity value.

(c) Computation of the effective torsional rigidity

The effective torsional rigidity of the ribs is defined as the torsional rigidity of an ideal system (as represented by the dashed line in Figure 3.7), free from secondary flexural deformations (the wavy line in Figure 3.7), in which the work of deformation due to torsion alone is equal to the work of deformation due to torsion and secondary flexure of the actual ribs. From this condition of equality of the energy consumed in both systems it follows that the torsional deformation of the ribs of the ideal system must be greater than the torsional deformation in the actual system, accounting only for a part of the total work consumed. Thus, with deformation being inversely

proportional to rigidity, the torsional rigidity of the ideal system, or the effective torsional rigidity of the ribs, is smaller than the rigidity value obtained without consideration of the secondary flexural deformations of the deck and the ribs, as has been already indicated in Section 3.3.3.1b.

The reduction of the theoretical rigidity value, based on the geometric properties of the rib cross section, is expressed by a reduction factor, μ , which is smaller than one.

The reduced torsional rigidity of the ribs, computed in the manner indicated above, is used to obtain the effective torsional rigidity, H , of a substitute orthotropic plate representing the actual deck.

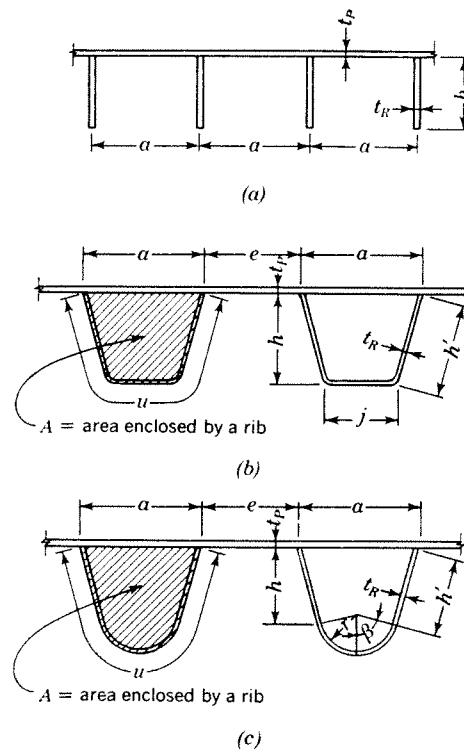


Fig. 3.9. Rib dimensions

Formulas for the reduction factor, μ , and the effective torsional rigidity, H , are given in Section 3.3.3.2. The derivations of these formulas may be found in reference [42].

The expressions for the reduction coefficient, μ , have been derived for simply supported ribs. Since the actual ribs are continuous over the floor beams, a substitute simple span, s_2 , of the ribs has to be used in the formulas. It is computed from the condition that the deflection under a wheel load in the midspan of a continuous rib is equal to the deflection of a substitute simple span of the length s_2 .

For design purposes an average value

$$s_2 = 0.81s \quad (3.12)$$

may be used.

The effective torsional rigidity, H , of a steel plate deck with closed ribs generally depends on the shape of the ribs, the plate thickness and the span and spacing of the ribs (Fig. 3.9).

The value of H increases with the area, A , enclosed by one rib, the plate thickness, t , and the rib span, s . With trapezoidal ribs, the maximum value of H is reached when the ratio of the bottom width to the top width of the rib, j/a , is approximately 0.4.

The value of H decreases sharply with increasing rib spacing, e .

Conversely, the reduction of the effective rigidity is the smallest when $e = 0$, since, in such case, the deck flexibility has little effect on the torsional rigidity. However, such an arrangement is not necessarily the most economical.

It should be noted that the load distributing capacity of the deck in the transverse direction depends on the relative rigidity ratio, H/D_v , rather than on the magnitude of H alone.

The correctness of the formulas for the effective torsional rigidity given in this Manual has been confirmed by model tests in which the measured stresses were found to be in a reasonable agreement with the computed values [42].

3.3.3.2 Formulas for Effective Torsional Rigidity

The effective torsional rigidity of an orthotropic plate representing a steel plate deck stiffened by closed ribs is expressed by the formula

$$H = \frac{1}{2} \left(\frac{\mu GK}{a + e} \right) \quad (3.13)$$

where

H = effective torsional rigidity of the orthotropic plate (k-in.²/in.)

G = modulus of elasticity of steel in shear
= 11.2×10 k/in.²

K = section property characterizing torsional resistance, as defined below (in.⁴)

a = top width of closed rib (in.) (Fig. 3.9)

e = width of deck plate between two ribs (in.)

μ = reduction coefficient, depending on flexibility of the deck plate and the span of ribs (dimensionless)

The factor $\frac{1}{2}$ in equation (3.13) is due to the conversion of the rib rigidity into the effective torsional

rigidity of the substitute orthotropic plate, as explained in Section 3.3.3.1a.

The rib section property, K , is computed by the formula

$$K = \frac{4A^2}{(u/t_R) + (a/t_P)} \quad (3.14)$$

where

A = area enclosed by one closed rib (in.²)

u = developed width of one rib plate (in.)

t_R = rib thickness (in.)

t_P = deck plate thickness (in.)

Formulas for reduction coefficients, μ , are given below for trapezoidal and round-bottomed ribs.

The following designations are used:

$$EI_P = \frac{Et_P^3}{12(1 - \nu^2)} = \frac{EI_P^3}{10.92} = \text{flexural rigidity of the deck plate (k-in.²/in.)}$$

$$\rho = \left(\frac{t_R}{t_P} \right)^3 = \text{ratio of the rib plate to the deck plate rigidity}$$

$$s_2 = 0.81s = \text{effective rib span used in the computation of the torsional rigidity}$$

Other designations are explained in Figure 3.9 or in the text.

(a) *Trapezoidal ribs (Fig. 3.9b)*

$$\frac{1}{\mu} = 1 + \frac{GK}{EI_P} \left(\frac{a^3}{12(a + e)^2} \right) \left(\frac{\pi}{s_2} \right)^2 \left[\left(\frac{e}{a} \right)^3 + \left(\frac{e - j}{a + j} + \lambda \right)^2 + \frac{\lambda^2}{\rho} \left(\frac{j}{a} \right)^3 + \frac{24}{\rho} \left(\frac{h'}{a} \right) \times \left(c_1^2 + c_1 c_2 + \frac{c_2^2}{3} \right) \right] \quad (3.15)$$

where

$$\lambda = \frac{(2a + j)(a + e)jh' - \rho a^3(e - j)}{(a + j)[2h'(a^2 + aj + j^2) + j^3 + \rho a^3]}$$

$$c_1 = \frac{\lambda}{2} \left(\frac{j}{a} \right)$$

$$c_2 = \frac{\lambda}{2} \left(\frac{a - j}{a} \right) - \left(\frac{a + e}{a + j} \right) \frac{j}{2a} \quad (3.15a)$$

(b) *Trapezoidal ribs, uniform deck plate divisions, $a = e$*

$$\frac{1}{\mu} = 1 + \frac{GK}{EI_P} \left(\frac{a}{48} \right) \left(\frac{\pi}{s_2} \right)^2 \left[1 + \left(\frac{a - j}{a + j} + \lambda \right)^2 + \frac{\lambda^2}{\rho} \left(\frac{j}{a} \right)^3 + \frac{24}{\rho} \left(\frac{h'}{a} \right) \left(c_1^2 + c_1 c_2 + \frac{c_2^2}{3} \right) \right] \quad (3.16)$$

where

$$\lambda = \frac{(2a + j)(2ajh') - \rho a^3(a - j)}{(a + j)[2h'(a^2 + aj + j^2) + j^3 + \rho a^3]}$$

$$c_1 = \frac{\lambda}{2} \left(\frac{j}{a} \right) \quad (3.16a)$$

$$c_2 = \frac{\lambda}{2} \left(\frac{a - j}{a} \right) - \frac{j}{a + j}$$

(c) *Ribs with rounded bottoms (Fig. 3.9c)*

$$\frac{1}{\mu} = 1 + \frac{GK}{EI_P} \left(\frac{a^3 r^2}{2A^2} \right) \left(\frac{\pi}{s_2} \right)^2 [J + L + M + N] \quad (3.17)$$

where

$$A = h \left(\frac{a + j}{2} \right) + r^2 \left(\beta - \frac{j}{2r} \cos \beta \right)$$

$$J = \left(\frac{2A}{r(a + e)} \right)^2 \left(\frac{1}{24} \right) \left(\frac{e}{a} \right)^3$$

$$L = \frac{1}{24} (\lambda - B)^2$$

$$M = \frac{1}{\rho} \left(\frac{r}{a} \right)^3 \left[\frac{\beta^3}{3} - 2(1 + \lambda) \left(\frac{j}{2r} - \beta \cos \beta \right) + \frac{(1 + \lambda)^2}{2} \left(\beta - \frac{j}{2r} \cos \beta \right) \right]$$

$$N = \frac{1}{\rho} \left(\frac{r^2 h'}{a^3} \right) \left(c_1^2 + c_1 c_2 + \frac{c_2^2}{3} \right)$$

$$\lambda = \frac{B + C}{1 + D} \quad (3.17a)$$

$$B = \frac{2A}{r(a + e)} - \frac{h}{r} - (1 - \cos \beta)$$

$$C = \frac{24}{\rho} \left(\frac{r}{a} \right)^3 \left[\frac{j}{2r} \left(1 + \frac{1}{2} \cos \beta \right) - \beta \left(\frac{1}{2} + \cos \beta \right) + \frac{h'(a + j)}{4r^2} \left(\beta - \frac{j}{2r} \right) + \frac{h'^2(2a + j)}{12r^3} (1 - \cos \beta) \right]$$

$$D = \frac{24}{\rho} \left(\frac{r}{a} \right)^3 \left[\frac{1}{2} \left(\beta - \frac{j}{2r} \cos \beta \right) + \frac{h'(a^2 + aj + j^2)}{12r^3} \right]$$

$$c_1 = \beta - \frac{j}{2r} (1 + \lambda)$$

$$c_2 = \frac{h'}{r} (1 - \cos \beta) - \lambda \left(\frac{a - j}{2r} \right)$$

(d) *Ribs with rounded bottoms, uniform deck plate divisions,*
 $a = e$

In this case formulas for case (c) are used with the following simplifications:

$$J = \left(\frac{A}{ar} \right)^2 \left(\frac{1}{24} \right) \quad (3.18)$$

$$B = \frac{A}{ar} - \frac{h}{r} - (1 - \cos \beta)$$

(e) *Ribs with rounded bottoms and vertical sides,*
 $a = j = 2r$

In this case formulas for case (c) are used with the following simplifications:

$$\beta = \frac{\pi}{2}, \quad h' = h$$

$$\frac{1}{\mu} = 1 + \frac{GK}{EI_P} \left(\frac{a^5}{8A^2} \right) \left(\frac{\pi}{s_2} \right)^2 (J + L + M + N) \quad (3.19)$$

where

$$A = ah + \frac{\pi a^2}{8}$$

$$J = \left(\frac{4A}{a(a + e)} \right)^2 \left(\frac{1}{24} \right) \left(\frac{e}{a} \right)^3$$

$$M = \frac{1}{8\rho} \left[\frac{\pi^3}{24} - 2(1 + \lambda) + \frac{(1 + \lambda)^2}{2} \left(\frac{\pi}{2} \right) \right]$$

$$N = \frac{h}{4\rho a} \left(c_1^2 + c_1 c_2 + \frac{c_2^2}{3} \right)$$

$$B = \frac{4A}{a(a + e)} - \frac{2h}{a} - 1 \quad (3.19a)$$

$$C = \frac{3}{\rho} \left[1 - \frac{\pi}{4} + \frac{2h}{a} \left(\frac{\pi}{2} - 1 \right) + 2 \left(\frac{h}{a} \right)^2 \right]$$

$$D = \frac{3}{\rho} \left(\frac{\pi}{4} + \frac{2h}{a} \right)$$

$$c_1 = \frac{\pi}{2} - (1 + \lambda)$$

$$c_2 = \frac{2h}{a}$$

3.4 LOADING

3.4.1 General

3.4.1.1 Dead Load

The dead load of a steel plate bridge deck consists of the weight of the steel construction of the deck and the weight of the wearing surface.

For the purposes of a preliminary computation, the weight of the steel deck construction, consisting of a $\frac{3}{8}$ -in. deck plate, longitudinal ribs and floor beams, may be assumed to range from 35 to 45 lbs per sq ft of the roadway area.

The weight of the wearing surface may range from approximately 25 lbs per sq ft for bituminous wearing surfaces to about 3 to 5 lbs per sq ft for thin lightweight wearing surfaces (see Chapter 8).

3.4.1.2 Live Load

The live load to be used in the design consists generally of the individual wheel, axle and truck loads, or the alternative uniformly distributed lane loads, as given by the AASHO specifications [1].

In the design of the bridge decks the uniformly distributed lane load never governs, because of the relatively short spans of the structural members of the deck.

In Step 1 of the design of the longitudinal ribs of a steel plate deck (ribs continuous over floor beams considered to be rigid) the critical loading consists of the individual wheel loads.

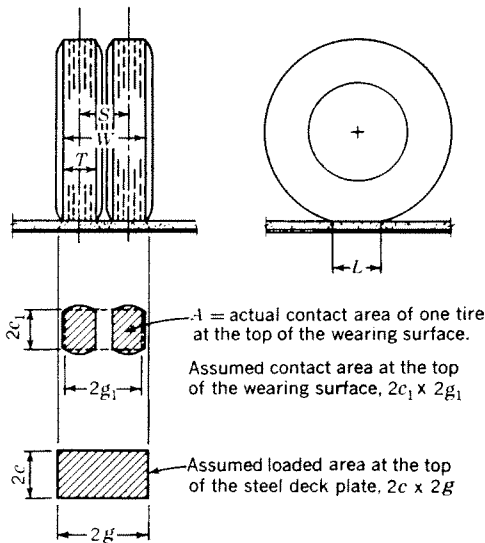


Fig. 3.10. Wheel load dimensions

In Step 2 of the design of the ribs, considering the effects of the floor beam elasticity, full axle and truck loads are used.

Full axle or truck loads are also used in the design of the floor beams.

The number and position of the individual wheel loads and the axle and truck loads causing maximum moments in the various structural members of the decks with open and with closed ribs are discussed in Chapter 10.

The rear truck wheels used in the design consist generally of two tires each (Fig. 3.10). The contact area between the tire tread and the roadway is an oval surface, depending on the total load, the dimensions and the inflation pressure of the tire.

The directly loaded area of the steel deck plate is larger than the contact area between the tire and the roadway because of the load distributing action of the wearing surface, depending on its thickness and rigidity. For asphalt wearing surfaces a 45° distribution is usually assumed.

For design purposes it is permissible to represent the actual loaded area of the steel plate deck under a wheel load by an equivalent rectangular area, $2c \times 2g$ (Fig. 3.10), which is assumed to be uniformly loaded.

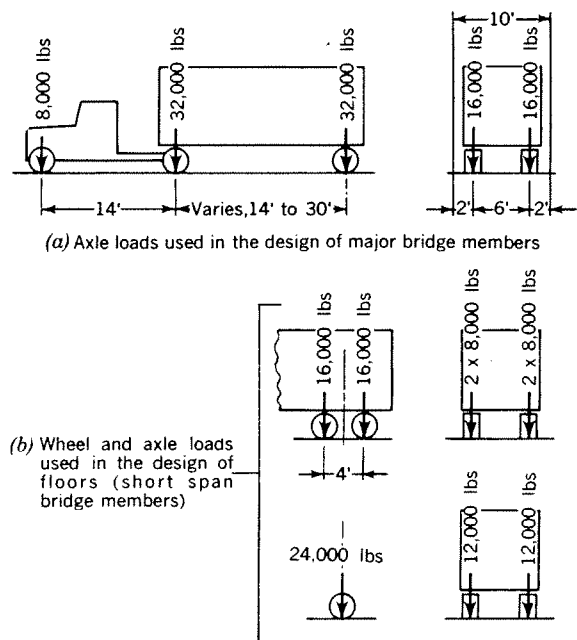


Fig. 3.11. Standard H20-S16-44 truck-trailer loading (AASHO specifications)

3.4.2 Application of the AASHO Loads in the Design of Steel Plate Bridge Decks

3.4.2.1 Wheel Loads

Major bridges on the Federal and State highways are designed, as a rule, for the heaviest type of truck-trailer loading.

This loading, designated H20-S16-44 by the AASHO specifications, consists of a standard truck with semi-trailer, having a total weight of $20 + 16 = 36$ tons, or 72,000 lbs, represented by three axles with a variable spacing, chosen to approximate the dimensions of tractor-trailers now in use, as shown in Figure 3.11a.

The 8 kip and 32 kip axle loads, convenient in the design of the bridge members of longer spans, do not represent correctly the actual local loading conditions governing the design of bridge floor members of short spans, since heavy tires, capable of supporting 32 kip single axle loads are not practical on trucks, and lighter tandem axles are used instead. This is reflected in the alternative design provision of the AASHO Design Specifications (Eighth Edition, 1961, Section 1.2.5(C), Figures 5 and 6, Footnote), permitting the use of two 16 kip axles 4 ft apart, or one 24 kip axle, instead of a 32 kip axle, for the design of bridge floors (Fig. 3.11b). This loading is recommended for the design of the deck plate and the longitudinal ribs of steel plate decks.

Several State Highway Departments specify using the 32 kip axle for the floors of bridges designed for the H20-S16-44 loading.

The Bureau of Public Roads specifies two 24 kip axles spaced 4 ft apart for the design of floor systems of bridges supporting interstate highways, with the total truck load corresponding to the basic H20-S16-44 loading.

However, these design provisions are expressly motivated by the need to overcome the deficiencies of conventional bridge floors [6]. Since steel plate bridge decks are distinguished by a remarkable reserve carrying capacity for local overloads, as has been shown in Chapter 1, the above provisions should not apply to the design of such decks.

It should be noted that the 16 kip wheel loads, in accordance with Figure 3.11a, are not always critical in the design of the longitudinal ribs of a steel plate deck.

In the design charts for the bending moments in the ribs due to the local wheel loads (Charts 3 to 14, Appendix), the effects of both types of loading, Figures 3.11a and 3.11b, are given.

In the computations of the effects of the floor beam flexibility on the rib moments and in the floor beam design the full H20-S16-44 truck-trailer loading, Figure 3.11a, is used.

3.4.2.2 Loaded Area Dimensions

The average actual dimensions of the standard truck tires (Fig. 3.10), corresponding to the 8, 12 and 16 kip wheel loads of the H20-S16-44 tractor-trailer, are given in Table 3.4.2.2, columns (2) to (6).

The assumed dimensions of the rectangular wheel load areas, $2c_1 \times 2g_1$, at the roadway surface, approximating the actual tire pattern dimensions, are given in columns (7) and (8). The dimensions for the 8 kip and 12 kip wheels are assumed, for the sake of simplicity, to be the same, with the width, $2g_1 = 20$ in., corresponding to that given by the AASHO specifications for the rear axle wheels of the standard 20-ton truck.

However, for a 16 kip wheel a 24 in. width is used, which is in better agreement with the actual tire dimensions of the standard tractor-trailer specified for the design.

The length, $2c_1$, is assumed to be 10 in. for all wheel loads.

To account for the load distribution through the wearing surface placed on the steel deck, an increase of the loaded area dimensions by 2 in. in each direction is assumed as an average value. This assumption is conservative for the usual 2-in. thick asphalt wearing surface or for an asphalt plank surfacing, and is somewhat too liberal for the thin epoxy wearing surfaces.

Thus the following design loaded areas, $2g \times 2c$, recommended for the design of steel plate decks are obtained: 22 in. \times 12 in. for the 8 kip and 12 kip wheels, and 26 in. \times 12 in. for the 16 kip wheels, as shown in columns (9) and (10) of Table 3.4.2.2.

These dimensions are used in the design charts given in the Appendix.

3.4.2.3 Impact Factors and Load Reduction Coefficients

Impact factors are applied to all live loads in accordance with the AASHO specifications, 1961, Section 1.2.12.

For the design of the deck plate and the longitudinal

TABLE 3.4.2.2
LOADED AREA DIMENSIONS OF TRUCK WHEELS (IN.)

Nominal Wheel Loads (kips) (1)	Actual Dimensions					Dimensions Used in Design			
						Top of Roadway		Top of Steel Plate	
	<i>T</i> (2)	<i>L</i> (3)	<i>A</i> (4)	<i>S</i> (5)	<i>W</i> (6)	$2g_1$ (7)	$2c_1$ (8)	$2g$ (9)	$2c$ (10)
8	7.0	8.9	62	11.4	18.4	20	10	22	12
12	7.9	10.8	85	12.8	20.7	20	10	22	12
16	10	11.0	110	16.2	26.2	24	10	26	12

NOTES: Dimensions are defined in Fig. 3.10. Columns (2), (4) and (5) are average data given by manufacturers for tires corresponding to nominal wheel loads in Column (1). Column (3) obtained by dividing (4) by (2).

ribs the maximum impact factor of 30% is used, because of the short spans of these members.

For the design of the floor beams the impact factor is computed by the formula given in the AASHTO specifications, using the actual floor beam span.

In the design of the floor beams and in the computations of the additional bending moments in the ribs due to floor beam elasticity, maximum effects are usually obtained with a simultaneous loading of more than two design traffic lanes. In such cases the load reduction coefficients are applied, as specified for multiple lane loading by Section 1.2.9 of the AASHTO specifications.

These reduction coefficients have been considered in Charts 16 and 32 for floor beam design.

3.5 FOURIER ANALYSIS OF LOADING

3.5.1 Introduction

For the purposes of computation of the bending moments in the deck with closed ribs, treated as an orthotropic plate, and for evaluation of the effects of floor beam flexibility on the moments in the deck with closed or open ribs, the wheel loads acting on the

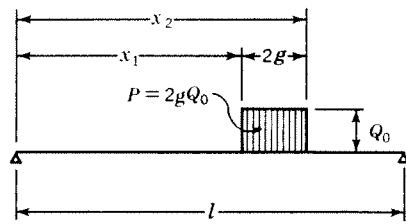


Fig. 3.12

bridge deck must be developed into *Fourier series*, representing the actual concentrated loads by a summation of sinusoidal component loads extending over the whole width of the bridge deck.

In the system shown in Figure 3.12 a load $P = Q_0(x_2 - x_1)$ may be represented by a series

$$Q_x = \sum_{n=1}^{\infty} Q_n \sin \frac{n\pi x}{l} \quad (3.20)$$

with

$$\begin{aligned} Q_n &= \frac{2Q_0}{l} \int_{x_1}^{x_2} \sin \frac{n\pi x}{l} dx \\ &= \frac{2Q_0}{n\pi} \left[\cos \frac{n\pi x_1}{l} - \cos \frac{n\pi x_2}{l} \right] \end{aligned} \quad (3.20a)$$

where

Q_x = load per unit width at the location x , represented by a Fourier series (k/in.)

Q_0 = actual load on bridge deck per unit width
 = $P/2g$ (k/in.)
 l = span length = width of bridge deck (in.)

The value of Q_n (Q_1, Q_2, Q_3, \dots), in kips per inch, represents the maximum value (the amplitude) of the n th sinusoidal component load of the series, as illustrated in Figure 3.13b.

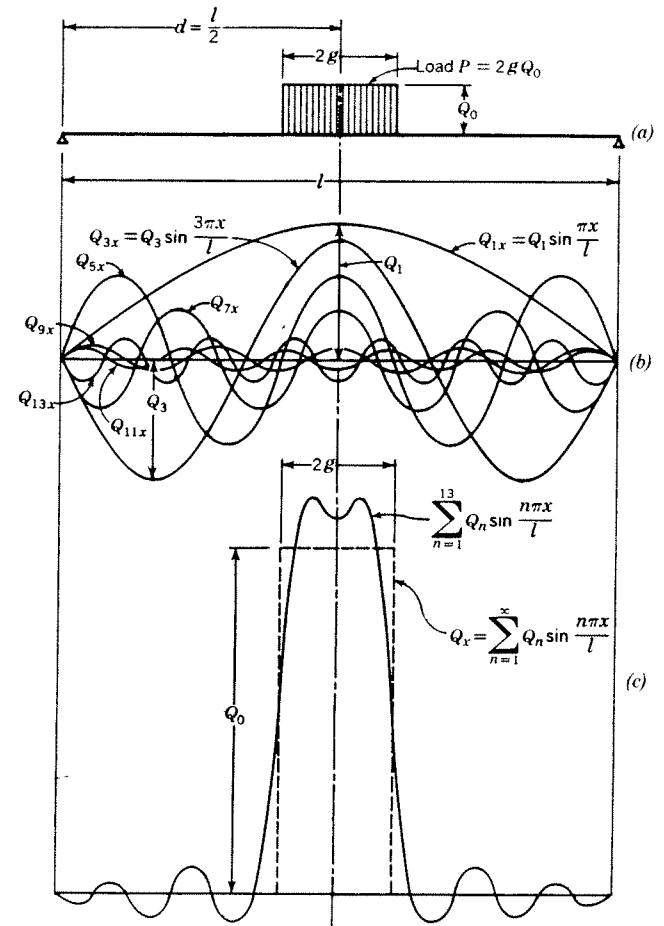


Fig. 3.13

At any point, x , the load intensity, Q_{nx} , of the n th component load of the series is (see Fig. 3.13b)

$$Q_{nx} = Q_n \sin \frac{n\pi x}{l} \quad (3.21)$$

An example of a load represented by a Fourier series is given in Figure 3.13. A wheel load of a width $2g$ and of an intensity Q_0 (Fig. 3.13a) is equivalent to a series of sinusoidal component loads $Q_{1x}, Q_{3x}, Q_{5x}, \dots, Q_{nx}$ (see Fig. 3.13b). In Figure 3.13c a summation of the component loads, Q_{nx} , is shown for n equal 1 through 13. With n approaching infinity, the summation of the component loads approaches the actual

load shown. In this example all component loads for even values of n are equal to zero, because of the symmetry of the loading.

In numerical computations it is convenient to use the dimensionless Fourier coefficients Q_{nx}/Q_0 , rather than the values of Q_{nx} . This has the advantage of making the intermediate steps of the calculations independent of the load intensity, Q_0 , which is introduced only in the final formulas for the bending moments.

3.5.2 Application of the Fourier Analysis to the Deck Design

The Fourier analysis of loading is needed in both Steps 1 and 2 of the design of a steel plate deck with closed ribs and in Step 2 of the design of a deck with open ribs.

In the design of the deck with closed ribs as an orthotropic plate continuous over infinitely rigid floor beams (Step 1 of the computation) the expressions for bending moments are given as infinite series, as explained in Section 2.3.

In order to evaluate these expressions, the loading must also be represented as a series consisting of sinusoidal component loads of the type discussed in Section 3.5.1 above.

In Step 1 of the design computations the width of the deck affected by a wheel load is always much smaller than the actual width, l , of the deck between the main girders. Therefore, a substitute width, b , smaller than l , may be used.

This has the advantage of considerably improving the convergence of the series, as will be shown in Chapters 4 and 10.

Numerical calculations are further simplified by using symmetrical loading only. This eliminates the Fourier coefficients for the even values of n .

Formulas for the Fourier coefficients Q_{nx}/Q_0 needed for computation of bending moments in closed ribs are given in Section 3.5.3.

In Step 2 of the computation, evaluating the effects of floor beam flexibility, it is necessary to represent the truck loads causing the floor beam deflection by Fourier series, in order to obtain a substitute loading proportional to the floor beam deflections at any point of the floor beam. This is discussed in Chapter 5.

It is sufficient for design purposes to use only the first Fourier component load, Q_{1x}/Q_0 , since the effect of the higher component loads, Q_{2x} , Q_{3x} , Q_{4x} , etc., on the floor beam deflections is negligible (see Chapter 5).

Formulas for the Fourier coefficients Q_{1x}/Q_0 needed for computations of the effects of flexibility of simply supported floor beams are given in Section 3.5.4.

3.5.3 Fourier Coefficients Q_{nx}/Q_0 Used in Computation of Moments in the Orthotropic Plate on Rigid Supports

In the computation of the bending moments in the orthotropic plate the Fourier coefficients, Q_{nx}/Q_0 , may be needed for the following cases:

3.5.3.1 One Wheel in Center of the Plate Strip Considered (Fig. 3.14)

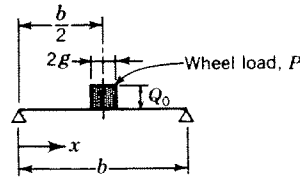


Fig. 3.14

(a) With a substitute span length, b , instead of the actual main girder spacing, l , as explained in Section 3.5.2, and with the values $x_1 = (b/2) - g$ and $x_2 = (b/2) + g$ (Fig. 3.12), the expression for Q_{nx}/Q_0 is obtained from equations (3.20a) and (3.21), for any point, x , of the span, b ,

$$\frac{Q_{nx}}{Q_0} = \frac{4}{n\pi} \sin \frac{n\pi g}{b} \sin \frac{n\pi}{2} \sin \frac{n\pi x}{b} \quad (3.22)$$

$$n = 1, 3, 5 \dots$$

(b) For the point at the center of the applied load (at the midspan), $x = b/2$, equation (3.22) becomes

$$\frac{Q_{nx}}{Q_0} = \frac{4}{n\pi} \sin \frac{n\pi g}{b} \quad (3.23)$$

$$n = 1, 3, 5 \dots$$

3.5.3.2 One Axle Symmetrically Placed (Fig. 3.15)

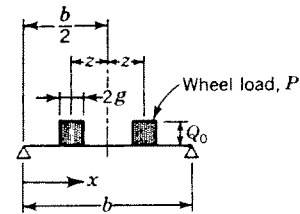


Fig. 3.15

(a) For any point, x , the value of Q_{nx}/Q_0 is obtained in a similar manner as above,

$$\frac{Q_{nx}}{Q_0} = \frac{8}{n\pi} \cos \frac{n\pi z}{b} \sin \frac{n\pi g}{b} \sin \frac{n\pi}{2} \sin \frac{n\pi x}{b} \quad (3.24)$$

$$n = 1, 3, 5 \dots$$

(b) For the point under one of the wheel loads, with $x = (b/2) - z$,

$$\frac{Q_{nz}}{Q_0} = \frac{8}{n\pi} \cos^2 \frac{n\pi z}{b} \sin \frac{n\pi g}{b} \quad (3.25)$$

$n = 1, 3, 5 \dots$

3.5.3.3 Axles Symmetrically Placed (Fig. 3.16)

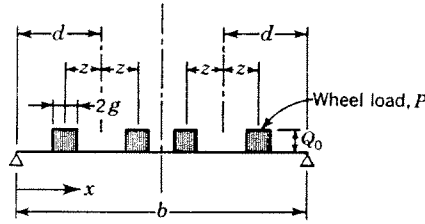


Fig. 3.16

For any point, x ,

$$\frac{Q_{nz}}{Q_0} = \frac{16}{n\pi} \cos \frac{n\pi z}{b} \sin \frac{n\pi g}{b} \sin \frac{n\pi d}{b} \sin \frac{n\pi x}{b} \quad (3.26)$$

$n = 1, 3, 5 \dots$

3.5.4 Fourier Coefficients Q_{1z}/Q_0 (Coefficients for $n = 1$) Used in Computation of the Effects of Floor Beam Flexibility

In determination of the effects of the floor beam flexibility on the bending moments in the ribs and the floor beams the Fourier coefficients may be needed for the loading cases given below.

The formulas are given for any position of the truck loads on the bridge. However, in design in accordance with the AASHO specifications, the position of the trucks within the specified design traffic lanes has to be observed (AASHO specifications, 1961, Section 1.2.6).

3.5.4.1 One Axle in Any Position (Fig. 3.17)

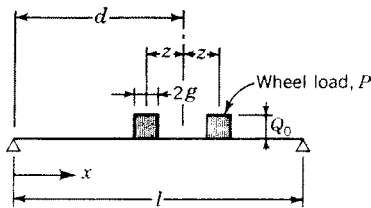


Fig. 3.17

(a) With the full effective floor beam span, l , the first Fourier coefficient is obtained for any position, d , of the truck on the bridge deck, for any point, x ,

$$\frac{Q_{1z}}{Q_0} = \frac{8}{\pi} \cos \frac{\pi z}{l} \sin \frac{\pi g}{l} \sin \frac{\pi d}{l} \sin \frac{\pi x}{l} \quad (3.27)$$

(b) For a maximum value of the coefficient Q_{1z}/Q_0 under a wheel, the truck shall be placed at $d = (l + z)/2$. With this position of loading, for the point under the wheel, $x = d - z$,

$$\frac{Q_{1z}}{Q_0} = \frac{4}{\pi} \cos \frac{\pi z}{l} \sin \frac{\pi g}{l} \left[1 + \cos \frac{\pi z}{l} \right] \quad (3.28)$$

3.5.4.2 Two Axles in Any Position (Fig. 3.18)

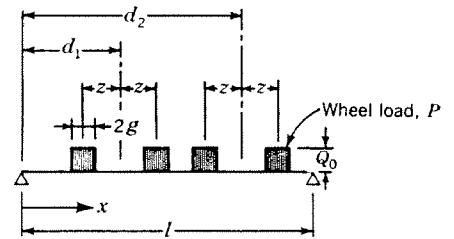


Fig. 3.18

(a) For two truck axles in any positions, d_1 and d_2 , for any point, x ,

$$\frac{Q_{1z}}{Q_0} = \frac{8}{\pi} \cos \frac{\pi z}{l} \sin \frac{\pi g}{l} \left[\sin \frac{\pi d_1}{l} + \sin \frac{\pi d_2}{l} \right] \sin \frac{\pi x}{l} \quad (3.29)$$

(b) For two truck axles symmetrically placed, $d_1 = d$, $d_2 = l - d$, equation (3.26) may be used, with $n = 1$ and $b = l$.

3.5.4.3 Many Axles in Any Position (Fig. 3.19)

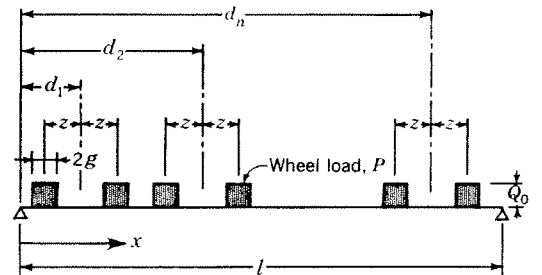


Fig. 3.19

Similarly as above, for any x ,

$$\frac{Q_{1z}}{Q_0} = \frac{8}{\pi} \cos \frac{\pi z}{l} \sin \frac{\pi g}{l} \left[\sin \frac{\pi d_1}{l} + \sin \frac{\pi d_2}{l} + \dots + \sin \frac{\pi d_n}{l} \right] \sin \frac{\pi x}{l} \quad (3.30)$$

Based on the above formulas, design Charts 28, 29 and 32 have been developed, giving the values of Q_{1z}/Q_0 at specific points for the various cases of loading. The use of these charts is explained in Chapter 10.

CHAPTER 4

Formulas for Steel Plate Decks on Rigid Supports

4.1 INTRODUCTION

In the first step of the design procedure outlined in this chapter, the bridge deck, consisting of the deck plate and the longitudinal ribs, is treated as a continuous structure supported on infinitely rigid (unyielding) uniformly spaced floor beams (Fig. 3.1a).

Since the torsional rigidity of the single-webbed floor beams is negligible, they are assumed to act as "knife-edge" supports, offering no flexural restraint to the ribs.

Formulas for the bending moments in the ribs are based on the simplifying assumptions discussed in Chapter 3.

4.2 DECK WITH OPEN RIBS

4.2.1 General

4.2.1.1 Differential Equation

With the assumptions $D_x = 0$ and $H = 0$, applicable to the deck with open ribs, as discussed in Chapter 3, the differential equation of the orthotropic plate (2.10) becomes

$$\frac{\partial^4 w}{\partial y^4} = \frac{p}{D_v} \quad (4.1)$$

which is the familiar equation of the deflection line of a beam. Thus the analysis of the deck with open ribs reduces to a linear problem and the ribs may be designed by continuous beam formulas.

4.2.1.2 Carry-over Factor

In a continuous beam of a constant moment of inertia on uniformly spaced rigid supports the magnitudes of bending moments, shears, deflections, etc. in

unloaded panels decrease with a constant coefficient κ (kappa), called the carry-over coefficient, as shown in Figure 4.1.

If M_0 is the bending moment at the support $m = 0$, then

$$\begin{aligned} M_1 &= \kappa M_0 \\ M_2 &= \kappa M_1 = \kappa^2 M_0 \\ M_3 &= \kappa M_2 = \kappa^3 M_0 \\ &\text{etc.} \end{aligned} \quad (4.2)$$

The value of the coefficient κ is obtained from the familiar three-moment equation, which, for the unloaded beam, is

$$M_0 + 4M_1 + M_2 = 0 \quad (4.3)$$

or, substituting equations (4.2),

$$M_0(1 + 4\kappa + \kappa^2) = 0 \quad (4.3a)$$

Hence

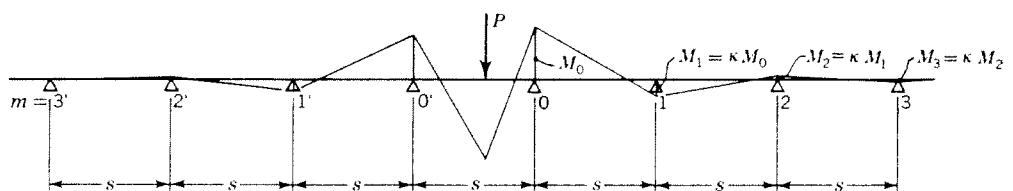
$$\kappa = -2 + \sqrt{3} = -0.2679 \quad (4.4)$$

4.2.1.3 Influence Lines

The bending moments and reactions of the open ribs are computed from the influence lines of a continuous beam.

The influence lines needed are obtained, in accordance with the Betti-Maxwell principle of reciprocity, as deflection lines of a continuous beam due to unit deformations. Thus, the influence line for the bending moment at any point of the continuous beam is defined as the deflection line of the beam due to a unit rotation applied at that point (Fig. 4.2a and b). Similarly, the influence line for the reaction at a support is the deflection line due to a unit deflection at the support where the reaction is sought (Fig. 4.2c).

Fig. 4.1. Bending moments of a continuous beam on rigid supports due to a concentrated load



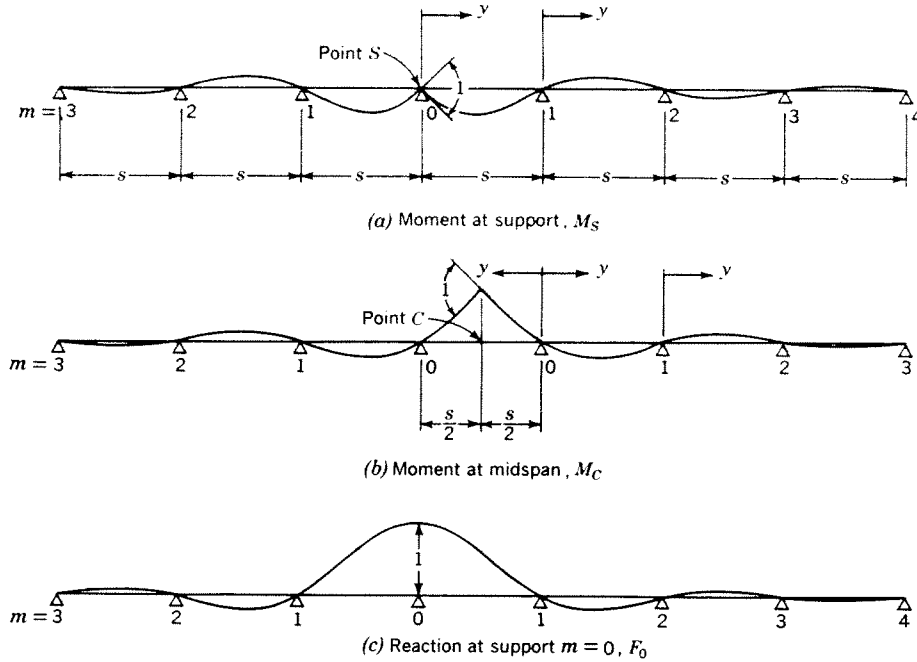


Fig. 4.2. Influence lines of a continuous beam on rigid supports

Formulas for influence lines given in Sections 4.2.2 to 4.2.4 are derived from the known relationship between the curvature of a beam and the bending moment, M . In this case, the moments M are caused by the unit deformations, as shown in Figure 4.2.

4.2.1.4 Computation of the Bending Moments in the Ribs

The bending moments in the ribs depend on the load P , the rib span s , and the variable load position along the rib, y . In the computation of the moments by means of influence lines it is convenient to use the dimensionless coefficients y/s and η/s , rather than the numerical values of y , s and η .

The bending moments are obtained from the general expression

$$M = \frac{\eta}{s} sP \tag{4.5}$$

where η/s is the influence line ordinate for a unit span, expressed as a function of the ratio y/s .

The bending moments acting on one rib, M_R , needed for the design of the ribs, are computed by the formula

$$M_R = M_{total}(R/P) \tag{4.5a}$$

where M_{total} is the moment computed by equation (4.5) and R/P is the ratio of the load on the rib under consideration to the total wheel load, which may be computed by the formulas given in Section 4.2.4.2, or obtained from Charts 2 or 3.

4.2.2 Bending Moment at the Support of Ribs

4.2.2.1 Concentrated Load at Any Point

(a) The equation of the influence line in panel 0-1 for the moment M_s at the support $m = 0$, is

$$\begin{aligned} \left(\frac{M_s}{sP}\right)_{01} &= \left(\frac{\eta_s}{s}\right)_{01} = \\ &= \frac{3}{2 + \kappa} \left[-\frac{(2 + \kappa)}{6} \frac{y}{s} + \frac{1}{2} \left(\frac{y}{s}\right)^2 - \frac{(1 - \kappa)}{6} \left(\frac{y}{s}\right)^3 \right] \\ &= -0.5 \frac{y}{s} + 0.8660 \left(\frac{y}{s}\right)^2 - 0.3660 \left(\frac{y}{s}\right)^3 \end{aligned} \tag{4.6}$$

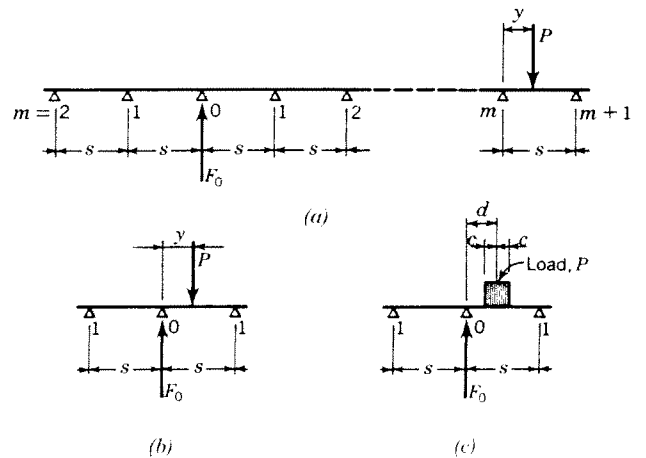


Fig. 4.3. Loads used in the computation of the moment M_s and reaction F_0 at support $m = 0$ of a continuous rib

(b) For panels 1-2, 2-3, 3-4 . . . (m)-(m+1) the expressions for the influence line are obtained by multiplication of equation (4.6) by the coefficient $(\kappa)^m$, where m is the smaller of the two support numbers enclosing the panel under consideration.

$$\left(\frac{M_s}{sP}\right)_m = \left(\frac{\eta_s}{s}\right)_m = \left[-0.5 \frac{y}{s} + 0.8660 \left(\frac{y}{s}\right)^2 - 0.3660 \left(\frac{y}{s}\right)^3\right] (-0.2679)^m \quad (4.6a)$$

(c) The maximum ordinate of the influence line occurs at the location $y/s = 0.3804$. At this location

$$\left(\frac{M_s}{sP}\right)_{0.38} = \left(\frac{\eta_s}{s}\right)_{0.38} = -0.0850 \quad (4.6b)$$

The bending moments M_s due to a concentrated load P are computed directly from the above formulas.

4.2.2.2 Distributed Load

Formulas for the bending moment M_s due to a distributed load P of a length $2c$ are needed only for the load located in the panel 0-1. The effect of a distributed load in a more distant panel may be obtained with sufficient accuracy by the concentrated load formula (4.6a).

(a) The bending moment M_s due to a distributed load located at a distance $y = d$ from the support $m = 0$ (Fig. 4.3c) is obtained by evaluation of the influence line, equation (4.6a) as

$$\left(\frac{M_s}{sP}\right) = -0.5 \left(\frac{d}{s}\right) + 0.8660 \left(\frac{d}{s}\right)^2 - 0.3660 \left(\frac{d}{s}\right)^3 + \left(\frac{c}{s}\right)^2 \left(0.2887 - 0.3660 \frac{d}{s}\right) \quad (4.7)$$

(b) The maximum value of the moment M_s is obtained with the load located at $d = 0.3804 s$. For this case

$$\left(\frac{M_s}{sP}\right)_{0.38} = -0.0850 + 0.1494 \left(\frac{c}{s}\right)^2 \quad (4.7a)$$

4.2.3 Bending Moment at the Midspan of Ribs

4.2.3.1 Concentrated Load at Any Point

(a) The equation of the influence line for the bending moment M_c at the midspan of the panel 0-0, for a load in panel 0-0 (Fig. 4.4a) is

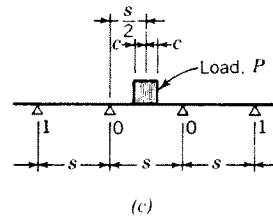
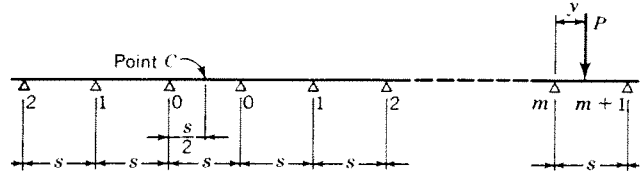
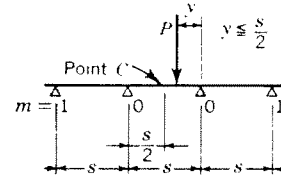


Fig. 4.4. Loads used in the computation of the moment M_c at the midspan of panel 0-0 of a continuous rib

$$\begin{aligned} \left(\frac{M_c}{sP}\right)_{00} &= \left(\frac{\eta_c}{s}\right)_{00} \\ &= \frac{1}{2} \frac{y}{s} - \frac{3}{2(5 + \kappa)} \left[\frac{y}{s} - \left(\frac{y}{s}\right)^2\right] \\ &= 0.1830 \frac{y}{s} + 0.3170 \left(\frac{y}{s}\right)^2 \end{aligned} \quad (4.8)$$

where $y < \frac{s}{2}$

(b) The maximum ordinate of the influence line is at the midspan of the panel 0-0, $y = 0.5 s$. At this location

$$\left(\frac{M_c}{sP}\right)_{0.5} = \left(\frac{\eta_c}{s}\right)_{0.5} = 0.1708 \quad (4.8a)$$

(c) The equation of the influence line in the distant panels 0-1, 1-2, 2-3, . . . (m)-(m+1), (Fig. 4.4b), is

$$\begin{aligned} \left(\frac{M_c}{sP}\right)_m &= \left(\frac{\eta_c}{s}\right)_m = \\ &= \frac{3}{5 + \kappa} \left[-\frac{(2 + \kappa)}{6} \frac{y}{s} + \frac{1}{2} \left(\frac{y}{s}\right)^2 - \frac{(1 - \kappa)}{6} \left(\frac{y}{s}\right)^3\right] \kappa^m \\ &= \left[-0.1830 \frac{y}{s} + 0.3170 \left(\frac{y}{s}\right)^2 - 0.1340 \left(\frac{y}{s}\right)^3\right] (-0.2679)^m \end{aligned} \quad (4.9)$$

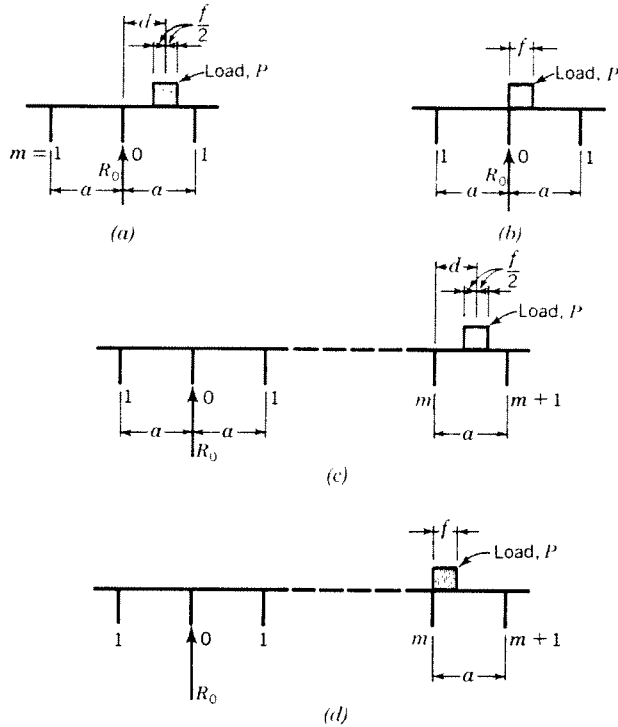


Fig. 4.5. Loads used in the computation of the reaction R_0 of a rib

where m is the smaller of the two support numbers enclosing the panel under consideration.

4.2.3.2 Distributed Load

The formula for the bending moment M_C at the midspan of the panel 0-0 is needed for the case of a wheel load located at the midspan (Fig. 4.4c). For other positions of the load the moment M_C may be obtained with sufficient accuracy from equations (4.8) and (4.9).

For the wheel load at midspan we obtain

$$\frac{M_C}{sP} = 0.1708 - 0.2500 \frac{c}{s} + 0.1057 \left(\frac{c}{s}\right)^2 \quad (4.10)$$

4.2.4 Reactions

4.2.4.1 Floor Beam Reactions on Ribs

In the computation of the floor beam reactions, F , on the ribs it is sufficient to represent the wheel loads, P , as concentrated loads.

(a) The equation for the influence line of the reaction F_0 at the support $m = 0$, for the load in the panel 0-1 (Fig. 4.3b) is

$$\begin{aligned} \frac{F_0}{P} = \vartheta_0 &= 1 - \frac{3(5 + \kappa)}{7 + 2\kappa} \left(\frac{y}{s}\right)^2 + \frac{8 + \kappa}{7 + 2\kappa} \left(\frac{y}{s}\right)^3 \\ &= 1 - 2.1962 \left(\frac{y}{s}\right)^2 + 1.1962 \left(\frac{y}{s}\right)^3 \end{aligned} \quad (4.11)$$

(b) For the load in any distant panel, $(m)-(m+1)$ (Fig. 4.3a) the equation of the influence line for F_0 is

$$\begin{aligned} \frac{F_0}{P} = \vartheta_0 &= \left\{ -\frac{6}{7 + 2\kappa} \left[\left(1 + \frac{\kappa}{2}\right) \frac{y}{s} - \frac{3}{2} \left(\frac{y}{s}\right)^2 + \frac{1 - \kappa}{2} \left(\frac{y}{s}\right)^3 \right] \right\} \kappa^{m-1} \\ &= \left[-0.8038 \frac{y}{s} + 1.3923 \left(\frac{y}{s}\right)^2 - 0.5885 \left(\frac{y}{s}\right)^3 \right] (-0.2679)^{m-1} \end{aligned} \quad (4.12)$$

where m is the smaller of the two support numbers enclosing the panel under consideration.

(c) Reactions $F_1, F_2, F_3, \dots, F_m$ at the distant floor beams due to a load in a certain position are obtained from equations (4.11) or (4.12) by placing the load in an appropriate position with respect to the support where the reaction is sought.

4.2.4.2 Rib Reactions on the Deck Plate

In distributing the local wheel load, the deck plate is assumed to act as a continuous isotropic plate on rigid supports (see Fig. 2.7c).

The rib reactions, or the loads acting on the individual ribs R_0, R_1, \dots, R_m , are computed by the formulas given below, based on the influence lines, equations (4.11) and (4.12). The formulas are given for a distributed load P , having a width, f , smaller than the rib spacing, a (Fig. 4.5). If the width of the actual wheel load, $2g$, is greater than the rib spacing, a , the rib reactions are obtained by superposition of the effects of the loads in the individual panels.

(a) Load in panel 0-1 in any position (Fig. 4.5a)

$$R_0 = P \left[1 - 2.1962 \left(\frac{d}{a}\right)^2 + 1.1962 \left(\frac{d}{a}\right)^3 + \left(\frac{f}{a}\right)^2 \left(-0.1830 + 0.2990 \frac{d}{a} \right) \right] \quad (4.13)$$

(b) Load in panel 0-1, at support 0 (Fig. 4.5b)

$$R_0 = P \left[1 - 0.7321 \left(\frac{f}{a}\right)^2 + 0.2990 \left(\frac{f}{a}\right)^3 \right] \quad (4.13a)$$

(c) Load in any panel, $(m)-(m+1)$, in any position (Fig. 4.5c)

$$R_0 = P \left[-0.8038 \frac{d}{a} + 1.3923 \left(\frac{d}{a}\right)^2 - 0.5885 \left(\frac{d}{a}\right)^3 + \left(\frac{f}{a}\right)^2 \left(0.1160 - 0.1471 \frac{d}{a} \right) \right] (-0.2679)^{m-1} \quad (4.14)$$

(d) Load in any panel, $(m)-(m + 1)$, at support m (Fig. 4.5d)

$$R_0 = P \left[- 0.4019 \frac{f}{a} + 0.4641 \left(\frac{f}{a} \right)^2 - 0.1471 \left(\frac{f}{a} \right)^3 \right] (-0.2679)^{m-1} \quad (4.14a)$$

The above formulas also may be used for the reactions $R_1, R_2 \dots$ etc., if the load, P , is appropriately placed with respect to the support where the reaction is sought.

4.2.5 Influence Line Ordinates

The ordinates of the influence lines for the bending moments at the support and at the midspan, and for the reaction at the support of a continuous beam on rigid supports, computed by the equations given in the foregoing sections, are given in Table 4.2.5. The influence lines are also represented graphically in Chart 5.

4.2.6 Charts for the Design of Decks with Open Ribs on Rigid Supports

Charts prepared with the purpose of facilitating the design computations are given in the Appendix.

In this section the derivation of the charts applicable to the design of the open ribs on rigid supports and the rigid floor beams is discussed.

The use of the charts in practical design computations is explained in Chapter 10.

Chart 1 gives the effective width ratio of the deck plate as a function of the spacing to span ratio of the ribs or the floor beams. The curve shown is based on the numerical values in Table 3.3.2.1 given and explained in Chapter 3.

Chart 2a, giving the ratio of the load, R_0 , on the rib directly under the load to the total wheel load, P , as a function of the wheel width, $2g$, and the rib spacing, a , is based on equations (4.13) and (4.14). It is seen that Case 1 (wheel centered over the rib) governs in most practical cases. Assuming the wheel width $2g = 22$ in., Case 2 (wheel between ribs) governs only with a rib spacing a smaller than 8 in.

Chart 2b, giving the effective rib spacing ratio, has been obtained with equation (3.5), given and explained in Chapter 3. The rib reactions, R_0 and R_1 , needed in equation (3.5), have been computed by equations (4.13) and (4.14).

Chart 3 gives the R_0/P ratios and the load per rib, R_0 , directly for the 8, 12 and 16 kip AASHO wheel loads, using the widths $2g = 22$ in. and 26 in., as discussed in Section 3.4.2. The 30% impact factor is included. The curves are based on equations (4.13) and (4.14).

Chart 4 gives the effective rib spacing, a_0^* , needed for the computation of the effective width of plate for the directly loaded rib, for the AASHO wheel loads. The formulas used in the preparation of this chart are the same as used for Chart 2b.

TABLE 4.2.5
INFLUENCE ORDINATES FOR A BEAM ON AN INFINITE NUMBER OF RIGID SUPPORTS
For point designations see Chart 5, Appendix

Point						0.5'	0.4'	0.3'	0.2'	0.1'	0.0
$\eta_{c/s}$ -Moment at Midspan						+0.1708	+0.1239	+0.0834	+0.0493	+0.0215	0
Point	0.0	0.1	0.2	0.3	0.4	0.5	0.6	0.7	0.8	0.9	1.0
$\eta_{c/s}$ -Moment at Midspan	0	-0.0153	-0.0250	-0.0300	-0.0311	-0.0290	-0.0246	-0.0187	-0.0121	-0.0056	0
$\eta_{s/s}$ -Moment at Support	0	-0.0471	-0.0683	-0.0819	-0.0849	-0.0792	-0.0673	-0.0512	-0.0331	-0.0154	0
ϑ -Reaction	+1	+0.9792	+0.9217	+0.8346	+0.7252	+0.6005	+0.4678	+0.3342	+0.2069	+0.0931	0
Point	1.0	1.1	1.2	1.3	1.4	1.5	1.6	1.7	1.8	1.9	2.0
$\eta_{c/s}$ -Moment at Midspan	0	+0.0041	+0.0067	+0.0080	+0.0083	+0.0078	+0.0066	+0.0050	+0.0033	+0.0015	0
$\eta_{s/s}$ -Moment at Support	0	+0.0112	+0.0183	+0.0220	+0.0227	+0.0212	+0.0180	+0.0137	+0.0089	+0.0041	0
ϑ -Reaction	0	-0.0671	-0.1098	-0.1317	-0.1364	-0.1274	-0.1082	-0.0823	-0.0553	-0.0247	0
Point	2.0	2.1	2.2	2.3	2.4	2.5	2.6	2.7	2.8	2.9	3.0
$\eta_{c/s}$ -Moment at Midspan	0	-0.0011	-0.0018	-0.0022	-0.0022	-0.0021	-0.0018	-0.0013	-0.0009	-0.0004	0
$\eta_{s/s}$ -Moment at Support	0	-0.0030	-0.0049	-0.0059	-0.0061	-0.0057	-0.0048	-0.0037	-0.0024	-0.0011	0
ϑ -Reaction	0	+0.0180	+0.0294	+0.0353	+0.0366	+0.0341	+0.0290	+0.0221	+0.0143	+0.0066	0

Chart 5 represents graphically the values of the influence ordinates for the bending moments at the midspan and at the support, and the reaction at the support of a continuous beam on rigid supports, given in Table 4.2.5. The values of the moment ordinates have been computed by equations (4.6), (4.6a), (4.8) and (4.9). The reaction ordinates have been obtained from equations (4.11) and (4.12).

Chart 6 gives the total value (over the entire effective width of the bridge deck) of the positive moment at the midspan of the deck between two floor beams caused by one wheel load, or a group of wheel loads aligned in the longitudinal direction of the bridge, as shown. The curves have been computed by equations (4.8), (4.9) and (4.10).

The loads used are in accordance with the AASHO design specifications, as discussed in Section 3.4.2.

The wheel loads placed at the location of the maximum positive moment (midspan, point "C") are considered to be distributed over the length $2c = 12$ in. The wheel loads at other points are treated as concentrated loads.

The loading cases **a**, **b** and **c** represent wheel loads in the deck panel under consideration. In the cases **a**₁, **b**₁ and **c**₁ additional effects of the rear and the front wheels in the more distant panels are considered. The rear wheels are placed in such a position, within the variable 14-ft to 30-ft distance from the center wheel, as to produce the maximum moment at point "C." The effect of the front 4 kip wheel, at the fixed distance of 14 ft from the center wheel, is included only if it produces a positive moment at "C." It is seen that the effect of the wheels in the distant panels is not very large, and does not exceed 7% of the effect of the center wheel alone.

The choice between the loading **a**, **b** or **c** and the loading **a**₁, **b**₁ or **c**₁ is determined by comparison of the effects of these loadings, with consideration of the floor beam flexibility.

The 30% impact allowance has been included.

It should be noted that *Chart 6*, as well as *Charts 7* and *8*, giving the values of the total moment at the midspan or at the support of the deck panel, are equally valid for the deck with open as well as closed longitudinal ribs. However, these charts can be directly used for the design of the open ribs only, by multiplication of the total moment values given in these charts by the R_0/P ratio given in *Chart 2a* or *3*. The moment per rib in the closed system, depending on the rigidity ratio H/D_v , cannot be obtained from these charts.

Although the spans of the open ribs are usually well under 10 ft, the range of *Charts 6*, *7* and *8* has been extended up to $s = 25$ ft, in the same way as the charts for closed ribs. Thus, these charts may also be used in the design of conventional bridge stringers.

Chart 7, giving the values of the total negative moment in the deck at the floor beam caused by the wheel loads shown, has been computed by equations (4.6) and (4.6a). All wheel loads are considered to be concentrated loads.

For other comments see the discussion of *Chart 6*.

Chart 8, giving the values of the negative moments at the midspan and the positive moments at the support of the ribs, is presented for the purpose of computing the alternating stresses in the ribs under moving loads.

Chart 15 gives the maximum floor beam reaction, F_0 , expressed as the ratio, F_0/P , of the reaction to the axle load of one vehicle. The floor beam is considered infinitely rigid.

Case **B** represents the standard H-S truck of the AASHO specifications. The maximum reaction, F_0 , is obtained with the closest specified axle spacing of 14 ft. The critical locations of the truck have been determined by means of the influence line, *Chart 5*. The values for the curve are computed by equations (4.11) and (4.12).

Chart 16 is presented to facilitate the computation of the maximum moment in the rigid floor beam. The maximum moment occurs under the wheel of the truck placed in an inside lane of the bridge. In computing the moment values, the trucks have been placed in such positions in the transverse direction of the bridge as to cause the maximum value of the moment under the critical wheel. The position of the trucks within the AASHO design lanes, W , and the load intensity reduction due to the multiple lane loading, in accordance with the AASHO specifications, has been taken in consideration. For bridges with 4 and more traffic lanes, a 4-ft wide center mall has been assumed.

4.2.7 Design of the Open Ribs on Rigid Supports with Consideration of the Effects of the Deck Plate Rigidity, D_P

4.2.7.1 General

The formulas for the rib reactions on the deck plate, R_0, R_1, \dots, R_m , given in Section 4.2.4.2 and *Charts 2, 3* and *4*, are based on the assumption that the wheel load distribution to the individual ribs depends only on the loading width and the rib spacing and does not depend on the rigidity of the deck plate, D_P , since both the flexural rigidity, D_P , and the deflection of the loaded rib relative to the adjoining ribs are small and may be disregarded in the usual cases. Thus, the deck plate is assumed to act as a continuous member supported on rigid

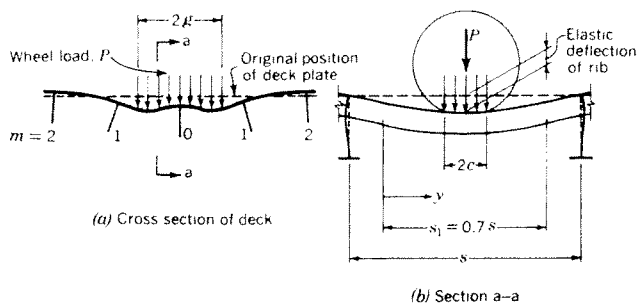


Fig. 4.6. Longitudinal ribs acting as elastic supports of the deck plate

(inflexible) ribs, and the rib reactions are computed accordingly (Fig. 2.7c).

However, with longer rib spans or a thick deck plate, the effects of the deck plate rigidity and the rib flexibility on the load distribution may have to be considered. In such cases the deck plate acts as a continuous member on elastic supports, relieving the rib directly under the load and distributing the load on the adjoining ribs, as shown in Figure 4.6, and the computation in accordance with the simplified procedure may be too conservative.

If a more accurate computation is desired, the moment relief in a rib, $\Delta' M_R$, due to the rib flexibility may be computed by the formulas given below and subtracted from the value of the moment computed for the rigid rib by the formulas given in the foregoing sections of this chapter.

4.2.7.2 Formulas for the Moment Relief, $\Delta' M_R$

The computation of the moment relief in the rib, $\Delta' M_R$, is based on considerations similar to those used in the computation of the moment relief, ΔM_F , in the flexible floor beams, as explained in Chapter 5. The formulas are similar except that the ribs are treated here as the "floor beams" of Chapter 5, and the deck plate as the "ribs," with the appropriate values of the spans and rigidities.

(a) The reduction of the positive moment, $\Delta' M_{RC}$, at the midspan of the rib, due to the elastic flexibility of the ribs under a wheel load at the midspan (Fig. 4.6b) is computed by the formula

$$\Delta' M_{RC} = Q_0' \left(\frac{s_1}{\pi} \right)^2 \frac{Q_{1y}}{Q_0'} \left(\frac{R_0}{P} - \sum_{m=0}^m \frac{R_m}{P} \bar{\vartheta}_0 \right) \quad (4.15)$$

with

$$Q_0' = \frac{P}{2c} \quad (4.15a)$$

The length s_1 is the equivalent simple span corresponding to the actual span, s , of the continuous ribs

$$s_1 = 0.7s \quad (4.16)$$

The load Q_{1y} in equation (4.15) is the loading per unit length at the location y of the first component load in the Fourier analysis of the loading in the y -direction, comparable to the value of Q_{1x} in Figure 3.13.

Corresponding to equation (3.23) the coefficient Q_{1y}/Q_0' is expressed by the formula

$$\frac{Q_{1y}}{Q_0'} = \frac{4}{\pi} \sin \frac{c}{s_1} \quad (4.17)$$

$R_0, R_1 \dots R_m$ are the rib reactions on the deck plate, computed under the assumption of rigid ribs.

The values of $\bar{\vartheta}_0$ are the influence line ordinates for the reactions of a beam on elastic supports, which may be obtained from Chart 19 as a function of the relative rigidity coefficient, γ' .

In this case, the value of γ' expresses the relative rigidity ratio of the deck plate and the ribs and is given by the formula

$$\gamma' = \frac{t_P^3}{10.92 I_R'} \frac{s_2^4}{a^3 \pi^4} \quad (4.18)$$

where

t_P = deck plate thickness

I_R' = moment of inertia of one longitudinal rib, including the effective width of plate

$s_2 = 0.81s$ = equivalent rib span computed by equation (3.12)

(b) The reduction of the negative moment, $\Delta' M_{RS}$, at the support of the ribs, due to the elastic flexibility of the ribs, may be computed by assuming, with accuracy sufficient for design purposes, that it is proportional to the moment reduction, $\Delta' M_{RC}$, at the midspan, computed by formula (4.15).

Thus, the value of $\Delta' M_{RS}$ is obtained from

$$\Delta' M_{RS} = \Delta' M_{RC} \frac{M_S}{M_C} \quad (4.19)$$

where M_S and M_C are the positive and the negative moments, respectively, obtained by the simplified procedure, as given in Sections 4.2.1 to 4.2.6.

4.2.7.3 Criteria for Determination of the Error Due to the Simplified Computation of the Moments in Ribs

In the design computations the following approximate criteria, based on an average width of wheel load of 24 in., may be used.

The moment reduction in the longitudinal rib, $\Delta' M_R$, due to the rib flexibility, will be smaller than 3% of the moment computed by the simplified procedure (Sections 4.2.2-4) if the relative rigidity coefficient, γ' , does not exceed the following values:

$$\text{with } a = 12 \text{ in.} \quad \gamma' \leq 0.006 \quad (4.20)$$

$$\text{with } a = 16 \text{ in.} \quad \gamma' \leq 0.004 \quad (4.20a)$$

4.3 DECK WITH CLOSED RIBS

4.3.1 General

4.3.1.1 Differential Equation and Its Solution

With the assumption $D_x = 0$, the admissibility of which has been discussed in Section 3.2.2, differential equation (2.10) of the orthotropic plate reduces to equation (3.1).

In the derivation of the formulas for the influence surfaces, used in the computation of the bending moments in the ribs, only the homogeneous equation of the unloaded plate is needed. The homogeneous equation corresponding to the non-homogeneous equation (3.1) is

$$D_y \frac{\partial^4 w}{\partial y^4} + 2H \frac{\partial^4 w}{\partial x^2 \partial y^2} = 0 \quad (4.21)$$

The general solution of this equation can only be given as an infinite series (see Chapter 2)

$$w = \sum_{n=1}^{\infty} w_n \quad (4.22)$$

with

$$w_n =$$

$$(C_{1n} \sinh \alpha_n y + C_{2n} \cosh \alpha_n y + C_{3n} \alpha_n y + C_{4n}) \sin \frac{n\pi x}{b} \quad (4.22a)$$

where

$$\alpha_n = \frac{n\pi}{b} \sqrt{\frac{2H}{D_y}} \quad (4.23)$$

C_{1n} , C_{2n} , C_{3n} , C_{4n} are the integration constants to be determined from the boundary conditions for each term, n , of the series.

In the following formulas the subscripts n , denoting that the constants α and C are functions of the number n , are generally omitted for convenience.

The derivatives with respect to y of the function w_n are

$$\begin{aligned} w' &= \alpha(C_1 \cosh \alpha y + C_2 \sinh \alpha y + C_3) \sin \frac{n\pi x}{b} \\ w'' &= \alpha^2(C_1 \sinh \alpha y + C_2 \cosh \alpha y) \sin \frac{n\pi x}{b} \\ w''' &= \alpha^3(C_1 \cosh \alpha y + C_2 \sinh \alpha y) \sin \frac{n\pi x}{b} \\ w'''' &= \alpha^4(C_1 \sinh \alpha y + C_2 \cosh \alpha y) \sin \frac{n\pi x}{b} \end{aligned} \quad (4.24)$$

4.3.1.2 Sinusoidal Affinity between the Loads and the Deformations, Shears and Moments

In the analysis of the deck the actual applied load is represented by a series of sinusoidal component loads $Q_{nx} = Q_n \sin(n\pi x/b)$, extending over the width, b , of the deck, as explained in Section 3.5.

It is the property of a *sinusoidal loading* (force or moment) applied across the width, b , of a plate simply supported along the edges $x = 0$ and $x = b$, that the *deflections*, *rotations*, *shears* and *bending moments* in the y -direction caused by it at any location, y , in any panel of the plate, are also *sinusoidal* and have the same frequency in the x -direction as the applied loading (Fig. 4.8b). This becomes apparent by observing that the expressions for w and its derivatives with respect to y , determining the values of the rotations, moments and shears in the y -direction, contain the function $\sin(n\pi x/b)$.

The sinusoidal affinity between the loading and the deformations is an important factor in the determination of the influence surfaces (Section 4.3.2).

4.3.1.3 Carry-over Factor

The carry-over factor, κ , needed in the analysis of a continuous orthotropic plate, is obtained from the three-moment equation, by considerations essentially similar to those used in determination of the carry-over factor of a continuous beam (Section 4.2.1.3).

In order to find the expression for the carry-over factor, κ , a simply supported plate panel 0-1 is considered (Fig. 4.7a).

At the right edge of the panel a sinusoidal bending moment, $M_1 = \bar{M}_1 \sin(n\pi x/b)$, is applied, which is distributed along the entire length, b , of the support and has the maximum value, \bar{M}_1 , at the location $x = b/2n$.

The rotations at supports $m = 0$ and $m = 1$ due to moment M_1 are computed from equations (4.24), with integration constants obtained from the boundary conditions

$$\begin{aligned} y = 0 & \quad w = 0 & \quad M_y = 0 \\ y = s & \quad w = 0 & \quad M_y = M_1 \end{aligned}$$

with the result:

$$C_1 = -\frac{\bar{M}_1}{D_y} \frac{1}{\alpha^2 \sinh \alpha s} \quad C_3 = \frac{\bar{M}_1}{D_y} \frac{1}{\alpha^3 s}$$

$$C_2 = C_4 = 0$$

with the value of α defined by equation (4.23).

With the above values of constants, the expressions for the rotations due to the moment M_1 at support $m = 1$ are:

$$w'_0 = -\frac{M_1}{D_y} \frac{1}{\alpha} \left(\frac{1}{\sinh \alpha s} - \frac{1}{\alpha s} \right)$$

$$w'_1 = -\frac{M_1}{D_y} \frac{1}{\alpha} \left(\coth \alpha s - \frac{1}{\alpha s} \right)$$

If bending moments are applied at both supports of the plate, $m = 0$ and $m = 1$ (Fig. 4.7b), the values of the rotations at each support are obtained as functions of both applied moments, M_0 and M_1 , by superposition of the above expressions.

The rotations at support $m = 1$ of the two adjoining panels of the plate may be expressed as a function of the moments M_0 and M_1 in panel 0-1, and a function of the moments M_1 and M_2 in panel 1-2. From the condition of equality of the rotations w'_{1L} and w'_{1R} in a continuous plate, the three-moment equation of an unloaded continuous plate is obtained as

$$M_0 + 2kM_1 + M_2 = 0 \quad (4.25)$$

where

$$k = \frac{\alpha s \coth \alpha s - 1}{\alpha^*} \quad (4.26)$$

$$\alpha^* = 1 - \frac{\alpha s}{\sinh \alpha s} \quad (4.27)$$

If a sinusoidal moment, $M_{0n} = \bar{M}_{0n} \sin(n\pi x/b)$, is introduced at the support $m = 0$, the moments at the more distant supports, $m = 1, 2, 3 \dots$ decrease by a carry-over factor, κ , similarly as in the case of a continuous beam (Fig. 4.1).

$$M_{1n} = \kappa_n M_{0n} \quad (4.28)$$

$$M_{2n} = \kappa_n M_{1n} = \kappa_n^2 M_{0n}$$

etc.

By substituting equations (4.28) into (4.25), the carry-over factor is obtained as

$$\kappa_n = -k + \sqrt{k^2 - 1} \quad (4.29)$$

It is seen that the carry-over factor, κ_n , has a different value for each term, n , of the solution of the plate equation (4.21). Generally, the value of κ decreases rapidly with increasing n . Thus the effect of the higher

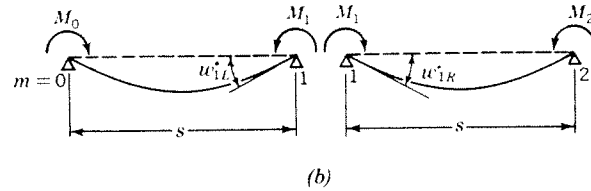
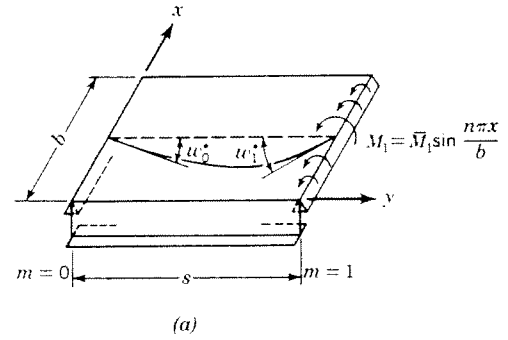


Fig. 4.7

component loads on the bending moments in the distant panels (see Sections 4.3.3 and 4.3.4) is not very significant.

4.3.2 General Expressions for the Bending Moments

4.3.2.1 Bending Moments M_y in a Continuous Plate Due to Sinusoidal Loading

The method of deriving the general expressions for the influence surfaces for the bending moments of a continuous orthotropic plate is essentially similar to that used in the derivation of the influence lines of a continuous beam (Section 4.2.1.3).

The basic system used in the derivation is shown in Figure 4.8.

First, the expression is obtained for the bending moment, M_y , at any cross section, $y = \text{constant}$, of the plate, due to a sinusoidal line load extending over the entire width, b , of the plate, located at any position, y .

At the cross section where the bending moment is sought, designated as line 1-1, a hinge is assumed, transmitting shear but no moment.

A sinusoidal unit moment, $1[\sin(n\pi x/b)]$, is applied at the hinge 1-1, (Fig. 4.8a) and a sinusoidal unit line load, $1[\sin(n\pi x/b)]$ is placed at any location, y , designated as line 2-2 (Fig. 4.8b). Both loadings cause deflections and rotations that change sinusoidally across the width, b , of the plate, as pointed out in Section 4.3.1.2. In Figure 4.8 the sinusoidal loads and deformations are illustrated for $n = 1$; the loads and deformations for higher values of n may be easily visualized.

The following deformations are needed:

$\vartheta_{11n} \sin(n\pi x/b)$ = rotation at 1-1, with the maximum value of ϑ_{11n} at the location $x = b/2n$, due to the sinusoidal unit moment at 1-1.

$\delta_{21n} \sin(n\pi x/b)$ = rotation at 1-1 due to the sinusoidal unit line load at 2-2.

$\delta_{21n} \sin(n\pi x/b)$ = deflection at 2-2 due to the sinusoidal unit moment at 1-1.

It can be shown that

$$\delta_{21n} = \vartheta_{12n} \quad (4.30)$$

Any sinusoidal load, $Q = Q_n \sin(n\pi x/b)$, applied at 2-2 causes a sinusoidal rotation at the hinge 1-1 equal to $Q_n \vartheta_{12n} \sin(n\pi x/b)$. In order to eliminate this rotation, to satisfy the condition of continuity of the actual plate at 1-1, a moment $M_n = \bar{M}_n \sin(n\pi x/b)$ must be introduced at 1-1 of such a magnitude as is necessary to cause at 1-1 a rotation equal and opposite to that caused by the load, Q .

Thus, the moment at 1-1 is obtained from the condition

$$\bar{M}_n \vartheta_{11n} \sin \frac{n\pi x}{b} = - Q_n \vartheta_{12n} \sin \frac{n\pi x}{b} \quad (4.31)$$

By substituting $\delta_{21n} = \vartheta_{12n}$ (equation 4.30), and $\bar{M}_n \sin(n\pi x/b) = M_n$, the following expression is obtained:

$$M_n = - Q_n \frac{\delta_{21n}}{\vartheta_{11n}} \sin \frac{n\pi x}{b} \quad (4.32)$$

In order to find the geometric interpretation of the ratio $\delta_{21n}/\vartheta_{11n}$ in equation (4.32) a sinusoidal unit rotation, $1[\sin(n\pi x/b)]$, is applied at 1-1 (Fig. 4.8c).

Referring to Figure 4.8a, it is seen that the unit rotation at 1-1 can be expressed as a function of the bending moment $M_1 \sin(n\pi x/b)$, required to sustain it,

$$1 \left(\sin \frac{n\pi x}{b} \right) = M_1 \vartheta_{11n} \sin \frac{n\pi x}{b}$$

Thus, the deflection at 2-2 may be given as

$$\Delta_{21n} \sin \frac{n\pi x}{b} = M_1 \delta_{21n} \sin \frac{n\pi x}{b} = \frac{\delta_{21n}}{\vartheta_{11n}} \sin \frac{n\pi x}{b}$$

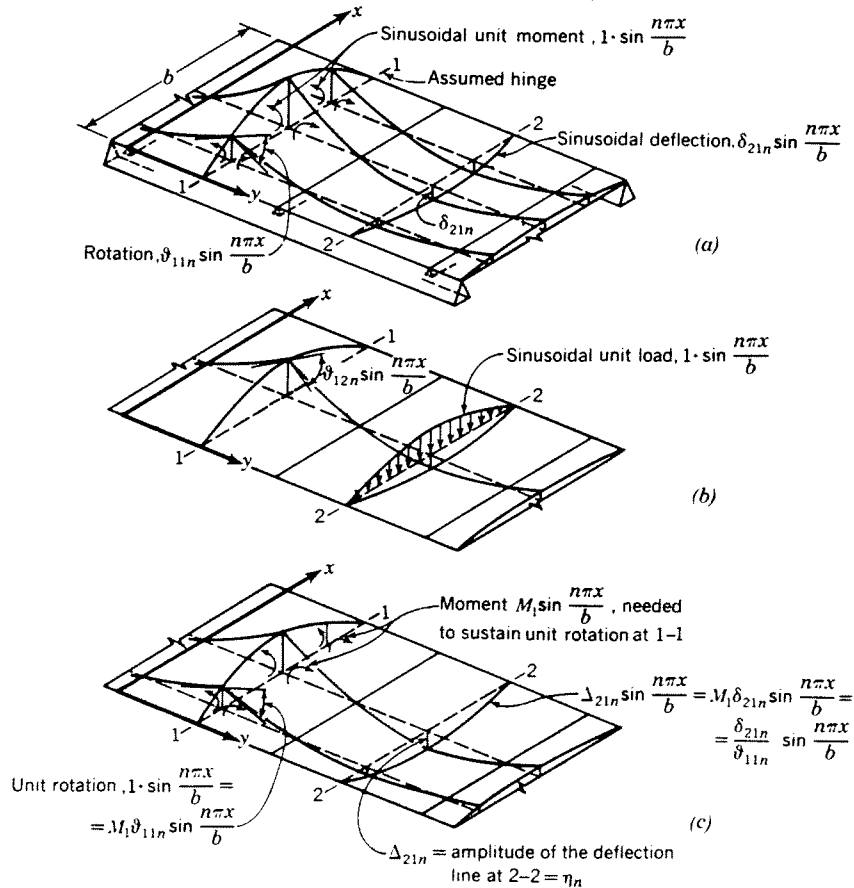


Fig. 4.8.

It is seen that the ratio $\delta_{21n}/\vartheta_{11n}$ represents the maximum ordinate (the amplitude), Δ_{21n} , of the deflection of the plate at Section 2-2 caused by a sinusoidal unit rotation 1 $[\sin(n\pi x/b)]$ at Section 1-1.

With the value of $-\Delta_{21n}$ designated as the influence ordinate, η_n

$$-\frac{\delta_{21n}}{\vartheta_{11n}} = -\Delta_{21n} = \eta_n \quad (4.33)$$

equation (4.32) may be expressed

$$M_n = Q_n \sin \frac{n\pi x}{b} \eta_n \quad (4.34)$$

Thus it is shown that the bending moment in the y -direction at any point, x , of a chosen line, $y = \text{constant}$, of a continuous plate due to a sinusoidal load in any position, y , is given by the magnitude of the load at the same value of x multiplied by the influence ordinate, η_n , which is a function of the position of the load, y , only, and is not a function of x . Therefore the expression for η_n may be called the influence line for the moment in the plate. Thus, the determination of the bending moments in the plate reduces to a one-dimensional problem.

4.3.2.2 Bending Moments in the Deck Due to Actual Loads

The actual deck loading, which is not sinusoidal, is expressed through the Fourier analysis as a summation of sinusoidal component loads, as discussed in Chapter 3,

$$Q_x = \sum Q_n \sin \frac{n\pi x}{b} \quad (3.20)$$

The total bending moment in the deck is then expressed as the sum of the moments, equation (4.34), due to the individual component loads,

$$M = \sum_{n=1}^{\infty} Q_n \sin \frac{n\pi x}{b} \eta_n \quad (4.34a)$$

or, using the designation

$$Q_n \sin \frac{n\pi x}{b} = Q_{nx}$$

and introducing the dimensionless ratios Q_{nx}/Q_0 and η_n/s ,

$$M = Q_0 s \sum_{n=1}^{\infty} \frac{Q_{nx}}{Q_0} \frac{\eta_n}{s} \quad (4.35)$$

Equation (4.35) gives the value of the bending moment M_y per unit width of the plate at any location, x .

The coefficient Q_{nx}/Q_0 , defined by the formulas given in Section 3.5.3, denotes the loading at the location, x , at which the moment is computed.

The bending moment acting on one rib of the actual steel plate deck is usually obtained by multiplication of the moment per unit width, computed by equation (4.35) at the location x , corresponding to the center of the rib, by the width of the rib, $a + e$, (Fig. 2.8)

$$M_R = M(a + e) \quad (4.35a)$$

A more accurate value may be obtained by integration of the moment distribution curve, M_y , over the width of the rib. The general expression for the moment in one rib then becomes

$$M_R = Q_0 s \sum_{n=1}^{\infty} \frac{\eta_n}{s} \int_{x=f-\frac{a+e}{2}}^{x=f+\frac{a+e}{2}} \frac{Q_{nx}}{Q_0} dx \quad (4.36)$$

where f designates the location of the center line of the rib where the moment is sought.

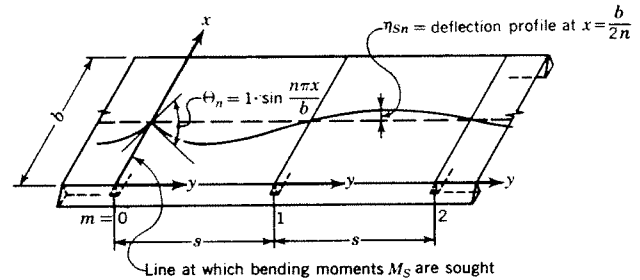


Fig. 4.9

If the loading consists of a single wheel placed at $x = b/2$ (Fig. 3.14) and the moment is sought in the rib located directly under the load, $f = b/2$, the coefficient Q_{nx}/Q_0 is expressed by equation (3.22). Then equation (4.36) becomes

$$M_R = Q_0 s \sum_{n=1}^{\infty} \frac{\eta_n}{s} \frac{8b}{(n\pi)^2} \sin \frac{n\pi g}{b} \sin \frac{n\pi(a+e)}{2b} \quad (4.36a)$$

The moment obtained by equation (4.36) is generally smaller than that computed by equation (4.35a), as discussed in Section 2.4.1.3. However, it should be noted that the actual stresses in the bottoms of the ribs may be somewhat higher than those corresponding to the moments computed by equation (4.36), due to the effect of the System III stresses in the rib walls (see Chapter 6).

For design purposes the values of bending moments in the deck are needed at the supports (moments M_S , Fig. 4.9) and at the midspan between the supports (moments M_C , Fig. 4.10).

The expressions for the corresponding influence lines, η_{Sn} and η_{Cn} , are given in the following sections.

4.3.3 Bending Moment at the Support, M_s

The influence line, η_{sn} , for the moment at the support $m = 0$ is obtained as the profile at the location $x = b/2n$ of the deflection surface caused by a unit rotation $1 [\sin(n\pi x/b)]$ at the support $m = 0$ (Fig. 4.9), as explained in Section 4.3.2.1.

The moment at support 0, $M_{0n} = \bar{M}_{0n} \sin(n\pi x/b)$, necessary to produce the unit rotation, is found to be

$$M_{0n} = \bar{M}_{0n} \sin \frac{n\pi x}{b} = \frac{\kappa}{(1 - \kappa^2)} \frac{D_y \alpha^2 s}{\alpha^*} \sin \frac{n\pi x}{b}$$

and the corresponding moment at support 1 is

$$M_{1n} = \kappa M_{0n}$$

With these moments applied at the edges of the plate panel 0-1, the four boundary conditions are obtained

$$\begin{aligned} y = 0 & \quad w = 0 & \quad M = M_{0n} \\ y = s & \quad w = 0 & \quad M = M_{1n} \end{aligned}$$

from which the four integration constants in equation (4.37) of the deflection line, η_{sn} , are computed.

The equation for η_{sn} , in any panel of the plate, is the same as equation (4.22a), except for the term $\sin(n\pi x/b)$.

For convenience, designations of constants in equation (4.22a) are changed from C to C' , resulting in

$$\eta_{sn} = C_1' \sinh \alpha y + C_2' \cosh \alpha y + C_3' \alpha y + C_4' \quad (4.37)$$

By introducing the dimensionless influence ordinate, η_{sn}/s , and expressing the constants in terms more convenient for numerical computations, equation (4.37) may be given as

$$\frac{\eta_{sn}}{s} = \frac{M_0^*}{s} \kappa^m \left(C_1 \sinh \alpha y + C_2 \cosh \alpha y + C_3 \frac{y}{s} + C_4 \right) \quad (4.38)$$

where

$$\begin{aligned} C_1 &= \frac{-\kappa + \cosh \alpha s}{\sinh \alpha s} & C_2 &= -1 \\ C_3 &= \kappa - 1 & C_4 &= +1 \end{aligned} \quad (4.39)$$

$$\frac{M_0^*}{s} = \frac{1}{\alpha^*} \frac{\kappa}{(1 - \kappa^2)} \quad (4.40)$$

The parameters α , α^* and κ are defined by equations (4.23), (4.27) and (4.29), respectively. They are functions of n , and have to be determined separately for each value of n used in the computations. It should be noted that for a symmetrical loading only the odd values of n ($n = 1, 3, 5, \dots$) are needed (see Section 3.5.1).

The ordinate y , determining the position of the load, is always measured from the support with the lower number (Fig. 4.9). The parameter m denotes

the smaller of the two support numbers enclosing the plate panel under consideration.

In computation of the moment at the support the effect of the wheel load distribution in the longitudinal direction (dimension $2c$, Fig. 3.10) is negligible, and the individual wheel loads are treated as line loads in the x -direction, represented by the sinusoidal component loads, Q_{nx} , as discussed in Chapter 3.

The bending moment M_s per unit width of the plate, at the support, at the location x , is computed by formula (4.35), by substituting $\eta_n = \eta_{sn}$, from equation (4.38).

Computation shortcuts applicable in the numerical determination of the moment M_s are given in Sections 4.3.5.2 and 4.3.5.3a.

4.3.4 Bending Moment at the Midspan, M_c

4.3.4.1 Influence Line

The influence line, η_{cn} , for the moment at the midspan of the panel 0-0 is obtained as a profile at the location $x = b/2n$ of the deflection surface caused by a unit rotation, $1 [\sin(n\pi x/b)]$, applied at the midspan of the panel 0-0 (Fig. 4.10).

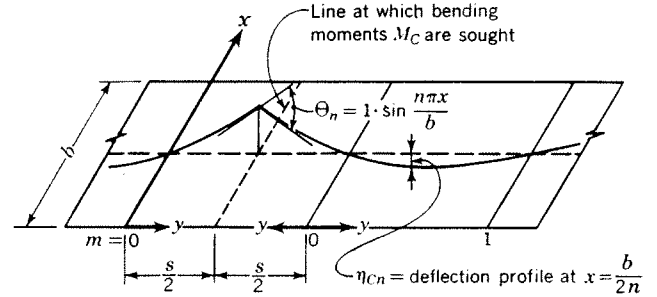


Fig. 4.10

The moment at the support 0, $M_{0n} = \bar{M}_{0n} \sin(n\pi x/b)$, corresponding to the unit rotation of the plate at $y = s/2$, is found to be

$$M_{0n} = \bar{M}_{0n} \sin \frac{n\pi x}{b} = \frac{\kappa}{2a_1 (1 - \kappa) \cosh(\alpha s/2)} \sin \frac{n\pi x}{b}$$

with

$$a_1 = \frac{\alpha^*}{D_y \alpha^2 s}$$

The boundary conditions at the edges $y = 0$ and $y = s/2$ of the half-panel considered are:

$$\begin{aligned} y = 0 & \quad w = 0 & \quad M = M_{0n} \\ y = s/2 & \quad w' = \frac{1}{2} \sin(n\pi x/b) & \quad V^* = 0 \end{aligned}$$

The magnitude V^* is the substitute shear, representing the combined shear and the twisting moment, which

have to be equal to zero at $y = s/2$ (Kirchhoff's boundary condition).

From the above boundary conditions the four integration constants in the expression for the deflection line, η_{cn} , in the panel 0-0, are computed.

The general form of the expression for η_{cn} is the same as for η_{sn} , equation (4.37).

The formulas used in the design computations and the values of constants for the two basic cases, (a) load in panel 0-0 and (b) load in other panels, are given below.

(a) *Load in panel 0-0*

For the load in panel 0-0 (Fig. 4.4a) the dimensionless influence ordinate η_{cn}/s may be represented in a form convenient for numerical computations as

$$\frac{\eta_{cn}}{s} = \frac{\sinh \alpha y}{2\alpha s \cosh(\alpha s/2)} + \frac{M_0^*}{s} (C_1 \sinh \alpha y + C_2 \cosh \alpha y + C_3 \alpha y + C_4) \quad (4.41)$$

with $y < \frac{s}{2}$

where

$$C_1 = \tanh(\alpha s/2) \quad C_2 = -1 \quad (4.42)$$

$$C_3 = 0 \quad C_4 = +1$$

$$\frac{M_0^*}{s} = \frac{\kappa}{\alpha^*(1 - \kappa)} \frac{1}{2 \cosh(\alpha s/2)} \quad (4.43)$$

The parameters α , α^* and κ are defined by equations (4.23), (4.27) and (4.29), respectively, as in Section 4.3.3.

(b) *Load in other panels*

The formula for the influence ordinate η_{cn}/s in panels 0-1, 1-2, etc. (Fig. 4.4b) is given by equation (4.38), the same as for the influence ordinate of the moment at the support, η_{sn}/s , with the values of the constants defined by equations (4.39), except for the value of the moment M_0^* , which, for η_{cn}/s , is given by equation (4.43).

The bending moment M_c , at the midspan of the plate at any location x , is computed by formula (4.35), by substituting $\eta_n = \eta_{cn}$, from equation (4.41), in conjunction with equations (4.42) and (4.43), or (4.39) and (4.43).

4.3.4.2 Bending Moment Due to a Distributed Load

The bending moment M_c , at any location x at the midspan of the plate, due to a distributed load

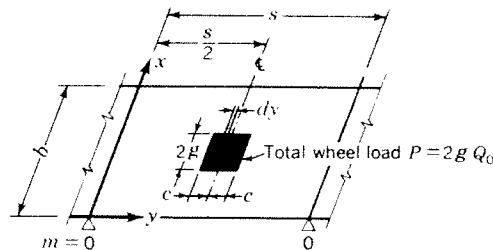


Fig. 4.11

placed at the midspan (Fig. 4.11), is obtained by integration of the influence line η_{cn} , equation (4.41), over the length of the loading, $2c$.

The load per unit width of the deck on the elementary strip, dy , at any point y under the distributed load, P , is $dQ = (Q_0/2c)dy$, or, expressed by sinusoidal component loads

$$dQ = \frac{Q_0 dy}{2c} \sum \frac{Q_{nx}}{Q_0} \quad (4.44)$$

The moment, dM_c , due to the elementary load, dQ , is, by equation (4.35)

$$dM_c = \frac{Q_0 s}{2c} \sum \frac{Q_{nx}}{Q_0} \frac{\eta_{cn}}{s} dy \quad (4.45)$$

By integrating over the length $2c$, the expression for the moment is obtained as

$$\begin{aligned} M_c &= 2 \int_{y=(s/2)-c}^{y=s/2} dM_c \\ &= \frac{Q_0 s}{c} \sum \frac{Q_{nx}}{Q_0} \int_{y=(s/2)-c}^{y=s/2} \frac{\eta_{cn}}{s} dy \\ &= Q_0 s \sum \frac{Q_{nx}}{Q_0} \frac{M_{cn}}{Q s} \end{aligned} \quad (4.46)$$

where M_{cn}/Qs represents the dimensionless component moment, expressed as

$$\begin{aligned} \frac{M_{cn}}{Qs} &= \frac{1}{2\alpha s \alpha c} \left[1 - \frac{\cosh \left[\alpha \left(\frac{s}{2} - c \right) \right]}{\cosh(\alpha s/2)} \right] + \\ &\quad \frac{M_0^*}{s} \left[1 - \frac{\sinh \alpha c}{\alpha c \cosh(\alpha s/2)} \right] \end{aligned} \quad (4.47)$$

with the value of M_0^*/s defined by equation (4.43).

4.3.5 Shortcut Formulas for Numerical Computations

4.3.5.1 General

In the numerical determination of the bending moments by formulas given in Sections 4.3.1 through

4.3.4, the accuracy to four decimal places will be generally required in the intermediate steps of the computations.

The various constants and parameters occurring in the formulas generally involve hyperbolic sines and cosines of the arguments $\alpha_n s$, $\alpha_n y$, $\alpha_n s/2$, etc. The numerical values of these functions increase very rapidly with the increasing values of the arguments. For example, the value of $\sinh x$ for $x = 7.5$ is 904.02... , and for $x = 50$ its value reaches the order of 5×10^{21} .

If hyperbolic functions occur in the denominator, the expressions in which they occur become equal to zero, within the computation accuracy, for sufficiently large arguments. Thus some formulas may simplify considerably.

If large values of two hyperbolic functions have to be subtracted (as, for example, in formula (4.38)), a direct computation might become quite difficult and might lead to a considerable error, since the values of hyperbolic functions for larger arguments are given in the tables in intervals too large for a sufficiently accurate interpolation. In such cases the numerical computations are simplified and much more accurate results are obtained by application of the shortcut formulas given below.

The term of the series, n , at which the simplified formulas are applicable, depends on the formulas and the values of the parameters s , b , y and H/D_y and on the desired accuracy of the computation, to be determined by the designer.

The simplified formulas listed below are accurate to 4 or 5 significant figures for the arguments equal to or larger than the values given with the formulas.

4.3.5.2 Constants

α^* , equation (4.27):

$$\alpha^* = 1.0000 \quad \text{for } \alpha s \geq 13.3 \quad (4.48)$$

k , equation (4.26):

$$k = \frac{\alpha s - 1}{\alpha^*} \quad \text{for } \alpha s \geq 5.3 \quad (4.49)$$

$$k = \alpha s - 1 \quad \text{for } \alpha s \geq 13.3 \quad (4.49a)$$

κ , equation (4.29):

$$\kappa = -\frac{1}{2k} \quad \text{for } \alpha s \geq 16.8 \quad (4.50)$$

4.3.5.3 Moment Formulas

(a) *Moment at support*

In equation (4.38) the following simplification may be substituted:

$$C_1 \sinh \alpha y + C_2 \cosh \alpha y = -e^{-\alpha y} - e^{-\alpha(s-y)}(\kappa - e^{-\alpha s}) \quad \text{for } \alpha y \geq 4 \quad (4.51)$$

Equation (4.40) simplifies to

$$\frac{M_0^*}{s} = \kappa \quad \text{for } \alpha s \geq 17 \quad (4.52)$$

(b) *Moment at midspan, concentrated load in panel 0-0*

In equation (4.41) the following expressions may be used

$$\frac{\sinh \alpha y}{2\alpha s \cosh(\alpha s/2)} = \frac{e^{-\alpha[(s/2)-y]}}{2\alpha s} \quad \text{for } \alpha[(s/2) + y] \geq 12 \quad (4.53)$$

$$C_1 \sinh \alpha y + C_2 \cosh \alpha y = -e^{-\alpha y} - e^{-\alpha(s-y)} \quad \text{for } \alpha s \geq 10 \quad (4.54)$$

Equation (4.43) simplifies to

$$\frac{M_0^*}{s} = 0 \quad \text{for } \alpha s \geq 17.4 \quad (4.55)$$

(c) *Moment at midspan, concentrated load in other panels*

The following simplifications apply in this case:

In equation (4.38) the expression given by equation (4.51) may be substituted.

Equation (4.43) simplifies to equation (4.55).

(d) *Moment at midspan due to a distributed load*

Equation (4.47) simplifies as follows:

$$\frac{1}{2\alpha s \alpha c} \left[1 - \frac{\cosh \left[\alpha \left(\frac{s}{2} - c \right) \right]}{\cosh(\alpha s/2)} \right] = \frac{1}{2\alpha s \alpha c} (1 - e^{-\alpha c})$$

for $\alpha s \geq 13$ and $c/s \leq 0.2$
or for $\alpha s \geq 20$ and $c/s \leq 0.5$ (4.56)

$$\frac{M_0^*}{s} \left[1 - \frac{\sinh \alpha c}{\alpha c \cosh(\alpha s/2)} \right] = 0 \quad \text{for } \alpha s \geq 17.4 \quad (4.57)$$

4.3.6 Charts for the Design of the Decks with Closed Ribs on Rigid Supports for AASHTO Loads

4.3.6.1 Range of Charts

The bending moments in the closed ribs, given in Charts 9 to 14 (Appendix I), are represented as functions of two parameters: the span, s , of the ribs, and the rigidity ratio, H/D_y , of the deck system.

The spans of the closed ribs of the existing steel plate deck highway bridges do not exceed 8 ft. However, comparative cost studies have shown that longer rib

spans would be more economical in American practice. A design example with $s = 15$ ft is given in Chapter 11.

Without attempting to establish the upper economic span limit, the charts have been arbitrarily extended to a span $s = 25$ ft.

The rigidity ratio, H/D_v , of the decks without additional stiffening diaphragms between the floor beams may range between very small values up to about 0.15 in exceptional cases, with the usual values being of the order of 0.04 to 0.08. The curves have been extended up to the value of $H/D_v = 0.6$, with the purpose of demonstrating the possible effect of a large torsional rigidity of the deck (such as might be achieved by adding transverse stiffening members connecting the ribs between the floor beams) on the load distribution in the deck. It is seen that if the rigidity ratio H/D_v is increased beyond the value of 0.2, the corresponding decrease of the bending moments is not very significant.

4.3.6.2 Loading

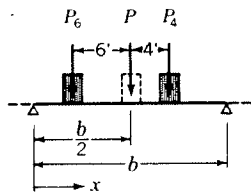
Charts 9 to 14 are computed for the wheel loads of the H20-S16-44 truck, in accordance with the AASHO, Standard Specifications for Highway Bridges, 1961 Section 1.2.5(C), using wheel load dimensions of 22 in. \times 12 in. for the 8 kip and 12 kip wheels, and 26 in. \times 12 in. for the 16 kip wheel, as discussed in Section 3.4.2 of this manual. The values of the moments include the effect of the 30% impact factor.

The loading type designations are the same as used in Charts 6, 7 and 8 for the total maximum moments in the ribs.

The bending moments given in Charts 9 to 14 are the moments M_v per unit width of the orthotropic plate at the location $x = b/2$ (Fig. 4.12), due to one wheel load at $x = b/2$, or several wheel loads at $x = b/2$, arranged in the longitudinal direction of the bridge as shown on the charts. The effect of the second wheel, or wheels,

TABLE 4.3.6.2

MOMENT INCREASE AT $x = b/2$ DUE TO ADDITIONAL WHEELS, IN TERMS OF EFFECT OF ONE WHEEL AT $x = b/2$



Upper values—effect of wheel P_6 , located at a transverse distance of 6 ft from the wheel at $x = b/2$.
 Lower values—effect of wheel P_4 , located at a transverse distance of 4 ft from the wheel at $x = b/2$.
 s = rib span.
 H/D_v = rigidity ratio of the deck.

H/D_v	Increase of Bending Moment at Midspan (Percent)					Increase of Bending Moment at Support (Percent)				
	$s = 5'$	$s = 10'$	$s = 15'$	$s = 20'$	$s = 25'$	$s = 5'$	$s = 10'$	$s = 15'$	$s = 20'$	$s = 25'$
0	—	—	—	—	—	—	—	—	—	—
0.01	—	—	—	—	1	—	—	—	—	—
0.02	—	—	1	3	4	—	—	—	1	1
0.04	—	1	3	5	8	—	—	1	2	4
0.06	—	2	4	7	11	—	1	2	4	7
0.08	—	3	6	10	14	—	1	4	7	9
0.10	1	4	8	12	16	—	2	5	8	11
0.20	2	8	14	19	23	—	4	9	13	16
0.30	3	11	18	23	28	1	6	13	17	20
0.60	2 6	8 17	14 25	20 31	24 36	1 2	4 11	10 21	14 25	17 28

of the same vehicle, located at a transverse distance of 6 ft from the wheel at the location $x = b/2$, or the effect of the wheels of the adjoining vehicle, which may be placed at a distance of 4 ft, is not included.

The reason for using one wheel only lies in the fact that this loading is sufficient for the design in most practical cases.

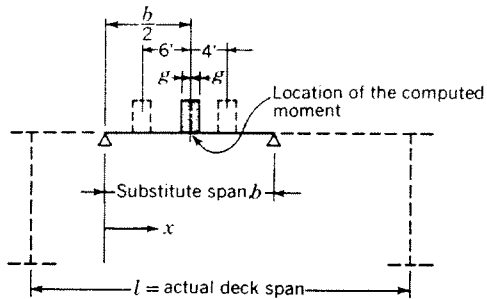


Fig. 4.12

The effect of the wheel 6 ft away on the magnitude of the moment is generally small in the usual range of spans and rigidity ratios.

The effect of the wheel of the adjoining vehicle 4 ft away is greater. However, it should be noted that position of the wheels exactly opposite each other does not necessarily correspond to the position causing the maximum increase of the moment due to the floor beam flexibility (see Chapter 5).

For the cases requiring consideration of the adjoining wheels, approximate values of the bending moment increments due to additional wheels 4 ft and 6 ft away are given in Table 4.3.6.2.

It is seen, by inspection of Table 4.3.6.2, that the effect of the additional wheels is considerable only for rib spans and rigidity ratios beyond the usual conditions.

It should also be noted that the formulas for the bending moments based on the simplifying assumption $D_x = 0$ (see Section 3.2.2.2) result in bending moments larger than the actual moments if the spans are large. Therefore, the larger effect of the additional wheel loads in the case of long rib spans may be considered to be partly compensated by the conservative values of the moments obtained from the formulas, or the charts based on them.

4.3.6.3 Computation of the Charts

Charts 9 to 14 for the design of closed ribs are based on the equations given in Sections 4.3.1–5 of this Chapter.

The values needed for plotting the charts have been computed with an accuracy better than 0.5% by means of the IBM 704 electronic computer. The substitute span, b (Fig. 4.12), used in the computations, has been determined to provide the desired accuracy of the results, as discussed in Chapter 10, with the ratio $(b - 2g)/s$ ranging between 1.0 and 1.8. The number n_{\max} , denoting the last term of the series, varied between 45 and 79, depending on the parameters used.

CHAPTER 5

Effects of Floor Beam Flexibility

5.1 INTRODUCTION

The computation of the bending moments in a steel plate deck given in Chapter 4 is based on the assumption of rigid (unyielding) floor beams (Step 1 of the computation).

In the actual system, a load placed on the deck will deflect the adjoining floor beams (Fig. 3.1), and the floor beam deflections will cause a redistribution of the bending moments and stresses.

The determination of the effects of the elastic flexibility of the floor beams (Step 2 of the computation) is presented in this chapter.

Generally, the deflection of a directly loaded floor beam will cause a distribution of the load to the floor beams over which there is no load, and a relief of the floor beam located directly under the load.

The deflection of the floor beams will also affect the ribs, increasing the positive bending moment under the load at the midspan of the ribs, and decreasing the negative bending moment at the supports of the ribs at the floor beams. The effect of the floor beam flexibility on the bending moments in the ribs will be greatest at the center line of the bridge deck midway between the main girders (Section A-A, Fig. 1.31), and will be negligible near the main girders, where the floor beam deflections are small (Section B-B, Fig. 1.31).

The computation of the effects of floor beam flexibility is based on the theory of a continuous beam on elastic supports, adapted to a plate supported along the edges $x = 0$ and $x = l$ and continuous over uniformly spaced floor beams treated as elastic supports (Fig. 3.1).

Influence lines of a continuous beam on elastic supports are discussed in Section 5.2.

Application of the influence lines of a beam on elastic supports to the problem of a plate continuous over simply supported floor beams of uniform rigidity, and the formulas for the bending moments in the ribs and in the floor beams, caused by floor beam deflections, are given in Section 5.3.

Procedures for computation of the effects of floor beam flexibility with floor beams of non-uniform

rigidity, or floor beams continuous over more than two main girders are discussed in Sections 5.4 and 5.5.

5.2 BENDING MOMENTS AND REACTIONS OF A CONTINUOUS BEAM ON ELASTIC SUPPORTS

The characteristic property of a continuous beam on elastic supports is that the reaction of the beam, \bar{F}_m , at any support, m , is proportional to the vertical movement, δ_m , of the support,

$$\bar{F}_m = \delta_m k_m \quad (5.1)$$

where k_m (in kips/inch) is the elastic spring constant of the support m , expressing the resistance of the support to the vertical movement.

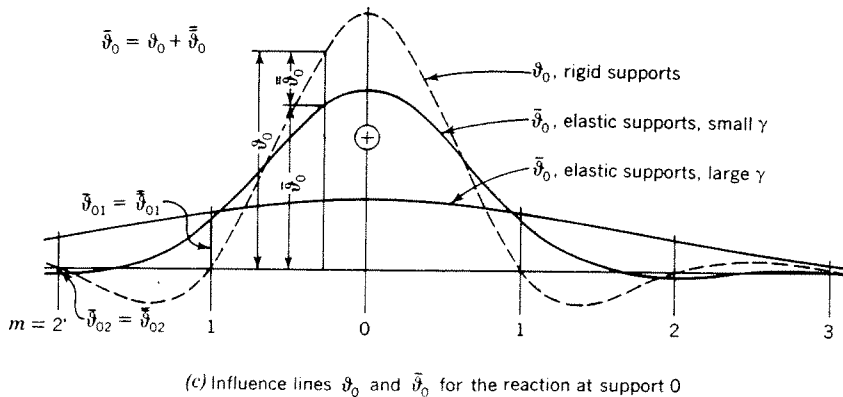
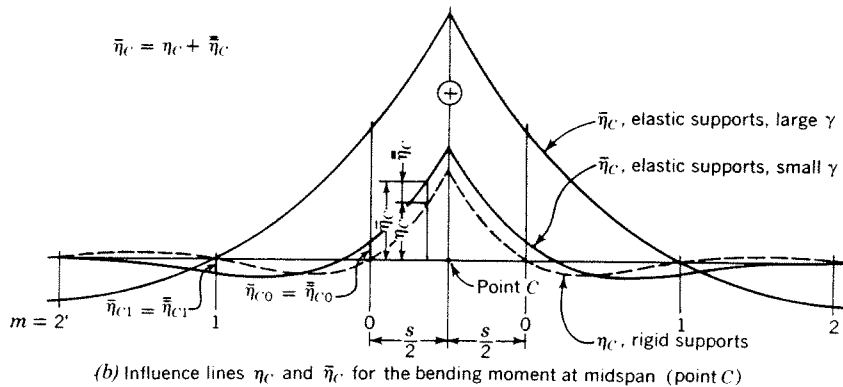
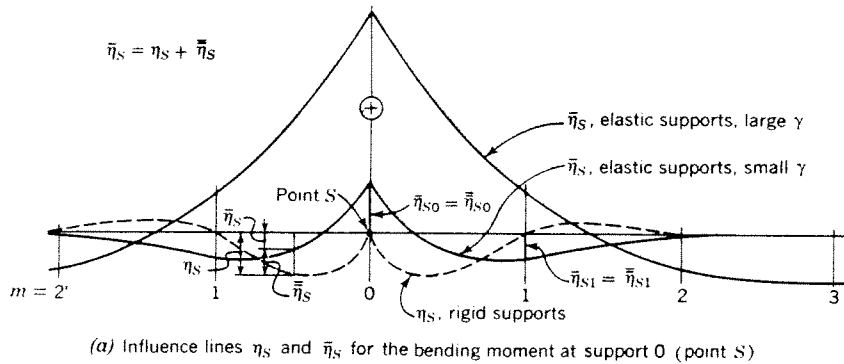
The bending moments and reactions of a loaded continuous beam on elastic supports depend on the dimensionless parameter γ , representing the ratio of the stiffness of the beam to the rigidity of the supports.

Influence lines for bending moments and reactions of a continuous beam on elastic supports are defined, similarly as in the case of a continuous beam on rigid supports (Section 4.2.1.3), as deflection lines due to a unit rotation (or deflection) at the point where the bending moment (or reaction) is sought.

Typical influence lines, $\bar{\eta}$ and $\bar{\vartheta}$, of a continuous beam on elastic supports, with equal span lengths, uniform beam rigidity and uniform elastic constant at all supports, are compared with similar influence lines, η and ϑ , of a beam on rigid supports in Figure 5.1.

The influence ordinates of a continuous beam on elastic supports may be computed by means of the *five-moment equation*, which may be found in [39, 42, 51] and other references.

In the computation of the effects of floor beam flexibility the ordinates of the influence lines $\bar{\eta}_s$, $\bar{\eta}_c$ and $\bar{\vartheta}_0$, for the bending moments at support and at midspan and for the reaction at support, respectively (Fig. 5.1), are needed only at the supports. These ordinates, computed for the various values of the relative rigidity coefficient, γ , are given graphically in Charts 17, 18 and 19.



5.3 APPLICATION OF THE FORMULAS FOR A BEAM ON ELASTIC SUPPORTS TO THE ANALYSIS OF STEEL PLATE DECKS CONTINUOUS OVER FLOOR BEAMS OF UNIFORM RIGIDITY

5.3.1 Basic Concepts

The effects of floor beam flexibility on the bending moments in the deck extend over the entire width of the deck, l . Thus, even the ribs not directly loaded by external loads are subjected to flexure.

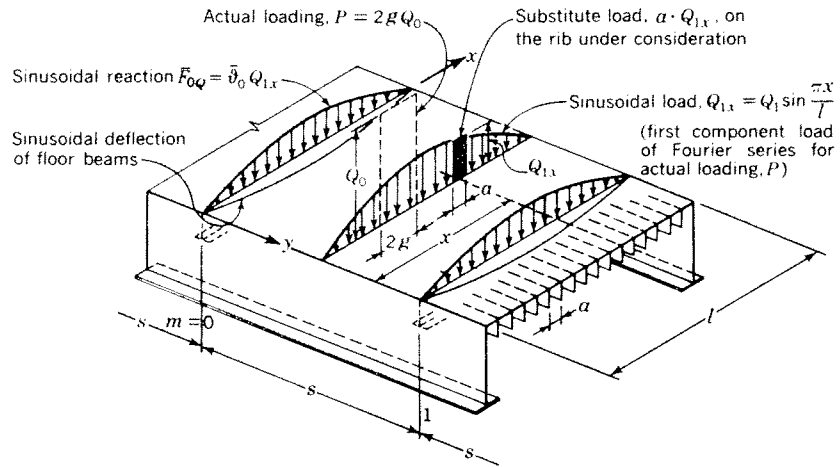
Because of the distribution of the floor beam flexi-

bility effects over the entire width of the deck, the deck may be treated as a plate, with the flexural rigidity of the open or closed longitudinal ribs assumed to be uniformly distributed.

The deck curvature in the transverse direction of the bridge, caused by the floor beam deflections, is very small compared with the deck curvature caused by local loads, so that the stresses in the deck in the x -direction due to floor beam flexibility may be considered negligible, and the transverse flexural rigidity of the deck, $D_x = D_p$, as well as the torsional rigidity, H , may be disregarded.

Fig. 5.1. Typical influence lines for continuous beams on elastic and on rigid supports

Fig. 5.2. Sinusoidal loading on the deck, causing sinusoidal reactions and deflections of the floor beams



Thus, for the purposes of computation of the effects of floor beam flexibility, assumptions $D_x = 0$ and $H = 0$ may be made, and the deck becomes, in effect, a series of parallel plate strips placed side-by-side, as represented graphically in Figure 2.7b, running continuously over the floor beams, which act as common elastic supports of the individual strips.

These strips may be treated as continuous beams on elastic supports, discussed in Section 5.2, if the basic condition requiring that the reactions at any support be proportional to the deflection of the support, as formulated by equation (5.1), is satisfied. Thus, the computation of the plate strips as continuous beams on elastic supports is possible only if the loading is distributed over the width of the deck in such a manner that the resulting floor beam deflections at each point of the floor beam are proportional to the plate strip reactions at those points.

In the usual case of floor beams simply supported at the main girders, this condition is satisfied by a *sinusoidal loading* extending over the entire width of the deck, causing sinusoidal reactions at any floor beam (see Section 4.3.1.2), which, in turn, cause sinusoidal deflections of the floor beams thus loaded, as may be seen from equations (5.3) and (5.4). Therefore, in the computation of the effects of floor beam flexibility, the actual load on the deck is represented by a Fourier series consisting of sinusoidal component loads, Q_{1x} , Q_{2x} , Q_{3x} ... Q_{nx} , as discussed in Section 3.5.

By inspection of the component loads, Figure 3.13, it may be easily seen that the deflection of a simply supported floor beam is determined almost entirely by the first sinusoidal component load, Q_{1x} , since the effect of the higher component loads, causing local deflections proportional to the fourth power of the decreasing effective spans, l/n , is insignificant (see equation 5.4).

Therefore it is sufficient for design purposes to

consider only the first sinusoidal component load, $Q_{1x} = Q_1 \sin \pi x/l$, as shown in Figure 5.2. In the computation of the effects of floor beam flexibility each plate strip of a unit width at the location x is loaded by the corresponding loading at the same location, Q_{1x} , and treated as a beam on elastic supports.

Formulas for the dimensionless loading coefficients, Q_{1x}/Q_0 , are given in Section 3.5.4.

Formulas for the bending moment corrections due to floor beam flexibility are given in Section 5.3.3.

5.3.2 Relative Rigidity Coefficient, γ

In the system shown in Figure 5.2 the floor beams act as elastic supports for the individual plate strips. Since both the plate strip reactions and their deflections vary sinusoidally along the floor beam, the spring constant, k , defined in accordance with equation (5.1) as the ratio of the reaction to the deflection of the support

$$k = \frac{\bar{F}}{\delta} \quad (5.2)$$

has the same value at all points along the floor beam.

For the system shown in Figure 5.2, loaded by sinusoidal component loads, Q_{nx} , the reaction at floor beam $m = 0$, $(\bar{F}_{0Q})_n$, due to the n th component load, is, generally

$$(\bar{F}_{0Q})_n = \bar{v}_{0n} Q_n \sin \frac{n\pi x}{l} \quad (5.3)$$

where \bar{v}_{0n} is the influence ordinate at the location of the load, Q_{nx} , for the sought reaction at support $m = 0$ of a beam on elastic supports, computed with the proper value of the relative rigidity coefficient, γ_n .

The floor beam deflection, δ_n , caused by the sinusoidal reaction $(\bar{F}_{0Q})_n$, on the floor beam is also a sinusoidal curve, given as

$$\delta_n = \frac{1}{EI_F} \iiint \int (\bar{F}_{0Q})_n dx^4 = \frac{\bar{\vartheta}_{0n}}{EI_F} \left(\frac{l}{n\pi}\right)^4 Q_n \sin \frac{n\pi x}{l} \quad (5.4)$$

where EI_F is the floor beam rigidity, and l is the floor beam span.

By substituting expressions (5.3) and (5.4) into equation (5.2), the value of the spring constant is obtained as

$$k_n = \frac{n^4 \pi^4 EI_F}{l^4} \quad (5.5)$$

The relative rigidity coefficient, γ_n , is defined as the ratio of the stiffness of the deck strip to the spring constant of the supports, k_n . For a deck with open ribs the expression for γ_n is

$$\gamma_n = \frac{EI_R/s^3 a}{k_n} \quad (5.6)$$

and for a deck with closed ribs

$$\gamma_n = \frac{EI_R/s^3(a+e)}{k_n} \quad (5.6a)$$

It is seen that the relative rigidity coefficient, γ , of a deck system is not constant for all cases of loading, but depends on the number n of the sinusoidal component loading applied.

Using only the first component load ($n = 1$) and disregarding the higher load components, as discussed in Section 5.3.1, the relative rigidity coefficient may be given by substituting equation (5.5) into equation (5.6) or (5.6a) as follows:

For a deck with open ribs

$$\gamma = \frac{l^4 I_R}{as^3 \pi^4 I_F} \quad (5.7)$$

and, for a deck with closed ribs

$$\gamma = \frac{l^4 I_R}{(a+e)s^3 \pi^4 I_F} \quad (5.7a)$$

If the rib sizes vary across the width of the deck, an appropriate average value of I_R may be used, with more weight given to the ribs near the midspan of the floor beam.

In the case of floor beams of a variable depth, an equivalent uniform moment of inertia, I_F , should be used, resulting in the same deflection at the midspan of the floor beam as is obtained with the actual variable moment of inertia of the floor beam.

The moments of inertia, I_R and I_F , should be determined in accordance with the formulas given in Section 3.3.2.2.

5.3.3 Bending Moment Corrections Due to Floor Beam Flexibility

5.3.3.1 Moment Increase, ΔM_R , in the Ribs

By inspection of the influence lines for the bending moments in a continuous beam on elastic supports, Figure 5.1a and b, it may be seen that the bending moment at any point of the beam consists of two parts.

One part, which may be regarded as due to the action of the loads, P , in a system with unyielding supports, corresponds to the influence ordinates η of a beam on rigid supports. For a deck plate strip this moment is computed, with consideration of the transverse load distribution, in Step 1 of the computation by formulas given in Chapter 4.

The other part of the moment is due to the vertical movement of the supports and corresponds to the differences, $\bar{\eta} = \bar{\eta} - \eta$, between the influence ordinates of the beam on elastic supports, $\bar{\eta}$, and the influence ordinates of the beam on rigid supports, η (Fig. 5.1a and b). Thus, the ordinates $\bar{\eta}$ represent the effect of the support elasticity only.

It may be shown that the additional moment, ΔM , at any point, i , of the beam, due to the vertical movement of the supports under a load, or a group of loads, P , may be expressed as

$$\Delta M = P \bar{\eta} = \sum_{m=0}^{\infty} F_m \bar{\eta}_{im} \quad (5.8)$$

where

P = load

F_m = reaction at support m of a continuous beam on rigid supports, due to load, P , or group of loads placed on the beam, expressed in terms of the load, P

$\bar{\eta}_{im}$ = influence ordinate at support m , for the bending moment at point i under consideration, of a continuous beam on elastic supports

If the dimensionless ratios, $\bar{\eta}_{im}/s$ and F_m/P , are introduced, equation (5.8) can be given as

$$\Delta M = P s \frac{\bar{\eta}}{s} = P s \sum \frac{F_m}{P} \frac{\bar{\eta}_{im}}{s} \quad (5.8a)$$

It should be noted that the ratio F_m/P is independent of the magnitude of the load, P , and represents the influence ordinate, ϑ_m , for the reaction at support m of a beam on rigid supports, or, in case of a group of loads expressed in terms of P , the properly modified sum of the influence ordinates at the locations of the individual loads.

In accordance with Section 5.3.1, application of the formulas for a beam on elastic supports for the computation of the bridge deck supported on flexible

floor beams requires that the actual loads, P , acting on the deck be replaced by their first sinusoidal component loads, Q_{1x} (Fig. 5.2). Thus in the computation of the additional bending moment, ΔM_R , in a rib due to floor beam deflections, the load on the rib under consideration at the location x is obtained as the product, $Q_{1x}(a)$, or $Q_{1x}(a + e)$, of the intensity of the first sinusoidal component load at the location x and the width of the rib, as indicated in Figure 5.2.

With these loading values and the dimensionless coefficient, Q_{1x}/Q_0 , equation (5.8a) becomes for open ribs

$$\Delta M_R = Q_0 s a \frac{Q_{1x}}{Q_0} \sum \frac{F_m}{P} \frac{\bar{\eta}_{im}}{s} \quad (5.9)$$

and for closed ribs

$$\Delta M_R = Q_0 s (a + e) \frac{Q_{1x}}{Q_0} \sum \frac{F_m}{P} \frac{\bar{\eta}_{im}}{s} \quad (5.9a)$$

where

ΔM_R = additional moment per rib due to floor beam deflections

$Q_0 = P/2g =$ wheel load per inch of width of the deck

$Q_{1x} =$ value at the rib under consideration (location x) of the first sinusoidal component load of the actual wheel load, P , as defined by equation (3.21)

Other designations have been defined above.

The values of the influence ordinates, $\bar{\eta}_{cm}/s$ and $\bar{\eta}_{sm}/s$, to be used in equation (5.9) or (5.9a) for the computation of the additional bending moments in the ribs at the midspan and at the supports, are given in Charts 17 and 18.

In the usual design cases, the additional moment, ΔM_R , computed by equation (5.9) or (5.9a) has a positive value, meaning a bending moment increment at the midspan and a moment relief at the support of a rib.

In the design computations in accordance with the AASHO specifications several traffic lanes may be loaded simultaneously. However, the wheel loads and the truck positions may be different in the lane where the moment is computed and in the adjoining lanes. This is discussed in Chapter 10.

In such cases, the total additional bending moment in a rib due to floor beam deflections is computed as the sum of the effects of the loads in the critical lane under consideration and in other lanes,

$$\Delta M_R = \Delta M_{R(\text{crit. lane})} + \sum \Delta M_{R(\text{other lanes})} \quad (5.10)$$

The bending moment correction, ΔM_R , computed by equation (5.10) is added to the moment M_R , com-

puted in Step 1 of the design, to obtain the final design moment.

In accordance with the AASHO specifications, Section 1.2.9, the total moment in a rib, $M_R + \Delta M_R$, has to be multiplied by a load reduction coefficient if it is due to more than two lanes simultaneously loaded.

5.3.3.2 Moment Relief, ΔM_F , in the Floor Beams

A load, P , placed near a floor beam on a deck supported by flexible floor beams will cause a floor beam reaction which will be smaller than the reaction in a system with unyielding floor beams, as may be seen by inspection of the influence lines, Figure 5.1c.

Consequently, the bending moments in the floor beam, which are proportional to the floor beam reaction, will be smaller in a flexible system than in the rigid system.

If the load P is represented by sinusoidal component loads, $Q_{nx} = Q_n \sin(n\pi x/l)$, the moment at any point of the floor beam $m = 0$, found by double integration of the loading, may be expressed, for a rigid floor beam, as

$$\begin{aligned} M_F &= \sum_{n=0}^{\infty} -\frac{F_0}{P} \iint Q_{nx} dx^2 \\ &= \sum_{n=0}^{\infty} \frac{F_0}{P} Q_n \left(\frac{l}{n\pi}\right)^2 \sin \frac{n\pi x}{l} \end{aligned} \quad (5.11)$$

and, for an elastic floor beam, as

$$\bar{M}_F = \sum_{n=0}^{\infty} \frac{\bar{F}_0}{P} Q_n \left(\frac{l}{n\pi}\right)^2 \sin \frac{n\pi x}{l} \quad (5.11a)$$

where the ratios F_0/P and \bar{F}_0/P are the influence ordinates, or, in case of a group of loads expressed in terms of P , the sums of the influence ordinates at the locations of the individual loads for the reaction at support $m = 0$ of a continuous beam on rigid or elastic supports, respectively.

The difference, $M_F - \bar{M}_F = \Delta M_F$, or the moment relief in the floor beam due to its elastic flexibility, is then

$$\Delta M_F = \sum_{n=0}^{\infty} \left[\frac{F_0}{P} - \frac{\bar{F}_0}{P} \right] Q_n \left(\frac{l}{n\pi}\right)^2 \sin \frac{n\pi x}{l} \quad (5.12)$$

If only the first term of the series is considered, as explained in Section 5.3.1, equation (5.12) becomes

$$\Delta M_F = \left[\frac{F_0}{P} - \frac{\bar{F}_0}{P} \right] Q_1 \left(\frac{l}{\pi}\right)^2 \sin \frac{\pi x}{l} \quad (5.12a)$$

With the load or group of loads, P , in any position on the deck, the ratio \bar{F}_0/P is obtained by evaluation of the influence line for the reaction of a beam on elastic supports (Fig. 5.1c), and is

$$\frac{\bar{F}_0}{P} = \sum_{m=0}^{\infty} \frac{F_m}{P} \bar{\vartheta}_{0m} \quad (5.13)$$

where

F_m = reaction at support m of a continuous beam on rigid supports, as defined in Section 5.3.3.1

$\bar{\vartheta}_{0m}$ = influence ordinate at support m , for the reaction at support $m = 0$ of a beam on elastic supports

By substituting equation (5.13) into equation (5.12a), using the definition, equation (3.21), and introducing the dimensionless ratio, Q_{1x}/Q_0 , the formula for the moment relief, ΔM_F , at any point x of an elastic floor beam is obtained as

$$\Delta M_F = Q_0 \left(\frac{l}{\pi} \right)^2 \frac{Q_{1x}}{Q_0} \left[\frac{F_0}{P} - \sum \frac{F_m}{P} \bar{\vartheta}_{0m} \right] \quad (5.14)$$

Formulas for the Fourier coefficients, Q_{1x}/Q_0 , for the various cases of floor beam loading, are given in Section 3.5.4.

The values of F_0/P and F_m/P , defined above, may be obtained from Chart 5c or Table 4.2.5.

The influence ordinates $\bar{\vartheta}_{0m}$ of a beam on elastic supports are given in Chart 19.

The values of $[(F_0/P) - \sum (F_m/P) \bar{\vartheta}_m]$ for the AASHO truck loads are given in Charts 30 and 31.

5.3.4 Shear Corrections Due to Floor Beam Flexibility

5.3.4.1 Shears in the Ribs

Due to the fact that in an elastic system the rib reactions on the floor beams are generally smaller than in the rigid system, the shears in the ribs will also be smaller.

Based on considerations similar to those in Section 5.3.3, shear corrections, ΔV_R , in the ribs could be computed.

However, since in the usual cases the shearing stresses in the ribs are low and do not govern the design, the computation of the shears in the ribs in the rigid system only will generally suffice.

5.3.4.2 Shears in the Floor Beams

Similarly as the bending moments, the shears in elastic floor beams will be generally smaller than those in rigid floor beams.

The expression for the shear relief, ΔV_F , in an elastic floor beam is found in a similar manner as the moment relief, ΔM_F , Section 5.3.3.2.

The load, P , placed at any location on the deck and represented by its sinusoidal component loads, $Q_{nx} = Q_n \sin(n\pi x/l)$, causes the shear, V_F , at any

point of the rigid floor beam $m = 0$, which is found by integration of the sinusoidal component reactions on the floor beam due to loads Q_{nx} as

$$V_F = - \sum_{n=0}^{\infty} \int \frac{F_0}{P} Q_{nx} dx = \sum_{n=0}^{\infty} \frac{F_0}{P} \frac{Q_n l}{n\pi} \cos \frac{n\pi x}{l} \quad (5.15)$$

Similarly, for the elastic floor beam

$$\bar{V}_F = - \sum_{n=0}^{\infty} \int \frac{\bar{F}_0}{P} Q_{nx} dx = \sum_{n=0}^{\infty} \frac{\bar{F}_0}{P} \frac{Q_n l}{n\pi} \cos \frac{n\pi x}{l} \quad (5.15a)$$

The ratios F_0/P and \bar{F}_0/P in the above equations are defined in Section 5.3.3.2.

With the first component loads only, the difference, $\Delta V_F = (V_F)_1 - (\bar{V}_F)_1$, is

$$\Delta V_F = \left[\frac{F_0}{P} - \frac{\bar{F}_0}{P} \right] \frac{Q_1 l}{\pi} \cos \frac{\pi x}{l} \quad (5.16)$$

If equation (5.13) is substituted into equation (5.16), the value of ΔV_F , or the shear relief in the floor beam due to its elastic flexibility under a given loading, at any point, x , of the floor beam is obtained as

$$\Delta V_F = \frac{Q_1 l}{\pi} \left[\frac{F_0}{P} - \sum_{m=0}^{\infty} \frac{F_m}{P} \bar{\vartheta}_{0m} \right] \cos \frac{\pi x}{l} \quad (5.17)$$

where Q_1 is the amplitude of the first sinusoidal component of the deck loading, which may be obtained for the various loading cases from the formulas given in Section 3.5.4 by means of the relationship

$$Q_1 = \frac{Q_{1x}}{\sin(\pi x/l)}$$

Other symbols in equation (5.17) have the same meaning as in the similar formula for the moment relief, equation (5.14).

The value of the shear correction at a specific point of the floor beam, $x = d$, due to a concentrated load, P , placed at the variable location, x , anywhere on the deck, is obtained by substituting into equation (5.17) the expression for Q_1 of the load P .

The value of the first component load, Q_1 , of the concentrated load, P , is

$$Q_1 = \frac{2P}{l} \sin \frac{\pi x}{l} \quad (5.18)$$

By substituting equation (5.18) into equation (5.17) and setting the value of x in equation (5.17) equal to the specified ordinate, d , the equation for the shear relief due to a concentrated load, ΔV_{FP} , at the location d of the floor beam is obtained as

$$\Delta V_{FP} = \frac{2P}{\pi} \left[\frac{F_0}{P} - \sum \frac{F_m}{P} \bar{\vartheta}_{0m} \right] \cos \frac{\pi d}{l} \sin \frac{\pi x}{l} \quad (5.19)$$

The final design value of shear, \bar{V}_F , in the floor beam is obtained by subtracting the shear relief, ΔV_F , from the value of shear, V_F , in the rigid floor beam,

$$\bar{V}_F = V_F - \Delta V_F \quad (5.20)$$

The shear, V_F , in a rigid floor beam due to loads P on the deck is usually obtained by evaluation of the influence line for shear at the point under consideration with the values of the deck reactions, F_0 , on the floor beam, as

$$V_F = \sum F_0 \vartheta_V \quad (5.21)$$

where ϑ_V are the influence ordinates for shear in the rigid floor beam.

In order to construct the influence line for the final design shear, \bar{V}_F , in an elastic floor beam, the acting loads, P , are represented as functions of their reactions, F_0 , on the floor beam

$$P = \frac{F_0}{(F_0/P)} \quad (5.22)$$

and equation (5.19) is rewritten as

$$\Delta V_{FP} = F_0 \frac{2}{\pi} \left[1 - \frac{\sum (F_m/P) \bar{\vartheta}_{0m}}{F_0/P} \right] \cos \frac{\pi d}{l} \sin \frac{\pi x}{l} \quad (5.19a)$$

Thus, with equations (5.19a), (5.20) and (5.21), the design shear, \bar{V}_F , may be given as

$$\bar{V}_F = \sum F_0 \left\{ \vartheta_V - \frac{2}{\pi} \left[1 - \frac{\sum (F_m/P) \bar{\vartheta}_{0m}}{F_0/P} \right] \cos \frac{\pi d}{l} \sin \frac{\pi x}{l} \right\} \quad (5.23)$$

The influence ordinates for shear in an elastic floor beam, given by equation (5.23) are represented graphically in Figure 5.3.

It should be noted that in equation (5.23), F_0 is the reaction of one truck on a rigid floor beam and P denotes the weight of one axle of the truck. In evaluating the influence lines shown in Figure 5.3 the values of $F_0/2$ at the locations of the wheels, rather than the full values of F_0 at the center lines of trucks are used for better accuracy.

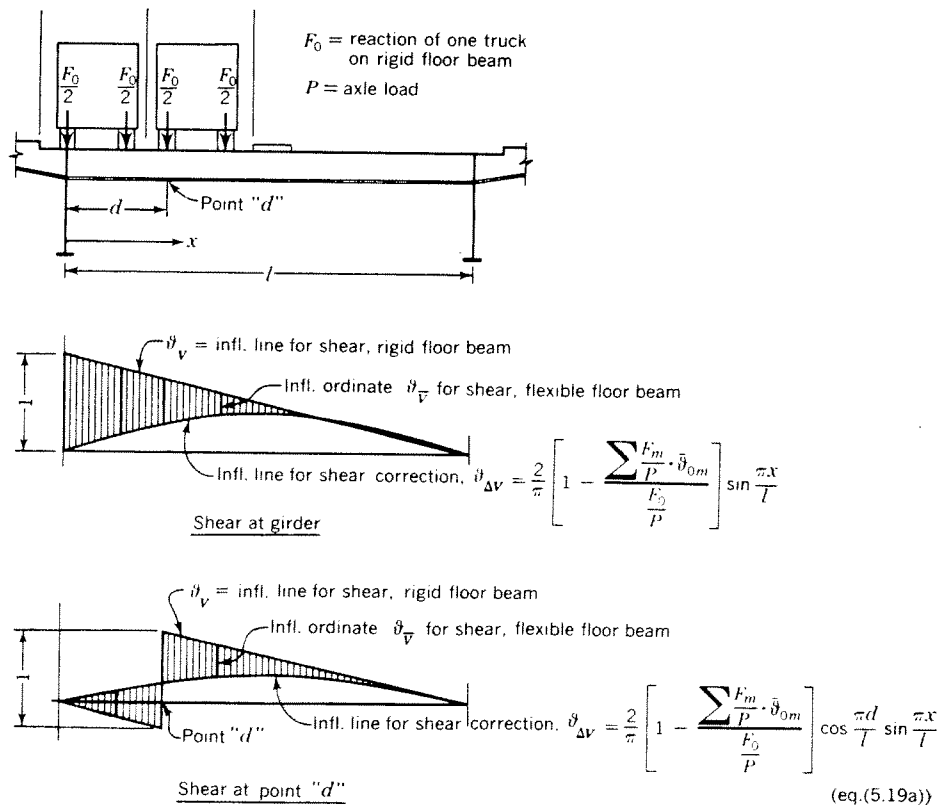


Fig. 5.3. Influence lines for shears in a flexible floor beam

5.3.5 Charts for the Determination of the Effects of Floor Beam Flexibility Due to AASHO Loads

In order to facilitate the computation of the effects of floor beam flexibility, design charts are given in the Appendix.

The derivation of the charts is discussed below.

The use of the charts in practical design computations is explained in Chapter 10.

Charts 17, 18 and 19 give the values of the influence ordinates for the bending moments at the midspan and at the support, and for the reaction at the support of a continuous beam on elastic supports, for the various relative rigidities, γ . The ordinate values have been obtained from Tables 165.1–3 of reference [42].

Charts 20, 21 and 22 give the values of the dimensionless coefficients, $\sum(F_m/\bar{\eta}_{c_m})(P/s)$, used in the computation of the bending moment correction at the midspan of the ribs by equation (5.9) or (5.9a), for loading cases **a**, **a**₁, **b**, **b**₁, **c** and **c**₁, used in the computation of the bending moment at the midspan of the ribs in a system with floor beams considered rigid (*Charts 6, 9, 10, 11 and 12*). The individual axle loads have been placed in the same positions as used in the computation of the *Charts 6, 9, 10, 11 and 12*. The chart ordinates have been obtained by numerical evaluation of the influence lines, *Charts 5c and 17*.

Chart 23 gives the values of $\sum(F/P)(\bar{\eta}_{c_m}/s)$, needed in the evaluation of equations (5.9) and (5.9a) for loadings **h** and **h**₁, as shown in sketch on *Chart 23*, representing the loading in the lanes other than the critical lane.

The trucks are placed in such positions as to cause maximum deflections of the floor beams $m = 0$ and $m = 0'$.

Charts 24, 25, 26 and 27 give coefficients $\sum(F/P)(\bar{\eta}_{s_m}/s)$ needed in the computation of the bending moment relief at the supports of the ribs by equation (5.9) or (5.9a) for loading cases **d**, **e**, **f** and **g**, used in the computation of *Charts 7 and 13*. The ordinates have been obtained in a similar manner as for *Charts 20–22*.

Chart 28 gives the values of the first Fourier coefficients, Q_{1x}/Q_0 , at the location x under the critical wheel, used in equations (5.9) and (5.9a). The values of Q_{1x}/Q_0 have been computed by equation (3.27), for positions of the truck consistent with the AASHO Design Specifications, Section 1.2.6. The truck load is placed in the critical lane only.

Chart 29 gives the values of the coefficients Q_{1x}/Q_0 at the critical rib for other than critical lanes loaded, as shown in a sketch on the chart. Equation (3.30) has been used to compute the chart ordinates.

Charts 30 and 31 give the values of the expression $(F_0/P) - \sum(F_m/P)\bar{\delta}_{0m}$, needed in the evaluation of equation (5.14). Influence lines, *Charts 5c and 19*, have been used to determine the chart ordinates for loading cases **A** and **B**, corresponding to those in *Chart 15*.

Chart 32 gives the coefficients Q_{1x}/Q_0 at the point of maximum moment in the floor beam, needed in the evaluation of equation (5.14), for the various numbers of lanes loaded. The values needed have been computed by equation (3.30).

5.4 BRIDGE DECKS WITH FLOOR BEAMS OF NON-UNIFORM RIGIDITY

5.4.1 General

The formulas for the bending moment corrections in the deck due to floor beam flexibility given in Section 5.3.3 are valid for bridge decks with a uniform rigidity of all floor beams.

However, the design and construction considerations usually require the use of heavier floor beams at certain intervals, acting as bridge cross frames or load distributing diaphragms between multiple main girders.

The effect of the heavier floor beams on the distribution of the stresses in the deck system will depend on the relative stiffness ratios of the structural members of the deck and on the loading.

Generally, the reactions and the bending moments in the heavier floor beams will be increased, compared with the system with uniformly rigid floor beams, while the light floor beams adjoining the heavy ones will be relieved.

In the continuous deck the maximum negative bending moments over the heavier floor beams will be larger than those in a system with floor beams of uniform rigidity. The maximum positive moments at the midspan of the ribs may decrease or increase, depending on the rigidity ratios of the system.

In most cases the effect of one heavy floor beam on the stresses at the location of the next heavy floor beam will be small. Therefore, for design purposes it may be sufficient to consider the effect on the stress distribution of one heavy floor beam only.

Formulas for such computations are given in Section 5.4.3 and illustrated by a numerical example in Section 11.2.2.3.

If, in the general case of floor beams of varying rigidity, a more accurate design computation should be required, the needed results may be obtained by application of the five-moment equation of a beam on elastic supports in its general form, as given in [51] or other references.

5.4.2 Designations

The following designations are used:

- P = load
- \bar{F}_{0P} = reaction of elastic support 0, due to P , in a system with all supports of uniform rigidity
- X_0 = internal redundant force at the more rigid support, 0, due to its surplus rigidity (Fig. 5.5b)
- $\Delta \bar{F}_{m0}$ = change of the reaction at support m , due to force X_0 at support 0
- $\Delta \bar{F}_{00}$ = change of the reaction at support 0, due to force X_0
- β = ratio of the rigidity of support 0 to the rigidity of the other supports, equal to the ratio I_0/I of the moment of inertia of the heavier floor beam, $m = 0$, to that of the other floor beams
- k = spring constant of the more elastic supports (k/in.)
- βk = $k + k_a$ = spring constant of the more rigid support, 0 (Fig. 5.4a and b)
- δ_a = relative deflection between the continuous beam and the redundant support, k_a , at support 0 (Fig. 5.5a, b)
- $\bar{\vartheta}_{m0}$ = influence ordinate at support 0, for the reaction at support m in a system with uniform rigidity of all supports
- $\bar{\vartheta}_{00}$ = influence ordinate at support 0, for the reaction at support 0 in a system with uniform rigidity of all supports
- $\bar{\eta}_{i0}$ = influence ordinate at support 0, for the bending moment at any point i , in a system with uniform rigidity of all supports
- $\Delta \bar{M}_{i0}$ = change of the bending moment in a continuous beam at point i , due to force, X_0 , at support 0

$\Delta \bar{M}_{Pm}$ = change of the bending moment in floor beam m , due to the surplus rigidity of floor beam 0

$\Delta \bar{M}_{Ri}$ = change of the bending moment in a rib at point i , due to the surplus rigidity of floor beam 0

5.4.3 Formulas for the Effect of One Heavier Floor Beam

5.4.3.1 Derivation for Beam on Elastic Supports

In the system shown in Figure 5.4a the spring constant, βk , of the elastic support, 0, is greater than the spring constant, k , of the remaining elastic supports, 1, 2, 3 The more rigid support, 0, is replaced by a light support, with a spring constant k , and an additional support, located very close to it, with a spring constant k_a (Fig. 5.4b). The additional supporting force, provided by the spring k_a will be treated as an external force acting on a system with uniform rigidity, k , of all supports.

The internal redundant force, X_0 , of the support k_a is obtained by analyzing the system as a statically indeterminate structure in the following manner:

If the connection between the redundant support, k_a , and the continuous beam is assumed severed, a load P will cause a relative deflection, δ_{aP} , at support 0, between the spring k_a and the continuous beam, as shown in Figure 5.5a.

The redundant reaction, X_0 , between the beam and the support k_a causes a relative deflection, δ_{aX} , in the opposite direction, between the beam and the support k_a (Fig. 5.5b). It is seen that the deflection δ_{aX} consists of two parts, one being the deflection of the end of the spring k_a from its original position due to the force X_0 , the other representing the motion in the opposite direction of the end of the spring k under the effect of the reaction, $X_0 \bar{\vartheta}_{00}$, caused by the force X_0 at support 0.

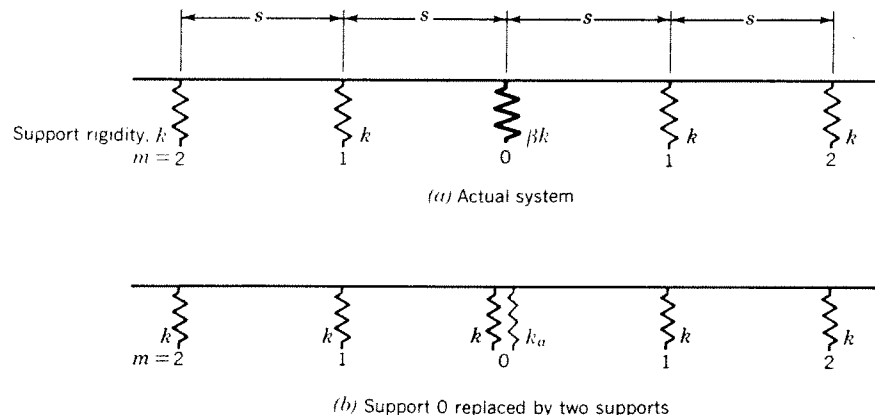


Fig. 5.4. Continuous beam on elastic supports with support 0 more rigid than the others

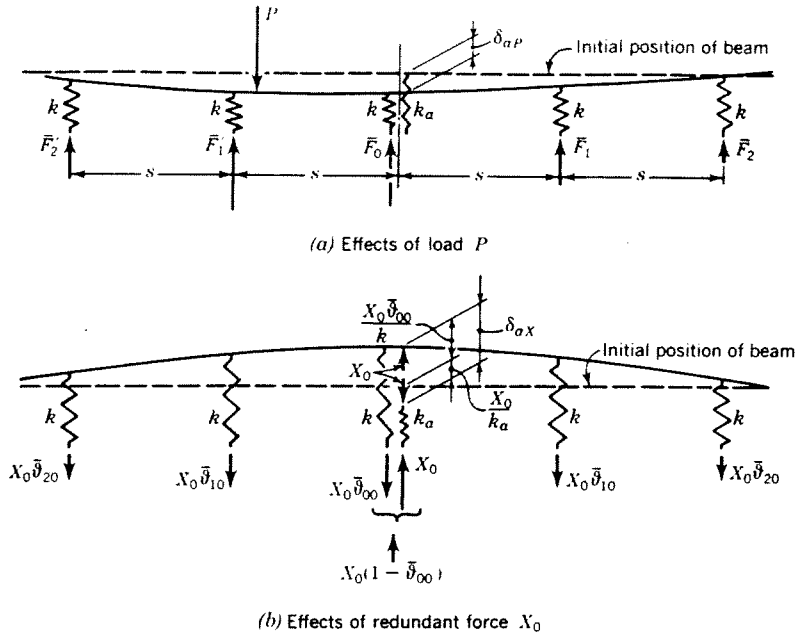


Fig. 5.5. Determination of redundant force in additional support k_a

From equation (5.1) with designations given in Section 5.4.2, the deflections, δ_a , are obtained as

$$\delta_{aP} = -\frac{F_{0P}}{k}$$

$$\delta_{aX} = \frac{X_0}{k_a} + \frac{X_0 \bar{\vartheta}_{00}}{k} = \frac{X_0}{k(\beta - 1)} + \frac{X_0 \bar{\vartheta}_{00}}{k}$$

The actual relative motion between the spring, k_a , and the beam must be equal to zero, or

$$\delta_{aP} + \delta_{aX} = -\frac{F_{0P}}{k} + \frac{X_0}{k} \left(\bar{\vartheta}_{00} + \frac{1}{\beta - 1} \right) = 0$$

hence

$$X_0 = F_{0P} \left(\frac{1}{\bar{\vartheta}_{00} + \frac{1}{\beta - 1}} \right) \quad (5.24)$$

With the redundant additional reaction, X_0 , known, its effects on the reactions and the bending moments in the system are obtained by the following formulas:

$$\Delta \bar{M}_{i0} = \bar{\eta}_{i0} X_0 \quad (5.25)$$

$$\Delta \bar{F}_{00} = (1 - \bar{\vartheta}_{00}) X_0 \quad (5.26)$$

$$\Delta \bar{F}_{m0} = \bar{\vartheta}_{m0} X_0 \quad (5.27)$$

with designations as defined in Section 5.4.2.

5.4.3.2 Change of the Bending Moments in Ribs

By adaptation of equation (5.25) to a system consisting of a steel plate deck continuous over elastic floor

beams, the effect of one heavier floor beam on the bending moments in the longitudinal ribs is computed in a similar manner as shown in Section 5.3.3.1.

By introducing into equation (5.25) the dimensionless ratios, X_0/P and $\bar{\eta}_{i0}/s$, and substituting the first Fourier component load, Q_{1z} , for the load P , the formulas for the bending moment change, $\Delta \bar{M}_{Ri}$, at point i of the longitudinal ribs are obtained. These are similar to equations (5.9) and (5.9a). For open ribs

$$\Delta \bar{M}_{Ri} = Q_{0sa} \frac{Q_{1z}}{Q_0} \frac{X_0}{P} \frac{\bar{\eta}_{i0}}{s} \quad (5.28)$$

and for closed ribs

$$\Delta \bar{M}_{Ri} = Q_{0s}(a + e) \frac{Q_{1z}}{Q_0} \frac{X_0}{P} \frac{\bar{\eta}_{i0}}{s} \quad (5.28a)$$

The ratio X_0/P is defined by equation (5.24) with (5.13), and should be computed for the same position of the loads P as used in the computations of the bending moments in the system with rigid floor beams (Chapter 4), and in the system with uniform rigidity of all floor beams (Section 5.3.3.1). The total bending moment in the rib is then obtained by superposition of all three effects.

The minus signs in equations (5.28) and (5.28a), as well as in equation (5.30), are due to the fact that the redundant force X_0 is acting upward (Fig. 5.5).

The influence ordinates, $\bar{\eta}_{i0}$ and $\bar{\vartheta}_{00}$, needed in the evaluation of equations (5.28) and (5.28a) may be obtained from Charts 17-19.

5.4.3.3 Change of the Bending Moments in Floor Beams

By introducing into equation (5.26) the dimensionless ratio X_0/P , and by substituting the first sinusoidal component load, Q_{1x} , for the load, P , the formula for the change of the bending moment in the heavy floor beam, $m = 0$, is obtained from equation (5.14) as

$$\bar{\Delta}M_{F0} = -Q_0 \frac{Q_{1x}}{Q_0} \left(\frac{l}{\pi}\right)^2 \frac{X_0}{P} (1 - \bar{\nu}_{00}) \quad (5.29)$$

Similarly, from equations (5.27) and (5.14) the formula for bending moment change in a light floor beam, m , is obtained as

$$\bar{\Delta}M_{Fm} = Q_0 \frac{Q_{1x}}{Q_0} \left(\frac{l}{\pi}\right)^2 \frac{X_0}{P} \vartheta_{m0} \quad (5.30)$$

where the ratio X_0/P is defined by equation (5.24) with (5.13).

5.5 BRIDGE DECKS WITH FLOOR BEAMS ELASTICALLY RESTRAINED AT THE MAIN GIRDERS OR CONTINUOUS OVER MORE THAN TWO MAIN GIRDERS

The condition of proportionality of the loading to the deflection at each point of the floor beam, necessary in the analysis of the deck strips as beams on elastic supports (Section 5.3.1), is satisfied by the sinusoidal component loads, obtained through Fourier analysis, only if the floor beams are simply supported. This may be considered the case if there are only two single-webbed main girders, having a negligible torsional rigidity.

If the floor beams are framed into bridge members of considerable torsional rigidity, such as box girders, or in the case of continuity of the floor beams over more than two main girders (Fig. 5.6), representation of the actual loading by simple sinusoidal components is no longer sufficient. In such cases, in order to rigorously satisfy the basic condition defined above, the loading must be expressed by functions, consisting of ordinary and hyperbolic sines and cosines, to be

determined separately in each case, known as *eigenfunctions* of the system. Application of this method of analysis, presentation of which would exceed the scope of this Manual, is given and illustrated in Reference [42], Section 151.3.

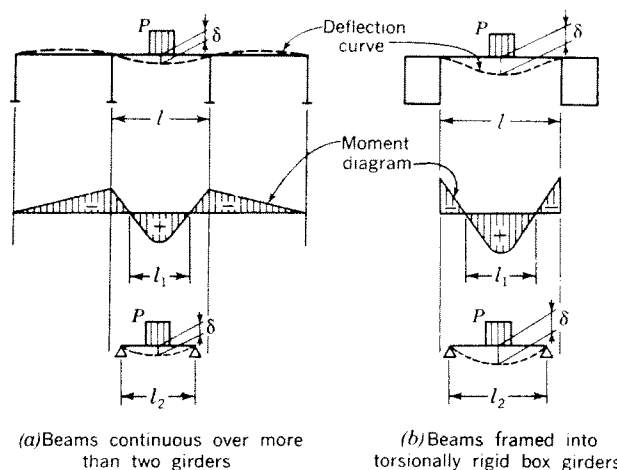


Fig. 5.6. Approximate determination of the effective spans of continuous floor beams

However, it may be sufficient for design purposes in most cases to use the Fourier analysis and the formulas given in Section 5.3, with an appropriately chosen value of the *effective simple span*, l_1 , of the floor beams. The effective span, l_1 , is the length of the positive portion of the moment diagram of the actual floor beam, as shown in Figure 5.6.

The value of the relative rigidity coefficient, γ , is determined from equation (5.7) or (5.7a) by substituting the effective simple span, l_2 , determined from the condition that the deflection at the center of the simple span, l_2 , due to the loads on the bridge be the same as the deflection at the center of the actual floor beam (Fig. 5.6).

The results of this approximate method are valid only for the ribs near the center of the floor beam.

CHAPTER 6

Design of the Deck Plate

6.1 DESIGN CRITERIA

The primary function of the deck plate is to directly support the traffic loads and to transmit the reactions to the longitudinal ribs. The deck plate acting as a member transmitting the wheel loads to the ribs constitutes a separate local structural system, defined as System III (see Section 1.2.2), which may be treated independently from structural Systems I and II, comprising the action of the deck plate as a flange of the primary and secondary carrying members of the bridge.

In the design of the deck plate as an independent structural member directly supporting the wheel loads, the following requirements have to be satisfied:

(a) *Carrying capacity*

The deck plate shall possess an adequate load carrying capacity to support the traffic loads. A reserve capacity in excess of the specified design loads is desirable to permit safe passage of occasional special heavy vehicles and to provide for unforeseen future loading increases.

The requirement of adequate strength is amply satisfied by steel bridge deck plates of usual proportions which have a very high carrying capacity for static concentrated loads. This is discussed in Section 6.2.2.

However, similarly as in the case of the longitudinal ribs (System II, see Section 1.2.4.2), the behavior of the deck plate (System III) under higher loads strongly deviates from that predicted by the ordinary flexural theory of first order.

Therefore, the deformations and the ultimate carrying capacity of the deck plate cannot be judged on the basis of the deflections and stresses under working loads and may be determined only by direct experiment. An empirical formula for an approximate evaluation of the ultimate static load is given in Section 6.3.

(b) *Fatigue strength*

The deck plate shall be capable of resisting the effects of the pulsating and alternating stresses occurring at critical points of the deck plate under the effects of the passing wheel loads.

The fatigue strength of the steel deck plate is discussed in Section 6.2.3.

(c) *Rigidity*

The local deflections of the deck plate between the ribs, even of a considerable magnitude, are not objectionable structurally, provided they are purely elastic.

However, an excessive flexibility of the deck plate may adversely affect the wearing surface placed on the deck.

For the usual asphaltic wearing surfaces a deck plate deflection between the longitudinal ribs of the order of $\frac{1}{300}$ of the rib spacing is not considered objectionable [31]. With thinner wearing surfaces (see Chapter 8) even larger deflections might possibly be tolerated.

An empirical formula for the computation of the deck plate deflection is given in Section 6.3.3.

It should be noted that the deflections of the deck may be considerably reduced by the stiffening effect of the wearing surface, as discussed in Section 8.2.4.1d.

In addition to the above design criteria based on consideration of the deck plate as an independent element, the following requirements have to be satisfied in the determination of the deck plate thickness.

(d) *Adequate cross-sectional area*

The deck plate has to provide a sufficient top flange area for the structural members of the bridge.

To be adequate as the flange of the main bridge girders (System I), the deck plate may have to be considerably thickened, in excess of the local requirements of System III, in the maximum moment areas of the main girders.

The shearing strength of the deck plate as a part of System I must also be checked.

In System II (see Section 1.2.2) the strength of the deck plate acting as the top flange of the longitudinal ribs and the floor beams is always ample, because of the markedly unsymmetrical cross sections of these members.

(e) *Fabrication and erection requirements*

With a great amount of welding necessary in the fabrication of the deck panels, warpage due to welding may become a problem if too thin a deck plate is used. Experience indicates that a $\frac{3}{8}$ -in. thick deck plate is still satisfactory in this respect.

For erection purposes the portions of the deck plating directly connected to the main girder webs may have to be thickened for strength and stability.

6.2 STRUCTURAL BEHAVIOR OF THE DECK PLATE ACTING AS AN INDEPENDENT STRUCTURAL ELEMENT (SYSTEM III)

6.2.1 Deck Plate Subjected to Small Loads

6.2.1.1 Tests on Decks Subjected to Design Loads

6.2.1.1.1 General

Tests made on models and on actual deck plates of steel plate deck bridges indicate that, under small loads of the order of the standard truck wheel loads, the deck plate behaves as an isotropic plate, in accordance with the flexural theory of the first order.

The correspondence of the computed and the measured stresses is, however, only approximate, in most cases.

This may be attributed, primarily, to the difficulties in analyzing the actual deck plate system, as discussed in Section 6.2.1.2.1.

Also, in measuring the local stresses in the deck plate (System III) it is not always possible to eliminate the effects of the action of the deck plate as a flange of the ribs, floor beams and the main girders (Systems I and II).

Some of the working load tests made on steel deck plates are briefly described below.

6.2.1.1.2 Tests on Battledeck Floor Plates

Stress measurements on models of battledeck-type bridge floors (Fig. 1.3) were made by the AISC [2, 34].

The results obtained indicated that the deck plate loaded by a wheel placed between the stringers behaved as a continuous member with the points of inflection at the toes of the stringer flanges, which is equivalent to a simply supported plate with a span equal to the clear distance between the flanges.

There were definite indications that in the more slender deck plate panels membrane stresses developed under the wheel load, in addition to the flexural stresses.

Based on these tests, empirical formulas were proposed for the maximum stress at the midspan of the deck plate under the wheel, which give results that are in good agreement with the theoretically computed stresses if the clear span of the plate between the toes of the wide-flange stringers is about 15 to 24 in. (see Section 6.3.1).

6.2.1.1.3 Tests on Decks with Open Ribs

Several tests on steel plate decks with open ribs were conducted by Prof. Kloeppel at the Technological University in Darmstadt [29, 30, 31, 76].

A typical pattern of the local stress distribution in the deck plate under a simulated wheel load, based on the results of the model tests [31] is shown in Figure 6.1.

It should be noted that the stresses in the deck plate over the rib drop sharply due to the strengthening of the plate by the weld and the rib, so that the maximum stress occurs at the toe of the weld.

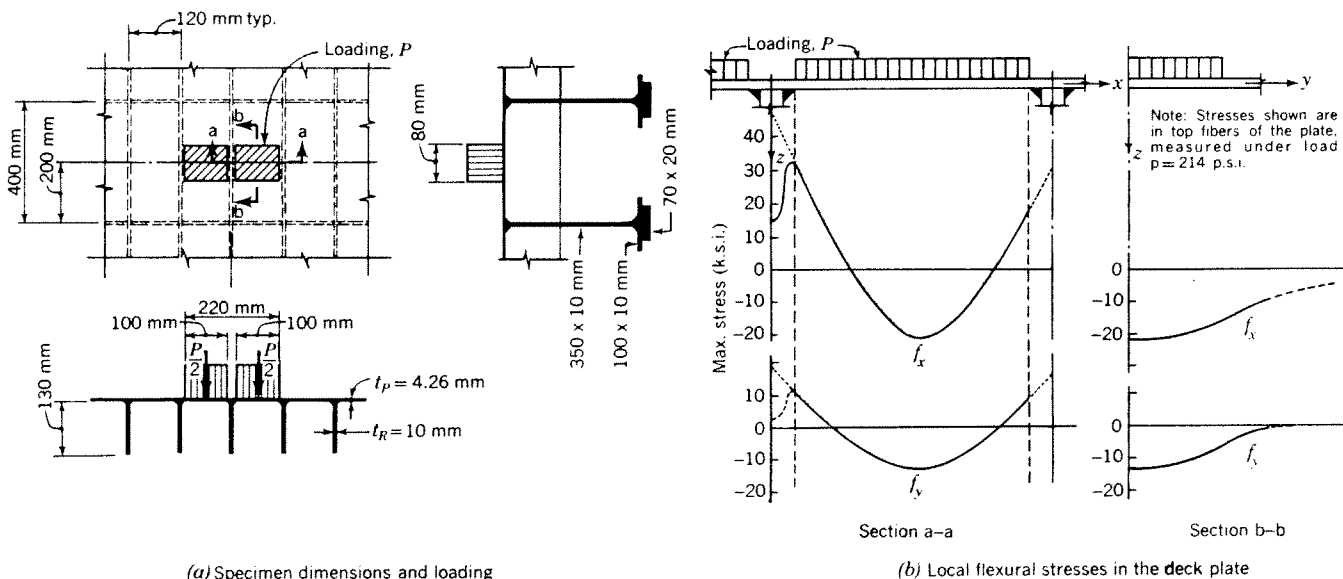


Fig. 6.1. Typical stress diagrams of a deck plate under a wheel load, obtained from strain measurements [31]

In addition to the stresses in the direction normal to the ribs, considerable stresses develop in the deck plate in the direction of the ribs, as predicted by the plate theory.

The local stresses in the deck plate (System III), represented by curves in Figure 6.1b, have been extracted from the measurements of the strains which also included the effects of the variable axial prestress in the y -direction, simulating the System I stress in the bridge deck, and the stresses in the plate as the flange of the ribs and the floor beams (System II).

Varying the longitudinal prestress from a uniform tension of 20 ksi to a compression of 17.3 ksi had almost no effect on the local stresses in the deck plate. This indicates that under the working loads no appreciable membrane conditions in the deck plate have developed in the y -direction.

For the purposes of comparison the local stresses in the system shown in Figure 6.1a were also determined analytically, using the clear span in the x -direction of 100 mm, and assuming full fixity at both edges. The maximum stresses obtained in this manner were found to be equal to about 6/5 of the measured values [31].

It should be noted, however, that the assumptions of a plate span shorter than the rib spacing and the full fixity of the plate, while possibly justified in the above case, where ribs were relatively rigid and thick compared to the deck plate, may not be appropriate in the analysis of the decks of usual proportions.

A full-scale test on a bridge deck plate supported by open ribs 12 in. o.c. and subjected to concentrated loads in the range of the design wheel loads is described in Section 192 of reference [42]. In this case a comparative computation made with the assumptions discussed in Section 6.2.1.2.2 results in stresses about 10% lower than those measured.

6.2.1.1.4 Tests on Deck with Closed Ribs

Test measurements of stresses in a deck with closed ribs are reported in Section 193.43 of reference [42].

Under the working loads the measured stresses in the deck plate and in the rib walls in the direction perpendicular to the ribs were found to be in reasonable agreement with the values computed by the method discussed in Sections 6.2.1.2.3 and 6.2.1.3.2.

6.2.1.2 Analytical Determination of the Local Stresses in the Deck Plate Under the Design Loads

6.2.1.2.1 General

The magnitudes of the local stresses occurring in the deck plate under the design loads provide no direct measure of the actual safety of the deck plate, as dis-

cussed in Section 6.2.2, and, therefore, the local stress analysis of the deck plate is, as a rule, omitted entirely in the design.

However, should the values of the local stresses be required, they may be obtained by methods indicated in this Section.

Generally, in the range of the working loads, the steel deck plate supported on the longitudinal ribs may be treated as a continuous isotropic plate.

A rigorous analytical determination of the stresses and deflections of the deck plate under wheel loads would be extremely complicated, because of the following factors:

(a) The plate supports at ribs cannot be regarded as "knife-edge" supports, since they have a definite width and may offer restraint against rotation.

This must be recognized, especially in the analysis of the deck plate supported on closed ribs.

(b) The exact magnitude and distribution of the stresses over the supports, where the deck plate is stiffened by welds, is practically impossible to determine analytically.

(c) Even under the design loads, small membrane stresses may occur in the deck plate. Thus the analysis based on the ordinary flexural theory of first order may not be adequate, especially with thin plates.

(d) The ribs acting as supports of the deck plate are not inflexible (see Fig. 4.6a). The elastic flexibility of the ribs will tend to increase the plate stresses between the ribs and decrease the stresses over the ribs.

(e) In an actual bridge deck the stresses and deflections of the deck plate may be considerably reduced by composite action of the deck plate with the wearing surface. The extent of such a composite action may vary and can only be determined experimentally.

With a 2-in. asphalt wearing surface the stress relief in the steel may reach the order of 75% and more at cold temperatures (see Section 8.2.4.1d). Even at high temperatures there may be a considerable composite action of the asphalt with the steel plate under impact loads.

An approximate method of analysis of the deck plate supported by open ribs is given in Section 6.2.1.2.2.

Stresses and deflections of the deck plate supported by closed ribs will be generally lower than those of the plate on open ribs with the same spans.

A discussion of the stresses in the deck plate supported by closed ribs is given in Section 6.2.1.2.3.

6.2.1.2.2 Deck Plate Supported by Open Ribs

(a) Deck plate on rigid supports

For the purposes of an approximate computation, the deck plate supported by open ribs is treated as an

isotropic plate continuous in the x -direction over the ribs acting as simple unyielding supports (Fig. 6.2).

It is assumed first that the applied wheel load, P , is supported by a plate strip having a width of $2c$, equal to the width of the load, distributed over the area $2g \times 2c$. In such a case the bending moments and stresses would occur predominantly in the x -direction and could be approximately computed by continuous beam formulas given in Sections 4.2.2 and 4.2.3.

In the actual case, the plate extends in the y -direction beyond the width of the applied load and the portions of the plate on both sides of the load also participate in the stresses. Thus the critical maximum moment in the x -direction in the 1-in. wide plate strip under the center of the applied load will be smaller in the full plate than in the plate strip of the first case treated as a continuous beam.

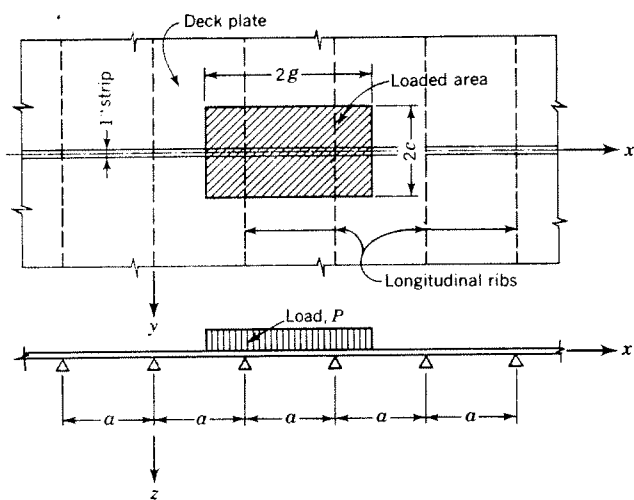


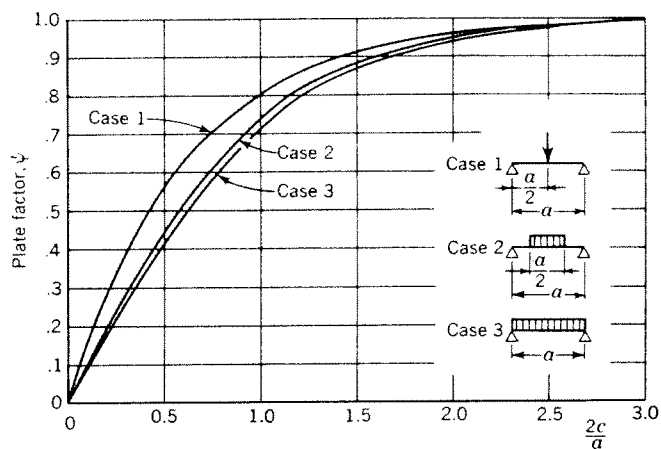
Fig. 6.2. Deck plate supported on open ribs treated as a continuous plate on rigid knife-edge supports

The ratio of the bending moment, M_P , in the x -direction of the full plate, to the corresponding moment, M_B , in the continuous beam, per inch of width, is defined as a plate factor, ψ

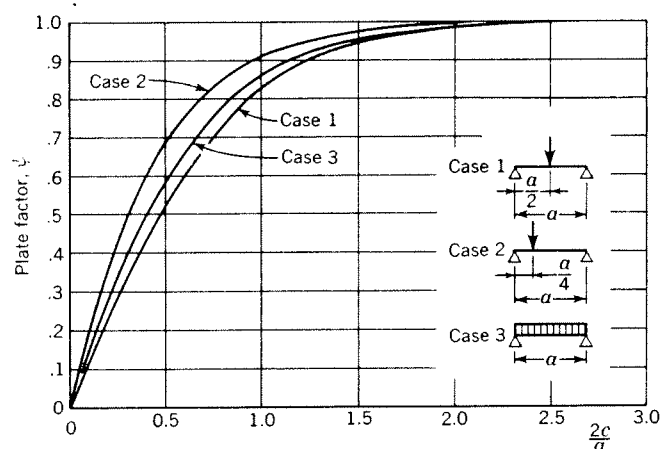
$$\psi = \frac{M_P}{M_B} \quad (6.1)$$

The value of the plate factor, ψ , which is always smaller than one, is independent of the plate thickness and varies with the ratio of the loading width to plate span, $2c/a$, the load distribution in the x -direction and the location of the bending moment computed.

Values of the plate factors, based on computations of the bending moments in a continuous isotropic plate on rigid supports, have been determined by Pelikan and Esslinger [42] for the bending moments at the



(a) Moment at midspan



(b) Moment at support

Notes: $2c$ = length of load in direction of supports.
Plate moment = ψ · moment in a beam.

Fig. 6.3. Plate factors for moments in a continuous isotropic plate [42]

midspan and over the supports of the deck plate and are given in Figure 6.3. The use of these factors is illustrated by numerical examples, Section 6.2.1.3.

In the computation of the maximum bending moments and stresses in the deck plate over the ribs the effect of the local strengthening of the plate by the rib and the welds may be accounted for by using the theoretical value of the moment at the toe of the fillet weld (Fig. 6.4a). Such procedure is justified by the test results (see Section 6.2.1.1.3)

Deflections of the deck plate between the ribs may be determined analytically or graphically by treating a one-inch wide plate strip as a simple beam and applying to it the bending moments computed for the continuous plate, as illustrated by a numerical example in Section 6.2.1.3.1. The plate rigidity, D_P , defined by equation (2.7) should be used in the computation.

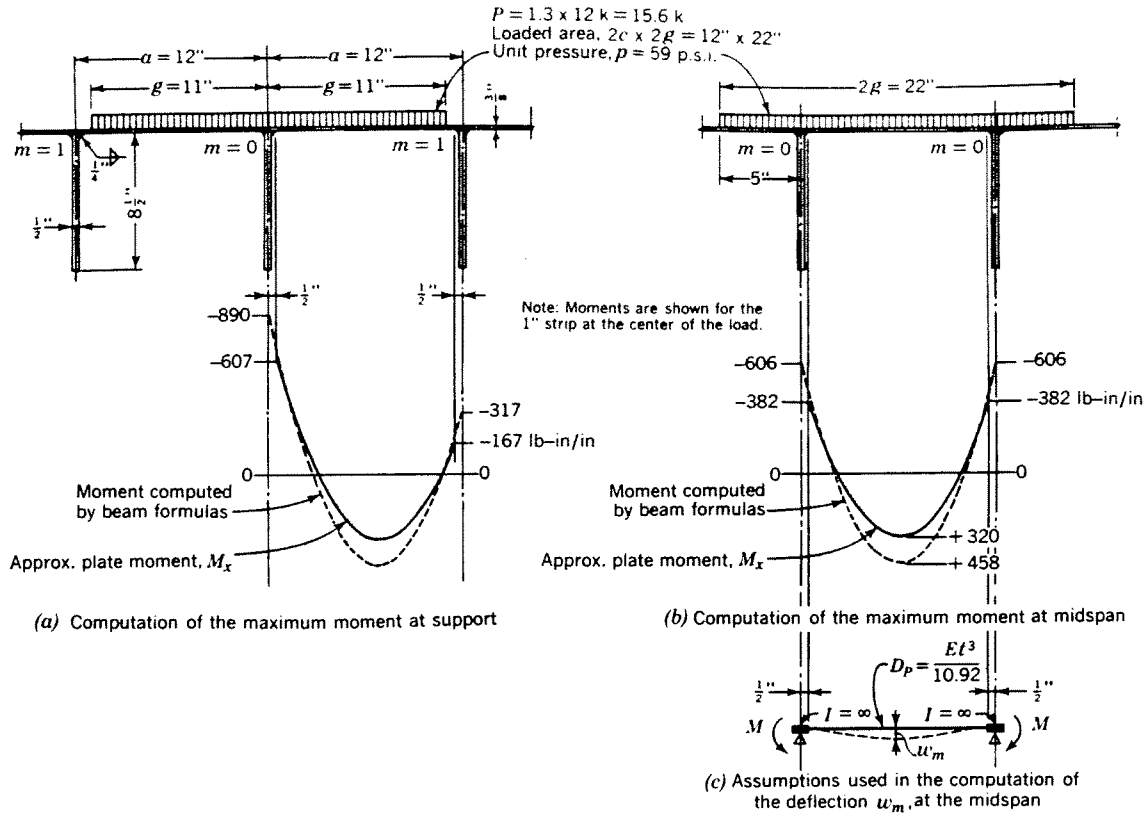


Fig. 6.4. Computation of the bending moments in a deck plate supported by open ribs

(b) *Effects of rib flexibility*

The elastic flexibility of the ribs will tend to decrease the maximum moments over the ribs and increase the moments at the midspan of the plate. However, these effects will be small in the usual cases.

If an analysis of the effects of the rib flexibility on the bending moments in the plate is desired, a method similar to that outlined in Section 4.2.7 may be used.

The limiting values of the relative rigidity coefficients, γ' , indicating the error due to disregarding the rib elasticity, given in Section 4.2.7.3, are also valid in the analysis of the deck plate.

6.2.1.2.3 Deck Plate Supported by Closed Ribs

The local stresses in the deck plate supported by closed ribs may be considered to consist of two parts:

(a) Stresses due to the direct loading of the deck plate supported by inflexible ribs, as shown in Figure 6.5a.

(b) Stresses due to the load transfer from the directly loaded rib to the adjoining ribs in the actual deck system acting as an orthotropic plate, as shown in Figures 3.7, 3.8 and 6.6a.

(a) *Stresses due to direct loading*

Stresses due to direct loading of the deck plate by a distributed wheel load may be obtained by analyzing the system shown in Figure 6.5a, consisting of a continuous isotropic plate rigidly connected to the rib walls which act as rigid frames and provide an elastic restraint of the plate at the points of support. The ribs, carrying their load to the floor beams, are assumed not to deflect under the load, which is indicated by rigid supports under each rib in Figure 6.5a.

For the purpose of determination of the maximum stresses, which will occur in the directly loaded rib, the system may be simplified by replacing the rigid connections of the plate to the adjoining ribs by knife-edge supports and assuming a uniform spacing, a , of these supports, as shown in Figure 6.5b. The use of a symmetrical loading further simplifies the computations.

The structure is first treated as a 1-in. wide frame. The final plate moments in the directly loaded rib are obtained from the frame moments by applying appropriate plate factors, as discussed in Section 6.2.1.2.2.

The system shown in Figure 6.5b is, theoretically, redundant to the infinite degree. However, in the present

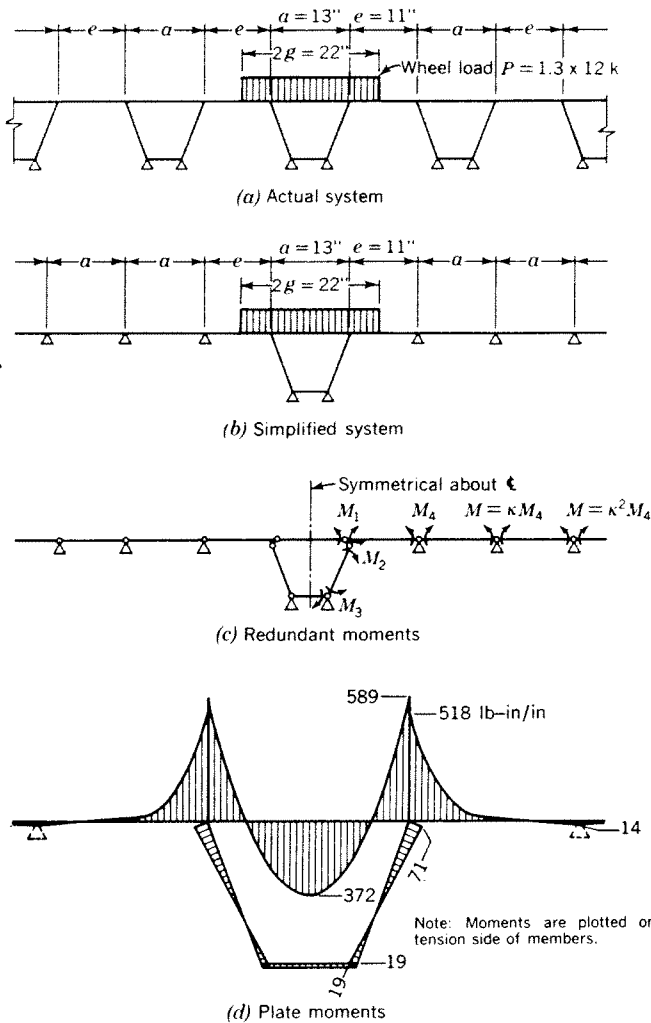


Fig. 6.5. Computation of the bending moments in a deck plate supported by closed ribs. Moments due to direct loading

loading case, the number of the independent redundants reduces to four, designated as M_1 , M_2 , M_3 and M_4 , since the redundant moments in the unloaded portions of the plate may be expressed as a function of the redundant M_4 and the carry-over coefficient, κ (Fig. 6.5c). This is discussed in Section 4.2.1.3.

The four redundant moments, M_1 , M_2 , M_3 and M_4 , are computed by the usual methods of indeterminate structural analysis.

A typical bending moment diagram obtained by the above procedure, with the moment values modified by the appropriate plate factors, is shown in Figure 6.5d.

(b) *Stresses due to transverse shear transfer*

In the actual deck system the ribs are not inflexible, as assumed in the computations under (a), above,

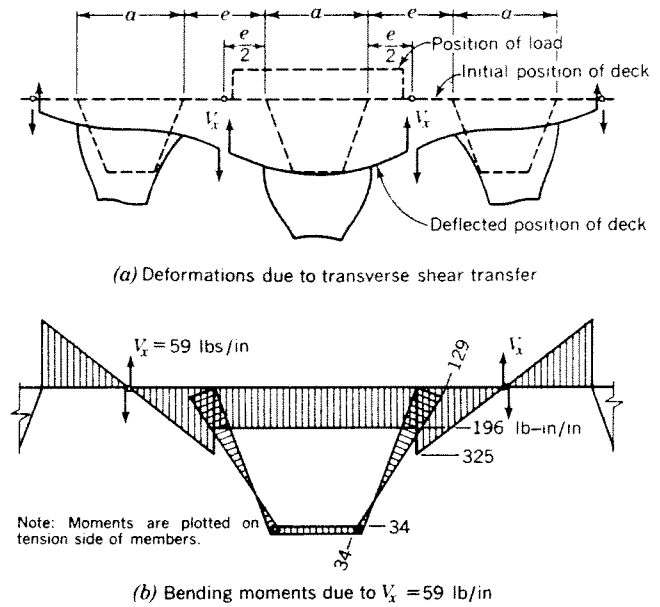


Fig. 6.6 Computation of the bending moments in a deck plate supported by closed ribs. Moments due to transverse shear transfer

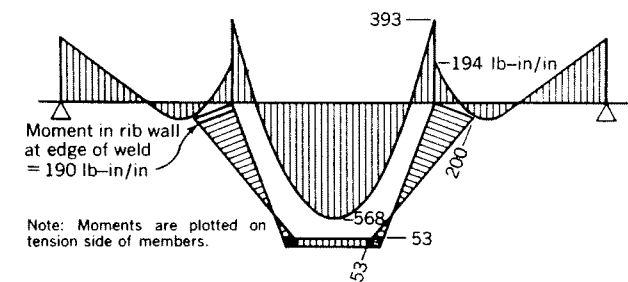


Fig. 6.7. Computation of the bending moments in a deck plate supported by closed ribs. Total bending moments in deck plate in x -direction, obtained by superposition of the effects of direct loading and transverse shear transfer (Figs. 6.5 and 6.6)

but deflect under loads, as shown in Figure 3.7. In addition to the rib directly loaded, the adjacent ribs also deflect and twist, thus participating in the load carrying action. The load transfer from the directly loaded rib to the distant ribs occurs through the transverse shearing forces, V_x , transmitted by the deck plate acting in flexure, as indicated by the wavy line in Figure 3.7. The shearing forces in the deck plate due to the load transfer are indicated near a rib not directly loaded in Figure 3.8a, and, in the deck plate at the rib directly loaded, in Figure 6.6a.

The magnitudes of the shearing forces, V_x , have to be obtained from considerations of the deck plate and the ribs acting as an idealized orthotropic plate with continuously distributed elastic properties, as discussed in Chapters 2, 3 and 4.

However, since the actual deck structure is discontinuous, with the smallest element having a width $a + e$, the shears computed in the idealized system are valid in the actual system only at midpoints between the ribs, as shown in Figure 6.6a.

The general expression for the shear, V_x , in an orthotropic plate is, with $\nu = 0$ (in accordance with equation 2.18)

$$V_x = -D_x \frac{\partial^3 w}{\partial x^3} - 2H \frac{\partial^3 w}{\partial x \partial y^2}$$

In the simplified treatment of the deck as an orthotropic plate the effect of the rigidity, D_x , of the idealized plate is assumed to be negligible in the overall considerations, as discussed in Section 3.2.2. Thus the above equation for shear simplifies to

$$V_x = -2H \frac{\partial^3 w}{\partial x \partial y^2} \quad (6.2)$$

For the wheel load position at the midspan of the rib the previously derived expressions for the bending moment, M_y , in the orthotropic plate may be utilized in computing the value of V_x , as follows:

With $\nu = 0$, the moment M_y is given by equation (2.17) as

$$M_y = -D_y \frac{\partial^2 w}{\partial y^2}$$

Substituting this into equation (6.2) results in

$$V_x = -2H \frac{\partial}{\partial x} \frac{\partial^2 w}{\partial y^2}$$

or

$$V_x = \frac{2H}{D_y} \frac{\partial(M_y)}{\partial x} \quad (6.3)$$

Substituting the expression for M_y at $y = s/2$, for a load at $y = s/2$, (equation 4.46) gives

$$V_x = \frac{2H}{D_y} \frac{\partial}{\partial x} \left(Q_0 s \sum \frac{M_{cn}}{Q_s} \frac{Q_{nx}}{Q_0} \right)$$

For the loading case shown in Figure 6.5a, the expression for the component load, Q_{nx}/Q_0 , is given by equation (3.22). Substituting this into the above expression for V_x results in

$$V_x = \frac{2H}{D_y} \frac{\partial}{\partial x} \left(Q_0 s \sum \frac{M_{cn}}{Q_s} \frac{4}{\pi} \sin \frac{n\pi g}{b} \sin \frac{n\pi}{2} \sin \frac{n\pi x}{b} \right)$$

The term M_{cn}/Q_s , given by equation (4.47), is not a function of x . By differentiation of the above expression the formula for V_x is obtained as

$$V_x = \frac{8Q_0 s H}{b D_y} \sum \frac{M_{cn}}{Q_s} \sin \frac{n\pi g}{b} \sin \frac{n\pi}{2} \cos \frac{n\pi x}{b} \quad (6.4)$$

with designations explained in Chapters 3 and 4.

For the determination of the stresses in the rib directly loaded (Fig. 6.6a), the shear, V_x , is computed by equation (6.4) at the location $x = (b/2) + (a + e)/2$, with the co-ordinate x measured as shown in Figure 3.14.

With the shear, V_x , obtained by equation (6.4), the bending moments in the deck plate and in the rib walls are computed, as shown in Figure 6.6b.

(c) Computation of the total stresses

The total local moments and stresses in the deck plate are obtained by superposition of the effects (a) and (b), as shown in Figure 6.7.

In computation of the stress in the deck plate over the rib wall the value of the bending moment at the face of the weld should be used, similarly as in the case of open ribs (see Section 6.2.1.2.2a).

It should be noted that the local stresses in the x -direction contribute to the stresses in the y -direction in the deck plate and in the rib walls. The stress increment, Δf_y , in the y -direction is, in accordance with Hooke's law in its general form,

$$\Delta f_y = \nu f_x$$

where $\nu = 0.3 =$ Poisson's ratio for steel and $f_x =$ stress in the x -direction.

Thus, the high axial stresses in the bottom of a closed rib may be further increased by the effect of the local stresses. This effect is, however, amply compensated by the conservative assumptions used in the computation of the longitudinal stresses in the ribs, as discussed in Section 2.4.1.3.

6.2.1.3 Numerical Examples of the Deck Plate Analysis

6.2.1.3.1 Deck with Open Ribs

In this example the deck plate of the numerical example given in Section 11.2, Figure 11.2, is analyzed. The plate thickness is $\frac{3}{8}$ in., the $8\frac{1}{2}$ in. \times $\frac{1}{2}$ in. ribs are spaced 12 in. o.c. The plate is loaded by a 12 kip wheel load with loaded area dimensions $2g \times 2c = 22$ in. \times 12 in. (see Section 3.4.2). The unit pressure, p , including the 30% impact factor, is 59 psi.

The deck plate is treated as a continuous plate (see Section 6.2.1.2.2).

(a) Beam moments

The moments in a 1-in. wide beam, loaded as shown in Figure 6.4a are computed by integration of the equations of the influence lines for continuous beams.

Moment at support 0:

By equation (4.6)

$$\begin{aligned}
 M_0 &= 2 \int_{x=0}^{11} \left[-0.5 \left(\frac{x}{a} \right) + 0.866 \left(\frac{x}{a} \right)^2 - \right. \\
 &\quad \left. 0.366 \left(\frac{x}{a} \right)^3 \right] p a dx \\
 &= 2(59)(12)^2 \left[-\frac{0.5}{2} \left(\frac{11}{12} \right)^2 + \frac{0.866}{3} \left(\frac{11}{12} \right)^3 - \right. \\
 &\quad \left. \frac{0.366}{4} \left(\frac{11}{12} \right)^4 \right] \\
 &= -890 \text{ lb-in.}
 \end{aligned}$$

Moment at support 1:

In a similar manner, using equations (4.6) and (4.6a) the moment at support 1, M_1 , is computed as

$$M_1 = -317 \text{ lb-in.}$$

Moment at support 0 at the toe of the weld:

The value of the shear, V_0 , at support 0, necessary in the computation, is obtained as

$$\begin{aligned}
 V_0 &= R_0 + \frac{(-M_0 + M_1)}{a} \\
 &= \frac{(59)(11)(6.5)}{12} + \frac{890 - 317}{12} = 399 \text{ lb}
 \end{aligned}$$

The bending moment at the toe of the weld, at a distance of $\frac{1}{2}$ in. from the center line of the rib is

$$M_T = -890 + (399)(0.5) - \frac{(59)(0.5)^2}{2} = -698 \text{ lb-in.}$$

The moment at midspan, for the loading position as shown in Figure 6.4b, is computed by integration of equations (4.8) and (4.8a), in a similar manner as above, as

$$M_C = +458 \text{ lb-in.}$$

The above bending moments may also be obtained by evaluation of the influence lines, Charts 5a and b.

(b) Plate moments and stresses

For the bending moment at support, the plate factor, ψ , is obtained from Figure 6.3b, Case 3. With the ratio $2c/a = 12/12 = 1.0$, the plate factor is obtained

$$\psi_s = 0.87$$

The maximum stress in the deck plate occurs at the toe of the weld, as discussed in Section 6.2.1.2.2.

The maximum bending moment in the plate at the toe of the weld is computed from the beam moment by equation (6.1) as

$$M_T = 0.87(-698) = -607 \text{ lb-in./in.}$$

With the section modulus of the $\frac{3}{8}$ -in. plate

$$S = \frac{(0.375)^2}{6} = 0.0234 \text{ in.}^3/\text{in.}$$

the maximum stress is obtained as

$$f_{\max} = \frac{607}{0.0234} = 25,940 \text{ psi}$$

For the bending moment at the midspan of the plate, the plate factor is obtained from Figure 6.3a, Case 3

$$\psi_c = 0.70$$

The values of the maximum moment and stress at the midspan of the plate are

$$M_C = 0.70(458) = 320 \text{ lb-in./in.}$$

$$f = \frac{320}{0.0234} = 13,680 \text{ psi}$$

(c) Maximum deflection

The maximum deflection of the plate is computed approximately by applying to a simple beam with a span $a = 12$ in. the computed bending moments shown in Figure 6.4b. The plate rigidity, $D_P = Et^3/10.92$, is used in the computation. The rigidity of the beam at the ribs is assumed to be infinitely large (Fig. 6.4c), to account for the plate stiffening at the supports.

The maximum deflection at the midspan is obtained in this manner as

$$w_c = 0.024 \text{ in.}$$

(d) Effects of rib flexibility

The value of the relative rigidity coefficient, γ' , computed in Section 11.2.1.4.2, is equal to 0.0041. Thus the error due to disregarding the effects of the rib flexibility on the bending moments in the deck plate is smaller than 3%.

6.2.1.3.2 Deck with Closed Ribs

The local stresses are computed for the closed rib system of the numerical example given in Section 11.3.

The dimensions of the system are given in Figures 11.9 and 11.10.

The loading consists of one 12 kip wheel, with a unit pressure $p = 59$ psi, as shown in Figure 6.5a.

The analysis is made in accordance with the outlines given in Section 6.1.2.3.

(a) Effects of direct loading

In computation of the effects of the direct loading, the ribs are considered rigid, as shown in Figure 6.5a.

The simplified system is shown in Figure 6.5b.

The redundant moments shown in Figure 6.5c are

obtained by a statistically indeterminate analysis and are, for a 1-in. wide frame, as follows:

$$\begin{aligned} M_1 &= -701 \text{ lb-in./in.} & M_3 &= +23 \text{ lb-in./in.} \\ M_2 &= -85 \text{ lb-in./in.} & M_4 &= +17 \text{ lb-in./in.} \end{aligned}$$

The moment at the midspan of the deck plate under the load is obtained as

$$M_C = +547 \text{ lb-in./in.}$$

The plate moments are obtained by application of the plate factors, based on the most heavily loaded span, $a = 13$ in. Thus,

$$\frac{2c}{a} = \frac{12}{13} = 0.92$$

From Figure 6.3, Case 3, the plate factors are:

$$\text{For moment at support: } \psi_S = 0.84$$

$$\text{For moment at midspan: } \psi_C = 0.68$$

Thus, the plate moments are:

$$M_1 = -(701)(0.84) = -589 \text{ lb-in./in.}$$

$$M_2 = -(85)(0.84) = -71 \text{ lb-in./in.}$$

$$M_3 = +(23)(0.84) = +19 \text{ lb-in./in.}$$

$$M_4 = +(17)(0.84) = +14 \text{ lb-in./in.}$$

$$M_C = +(547)(0.68) = +372 \text{ lb-in./in.}$$

These moments are shown in Figure 6.5d.

(b) Effects of transverse shear transfer

The shear resulting from the transverse load transfer at the point midway between the loaded rib and the adjacent rib (Fig. 6.6a) is computed by equation (6.4), using the values of M_{Cn}/Q_S given in Table 11.3.2.1.5.

The value of

$$\sum_{n=1}^{35} \frac{M_{Cn}}{Q_S} \sin \frac{n\pi g}{b} \sin \frac{n\pi}{2} \cos \frac{n\pi x}{b}$$

at the location

$$x = \frac{b}{2} + \frac{a + e}{2} = \frac{154}{2} + \frac{13 + 11}{2} = 89 \text{ in.}$$

is computed to be -0.174 .

From equation (6.4), using the parameters computed in Section 11.3

$$V_x = -\frac{(8)(0.709)(180)}{154} (0.051)(0.174) = -0.059 \text{ k/in.}$$

The moments in the deck plate and in the rib walls due to the shears of 59 lbs/in. on both sides (Fig. 6.6b), are computed to be as follows:

$$M_1 = +196 \text{ lb-in./in.} \quad M_2 = -129 \text{ lb-in./in.}$$

$$M_3 = +34 \text{ lb-in./in.}$$

No plate factors are applied to these moments since the shear, V_x , computed by equation (6.4), is obtained from considerations of the deck acting as a plate, as discussed in Section 6.2.1.2.3.

(c) Total moments and stresses

The total moments in the deck plate and in the rib walls are obtained by superposition of the effects (a) and (b), above, as shown in Figure 6.7.

The maximum stress in the $\frac{3}{8}$ -in. deck plate occurs at the midspan of the plate and is

$$f = \frac{M}{S} = \frac{568}{(0.375)^2/6} = \pm 24,200 \text{ psi}$$

The stress in the side wall of the rib at the junction with the deck plate is

$$f = \frac{190}{(0.250)^2/6} = \pm 18,200 \text{ psi}$$

and at the bottom of the rib

$$f = \frac{53}{(0.250)^2/6} = \pm 5090 \text{ psi}$$

The stress increments in the y -direction due to the stresses in the plate in the x -direction are, with Poisson's ratio for steel $\nu = 0.3$:

$$\text{In the deck plate: } \Delta f_y = \pm (0.3)(24,200) = \pm 7250 \text{ psi}$$

$$\text{In the bottom of rib: } \Delta f_y = \pm (0.3)(5090) = \pm 1530 \text{ psi}$$

6.2.2 Deck Plate Subjected to Large Loads

6.2.2.1 General

For the purposes of this discussion, "large loads" are defined as those loads under which the stresses in the deck plate computed in accordance with the ordinary plate theory of the first order exceed the normally allowed limits.

Tests on steel deck plates subject to static concentrated loads have established the fact that under increasing loads the elastic behavior of the plate, evidenced by the lack of permanent deformations after unloading, extends considerably beyond the limits predicted by the ordinary flexural theory [29, 30, 31, 34].

As the loads and the deflections increase, membrane stresses develop in the plate, causing horizontal reactions at the supports and internal compressive stresses in the portions of the plate adjoining the loaded area. At higher stages of loading, plastic hinges form over the supports and the flexural stresses are almost entirely replaced by membrane stresses. In spite of the plastic

conditions at the critical locations of the plate, the deflections are limited because of the restraining effect of the adjoining unloaded portions of the plate. In the final stage of loading the strain hardening phase is observed in the plate. Thus the full tensile strength of the material is developed before rupture occurs at the ultimate load.

6.2.2.2 Ultimate Load Test on a Deck Plate

Results of a full scale loading test [30, 76] of a 3/8-in. thick deck plate supported on ribs spaced 12 in. o.c. are shown in Figure 6.8.

In this test a wheel load was simulated by two loaded areas straddling the rib (Fig. 6.8a). After the total load reached 122 metric tons, only the area on the left side of the center rib continued to be loaded until the ultimate load was reached. The deck plate was made of St 37 steel, corresponding roughly to the American A7 carbon structural steel.

The load-deflection diagram of the test is shown in Figure 6.8b. The behavior of the test specimen was fully elastic, with no measurable permanent deflections, until the load of 32.5 metric tons was exceeded, corresponding to 3.25 times the German standard design wheel load. In the range between 32.5 and 75 tons the load-deflection curve is flatter, indicating plasticity in the plate. The deflection increments under loads larger than 75 tons are again smaller,

which is attributed to the strain-hardening effects in the plate. The ultimate capacity of the plate was reached at the load $P/2 = 276/2$ tons.

Thus, with the design load P of 10 tons, the safety against rupture was $276/10 = 27.6$.

If the system shown in Figure 6.8a is analyzed as a continuous isotropic plate, as discussed in Sections 6.2.1.2.2 and 6.2.1.3.1, a theoretical "allowable load" of about 5.3 metric tons is obtained if the allowable stress of 1600 kg/cm² or 22.7 ksi should not be exceeded at the toe of the weld (see Fig. 6.1b). The load of 32.5 tons, which, according to the test, caused no permanent deformation of the plate, would, by the above analysis, correspond to a stress of 136 ksi, which by far exceeds the ultimate strength of the material.

It is seen that the analysis of the deck plate in accordance with the first order plate theory is entirely inappropriate and misleading if the loads exceed the usual limits.

It is also obvious that the stresses in the plate under the working loads cannot be used to judge the ultimate static strength and the actual factor of safety of the plate.

6.2.2.3 Effects of Axial Prestress and Initial Dishing of the Plate

Theoretical and experimental investigations conducted by Kloeppe [30] indicate that in the elastic range (see Fig. 6.8b) the stresses and deflections of a

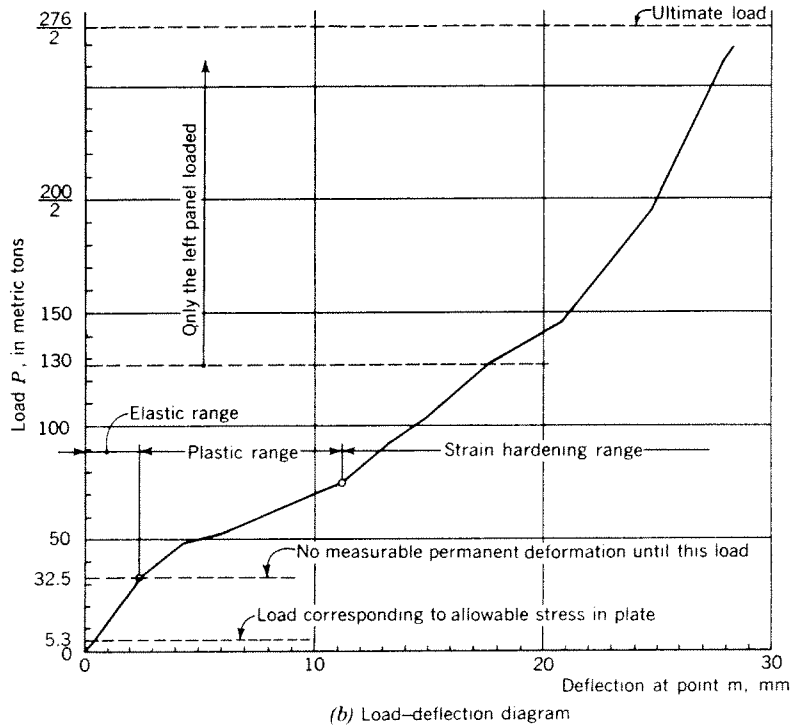
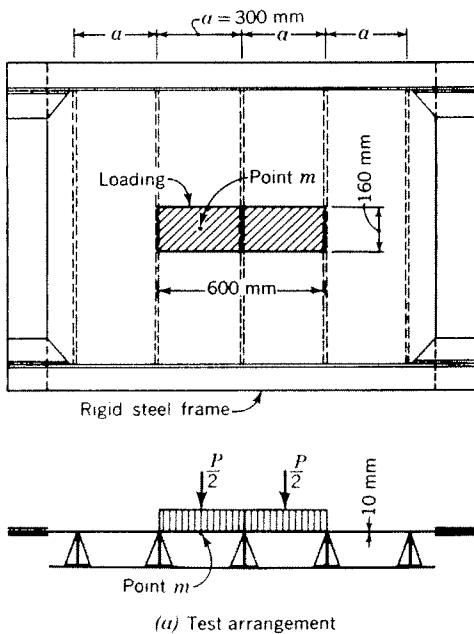


Fig. 6.8. Ultimate load test on a steel deck plate [30, 76]

steel plate acting in combined flexure and tension may be considerably affected by axial prestress and initial dishing of the plate.

The effect of a tensile prestressing force, H , on the deflection of a loaded slender flat bar made of carbon structural steel St 37 is shown in Figure 6.9. It is seen that prestressing considerably reduces the deflections under a given vertical load.

It should be noted that in a steel plate deck a prestress in the deck plate may develop as a result of the transverse contraction of the fillet welds connecting the deck plate and the ribs. Such residual stresses due to weld shrinkage up to 5000 psi have been observed in the deck plates [30].

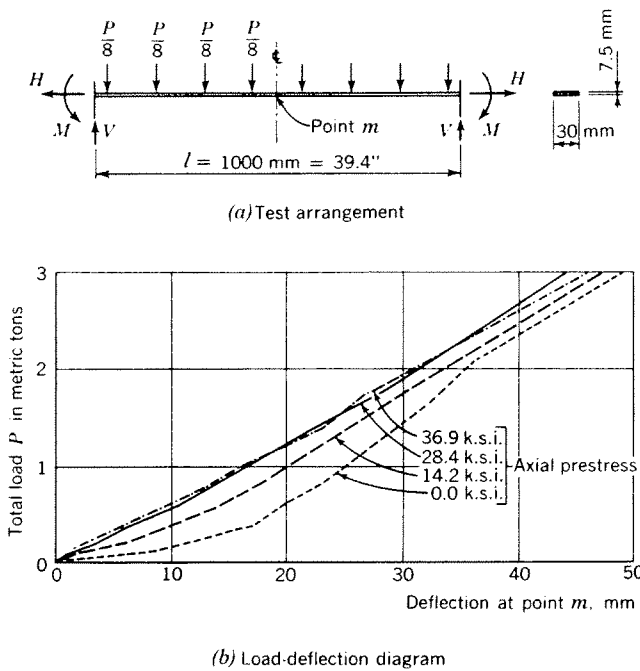


Fig. 6.9. Effect of axial prestress on deflection of a slender flat bar [30]

Initial dishing of the deck plate between the ribs tends to reduce both the stresses and the deflections of the plate.

The effects of the initial dishing of a slender flat bar, obtained by computation, are shown in Figure 6.10.

Figure 6.10a shows that even a small initial deflection of less than $\frac{1}{300}$ of the span may markedly decrease the deflection under an applied load. An initial dishing of the order of 5% of the span stiffens the system considerably.

Pre-dishing of the plate also increases the load under which the design stress or the yield stress in the plate is attained, as shown in Figure 6.10b.

Unintended dishing of the deck plate may occur as

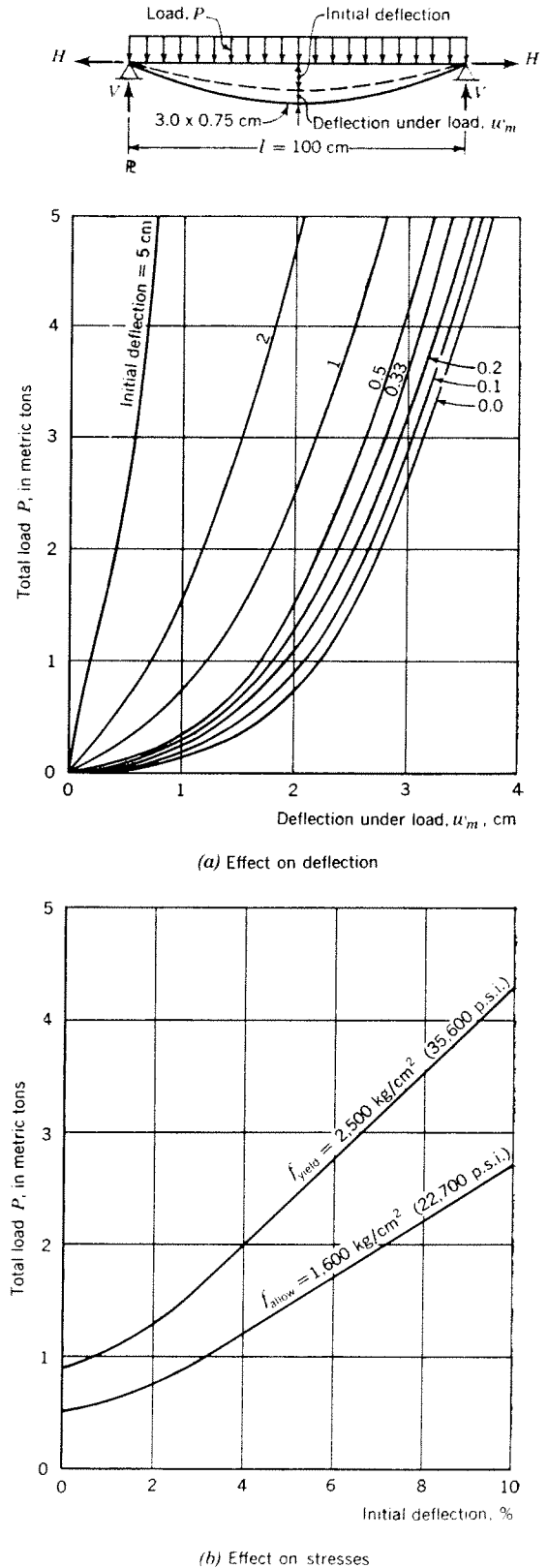


Fig. 6.10. Effects of initial deflection of a slender flat bar on deflection and stresses (computed values) [30]

a result of warpage of the deck structure due to weld shrinkage.

An intentional application of prestressing and pre-dishing in the fabrication of steel plate decks may offer interesting possibilities, if the design is governed by deflections under working loads.

It should be noted, however, that prestressing and initial curvature have no effect on the ultimate strength of the plate.

6.2.3 Fatigue Strength of the Deck Plate

6.2.3.1 Fatigue Tests

Tests to determine the strength of the deck plate under the effects of pulsating concentrated loads were conducted at the Technological University in Darmstadt [31].

The arrangement of Tests 1 and 2 was the same as used in the static tests of the deck plate, Figure 6.1a. Thus, in addition to the local stresses (System III), the deck plate tested was also subjected to the tensile longitudinal prestress in the y -direction, simulating the System I stresses, and to the System II stresses, as the flange of the ribs and the floor beams.

Tests 3 and 4 were made on smaller deck panels, without longitudinal prestress.

The dimensions of the test models, having a reduction ratio of 2.5, corresponded to a 10.6-mm ($\frac{7}{16}$ -in.) deck plate supported by 1 in. thick longitudinal ribs spaced 300 mm (11.8 in.) o.c. and floor beams spaced 1000 mm (39.4 in.) o.c. The loaded area of the model, corresponding to a 21.6-in. \times 8-in. gross contact area, was intended to simulate the standard wheel of the German design specification, without allowance for the load distribution through a wearing surface.

Since the model dimensions and the loaded area dimensions are reduced in the same proportion, the stresses measured in the deck plate of the model are the same as would occur in a full-scale deck under the same unit pressure of the applied load.

The load was applied by means of a pulsator, with a frequency of 220 load cycles per minute in Tests 1 and 2, and 1800 cycles per minute in Tests 3 and 4.

The test results, with the unit pressures under the applied loading expressed in psi are given in Table 6.2.3.1.

A comparison of the test loads to the actual wheel loads acting on deck plates may be expressed by the ratio of the upper values of the unit pressures used in the tests and the pressure under the standard 12 kip wheel of the AASHO specifications (59 psi, including 30% impact, see Section 6.2.1.3.1), which ranged from 3.3 to 7.8. However, it should be noted that if the test pressures were applied to the design loaded area

TABLE 6.2.3.1
FATIGUE TESTS ON STEEL DECK PLATE

(Test arrangement as shown in Figure 6.1)

Test No.	Unit Pressure of Applied Pulsating Loading (psi)		No. of Load Cycles	Remarks
	From	To		
1	18	195	2.2×10^6	Test discontinued with no crack apparent
2	18	311	6.75×10^6	Test made after completion of Test 1 on the same specimen. Visible crack at 6.75×10^6 cycles
3a	80	240	5×10^6	Test discontinued with no crack apparent
3b	80	300	5×10^6	Test continued on the same specimen. No crack apparent
3c	107	461	2.2×10^6	Test continued on the same specimen. Crack along longitudinal rib at 2.2×10^6 cycles
4	226	338	6.88×10^6	Visible crack at 6.75×10^6 cycles. Failure at 6.88×10^6 cycles

of the 12 kip AASHO wheel of 22 in. \times 12 in. (see Section 3.4.2.2), which is larger than the equivalent full-scale loaded area of the tests of 21.6 in. \times 8 in., all other conditions being equal, the maximum stress in the deck plate would be about 20% higher.

Strain measurements for the purpose of computation of the stresses in the deck plate were made in Tests 1, 2 and 4. In Test 1 a drop of the residual stresses in the deck plate was observed under the action of the pulsating loading.

Because of the limited number of the strain gages used in the fatigue tests, the stresses in the deck plate could be only approximately determined. In Test 2 the maximum principal tensile stress in the top fiber of the plate above the toe of the weld, where the crack occurred, was found to be greater than 45 ksi. The yield point stress of the thin carbon steel deck plate, obtained by tensile test of the specimen, was determined to be 47.5 ksi. Thus the fatigue strength of the deck plate was, in this case, approximately equal to the yield point stress.

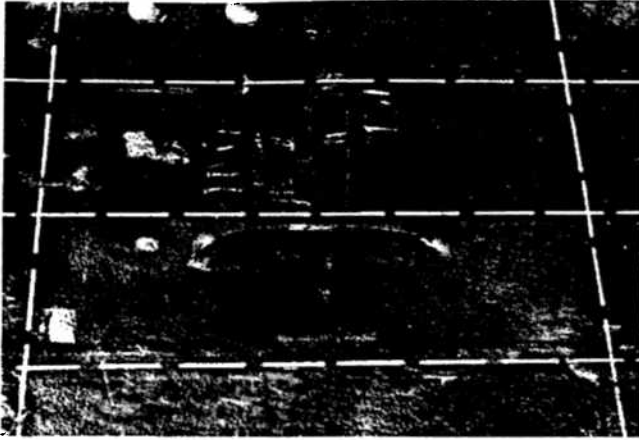


Fig. 6.11. Fatigue tests on steel deck plate [31]. Fatigue rupture of deck plate in Test 3c (See Table 6.2.3.1)

The fatigue rupture of the deck plate in Test 3 is shown in Figure 6.11.

6.2.3.2 Discussion of the Factors Affecting the Fatigue Strength of the Deck Plate

The fatigue strength of the deck plate of the model test described above was found to be very high.

This is partly explained by the fact that at the critical section of the deck plate at the rib, where fatigue cracks occurred, the weld is located on the compressive side of the plate. Thus the local stress concentrations, occurring at the toe of the weld, could not affect the maximum tensile stress in the top fibers of the deck plate.

Another factor contributing to the high fatigue strength is seen in the rapid decrease of the stress in the direction of the depth of the critical cross section of the thin deck plate and in the relatively large elasticity of the deck plate [31].

The results of the model tests may be used as an indication of the probable fatigue behavior of full-scale steel decks of similar geometric proportions and material properties, under similar loading conditions.

In comparing the test model with the actual deck designs, the high mechanical properties of the carbon steel plate used in the test may be reasonably expected to be matched or exceeded by low-alloy steel plate commonly used in the design of the decks, which has an additional advantage of a higher resistance to corrosion.

While no fatigue test results are available for the decks with closed ribs, it may be assumed that the fatigue behavior of the deck plate in this system is essentially similar to that of the deck supported by open ribs, since the maximum local stresses in the deck plate under the working loads are of the same order

if geometric conditions are similar (see Section 6.2.1.3).

In evaluating the results of the tests it is seen that the values of the pressures under the loads causing fatigue failure of the plate (Table 6.2.3.1) exceed by far the unit pressures of the standard truck wheels used in the design of the bridge decks (see Section 3.4.2.2).

It should be noted that even under the heaviest tires of special vehicles, the actual contact pressures normally do not exceed 80–100 psi, because of the limitations of the tire inflation pressures. The highest contact pressure practically possible with the existing equipment would occur under special earth compactor tires and may reach the order of 130 psi, which is still considerably below the pressures used in the tests. Moreover, the actual pressures on the steel deck would be lower, because of the load distributing action of the wearing surface.

Since the stresses in the deck plate, with rib spacing and wheel dimensions of the common order, depend directly on the contact pressure under load, as already mentioned in Section 6.2.3.1, the design wheel loads appear to be far from causing conditions leading to a fatigue failure of the deck plate of low-alloy steel with the usual minimum thickness of $\frac{7}{16}$ in. or $\frac{3}{8}$ in.

This view is further supported by the following observations:

(a) Pulsating loads causing maximum stresses below the critical level do not seem to affect the fatigue strength of the plate [31].

It should be noted that a realistic judgment of the danger of fatigue should be based not on the maximum loads, but on the average actual loads to which any particular panel of the deck plating may be subjected. The actual bridge loading, which may include occasional to frequent design loads and even some loads exceeding the design limits, will probably consist predominantly of lighter loads, which will not affect the fatigue life of the plate.

It is also unlikely that all, or even the majority, of the wheel loads will exert the full additional impact load of 30%.

(b) The actual stresses in the steel deck plate are likely to be smaller than the computed values, as a result of the composite action of the plate with the wearing surface, as discussed in Section 6.2.1.2.1e.

(c) It should be noted that if a fatigue crack in the deck plate develops, it occurs in the direction of the rib (Fig. 6.11), which is the longitudinal direction of the bridge.

Thus a fatigue crack does not endanger the deck acting as the top flange of the main girders and its effects are purely local. Such a crack in the deck plate may be repaired by welding.

6.2.3.3 Conclusion

Based on the above discussion of the fatigue behavior of the steel bridge deck plate and on the satisfactory performance of the steel plate decks of the existing bridges the conclusion may be reached that, under normal loading conditions and with the usual rib spacings and deck plate thicknesses (see Chapter 7), fatigue of the deck plate of low-alloy steel should not be regarded a critical design factor.

6.3 EMPIRICAL FORMULAS FOR THE DESIGN OF STEEL DECK PLATES

6.3.1 AISC Formulas for the Deck Plate of Battle-deck Bridge Floors

Empirical formulas for the design of steel deck plate subject to standard wheel loads are given in reference [2].

The plate thickness is determined by the maximum flexural stress at the midspan of the deck plate between the stringers (Fig. 1.3).

For the deck plate of structural carbon steel, a 40% increase of the allowable stress was recommended, resulting in a design stress of 28,000 psi.

The AISC formulas are meaningful only for the deck plate supported on wide-flange beam stringers (see Section 6.2.1.1.2), and are not applicable to the plate supported by open or closed ribs of the type shown in Figure 1.2.

6.3.2 Formula for the Plate Thickness Based on Allowable Deflection

A formula for an approximate determination of the thickness of the deck plate based on a specified deflection of the plate under a wheel load was proposed by Kloepfel [30, 31].

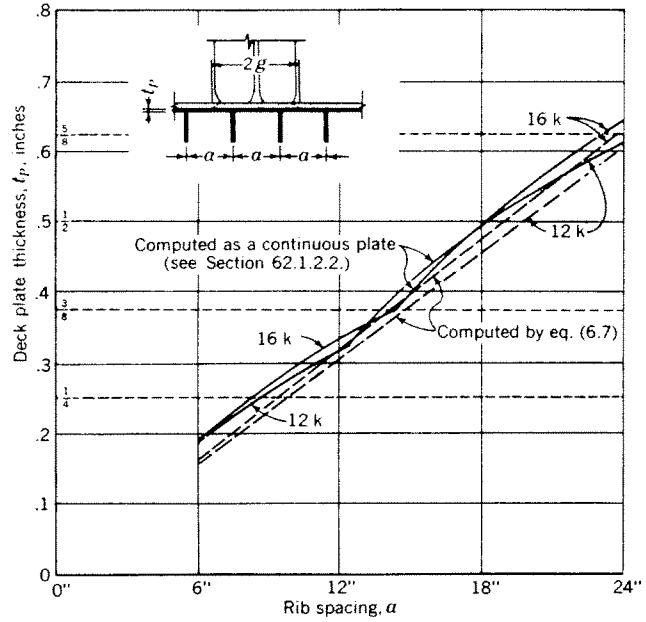
In accordance with this semi-empirical formula the maximum deflection, w_m , of the deck plate at the midspan between the ribs, under a wheel load extending over the full span of the plate, equals the deflection of a fixed beam of the same span and thickness subject to the same unit loading times a factor of $\frac{5}{6}$.

Thus the deflection of the plate is expressed as

$$w_m = \frac{5}{6} \frac{1}{384} \frac{pa^4}{EI} \tag{6.5}$$

where

- w_m = maximum deflection of the deck plate under a wheel load
- p = wheel load unit pressure
- a = rib spacing
- I = $t_p^3/12$, with t_p = plate thickness



Note: AASHTO wheel loads and dimensions are used as follows:
 12 k wheel: $P = 12 \times 1.3 = 15.6$ k, loaded area = 12" x 22"
 16 k wheel: $P = 16 \times 1.3 = 20.8$ k, loaded area = 12" x 26"

Fig. 6.12. Deck plate thickness required for a deflection $w_m = (1/300) \times$ plate span

The deck deflections computed by formula (6.5) are in a fair agreement with the test measurements made [30]. However, the range of the tests is probably too limited for a complete verification.

If the deflection of the deck plate should not exceed $\frac{1}{300}$ of the spacing of the deck plate supports (i.e., the open ribs, or the side walls of the closed ribs), the following condition is obtained

$$w_m = \frac{5}{6} \left(\frac{12}{384} \right) \left(\frac{pa^4}{Et_p^3} \right) \leq \frac{a}{300}$$

and hence

$$t_p \geq a \sqrt[3]{\frac{125}{16} \left(\frac{p}{E} \right)} \tag{6.6}$$

With $E = 29 \times 10^6$ psi, the approximate formula for the plate thickness is obtained as

$$t_p \geq 0.0065a \sqrt[3]{p} \tag{6.7}$$

The unit pressures, p , under the standard AASHTO wheel loads, including 30% impact, are 59 psi and 67 psi, respectively, for the 12 kip and 16 kip wheels (see Section 3.4.2).

Deck plate thicknesses obtained by equation (6.7) with the above wheel load pressures are shown for the various rib spacings in Figure 6.12.

For comparison, the thickness obtained from deflections computed under an assumption of a continuous

deck plate and with the actual wheel dimensions, as illustrated in the numerical example, Section 6.2.1.3.1, are also plotted.

It is seen that the values obtained from the semi-empirical formula (6.7) are somewhat smaller than those computed analytically, with the simplifying assumptions discussed in Section 6.2.1.2.2.

While a rigorous determination of the deck plate deflections presents great difficulties, it is believed that the values of the minimum deck thickness, t_P , based on the deflection ratio of $a/300$, may be computed conservatively by formula (6.7a) given below, obtained by a small modification of the numerical coefficient in equation (6.7)

$$t_P \geq 0.007a\sqrt[3]{p} \quad (6.7a)$$

It should be noted that the condition of a constant deflection ratio of the deck corresponds, with the constant unit load extending over the entire span of the deck plate between the ribs, to an approximately constant value of the stresses in the plate, for any deck plate span. Thus, in a deck with open ribs, the maximum theoretical stress in the deck plate having a thickness determined by formula (6.7a), computed in accordance with the assumptions used in Section 6.2.1.3.1 will be of the order of 33 to 35 ksi. The computed stresses in the actual designs will usually be lower because the plate thickness is rounded to the next higher standard size.

Composite action of the wearing surface with the steel plate will tend to further decrease the actual deck deflections and stresses, see Section 6.2.1.2.1e.

6.3.3 Formula for Ultimate Capacity of the Plate

A formula for the ultimate strength of the deck plate, based on the behavior of a flat bar, has been obtained by Kloepfel [30] as follows:

Tests have shown that a flat steel bar, fixed at both ends and loaded with a uniformly distributed load, p , per unit length (Fig. 6.9), acts at failure as a cable, with the load carried by axial stresses only, sustained by the reactions at supports. The total elongation at failure was found to be approximately equal to the elongation at maximum load in a tensile load test of a specimen of equal length.

For a bar of a span a and a cross section A acting as a cable, the following relationship is true:

$$H = \frac{p a^2}{8w_m} \quad (6.8)$$

where

- H = horizontal reaction at supports
- p = loading, per unit length of bar
- w_m = maximum deflection at midspan

The total elongation, Δa , may be approximately expressed as

$$\Delta a \cong \frac{8}{3} \frac{w_m^2}{a} \quad (6.9)$$

The unit elongation, ϵ , may then be given as

$$\epsilon = \frac{\Delta a}{a} = \frac{8}{3} \frac{p^2 a^2}{64H^2} = \frac{1}{24} \frac{p^2 a^2}{H^2} \quad (6.10)$$

With the ultimate value of the horizontal reaction, H_u , expressed as a function of the known ultimate tensile stress, f_u , of the material

$$H_u \cong F_u A \quad (6.11)$$

equation (6.10) becomes

$$\epsilon_u = \frac{1}{24} \left(\frac{p a}{f_u A} \right)^2 \quad (6.12)$$

Hence, the ultimate load on bar is obtained as

$$p_u = \frac{4.9 f_u A}{a} \sqrt{\epsilon_u} \quad (6.13)$$

The value of ϵ_u in the above equation may be set equal to the ultimate unit elongation at maximum load, obtained from the tensile ultimate load test of a specimen of the same length. For the carbon steel bars of the above tests the value of ϵ_u thus obtained was 14%.

The ultimate loading capacity of a plate with a uniformly distributed load extending only over a portion of the width of the plate (Fig. 6.2) is, obviously, greater than that of a bar loaded over its full width. For the bridge decks and wheel loads of the average proportions an empirical correction coefficient, $k = 1.25$, based on the test shown in Figure 6.7 has been proposed by Kloepfel.

Thus, the formula for the ultimate uniform load, p_u , of a deck plate loaded over its entire span between the longitudinal ribs, obtained from equation (6.13), is

$$p_u = 1.25 \frac{4.9 f_u t}{a} \sqrt{\epsilon_u} \quad (6.14)$$

where

- p_u = ultimate loading, psi
- t = plate thickness, in.
- f_u = ultimate tensile strength, psi
- a = longitudinal rib spacing, in.
- ϵ_u = ultimate elongation of the material, corresponding to the stress, f_u

A further experimental verification of this formula is desirable.

6.4 SUMMARY AND CONCLUSIONS

The deck plate of a steel plate deck bridge, acting locally in transmitting the wheel loads to the longitudinal ribs, behaves under the design loads as a continuous isotropic plate.

However, under loads exceeding the usual design loads *membrane stresses* occur in the plate and the stress increments are no longer proportional to the loads.

The *ultimate load* of the deck plate, near which the plate acts, practically, as a membrane, is very large and reaches the order of 15–20 times the ultimate load computed in accordance with the ordinary flexural plate theory. Thus the bridge deck plate possesses an ample local overload capacity.

Since the relationship between the loads and stresses

under higher loads is non-linear, the *local stresses* in the deck plate under the design loads cannot be used as a measure of the actual strength of the deck. Therefore the computation of the local stresses in the deck plate is usually not required.

The *fatigue strength* of the deck plate subjected to pulsating loads has been found to be high. Therefore, fatigue of low-alloy deck plate of usual proportions subjected to the standard wheel loads is not considered a critical design factor.

The minimum thickness of the deck plate may be determined by the allowable deflection of the deck plate under the wheel. Formula for the deck plate thickness based on a plate deflection of $\frac{1}{300}$ of the rib spacing is given in Section 6.3.2.

CHAPTER 7

Construction Details

7.1 CONSTRUCTION ELEMENTS

7.1.1 Open Ribs

7.1.1.1 General

In the open rib deck system flat bars, bulb sections, angles and split I-beam sections have been used, as shown in Figure 7.1.

The flat bars and the bulb sections (Fig. 7.1a and c) are most frequently used. The deep and slender rib sections of this type may have to be investigated for elastic stability (see Appendix II).

As a rule, the ribs are arranged in the longitudinal direction of the bridge and run continuously through slots in the transverse floor beams.

Because of the high flexural stresses in the ribs, which are superimposed on System I stresses, low-alloy structural steel is usually required. However, the use of the heat-treated high-strength constructional steels does not seem to be warranted, since it may result in excessive deflections of the ribs.

7.1.1.2 Evaluation of the Open Rib System

The open ribs are simple to fabricate and may be easily spliced in the field. The rib depth and thickness may be varied as required in the various parts of the bridge deck. All rib surfaces and the bottom of the deck plate are accessible for inspection and maintenance during the lifetime of the structure.

The disadvantages of the open rib system are in its small wheel load distribution capacity in the transverse direction and in a relatively close floor beam spacing required with the flat bar ribs of the usual depths. The T-section ribs, which have to be spaced farther apart, require a heavier deck plate. Thus the weight of steel per sq ft of deck is usually considerably higher in the open than in the closed rib system (see Fig. 7.2).

It should also be noted that the total length of welds required in the fabrication of the deck with open ribs is about twice as large as in the deck with closed ribs.

7.1.1.3 Optimum Spacing and Span

The rib spacing is governed by the strength and the deflections of the deck plate and is determined by the criteria discussed in Chapter 6.

The choice of the rib span may depend on such diverse factors as the type of rib, type of steel, loading, the span and rigidity of the floor beams, ratio of the System II stresses to System I stresses in the ribs, design stresses used, fabrication and erection methods, etc. Therefore an analytical determination of the optimum floor beam spacing, as attempted in [17], does not seem to be practical. The floor beam spacing to be used in each particular case is best decided by comparative weight and fabrication cost estimates for the various alternatives.

Generally, the floor beam spacing should be larger if the span between the main girders is large, and smaller if the floor beam span is relatively short.

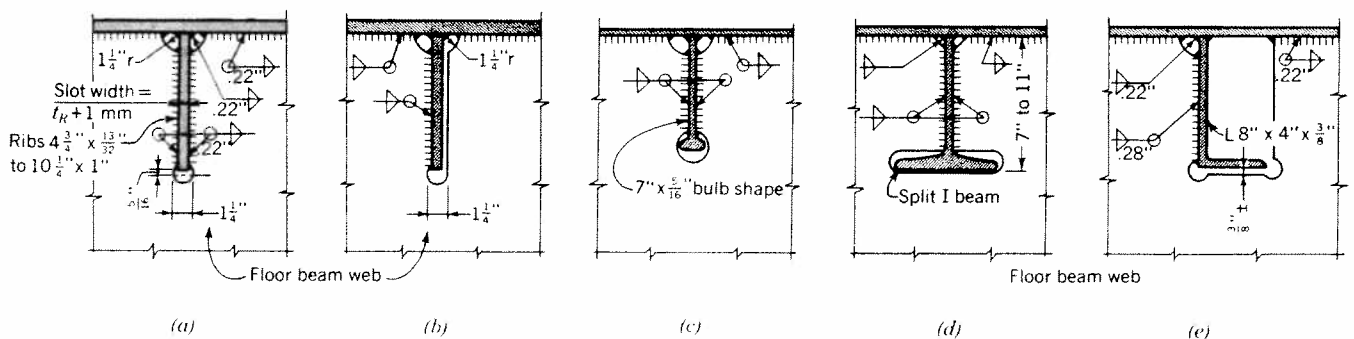
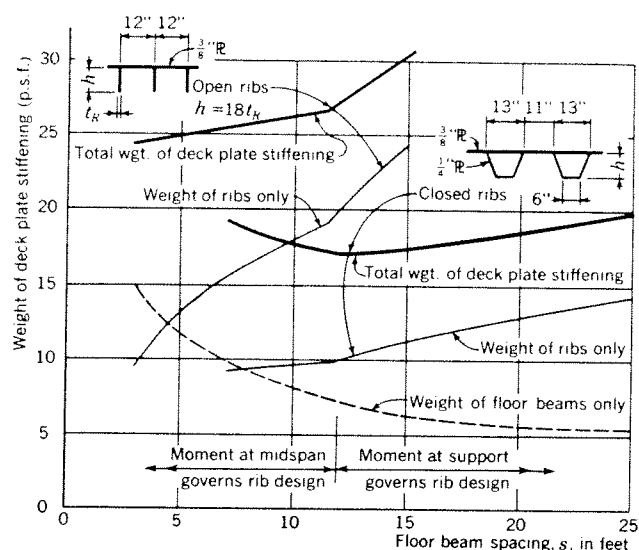


Fig. 7.1. Typical open rib cross sections: (a) Save River Bridge [42, 76], see Fig. 1.8. (b) Possible arrangement, minimizing residual welding stresses. (c) Cologne-Meulheim Bridge [74, 80], see Fig. 1.21. (d) Duesseldorf-Neuss Bridge [68, 78], see Fig. 1.10. (e) Duesseldorf-North Bridge [59, 73], see Fig. 1.15



Note: The weight of stiffening includes the ribs and the floor beams.
The weight of the deck plate is not included.

Design conditions:

- (1). Material: low alloy structural steel except as noted under (7).
- (2). Loading application: see Section 3.4.2.
- (3). Design stresses:
Max. local stress in ribs (System II) 17.0 k.s.i.
Max. stress in low alloy floor beams 27.0 k.s.i.
- (4). Floor beam span 50'-0".
- (5). Deck plate and rib sizes as shown.
- (6). Floor beams spaced more than 9'-0" o.c. are of the type shown in Figs. 11.9 and 11.10(c).
- (7). Floor beams spaced less than 9'-0" o.c. are of two types:
(a). Heavy floor beams of low-alloy steel, spaced 21 to 28 ft. o.c., Fig. 11.3(d).
(b). Intermediate floor beams of carbon steel, Fig. 11.3(c).

Fig. 7.2. Weight of deck plate stiffening of a bridge deck 50 ft wide between girders, AASHO loading, as a function of floor beam spacing

The spans of the open ribs of the existing steel plate deck bridges in Europe, governed primarily by the material economy, do not exceed 7 ft. It is likely that the upper economical span limit for open ribs will be higher in American practice.

If longer rib spans are used, their deflections under the wheel loads may have to be investigated.

The relationship between the weight of the deck stiffening members (longitudinal ribs and floor beams, not including the deck plate) and the floor beam spacing for the specific case of the bridge treated in the numerical examples of Chapter 11 is shown in Figure 7.2. The weights of the ribs and floor beams shown in this figure are based on the following assumptions: the ribs are flat bars; the deck plate is $\frac{3}{8}$ in. thick; the 50-ft long floor beams also serve as erection supports for the deck plating, as shown in Figures 11.2 and 11.9; the material is low-alloy steel, except for the intermediate floor beams spaced closer than 9 ft o.c., which are of carbon steel. The maximum local stress in the longitudinal ribs under the AASHO wheel loads is equal to 17 ksi.

Figure 7.2 also includes the weights of the closed rib system with trapezoidal ribs.

While the curves shown in Figure 7.2 are valid only for the conditions under which they were derived, the weight data for other structural conditions would indicate similar trends.

It is seen that the total weight curve does not increase very sharply with increasing rib spans. Thus the floor beam spacing may depend to a considerable degree on the economy of fabrication.

7.1.2 Closed Ribs

7.1.2.1 Types of Closed Ribs

The most often used *trapezoidal* rib section is shown in Figure 7.3a. The rib width at the top, a , and the deck plate span between the ribs, e , are determined by the strength of the deck plate (see Chapter 6). The trapezoidal cross section possesses considerable torsional rigidity, resulting in a good transverse load distributing capacity of the deck, as discussed in Chapter 3.

The rib type with a *rounded* bottom (Fig. 7.3b) has the advantage of avoiding the sharp bends which may cause overstraining of the plate material during fabrication. However the effective torsional rigidity of the ribs with rounded bottoms is much smaller than that of the trapezoidal ribs.

Figure 7.3c represents a compromise solution. The torsional rigidity of this type of rib lies between types (a) and (b).

Triangular ribs have also been used, with or without additional inverted T-sections to increase their flexural rigidity (see Fig. 7.3d and e).

The closed ribs of the European steel plate deck bridges are, as a rule, cut at the floor beams and butt-welded to the floor beam webs, as shown in Figures 7.3a and b. However, the continuity of the ribs through the cutouts in the floor beam webs (Fig. 7.3c) is much to be preferred, especially in the portions of the deck subjected to tension.

The rib thickness varies from $\frac{3}{16}$ in. to $\frac{5}{16}$ in. Since the box rib sections are welded air-tight, no corrosion is expected in the interior of the ribs. This is discussed in Section 7.4.

The load distributing capacity of the deck with closed ribs will be considerably increased by additional *stiffening diaphragms* between the ribs, as shown in Figure 7.4. However, because of the additional cost of fabrication, the economy of such a construction in American practice is doubtful.

The ribs are arranged, as a rule, in the longitudinal direction of the bridge. Such an arrangement has the advantage of utilizing the cross-sectional area of the

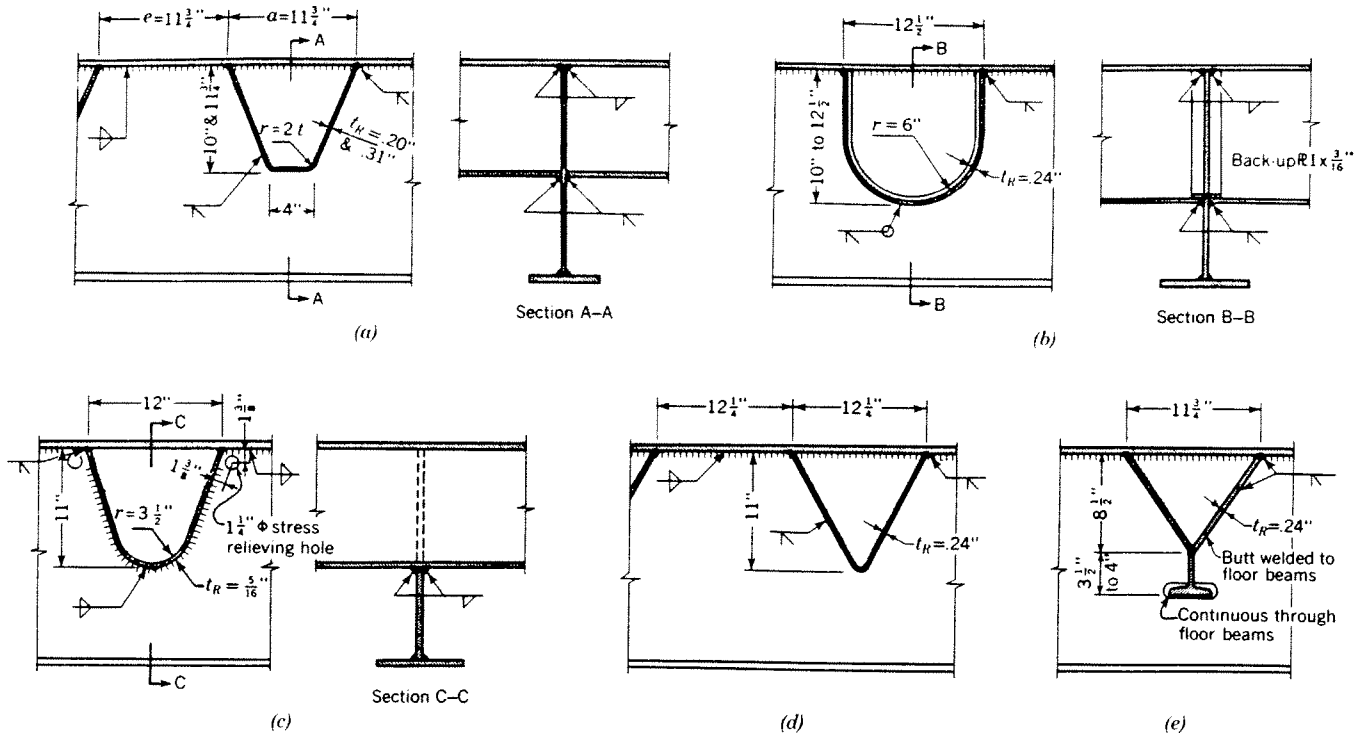


Fig. 7.3. Typical cross sections of closed ribs: (a) Mannheim-Ludwigshafen Bridge [77], see Fig. 7.20. (b) Weser Bridge Porta [60], see Fig. 1.12. (c) Port Mann Bridge [22, 62], see Fig. 1.24. (d) Haseltal Bridge on the Frankfurt-Wuerzburg Autobahn [72]. (e) Fulda River Bridge, Bergshausen [72], see Fig. 1.26

ribs as a part of the flanges of the main bridge members, and avoids the superposition of the large System III stresses and System I stresses in the deck plate. However, if the System I stresses are low and the main members are closely spaced, it may be advantageous to span the ribs in the transverse direction of the bridge. An example of such a structure is the combined railroad and highway truss bridge shown in Figure 7.5.

7.1.2.2 Evaluation of the Closed Rib System

The bridge deck stiffened by closed ribs has a considerably better load distributing capacity than a deck with open ribs.

The hollow, thin-walled rib sections are efficient as flexural members and also possess a high degree of elastic stability.

Thus a relatively wide spacing of the floor beams becomes possible, which results in a lower weight of the bridge deck (Fig. 7.2) and reduces the fabrication and erection labor. The amount of welding required in the closed rib system is also considerably smaller than in the open rib deck, as mentioned in Section 7.1.1.2.

The disadvantage of the deck with closed ribs is in the more difficult fabrication of the rib profiles and the more complicated field splices of the ribs.

The closed rib system also requires a higher degree of precision in fabrication and erection of the deck panels to insure proper fit at splices.

7.1.3 Floor Beams

The transverse floor beams are shaped as inverted T-sections using the deck plate as the upper flange.

If the main girder spacing is large, it may be advantageous to use the floor beams as erection supports for the deck plating panels, in a manner indicated in Figures 11.2 and 11.9. In such a case the lower part of the floor beam may consist of an I-section fabricated separately, to which the upper part of the floor beam web, fabricated together with the deck plating, is welded in the field after placing the deck panels into position.

Heavier floor beams or deep diaphragms are generally required at certain intervals to act as wind frames and to increase the torsional rigidity of the bridge cross section. However, in some structures the heavy transverse members have been omitted, due to special considerations (see Figs. 1.23, 1.24).

Cutouts have to be provided in the floor beam webs at the intersections with the continuous longitudinal ribs.

The usual detail at the intersection with the flat

bar ribs is shown in Figure 7.1a. The circular cutouts at the top and at the bottom of the slots in the floor beam web are made to reduce the stress concentrations in the web plate and to avoid intersections of the welds connecting the floor beams and the longitudinal ribs to the deck plate. With the arrangement shown, the welds between the ribs and the deck are continuous, while the welds connecting the ribs to the floor beams and the floor beams to the deck form closed loops.

The shears transmitted by the ribs to the floor beams are usually low, and it is sufficient to weld the ribs to the floor beam webs on one side only, as shown in Figure 7.1b. This has the advantage of minimizing the stresses in the floor beam web developing as a result of the shrinkage of the vertical welds at the ribs. Such stresses have occasionally caused cracks in the vertical welds. However, the arrangement shown in Figure 7.1b impairs the continuity of the floor beam web, which may be needed where the shearing stresses in the floor beam web are large.

Details at intersections of other types of ribs with the floor beams are given in Figures 7.1c, d, e and 7.3.

The depths and sizes of the floor beams may be governed by the erection requirements and the allowable deflections, especially with longer floor beam spans. In such cases the use of structural carbon steel for the floor beams might be indicated.

7.1.4 Main Bridge Members

Examples and a general discussion of the main bridge members acting in conjunction with the steel plate deck are given in Sections 1.1.3 and 1.2.3.

Single-web girders have often been riveted (see Figs. 1.6, 1.7, 1.8, 1.21), since welded fabrication and field splicing of the heavy bottom flanges often required in long span bridges were not considered practical until recently. However, the development of new welding techniques for use with heavy plates of weldable high-strength steel now make it possible to design welded girders with flange areas of large cross section.

A possible cross section of a heavy welded girder bottom flange is indicated in Figures 11.2 and 11.9.

The single-web main girders of steel plate deck bridges are, in most cases, fabricated without the top flanges

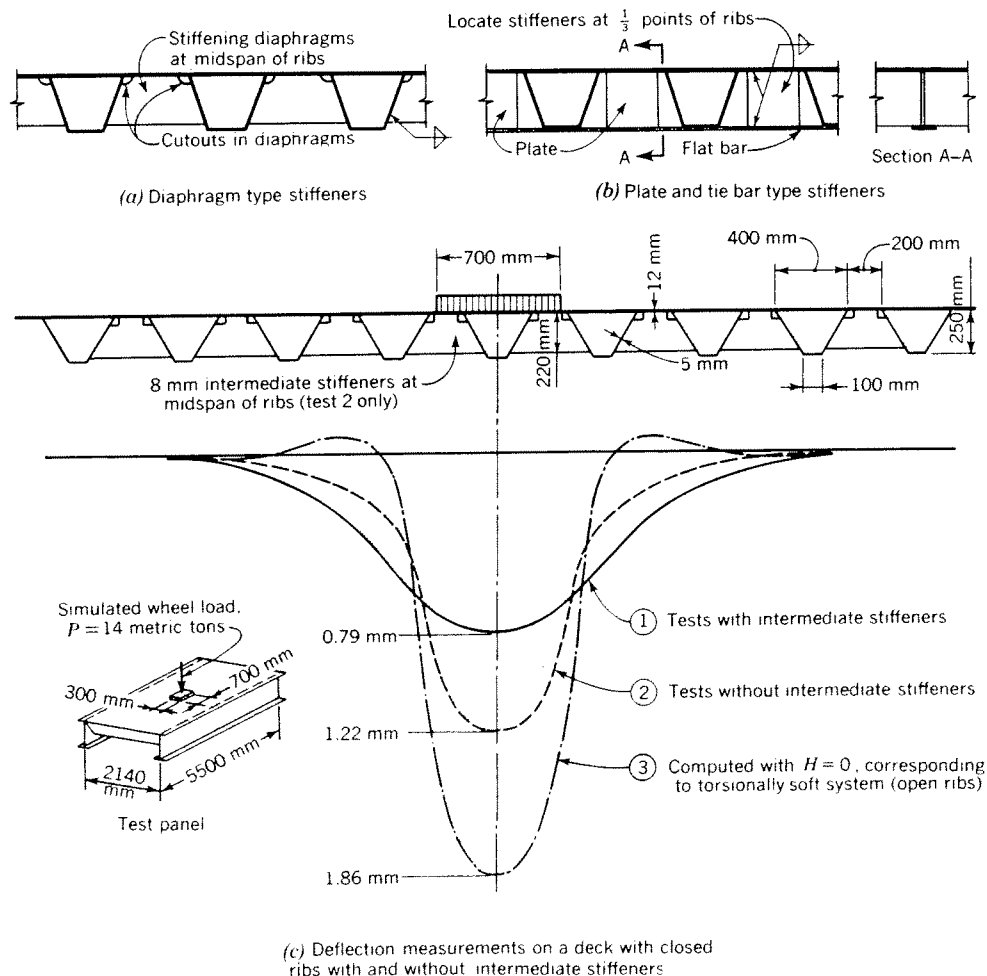


Fig. 7.4. Intermediate stiffeners between closed ribs [77]

(c) Deflection measurements on a deck with closed ribs with and without intermediate stiffeners

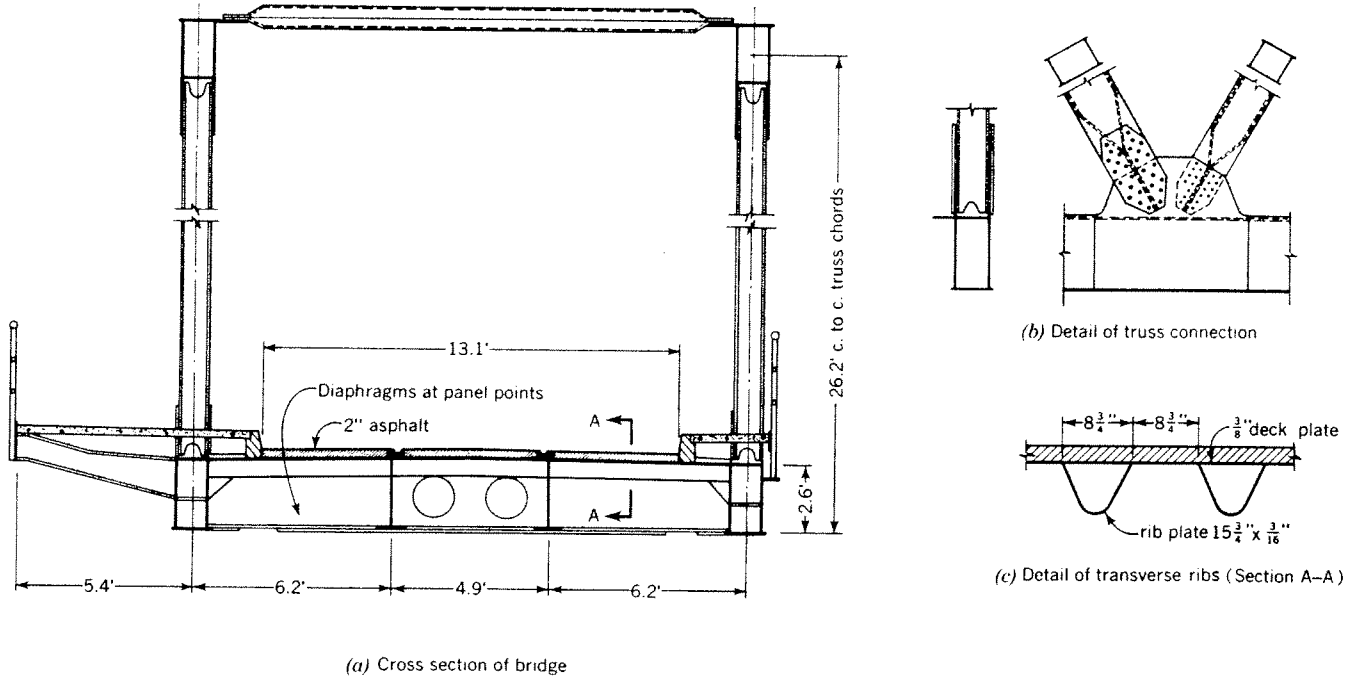


Fig. 7.5. Combined railroad and highway bridge over the Lippe-Seiten Canal with transverse orientation of the deck ribs [61] (simple span—190 ft)

(Fig. 1.8), or with only nominal top flanges (Fig. 1.29b), to which the deck plating is connected in the field. However, the main girder sections may also be fabricated together with a strip of the deck plating, of a width governed by the transportation facilities, as shown in Figures 11.2 and 11.9.

The girder web thickness may be kept small by appropriate web stiffening. Using several rows of

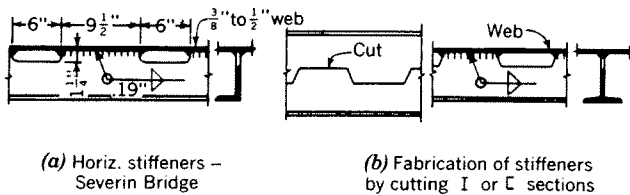


Fig. 7.6. Girder web stiffeners

horizontal web stiffeners is a standard practice in European bridge construction, resulting in webs seldom exceeding $\frac{9}{16}$ in. in thickness, even with very deep girders (see Fig. 1.8).

In welded construction it may be advantageous to cut out the stiffeners as shown in Figure 7.6, to decrease the amount of welding and the resulting warpage and residual stresses in the web.

Box girders of conventional types, using the steel deck as their upper flange, are illustrated by Figures 1.15, 1.23 and 1.24.

In many cases wide box girders have been used, with the top and bottom flanges stiffened by longitudinal ribs (Figs. 1.10, 1.12, 1.14, 1.17).

The advantages of this design are a large torsional rigidity of the girder sections and additional weather protection of the longitudinal ribs. However, if the bottom flange is curved, strong transverse members are needed to transmit the radial components of the flange forces to the vertical webs.

Truss bridges with steel plate decks utilize the steel deck as a part of the upper or the lower chord.

An example of the former type is shown in Figure 1.26.

A bridge with the deck plate forming a part of the lower chord of a truss is shown in Figure 7.5.

7.1.5 Miscellaneous Details

Sidewalks may consist of precast or cast-in-place concrete panels, steel plate with or without a wearing surface, metal grating, etc., as shown in the various bridge cross sections in Chapter 1.

Figure 7.7a shows a precast concrete sidewalk with an edge formed to protect the exposed steel fascia stringers against the weather.

Generally, the concrete sidewalks, curbs and malls on steel plate bridges are less desirable than those of steel. The cast-in-place concrete sidewalks may add considerably to the dead weight of the structure. The

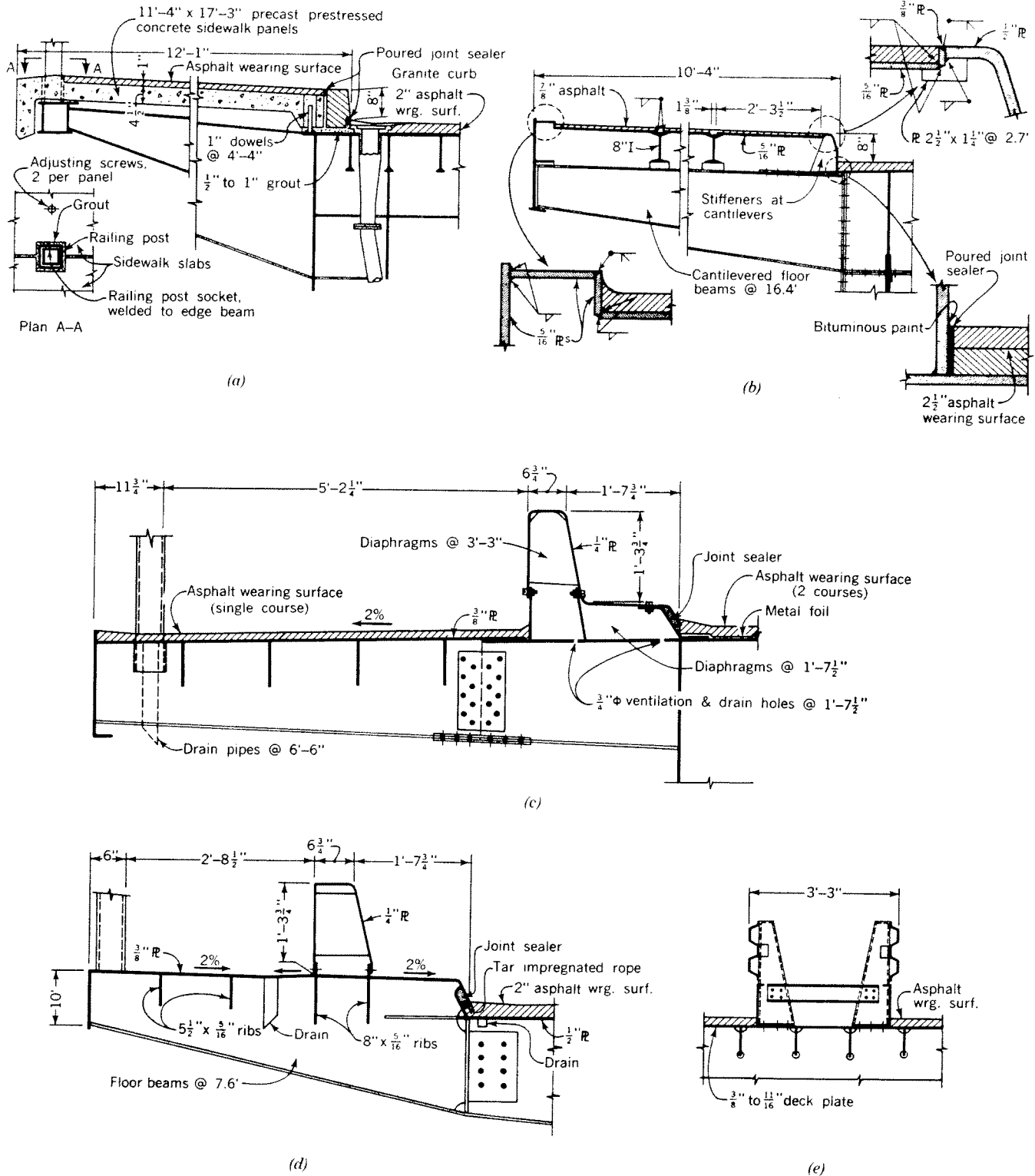


Fig. 7.7. Miscellaneous details: (a) Sidewalk and curb, Rhine River Bridge at Speyer [79]. (b) Sidewalk and curb, St. Alban Bridge, Basle [67]. (c) Sidewalk, traffic barrier and curb, Fehmarnsund Bridge [72]. (d) Sidewalk, traffic barrier and curb, Haseltal Bridge [72]. (e) Center traffic divider, Europe Bridge [58]

use of the lighter precast concrete panels leads to problems of maintenance of the underlying steel members.

The steel sidewalks, which may form an integral part of the bridge superstructure, are usually preferred. Typical details of such sidewalks are given in Figures 7.7b, c and d. Details at *curbs* must be carefully worked out to prevent intrusion of water to the deck plate surface (see Section 8.2.5.2). Appropriate joint sealers and drainage scuppers should be provided, as illustrated by the examples in Figure 7.7.

Median barriers and *traffic guide rails* may be of the type shown in Figures 7.7c, d and e. The traffic barriers shown are connected to the deck structure by means of bolts and are removable.

Expansion joints in the deck at the ends of the bridge structure may be essentially similar to those used on conventional bridges.

7.2 FABRICATION

7.2.1 General Comments on Welding of Steel Plate Decks

The stresses in the welds connecting the deck plate with the longitudinal ribs and the floor beam webs are usually low, so that nominal amounts of welding are theoretically sufficient in most joints.

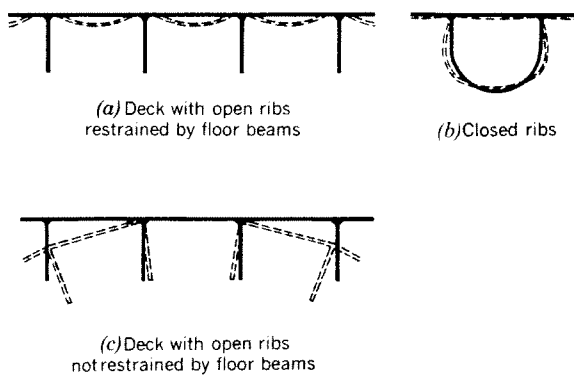


Fig. 7.8. Welding deformations (exaggerated)

Thus, the use of continuous fillet welds for these joints, in accordance with the bridge specification requirements, while justifiable by fatigue safety considerations, results, practically, in considerable overwelding. This may be aggravated by the tendency of designers and steel fabricators to shun the minimum weld size of $\frac{3}{16}$ in. allowed by the bridge code for thin members in favor of $\frac{1}{4}$ in. and heavier weld sizes, and by further scaling up of specified weld sizes in the fabricating shop in order to be "safe."

If it is considered that the total length of welds per

pound of a steel plate deck is rather high, especially in the open rib system, and that the amount of weld metal increases as the square of the weld size, it becomes apparent that overwelding may lead to serious fabrication problems and may increase cost considerably.

Figures 7.8a and b show in an exaggerated manner the *deformations* that tend to develop during fabrication of a deck with open ribs due to fillet weld shrinkage. The deformations increase as deck plate thickness decreases and as weld size increases. The deformations in the closed rib system are shown schematically in Figure 7.8c. It is seen that, in this case, warpage develops primarily in the rib walls, which are usually much thinner than the deck plate.

Warpage of the deck panels must be controlled by appropriate fabrication measures and corrected by flame-shrinkage or other means after fabrication.

Weld shrinkage and the resulting distortions are associated with the *residual welding stresses* in the structural members. The magnitudes of these stresses, which can never be entirely avoided, remain largely unknown, and may be quite high if the rules of good welding practice are not followed. From the point of view of safety, such residual stresses may be considered as undesirable as the local stress concentrations caused by intermittent or spot welding.

Generally, with other factors being equal, the welding distortions and residual stresses depend directly on the amount of welding involved in the fabrication.

Thus, the first rule in the fabrication of steel plate bridge decks should be to *avoid overwelding*.

Another means to reduce welding distortions is the application of the fast *automatic welding* techniques, inducing less heat in the material surrounding the weld than the less efficient manual welding. Therefore the construction details of steel plate decks should be such as to permit the most extensive use of automatic welding.

A proper *welding sequence* should be carefully determined at each joint, to minimize the residual stresses.

Welded shop or field splices of the highly stressed ribs and floor beam flanges should be made with particular care.

Intersections of welds should be avoided where possible, as shown in Figures 7.1 and 7.16, to avoid bi-axial stress conditions in the welds.

7.2.2 Fabrication of the Deck Plating Panels

Welding of longitudinal ribs and floor beams to the underside of the deck plate is usually performed in the trough position on tilt tables, as shown in Figure 7.9.

In the fabrication of decks with *open ribs* the floor beams are usually tack-welded first, then the ribs are threaded through the cut-outs in the floor beam webs and welded.

Welding longitudinal ribs first, before placing the floor beams, has the advantage of convenient execution of the rib welds along their entire length; however, it causes deck plate warpage as indicated in Figure 7.8b, and makes the subsequent fitting of the floor beams difficult. These difficulties may be avoided by welding the ribs to the deck plate pre-bent in the direction opposite to that shown.

It should be noted that if the open ribs are deep and closely spaced, application of the automatic welding processes may be difficult and may require special equipment.

• In the fabrication of European bridges with flat bar ribs a method known as Elin-Hafergut welding has often been applied [56]. In this method coated electrodes are laid flat end to end along the joint to be welded and then covered by hollowed copper bars about 2 in. \times 2 in. After closing of the circuit, welding proceeds automatically by progressive melting of the electrode. Continuous welds can also be obtained by this method through the cutouts in the floor beams (Fig. 7.1a). The advantages of this method are: (a) uniform weld quality; (b) reduced warpage and residual stresses, since the copper bars absorb much of the heat generated by welding; (c) welding can proceed simultaneously on several ribs; (d) qualified welders are not necessarily required. The disadvantages are in the relatively slow speed of the method and in the inconvenience of handling the copper bars in lengths to fit the required length of the weld.

Closed ribs are usually fabricated by cold bending of flat plate cut to size and beveled along the edges for the V-groove welded connection to the deck plate (Fig. 7.3a). The bends should not be too sharp, to prevent ageing effects in the steel. However, a large radius of curvature at the bottom of the rib impairs its torsional rigidity.

Fabrication of the $\frac{3}{16}$ -in. to $\frac{5}{16}$ -in. thick ribs on bending presses of the required capacity does not present unusual difficulties. However, bending heavier plates of low-alloy steel may make the fabrication expensive and uneconomical.

The welds connecting the rib walls to the deck plate and the end diaphragms are made air tight, to prevent corrosion of the inside surfaces (see Section 7.4).

The *dimensions* of the shop-fabricated *panels* of the deck plating are governed by transportation and erection facilities. Deck panels up to 58 ft \times 18 ft and 47 ft \times 21 ft have been fabricated as one weldment for transportation by barges. Panels 38 ft \times 26 ft, weighing up to 45 metric tons, have been transported by highway truck platforms. For railroad transportation the width of the panels is usually limited to 10–13 ft.

The deck panels may be fabricated with their long

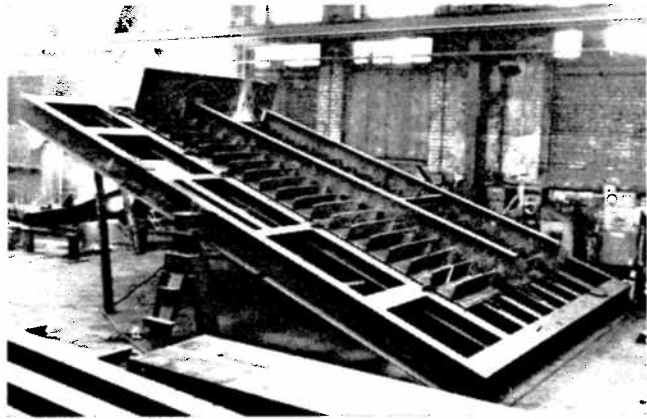


Fig. 7.9. Welding of a deck panel of the Save River Bridge on a tilt-table

sides parallel to the longitudinal ribs (*longitudinal orientation*, see Fig. 7.20) or to the floor beams (*transverse orientation*, see Fig. 7.9). The choice depends on the intended erection method of the panels. Generally, longitudinal orientation, requiring fewer transverse field splices of the deck plate and the ribs, should be preferred.

In the fabrication of the deck panels, necessary allowances must be made to insure *fit* under the field erection conditions (see Section 7.3).

7.2.3 Thoughts on the Economy of Fabrication of Steel Plate Decks

The economy of steel plate deck bridge construction might be considerably enhanced by *standardization* of the deck types and *prefabrication* of the deck plating panels in units suitable for the various design conditions. Such units, if fabricated by mass production methods, could possibly be used also for bridges of shorter spans, where steel plate deck construction would normally be uneconomical (see Section 1.3).

In the fabrication of the deck plating with open ribs, some techniques of steel grating fabrication might be applied.

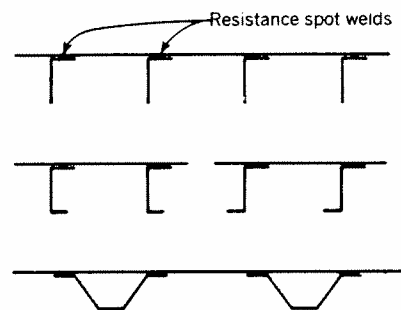


Fig. 7.10. Suggested welding of the ribs to the deck plate by means of resistance welds [44]

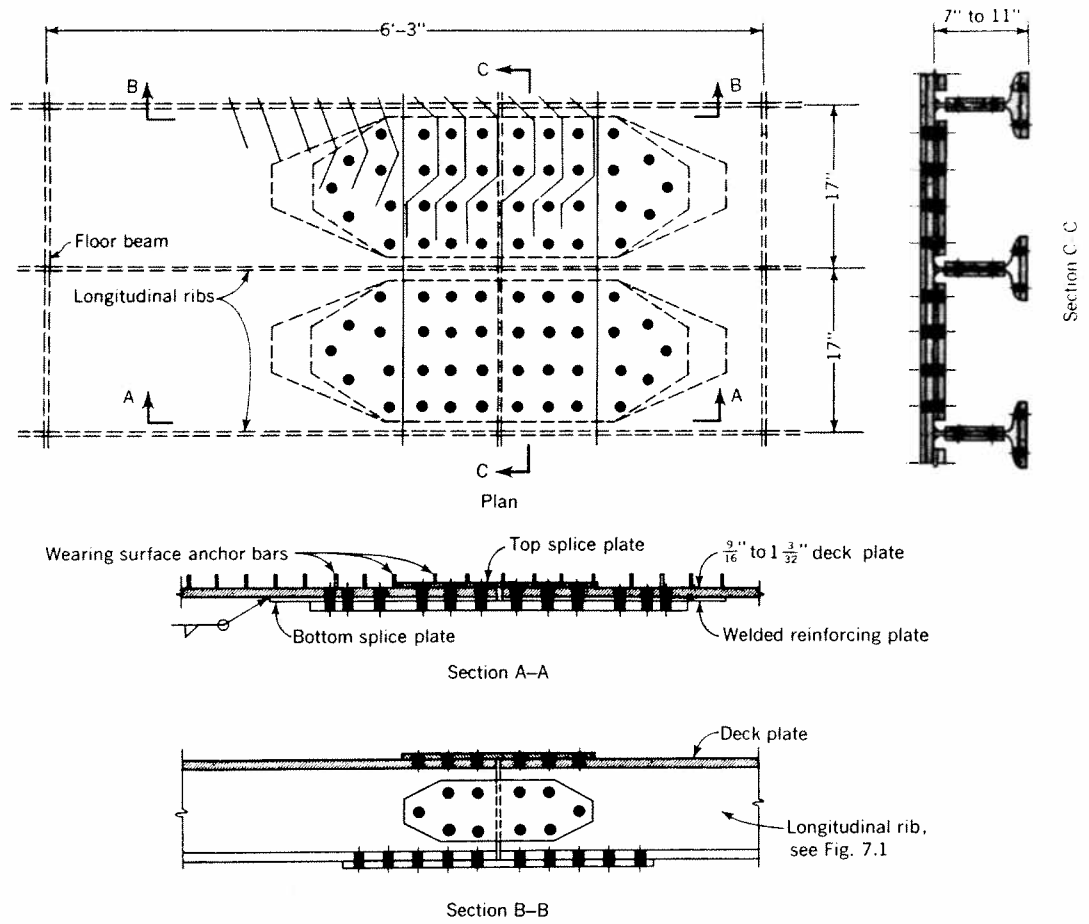


Fig. 7.11. Riveted deck splice, Duesseldorf-Neuss Bridge [68]

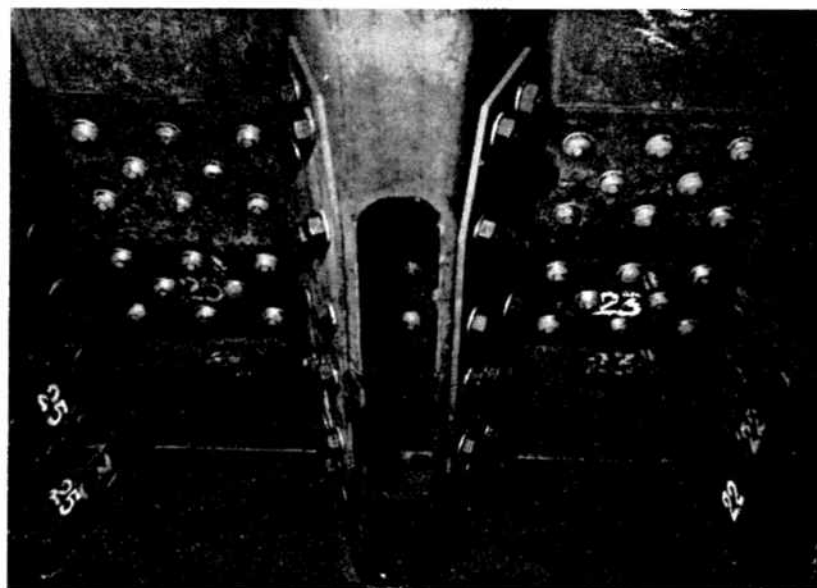
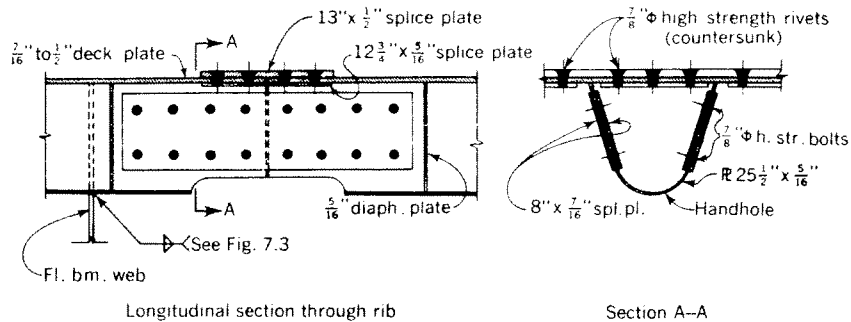


Fig. 7.12. Bolted and riveted deck splice, Duisburg-Homberg Bridge [65, 81]

Fig. 7.13. Bolted and riveted deck splice, Port Mann Bridge [22, 62]



For the closed-rib type of decks prefabricated trapezoidal or U-sections, made by bending or rolling, would be very desirable. Extending the spans of closed ribs beyond the lengths used in existing bridges would also contribute to economy by reducing the number of costly intersections of the ribs with the floor beams.

A suggestion to use resistance spot welds rather than continuous welds, with the purpose of simplifying the fabrication and reducing the amount of welding and of residual stresses associated with it (see Section 7.2.1) should also be mentioned [44]. The proposed details are shown in Figure 7.10. Resistance spot-welding machines with an arm length of about 5 ft, capable of spot-welding two plates, each up to $\frac{3}{4}$ in. thick, with a weld diameter of up to $\frac{3}{4}$ in. are now available. Thus deck plating panels up to 10 ft wide could be fabricated in this manner.

7.3 ERECTION

7.3.1 Field Splice Details

7.3.1.1 Riveted and Bolted Splices

Riveted and bolted connections have often been used in the field splices of steel plate decks. The relative advantages of such splices, compared with welded connections are: (a) fitting of the members is easier, because no deformations develop in the field as with welded splices; (b) connections can also be made during cold weather periods, when welding might be objectionable.

The disadvantages of riveted and bolted splices of the deck are in the loss of net cross-sectional area of the members at splices, additional material required for the splice plates, complicated and not very satisfactory details of the bolted splices of the closed ribs, more difficult maintenance and a greater susceptibility to corrosion of such connections.

For riveting or bolting of the splices of the closely spaced longitudinal ribs, special tools may be required.

Protruding splice plates and rivet heads of the deck plate splices also make a satisfactory construction of

the wearing surface more difficult and preclude the use of the thin lightweight wearing surfaces (see Chapter 8).

An example of a riveted field splice of a deck with *open ribs* is given in Figure 7.11, showing the deck splice details of the Duesseldorf-Neuss Bridge (see Fig. 1.10). In this case the $\frac{9}{16}$ -in. to $1\frac{3}{32}$ -in. thick deck plates, required as the upper flanges of the main girders, were strengthened at splices by additional shop-welded plate strips in order to minimize the loss of cross-sectional area.

Splices of *closed ribs* require handholes in the bottom of the rib section, as shown in Figure 7.12, through which the bolts or rivets are handled.

In the existing splices of this type the deck plate splice is riveted, the rib walls are high-strength bolted.

The compatibility of bolting and riveting in a splice of this type has been investigated experimentally. It is reported that the splice is satisfactory and that the rivets transmit their full share of the load, even under small loads [77].

In order to compensate for the loss of rigidity and the cross-sectional area of the rib at the handhole, thicker rib material may be used at splices.

A splice of a similar type has been adopted for the deck of the Port Mann Bridge (see Fig. 1.24), as shown in Figure 7.13. The air-tightness of the rib on each side of the splice is achieved by diaphragm plates welded inside of the rib section.

The field connections between the deck plating and the main girders are riveted in most existing bridges, as indicated schematically in Figures 1.10 and 1.29b.

If the deck plating is fabricated together with the upper portions of the main girders, the connection between the girders and the deck is made as a longitudinal girder splice (see Figs. 1.8 and 7.14).

Another splice detail at the main girder is shown in Figure 7.15b.

7.3.1.2 Welded Splices

(a) General

Welded field splices of the deck plating require a considerable degree of precision in the shop fabrication

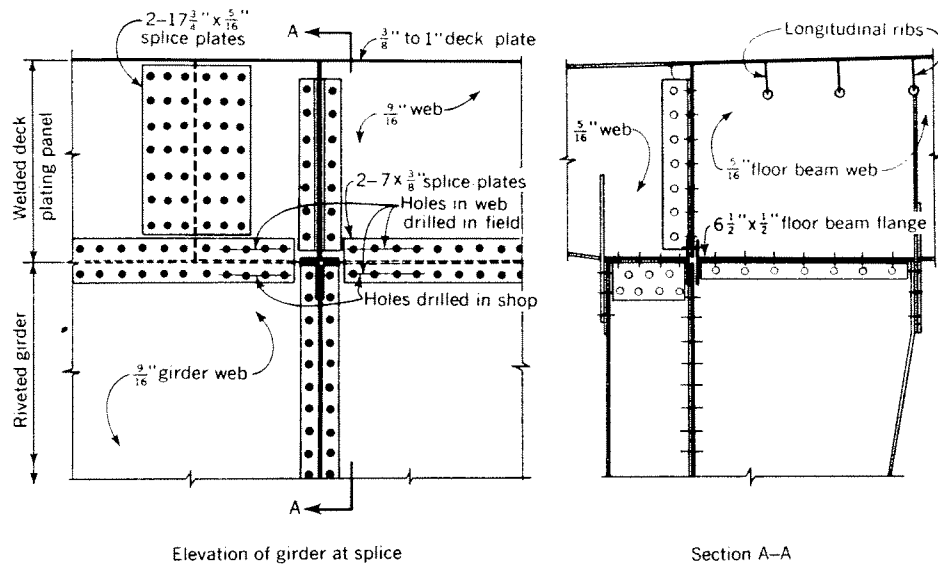


Fig. 7.14. Detail of splice between the deck plating and the main girder, Save River Bridge, see Fig. 1.8

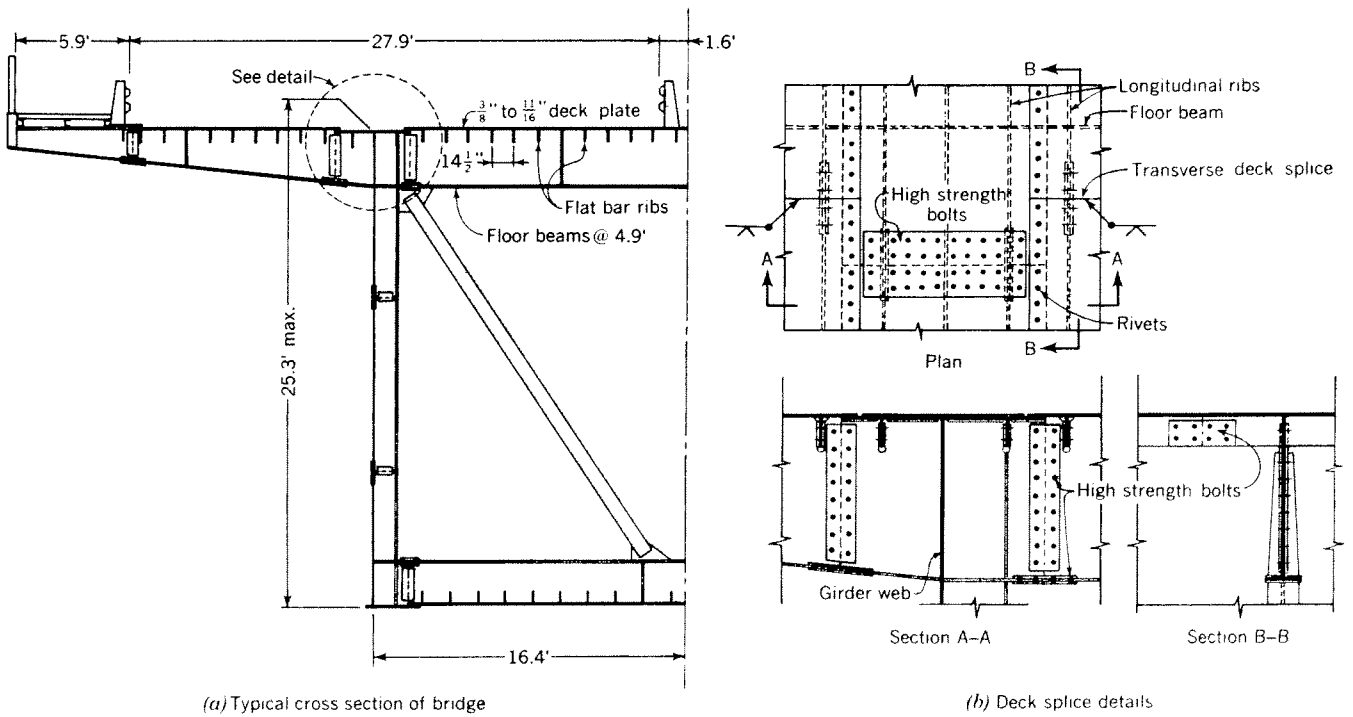


Fig. 7.15. Cross section and field splice details of the Europe Bridge over the Sill Valley, Austria (266-354-650-354-266-266 ft. spans [58])

and in the erection of the steel superstructure to obtain a satisfactory fit for welded connections.

However, unlike riveted construction, final fit of the deck plating to be spliced in the field cannot be assured in the shop by pre-assembling, since the transverse and longitudinal shrinkage of the field welds will tend to deform the plating out of its correct alignment. Such welding deformations, depending on structural details, size of welds, welding methods used and other factors, must be anticipated and correctly allowed for.

In spite of all precautions, some *field cutting* of the plating is usually necessary.

In the erection of steel plate deck bridges with large deck plating panels intended to be spliced by combina-

tion of welding and riveting, it was found practically impossible to obtain the required fit of the deck plate, ribs and floor beam connections by careful fabrication and erection alone. Therefore, field cutting of the deck plate and ribs and field drilling of the rivet holes at certain splices was included in the planned erection procedure, to compensate for the unavoidable accumulation of small fabrication and erection inaccuracies and errors in the estimates of the weld shrinkage.

Such adjustments involved a considerable amount of field work, especially when edge preparation of the joints was required.

Residual welding stresses in the field-welded splices should be kept to a minimum by providing for an

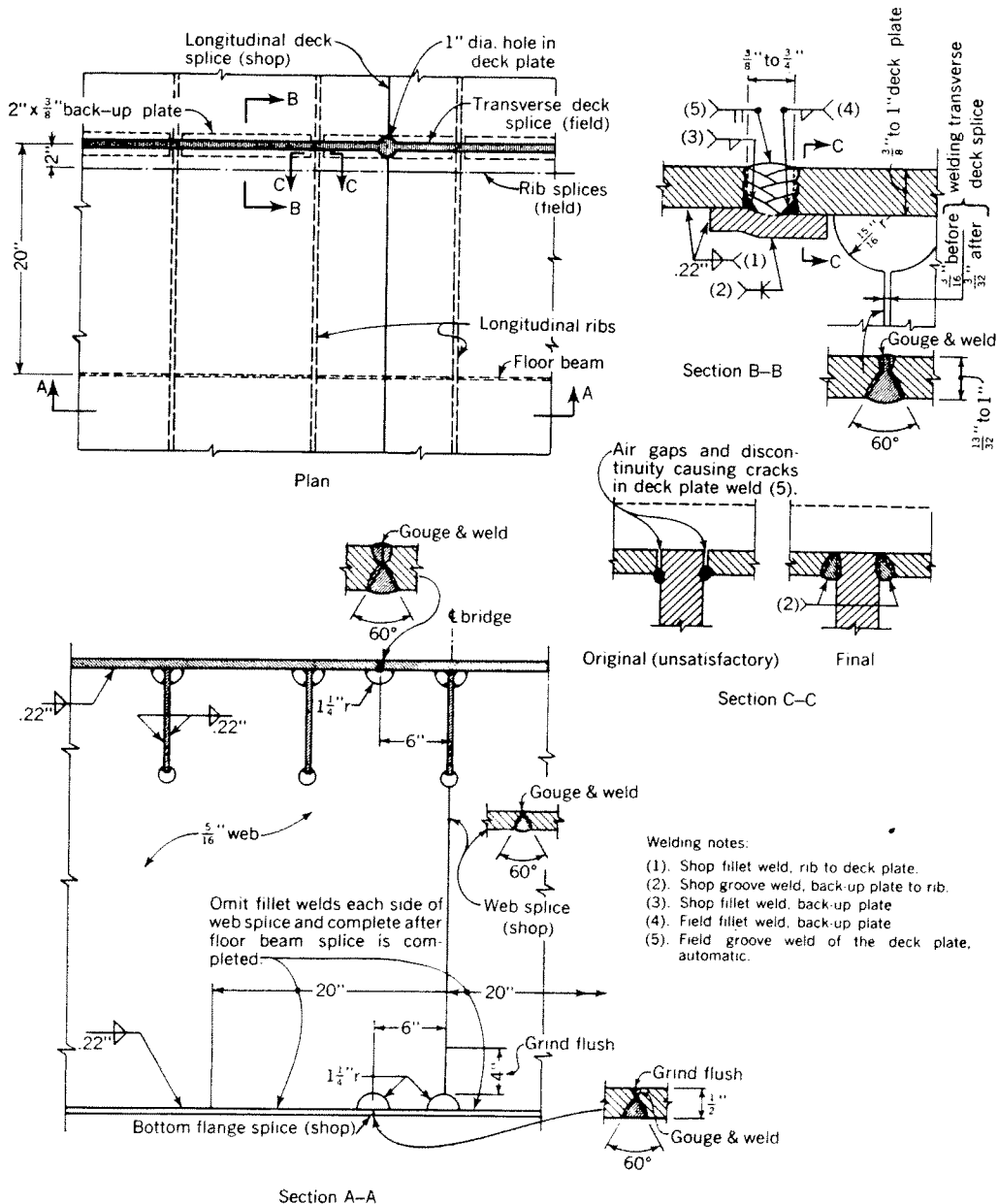


Fig. 7.16. Deck splice details, Save River Bridge [42, 76]

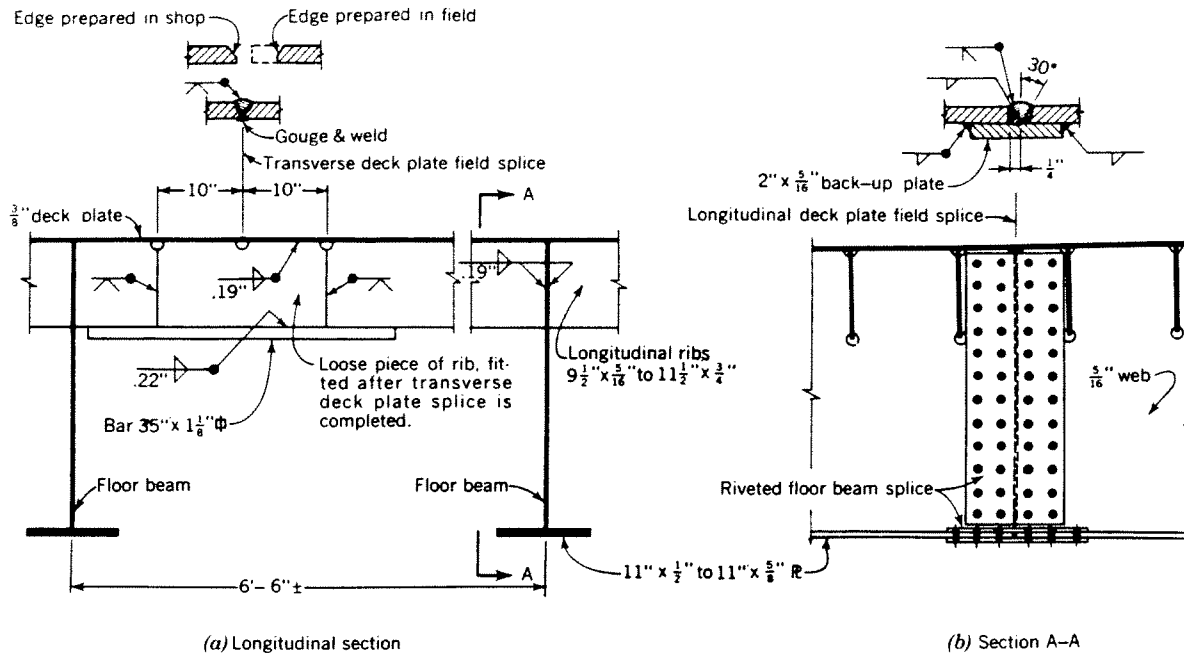


Fig. 7.17. Deck splice details, Severin Bridge [63, 69], see Fig. 1.17

unrestrained motion of the deck panel being connected in the direction perpendicular to the welds made.

The type, execution and sequence of the field welds used in the joints have to be carefully planned.

In making the transverse splices of the deck panels it may be advisable to leave out the longitudinal welds connecting the ribs to the deck plate for a certain distance on both sides of the splice, and to complete these welds after welding the transverse joints. Such procedure, in addition to minimizing the residual welding stresses in the rib splices, allows a slight adjustment of the rib alignment.

(b) Deck with open ribs

As an example of the welded splices of a bridge deck with open ribs, the splice details of the Save River Bridge (Fig. 1.8) are shown in Figure 7.16.

The transverse deck plate welds (Section B-B) were made in several passes by an automatic welding process.

The 2-in. \times $\frac{3}{8}$ -in. back-up plates used in the deck splice were first made discontinuous at their intersections with the longitudinal ribs (see Section C-C). However, cracks appearing in the weld, which were attributed to the air gap and discontinuity, led to an improved detail, as shown.

Intersections of the welds and the end craters have been avoided, where possible, by semicircular cutouts in the webs of the ribs and the floor beams, indicated in Sections A-A and B-B. Circular holes have been drilled in the deck plate at the intersections of the

transverse field welds and the longitudinal shop welds of the deck plate, as shown in the plan view.

Approximately 70% of the total length of the field butt welds of the deck plate and the longitudinal ribs have been X-rayed.

A transverse deck splice of a different type, used in the Severin Bridge (Fig. 1.17) is shown in Figure 7.17.

As a result of the field sub-assembling by welding of the smaller deck plating panels into large erection units (see Section 7.3.2), the deformations of the transverse edges of the panels and a longitudinal misalignment of the deck units with respect to the main box girders had to be anticipated. Therefore only the forward transverse edges of the deck panels were cut to the required length and beveled in the shop (Fig. 7.17a). The other edge of the plate was cut and prepared in the field, after fitting the connections between the deck unit and the floor beams.

The longitudinal ribs were cut off short on each side of the splice, which made it possible to weld the transverse joint in the deck plate continuously from both sides of the plate, and to check the weld quality by X-rays. Then the 20-in. long pieces of the longitudinal ribs were fitted in and welded. The splice was then additionally reinforced by a $1\frac{1}{8}$ -in. square bar, as shown in Figure 7.17a.

The longitudinal deck plate field splice was welded from the top only, as shown in Figure 7.17b.

The field splices of the floor beams were riveted, with the holes reamed after welding the longitudinal deck

splices. In this manner the planned cross slope of the bridge deck could be exactly controlled.

It is claimed that, in this case, the use of welding and riveting in one joint is not objectionable, since any slip in the riveted part of the splice will merely cause a slight rotation around the joint in the deck plate without additional stresses in the weld.

A similar combination of a field welded transverse splice of the deck plate and bolted longitudinal rib splices is planned for the Europe Bridge, Figure 7.15b.

(c) Decks with closed ribs

The field splices of the entire cross section of the Weser Bridge Porta (Fig. 1.12) were welded.

The U-shaped ribs and the deck plate were spliced as shown in Figure 7.3b.

The longitudinal splices of the deck plate and of the bottom plate of the box girder were spliced by overlapping, as indicated in Figure 1.12. This considerably simplified the fitting.

In making the total splice, the transverse splices of the deck and the bottom were welded first, while precautions were taken to allow for the longitudinal motion of the parts joined due to the shrinkage of the butt welds. During the subsequent welding of the butt joints of the girder webs, the deck and the bottom were kept warm at the location of the splice so that they could follow the contraction of the web joints while cooling off. In this manner it was attempted to minimize the residual welding stresses in the girder plating.

The proposed welded field splices of the trapezoidal ribs are shown in Figure 7.18.

In the splice shown in Figure 7.18a, a deck plate strip 2 to 3 ft wide is left out over the rib splice, which can be welded from above and X-rayed, if necessary. Then the missing strip of the deck plate is fitted in and welded. Lastly, the welds connecting the rib side walls to the deck are completed. The direct butt

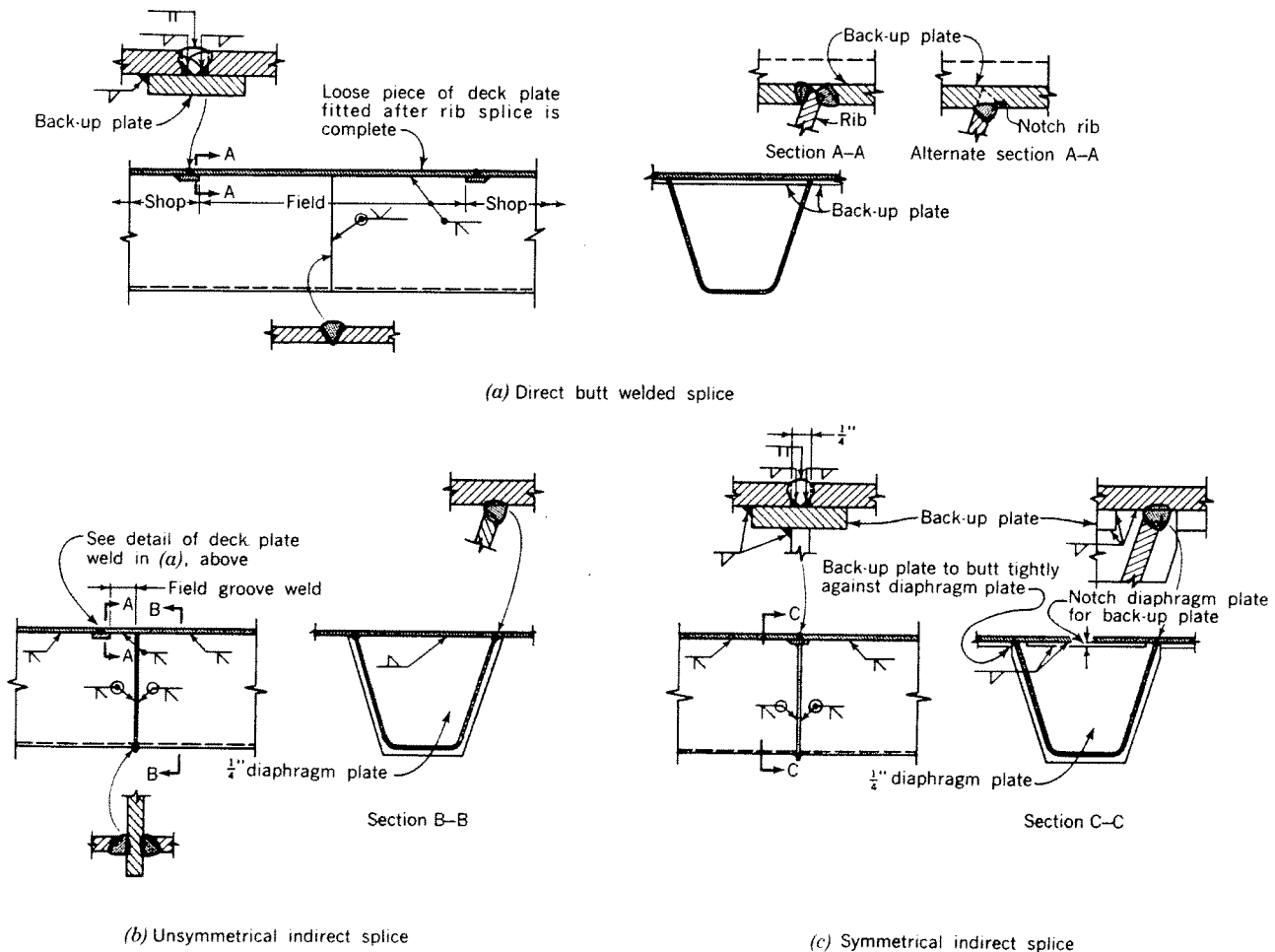


Fig. 7.18. Proposed welded field splices of closed ribs

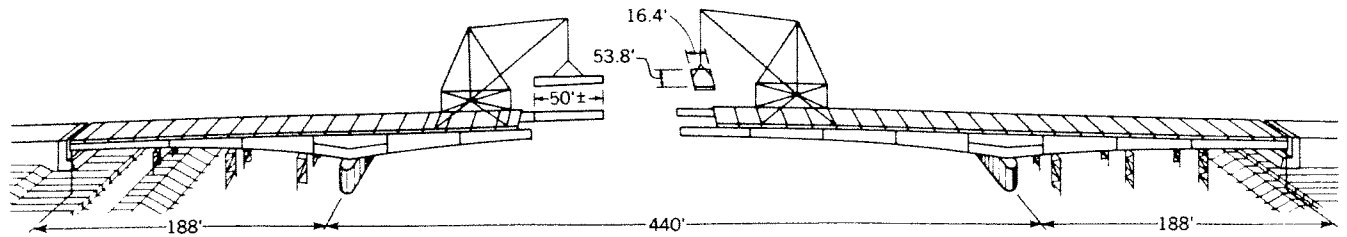


Fig. 7.19. Erection of the St. Alban Bridge in Basle, Switzerland [67]

welding of the ribs in this splice permits full utilization of the rib cross section [42].

A splice using an intermediate plate diaphragm to which both ends of the rib are welded is shown in Figures 7.18b and c. Only one transverse weld of the deck plate is required. Fitting of the splices of this type does not require as high a degree of fabrication and erection precision as may be needed in the case of direct splicing of the ribs (Fig. 7.18a).

7.3.2 Erection Procedures

The erection procedure depends on the structural system of the bridge, the site conditions, dimensions and orientation of the shop-fabricated steel deck plating panels, equipment used and other factors.

The erection problems of a girder bridge with the deck panels oriented in the *transverse direction* are illustrated by the construction of the St. Alban Bridge in Basle, Switzerland (see Fig. 7.19).

The deck plating panels delivered to the construction site measured 16.4 ft in the longitudinal direction and 53.8 ft in the transverse direction of the bridge, and included the open ribs, the floor beams and the upper portions of the main girder webs, to be connected to the lower portions in a manner similar to that shown in Figure 7.14.

After the short side spans were constructed on temporary supports, the erection of the center span proceeded by cantilever method, with the help of derricks

running directly on the completed portion of the deck. First the lower portions of the main girders were cantilevered in sections up to 50 ft long; then the deck plating panels were laid across the girders.

After a deck panel was placed in position, the transverse splice of the deck plate and of the longitudinal ribs was welded. During the welding operation precautions were taken to minimize friction between the deck panel and the main girder, in order to allow unrestrained shrinkage of the welds.

The cantilevered sections of the main girders, having no upper flanges, and not yet connected to the deck plating panel being welded, deflected considerably. In order to make the connections between the girders and the deck plating in the planned position, the ends of the cantilevered girder portions were raised the necessary amount by the erection derrick and, in such position, the longitudinal splices of the girder webs were riveted. Thus the residual erection stresses in the girders were largely eliminated.

Because the exact amount of shrinkage of the transverse field welds of the deck could not be estimated with certainty, the rivet holes for the longitudinal splice in the upper parts of the main girder webs had to be drilled in the field in final position before riveting.

For the same reason every third or fourth deck plating panel was fabricated somewhat longer in the longitudinal direction of the bridge and was cut off in the field to fit.

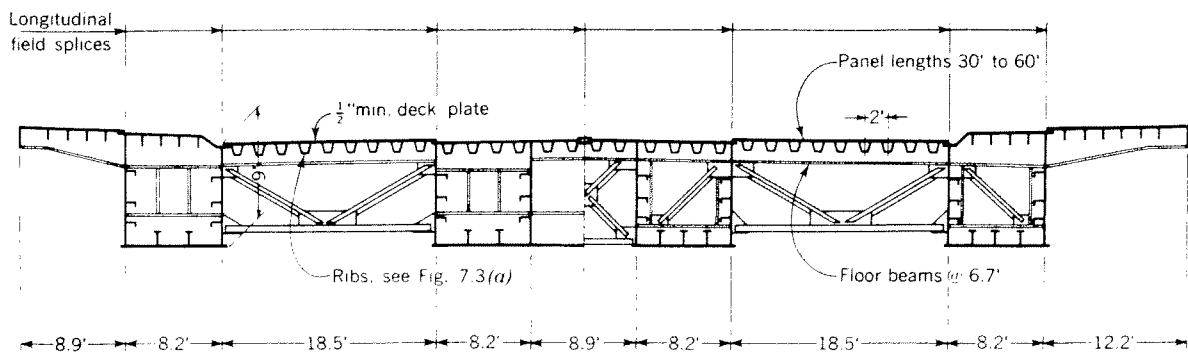
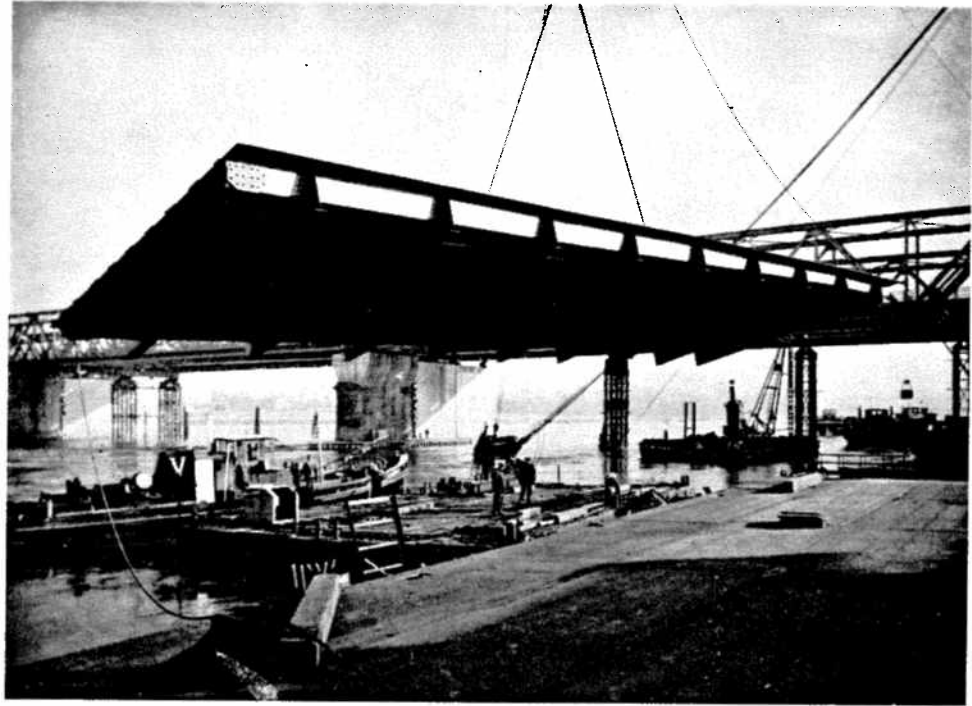


Fig. 7.20. Cross section of the Mannheim-Ludwigshafen Bridge over the Rhine (300-300-300 ft spans) [77]

Fig. 7.21. A 60-ft x 18.5-ft panel of the deck plating of the Mannheim-Ludwigshafen Bridge being lifted into position



The *longitudinal orientation* of the deck panels, requiring fewer transverse field splices is definitely advantageous. Such arrangement was used in the Mannheim-Ludwigshafen Bridge, Figure 7.20. Here the deck panels 18.5 ft wide and 30 to 60 ft long were transported by river barges and riveted into position between the cantilevered main girder box sections. The transverse splices of the deck plate and the welded girders were also riveted; the splices of the closed ribs were bolted (see Section 7.3.1.1).

Figure 7.21 shows a 60-ft x 18.5-ft panel of the deck plating being lifted into position.

If the main girders are widely spaced, the longitudinal arrangement of the deck panels is possible if the lower portions of the floor beams are used as erection supports of the deck panels, as shown schematically in Figures 11.2 and 11.9.

Another solution may be provided by sub-assembly in the field of the longitudinal deck plating panels into larger erection units extending over the entire width of the deck. However, handling of such deck plating units requires erection equipment of large lifting capacity.

Such procedure was used in the erection of the Severin Bridge in Cologne (see Fig. 1.17), as shown in Figure 7.22.

The 22.5-ft and 17.8-ft wide shop-fabricated panels, 47 to 54 ft long, were sub-assembled into 62.8-ft wide units, using the completed portion of the deck as a working platform. First the longitudinal deck plate splices were welded, then the floor beam splices were

riveted, as shown in Figure 7.17b. After sub-assembly the unit was brought forward by a portal crane running on the box girders and placed between the cantilevered ends of the girders.

The rear edge of the deck plate was then cut off, with the floor beam connections of the deck plate unit matching, and then the transverse splice of the deck-plating was welded as shown in Figure 7.17a.

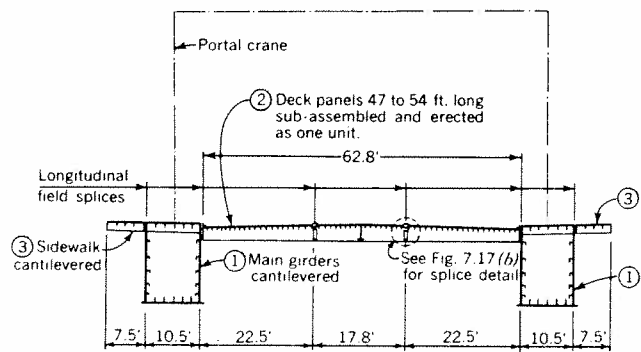


Fig. 7.22. Erection scheme of the Severin Bridge, see Fig. 1.17

The holes in the deck plate for the longitudinal riveted splice between the deck and the box girders were drilled in the field.

A complete description of the complex erection procedure of the cable-stiffened superstructure of this bridge may be found in [82].

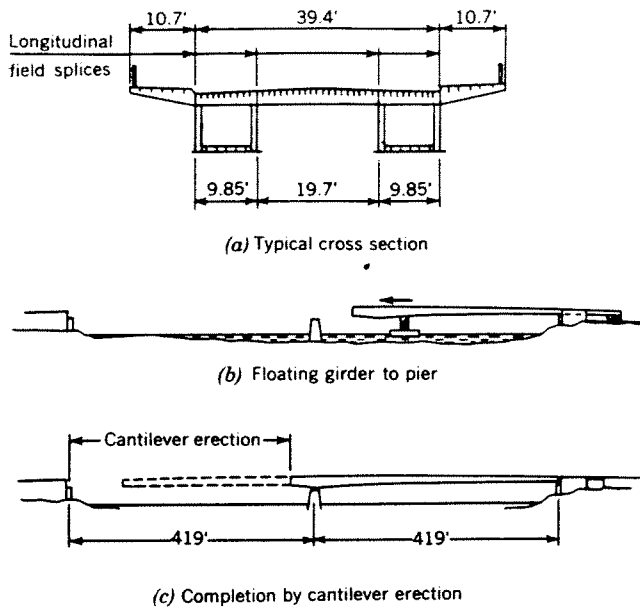


Fig. 7.23. Erection of the Bridge over the Rhine at Kehl [72]

An original erection procedure was used for the two-span highway bridge over the Rhine at Kehl, Figure 7.23. First, one of the two box girders of the right-bank span was erected on the shore, with the abutment end resting on a moving platform. Then the girder was moved forward and the front end supported on a floating platform. In such position the girder was pulled across the river and the front end deposited on the center pier. After the second girder was installed in a similar manner, the deck plating panels connecting the two girders were welded into position.

The erection of the left-bank span proceeded from the center pier by cantilever method.

7.3.3 Effects of the Erection Procedure on the Final Stresses in the Bridge System

In the design of statically indeterminate bridge structures it is customary to compute the dead load bending moments and stresses by assuming that the entire dead load is applied to a weightless structure, fitting stresslessly at all external supports.

However, it must be kept in mind that the dead load stresses are introduced into the actual structure in a much different way, with the final moments and stresses being the end result of the successive erection conditions. The final dead load moment line is usually made to coincide with the conventionally computed moment line, by shop-fabricating the members in such a manner that, if weightless, the structure would fit

stresslessly at the supports (see Fig. 7.24). However, this moment line is only one of many possible dead load moment lines that may be introduced into the system.

This is illustrated by the example of a three-span continuous girder bridge.

Figure 7.24 shows that the final dead load moment line of such a structure, erected by the usual cantilever method, consists of three basic components: (1) bending moments due to a double cantilever condition prior to closure at the midspan; (2) moments due to bringing the ends of girder into correct elevation after closure; and (3) moments due to the dead loads superimposed on the continuous structure after erection.

The moments (2) are, theoretically, entirely arbitrary and may be introduced in any desired positive or negative amount, depending on the magnitude and the direction of the end support adjustment, as required by the camber provided. Thus various final dead load moment lines may be obtained in the structure, as shown in Figure 7.24d. It should be noted that the erection procedure is exactly the same in all three cases shown, of which Case I represents the conventional moment distribution.

For design purposes, that moment line may be chosen which results in the most economical utilization of the material. Such arbitrary *adjustment of the dead load moments* was used in the design of several major steel plate deck bridges [42, 67, 82]. An example of an advantageous re-distribution of the bending moments (which may also be referred to as "prestressing") is given in Figure 7.25.

Unlike conventional fabrication procedure, the camber line of a girder which is to obtain a predetermined desired dead load moment line by adjustments at supports, equal to the negative of the deflection line corresponding to the desired final bending moment line, generally does not pass through all points of support of the girder. This is illustrated in Figures 7.24e and 7.25d.

The accuracy of the moment adjustment depends on the accuracy with which the actual deflection line of the girder can be determined by computation. However, the degree of accuracy required in determining the deflections should not be exaggerated, since the dead load moments are subject to other unavoidable inaccuracies due to departures of the weights of the structural members from the nominal weights, local departures from the design thickness of the wearing surface, etc.

The magnitudes of the final dead load moments are also affected by the accuracy with which the computed camber line is actually reproduced in the field. *Erection errors*, incorrect reaming of the field rivet or

bolt holes, rivet slip or non-uniform weld shrinkage at the field splices may result in an incorrect shape of the girders, which, in turn, affects the bending moment line after closure.

It should be noted that erection errors at splices have the same effect on final moments in conventional cases (e.g. Case I, Fig. 7.24) with no intentional changes of the moments by adjustment of supports.

Therefore, the geometry of the bridge members must be carefully controlled during erection in all cases and corrective measures taken, if necessary, at each splice.

Another factor to be considered in the determination of the final dead load stresses and of the camber line of the bridge members are the *residual* (or the locked-in) stresses and deformations of the members resulting from

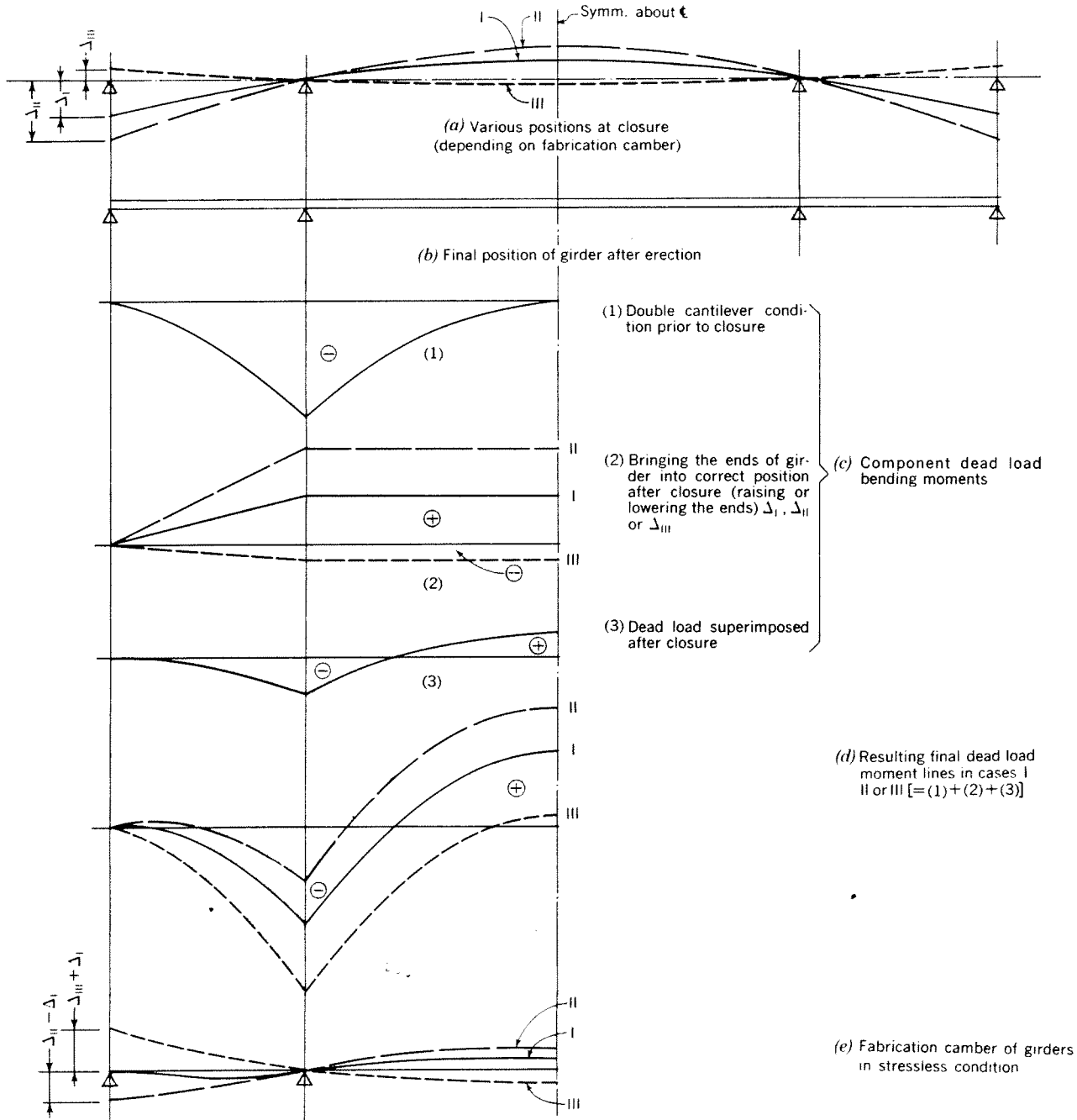


Fig. 7.24. Dead load moments in a three-span continuous girder

the erection procedure. Such stresses occur, for example, in the cantilevered main girder sections (see Fig. 7.19) which have to carry their own weight before being joined with the deck plating acting as their top flange.

A similar condition occurs in the floor beams erected in a two-step procedure (see Figs. 11.2 and 11.9 and Sections 11.2.2.4.2 and 11.3.2.3 of the numerical examples).

Such stresses and deformations must be accounted for in the design, fabrication and erection of the bridge members.

7.4 PROTECTION AGAINST CORROSION

The problem of protecting a steel plate deck bridge against corrosion is essentially the same as with other types of steel bridges, except for the top surface of the deck plate, which requires special treatment, and the insides of closed hollow sections, which have a much higher resistance to corrosion than conventional steel bridge members.

7.4.1 Steel Deck Plate

The top surface of the deck is usually shipped without paint, sandblasted after erection and given a coating of corrosion protective and bonding material, prior to placing of the wearing surface.

This is discussed in Chapter 8, Section 8.2.3.

The unpainted surface of the steel deck may be protected until erection by coating with linseed oil or other means.

7.4.2 Insides of Closed Ribs and Other Inaccessible Closed Hollow Sections

The question of corrosion inside of closed sections has been extensively investigated in Germany [99, 100, 101].

A series of investigations on bridges up to 50 years old with hollow members has revealed no moisture and no corrosion inside the hollow members, except in a few cases where external damage made it possible for water to enter.

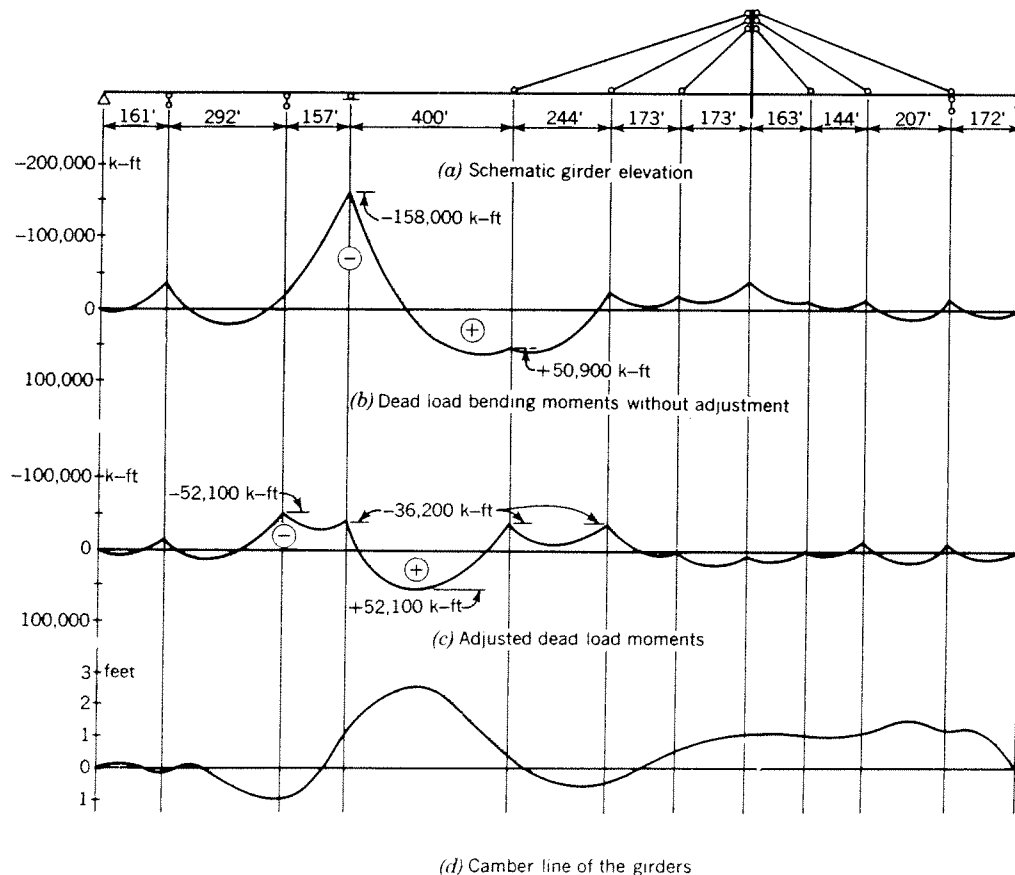


Fig. 7.25. Dead load moments and camber line of the Severin Bridge in Cologne [82], see Fig. 1.17

Note: The camber line shown is the sum of the cambers required for the adjusted dead load moments, the effects of the eccentricity of the cable connections and the residual erection stresses. The vertical curvature camber is not shown.

Many of the members investigated were painted on the inside; the paint, even inside of members which water had entered, was in excellent condition, except in the portions where water had accumulated and some rusting has occurred.

A further series of planned experiments on pipes and some field investigations on transmission towers fabricated from pipes, all unpainted on the inside, showed not the slightest sign of corrosion inside of sealed sections, even after many years in service. Where water was able to enter through holes provided in the planned experiments or through damage in the transmission towers, corrosion took place mainly where water had come into contact with or run down along the steel. Other portions were practically unaffected.

These investigations indicate that there is no danger of corrosion inside the closed ribs or closed truss members (see Fig. 7.5), since such members can easily be made air-tight. Moreover, the closed ribs, located under the bridge deck, are well sheltered against direct effects of precipitation and are not subject to danger of accidental damage after the bridge is completed. Thus no provisions for corrosion protection inside the closed ribs are necessary, other than making the ribs air-tight in the course of normal fabrication and erection.

It should also be noted that the smooth exterior surfaces of the closed ribs have a low susceptibility to corrosion and can be easily inspected and maintained during the lifetime of the structure.

The above findings are reflected in the details of recent steel plate deck bridges, where $\frac{3}{16}$ -in. thick closed ribs are often used, unpainted inside.

Other types of hollow sections which cannot be entered (such as truss members, columns, etc.), or which are entered with difficulty, should in all cases be welded air-tight or provided with rubber sealed manholes. In such cases no corrosion protection is necessary.

Should air-tight construction be impossible, a somewhat simpler corrosion protection than on the outside of the member should be provided before welding the member. The zinc-powder paints are more suitable for this purpose than other types of paints, since they are less affected by welding heat and, generally, do not affect the quality of the welds, should the paint cover the location of the welds to be made in joining the member.

Another possibility is the use of ordinary paints, leaving unpainted strips at the locations of the welds.

Inside painting could also be done after welding by spraying apparatus inserted into the members.

7.4.3 Box Girder Sections

A survey of large box girders of the type shown in Figures 1.10 and 1.12 has led to the conclusion that the insides of such sections are considerably less susceptible to corrosion than the outside surfaces [101].

The findings of the survey may be summarized as follows:

1. The moisture formation as a result of condensation inside the large box sections is insignificant and of little consequence.

2. Even large box sections which can be entered should be constructed air-tight, if possible. Closing of the box section does not increase the moisture condensation in a degree that might have an effect on corrosion.

If closed box girder sections are made air-tight by doors or manholes with rubber gaskets, protective measures against inside corrosion may be omitted.

3. If, for any reason, the large box sections cannot be made air-tight, sufficient ventilation openings must be provided in the front and the side walls of the boxes. Openings in the bottom plate are not suitable for ventilation purposes and might have the adverse effect of admitting moist air (from the river below), or corrosive industrial gases into the box section.

4. If water pipes are carried inside the box section, openings in the bottom plate, as a safeguard against a pipe burst, cannot be avoided. In such cases it may be advisable to provide such openings with safety covers from below, which would open under pressure from inside.

The water pipes should be well insulated, to prevent moisture condensation.

5. No open drainage troughs should be located inside the box section.

6. Inside the large accessible box sections which are not made air-tight, a somewhat simpler corrosion protection than that on the outside is generally sufficient, except in the vicinity of ventilation and other openings, where a normal protection is indicated.

CHAPTER 8

Wearing Surfaces

8.1 GENERAL REQUIREMENTS

Steel plate bridge decks are generally topped with a wearing surface to improve traction and to protect the steel deck against the direct effects of atmospheric conditions and traffic.

It should be noted, however, that there are several bridges in existence having unprotected checkered or patterned steel plate decks. Experience with these structures and trial installations indicate that the resistance to corrosion and wear of the unprotected exposed steel plate decks is good; however, the surface friction of such decks is less satisfactory, especially if the deck is subject to icing.

While some improvement of the surface roughness may be obtained by such means as welding protruding studs, bars, etc. to the steel plate, the use of a proper wearing surface must, at the present time, be regarded as a standard solution.

The principal requirements which a wearing surface on a steel plate deck bridge must satisfy may be summarized as follows:

1. *Light weight.* This is an obvious requirement for a steel plate deck bridge, aiming at a maximum dead weight saving. For this reason alone conventional pavements requiring a thickness of several inches must be excluded.

2. *Skid resistance.* The wearing surface should have a high surface friction coefficient, dry or wet. The surface texture should be rough and abrasive to increase friction and to minimize the effects of icing of the deck.

3. *Stability and durability.* No shoving, rippling or other deformation should develop in the wearing surface due to traction and braking forces of the vehicles. The stability of the surfacing should be maintained over the entire expected temperature range.

The wearing surface should be resistant to surface deterioration, potholing and raveling and should not be affected by oils, gasoline, de-icing salts and other chemicals. For thin surfacings a high resistance to abrasion is essential.

The required surface roughness should be little affected by wear and ageing.

4. *Sufficient thickness* is required to provide an even and plane surface, true to the specified slopes and grades.

The steel plate deck surface will not be geometrically perfect, even if fabricated and erected with all precautions. Therefore the minimum design thickness of the surfacing should include an allowance for unavoidable departures from the correct deck elevations due to welding distortions of the deck plate, errors in cambering of members, etc.

Increased thickness of the wearing surface will be needed on decks using variable steel plate thickness, protruding deck splice plates, bolt and rivet heads.

5. *Positive and lasting protection of the deck against corrosion.* The wearing surface may aggravate rather than relieve the danger of steel deck corrosion if it is faulty, cracked or insufficiently bonded to the deck, forming pockets in which moisture may accumulate. If, under such circumstances, deck corrosion sets in, it may spread undetected under the surfacing.

Therefore the wearing surface should be impervious to water or chemical agents, should develop no cracks enabling the moisture to penetrate to the steel deck and should have a good bond to the top of the steel under all circumstances. The bond between the wearing surface and the deck should be sufficiently strong to withstand the traction and braking forces of vehicular traffic, the shearing forces due to composite action of the surfacing with the deck plate and should not be loosened by local vibrations of the steel deck plate.

6. *Easy maintenance and repairs.* The wearing surface should require a minimum of maintenance work. If any damage occurs, it should be possible to make the necessary repairs quickly, easily and inexpensively. It should also be possible to remove and replace portions of the wearing surface if necessary, without disrupting traffic for a prolonged period of time.

It is seen that the wearing surface on a steel plate deck bridge is subject to more severe requirements and service conditions than the surfacing of a concrete deck bridge. Therefore the choice of the proper type and composition of the wearing surface should be a matter of careful study in each case. Final selection of the

surfacing will depend on local traffic demands, climatic conditions, relative importance of dead weight saving, structural details of the deck, cost of the various types of surfacing and the engineer's preference, based on local experiences and the performance record of the various materials.

While the development of wearing surfaces on steel plate decks is still in progress and no present surfacing may be termed ideal in all respects, several types of surfacings on existing steel deck bridges have proved to be satisfactory.

The various possible types of wearing surfaces on steel decks are discussed in the following sections.

8.2 BITUMINOUS-MIX WEARING SURFACES

8.2.1 General

The bituminous-mix wearing surface is, at present, the predominant type of surfacing on steel plate deck bridges, and has been used on all major structures of this type.

A proportioned mixture of a properly graded mineral aggregate and an asphalt binder is called *asphalt concrete*.

A mixture of asphalt and fine aggregate containing a large proportion of small particles and dust is known as *asphalt mastic*. Both types of mixes have found application as wearing surfaces on steel plate decks.

A comprehensive discussion of the composition and construction of bituminous pavements and the properties of materials may be found in general engineering handbooks and reference works ([84], [105] or similar references).

A brief review of material properties is given below, inasmuch as it is necessary in the discussion of the bituminous pavements on steel decks.

8.2.2 Materials for Bituminous Wearing Surfaces

8.2.2.1 Asphalt

Asphalt used in bituminous pavements is a black semi-solid or solid cementitious material consisting of approximately 99% of pure bitumen (hydrocarbon material soluble in carbon disulfide) and 1% of mineral matter. It is obtained through fractional distillation of crude petroleum or by refining natural lake asphalt (Trinidad, Bermudez). The origin of the asphalt has an effect on its physical properties; however, by proper blending operations, asphalts of desired characteristics may be produced from many sources of crude.

Asphalt is a thermoplastic material since it liquefies gradually when heated.

It is characterized by its *hardness* at a specified temperature. The hardness of an asphalt is determined by

a standard *penetration test*. The *penetration grade* of an asphalt, as determined by this test, is the depth, measured in tenths of a millimeter, that a standard needle penetrates the asphalt under a load of 100 g applied for 5 seconds at a temperature of 77°F (ASTM Test Designation D5).

An asphalt specially prepared for use in paving is known as *asphalt cement*.

For highway hot-mix bituminous pavements the asphalt penetration grades ranging from 60 to 150 are usually suggested [84]. For wearing surfaces on existing orthotropic steel plate deck bridges harder penetration grades of asphalt have been used, ranging from 20 to 50.

The relationship between temperature and consistency of an asphalt may not be the same for different sources and types of asphaltic material. Several asphalts having the same penetration grade (100 g, 5 seconds) at 77°F may have penetration characteristics differing from each other at another temperature. The factor characterizing the extent to which the consistency of an asphalt changes with temperature is called *temperature susceptibility*. It is usually given as a ratio of the penetration values at two standard temperatures.

Another method of describing the consistency of an asphalt, often used in European specifications, is given by a test determining the *softening point*.

The softening point, as determined by this test, is the temperature at which a standard sample of asphalt mounted in a brass ring sags 1 in. under the weight of a $\frac{3}{8}$ -in. steel ball ("Ring and Ball" test, ASTM D36).

The softening point value, in conjunction with the penetration grade, may be used as a measure of the temperature susceptibility of an asphalt.

It should be noted that the hardness and consistency tests of the original asphalt material before its use in a pavement do not directly reflect the final asphalt properties, which undergo significant changes after heating the asphalt to high temperatures, especially in thin films. Such conditions prevail during mixing and placing of the hot-mix pavements and lead to a considerable hardening of the asphalt after cooling. The penetration value may decrease up to 50% and the softening point temperature may be raised by 10–30°F, depending on the type of asphalt, mixing temperature and duration, and the conditions of placement.

Therefore the desired qualities of asphalt and asphalt-aggregate mixtures essential to proper pavement performance would be more properly defined by tests and specifications based on properties of the finished pavement and of the asphalt extracted from it, rather than on the characteristics of the original materials.

Until such improved specifications are adopted, proved and standardized, the selection of a proper type

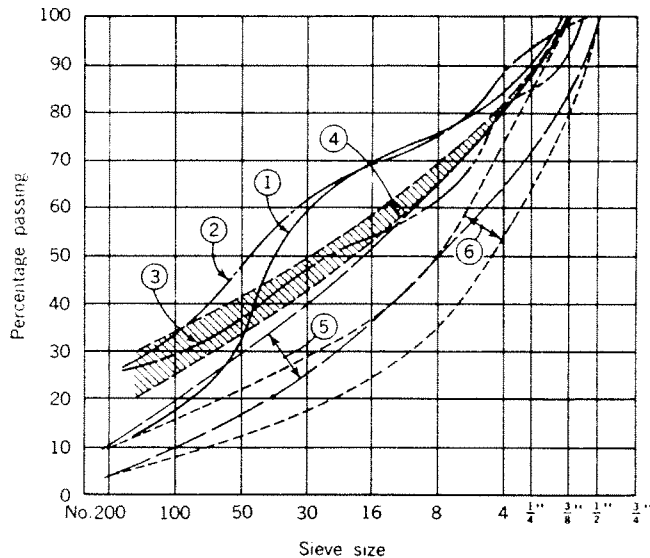


Fig. 8.1. Typical gradation curves of aggregates used in bituminous mix wearing surfaces: (1) Binder and surface courses, west end, Cologne-Muelheim Bridge (Section 8.2.4.2a). (2) Binder course, east end, Cologne-Muelheim Bridge (Section 8.2.4.2a). (3) Surface course, east end, Cologne-Muelheim Bridge (Section 8.2.4.2a). (4) Tentative German specifications for asphalt concrete mixes on steel decks [86]. (5) Fine-graded mix, Composition Type Va, The Asphalt Institute. Gradation used for surface courses [105]. (6) Dense-graded mix, Composition Type IVa, The Asphalt Institute. Gradation used for surface courses [105]

and grade of asphalt to be used in a wearing surface will have to be determined by a cautious use of the various existing specifications and by direct trial and experimentation.

8.2.2.2 Aggregate

(a) Definitions, gradation

The term *aggregate* defines a properly graded agglomeration of crushed or natural stone, gravel, sand and fine inert mineral particles used in bituminous or cement concrete.

Physical composition of the aggregate is characterized by the weight proportion of the component particles of the various sizes, known as *gradation* of the aggregate. Gradation is usually given as a total weight percentage passing each of a series of standard sieves of decreasing mesh size, and is represented by gradation curves or tables.

In bituminous mix construction the component parts of an aggregate are designated as follows [105]:

coarse aggregate—retained on No. 8 sieve (square opening of 0.0937 in., or approximately $\frac{3}{32}$ in.)

fine aggregate—passing the No. 8 sieve and retained on the No. 200 sieve (0.0029-in. opening)

mineral dust—passing the No. 200 sieve. Fine mineral material 65% of which will pass the No. 200 sieve is designated as *mineral filler*

The relative amount of the mineral filler can greatly affect such properties of a bituminous mix as density, strength and resistance to weathering.

On the basis of gradation, aggregates may be divided into the following categories:

dense graded, including particles of all sizes in proportions necessary to fill the voids between the particles

open graded, having an incomplete grading, with certain sizes omitted and containing a smaller amount of mineral filler

one-sized, consisting of particles of one size

Bituminous pavements on steel plate deck bridges have been made, in most cases, with a dense-graded aggregate having a maximum particle size of approximately $\frac{3}{8}$ in. and including a high proportion of mineral filler. One-sized aggregate $\frac{1}{4}$ in. to $\frac{3}{4}$ in. is frequently used in surface treatments.

Typical gradation curves of the aggregates used in the wearing surfaces on steel plate deck bridges are shown in Figure 8.1.

(b) Desirable properties

The aggregate content in a bituminous mix ranges from 88% to 96%; therefore, the aggregate characteristics determine to a great extent the structural properties of a bituminous pavement.

The desirable properties of an aggregate for use in bituminous construction may be described as follows [105]:

1. *Appropriate gradation and size.* Gradation of an aggregate significantly affects the density, strength, mechanical stability, workability and the asphalt content of a bituminous mix.

Aggregate in a finished mix is subject to partial breaking up or *degradation*, due to crushing or abrasion of the particles under loads. Since degradation will increase the total surface area of the aggregate, the amount of bitumen binder in the mix may no longer be sufficient to coat each particle of the aggregate. This may result in a deterioration of the pavement properties. Open-graded aggregates tend to be more affected by degradation than the dense ones.

Appropriate aggregate gradations for bituminous pavements are recommended by the various specifications for bituminous mixtures.

2. *Strength and durability.* This property is determined by the resistance to crushing and abrasion of the mineral material. High strength is required to provide a proper wear resistance of the pavement and to prevent excessive degradation of the mix.

3. *Angular particle shape* providing mechanical interlock of the mix is essential to proper pavement stability, especially if open-graded aggregate is used. Angularity of the fine aggregate is especially important.

4. *Rough surface texture* is equally important to mixture stability. Rough texture also helps in holding the asphalt film in place.

5. *Low porosity* of an aggregate is desirable to prevent selective absorption and the resulting decomposition of the bitumen.

6. *Hydrophobic character*. In order to prevent displacing of the bituminous film from the aggregate by water, the aggregate should have a greater affinity for bitumen than for water, or should be hydrophobic ("water-hating") in nature. Limestone is an example of a hydrophobic material. Hydrophilic ("water-loving") minerals, like silicates, are less suitable as aggregates for bituminous construction because the bituminous film may be stripped from them more easily.

Adhesion of the bituminous films to aggregates may be improved by adding anti-stripping agents to the asphalt, which, however, may not be permanently effective.

8.2.3 Corrosion Protection and Bonding

8.2.3.1 Purpose, Desirable Properties

Experience has shown that placing a bituminous concrete wearing surface directly on a steel plate deck does not give satisfactory results. Good bond between asphalt concrete and steel is difficult to achieve and may be broken due to the effects of temperature stresses, shearing stresses between the asphalt and the deck due to composite action, and deck plate vibrations. Loosening of the bond and the consequent separation of the wearing surface from the deck could expose the steel plate to corrosive effects of moisture that might penetrate to the surface of the steel if deep cracks developed in the bituminous pavement. Breaking of the bond would also subject the asphalt concrete to greater local stresses under the wheel loads and precipitate its deterioration.

Therefore appropriate sealing materials must be applied to the steel deck, prior to placement of the bituminous surfacing, to perform the following functions:

(a) provide positive *protection* of the steel deck *against corrosion*, which should safeguard the deck even if imperfections in the bituminous wearing surface develop;

(b) provide *satisfactory bond* between the wearing surface and the steel plate deck.

Thus, the desirable properties of materials to be

used under a bituminous pavement on a steel plate deck may be defined as follows:

1. Perfect adhesion to the steel deck, to preclude penetration of moisture to the steel deck, and to assure good bonding to the bituminous concrete course.

2. Impermeability to moisture and resistance to the action of oils, gasoline, de-icing salts and other chemicals that might penetrate through the wearing surface.

3. Adequate shearing strength, to resist shoving of the wearing surface.

4. Low temperature susceptibility. The protective coating should not become brittle at cold temperatures, nor should it be affected by high temperatures during placing of the hot asphalt mix.

A brief review and discussion of experiences with the various types of protective materials used or experimented with on steel plate deck bridges is given below.

8.2.3.2 Protective Materials

(a) *Bituminous paints and tack coats*

Bituminous paints, consisting of a high penetration bitumen and a solvent as well as various commercial products on bituminous bases, have been used on steel decks. Paint is applied in one or two coats immediately after cleaning the steel deck of oil, grease, rust and mill scale. Paint should be quick-drying and heat resistant.

Field tests with hard mastic asphalt wearing surfaces placed on orthotropic steel plate deck panels primed with bituminous paint have been made by the Road Research Laboratory in England [103]. Inspection of test panels that were subjected to heavy highway traffic for a period of $4\frac{1}{2}$ years has revealed local corrosion of the steel plate over the ribs where cracks have formed in the 1-in. thick wearing surface. No corrosion was found where cracks formed but did not penetrate through to the steel plate (surfacing of $1\frac{1}{2}$ in. and 2 in. thickness).

Bond between the wearing surface and the deck was found locally loosened in these tests, and at such locations considerable corrosion has occurred, in spite of the bituminous priming of the steel deck.

The above test results indicate that bituminous paints *alone* are not sufficient to protect the steel deck against corrosion, and do not provide a satisfactory bond.

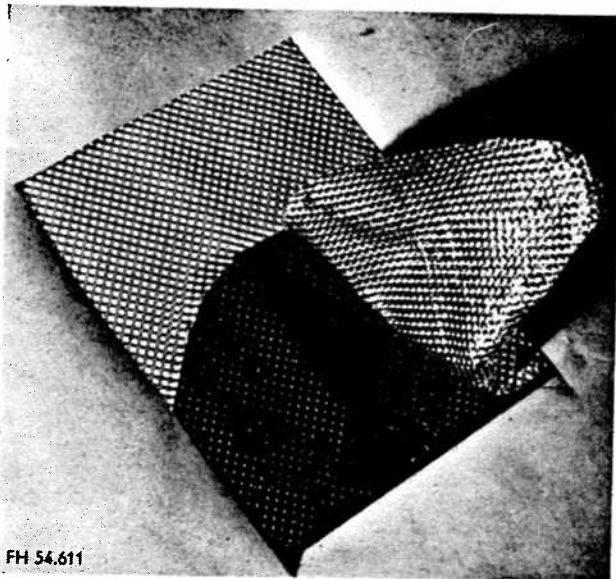
German tests [72] have shown that the bond between asphalt concrete surfacing and a bitumen-primed steel plate decreases considerably with temperature and becomes unsatisfactory at temperatures of 0–15°F. Somewhat better results are obtained with special bituminous tacking compounds.

(b) *Resinous paints*

Resinous paints, modified with red lead or drying oils, have also been tried.

A protective coating consisting of two coats of a resinous paint mixed with 50% of red lead, a 0.02-in. thick coat of a bituminous adhesive compound (61.7% bitumen of a 100–200 penetration grade, 3.3% Latex-powder and 33% solvent) and a 0.04-in. thick felt cloth has been used on the St. Alban Bridge in Basle, Switzerland (1955), (Fig. 8.8).

The felt cloth was placed to prevent blistering of the overlaying bituminous-mix courses and to improve the bond with the overlaying asphalt wearing surface.



FH 54.611

Fig. 8.2. Rippled aluminum foil bonded to a steel plate



FH 54.617

Fig. 8.3. Rippled aluminum foil sheets being placed on a steel plate deck. Bonding compound used for adhesion to steel

However, this installation was not successful (see Section 8.2.4.2.3).

(c) *Asphalt mastic*

This type of coating has been used on several steel plate deck bridges built in Germany.

Asphalt mastic is a dense, impervious, voidless mixture of asphalt, fine aggregate and mineral dust that may retain its plasticity after setting in a degree depending on its bitumen content. It has been applied on the bitumen-coated steel plate in a thickness of $\frac{1}{4}$ in. to $\frac{3}{8}$ in.

Occasionally the mastic was topped by a layer of paper in order to prevent bleeding of the bitumen from the mastic into the overlaying asphaltic wearing course. Another advantage of the paper layer may be seen as facilitating future replacement of the wearing surface. However, a separation of the individual courses by paper may lead to shoving of the wearing surface and is no longer recommended.

Satisfactory performance of the mastic-type sealant in protecting the steel deck plate against corrosion is illustrated by several German steel plate deck bridges built in the 1930's. During the war the bridges were poorly maintained and cracks up to a finger-width have formed in the asphaltic wearing surfaces.

Despite these conditions, inspection of the steel plate decks after the war has shown that in no case have the cracks in the surfacing continued through the mastic layer, and no trace of corrosion was found.

The tentative German specifications for wearing surfaces on steel plate deck bridges [86] call for a mastic coating $\frac{5}{16}$ in. to $\frac{3}{8}$ in. thick of the following composition:

Mineral aggregate: maximum particle size 2 mm (passing sieve No. 8); at least 30% of the aggregate should be smaller than 0.09 mm (passing sieve No. 140). A high content of mineral filler is essential for obtaining sufficient stability of the mastic.

Bitumen content: 12% to 17% max., desirable 14% to 16%. Softening point (ring and ball) of the bitumen *after extraction* from mastic 105°F to 140°F; desirable 122°F to 140°F (corresponding, with an average type of asphalt, to a penetration grade 77°F, 100 g, 5 seconds of 30 to 70). To achieve this consistency after extraction, an asphalt with a correspondingly higher original penetration grade must be used (see Section 8.2.2.1).

As an alternative, a mastic layer $\frac{1}{8}$ in. to $\frac{3}{16}$ in. thick is specified, consisting of mineral dust and asphalt of an original penetration grade of 200, with 2% raw rubber added. The mix of mineral filler and asphalt should have a softening point (ring and ball) of 180°F to 185°F, before addition of rubber.

A proper content of asphalt in the mastic is of great importance to the wearing surface stability. This is indicated by experiences with the surfacing of the Cologne-Muelheim suspension bridge (Fig. 1.21). On the East end of the bridge the 1 $\frac{3}{4}$ -in. thick asphalt concrete surfacing placed on a $\frac{5}{16}$ -in. thick mastic layer containing 22% bitumen soon developed surface ripples due to shoving of the surfacing under traffic and had to be replaced. On the West end, the wearing surface of an almost identical composition placed on a mastic course with 16% bitumen has shown no signs of shoving or rippling and is performing satisfactorily (Fig. 8.6).

(d) *Rippled metal foil*

Aluminum or copper foil is being used as a sealing membrane over steel plate decks.

The aluminum foil used is approximately 0.008 in. thick and has wart-like ripples approximately $\frac{1}{16}$ in. deep (Figs. 8.2 and 8.3). It is bonded to the bitumen-primed deck by means of a hot bituminous adhesive compound. Prior to placing the foil, any irregularities of the deck surface, such as rivet heads, splice plates, etc., must be leveled out by application of a bituminous caulking compound. No air should be entrapped under the foil, since it would affect the bond and cause blisters in the asphaltic wearing surface.

Adhesion of the rippled aluminum foil to the steel deck surface is reported to be very good (Fig. 8.2).

Tests have indicated that a good bond is maintained even at a temperature of -5°F [91].

The metal-foil type of deck protection is considered highly satisfactory and has been used on several important steel plate deck bridges, among them the 856-ft span Save River Bridge in Belgrade, Yugoslavia (Fig. 1.9) and the Severin Bridge in Cologne (Fig. 1.18).

However, it should be emphasized that the success of an installation of this type depends entirely on careful placement of the foil, which should be thoroughly bonded to the deck. Any air contained in void spaces under the foil may eventually cause a general loosening of the bond and a deterioration of the overlaying wearing surface [95].

(e) *Zinc coating*

Good protection against corrosion is provided by spraying the properly prepared steel plate deck with metallic zinc.

British tests with steel plate deck panels sprayed with a 0.001-in. thick coating of metallic zinc prior to surfacing by an asphaltic mix (see Section 8.2.3.2a) have shown no trace of corrosion in the steel plates after 4 $\frac{1}{2}$ years, even where cracks in the asphaltic mix

penetrated through to the steel plate, or where the bond was loosened [103].

Zinc spraying topped with a bituminous adhesive compound for bonding with the overlaying asphaltic wearing surface has been specified on some recent German bridges with steel plate decks.

A 0.005-in. thick zinc coating will be used on an experimental short span steel deck bridge near Troy, Ill. It will be topped with four different types of sealants: coal tar epoxy, pure epoxy resin, asphalt mastic and latex.

The disadvantage of zinc metallizing, in addition to its cost, is in the poor adhesion of the wearing surface materials to the zinc coated surface of the deck. Therefore many engineers consider zinc metallizing of the steel decks to be unwarranted, especially if used in conjunction with additional sealants.

The possibility of using organically or inorganically bound zinc rich protective coatings has also been suggested.

(f) *Plastic membranes*

Polyisobutylene plastic membranes bonded by means of appropriate adhesive paints have been experimented with; however, no firm conclusions regarding suitability of this type of deck protection have been reached. Protective properties of plastic membranes were found satisfactory; however, plastics of insufficient heat resistance may be damaged when topped by hot asphaltic mixes. In some cases poor adhesion of the asphaltic wearing surface to the plastic has been observed, in spite of the tack coats applied [90, 91, 92].

The use of plastic tapes, of the type used for coating of steel pipelines [94], might also be considered.

(g) *Latex compounds*

Latex rubber compounds have been successfully applied both as a protective coating under bituminous wearing surfaces and as a final surfacing. This type of surfacing has been developed in England and is known under the commercial designation of "Semtex".

The compound is applied cold. It has been proved to have a very strong bond with a steel deck, thus providing a reliable protection of the deck against corrosion.

The Semtex surfacing has a rough and skid resistant surface; it is tough and is not affected by vibrations or temperature changes.

When used as a protective coating, a $\frac{3}{32}$ -in. thickness suffices. Final wearing surfaces approximately $\frac{1}{2}$ in. thick have been used. An example of such application is a bascule bridge of the Surrey Commercial Docks in London (1954) [92].

(h) *Epoxy resins*

Epoxy resins, discussed in more detail in Section 8.4 below, may provide a good protective coating under bituminous wearing surfaces.

For a sealing membrane applied directly on a sand-blasted steel surface, epoxy resin containing no coal tar is considered preferable to coal tar epoxy, since the latter contains volatile elements that may cause shrinkage of the membrane.

Grits embedded in the epoxy seal coating will produce a good bond for the subsequent wearing course. Since water-tightness of the seal coating is essential, the amount and size of grit must be properly balanced against the volume of liquid epoxy to prevent pinholing.

A reliable seal coat will probably require an adequate quantity of epoxy resin in the first coat onto which a moderate amount of small size grit is placed, followed by a light final pass of the resin.

8.2.3.3 Mechanical Anchorage Devices

In addition to the protective and bonding materials described above, mechanical anchorage devices have been used to improve the bond of a bituminous wearing course with the steel deck.

Tests have been made on *asphalt concrete* wearing surfaces with wire mesh and expanded metal spot welded to the deck [92]. The results indicated that the presence of metal reinforcement is not always advantageous and may increase the tendency of a bituminous surfacing to crack.

It has also been found that the contact of the asphalt concrete course with the deck tends to be incomplete, resulting in pockets of entrapped air causing blisters in the surfacing.

However, this type of anchorage of the asphalt concrete surfacing may become necessary in special cases such as bascule bridges (Fig. 1.27).

For stabilization of *asphalt mastic* wearing surfaces, flat bar anchors spot welded to the deck are being used. The bars are approximately $\frac{3}{4}$ in. high and are arranged in a zig-zag fashion across the deck, spaced 3 to 6 in. o.c. (Figs. 7.11 and 8.7). This type of anchorage of the wearing surface has been used on two bridges in the city of Duesseldorf (see Section 8.2.4.2.2).

Prior to placing of the mastic surfacing, the bars are coated with a bituminous tack compound.

Some engineers contend that the spot welds between the flat bars and the deck plate may act as local stress raisers to impair the fatigue strength and corrosion resistance of the deck plate. However it is doubtful that such apprehensions are warranted.

A more definite disadvantage of the flat bar anchorage is the considerable amount of labor involved in this installation, resulting in higher costs.

8.2.4 Binder and Surface Courses**8.2.4.1 Composition and Properties of Bituminous-Mix Pavements on Steel Plate Decks**(a) *Composition and thickness*

Bituminous-mix wearing surfaces on steel decks usually consist of a high quality hot-mix of a low penetration asphalt and a dense graded aggregate. The asphalt content is determined by the aggregate gradation and usually ranges from 4% to 12% (See Section 8.2.4.1b).

Occasionally asphalt-mastic mixes containing a high proportion of mineral filler have been used in the wearing surfaces.

Typical data on the composition of bituminous mixes used on existing structures are given in Section 8.2.4.2.

The total thickness of the wearing surface may range from $1\frac{1}{4}$ in. to $2\frac{1}{2}$ in. and is usually placed in two courses, with the lower (binder) course somewhat softer than the upper (surface) course. According to British tests with mastic-type wearing surfaces, a thickness of over $1\frac{1}{2}$ in. is desirable, in order to prevent the cracks from reaching to the steel surface [103]. This requirement, however, may not be too important if the deck is properly protected (see Section 8.2.3).

Where bolt and rivet heads and the splice plates of the steel deck have to be covered, the total thickness of the wearing surface should be such as to provide a coverage of at least 1 in. over the protruding parts. Separation of the surface course from the binder course by a layer of paper, as has been occasionally done to facilitate future replacement of the surface course, is not recommended.

(b) *Stability and durability*

Stability of the pavement is defined as its resistance to deformation (shoving, rippling) under the action of traffic loads. Stability is determined by the frictional or interlocking resistance of the aggregate and by the cohesive resistance of the asphalt cement. Cohesive forces acting between two adjoining bitumen coated aggregate particles are greatest if the bitumen film is thin. An excessive amount of asphalt decreases the cohesive forces and acts as a lubricant, thus lowering the stability of the mix.

Resistance of the wearing surface to shoving and rippling also depends on a good bond of the surfacing with the underlying seal coating and an adequate shearing strength and stability of the sealant itself (see Section 8.2.3).

The effects of temperature on pavement stability are discussed under (c), below.

Durability is the resistance of a pavement to disintegration (raveling, potholing, cracking, rutting). The durability and the density of a bituminous pavement is largely determined by its asphalt content.

Thus the asphalt content and its penetration grade must be determined as a compromise between stability and durability requirements.

Experiences with bituminous wearing surfaces indicate that it is possible to achieve a proper balance, resulting in surfacings that do not become too soft at high temperatures, nor crack in the wintertime.

Generally, in the design of the mixes to be used on steel decks the stability of the surfacing at high temperatures should be regarded as more important than durability. Ruts and washboard ripples in a surfacing that was made too soft are difficult to eliminate once they have developed, and may necessitate replacement of the entire pavement (see Section 8.2.3.2c). Should moderate winter cracking occur as a result of a too hard grade of asphalt, it may be of a relatively small consequence, since such cracks may be easily sealed in the course of routine maintenance of the deck. It should also be noted that, with a proper seal coating under the wearing course, cracks do not directly expose the deck to corrosion (see Section 8.2.3.2).

As a safeguard against cracking of asphalt wearing surfaces, arbitrarily increased deck plate thicknesses have been proposed for the various rib spacings, with the purpose of limiting the deck plate deflections under loads. However, the appropriateness of unduly increasing the deck plate thickness beyond the actual structural requirements is open to question. Cracking may be caused primarily by factors not related to deflections, such as the grade and quality of the asphalt, temperature and aging effects, etc. Available experience with steel deck bridges does not indicate any direct correlation between deck plate thickness and pavement cracking, as may be seen from the fact that on some bridges with a $\frac{3}{8}$ -in. thick deck no cracks are apparent, while pavement cracking has occurred on bridges having thicker deck plates with the same rib spacing.

(c) Temperature effects

A black bituminous pavement subject to heat radiation acts as a "black body" and absorbs large amounts of heat. On hot summer days, temperatures of asphalt pavements of over 140°F have been recorded [92].

Overheating of a thin bituminous wearing surface on a steel deck is likely to be especially severe because a steel plate does not have the heat absorbing and dissipating capacity of a normal pavement subgrade or a concrete slab. A typical relationship between air, wearing surface and steel plate temperature on a hot summer day, measured on the Save River Bridge in

Belgrade, is shown in Figure 8.4. It is seen that the temperature lag between the asphalt and the steel plate is not very large [76].

On the lower end of the temperature scale, the wearing surface on a steel deck may be subject to rapid cooling in the winter time in cold climatic zones.

The thermoplastic properties of the asphalt are imparted to the bituminous mixes, which gradually soften when heated. This may drastically decrease the stability and the load carrying capacity of the wearing surface as the temperature is increased.

At low temperatures the asphalt becomes brittle and its modulus of elasticity increases considerably. Since the thermal contraction coefficient of asphalt is greater than that of steel, an intense and rapid cooling

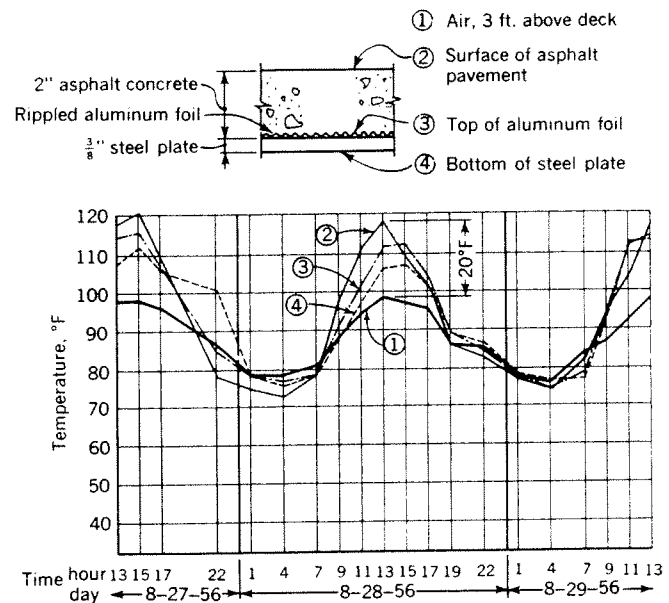


Fig. 8.4. Temperature variation in a wearing surface on a steel plate deck. Test measurements on the Save River Bridge

of the bituminous surfacing, combined with the flexural stresses, may lead to cracking.

The design of a bituminous mix for a wearing surface must take into consideration the adequacy of the pavement over the entire temperature range to be expected, which may be of the order of 150°F. A low temperature susceptibility of the asphalt used is, therefore, highly important; however, it should not be achieved at the expense of other desirable characteristics.

(d) Strength and elastic properties

The flexural strength and rigidity of a bituminous pavement is largely determined by the tensile and the shearing strength of the asphalt binder film surrounding

the aggregate particles, depending chiefly on cohesive forces acting in thin asphalt films and is affected by such factors as the asphalt grade, asphalt content in the mix, temperature, etc.

The compressive (crushing) strength of a pavement depends primarily on the strength of the aggregate particles, gradation of the aggregate and the lateral support of the loaded portion of the pavement.

The *loading duration* and the rate of load application are further important factors in determining the strength of a bituminous pavement. Under a permanently applied load, a pavement would act plastically and deform, while it may sustain a much greater load and act elastically if the load is applied suddenly for a short time, as in the case of a passing wheel of a vehicle.

Due to its elastic properties under instantaneously applied loads, a bituminous pavement bonded to the deck may develop considerable *composite action* with the underlying steel plate deck to which it is bonded.

The extent of composite action of a bituminous concrete wearing surface with a steel plate was investigated in connection with the design of the Cologne-Muelheim Bridge over the Rhine [93].

The effect of the loading duration on the flexural rigidity of a $\frac{5}{16}$ -in. thick steel plate topped with a 2-in. thick bituminous wearing surface, as determined by these tests, is illustrated by the following table:

TABLE 8.2.4.1
EFFECT OF LOADING DURATION ON COMPOSITE SECTION PROPERTIES

Test Conditions	Loading Duration	Relative Rigidity of Composite Section
$\frac{5}{16}$ -in. steel plate with 2 in. bituminous wearing surface, 122°F	Instantaneous	150%
	2 sec.	133%
	4 sec.	128%
	8 sec.	115%
Bare $\frac{5}{16}$ -in. steel plate	...	100%

The composition of the bituminous wearing surface corresponded to that described under Section 8.2.4.2a, below.

The test temperature of 122°F was chosen to approach the actual conditions on a steel bridge deck on a hot summer day.

The flexural modulus of elasticity of the bituminous wearing surface under the effect of an instantaneously applied load was determined from a series of vibration tests made with a 2-in. wearing surface bonded to a $\frac{5}{16}$ -in. thick steel plate, as described above, and was found to be a function of temperature. For the bitu-

minous mix used, its value ranged from approximately 28,000 psi at +120°F to 750,000 psi at -20°F, with a value from 70,000 to 200,000 psi at a temperature of 50°F.

Based on the above test data, the contribution of a 2-in. thick wearing surface to the flexural rigidity of a $\frac{1}{2}$ -in. steel plate subject to an instantaneously applied wheel load has been determined.

The results, represented graphically in Figure 8.5, indicate that the effect of composite action of the wearing surface with the steel deck is considerable in the lower and medium temperature range, and may still be significant at higher temperatures.

Contribution of a bituminous wearing surface to steel plate rigidity was confirmed by British tests with 1-in. and $1\frac{1}{2}$ -in. thick mastic asphalt wearing surfaces. The increase of the rigidity of a $\frac{1}{2}$ -in. thick plate was of

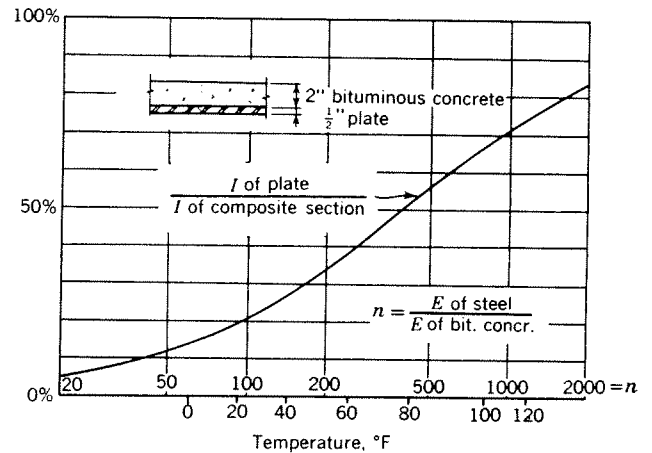


Fig. 8.5. Composite action of bituminous concrete wearing surface and steel deck plate under an instantaneously applied load. M.A.N. tests, 1951

the order of 60% to 80%, at temperatures of 30°F to 50°F. However, no significant effects were recorded at the temperature of 85°F [103].

While the elastic properties of a bituminous wearing surface will be affected by the type of mix, the asphalt content and its penetration grade, it may be concluded that the contribution of the wearing surface to deck plate rigidity will be significant in most cases. The resulting stress reduction in the steel plate is likely to outweigh the specified 30% stress increase due to the impact action of the wheel loads. Thus the wearing surface contribution to the steel deck plate strength, disregarded in the design, may represent an important additional safety factor in the design of the deck plate.

Regarding the stresses in the wearing surfacing, it should be noted that, at low temperatures, the stresses in the asphalt are lower in the case of composite action

of the surfacing bonded to the deck than in the case of the surfacing resting loosely. Thus breaking of the bond between the wearing surface and the steel may cause cracking and deterioration of the surfacing in the wintertime.

(e) *Skid resistance*

A friction coefficient between a given pavement and an automobile tire is not constant and may decrease considerably at higher vehicle speeds, depending on the type of pavement. The friction coefficient is further affected by the presence of water, ice, oil film or dirt on the pavement and is subject to decrease with time, as the wear and polishing of the pavement progresses.

On bridges a higher surface friction coefficient of the pavement is generally required than on open highway portions.

For safe performance, a friction coefficient of at least 0.5 between a wet pavement and a worn tire at a vehicle speed of 40 mph is desirable.

The surface friction coefficient of a bituminous pavement is determined largely by the following factors:

(1) *Aggregate properties.* For best results the aggregate must be tough, must resist wear and degradation and be polish-resistant.

(2) *Pavement composition and gradation.* The mix should have no excess of bitumen causing surface "bleeding" on hot summer days, resulting in a slippery condition. Surface roughness is also an important factor in determining skid resistance; however, there is considerable disagreement as to which type of pavement provides better anti-skid characteristics: an open-graded type, having large voids in the surface (Fig. 8.9) or a dense graded pavement, with a harsh, close-textured surface.

The open-graded pavements, of the type described in Section 8.2.4.2c are not subject to asphalt flushing and are reported to have very good skid resistance, which is little affected by the speed of the vehicle [89]. However, it is also contended that, in the long run, this type of pavement is more subject to aggregate polishing and degradation, which decreases the friction coefficient [105]. Furthermore, the open-type pavement tends to be less durable and more pervious to water, due to its smaller bitumen content.

Wearing surfaces on steel plate deck bridges are subject to an increased danger of *icing* in the winter time because of rapid cooling of the steel deck due to its high thermal conductivity. Slipperiness due to icing may be reduced by surface roughness of the bridge pavement, since an ice film would form less easily and might be sooner crushed by traffic on the sharp, abrasive protruding surface particles.

The skid resistance of a pavement may be improved

by an appropriate *surface treatment*, consisting usually of an application to the pavement surface of a fine-grained abrasive material held in place by a bituminous or other binder.

A comprehensive discussion of the skid resistance of various types of pavements may be found in [105], Chapter 20.

(f) *Additives to asphalt*

Certain properties of asphalt and asphalt-aggregate mixes may be affected by the admixture of additives.

The two most commonly used types of additives to asphalt are:

(1) Various chemicals used to improve coating and adhesion of the asphalt film to the aggregate ("anti-stripping" agents).

(2) Rubber in various forms (raw or synthetic rubber, latex, neoprene), used to improve such properties as temperature susceptibility, low-temperature ductility, and the cementing qualities of the asphalt.

The additives are usually applied at a rate of approximately 1% to 5% of the asphalt weight.

While improvements of the pavement properties due to addition of rubber materials have been reported in many cases, there is no general agreement as to the long-run effects and the economic value of such additives.

8.2.4.2 Typical Wearing Surfaces on Existing Steel Deck Bridges

Data on the composition of typical bituminous wearing surfaces on existing steel plate deck bridges are given below.

8.2.4.2.1 Double-Course Bituminous Concrete Surfacing on Mastic Seal Coat

On the *Cologne-Muelheim Bridge* (Fig. 1.21) two types of surfacing were used, made up as follows:

Type A (West end of bridge); Figure 8.6.

1. Seal coat:

- a. Bituminous heat-resistant paint approximately $\frac{3}{64}$ in. thick, on sand-blasted deck.
- b. $\frac{5}{16}$ -in. thick asphalt mastic, containing 16% bitumen (see Section 8.2.3.2c).

2. Binder and surface courses:

- a. $\frac{3}{4}$ -in. thick hard asphalt concrete. Asphalt content 9%, original asphalt penetration grade (77°F, 100 g, 5 seconds), 35–50. Aggregate gradation as shown in Figure 8.1.
- b. Paper layer, bitumen-impregnated.
- c. $\frac{7}{8}$ -in. thick hard asphalt concrete. Asphalt content 8.5%, original penetration grade 20–30. Aggregate—same as under 2a.

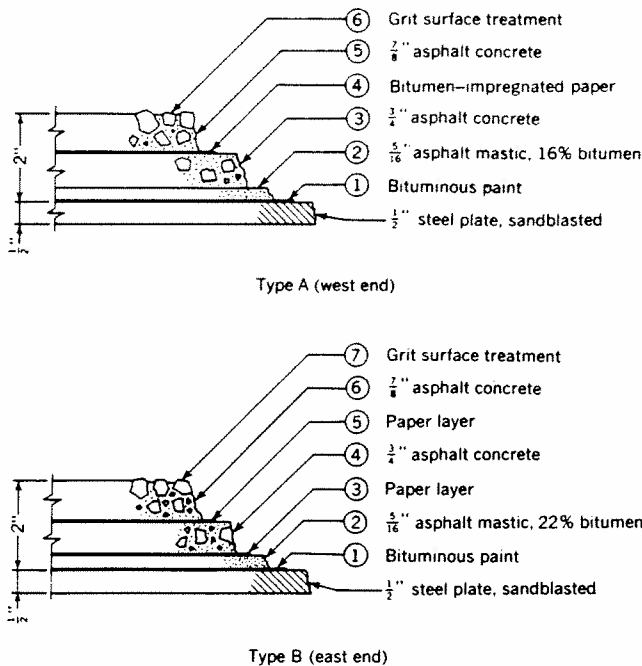


Fig. 8.6. Cross sections of the wearing surface on the Cologne-Muelheim Bridge

3. Surface treatment:

- a. Bitumen coated grit, size $\frac{1}{4}$ in. to $\frac{1}{2}$ in. rolled into the surface course while still hot, in the amount of 2–3 lbs per sq ft.

Type B (East end of bridge):

1. Seal coat:

- a. and b. Same as type A, except that mastic containing 22% of bitumen was used. This led to instability and rippling of the wearing surface (see Section 8.2.3.2) [92].

c. Paper layer.

2. Binder and surface courses:

- a. $\frac{3}{4}$ -in. thick asphalt concrete. Asphalt content 11%, penetration 20–30. Trinidad-Epuré natural asphalt was added. The aggregate was somewhat finer than in type A, as shown in Figure 8.1.
- b. Paper layer.
- c. $\frac{7}{8}$ -in. thick asphalt concrete, asphalt content 8.5%, penetration 20–30. Aggregate as shown in Figure 8.1.

3. Surface treatment: Same as type A.

The hot asphalt concrete mix was placed by hand and stomped with wooden blocks. No rollers were used to compact the mix. The total thickness of the wearing surface is 2 in.

The wearing surface on the West end of the bridge, with the type A composition, performs satisfactorily

under heavy traffic on the bridge and is in good condition. The type B pavement, however, had to be replaced, due to a too soft mastic layer.

The protection of the steel deck against corrosion is apparently good, as revealed by inspection.

8.2.4.2.2 Mastic Asphalt Surfacing with Flat Bar Anchorage

This type of surfacing is used on the *Duesseldorf-Neuss Bridge* (Fig. 1.10).

The wearing surface is about $1\frac{1}{2}$ in. thick and consists of an asphalt mastic placed between the flat 1-in. \times $\frac{1}{4}$ -in. anchorage bars welded to the deck 3 in. o.c. (see Section 8.2.3.3).

Before pouring the mastic, the deck and the anchorage bars were sprayed with a hot bituminous adhesive compound.

The mastic had an asphalt content of 14% to 16%; the softening point of the asphalt after extraction from the mix was 140°F (corresponding to a penetration of approximately 30–40). The mineral filler content in the mastic was over 25%. The hot mastic was poured flush with the 1-in. flat bars and then heated bitumen-coated basalt aggregate, size $\frac{1}{2}$ in. to $\frac{7}{8}$ in., was cast and rolled in up to the desired $1\frac{1}{2}$ -in. total thickness.

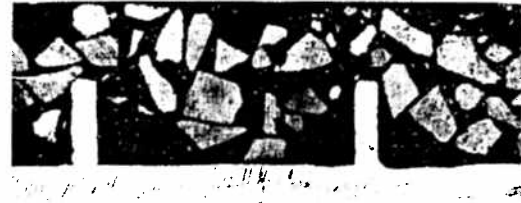


Fig. 8.7. Cross section of the wearing surface on the Duesseldorf-Neuss Bridge. Bituminous-mix between flat bars

The adhesion of the bituminous mix to the steel plate and the flat anchorage bars was found to be excellent, even after strenuous vibration tests [91].

A similar surfacing with flat bar anchorage is used on the *Duesseldorf-North Bridge* (Fig. 1.15).

This type of wearing surface, while expensive to install, is considered “foolproof” by many engineers, since the dense mastic course, which can be made sufficiently soft, provides excellent protection of the deck against corrosion, and cannot shove because of the bar anchorage. Another advantage is that no joints are required with this surfacing [95].

Anchored mastic pavements have, in the past, been regarded with some suspicion by German engineers. However, in view of their very good performance record on the above two structures in Duesseldorf, this

type of surfacing may be expected to gain favor, particularly on bridges with steep grades. Such a wearing surface is planned for the *Europe Bridge* in Austria (Fig. 7.15), which will have a uniform longitudinal slope of 4%.

8.2.4.2.3 Open Graded Asphalt Concrete on Mastic Asphalt Concrete and Resinous Seal Coat

A bituminous wearing surface approximately $2\frac{1}{2}$ in. thick, with an open-graded surface course has been used on the *St. Alban Bridge* in Basle, Switzerland (Fig. 7.19).

1. Seal coat: (see Section 8.2.3.2b)
 - a. 2 coats of resinous paint.
 - b. Bituminous adhesive compound.
 - c. 0.04-in. thick felt cloth.
2. Binder and surface courses:
 - a. $1\frac{1}{2}$ -in. thick mastic asphalt concrete with an asphalt content of 7.7%. The mix consisted of 58% mastic and 42% broken aggregate, size $\frac{1}{8}$ in. to $\frac{1}{2}$ in. The hardness of the mix in place is described by the "hardness index" of 9 (corresponding to a penetration of 0.9 mm, or 0.0354 in. of a steel rod with a $\frac{1}{4}$ in. diameter loaded with 70 lbs during one minute at a temperature of 77°F).
 - b. Bituminous adhesive compound, applied at a rate of 0.5 lb per sq yd, consisting of 50% bitumen, penetration grade 80-100, and 50% solvent.
 - c. A $\frac{3}{8}$ -in. layer of powdered asphalt (corresponding to approximately 22 lbs per sq yd) was placed.
 - d. A layer of a uniform-sized $\frac{3}{4}$ -in. broken hard, bitumen-coated aggregate, heated to 195°F to 215°F was placed. The bitumen used was of a penetration grade 280-320; its content was 2% of the aggregate weight. The aggregate was coated at a temperature of approximately 280°F. A small quantity of powdered asphalt was added to avoid lumping of the coated aggregate during transportation. The aggregate was rolled in after placing with a 6 to 8 ton roller.

- e. Powdered asphalt was applied and brushed in at a rate of approximately 1.8 lb per sq yd on top of the rolled surface course.

This surfacing, installed in 1955, was performing satisfactorily until the summer of 1962, when rippling developed similar to that on the east portion of the Cologne-Muelheim Bridge (see Section 8.2.4.2), which necessitated replacement of large portions of the surfacing.

8.2.4.2.4 Current German Specifications for Bituminous Wearing Surfaces on Steel Deck Bridges

The tentative German specifications for bituminous wearing surfaces on steel deck bridges [86], issued in 1961, contain general recommendations and describe five basic types of surfacings which may be used.

The general requirements are: the surfacing should not shove or ripple under traffic at high temperatures, should not crack in the winter, should have a low susceptibility to aging and fatigue, and should be well bonded to the steel deck. The specification also stipulates that only selected firms, possessing the necessary special knowledge and experience with bituminous surfacings on steel decks, should be entrusted with the preparation and placing of such surfacings.

The following types of bituminous wearing surfaces are suggested:

(a) *Double course of asphalt concrete on a seal paint and tack coat*

The deck must be cleaned by sandblasting or equivalent methods. The seal coat may consist of zinc powder paint, or other coatings, not further specified. The tack coat, placed subsequently, must be reasonably thin and contain no materials that may adversely affect the seal coat.

The asphalt concrete is placed in two courses—a $\frac{3}{4}$ -in. to 1-in. thick binder course and a 1-in. to $1\frac{1}{4}$ -in. thick surface course.

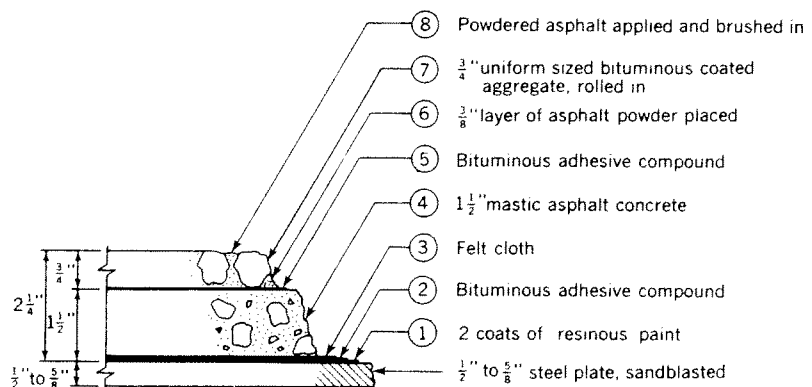


Fig. 8.8. Composition of the wearing surface on the *St. Alban Bridge*, Basle, Switzerland

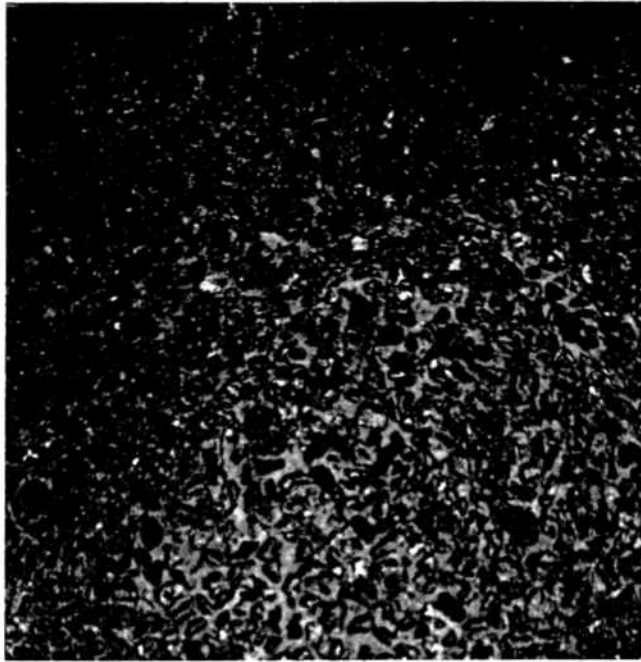


Fig. 8.9. Rough surface texture of the wearing surface on St. Alban Bridge, Basle

The asphalt content in the mix should be 7% to 9%, with the recommended aggregate gradation as shown in Figure 8.1.

The asphalt should have a softening point (standard ring and ball test) of 158°F max., after extraction from the mix (see Section 8.2.2.1), corresponding approximately to a penetration grade of 10–15. However, a softening point under 150°F (penetration 15–20) is preferred.

The softening point of the original asphalt must be correspondingly lower. A value of 140°F (approx. penetration 25–40) is recommended for the harder surface course, and 130°F (penetration 40–60) for the binder course.

The hardness of the finished wearing surface is checked by the penetration test for bituminous pavements, DIN 1996, new version. In this test the penetration of a round steel bar with a cross-sectional area of 5 cm² (approximately 1 in. dia.) loaded with 116 lbs during 30 minutes at a temperature of 104°F is measured. For the binder course a penetration of 4–8 mm (0.16–0.32 in.) is recommended; for the harder surface course this value should be 2–6 mm (0.08–0.24 in.).

Mechanical anchorage of the asphalt-concrete wearing surface by means of flat steel bars spaced far apart is considered ineffective.

Separation of the two asphalt-concrete courses by a layer of paper is not recommended.

(b) *Double course of asphalt concrete on mastic seal and tack coat*

The required composition of the mastic sealant is as described in Section 8.2.3.2c.

The asphalt concrete is placed in two courses, as under (a), above.

(c) *Double course of asphalt concrete on aluminum or copper foil and tack coat*

The required properties and placement of the metal foil are as given in Section 8.2.3.2d.

The asphalt concrete specifications are the same as under (a), above.

(d) *Mastic wearing surface with special anchorage*

The anchorage consists of flat bars, as described in Section 8.2.3.3.

The required composition and placement of the mastic surfacing is as given in Section 8.2.4.2.2.

(e) *Mastic wearing surface without special anchorage*

The asphalt mastic wearing surface without mechanical anchorage is placed in two courses, approximately $\frac{3}{8}$ in. thick. While the first course of mastic is still hot $\frac{3}{4}$ -in. to 1-in. lightly bitumen-coated aggregate is cast and rolled in. After pouring the second course $\frac{1}{4}$ -in. to $\frac{1}{2}$ -in. or $\frac{1}{2}$ -in. to $\frac{3}{4}$ -in. coated aggregate is cast and rolled, until a total thickness of about $1\frac{3}{8}$ in. is obtained. The total amount of mastic used for both courses is approximately 8.5 lbs per sq ft; the total weight of aggregate needed is also about 8.5 lbs per sq ft.

Mastic surfacings without bar anchorage have been tried in experimental installations. It is claimed that surfacings of this type are equally satisfactory and reliable as the mastic surfacings with bar anchorage [95].

Specifications also include recommendations regarding placing of the bituminous-mixes and construction of the joints in the surfacing (see Section 8.2.5).

8.2.5 Construction and Maintenance

8.2.5.1 Preparation of the Steel Surface

It is essential to achieving a good bond between the wearing surface and the steel that the steel surface be properly cleaned of oil, grease, water, dirt, rust and mill scale.

Oil and grease should be removed first by washing the surface with benzene, carbon tetrachloride or other suitable solvents.

Rust and mill scale are removed by mechanical means including chipping, wire brushing, sandblasting or shotblasting and flame cleaning. The degree of cleanliness required for a proper application of protective materials described under Section 8.2.3.2 may be best achieved by sandblasting.

The first coating of protective material has to be applied immediately (within two hours) after the deck cleaning.

Although the deck cleaning and sandblasting, followed by protective coating, could be more economically done in the shop after fabrication of the deck panels, the following practical considerations make it desirable to clean the deck in the field, after its complete erection.

(a) Straightening of warped deck plating panels by means of heat application is often necessary during erection. This could not be done with protective coating applied on the deck.

(b) The edge strips of the deck plating panels have to remain uncoated until the welded or bolted deck field splices are completed, and must be cleaned and sandblasted after the deck erection. Thus cleaning and coating the deck in the shop does not eliminate the need for the special equipment in the field.

(c) Protective coatings and final wearing surfaces are most effectively applied in a continuous operation. Additional cleaning and coating of the strips over the field splices may result in gaps in the protective coating and a wearing surface of non-uniform quality.

8.2.5.2 Placing of the Wearing Surface

Procedures and methods of placing the wearing surface depend on the type of surfacing used.

It must be emphasized that, because of the severe service conditions that must be satisfied by a wearing surface on a steel deck, preparation and placing must be performed with great care, beyond the routine precautions and general rules of good practice for bituminous pavement construction.

It is essential that all specification requirements regarding the quality and penetration grade of asphalt, gradation of the aggregate, mixing proportions and temperatures be strictly observed.

The wearing surface should be placed only during a warm and dry weather period. Placing the hot-mix at outside temperatures below 50°F should be avoided, since the mix would be subject to rapid cooling and would develop internal temperature stresses leading to subsequent cracking.

Rigorous supervision of all phases of the wearing surface construction will be required, since even the best mix may give inferior results if placed carelessly.

Certain cases of failures of bituminous wearing surfaces on steel decks may be directly attributed to the fact that the need for highest quality of workmanship in the installation of such pavements was not sufficiently appreciated. Therefore the construction of the wearing surfaces on steel plate decks should be entrusted only to highly reputable paving firms.

8.2.5.3 Joints

Appropriate longitudinal and transverse *joints* are generally required in *asphalt concrete* wearing surfaces. The joints are usually made $\frac{1}{4}$ in. to $\frac{3}{8}$ in. wide and are filled with an appropriate joint filler material.

Joints between the working batches of the asphalt concrete are required only in the upper course of the wearing surface [86].

Full-depth joints have to be made at all curb, mall and expansion joint steel plates in contact with the asphalt concrete wearing surface. Since these plates may become very hot because of their direct exposure to the sunshine, the joint filler material in direct contact with these parts should be of the lowest possible temperature susceptibility.

The sealing qualities of the joint filler used at the curbs and malls are especially important, since these areas, where dirt, water and snow would normally accumulate, are highly susceptible to corrosion. British tests have indicated that mastic-type joint fillers at the edges of the steel plate panels did not provide an adequate protection [103]. Good results were obtained with asphalt-rubber compounds.

In the *asphalt mastic* type of wearing surfaces no filled joints are required [86].

8.2.5.4 Maintenance

The wearing surface should be carefully inspected after each cold season. If cracks occur, they should be sealed by appropriate sealing compounds.

It is essential that accumulation of water on the deck be avoided. This may be achieved in the design of the bridge by providing sufficient cross slopes of the deck and adequate scuppers at curbs.

For the purpose of keeping the deck skid-free during ice-forming weather conditions, abrasives (coarse sand, cinders) or non-corrosive chemicals are to be preferred.

While a properly maintained wearing surface constructed in accordance with the recommendations of the foregoing sections may be regarded a sufficient protection of the steel deck against the corrosive effects of the ordinary salts used for ice removal, avoidance of their use would provide an additional safety measure.

8.2.6 Conclusions

Experience with bituminous wearing surfaces on orthotropic steel plate deck bridges in Europe shows that on a great majority of the structures such surfacings are giving satisfactory service. Although there are more than 40 existing structures of this type, only a few cases of serious damage to the surfacing have occurred

which required major repairs or replacement of the surfacing. These include one case of severe winter cracking (the Hedemuenden Bridge, Fig. 1.29), and three cases of instability of the surfacing (the Cologne-Muelheim Bridge (see Section 8.2.4.2), the St. Alban Bridge (see Section 8.2.4.2.3), and the Breitscheid Bridge—a short span experimental installation).



Fig. 8.10. Asphalt plank wearing surface on the Harlem River Lift Bridge, New York City

There are strong reasons to expect that a bituminous surfacing, designed in accordance with the criteria outlined in the foregoing sections and placed with proper care, should be successful. The cost of such a surfacing must, understandably, be higher than that of an ordinary bituminous wearing surface.

On the other hand, no wearing surface should be expected to last indefinitely, and occasional repairs and overhaul must be taken in stride. Exaggerated requirements or undue apprehensions regarding the performance of the surfacing may result in unnecessarily complex designs which are likely to be unduly costly.

8.3 ASPHALT PLANK WEARING SURFACES

8.3.1 General

Asphalt planks are composed of low-penetration asphalt, fibers and mineral filler, mixed at high tem-

perature and extruded to size under high pressure. This process results in a dense and durable internal structure.

For bridge paving purposes the *mineral-surfaced* plank is used, produced by forcing coarse trap rock aggregate under pressure into the surface of the plank in such a manner as to interlock the stone permanently with the fibrous body of the plank. The skid-resistance of the mineral-surfaced asphalt plank is comparable to that of asphalt concrete with surface treatment (see Section 8.2.4.1f).

The asphalt planking weighs approximately 100 lbs per cu ft. The standard size of the mineral-surfaced planks is 24 in. \times 12 in., with a thickness of 1, 1 $\frac{1}{4}$, 1 $\frac{1}{2}$ and 2 in.

For applications on solid smooth surfaces a thickness of 1 in. is considered sufficient.

8.3.2 Composition and Physical Properties

Asphalt planking for paving purposes, as presently manufactured, consists of approximately 40% to 48% low penetration asphalt, 35% to 45% mineral filler and 8% to 22% organic fiber. The hardness and toughness requirements for asphalt planking are given by ASTM Specification D517-50 and the similar AASHTO specification M46-38.

The asphalt planks for the steel plate deck Harlem River lift bridge of the west approach to the Triborough Bridge in New York City (1936), still in very good condition after 26 years of service (Fig. 8.10), were manufactured to a special specification with the following principal requirements: Composition—*asphalt* up to 50%; *mineral filler* 35% to 45%; *organic fiber*—not less than 12%, by weight.

The softening point of the asphalt after extraction from the plank—180°F to 225°F; standard penetration at 77°F—5 to 25.

The fiber should be free from decomposed or decayed material, mineral wool, metal, straw, leather, wood or sawdust and should contain at least 16% of shredded long cotton fabric, properly flocculated.

The mineral filler should possess physical characteristics making it suitable for use in bituminous mixes. At least 50% of the mineral filler should pass the No. 200 sieve.

The *hardness* of the finished plank was defined by the penetration test as follows: The underside of the 6-in. \times 6-in. sample shall be loaded by a 1-in. cylindrical steel point with an end radius of curvature of 2 in. Under a 56 lb load applied at a temperature of the sample of 140°F, a penetration reading at 15 seconds subtracted from that at 75 seconds after load application should not exceed 0.07 in.

The required *toughness* was defined by the following test: a steel pin with a $\frac{1}{32}$ -in. point is placed against the underside of the plank at a distance of 1 in. from the two edges of the 6-in. \times 6-in. sample at a temperature of 32°F. A 10 lb weight is dropped on the top of the pin from a height of 17 in. The plank should not split or crack.

8.3.3 Laying the Planks

According to the plank manufacturers' specifications, the planks shall be placed on a swept, broom-clean deck surface, and cemented in place by an appropriate asphalt plank cement [88, 96].

The asphalt plank cement usually consists of an asphalt cut back by volatile solvents to such consistency as is required for uniform application.

The cement shall be applied not less than $\frac{1}{32}$ in. thick and not more than $\frac{1}{16}$ in. thick (40 to 50 sq ft per gallon). All vertical surfaces of the curbs, stop bars, etc. which will come in contact with the wearing surface planks shall be likewise coated.

The planks shall be laid not less than 15 minutes and not more than 2 hours after application of the cement, with the 24 in. dimension of the plank parallel to the longitudinal axis of the bridge and the transverse joints of the adjoining planks offset by 12 in. Each plank shall be laid as close as possible to its final position and pressed or wedged firmly in place against the adjoining planks.

In order to assure complete lateral stability of the plank surfacing, transverse stop bars welded to the deck at 5-ft to 20-ft intervals are recommended. The stop bar spacing should be exactly adjusted to the plank dimensions, to reduce the field cutting and fitting of the plank to a minimum.

If no tight fit is obtained at the curbs and the stop bars, the gap shall be filled with a strip of asphalt-impregnated laminated felt.

All planks shall be pressed, rolled or weighted after placing to secure solid bearing in the asphalt cement coating.

On the Harlem River Bridge, mentioned above, the plank was laid on top of the steel deck painted in the usual manner and broom-cleaned. The asphalt cement prescribed for bonding of the plank consisted of 65% to 77% bitumen and 23% to 35% volatile solvent. For a uniform application the use of an air gun was prescribed at a pressure of not less than 60 psi. Spraying, or spreading of the asphalt cement by means of a brush or squeegee was not allowed. No application of the asphalt cement at a temperature below 50°F was permitted.

8.3.4 Performance

Experiences with asphalt plank surfacing indicate that the performance of the surfacing depends largely on the quality of the plank, careful placing and traffic intensity.

With the planks tightly fitted, the joints between the planks usually fill with bitumen extruded from the plank under the effects of traffic and heat, thus providing additional sealing of the underlying deck.

Moderately heavy traffic is helpful in maintaining an even riding surface. Curling up and lifting of the corners of the planks have occasionally been reported in pavement areas subject only to very light or infrequent traffic. For this reason mechanical anchorage of the plank corners has sometimes been used.

According to the Triborough Bridge Authority, performance of the $1\frac{1}{4}$ -in. thick asphalt plank surfacing on the Harlem River Bridge has been excellent, and only infrequent replacements of the individual planks have been found necessary.

However, the performance of similar planking on another of the Triborough approach bridges with a steel deck, the Bronx-Kill Bridge, has been less satisfactory and the plank replacement ratio on this structure is considerably higher. This may be due to a somewhat inferior plank composition, a less careful original placing procedure and extremely heavy truck traffic on this structure.

It is reported that the plank failure, necessitating its replacement, usually starts with a widening of a joint between the planks, followed by progressive chipping and crumbling of the plank edge.

Removing of the faulty plank usually reveals some deterioration of the asphalt cement coating directly under the damaged edges, accompanied by traces of rusting of the steel plate along the plank edge. However, except for the narrow strip along the edge, the bond of the plank to the deck is very strong, so that the plank has to be removed with a chisel. The area under the plank is reported to be sound, with no traces of corrosion.

8.3.5 Conclusions

Asphalt planking may provide a satisfactory wearing surface on steel plate deck, provided quality of the planks is high, rich in bitumen and organic fiber, and provided the planks are carefully placed.

One of the advantages of asphalt planking, as compared with bituminous concrete surfacing, is dead load saving. The 1-in. planking weighs approximately 9 lbs per sq ft, while the weight of the 2-in. bituminous wearing surface is approximately 23 lbs per sq ft. Another advantage may be seen in the easier installa-

tion, requiring no costly preparation of the steel deck surface in the field, as is needed with bituminous mix surfacing (Section 8.2.5.1).

However, an improvement of the presently used cementing materials and steel deck protection methods under the planking is desirable to assure a more reliable protection of the deck against corrosion.

Application of a metal foil or other protective materials (Section 8.2.3.2) might provide a satisfactory solution.

Since the surface on which the planks have to be laid must be perfectly even, application of the planking on steel decks having protruding splice plates, rivet heads, etc. is not possible.

Should the deck surface be locally dished or otherwise depart from prescribed deck elevations, due to welding deformations or imperfections due to fabrication and erection of the deck, local corrections of the deck elevations by adjustment of the planks would not be practical, since a uniform thickness of the cementing material used with the planks is required. Thus, steel decks to be surfaced with asphalt planks would have to be fabricated and erected to stricter geometric specifications and smaller tolerances than would be required in the case of a bituminous-mix surfacing.

8.4 EPOXY RESINS

8.4.1 General

Epoxy resin surfacings represent a new development in the field of highway paving. Surfacing of this type consist of specially prepared epoxy resin compounds which act as a binder to hold in place an appropriately graded abrasive grit, providing a tough and skid-resistant surface.

On the basis of the manner of application, two types of epoxy resin wearing surfaces may be distinguished:

(a) *Spray applications.* In this method the resin binder is applied to the surface in a liquid state and the grit is then broadcast over the surface. When the resin sets chemically, the grit is permanently fixed in place.

(b) *Epoxy concrete.* The epoxy binder, with or without an admixture of asphalt, and the aggregate are mixed, in a similar manner as a cement concrete or an asphalt concrete, prior to application to the roadway. The epoxy concrete is then placed on a prepared surface in a desired thickness.

Both types of surfacing are discussed below.

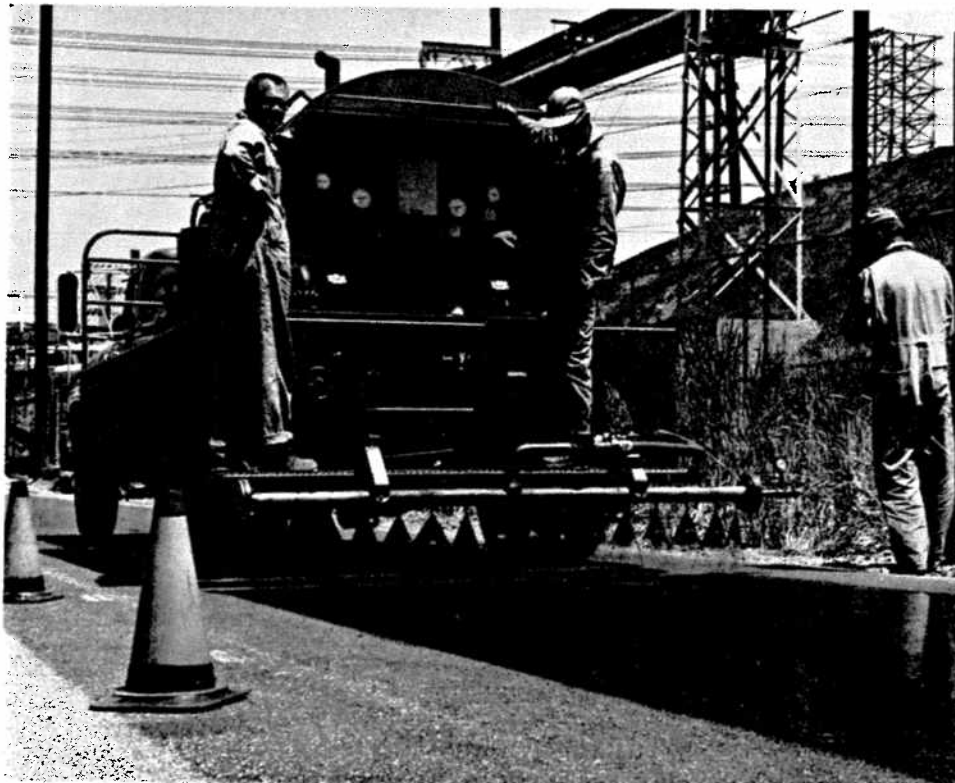


Fig. 8.11. Application of epoxy resin compound by spray truck

8.4.2 Material Properties

*Epoxy*s belong to the general family of *synthetic resins* whose molecules contain the reactive epoxide group. Through the use of a hardener, or catalyst, the reactive groups may be made to link together, thus producing the epoxy polymer system.

The reaction is exothermic (heat-generating), will take place at normal temperatures, and is irreversible. Once an epoxy plastic has set, it cannot be appreciably softened or remolded by heat. The epoxy resin compounds are designated thermosetting materials, in distinction from thermoplastic materials, such as asphalt, which melt upon heating and solidify upon cooling.

To produce certain desirable physical characteristics, as hardness, elasticity, etc., plasticizers and reinforcing fillers are added.

The epoxy compounds for use in wearing surfaces usually consist of two equal parts of an epoxy resin modified for maximum elasticity, and a catalyst hardener containing coal tar and an organic amine curing agent. The epoxy resin is a clear, oily fluid; the hardener is a black fluid, due to the coal tar content. The color of the compound after mixing is black.

Epoxy compounds without coal tar or pine oils, which are non-reactive fillers, are also available. They are more expensive because of a higher content of the pure epoxy resin. The mixture is clear and the color of the finished surfacing depends on the aggregate used.

It is currently felt that on steel plates pure epoxy resin, without coal tar, should be preferred, since it will achieve a better bond and decrease shrinkage of the epoxy film.

The epoxy compounds for paving purposes are known under various commercial names. The compounds are delivered in dual containers, containing the two components.

The hardening reaction, causing a gradual increase in viscosity, starts immediately after mixing the two components. The time from mixing the components until the mixture can no longer be placed is called the *pot life* of the compound.

The pot life of the epoxy compounds used in spray applications is rather short and may range from 30 to 90 minutes at a temperature of 50°F, 15 to 45 minutes at 70°F and 5 to 15 minutes at 90°F. The curing time of the compound is 8 to 13 hours at 60°F, 5 to 7 hours at 70°F and 1½ to 4 hours at 95°F. Complete hardening will require up to 24 hours.

The compressive *strength* of the epoxy compounds after hardening is reported to be of the order of 4000–5000 psi, with a modulus of elasticity of about 400,000 psi at lower temperatures to 100,000 psi at higher temperatures.

The compressive and flexural strength of an epoxy concrete (mix proportion: 1 part epoxy-coal tar compound, 2.8 parts sand, 2.6 parts coarse basalt aggregate, by weight) has been found to be inversely proportional to the test temperature, as follows [102]:

Compressive strength: (2-in. cubes) 7000 to 11,000 psi at 0°F; 5000 to 6000 psi at 70°F; 1200 psi at 140°F. There were indications of strength recovery after cooling.

Flexural strength (4-in. × 4-in. × 15-in. beams): 2900 psi at 0°F; 2500 psi at 70°F.

The unit weight of the epoxy concrete of the above composition was 139 lbs per cu ft.

The epoxy compounds, when properly mixed and hardened, are tough and resistant to the action of water, gasoline, oils, greases, solvents and de-icing salts. Adhesion to steel is excellent, provided the steel surface is clean and sound.

8.4.3 Spray Applications

8.4.3.1 Existing Installations

Epoxy compound surfacings with embedded grit have been applied on many occasions during recent years of bituminous and concrete pavements to improve their skid resistance in critical areas such as steep bridge slopes, sharp curves, stopping areas, etc. One example of such application is the downhill portion of the East-bound roadway of the Triborough Bridge in New York City where a single coating of an epoxy surfacing with emery aggregate was placed on the concrete deck in 1959. The surfacing possesses a very good friction coefficient and is in satisfactory condition after more than 2 years of service under heavy truck and car traffic.

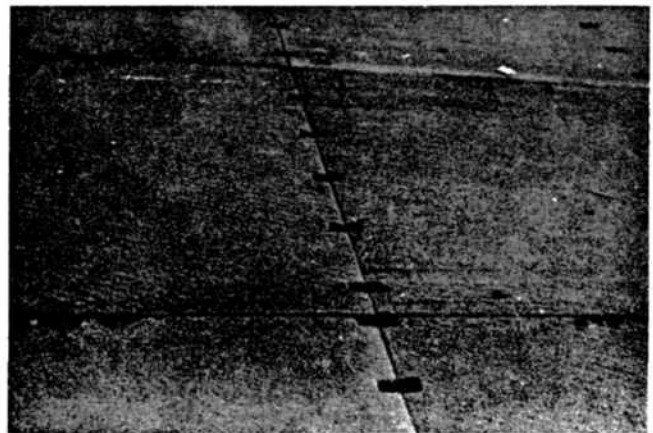


Fig. 8.12. Epoxy and grit surfacing on prefabricated stiffened steel deck panels installed on the Strawberry Mansion Bridge in Philadelphia (1960)

Test installations of epoxy surfacings on concrete slabs have indicated that if bond failures occur, they may be attributed to an unsound concrete surface, not perfectly dry or clean, saturated with oils, etc. In this respect applications on steel decks promise better results, since a steel plate, unlike a concrete or bituminous surface, does not absorb moisture and may be cleaned more perfectly prior to placing the surfacing.

Applications on steel plate decks have been less numerous. In 1958 a steel plate deck with a coal tar epoxy compound wearing surface was installed on the Pennypack Creek Bridge in Philadelphia. One half of the epoxy-coated steel panels were made with expanded metal reinforcement, the other half without the reinforcement. For three years no difference in the performance of the two halves was apparent; subsequently, however, a small failure appeared on the portion that did not have expanded metal. This was repaired with no interruption of service of the bridge. The surfacing has lost some of its original roughness and there are small pock marks where larger pieces of grit have been knocked out of the resin matrix; however, this action apparently has stopped and the general condition of the wearing surface, four years after its installation, is satisfactory. Emery aggregate passing through No. 12 mesh and retained by No. 20 mesh was used on this deck.

Another example of epoxy surfacing on steel is the deck of the Strawberry Mansion Bridge in Philadelphia, consisting of prefabricated stiffened steel plating panels coated with an epoxy compound with embedded abrasive aggregate (Fig. 8.12), installed in 1960 to replace a deteriorated concrete deck. Expanded metal reinforcement was used. After two years of service the surfacing was reported to be in good condition.

In both cases the total thickness of the surfacing is approximately $\frac{5}{16}$ in. The surfacing was applied in two layers in the shop and cured at a temperature of 200–250°F.

An epoxy surface treatment was applied in 1959 to eliminate the slipperiness of the wide flange steel expansion dams on the east bound ramp from the Interchange No. 14A on the Newark Bay Extension of the New Jersey Turnpike. The finger plates were coated with an epoxy compound and, while it was still tacky, sharp broken sand was spread on the surface. The surface treatment has proved to be successful [87].

8.4.3.2 Application Methods

Surface preparation. The steel deck must be clean and dry, free from rust, paint or grease. Best results may be obtained by solvent cleaning followed by sand-

blasting (see Section 8.2.5.1). However, in the opinion of some engineers, solvent cleaning of the steel surface may be sufficient for a good bond of the epoxy compound to the deck.

According to the manufacturers' recommendations [98, 102], the *quantity* of epoxy compound required for a single-layer coating is 1 gallon per 30 sq ft, which gives a thickness of epoxy matrix of approximately $\frac{1}{16}$ in.

Mixing of the two components of the epoxy compound may be done in conventional mortar mixers, when small areas have to be coated. The compound is then poured on the surface and spread with a trowel, brush or squeegee.

For applications involving large areas, a continuous automatic mixer-sprayer is recommended (Fig. 8.11).

The *grit* should be broadcast over the surface at a rate of approximately 15 lbs per sq yd, which is in excess of the quantity needed. After the epoxy matrix has sufficiently hardened, the excess grit (about 6 to 9 lbs per sq yd) is swept away. The resulting overall thickness of this type of surfacing is approximately $\frac{1}{8}$ in.

The grit should be clean, dry and sharp and contain no dust. The size should be such that 90% of the grit falls between the No. 12 to No. 20 mesh, with nothing finer than the No. 30 mesh.

Since the aggregate is largely exposed, with only the lower portions of the particles embedded in the matrix, a durable and wear-resistant aggregate is essential. The following aggregate materials, listed in the order of increasing cost, and, in general, increasing hardness, may be used: silica sand, iron ore tailings, emery, corundum.

The grit should be broadcast immediately after spreading the epoxy compound. The compound applied to the deck surface is workable for about $\frac{1}{2}$ hour at a temperature of 95°F, and longer at lower temperatures.

Application at temperatures below 60°F is not recommended because of the long curing time required.

Where thicker wearing surfaces are required, two or more layers of the epoxy compound may be applied. In such cases the lower course might be made with a less expensive aggregate.

A final light pass of the epoxy, after the aggregate has been cast and cemented in place, may provide a better coating of the exposed aggregate particles and prevent the knocking out of larger particles from the matrix.

The use of *expanded metal reinforcement* appears to be warranted, although it increases the cost of the surfacing. The reinforcement, tack-welded to the deck, may secure a constant thickness of the epoxy coating and prevent

or localize a deterioration of the surfacing, should such develop (see Section 8.4.3.1).

Shop application of the surfacing on steel plate deck panels is advantageous from the point of view of the quality of the wearing surface. The deck cleaning may be performed better and less expensively in the shop, and better quality of the surfacing may be obtained if it is applied under controlled temperature conditions. Application in the shop permits temperature curing, usually at a temperature of 200–250°F, which further increases the hardness and durability of the epoxy surfacing.

However, as has already been mentioned in Section 8.2.5.1, the edge strips of the deck plating panels have to be left uncoated, and must be cleaned and surfaced in the field, after completion of the deck splices. This would raise the problem of proper bonding of the shop- and field-applied portions of the surfacing. Adjustments of the steel deck geometry after erection, to conform exactly to the required deck elevations and grades, would hardly be possible with the surfacing already applied.

8.4.3.3 Conclusions

A sprayed-on epoxy coating represents a very desirable wearing surface on a steel deck from the point of view of weight saving and skid-resistance. It has a very good adhesion to steel and may be easily repaired by patching the damaged areas with an epoxy mortar.

The epoxy surfacing will certainly participate in the local flexural stresses of the steel deck plate. However, the strength and elasticity of the epoxy appear to be sufficient to prevent cracking.

The fatigue strength of the epoxy surfacing would still have to be determined experimentally.

A double course sprayed-on epoxy surfacing of a steel deck is still rather expensive, compared with a bituminous wearing surface, and may cost up to \$1 per sq ft. However, the additional cost of this type of surfacing would be partly offset by the steel weight saving due to the dead load reduction.

The thinness of the surfacing, while helpful in reducing the dead weight of the structure, is a disadvantage from the construction point of view. With wide steel decks, deviations from the specified deck elevations after erection are unavoidable and may be of the order of $\pm 3/8$ in. This may be due to imperfect cambering of the steel members, differences in the elevations of individual floor beams due to welding distortion, fabrication and erection inaccuracies, deck plate warping, etc. While evening out of the geometric imperfections of the deck may be accomplished by varying the thickness of a more substantial wearing surface, it would

not be possible with the thin sprayed-on epoxy surfacing requiring a uniform thickness of application. A partial adjustment would be possible by additional coatings applied to the depressed deck areas; however, this may materially increase the cost of the surfacing. Therefore the steel deck framing and plating would have to be fabricated and erected with smaller geometric tolerances than would be required for a thicker wearing surface.

The thinness of the epoxy surfacing would also preclude the use of bolted or riveted splices of the deck plate.

Application of sprayed-on epoxy surfacing to large steel deck areas, requiring well coordinated and rapid operations of deck cleaning, immediately followed by the epoxy spraying and grit casting, may present difficult practical problems, especially when the surfacing is installed in the field. Lengthening of the pot life and of the workability period of the epoxy compounds appears to be desirable.

As with the other types of wearing surfaces on steel plate decks, a high quality of workmanship is one of the most important requirements for a successful application.

The final answer to the problem of finding the most economical method of application of epoxy surfacings on steel bridge decks will have to evolve from the actual practice.

8.4.4 Epoxy Concrete

Epoxy concrete, using a mixture of epoxy and asphalt as a binder cementing the aggregate, has been experimented with as a wearing surface on concrete and bituminous pavements and industrial floors. A *hot mix* epoxy asphalt concrete with a binder content of 7% to 12% has been tried in thicknesses of approximately 1 in., with varying success. The short pot life of the epoxy component is reported to handicap the placing operations. The epoxy-asphalt concrete has the advantage of resisting jet fuel spillage and does not soften under high heat.

A *cold-mix* epoxy-asphalt concrete has also been developed [97]. The binder consists of 80% equal parts epoxy resin and a synthetic high-penetration bitumen and 20% hardener, wetting agents and flexibilizers. The binder content in the concrete is approximately 7%. The pot life of the binder components and the working life of the concrete are reported to be longer than those of the hot-mix type.

The epoxy-asphalt concrete surfacing should be placed on a prepared surface coated with an epoxy-asphalt binder. It may be screeded and rolled to the desired profile. The concrete is claimed to be water-

proof, resilient, very adhesive and less expensive than a sprayed-on epoxy surfacing. These properties make the cold-mix epoxy-asphalt concrete appear well suited for application on steel plate bridge decks. A $\frac{1}{2}$ -in. to $\frac{3}{4}$ -in. thickness is recommended by the manufacturers. However, experience with the cold-mix epoxy-asphalt concrete on steel decks is still lacking, since the only applications of this material to date have been on concrete or bituminous pavements.

8.5 OTHER MATERIALS

Latex-rubber compounds consisting of synthetic rubber, portland cement and fine aggregate, may be applied as a surfacing on steel plate decks.

A latex-rubber product known under the commercial name of "Semtex" (see Section 8.2.3.2g) has been used successfully on the steel decks of several short span bridges in England and Germany [92].

A similar product, commercially known as "Tivoplan" is being used for surfacing of ships' decks. One example of such application is the deck surfacing of the passenger liner *United States*.

A latex modified portland cement mortar is being recommended for patching of concrete pavements [85]. This product might also be applicable to steel decks.

A $\frac{3}{8}$ -in. thick latex compound surfacing weighs approximately 4 lbs per sq ft. The surfacing is reported to be very durable, resilient, water-tight and adhesive to metallic surfaces. A disadvantage of this surfacing is seen in a relatively long curing and hardening period (1 to 3 days), during which the surfacing is sensitive to weather conditions [91].

The use of a *rubber-latex asphalt* emulsion with a fine

aggregate on a steel deck has been tried with good results by the Department of Public Works of the State of California.

8.6 SUMMARY AND CONCLUSIONS

Bituminous-mix surfacings, in conjunction with appropriate sealants and tack coats, asphalt planks, epoxy compound surfacings and other materials, are available to provide a good riding surface on a steel plate bridge deck and to protect it against corrosion.

The bituminous-mix wearing surfaces are predominant and have been used on all major bridges with steel plate decks. Bituminous-mix surfacings may be expected to give satisfactory, economical service, provided errors in the design are avoided and the surfacing is placed with proper care. The disadvantage of a bituminous-mix surfacing is in its relatively large dead weight.

The development of the new synthetic surfacing materials, promising savings in dead weight and an improved skid resistance, is in progress.

Ideally, such a surfacing should be $\frac{1}{2}$ in. to $\frac{3}{4}$ in. thick and should be placed in one application. Surfacing containing epoxies appear to be most promising.

While a bridge surfacing ideal in all respects has not yet been developed, the imperfections of the existing types should not be exaggerated and should be viewed in the same light as the known deficiencies of all current paving materials and methods in general.

In conclusion it may be said that construction of reasonably good and reliable wearing surfaces on steel decks is entirely feasible. Thus bridge engineers need not be deterred from using the steel plate deck bridge system because of apprehensions regarding the surfacing.

CHAPTER 9

Design Criteria and Specifications

9.1 MAIN STRUCTURAL MEMBERS OF THE BRIDGE (SYSTEM I)

9.1.1 General

The basic criteria of *functionality*, *economy* and *aesthetics* governing the choice of the structural system, the spans and other principal features of steel bridges remain essentially the same in the design of bridges with steel plate decks.

However, the characteristic features of the steel plate deck bridge system, discussed in Chapter 1, are necessarily reflected in basic planning and design decisions.

Thus, for example, in the design of continuous girder bridges overall economy may dictate a choice of longer spans than would be economical in conventional design, because of the efficiency and the light weight of the steel deck superstructures.

In the design of tied arch and suspension bridges the vertical, lateral and torsional rigidity which may be provided by the steel deck system is taken into consideration and advantageously utilized.

Often the use of a steel deck may affect the choice of the structural system of the bridge, as in the cases illustrated in Figures 1.38b and c, where steel plate deck girder bridges proved to be more economical and more aesthetically appealing than the truss or suspension bridges which they replaced.

In all cases a steel plate deck bridge should be viewed as an integral three-dimensional space structure, and the close interdependence of its individual members should be kept in mind.

9.1.2 Dead Load and Live Load Stresses

The bending moments and stresses in the main system are computed and the bridge members proportioned by the usual methods, with loads and allowable stresses in accordance with the bridge specifications used.

In computations of rigidities or stresses the steel plate deck, or an appropriate portion of it, is included as a part of System I (see Section 1.2.3). In proportioning the steel deck the superposition of the System I and System II stresses has to be considered, as discussed in Section 9.3.

In the design of continuous girder bridges it is often advantageous to adjust the *dead load moments* in such a manner as to obtain a desired distribution of the moments, as discussed in Section 7.3.3. Since the full cross section of such bridges is usually built up in the individual construction steps, the residual erection bending moments and stresses have to be considered in the design.

Steel plate deck bridges are generally characterized by a much smaller proportion of the dead load moments and stresses, compared with structures of conventional types, because of a considerably smaller weight of the steel plate deck superstructures. Thus, the design *live load moments* and stresses become relatively more important.

However, it should be noted that developing the maximum values of the calculated live load stresses in the main members of long span bridges under actual service conditions is very unlikely, except under load test conditions, as confirmed by the surveys made. Thus, the maximum live load stresses actually attained in main bridge members are, as a rule, well below the level of the maximum design stresses.

9.1.3 Dynamic Effects

The vibration characteristics of bridge members depend essentially on their mass to rigidity ratio.

While the vibration characteristics of *girder bridges* with steel decks may differ somewhat from those of comparable bridges with concrete decks, more noticeably so in the shorter span range, no objectionable vibrations will occur under normal conditions and there is no need for revision of the usual *impact factors* stipulated by current bridge specifications.

The dynamic behavior of steel plate deck stiffening members of *suspension bridges* has to be investigated in each case by the methods used in the design of such bridges.

The *local vibrations* of steel plate decks are discussed in Section 9.2.4.

9.1.4 Deflections under Live Load

The live load deflection of *girder bridges* is a function of the span and of the ratio of the live load stress, f_L ,

in the bottom flange to the distance, c , between the bottom fiber and the neutral axis of the girder. In steel deck bridges both values, f_L and c , tend to increase, compared with concrete deck structures; the former because of the larger proportion of live load stress in the total stress, the latter because of the generally unsymmetrical cross section of the girder, with the neutral axis located in the upper half of the section. Thus, for a given span, the live load deflections would tend to be approximately the same in both cases if the depths of the girders are equal, and may be larger in the steel deck alternative if shallower girders are used in this case.

Generally, the amount or ratio of the live load deflection is hardly of direct importance for satisfactory performance of a bridge structure. It is well to note that some newer bridge design specifications do not contain provisions restricting the deflections under live loads.

However, an excessive relative deflection of the bridge girders under an unsymmetrical bridge loading, which may lead to a reversal of the design cross slope of the bridge deck, should be avoided.

9.1.5 Fatigue Strength

While the problem of fatigue strength of bridges with steel decks is essentially similar to that of conventional steel bridges, the generally larger proportion of live load design stresses in the total stresses of the members of steel deck bridges, resulting in a larger amplitude between the maximum and the minimum stresses, indicates the need for closer attention to the fatigue problem in the design of such structures. However, the actual maximum live load stresses in main bridge members tend to be considerably smaller than the calculated design values, as pointed out in Section 9.1.2. Furthermore, fatigue strength is governed by the *average* amplitude of stress fluctuation rather than the infrequent maximum amplitudes under peak loads.

Thus, as in conventional cases, the fatigue problem is hardly a critical factor in the design of the main members of steel deck bridges and should be regarded sufficiently covered by current design provisions for members subject to fluctuation of stress intensity.

9.2 BRIDGE DECK STRUCTURE (SYSTEM II)

9.2.1 General

The bridge deck, consisting of longitudinal ribs and transverse floor beams, both using the deck plate as their common flange, is treated for design purposes as a separate structure transmitting local traffic loads to the main bridge members, as discussed in Section 1.2.4.1.

The general criteria determining the choice of the stiffening system and the optimum spacing of the ribs and floor beams are discussed in Section 7.1.

The method for computation of the stresses in the ribs and the floor beams under design loads is given in Chapters 3, 4 and 5.

9.2.2 Static Strength

The strength of *longitudinal ribs* of the usual types loaded by concentrated wheel loads is very large and exceeds several times the values computed by ordinary flexural theory, as discussed in detail in Section 1.2.4.2.

Therefore, the "allowable stress" criterion, assuming a linear relationship between the loads and the stresses in the structure, is not appropriate for the determination of the actual safety factor of the ribs against failure.

Criteria currently used in the design of steel bridge decks, based on a partial recognition of the high strength of the longitudinal ribs under local loads, are discussed in Section 9.3.

The strength of the *floor beams* of steel decks has not yet been experimentally verified; however, the behavior of the floor beams under higher loads is likely to be essentially similar to that of the longitudinal ribs.

9.2.3 Deflections

Elastic deflections associated with the normal load carrying and load distributing action of the longitudinal ribs and the floor beams should be regarded as being desirable and should not be subject to restrictions, unless perceptible deck deformations should occur under loads.

Generally, the deflections of the longitudinal ribs cause a favorable distribution of the local wheel loads through a better utilization of the flexural rigidity of the deck plate.

It should be noted that, since the flexural rigidity of the deck plate is disregarded entirely in the simplified computation of the deck with open ribs (Section 3.2.2.3) and is only indirectly considered in the computation of the deck with closed ribs (Section 3.2.2.2), the stresses in the ribs computed by the above methods will tend to be somewhat larger than the actual stresses if the rib deflections are relatively large.

If the ribs are very flexible, deflections under loads may cause a further favorable load distribution due to membrane stresses in the deck plate which may occur even in the elastic stress range (see Section 1.2.4.2b).

9.2.4 Dynamic Effects

Investigations of local vibrations of steel bridge decks indicate that the *structural effects* of the rib and floor beam vibrations caused by the traffic loads, are ade-

quately provided for by the usual impact factors specified for the design of bridge members of short spans.

The question of *human perception* of deck vibrations may have to be studied if extensive *pedestrian traffic* is anticipated on the bridge.

In such cases computation of the vibration characteristics of the deck may be required.

A general method of computation of the vibration frequency and amplitude of a structural member under the effect of a moving load is given by Stuessi [52]. A method of determination of the vibration frequency of the floor beams of steel plate bridge decks has been presented by Naruoka and Yonezawa [40].

The natural frequency of vibration of steel deck floor beams supporting sidewalks generally increases with rigidity and decreases with span and mass of the floor beams and is, in most cases, greater than 5 cycles per second.

Application of the above methods involves considerable numerical work. However, the need for an accurate investigation of the vibration characteristics of a bridge deck will arise only in rare cases.

Studies of human sensitivity to vibrations sustained with a constant intensity over a period of time are reported by Postlethwaithe [47], Dieckmann [11], and other authors. Generally, the feeling of discomfort associated with vibrations increases as both the amplitude and the frequency increase. If the vibration frequency is less than 5 cycles per second, the maximum *acceleration* of the vibratory motion governs the perception, while with frequencies greater than 5 cycles per second the maximum *velocity* of the vibratory motion appears to be the factor determining human sensitivity [11]. Based on these studies, values of vibration frequencies and amplitudes are given corresponding to various degrees of relative discomfort or impairment of working ability. These values also may be expressed in terms of critical accelerations or velocities of the vibratory motion.

However, data on human sensitivity to *sustained* vibration of constant characteristics cannot be directly used to judge the relative discomfort of a person walking on a bridge, who will be subjected to the maximum vibration effects only for a rather short period of time during which the maximum vibration amplitudes will actually occur in the bridge member affected (for example, when a heavy truck passes over a floor beam above which the pedestrian stands). Under such conditions a much higher tolerance is certainly to be expected. Also, as has been pointed out in the Progress Report of the ASCE Committee on Deflection Limitations [3], "it is not clear whether unfavorable psychological reactions result from actual discomfort as a result of the bridge vibration or simply from the unexpected motion of

structure which the layman might logically expect to be rigid. If the latter situation exists, a program of consumer education might prove to be helpful in reducing complaints of objectionable vibrations."

Based on the above considerations, the following values might possibly serve as guides in the evaluation of the vibration characteristics of a deck. If the frequency of vibration is less than 5 cycles per second, the maximum tolerable acceleration may be of the order of about 1.5 to 4 ft/sec². For frequencies greater than 5 cycles per second the tolerable upper limit of velocity of about 0.04 to 0.12 ft/sec could be used. The critical values should be determined at the location of the sidewalks.

Generally, in order to minimize the effects of deck vibrations on pedestrians, sidewalks should be located close to the main girders of the bridge. Placing sidewalks on the ends of long cantilevered floor beams should be avoided.

It should be noted that bridge users seated in moving automobiles will hardly perceive any bridge vibrations at all, since these will be overshadowed by the vibrations of the vehicles themselves.

9.2.5 Fatigue Strength

The ribs and floor beams of steel plate decks are subject to variation of the stress intensity, similarly as the stringers and floor beams of conventional bridges, and should be treated in accordance with the usual fatigue design provisions.

It should be noted that the maximum design stresses in the longitudinal ribs, obtained from superposition of the System II and System I stresses may, practically, never be reached, as discussed in Section 9.1.2, and the actual regularly occurring maximum stresses in the ribs will be, as a rule, considerably below the critical fatigue stress level. Therefore suggestions have been made to treat the theoretical peak stresses in the ribs obtained by unlikely superpositions of the most unfavorable loading cases in Systems I and II as static rather than dynamic stresses [44].

9.3 SUPERPOSITION OF SYSTEM I AND SYSTEM II STRESSES

9.3.1 General

The maximum theoretical stresses in the ribs and in the deck plate in the longitudinal direction of the bridge are obtained by superposition of the System I and System II stresses, as discussed in Section 1.2.6 and illustrated by numerical examples in Sections 11.2.2.4 and 11.3.2.3.

However, it should be kept in mind that the values of the local peak stresses in the ribs obtained by such superposition of the System I and System II effects are in no way directly indicative of the actual safety of the deck structure, since the structural behavior and the factors of safety against failure are basically different in the two systems, as discussed in Chapter 1, with System II having very large inherent strength reserves in excess of the values obtained by a linear flexural theory.

Thus the need for a rational design procedure based on an appropriate evaluation of the actual structural characteristics of the steel plate decks becomes apparent.

Within the conventional "allowable stress" approach such a procedure is possible either (a) by applying a reduction factor to the System II stresses prior to adding them to the System I stresses and requiring that the sum should not exceed the prescribed allowable stress of the material, or (b) by allowing higher values of the stresses due to combined System I and System II effects.

Both methods have been used, as discussed in Sections 9.3.2 and 3.

The contribution of the local System III stresses in the deck plate and in the walls of closed ribs to the longitudinal rib stresses is generally disregarded in design computations. However, in special cases, these effects may have to be considered, for example in the evaluation of the stress measurements in the loading tests.

The second order effects associated with superposition of System I and System II stresses are discussed in Section 9.3.4.

9.3.2 Reduction of System II Stresses

In the design of the Save River Bridge in Belgrade (Fig. 1.8) the System II stresses in the longitudinal ribs were multiplied by a factor of $1/2.35 = 0.425$, and the reduced values of the stresses were added to the System I stresses in the deck [42].

The reduction factor of $1/2.35$ was obtained from the load test described in Section 1.2.4.2b (Fig. 1.32) as follows [42, 44]:

For a theoretical limit case of a rib loaded by a concentrated load and acting in flexure only (no axial stresses due to System I action) a factor of safety against breaking of 10 was chosen. With the value of the load at which the first crack occurred in the rib of 48 metric tons, the allowable load was obtained as

$$P_{\text{allow}} = 48/10 = 4.8 \text{ metric tons}$$

At this load the permanent deflection measured on the half-scale model was 0.25 mm, corresponding to a permanent deflection of 0.5 mm of the full scale rib. It should be noted, however, that no permanent deflection was intended under the design conditions in the

actual deck, since the actual stress in the rib consisted of the flexural System II stress and the axial System I stress, the latter not subject to a stress reduction, as explained below.

The theoretical "allowable load", computed by the linear flexural theory, with the allowable stress of 1.4 t/cm^2 for the carbon structural steel St 37 of the test model, was 2.06 metric tons. The ratio of the allowable load determined by ultimate load considerations to the theoretical allowable load was then

$$4.8/2.06 = 2.35$$

This ratio was used in the final design to reduce the computed values of the local flexural stresses in the ribs, although the material and the sizes of the ribs (see Fig. 1.8) did not correspond to those of the scale model tested.

The following conditions had to be satisfied:

$$(a) \quad f_I + \frac{f_{II}}{2.35} \leq f_{\text{allow}}$$

$$(b) \quad f_I \leq f_{\text{allow}}$$

where

- f_I = axial stress in the deck due to its action as the top flange of the main girders of the bridge
- f_{II} = flexural stress in the ribs due to local wheel loads, computed in accordance with the ordinary flexural theory
- f_{allow} = allowable stress of 2.1 t/cm^2 , or 29.9 ksi, as stipulated by the Yugoslavian specifications for the St 52 (a low-alloy steel) used. A 25% increase of the allowable stress was permitted for the effects of the heavier German regulation truck load

It is of interest to discuss in more detail the actual stress conditions in the deck of this structure, designed in accordance with the above design conditions.

According to condition (a), the computed flexural stress, f_{II} , in the ribs could exceed the yield point stress of 3.6 t/cm^2 of the St 52 only if the axial stress, f_I , were smaller than $0.27f_{\text{allow}}$ or 0.57 t/cm^2 .

Actually, due to the location of the neutral axis near the mid-depth of the girders, the theoretical System I stresses, f_I , constituted a major part of the total rib stresses and varied between $1.6\text{--}2.0 \text{ t/cm}^2$. The local theoretical System II stresses, f_{II} , were generally low, because the rib and deck sizes were governed in most parts of the deck by the System I considerations, and reached a maximum value of 1.2 t/cm^2 (tension) in the $6\frac{1}{2} \times \frac{1}{2}$ -in. ribs with a $\frac{3}{8}$ -in. thick deck plate. Thus the maximum total *theoretical* design stress, $f_I + f_{II}$, never exceeded the value of 2.7 t/cm^2 , which is

considerably below 3.6 t/cm², the yield point of the steel used, and no permanent rib deformation could take place. The *actual* total maximum stresses in the ribs under traffic are certainly still much lower, because of the unlikelihood of developing the full design values of the f_I stresses in the deck, as discussed in Section 9.1.2.

It is seen that the design condition (a), which may at first appear very radical, is, in fact, rather conservative.

A similar procedure was used in the design of the Europe-Bridge (Fig. 7.15), where the stresses due to the local loads were multiplied by a factor of 0.5, chosen by analogous considerations, prior to the superposition with the System I stresses in the ribs. Another stipulation was added requiring that the maximum total design stress (without reduction of the local stresses) shall at no point exceed the yield stress [58].

9.3.3 Increase of the Allowable Stresses for Superposition of the System I and System II Effects

An increase of the allowable stresses for the superposition of the System I and System II effects by a logical extension of the existing allowable stress provisions for the principal (Group H) and additional (Group Z) loads to the design of steel deck bridges has been proposed for the new issue of the *German Specifications for Steel Highway Bridges* (DIN 1073).

Group H loads, or the principal loads, as defined in the existing general German bridge specifications, include: dead load, live load, impact, effects of the support settlements, concrete shrinkage and plastic flow.

Group Z loads, or the additional loads, are the effects of temperature, wind, snow, braking and inertia forces, friction at supports and the railing loads.

In accordance with the proposed design provisions for steel deck bridges, the System I and System II stresses, considered separately, should each be smaller than the allowable stresses for the H-loads, while for superposition of the System I and System II stresses in the longitudinal ribs the allowable stresses for H + Z-loads should be permitted, or

$$(c) f_I \leq f_H$$

$$(d) f_{II} \leq f_H$$

$$(e) f_{I+II} \leq f_{H+Z}$$

where f_H and f_{H+Z} are the allowable stress values for Group H loads, or Group H and Group Z loads combined, respectively, and f_I and f_{II} are the System I or System II stresses.

The proposed values of the allowable stresses, f_H and f_{H+Z} , which are equal to the allowable stresses of the

German Railroad Bridge Specifications (BE), adjusted earlier, are given in Table 9.3.3.

Design provisions (c), (d) and (e), with allowable stresses given in Table 9.3.3, have already been applied in the design of several steel deck bridges.

TABLE 9.3.3

PROPOSED ALLOWABLE STRESSES FOR STEEL HIGHWAY BRIDGES, GERMAN SPECIFICATIONS DIN 1073
Stresses in t/cm² (ksi)

Stress	St 37 (Carbon Steel) $f_y = 2.4 \text{ t/cm}^2 \text{ (34.1 ksi)}$		St 52 (Low-Alloy Steel), $f_y = 3.6 \text{ t/cm}^2 \text{ (51.2 ksi)}$	
	H	H + Z	H	H + Z
Tension	1.6 (22.7)	1.8 (25.6)	2.4 (34.1)	2.7 (38.4)
Compr.	1.4 (19.8)	1.6 (22.7)	2.1 (29.9)	2.4 (34.1)
Shear	0.92 (13.1)	1.04 (14.8)	1.39 (19.8)	1.56 (22.2)

Provision (e) is entirely warranted and conservative, in view of the high local load capacity of the deck and a small probability of reaching the maximum design stresses in Systems I and II simultaneously, as discussed before.

Adoption of a similar provision in the AASHTO Specifications for Highway Bridges is suggested in Section 9.5.1.

9.3.4 Second-Order Effects in the Superposition of Stresses

In adding up the stresses in the individual component structural systems of a bridge deck to obtain the maximum effects, it is assumed that the relationship between the loads and the stresses in each system remains linear and is not affected by the interaction.

This assumption is, however, not strictly true, since the interaction of structural Systems I, II and III will tend to affect the stresses in the individual systems.

For example, the local flexural stresses in the ribs (System II) will be somewhat increased or decreased by an amount proportional to the axial stress in the rib acting as a part of System I and the rib deflection under the local load. If both the axial stresses and the deflections are relatively large, the effects on the stresses in the ribs may no longer be negligible.

The stress interaction will become much more complicated under increasing local loads, or in very slender deck panels, where the second-order effects will tend to develop in the local Systems II and III, as discussed in Sections 1.2.4.2 and 6.2.2.

While theoretical research in this field is in progress, results applicable to design are not yet available, and the secondary interaction effects are being disregarded in present design practice.

It is, however, believed that interaction does not significantly affect the high ultimate local load carrying capacity of Systems II and III.

9.4 DECK PLATE (SYSTEM III)

The criteria for design of the deck plate acting as an independent structural member supported by the longitudinal ribs are discussed in Chapter 6.

In accordance with the conclusions summarized in Section 6.4, the deck plate thickness should be determined by the allowable deflection rather than by the local stresses under the wheel loads.

It should be mentioned that, for checking the combined stress in the deck plate resulting from a superposition of the System I, II and III stresses, a design condition

$$f_c \leq 0.9f_y$$

is occasionally specified, where f_y is the yield point stress of the deck plate and f_c the value of the "comparative stress" computed by the Huber-V.Mises-Hencky formula

$$f_c = \sqrt{f_x^2 - f_x f_y + f_y^2 + 3v_{xy}^2}$$

where f_x and f_y are the values of the axial stresses in the x - and y -directions, respectively, and v_{xy} is the shearing stress. The value of f_c is considered, in accordance with the hypothesis of constant work of deformation, to be the criterion for yielding of steel under a bi-axial stress condition [49].

However, in the particular case of stresses in the deck plate under the effects of a local wheel load (see Fig. 6.1) the "comparative stress" value by the above formula does not provide a valid criterion for yielding of the deck plate, since the area of the plate where the critical stress condition occurs is confined to a local stress peak at a point under the wheel, surrounded by material with a lower stress intensity, which prevents the occurrence of yielding at the critical point.

It should also be noted that the "comparative stress" criterion is not well applicable to the weld material or to the plate areas in the immediate vicinity of the welds, where the maximum stresses occur.

9.5 DESIGN SPECIFICATIONS

9.5.1 Proposed Tentative Design Provisions

In order to permit a more advantageous utilization of the structural characteristics of steel deck bridges than is possible under the current Standard Specifications for Highway Bridges of the AASHO [1], the following tentative special design provisions for steel deck bridges are suggested:

Steel deck highway bridges shall be designed in accordance with the current specifications of the AASHO except as noted below:

1. Wheel Loads

In the design of steel plate bridge decks for H20 or H20-S16 loading, single axle loads of 24,000 pounds or double axle loads of 16,000 pounds each, spaced 4 ft apart, shall be used in the computation of the direct effects of the wheel loads on the deck plate and the longitudinal ribs, instead of the 32,000-pound axles of the standard truck loading.

The contact area of one 12,000-pound or 8000-pound wheel shall be assumed 20 in. wide and 10 in. long at the surface of the roadway. A further increase of the loaded area shall be considered by assuming a 45° load distribution by the wearing surface.

In the computation of the indirect effects on the stresses in the longitudinal ribs (effects of floor beam flexibility due to truck loads in lanes adjoining the critical lane under consideration), and in the design of the floor beams the full H20 or H20-S16 loading is used.

2. Design of the Deck Plates

2.1 Deck Plate of Low-Alloy Steel

The thickness of the deck plate made of low-alloy steel with a yield point stress of 46,000 psi or more, normally used in the design of the deck, shall be determined by the allowable deflection under a wheel, which shall not exceed 1/300 of the spacing of the deck plate supports, unless a greater thickness is required for the deck plate acting as the flange of the ribs, floor beams or the main structural members of the bridge.

The plate thickness, t_p , satisfying the above condition may be determined, provided that the spacing of the deck plate supports does not exceed 24 in., by the formula

$$t_p \geq 0.007a \sqrt[3]{p}$$

where

a = spacing of the open ribs, or the maximum spacing of the walls of the closed ribs, in inches

p = design unit pressure at the top of the steel plate under the standard 12,000-pound wheel, computed in accordance with the assumptions of Provision 1, above

Computation of the local flexural stresses in the deck plate satisfying the above allowable deflection provision is not required.

2.2 Deck Plate of Carbon Structural Steel

For the design of the deck plate in carbon structural steel special design provisions have to be established, subject to approval by the Bridge Engineer.

2.3 Minimum Thickness

The minimum thickness of the deck plate shall be 3/8 in.

3. Design of the Longitudinal Ribs

3.1 Allowable Stresses

(a) Tension and Shear

The following percentages of the basic allowable stresses of the AASHO specifications shall be used:

- Condition (I)—stresses in the ribs and in the deck plate acting as the flange of the main girders.....100%
- Condition (II)—stresses due to the local flexure of the ribs under the wheel loads.....100%
- Condition (I)+(II)—superposition of the above effects125%

(b) Compression

The allowable compressive stresses shall be governed by the safety against overall and local buckling of the ribs, determined in accordance with procedures and formulas given in Appendix II of this Manual, with the following factors of safety:

- Condition (I)—compression in the ribs and in the deck plate acting as the flange of the main girders.....1.85
- Condition (II)—compression due to the local flexure of the ribs under the wheel loads.....1.85
- Condition (I)+(II)—superposition of the above effects1.5

(c) Special Provisions

Allowable stresses higher than those stipulated in Provisions 3.1a and b above may be specified for Conditions (II) and (I)+(II), subject to special permission by the Bridge Engineer, provided the appropriateness of such stress increase is proven by tests.

3.2 Slenderness of Ribs

The slenderness ratio of the ribs, h/t_R , where h is the depth and t_R the rib plate thickness, shall not be subject to limitations if the ribs are designed in accordance with Provisions 3.1a and b, above.

4. Minimum Thickness of Closed Ribs

A minimum thickness of 3/16 in. of the closed ribs may be used, provided the ribs are welded airtight.

9.5.2 Commentary on the Proposed Design Provisions for Steel Deck Bridges

The justification and background of the design provisions suggested in Section 9.5.1 may be found in the preceding chapters of this Manual.

1. Wheel Loads

A discussion of the wheel and axle loads of the AASHO specifications and their application to the design of steel bridge decks is given in Section 3.4.2.

For suggestions regarding simplification of the loading assumptions see Section 9.5.3.

2. Design of the Deck Plate

The proposed provisions are based on the structural behavior of the deck plate under wheel loads, discussed in detail in Chapter 9.

The inappropriateness of the "allowable stress" approach in predicting the elastic behavior and the static strength of the deck plate has been pointed out in Section 6.2.2.2. A discussion of the fatigue factor in the design of the deck plate is given in Section 6.1c.

The value of the allowable deflection of the deck plate of $1/300$ of the plate span, replacing the "allowable stress" provision, is arbitrary, as discussed in Section 6.3.2. The recommended formula for the plate thickness is based on the empirical formula by Kloeppe, see equations (6.5) to (6.7a).

The extension of Kloeppe's formula to the deck plate supported by closed ribs, with the stipulation that the longer of the two deck plate spans be used, is conservative.

It should be noted that, with the usual geometric conditions and wheel loads, the maximum *theoretical* stress in the deck plates proportioned by the above deflection formula is approximately constant, regardless of the rib spacing, and is well within the elastic range of the low-alloy plate. The *actual* stresses and deflections occurring in the bridge deck may be considerably lower (see Sections 6.2.1.2.1e and 6.2.2.3). Thus the proposed design provisions for the deck plate are reasonably conservative.

3. Design of the Longitudinal Ribs

The proposed provisions for the design of the longitudinal ribs, increasing the allowable stresses for the case of superposition of the System I and System II stresses in the ribs, reflect both the small structural significance and the low probability of the occurrence of the local stress peaks in the ribs.

The provisions are patterned on the similar proposed German specifications for steel deck bridges (see Section 9.3.3), and are essentially similar to the existing provisions of the AASHO specifications [1] for the combined loading conditions (AASHO specifications, Section 1.4.1, loading Groups II-IX).

The structural behavior and stresses underlying the proposed provisions are discussed in the following sections of this Manual: System I—Sections 1.2.3 and 9.1; System II—Sections 1.2.4 and 9.2; superposition of Systems I and II—Sections 1.2.6 and 9.3.

The proposed 25% increase of the allowable stresses in *tension* and *shear* corresponds to the lowest percentage increased provided by the AASHO specifications, Section 1.4.1, for combined loading.

A similar application of the allowable stresses in *compression* of the AASHO specifications is not possible, since the present criteria underlying the choice of the allowable stresses of the specifications (column buckling, based on the secant formula, and lateral buckling of the compressive flanges of girders) are not applicable to the design of steel decks.

In the determination of the allowable compressive stresses in the longitudinal ribs, the following conditions have to be considered: (a) buckling of the entire deck between the floor beams, and (b) local buckling of the rib plate.

The methods of determining the critical compressive stresses for these cases are given and discussed in Appendix II.

The uniformly distributed System I compression in the deck may cause either of the above buckling phenomena. The local flexural compression in the rib walls, due to the System II action of the ribs, may, theoretically, cause the local buckling of the rib plate; however, the possibility of developing a dangerous local buckling deformation in a rib is remote because of geometric conditions (see Appendix II).

Since the local plate buckling due to System II stresses does not affect the ultimate capacity of the rib, and since such local buckling of a rib plate of the directly loaded rib cannot precipitate the overall buckling of the entire deck under System I stresses, the decrease of the required factor of safety for the combined System I + II compressive stresses is justified, similarly as in the case of tensile stresses.

The proposed factors of safety of 1.85 and 1.5 are chosen for consistency with the safety factors of the proposed provisions for the allowable tensile stresses.

It should be noted that for decks of usual proportions, the danger of rib buckling is small, especially in the closed rib system, and, therefore, the allowable compressive stresses obtained in accordance with the proposed provisions will not be much below the allowable tensile stress values.

The proposed provision (c) would make it possible to apply semi-empirical design procedures, similar to those discussed in Section 9.3.2. This provision would

be particularly appropriate in the design of decks in which System I stresses predominate, as may be the case in steel deck bridges with very long spans.

4. Minimum Thickness of Closed Ribs

The recommendation of reducing the minimum required thickness of the walls of the closed airtight ribs to $\frac{3}{16}$ in. is based on the good corrosion resistance of the closed ribs (see Section 7.4.2) and conforms to current practice.

9.5.3 Thoughts on Future Design Specifications for Steel Deck Bridges

In the development of future design specifications, which would reflect the structural characteristics of steel deck bridges more adequately than the proposed tentative provisions outlined above, consideration of the following problems would be desirable:

(a) A more consistent and far-reaching application of *ultimate design principles*, coupled with a judicious re-evaluation of the basic factors of safety for all bridge members. This would require a further study of ultimate behavior as well as fatigue behavior of steel bridge decks.

(b) Realistic evaluation of the actual *System I live load stresses* in the decks of long span bridges, to be superimposed with local System II stresses.

(c) Consideration of *second order interaction effects* in the superposition of the System I and System II action of the bridge deck.

(d) *Simplification of the loading assumptions* used in the design of the longitudinal ribs in System II. It should be noted that the application of the truck loads of the current AASHO specifications, with the variable axle spacings and wheel loads, unduly complicates the design computations, as is evident from the Design Charts given in Appendix I. The use of a single axle in the computation of the maximum positive moment in a rib and application of two axles with a constant spacing in the computation of the negative moment and the effects of floor beam flexibility may suffice.

(e) Elimination of the restrictive *live load deflection* provision limiting the deflection to $\frac{1}{800}$ of the span length.

(f) Revision of the *web design* provisions in order to make possible the use of efficient thin webs for deep girders.

CHAPTER 10

Computation Procedure for Practical Design

10.1 INTRODUCTION

In this Chapter procedures are summarized for the design of steel plate bridge decks with open and with closed ribs, based on the formulas presented and explained in Chapters 3, 4 and 5 and the design charts given in the Appendix.

The determination of the *deck plate thickness*, governed by considerations given in Chapter 6, is not discussed in this chapter.

The computation of the characteristic *section properties* and *rigidity values* of the deck is made by formulas given in Chapter 3.

In a *general case* of loading, the bending moments in the deck system will have to be computed by the formulas given in Chapters 4 and 5, with the general Charts 1, 2, 5, 17, 18 and 19.

For the standard bridge loadings of the *AASHTO specifications* the maximum values of the bending moments needed in the design may be obtained more directly by Charts 3, 4, 6-16 and 20-32, which will be sufficient in most cases.

However, computations by formulas will still be required for such problems as determination of the stresses in ribs not directly loaded, more refined computation of the bending moments in open ribs with consideration of the deck plate rigidity, more accurate computation of the bending moments per rib in the closed rib system, determination of the effects of floor beams of non-uniform rigidity, etc.

Both design procedures, by formulas and general charts and by charts for AASHTO loads, are outlined in detail.

The computation is made in *two steps*. In the first step the bending moments in the longitudinal ribs and in the floor beams are computed under the assumption that the floor beams are rigid. In the second step the effects of the elastic flexibility of the floor beams are determined.

The stresses in the deck due to its action as a flange of the main carrying members of the bridge (System I) are not considered. These stresses are computed by the conventional methods and superimposed on the stresses due to the local action of the loads on the deck (System II), computed in accordance with the procedure outlined in this chapter.

The general *designations* used in the computations are given in the nomenclature in the front of this Manual. The special terms used in the computation of the effects of floor beam flexibility are defined and explained in Section 3.5 and in Chapter 5.

The system dimensions and the axes of co-ordinates are given in Figure 3.1, the rib dimensions in Figure 3.9, and the wheel load dimensions are shown in Figure 3.10.

The design procedures given in this Chapter are illustrated by numerical examples in Chapter 11.

10.2 BENDING MOMENTS IN THE DECK WITH OPEN RIBS

10.2.1 General

A typical deck with open ribs is shown in Figure 1.2a.

The spacing of the open ribs is governed by the loading and the deck plate thickness used, and ranges between 11 and 16 in. in most cases.

The usual spacing of the floor beams in the deck with open ribs is between 5 and 7 ft.

In determination of the sizes of flat bar longitudinal ribs, safety against buckling of the slender ribs subject to compression should be investigated by means of the formulas given in Appendix II.

10.2.2 Section Properties and Relative Rigidities

In the design computations of the deck system the moments of inertia and the section moduli of the longitudinal ribs and the floor beams are needed.

In computation of these section properties, appropriate effective widths of the deck plating have to be used, as discussed in Chapter 3.

10.2.2.1 Longitudinal Ribs

The assumptions and formulas used in the computation of the section properties of the ribs are summarized in Table 3.3.2.2, lines 1 and 2.

(a) *Values of I_R' , and S_R' , for computation of the live load stresses in the ribs on rigid supports*

1. The effective rib spacing, a_0^* , is obtained in a general case from Chart 2b, as a function of the

width, $2g$, of one wheel, with consideration of the load distribution by the wearing surface. Case 1 (wheel centered over the rib) should be used, unless the wheel width, $2g$, is greater than $2.8a$.

In design in accordance with the AASHTO specifications, the effective rib spacing, a_0^* , may be obtained directly from Chart 4. The use of the 8 kip and 12 kip wheels, Figure 3.11b, is recommended in the design of the ribs, as discussed in Section 3.4.2.1.

2. With the effective rib spacing, a_0^* , determined, the effective width of plate, a_0' , is obtained from Chart 1, using the effective rib span, $s_1 = 0.7s$.

3. The moment of inertia, I_R' , and the section moduli, S_{RB}' and S_{RT}' are computed with the effective width of plate, a_0' .

(b) *Values of I_R and S_R , for computation of the effects of floor beam flexibility*

The effective width, a_0 , is equal to 1.1a.

With this value, the moment of inertia, I_R , and the section moduli, S_{RB} and S_{RT} , are computed.

10.2.2.2 Floor Beams

The effective width of plate, s_0 , acting with one floor beam is obtained from Chart 1, using $s^* = s$, and l equal to the main girder spacing, if floor beams may be assumed to be simply supported (see line 6, Table 3.3.2.2).

In a case of floor beams framed into torsionally stiff box girders, or continuous over more than two main girders, an effective span $l_1 = 0.7l$ may be used for the purpose of determination of the effective width.

If greater accuracy is desired in the computation of the live load stresses in the deck plate acting as the top flange of a floor beam, the effective width of the deck plate, s_0' , may be computed by the formulas given in line 7 of Table 3.3.2.2.

10.2.2.3 Relative Rigidity Coefficients, γ

The relative rigidity coefficient of the ribs and the floor beams, γ , is computed by equation (5.7), with the values of I_R and I_F determined in accordance with lines 2 and 6, respectively, of Table 3.3.2.2.

If the rib sizes and the moments of inertia of the floor beam vary along the length of the floor beam, appropriate average values have to be used in the computation of the coefficient γ , as discussed in Section 5.3.2.

If a more refined computation of the bending moment in the ribs is desired, the relative rigidity coefficient of the deck plate and the ribs, γ' , is computed by equation (4.18), with the value of I_R' computed in accordance with line 1 of Table 3.3.2.2.

10.2.3 Computation of the Bending Moments by General Formulas

10.2.3.1 Bending Moments in a System with Rigid Floor Beams (Step 1 of the Computation)

10.2.3.1.1 Bending Moments in the Ribs—Usual Conditions

In the usual cases, with the open rib spans not exceeding 6 ft, the bending moments in the ribs depend, practically, only on the span and the spacing of the ribs and the magnitudes and the dimensions of the wheel loads, and are independent of the rigidities of the system.

Critical bending moments are caused by one or several wheel loads aligned in the longitudinal direction of the bridge over the rib under consideration. In Step 1 of the computation (rigid floor beams) additional wheels placed over other ribs have no effect on the bending moments in the rib considered.

(a) *Positive moment at the midspan*

1. The total positive moment, M_C , at the midspan of the ribs due to a wheel load, P , at the midspan (Fig. 4.4c) is computed by equation (4.10).

2. Additional bending moment increments at the midspan of the panel 0-0 are obtained by placing the wheel loads, P , represented by concentrated loads, in the distant panels (Fig. 4.4b).

The values of the bending moments are obtained by equation (4.9), or by means of the influence line, Chart 5a, or Table 4.2.5.

3. The bending moment per rib is obtained from the total bending moment by equation (4.5a).

The ratio R/P is obtained from Chart 2a, or may be computed by equations given in Section 4.2.4.2.

(b) *Negative moment at the support*

The negative moment in the rib at the floor beam is computed in a similar manner by equation (4.6), (4.6a) or (4.6b) or by means of the influence line, Chart 5b, or Table 4.2.5.

10.2.3.1.2 Correction of the Bending Moments in the Ribs Due to Effects of Deck Plate Rigidity

If the relative rigidity coefficient, γ' (see Section 10.2.2.3), is smaller than the values given by equation (4.20) or (4.20a), the bending moments computed in Section 10.2.3.1.1, above, which are always on the safe side, may be considered sufficiently accurate for design purposes.

If, in the case of longer rib spans, the values of γ' are larger, or if a greater accuracy is desired, the moment

corrections, $\Delta M_R'$, which represent a reduction of the bending moments, may be computed by equation (4.15) or (4.19), in conjunction with equations (4.15a), (4.16) and (4.17).

The reactions R_0, R_1, \dots, R_m , needed in the computations, are obtained from the influence line, Chart 5c or Table 4.2.5, or by equations given in Section 4.2.4.2.

10.2.3.1.3 Bending Moments in the Floor Beams

The loads on rigid floor beams due to truck axles in various positions on the bridge are computed by equations (4.11) and (4.12), or by means of the influence line, Chart 5c or Table 4.2.5.

Bending moments in the floor beams due to these loads are determined by the usual methods.

10.2.3.2 Bending Moment Corrections Due to Floor Beam Flexibility (Step 2 of the Computation)

10.2.3.2.1 Loading

In determination of the effects of floor beam flexibility on the bending moments at any point of the deck the loading on the entire deck has to be considered.

In the computation of the bending moment increase at the midspan of a rib, the position and the magnitude of the wheel loads in the lane enclosing the rib under consideration must be the same as used in Step 1 of the computation, with second wheels added in each axle (Fig. 10.1). The truck loads in the adjoining lanes must be placed in such a manner as to cause maximum deflections of the floor beams enclosing the panel under consideration.

In the computation of the effects of the floor beam flexibility on the bending moments in the floor beams, the truck loads must be in the same positions as used in Step 1 of the computation.

In all cases the actual loadings are replaced by their first sinusoidal component loads, obtained through the Fourier analysis, as explained in Section 3.5.

10.2.3.2.2 Bending Moment Increase in the Ribs

The bending moment increase in a rib, ΔM_R , due to floor beam flexibility is computed by equation (5.9) if only one lane is loaded and by equation (5.10) if several lanes are loaded simultaneously, with different loads and load positions in each lane.

The ratios F_m/P and $\bar{\eta}_{tm}/s$ in equation (5.9) are defined in Section 5.3.3.1. In this case the load P denotes the weight of one wheel or axle placed in the lane under consideration. The values of the reactions,

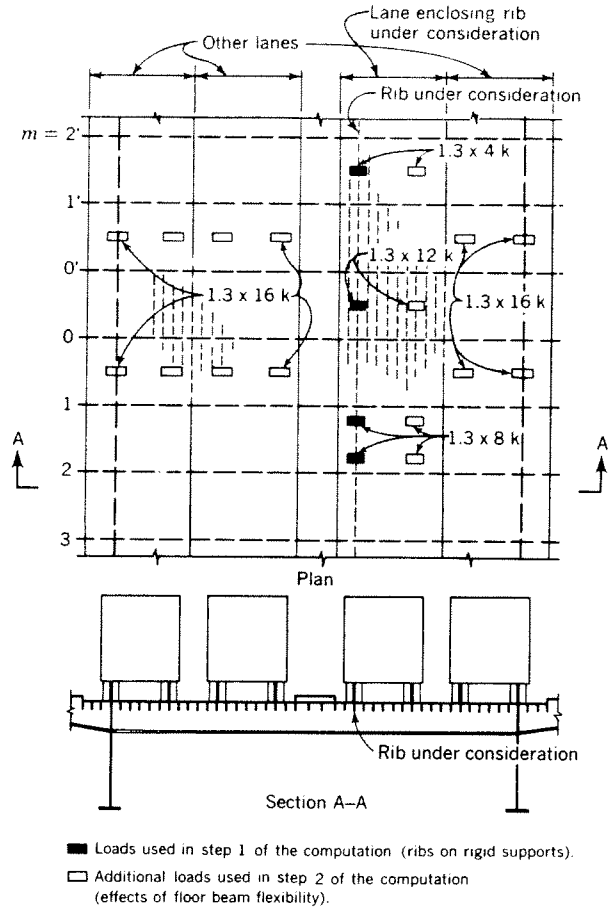


Fig. 10.1. Typical position of loads in the computation of the bending moment at the midspan of the critical rib

F_m , are obtained from the influence line, Chart 5c, or by equations (4.11) and (4.12) (see Section 4.2.4.1c).

In the computation of the moment increase ΔM_{RC} , at the midspan of the ribs, the values of $\bar{\eta}_{cm}/s$ are obtained from Chart 17, using the value of the relative rigidity coefficient, γ , for the system considered.

In the computation of the moment correction ΔM_{RS} , at the support of the ribs, the values of $\bar{\eta}_{sm}/s$ are obtained from Chart 18.

In most practical cases the bending moment increments, ΔM_{RC} and ΔM_{RS} , are positive, resulting in an increase of the total positive moment at the midspan and a decrease of the total negative moment at the support of the ribs. Therefore, in the cases where the negative bending moment at the support does not govern the design of the ribs, the bending moment increment, ΔM_{RS} , does not have to be computed.

10.2.3.2.3 Bending Moment Relief in the Floor Beams

The bending moment relief in a floor beam due to

floor beam flexibility is computed, for any point, x , of the floor beam, by equation (5.14).

The values of the reactions, $F_0 \dots F_m$, of a beam on rigid supports, due to axle loads, P , needed in equation (5.14) are obtained from the influence line, Chart 5c, or by equations (4.11) and (4.12).

The values of influence ordinates, $\bar{\theta}_{9m}$, of a beam on elastic supports are obtained from Chart 19.

The length, l , is the actual span of the floor beams, considered to be simply supported at the main girders. If this assumption is not valid, see Section 10.2.3.2.5.

10.2.3.2.4 Additional Effects of Heavier Floor Beams

If all floor beams of the bridge are of the same rigidity, the effects of the floor beam flexibility are obtained by procedures outlined in Sections 10.2.3.2.2 and 10.2.3.2.3 above.

If heavier floor beams or diaphragms are used at certain intervals, bending moment adjustments, in addition to the corrections computed in Sections 10.2.3.2.2 and 10.2.3.2.3, have to be made.

Generally, the bending moments will be increased in the heavier floor beams and will be decreased in the lighter floor beams adjoining the heavy ones.

The negative bending moments in the ribs over the heavy supports will be increased, while the bending moments at other points may be increased, or decreased, depending on the relative rigidities.

The change of the bending moments in ribs, $\bar{\Delta}M_{Ri}$, due to *one* heavier floor beam, is computed by equation (5.28), with equations (5.24) and (5.13), using designations given in Section 5.4.2. The effects of *additional* heavy floor beams are obtained in a similar manner and the results are superimposed.

The change of the bending moments in the floor beams, $\bar{\Delta}M_F$, due to one heavy floor beam, is computed by equations (5.29) and (5.30), with equations (5.24) and (5.13).

10.2.3.2.5 Effects of Flexibility of Continuous or Elastically Restrained Floor Beams

In the case of floor beams continuous over more than two main girders, or framed into torsionally stiff box girders, the effects of floor beam flexibility are determined by procedures indicated in Section 5.5.

10.2.4 Computation of the Bending Moments by Charts for AASHO Loads

Prior to the determination of the bending moments by charts, the section properties and the relative rigidity coefficients of the system have to be computed in accordance with Section 10.2.2.

10.2.4.1 Bending Moments in a System with Rigid Floor Beams (Step 1 of the Computation)

10.2.4.1.1 Bending Moments in the Ribs

In Step 1 of the computation of the bending moments in the ribs the use of the 8 kip and 12 kip wheels is recommended (see Section 3.4.2.1) with an impact factor of 30%.

(a) Positive moment at the midspan

1. The total positive moment, M_C , at the midspan of the ribs is obtained from Chart 6. Both loading cases, consisting of a single wheel load at the midspan of the rib with or without additional wheels in other rib panels, have to be evaluated.

2. The bending moment per rib is obtained by multiplication of the moment obtained from Chart 6 by the ratio R_0/P from Chart 3(a).

(b) Negative bending moment at the support

The negative bending moment per rib is obtained in a similar manner from Charts 7 and 3(a).

(c) Correction of the bending moments due to effects of deck plate rigidity

The necessity for such correction is determined by the magnitude of the relative rigidity coefficient, γ' (see Section 10.2.3.1.2). If necessary, the bending moment correction is computed by formulas indicated in Section 10.2.3.1.2.

10.2.4.1.2 Bending Moments in the Floor Beams

Trucks are to be placed in design traffic lanes, in accordance with the AASHO specifications, Section 1.2.6. Full axle loads are used, as specified in the AASHO specifications, Section 1.2.5, with an impact factor in accordance with Section 1.2.12 of the AASHO specifications.

1. Reactions F_0 , due to one lane loaded, are obtained from Chart 15 for one axle load (Case **A**) and for a full truck load (Case **B**).

2. The maximum floor beam moment is obtained from Chart 16. The floor beam is assumed to be simply supported at the main girders. The load reduction coefficients for multiple lane loading (see AASHO specifications, Section 1.2.9) are included in Chart 16.

3. If the floor beam is elastically restrained by torsionally stiff main girders or continuous over more than 2 main girders, the bending moments are computed in accordance with these conditions by the usual methods.

10.2.4.2 Bending Moment Corrections Due to Floor Beam Flexibility (Step 2 of the Computation)

10.2.4.2.1 Bending Moment Increase in the Ribs

In addition to the wheel loads used in Step 1 of the computation, Section 10.2.4.1.1, other wheel loads are added in the lane under consideration and in the adjoining lanes, as discussed in Section 10.2.3.2.1 and shown in Figure 10.1. In the lanes other than the lane under consideration, full AASHO truck loads are used.

The bending moment increments in the ribs are computed by equations (5.9) and (5.10), used in the "Computation by Formulas," Section 10.2.3.2.2, except that the values needed in the evaluation of these equations are obtained directly from the charts.

1. In the computation of the bending moment increment, ΔM_{RC} , at the midspan of the ribs the value of $\Sigma(F/P)$ (η_c/s), needed in equation (5.9), is obtained for the same loading cases as used in Section 10.2.4.1.1 from Charts 20, 21 or 22.

2. The value of Q_{1x}/Q_0 at critical rib is obtained from Chart 28.

3. With the above values, the moment increment, ΔM_{RC} , due to critical lane loaded, is computed by equation (5.9).

4. The effect of other lanes loaded is obtained in a similar manner, by means of Charts 23 and 29.

5. The total moment increment is computed by equation (5.10).

6. The change, ΔM_{RS} , of the negative bending moments at the supports of ribs is computed, if needed, in a similar manner as the moment increment ΔM_{RC} , by means of equations (5.9) and (5.10) with Charts 24–29, inclusive.

10.2.4.2.2 Bending Moment Relief in the Floor Beams

The bending moment relief, ΔM_F , in floor beam is computed by equation (5.14), with the value of $(F_0/P) - \Sigma(F_m/P)\bar{\nu}_{m0}$ obtained from Chart 30 and 31, and the value of Q_{1x}/Q_0 at the critical point of the floor beam obtained from Chart 32, which includes the AASHO reduction coefficient for multiple lane loading.

10.2.4.2.3 Additional Effects of Heavier Floor Beams

The computation of the additional effects of heavier floor beams is outlined in Section 10.2.3.2.4.

The value of F_0/P , equation (5.13), may be easily found from the influence line, $\bar{\nu}$, obtained by connecting

the influence ordinates at the supports, $\bar{\nu}_{m0}$ (Chart 19), with a smooth curve (see numerical example, Section 11.2.3.3.1).

10.2.4.2.4 Effect of Flexibility of Continuous or Elastically Restrained Floor Beams

The effects of floor beam flexibility in such cases may be obtained in an approximate manner by procedures outlined for simply supported floor beams, Sections 10.2.4.2.1 and 10.2.4.2.2, with the following modifications:

The relative rigidity coefficient, γ (Section 10.2.2.3) is determined with an effective span, l_2 , of the floor beams, rather than the actual span, l (see Section 5.5).

Charts 28, 29 and 32 should be entered with the effective span value, l_1 , as defined in Section 5.5.

Charts 20–27 and 30–31 are valid.

10.3 BENDING MOMENTS IN THE DECK WITH CLOSED RIBS

10.3.1 General

A typical deck with closed ribs is shown in Figure 1.2b.

In tentative determination of the sizes of the ribs it should be kept in mind that in the closed ribs system the wheel loads applied to the deck are distributed laterally to a considerable degree, unlike in the deck system with open ribs.

Relatively thin rib plates may be used if the ribs are designed to be air-tight.

The closed ribs of usual proportions may be considered safe against buckling under the action of the compressive stresses in the ribs.

The spacing of the closed ribs is usually about 2 ft.

The floor beam spacing is generally greater than 7 ft and should be determined by economic considerations. If large floor beam spacing is used, deflections of the ribs should be checked.

With floor beam spacing larger than in a system with open ribs the floor beams are, generally, more rigid, and the effects of their flexibility on the stresses in the deck are less significant than in the open rib system.

10.3.2 Section Properties and Relative Rigidities

10.3.2.1 Flexural Rigidity of the Ribs

The assumptions and formulas used in the computation of the section properties of the ribs and the flexural rigidity, D_v , of the deck system are summarized in Table 3.3.2.2, lines 3, 4 and 5.

(a) *Value of I_R , for computation of the flexural rigidity, D_v*

1. Using the assumption $s_1 = 0.7s$, the effective width of the deck plate, $a_0 + e_0$, acting with the rib $m = 0$, is obtained from Chart 1 and equation (3.6).

2. The above value of $a_0 + e_0$ is used in the computation of the moment of inertia, I_R , of one rib.

3. The flexural rigidity, D_v , is computed by equation (3.7).

(b) *Values of I_R' and S_R' , for computation of the stresses in the ribs on rigid supports*

The value of the effective spacing, e^* , can be computed by equation (3.8a) only if the bending moments M_0 , in the rib directly loaded, and M_1 , in the adjoining rib, are computed by formulas given in Chapter 4. It should be noted that the bending moment M_1 cannot be obtained by charts given in the Appendix.

However, in most cases, the stresses obtained by using the section moduli based on the value I_R , Section 10.3.2.1a, above, will be sufficiently accurate for design purposes, as explained in Section 3.3.2.2.c.

(c) *Values of I_R and S_R , for computation of the stresses due to floor beam flexibility*

These values are obtained by formulas given in line 5, Table 3.3.2.2.

10.3.2.2 Torsional Rigidity of the Ribs

The effective torsional rigidity, H , of the deck system with closed ribs is computed by formulas given in Section 3.3.3.2.

1. The rib section property, K , is computed by equation (3.14).

2. The reduction coefficient, μ , for the various types of closed ribs, is obtained by the appropriate equations (3.15) to (3.19a).

3. The value of H is computed by equation (3.13).

10.3.2.3 Flexural Rigidity of the Floor Beams

The flexural rigidity and the section properties of the floor beams are computed in accordance with Section 10.2.2.2.

10.3.2.4 Relative Rigidities

The following relative rigidity coefficients are needed:

1. The relative transverse rigidity of the deck, H/D_v (see Sections 10.3.2.1a and 10.3.2.2).

2. The relative rigidity of the ribs and the floor beams, γ .

The latter is computed by equation (5.7a), with the values of I_R and I_P determined in accordance with lines 5 and 6, respectively, of Table 3.3.2.2.

For other comments see Section 5.3.2.

10.3.3 Computation of the Bending Moments by General Formulas

10.3.3.1 Bending Moments in the Ribs in a System with Rigid Floor Beams

10.3.3.1.1 Loading Arrangement

As a rule, the loading used in the computation of the bending moments in a rib consists of one wheel or several wheels aligned in the longitudinal direction over the rib under consideration, as shown on sketches, Charts 9–14.

The effect of wheels placed over adjacent ribs, i.e. second wheels of the same vehicle or the wheels of the adjoining vehicle (Fig. 4.12) on the bending moments in the rib under consideration is small for the rib spans and the relative rigidity ratios, H/D_v , in the usual range (see Section 4.3.6.2). Approximate values of the bending moment increments due to loads over adjacent ribs are given in Table 4.3.6.2.

The computation of the bending moments due to more than one wheel in the transverse direction of the bridge requires the use of a longer substitute span, b , which, in turn, retards the convergence of the series expressing the moments.

In all cases it is advantageous to use only symmetrical loading with respect to the center of the substitute span, b (Figs. 3.14–3.16), since, in such case, only the odd terms of the series, $n = 1, 3, 5 \dots$, enter into the computations, the even terms being equal to zero.

The positions of the wheel loads in the longitudinal direction of the bridge may, for the computation of the bending moments, be determined by means of the influence lines, Charts 5a and b.

10.3.3.1.2 Choice of the Substitute Deck Span in the x -Direction, b , and the Number of Terms of the Series Needed

In the computation of the bending moments in the ribs in a system with rigid floor beams a substitute span, b , rather than the actual deck span in the x -direction, l , is used (Fig. 4.12), as explained in Section 3.5.2, in order to improve the convergence of the series.

For a given computation accuracy, the required substitute span, b , increases with the span, s , of the longitudinal ribs and with the ratio H/D_v of the system.

Generally, the substitute span, b , should be longer than the width of the deck affected by the loading applied, so that the supports assumed at $x = 0$ and $x = b$ (Fig. 4.12) have no effect on the bending moments in the deck system.

For the usual case of loading consisting of one wheel or a number of wheels arranged in the longitudinal

direction of the bridge (Fig. 3.14) the relationship between the accuracy of the results and the width to span ratio, $(b - 2g)/s$, and the relative rigidity ratio, H/D_y , is shown in Figure 10.2, based on numerical computations using a sufficiently large number of terms of the series. This diagram may be used to determine the minimum value of the substitute span, b , needed in the computation.

If the effect of the wheels placed over adjacent ribs, as shown with dashed lines in Figure 4.12, should be included in the computation, the value of b has to be appropriately increased.

Additional criteria for the choice of the substitute span, b , are obtained by inspection of Figure 10.3, illustrating the computation by equation (4.46) of the positive moment, M_C , at the midspan of the ribs due to one wheel load. The alternating positive and negative half-waves of the successive moment increments, δM , are determined by the loading function, Q_{1x}/Q_0 , expressed, in this case, by equation (3.23). In order to obtain a repeating sine function in each wave, the length b must be a multiple of the half-width of the wheel, g . It is furthermore desirable that each half-wave contain an odd number of terms. The above conditions are satisfied with the ratios b/g equal to 6, 10, 14, 18, ..., resulting in 3, 5, 7, 9 ... terms, respectively, in each half-wave.

The last term, n_{max} , included in the computation of the bending moment should be the middle term in a positive or a negative half-wave, as is seen from Figure 10.3. Generally, the computation may be discontinued if the total moment change due to the next half-

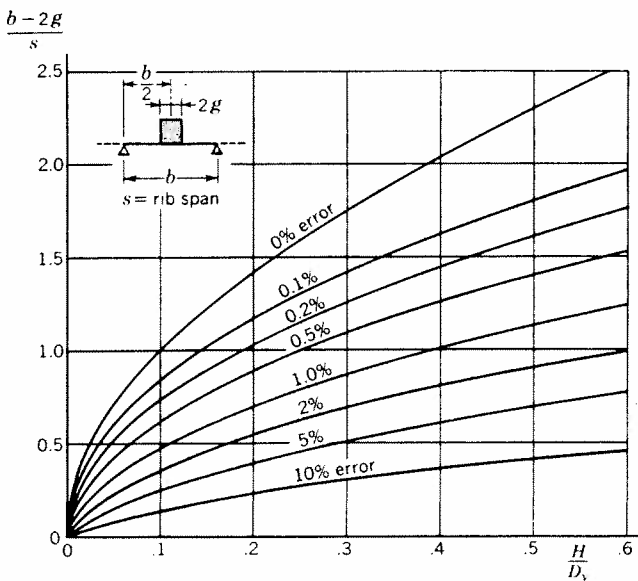


Fig. 10.2. Accuracy of the computation of the bending moment M_c at midspan of the closed ribs as a function of the width-to-span ratio of the deck strip and the relative rigidity ratio

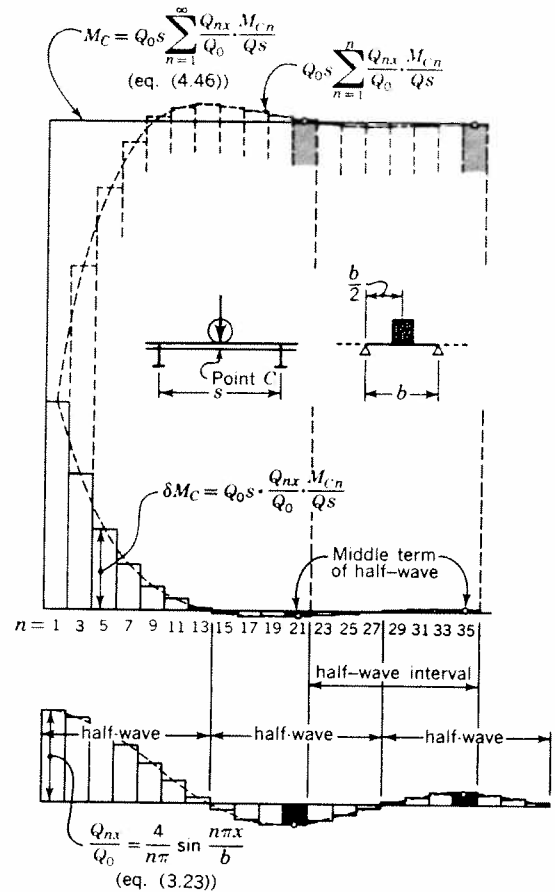


Fig. 10.3. Graphic representation of the computation by equation (4.46) of the bending moment M_c of the closed ribs due to a single load

wave interval of the moment increments is smaller than the desired accuracy of the results (see Fig. 10.3).

10.3.3.1.3 Fourier Analysis of Loading

The actual wheel loads on the deck are represented by sinusoidal component loads, as discussed in Section 3.5.2.

The Fourier coefficients, Q_{nx}/Q_0 , are needed at the location x of the substitute span, b (Figs. 3.14–3.16), where the bending moment is sought.

The maximum bending moment occurs in the rib located directly under the wheel load. For the usual case of loading by one wheel (Fig. 3.14), the coefficient Q_{nx}/Q_0 at the critical location, $x = b/2$, is computed by equation (3.23).

If the bending moments in other ribs are needed, or a moment distribution curve is desired, as shown in Figure 2.8, the coefficients Q_{nx}/Q_0 for additional locations x may be computed by equation (3.22).

Formulas for other cases of symmetrical loading are given in Section 3.5.3. Additional formulas may be

derived, if needed, from the general equations (3.20a) and (3.21).

The values of Q_{nz}/Q_0 are computed in tables for the necessary number of terms (see Section 11.3.2.1).

It should be noted that the coefficients Q_{nz}/Q_0 enter the formulas for the bending moments only at the end of the computation procedure (Section 10.3.3.1.5). Thus, with the basic numerical computations completed, the values of the bending moments at the various locations, x , of the substitute span b may be easily obtained by using appropriate sets of the Q_{nz}/Q_0 coefficients.

10.3.3.1.4 Computation of Constants

1. The basic constant, α_n , is computed, for the values of n used, by equation (4.23).

2. The following functions are needed in the computation of the positive bending moments at the *midspan* of the ribs due to a *distributed wheel load* (Fig. 4.11):

$$(1) \quad \alpha s \qquad \sinh \alpha s \qquad \coth \alpha s$$

$$(2) \quad \alpha s/2 \qquad \cosh (\alpha s/2)$$

$$(3) \quad \alpha c \qquad \sinh \alpha c$$

$$(4) \quad \alpha \left(\frac{s}{2} - c \right) \qquad \cosh \left[\alpha \left(\frac{s}{2} - c \right) \right]$$

$$(5) \quad e^{-\alpha c}$$

The numerical values of these functions, obtained from [4], [24], or similar references, are tabulated, as shown in Section 11.3.2.1.

The values for each n used should be filled in only as needed. The values of $\sinh \alpha s$ are computed only until the ratio $\alpha s/\sinh \alpha s$ becomes equal to 0 within the computation accuracy. The value of $\coth \alpha s$ need be computed only until it becomes equal to 1 within the computation accuracy. Lines (2), (3) and (4) above have to be computed only if the values of the parameter αs are smaller than the values given with equations (4.56) and (4.57). For larger values of αs , line (5) is needed instead.

3. In the computation of the bending moments at the *support* due to *concentrated loads* at various locations, y (Fig. 4.3a), the following functions, in addition to those in line (1) above, are needed:

$$(6) \quad \cosh \alpha s$$

$$(7) \qquad \sinh \alpha y \qquad \cosh \alpha y$$

$$(8) \quad e^{-\alpha y} \qquad e^{-\alpha(s-y)}$$

$$(9) \quad e^{-\alpha s}$$

The functions in lines (6) and (7) are computed only if $\alpha y < 4$, see equation (4.51). For larger values of αy lines (8) and (9) are needed instead.

4. In the computation of the bending moments at the *midspan* due to *concentrated loads* at various locations, y (Figs. 4.4a and 4.4b), the following functions, in addition to those in lines (1), (2) and (6) through (9), are needed.

$$(10) \quad \tanh (\alpha s/2)$$

$$(11) \quad e^{-\alpha \left(\frac{s}{2} - y \right)}$$

The value of $\tanh (\alpha s/2)$ is computed only if $\alpha[(s/2) + y] < 12$; the function in line (11) is computed only if $\alpha[(s/2) + y] > 12$, see equation (4.53). In computation of lines (2), (7) and (8) equations (4.33) to (4.55) have to be considered.

5. With the functions given in line (1), above, the constants α^* and κ are computed, for all values of n used, by equations (4.26), (4.27) and (4.29), or by equations (4.48) to (4.50) for larger values of αs (see Section 4.3.5.2).

10.3.3.1.5 Bending Moment at the Midspan of Ribs

(a) *Bending moment due to a distributed load at the midspan (Fig. 4.11)*

1. The dimensionless values of M_{Cn}/Qs are computed by equation (4.47) with equation (4.43). If the values of αs are large, equations (4.56) and (4.57) are used instead. The necessary number of terms is determined in accordance with Section 10.3.3.1.2. The intermediate computation steps and the end results should be tabulated.

2. The terms M_{Cn}/Qs are multiplied by the Fourier coefficients Q_{nz}/Q_0 (see Section 10.3.3.1.3), and the final bending moment per one inch of width of the deck at the location x is obtained by equation (4.46).

(b) *Bending moment due to a concentrated load in panel 0-0 (Fig. 4.4a)*

1. The values of η_{Cn}/s are computed by equation (4.41) with equations (4.42) and (4.43). If the values of αs become large, equations (4.53) to (4.55) are used instead.

2. The bending moment is computed in a similar manner as in case (a), above, by equation (4.35).

(c) *Bending moment due to a concentrated load in other panels (Fig. 4.4b)*

1. The values of η_{Cn}/s are computed by equation (4.38) with equations (4.39) and (4.43) (see Section 4.3.4.1b). If the values of αy and αs become large, equations (4.51) and (4.55) are used instead.

2. The bending moment is computed by equation (4.35).

10.3.3.1.6 Bending Moment at the Support of Ribs

In the computation of the bending moment at the support of ribs, only *concentrated loads*, P , at locations $y_1, y_2 \dots$ etc. are used (Fig. 4.3a). The values of y are measured from the nearest support with the lower number, m , in all cases. The bending moment due to several loads, P , at various locations, y , is obtained by superposition of the individual effects.

1. The values of η_{cn}/s are computed by equation (4.38) with equations (4.39) and (4.40). If the values of αs and αy become large, equations (4.51) and (4.52) are used instead.

2. The bending moment is computed by equation (4.35).

10.3.3.1.7 Computation of Bending Moments Per Rib

The bending moments computed in accordance with Sections 10.3.3.1.5 and 10.3.3.1.6 are obtained in units of kip-in./in., at the location x used in the computation of the coefficients Q_{nx}/Q_0 (Section 10.3.3.1.3).

In the usual cases it is sufficient to compute the bending moment acting on the critical rib by multiplying the moment obtained by equation (4.35) by the rib width, $a + e$, equation (4.35a). This value of the bending moment per rib is conservative (see Fig. 2.8).

If greater accuracy is desired, the moment per rib may be computed by equation (4.36).

In the special case of one load placed at the midspan of the plate strip, b , (Fig. 3.14), the moment in the rib located under the load may be obtained by equation (4.36a).

10.3.3.2 Bending Moments in Rigid Floor Beams

Bending moments in the rigid floor beams in a system with closed ribs are computed in the same manner as in that with open ribs (see Section 10.2.3.1.3).

10.3.3.3 Additional Bending Moments Due to Floor Beam Flexibility

The effects of floor beam flexibility on the bending moments in the deck system with closed ribs are computed by procedures given in Section 10.2.3.2, except that in the computation of the additional bending moments in the ribs equation (5.9a) is used instead of equation (5.9).

10.3.4 Computation of the Bending Moments by Charts for AASHO Loads

Before the computation of the bending moments the section properties and the rigidity coefficients of

the deck system have to be determined in accordance with Section 10.3.2.

10.3.4.1 Bending Moments in a System with Rigid Floor Beams

10.3.4.1.1 Bending Moments in the Ribs

(a) General

The charts for the determination of the bending moments in the closed ribs are computed for the standard wheel loads of the AASHO trucks. The use of the 8 kip and 12 kip wheel loads over the ribs where the bending moment is sought, with an impact factor of 30%, is recommended (see Section 3.4.2.1).

Charts 9–14 give the bending moments per unit width due to one wheel load or several wheel loads placed directly over the rib under consideration. Additional possible wheel loads 6 ft or 4 ft away over adjacent ribs are not considered in these charts (see Section 4.3.6.2).

If consideration of the additional wheels 6 ft or 4 ft away is required, the correction factors given in Table 4.3.6.2 may be used.

It should be noted that if additional wheels 4 ft away are used directly opposite the wheels placed over the rib under consideration, Chart 23 for the computation of the bending moment increment in the ribs due to loads in adjoining lanes cannot always be used.

(b) Bending moment at the midspan

1. The bending moment per unit width is obtained for one wheel over the midspan, with or without additional wheel loads over the rib considered, from Charts 9 and 11, or from Charts 10 and 12, depending on the loading used.

The decision as to whether one wheel or several wheels over the rib considered constitute the critical loading is made by comparing the maximum moments obtained with consideration of the effects of floor beam flexibility in both cases (see Section 10.3.4.2).

2. The bending moment per rib is obtained by multiplying the value from Charts 9–12 by the rib width, $a + e$ (equation 4.35a).

(c) Bending moment at the support

The bending moment at the support of the ribs is obtained in a similar manner by Chart 13 and equation (4.35a).

10.3.4.1.2 Bending Moments in the Floor Beams

The procedure for the computation of the bending moments in the rigid floor beams by Charts is given in Section 10.2.4.1.2.

10.3.4.2 Additional Bending Moments Due to Floor Beam Flexibility

The procedure is the same as given for the system with open ribs (Section 10.2.4.2), except that equation (5.9a) is used instead of equation (5.9) in the determination of the additional moments in the ribs.

10.4 COMPUTATION OF STRESSES

10.4.1 Stresses in System II

Stresses in System II are defined as flexural stresses in the longitudinal ribs and in the floor beams, acting together with appropriate portions of the deck plate as their flanges, due to the local action of the loads placed on the deck (see Sections 1.2.2 and 1.2.4.1).

10.4.1.1 Flexural Stresses in the Ribs

Stresses in the ribs are computed separately for the following loading cases:

- (A) Live load—ribs on rigid floor beams
- (B) Live load—additional effects of floor beam flexibility
- (C) Dead load

The section moduli for the live load stresses are computed in accordance with Sections 10.2.2.1 and 10.3.2.1. For computations of the dead load stresses, section moduli computed in accordance with lines (2) or (5) of Table 3.3.2.2 may be used.

In computing the live load stresses several groups of loads may have to be compared in order to determine which loading produces the maximum stress at the point under consideration due to cases (A) + (B), above.

The bending moments in the ribs due to dead load are computed, with consideration of the erection procedure, by the usual formulas for continuous beams on rigid supports. The steel dead weight and the superimposed dead weight (wearing surface) are treated separately. The effect of the heavier floor beams on the dead load stresses in the ribs may be computed in a similar manner as discussed in Section 5.4.

10.4.1.2 Flexural Stresses in the Floor Beams

Stresses in the floor beams are computed separately for loading cases (A), (B) and (C) (Section 10.4.1.1).

The floor beam section moduli are computed in accordance with Section 10.2.2.2.

The erection stresses have to be considered in the computation of the dead load stresses.

10.4.2 Stress Superposition, System I + II

Maximum stresses in the deck are obtained by superposition of the System II stresses in the longitudinal direction of the bridge (Section 10.4.1.1) and the System I stresses in the deck acting as the flange of the main carrying members of the bridge (girders or trusses).

Points of the bridge deck where the maximum tensile and compressive stresses occur in the usual cases are designated "A" and "B" in Figure 1.37. For additional comments regarding stress superposition, see Section 1.2.6.

The System I stresses are computed by the usual methods (see Section 1.2.3). In the computation of the dead load stresses the erection procedure has to be considered. Stresses at the top or the bottom of the ribs are computed with consideration of the distance of the point under investigation from the neutral axis of the bridge cross section (Fig. 1.37). In the cases of unsymmetrical bridge loading the stress is assumed to vary linearly between the main girders (Fig. 1.30b).

10.4.3 Shearing Stresses

Shearing stresses in the deck plate and in the welds have to be computed in System I and System II.

Maximum shears in the longitudinal ribs in System II may be conservatively estimated by placing wheel loads over the rib near the floor beam and assuming that the entire load is transmitted to the floor beam by the rib under consideration.

Maximum shears in the floor beams are computed with consideration of the floor beam flexibility by methods discussed in Section 5.3.4.2.

Shearing stresses in the floor beam webs and in the welds between the webs and the deck plate have to be computed with proper consideration of the cutouts in the floor beam webs for the longitudinal ribs.

10.4.4 Alternating and Pulsating Stresses

Alternating and pulsating stresses in the ribs and the floor beams may have to be investigated in the design.

Greatest amplitudes between the maximum and the minimum values of the stresses at any point of a rib are usually obtained if the maximum variation of both System I and System II stresses is considered.

For computation of the alternating stresses in System II, Charts 8 and 14 may be used.

CHAPTER 11

Numerical Examples

11.1 INTRODUCTION

The use of the formulas given in Chapters 3 to 5 and of the charts given in Appendix I is illustrated by the design computations of a steel plate deck of a continuous plate girder bridge with the following principal dimensions:

- Spans: 270-375-270 ft
- Width: 68 ft-0 in. o. to o. of fascias
- Main girder spacing: 50 ft-0 in.

Designs are presented for both principal deck systems: with open ribs (Section 11.2) and with closed ribs (Section 11.3).

The loads and stresses are in accordance with the current AASHO Standard Specifications for Highway Bridges [1], as interpreted in Section 3.4 of this Manual.

For each system the design computation is made twice: by the general formulas, and by the charts for the AASHO loading, to provide a comparison of the two design procedures. It is seen that the use of the charts significantly reduces the time needed for the design, especially in the case of a deck with closed ribs.

Numerical computations are presented in detail only for the bending moments and stresses in the deck acting as an independent structural element (System

II). Computations of the stresses in the deck as the top flange of the main girders (System I), the design of welds, and other computations made by routine methods are not included.

The design computations are made in accordance with the procedures outlined in Chapter 10, where additional comments on the individual computation steps may be found.

It should be emphasized that the layout of the deck plating panels, spacing of the ribs and floor beams, and other structural details shown in the numerical examples are not the only possible solutions, and that, in each practical case, a study of various alternative arrangements and details will be required to determine the design which will best satisfy the given conditions.

11.2 DECK WITH OPEN RIBS

11.2.1 General

11.2.1.1 Dimensions and Details

The general layout of the deck is shown in Figure 11.1.

Figure 11.2 shows typical deck dimensions and details. In general, it may be more economical to vary the size of the longitudinal ribs in the longitudinal as well as in

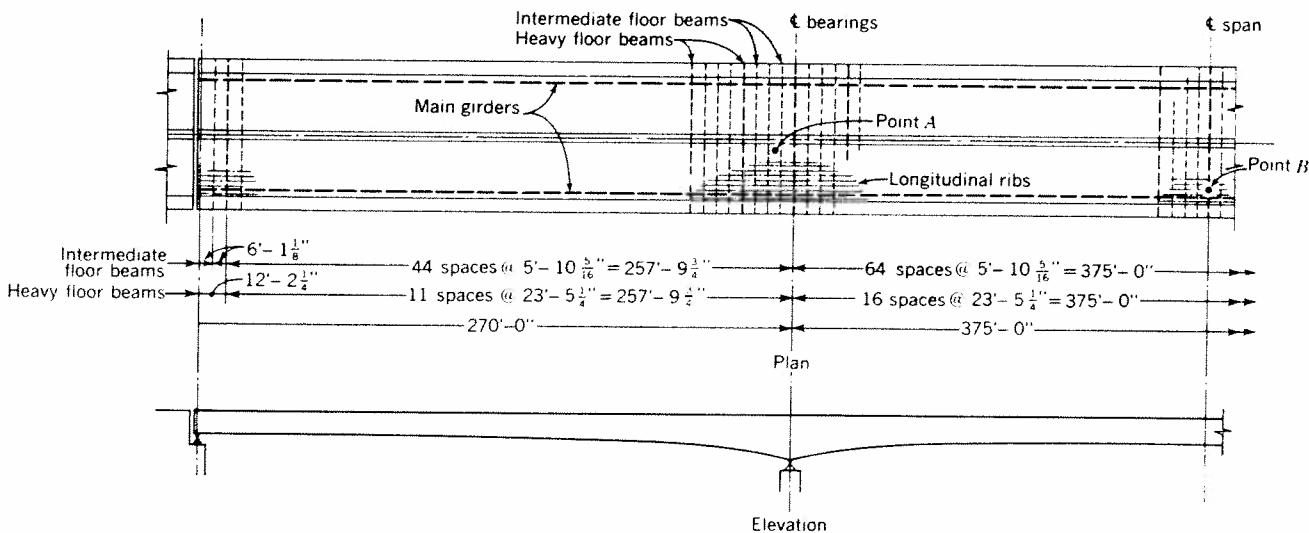


Fig. 11.1. Deck with open ribs — general layout

the transverse direction of the bridge, as required. However, in order to limit the scope of the design computations, only one rib size is used in this numerical example.

All material is low-alloy structural steel, except for the intermediate floor beams which, in this case, are designed in carbon structural steel in order to limit the deflections of the deck.

The heavier floor beams, spaced 23.44 ft o.c., provide the cross frames of the bridge and serve, in this case, as erection supports for the deck plating panels (see Fig. 11.2).

11.2.1.2 Choice of Deck Plate Thickness

The thickness of the deck plate is determined in accordance with the recommendations outlined in Chapter 6.

Applying the allowable deflection criterion of $\frac{1}{300}$ of the deck plate span between the ribs, the deck plate thickness theoretically required for the chosen spacing of the ribs is obtained from equation (6.7a).

With rib spacing $a = 12$ in., and the design pressure of a 12,000-lb wheel, including impact, $p = 59$ psi

(see Section 3.4.2), the plate thickness, t_P , is obtained as

$$t_P \geq (0.007)(12)(\sqrt[3]{59}) = 0.328 \text{ in.}$$

A thickness of $\frac{3}{8}$ in. is chosen.

It should be noted that the maximum value of the local flexural stress in the $\frac{3}{8}$ -in. deck plate of this design example is 25.9 ksi, and the maximum deflection is approximately $\frac{1}{500}$ of the deck plate span between the ribs, as computed in Section 6.2.1.3.1.

The $\frac{3}{8}$ -in. thickness of the deck plate as the top flange of the main girders, the longitudinal ribs and the floor beams is ample, as indicated by the relatively low axial stresses in the deck plate (see Sections 11.2.1.6, 11.2.2.4.1 and 11.2.2.4.2).

The shearing strength of the $\frac{3}{8}$ -in. deck plate acting as the top flange of the main girders is also satisfactory.

11.2.1.3 Section Properties

11.2.1.3.1 Longitudinal Ribs

(a) Values of I_R' and S_R' for computation of the live load stresses in the ribs on rigid supports

For the 8-kip and 12-kip wheels used in the rib design, with the width $2g = 22$ in., the ratio of the

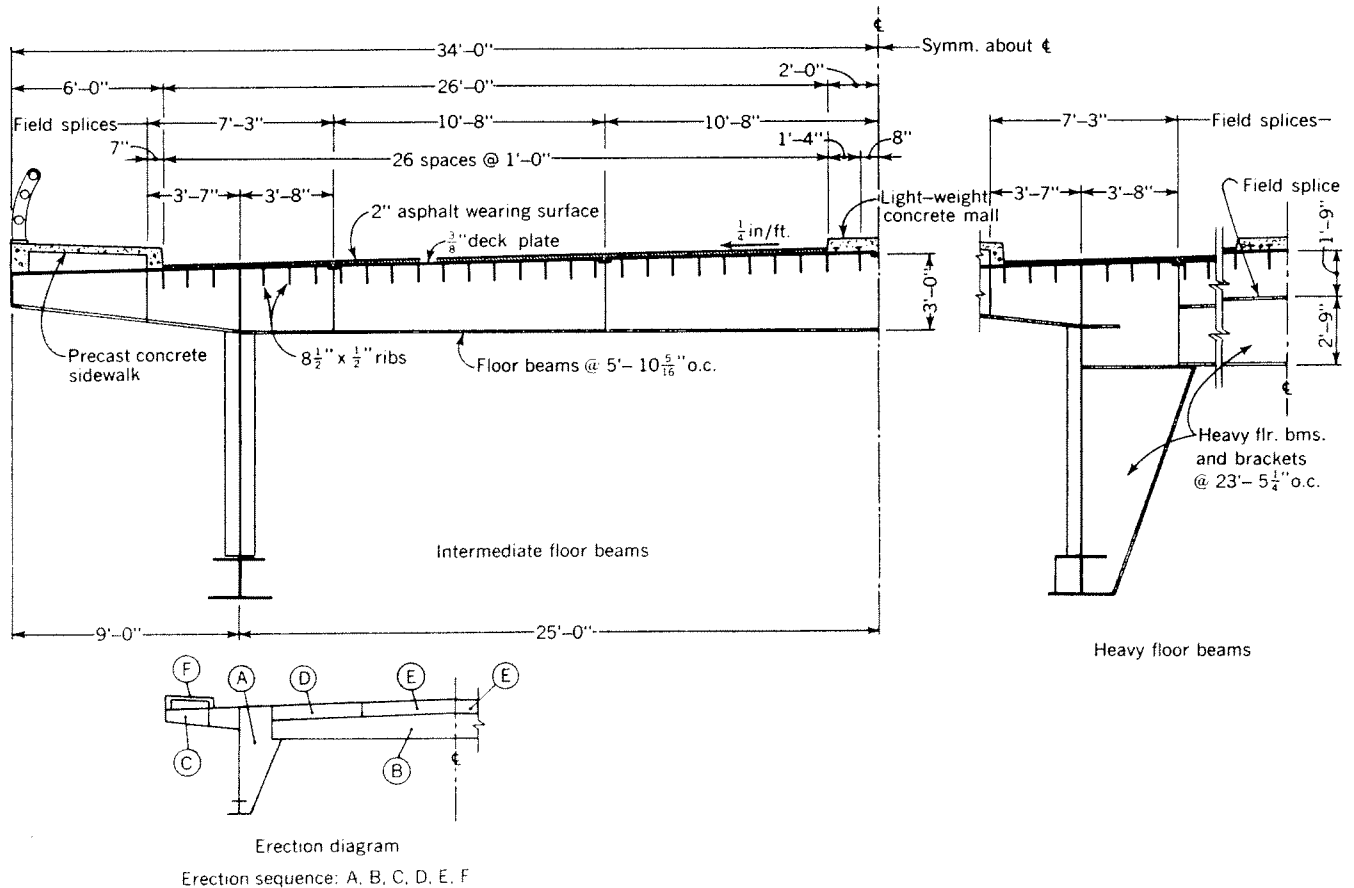


Fig. 11.2. Deck with open ribs — typical sections and details

loading width to rib spacing is computed

$$\frac{2g}{a} = \frac{22}{12} = 1.83$$

With this value, the effective rib spacing is obtained from Chart 2, Case 1, as

$$a_0^* = \left(\frac{a_0}{a}\right) a = (1.47)(12) = 17.6 \text{ in.}$$

This value may also be directly obtained from Chart 4. By formula, Line 1, Table 3.3.2.2, the effective rib span is computed as

$$s_1 = 0.7s = (0.7)(5.86)(12) = 49.3 \text{ in.}$$

Entering Chart 1 with the value

$$\frac{a_0^*}{s_1} = \frac{17.6}{49.3} = 0.357$$

the effective width of deck plate acting with the directly loaded rib is obtained as (Fig. 11.3a)

$$a_0' = \left(\frac{a_0}{a_0^*}\right) a_0^* = (0.85)(17.6) = 15.0 \text{ in.}$$

The section properties of one rib consisting of an $8\frac{1}{2} \times \frac{1}{2}$ -in. stiffener and the deck plate with the effective width a_0' are obtained as follows:

$$I_R' = 73.4 \text{ in.}^4 \quad S_{RT}' = 34.9 \text{ in.}^3 \quad S_{RB}' = 10.8 \text{ in.}^3$$

(b) *Values of I_R and S_R for computation of the effects of floor beam flexibility*

By formula, Line 2, Table 3.3.2.2 the effective width of deck plate is (Fig. 11.3b)

$$a_0 = 1.1a = (1.1)(12) = 13.2 \text{ in.}$$

The corresponding rib section properties are

$$I_R = 70.7 \text{ in.}^4 \quad S_{RT} = 31.5 \text{ in.}^3 \quad S_{RB} = 10.7 \text{ in.}^3$$

11.2.1.3.2 Floor Beams

(a) *Intermediate floor beams*

By formulas, Line 6, Table 3.3.2.2 and Chart 1

$$s^* = s = 70.3 \text{ in.}$$

$$\frac{s^*}{l} = \frac{70.3}{(50)(12)} = 0.117$$

The effective width of deck plate acting with one floor beam is (Fig. 11.3c)

$$s_0 = \left(\frac{s_0}{s^*}\right) s^* = (1.06)(70.3) = 74.5 \text{ in.}$$

With this value of s_0 the following section properties are computed:

At midspan:

$$I_F = 7810 \text{ in.}^4 \quad S_{FT} = 905 \text{ in.}^3 \quad S_{FB} = 276 \text{ in.}^3$$

At quarter-points:

$$I_F = 6350 \text{ in.}^4$$

(b) *Heavy floor beams*

The section properties are computed with the same effective width of deck plate, and are (Fig. 11.3d):

At midspan:

$$I_F = 22,740 \text{ in.}^4, \\ S_{F1} = 1370 \text{ in.}^3 \quad S_{F2} = 5170 \text{ in.}^3 \quad S_{F3} = 608 \text{ in.}^3$$

At quarter-points:

$$I_F = 19,920 \text{ in.}^4$$

Average value:

$$I_{F(\text{avg})} = \frac{22,740 + 19,920}{2} = 21,330 \text{ in.}^4$$

For the lower portion of the floor beam, carrying the erection dead load, the values at the midspan are:

$$I_F = 4415 \text{ in.}^4 \quad S_{F2} = S_{F3} = 268 \text{ in.}^3$$

11.2.1.4 Relative Rigidity Coefficients

11.2.1.4.1 Rigidity Ratio of the Ribs and the Floor Beams, γ

The average moment of inertia of the floor beam, resulting in the same floor beam deflection at midspan under the design loading as that of the actual floor beam (see Section 5.3.2), may be approximately computed as the average of the moments of inertia at the midspan and at the quarter-point.

$$I_{F(\text{avg})} = \frac{7810 + 6350}{2} = 7080 \text{ in.}^4$$

By equation (5.7)

$$\gamma = \frac{l^4 I_R}{a s^3 \pi^4 I_F} = \frac{(600)^4 (70.7)}{(12)(70.3)^3 (\pi^4)(7080)} = 3.2$$

11.2.1.4.2 Rigidity Ratio of the Deck Plate and the Ribs, γ'

The ratio γ' is computed by equation (4.18) as

$$\gamma' = \frac{t_P^3 s_2^4}{10.92 I_R' a^3 \pi^4} = \frac{(0.375)^3 [(0.81)(70.3)]^4}{(10.92)(73.4) 12^3 \pi^4} \\ = 0.0041$$

Since the value of γ' is smaller than 0.006 (see equation 4.20), no correction for the effects of the deck plate

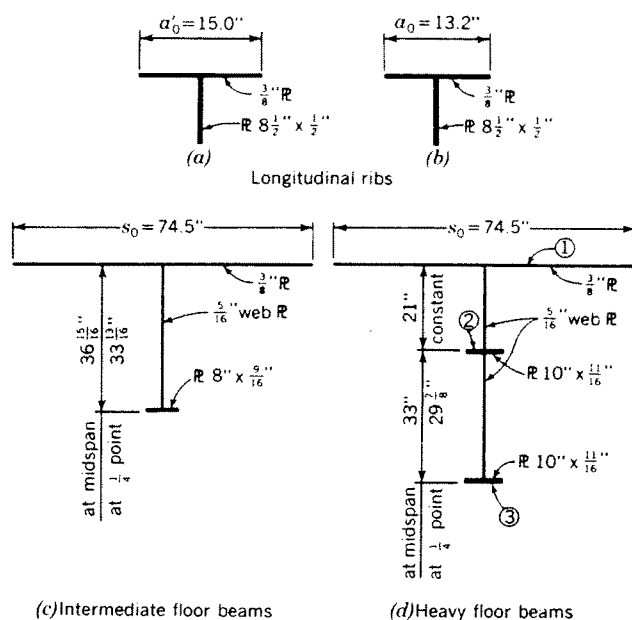


Fig. 11.3. Cross sections of structural elements of the deck with open ribs

rigidity (Section 4.2.7) is needed in the computation of the bending moments.

11.2.1.4.3 Rigidity Ratio of the Heavy and the Intermediate Floor Beams, β

The coefficient β , needed in the computation of the effects of the heavy floor beams (Section 5.4) is computed as

$$\beta = \frac{I_0}{I} = \frac{21,330}{7080} = 3.01$$

11.2.1.5 Elastic Stability of Ribs

The elastic stability of ribs subject to compression is investigated by formulas given in Appendix II.

Maximum compressive stresses in the ribs are obtained by superposition of the System I and System II stresses.

In order to evaluate the *local buckling strength* of the $8\frac{1}{2} \times \frac{1}{2}$ -in. ribs used in the design (Fig. 11.3), the ideal buckling stress, f_t , is computed by equation (II.1a).

With

$$\frac{t_R}{h} = \frac{\frac{1}{2}}{8\frac{1}{2}} = \frac{1}{17}$$

and $k = 1.0$ (see Appendix II, Section II.1.3.1.1), the ideal buckling stress is

$$f_t = (26,200)(1.0) \left(\frac{1}{17} \right)^2 = 90.7 \text{ ksi}$$

Since the above value of f_t is greater than the proportional limit of the low-alloy steel used, the critical buckling stress in the inelastic range, f_{cr} , has to be computed.

With the ratio

$$\frac{f_y}{f_t} = \frac{50}{90.7} = 0.55$$

the ratio f_{cr}/f_y is found from Figure II.2, Curve 1, as

$$\frac{f_{cr}}{f_y} = 0.95$$

Thus the critical buckling stress is

$$f_{cr} = (0.95)(50) = 47.5 \text{ ksi}$$

With the factor of safety of 1.5, as recommended in Section 9.5.1, the allowable compressive stress for the superposition of the System I and System II effects in a rib is

$$f_{\text{allow}} = \frac{47.5}{1.5} = 31.7 \text{ ksi}$$

The actual maximum combined compressive stress in the rib is 18.8 ksi (Section 11.2.2.4.1). Thus the local buckling safety of the $8\frac{1}{2} \times \frac{1}{2}$ -in. ribs is ample.

The *overall buckling strength* of the deck acting as the top flange of the main girders is even more adequate, as may be verified by formulas given in Section II.2 of Appendix II.

11.2.1.6 Stresses in the Deck as the Flange of the Main Girders

The maximum stresses in the deck acting as the upper flange of the main girders (System I), computed at points *A* and *B* of the deck (Fig. 11.1), as discussed in Section 1.2.6, are

Point	A	B
Top of deck plate, ksi	12.5	-11.2
Bottom of rib, ksi	11.3	-9.5

11.2.2 Design by General Formulas

11.2.2.1 Bending Moments in a System with Rigid Floor Beams

11.2.2.1.1 Loading

(a) Ribs

In the design of the ribs the 12-kip and 8-kip wheel loads are used, in accordance with Figures 5 and 6 and footnote, Section 1.2.5(C) of the 1961 AASHTO specifications (see Section 3.4.2.1 of this Manual).

The positions of the wheels used in the design are

shown in Figure 11.4. The position of the 8-kip wheels to obtain the largest effect in loading cases **a**₁ and **d** is determined by inspection of the influence lines, Charts 5a and 5b, respectively.

Using the wheel width, $2g$, of 22 in. (Section 3.4.2.2) it is seen from Chart 2a that the load on one rib, R_0 , is greatest if the wheel is centered over the rib (Case 1). With the value of $2g/a = 1.83$, the load per rib is

$$R_0 = \left(\frac{R_0}{P}\right) P = 0.615 P$$

A 30% impact factor is used in the design of the ribs.

(b) Floor beams

In the design of the floor beams, 32-kip truck axles are used.

The loading cases used in the design are shown in Figure 11.5.

The impact factor, computed in accordance with Section 1.2.12 (C) of the AASHO specifications, is

$$I = \frac{50}{L + 125} = \frac{50}{50 + 125} = 0.286$$

Thus, the axle load, P , is

$$P = 32(1.286) = 41.1 \text{ kips}$$

The loads on the floor beam, F_0 , due to one truck are, for loading case **A**,

$$F_0 = 41.1 \text{ kips}$$

and for loading case **B** (eqs. 4.11 and 4.12),

$$\begin{aligned} F_0 &= 41.1 + \left(41.1 + \frac{41.1}{4}\right) \left[-0.8038 \left(\frac{2.28}{5.86}\right) + \right. \\ &\quad \left. 1.3923 \left(\frac{2.28}{5.86}\right)^2 - 0.5885 \left(\frac{2.28}{5.86}\right)^3 \right] (-0.2679) \\ &= 41.1 + 1.9 = 43.0 \text{ kips} \end{aligned}$$

11.2.2.1.2 Live Load Moments at Midspan of Ribs

For loading case **a** (Fig. 11.4a), the bending moment per rib, M_{RC} , at the midspan is computed by equation (4.10) with equation (4.5a), using $c = 0.5$ ft, as

$$\begin{aligned} M_{RC} &= (12)(1.3)(0.615)(5.86) \times \\ &\quad \left[0.1708 - 0.25 \left(\frac{0.5}{5.86}\right) + 0.1057 \left(\frac{0.5}{5.86}\right)^2 \right] \\ &= 8.46 \text{ k-ft} \end{aligned}$$

For loading case **a**₁ the moment at midspan is obtained

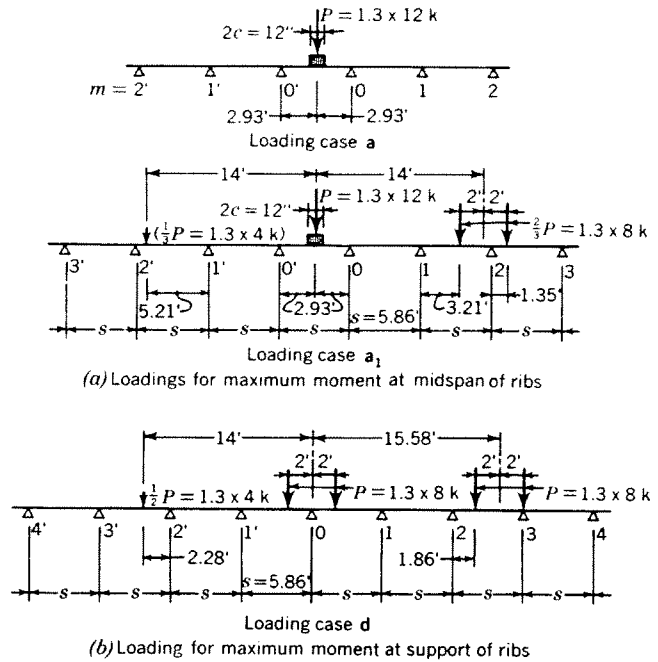


Fig. 11.4. Loadings used in the design of the open ribs in a system with rigid floor beams

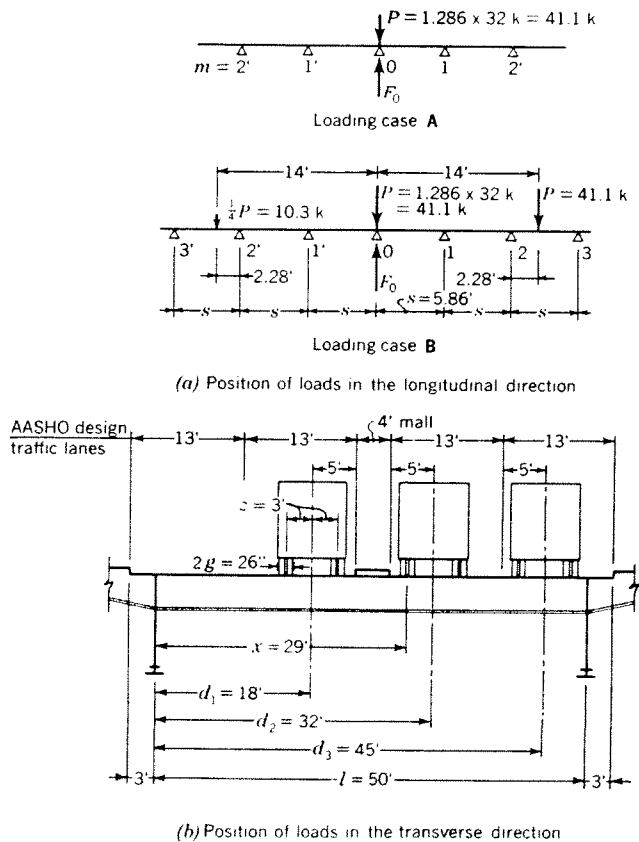


Fig. 11.5. Loadings used in the design of floor beams

by equations (4.10), (4.9) and (4.5a), as

$$\begin{aligned}
 M_{RC} &= 8.46 + 4(1.3)(0.615)(5.86) \times \\
 &\quad \left[-0.1830 \left(\frac{5.21}{5.86} \right) + 0.3170 \left(\frac{5.21}{5.86} \right)^2 - \right. \\
 &\quad \quad \left. 0.1340 \left(\frac{5.21}{5.86} \right)^3 \right] (-0.2679) + \\
 &\quad (8)(1.3)(0.615)(5.86) \times \\
 &\quad \left[-0.1830 \left(\frac{3.21}{5.86} \right) + 0.3170 \left(\frac{3.21}{5.86} \right)^2 - \right. \\
 &\quad \quad \left. 0.1340 \left(\frac{3.21}{5.86} \right)^3 \right] (-0.2679) + \\
 &\quad (8)(1.3)(0.615)(5.86) \times \\
 &\quad \left[-0.1830 \left(\frac{1.35}{5.86} \right) + 0.3170 \left(\frac{1.35}{5.86} \right)^2 - \right. \\
 &\quad \quad \left. 0.1340 \left(\frac{1.35}{5.86} \right)^3 \right] (-0.2679)^2 \\
 &= 8.46 + 0.03 + 0.27 - 0.07 = 8.69 \text{ k-ft}
 \end{aligned}$$

with the 4-kip wheel included, and

$$M_{RC} = 8.46 + 0.27 - 0.07 = 8.66 \text{ k-ft}$$

without the 4-kip wheel.

11.2.2.1.3 Live Load Moment at Support of Ribs

The bending moment per rib, M_{RS} , is computed for loading case **d** (Fig. 11.4b) by equation (4.6a) with (4.5a) as

$$\begin{aligned}
 M_{RS} &= (2)(8)(0.615)(5.86) \times \\
 &\quad \left[-0.5 \left(\frac{2.00}{5.86} \right) + 0.866 \left(\frac{2.00}{5.86} \right)^2 - \right. \\
 &\quad \quad \left. 0.366 \left(\frac{2.00}{5.86} \right)^3 \right] + \\
 &\quad 8(0.615)(5.86) \times \\
 &\quad \left[-0.5 \left(\frac{1.86}{5.86} \right) + 0.866 \left(\frac{1.86}{5.86} \right)^2 - \right. \\
 &\quad \quad \left. 0.366 \left(\frac{1.86}{5.86} \right)^3 \right] (-0.2679)^2 + \\
 &\quad (4)(0.615)(5.86) \times \\
 &\quad \left[-0.5 \left(\frac{2.28}{5.86} \right) + 0.866 \left(\frac{2.28}{5.86} \right)^2 - \right. \\
 &\quad \quad \left. 0.366 \left(\frac{2.28}{5.86} \right)^3 \right] (-0.2679)^2 \\
 &= -6.23 - 0.23 - 0.11 = -6.66 \text{ k-ft}
 \end{aligned}$$

11.2.2.1.4 Live Load Moments in Floor Beams

The maximum bending moments at a point under the wheel nearest to the center of the bridge, $x = 29$ ft (Fig. 11.5b), computed for truck loads, F_0 , obtained in Section 11.2.2.1.1b for loading cases **A** and **B** (Fig. 11.5a), are given below. The load intensity reduction coefficients for multiple lane loading of 10% for 3 lanes loaded and 25% for 4 lanes loaded (AASHTO specifications, Section 1.2.9) have been considered.

Lanes Loaded	Max. Bending Moments (k-ft)	
	Loading A	Loading B
2	741	775
3	774	810
4	709	742

It is seen that loading of 3 lanes governs.

11.2.2.1.5 Dead Load Moments

The erection procedure assumed in this case (Fig. 11.2) requires the ribs to carry the erection load of the deck panels to the heavy floor beams, spaced 23.44 ft o.c.

The lower portions of the heavy floor beams carry the erection load, the completed sections of the heavy floor beams and the intermediate floor beams carry the superimposed dead load.

The dead loads used in the computation are as follows:

Member	Erection Load	Superimposed Dead Load	
		Wearing Surface	Center Mall
Ribs (incl. weight of interm. floor beams), lbs/ft	36	25	—
Intermediate floor beams, lbs/ft	—	147	352
Heavy floor beams, lbs/ft	920	147	352

With the above weights the following dead load moments are obtained:

(a) Ribs

Erection load:

Moment at heavy floor beams

$$= \frac{(-0.036)(23.44)^2}{12} = -1.64 \text{ k-ft}$$

Moment midway between heavy floor beams

$$= +0.82 \text{ k-ft}$$

Superimposed dead load:

Moment at floor beams

$$= \frac{(-0.025)(5.86)^2}{12} = -0.07 \text{ k-ft}$$

Moment at midspan

$$= +0.04 \text{ k-ft}$$

(b) Floor beams

The sidewalk load causes the following negative moments in the floor beams:

- Heavy floor beams, erection condition: -14 k-ft
- All floor beams, superimposed dead load: -13 k-ft

With the weights given above, the bending moments at the midspan of the floor beams are:

- Heavy floor beams, erection loads:
288 - 14 = 274 k-ft
- All floor beams, superimposed loads:
56 - 13 = 43 k-ft

11.2.2.2 Effects of Floor Beam Flexibility, All Floor Beams Uniform

11.2.2.2.1 Additional Bending Moments in Ribs

(a) Positive moment increment

The maximum positive bending moment increment is obtained in the rib under the wheel near the midspan of the floor beam (Fig. 11.6b).

For computation of the effects of floor beam flexibility, the loads over the critical rib are the same as used in Section 11.2.2.1.2. Other loads used in the computation are shown in Figure 11.6a. Placing loads in additional lanes would cause a decrease of the bending moment, due to the AASHO load reduction coefficients for multiple lane loading.

The values needed in the evaluation of equation (5.9) for the bending moment increment are computed as follows:

The values of Q_0 , with consideration of the 30% impact factor, are:

For a 12-kip wheel load,

$$Q_0 = \frac{P}{2g} = \frac{(12)(1.3)}{22} = 0.709 \text{ k/in.}$$

For a 16-kip wheel load,

$$Q_0 = \frac{P}{2g} = \frac{(16)(1.3)}{26} = 0.800 \text{ k/in.}$$

The first Fourier coefficients, Q_{1x}/Q_0 , are computed at the location $x = 29$ ft (Fig. 11.6b) by equation (3.27).

For the truck in the critical lane,

$$\frac{Q_{1x}}{Q_0} = \frac{8}{\pi} \cos \frac{3\pi}{50} \sin \frac{11\pi}{(12)(50)} \sin \frac{32\pi}{50} \sin \frac{29\pi}{50} = 0.126$$

For the axle in the adjoining lane, with 16-kip wheels and $2g = 26$ in.,

$$\frac{Q_{1x}}{Q_0} = \frac{8}{\pi} \cos \frac{3\pi}{50} \sin \frac{13\pi}{(12)(50)} \sin \frac{18\pi}{50} \sin \frac{29\pi}{50} = 0.149$$

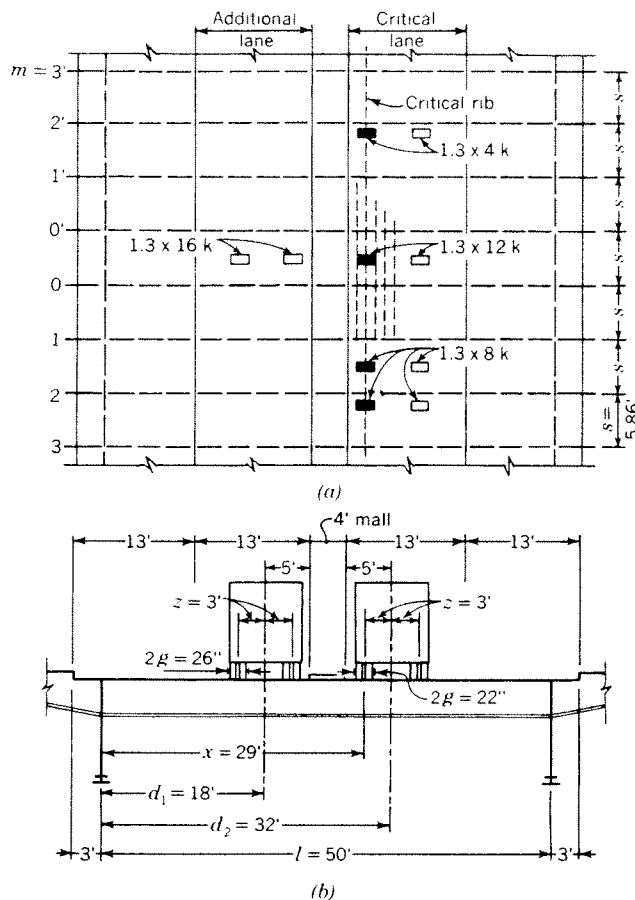


Fig. 11.6. Loading used in the computation of the maximum bending moments at the midspan of open ribs with consideration of floor beam flexibility

Computation of the expression $\sum(F_m/P)(\bar{\eta}_{Cm}/s)$ for loading cases **a** and **a₁** in the critical lane and for loading **h** in the adjoining lane is given in Table 11.2.2.2.1.

The values of F_m/P , defined in Section 5.3.3.1, are obtained separately for each wheel load by Chart 5c or equations (4.11) and (4.12). The load P is the 12-kip wheel load. The 8-kip and 4-kip wheel loads are expressed as fractions of P (see sketch, Table 11.2.2.1).

The dimensionless influence ordinates $\bar{\eta}_c/s$ for the bending moment at the midspan of the panel 0-0', are obtained from Chart 17 for $\gamma = 3.2$.

The bending moment increments per rib, ΔM_{RC} , are computed by equation (5.9) as follows:

Loading **a** in critical lane,

$$\Delta M_{RC} = (0.709)(5.86)(12)(0.126)(0.314) = 1.97 \text{ k-ft}$$

Loading **a₁** in critical lane, 4-kip wheel included,

$$\Delta M_{RC} = (0.709)(5.86)(12)(0.126)(0.177) = 1.11 \text{ k-ft}$$

Loading **a₁** in critical lane, 4-kip wheel not included,

$$\Delta M_{RC} = (0.709)(5.86)(12)(0.126)(0.207) = 1.30 \text{ k-ft}$$

TABLE 11.2.2.1
BENDING MOMENT INCREMENT AT MIDSPAN OF RIBS. COMPUTATION OF $\Sigma(F_m/P)(\bar{\eta}_{cm}/s)$

Loading (Figs. 11.4a & 11.6)	Values computed	Reference												$\Sigma \frac{F_m \bar{\eta}_{cm}}{P s}$
			Support (m)	4'	3'	2'	1'	0'	0	1	2	3	4	
	$\bar{\eta}_{cm}/s$	Chart 17	-0.062	-0.090	-0.088	+0.004	+0.266	+0.266	+0.004	-0.088	-0.090	-0.062		
Case a†	F_m/P	Eq. 4.11-12	+0.002	-0.009	+0.034	-0.127	+0.601	+0.601	-0.127	+0.034	-0.009	+0.002		
	$F_m/P(\bar{\eta}_{cm}/s)$		0	+0.001	-0.003	-0.001	+0.160	+0.160	-0.001	-0.003	+0.001	0	+0.314	
Case a ₁ with wheel (4)	F_m/P	Wheel (1)	Eqs. 4.11	+0.002	-0.009	+0.034	-0.127	+0.601	+0.601	-0.127	+0.034	-0.009	+0.002	
		Wheel (2)	& 4.12	0	0	+0.001	-0.006	+0.021	-0.079	+0.358	+0.442	-0.089	+0.024	
		Wheel (3)	or	0	0	0	+0.002	-0.006	+0.021	-0.079	+0.599	+0.163	-0.042	
		Chart 5c	+0.007	-0.024	+0.325	+0.035	-0.009	+0.002	-0.001	-0.001	0	0		
	Total F_m/P		+0.009	-0.033	+0.360	-0.096	+0.607	+0.545	+0.151	+1.075	+0.065	-0.016		
	$(F_m/P)(\bar{\eta}_{cm}/s)$		-0.001	+0.003	-0.032	0	+0.161	+0.145	+0.001	-0.095	-0.006	+0.001	+0.177	
Case a ₁ without wheel (4)	F_m/P		+0.002	-0.009	+0.035	-0.131	+0.616	+0.543	+0.152	+1.075	+0.065	-0.016		
	$(F_m/P)(\bar{\eta}_{cm}/s)$		0	+0.001	-0.003	-0.001	+0.164	+0.145	+0.001	-0.095	-0.006	+0.001	+0.207	

† Case a consists of wheel (1) only. Case h, additional lane loaded, is the same as Case a except that $P = 1.3 \times 16$ kips.

TABLE 11.2.2.2
MOMENT RELIEF IN FLOOR BEAMS. COMPUTATION OF $(F_0/P) - (F_0/P)$

Loading (Fig. 11.5)	Value computed	Reference											F_0/P , Eq. (5.13)	$(F_0/P) - (F_0/P)$
			Support, m	4'	3'	2'	1'	0	1	2	3	4		
	$\bar{\delta}_{0m}$	Chart 19	+0.010	+0.052	+0.125	+0.212	+0.264	+0.212	+0.125	+0.052	+0.010			
Case A†	F_m/P	Eqs. 4.11-4.12					+1.000							
	$(F_m/P)\bar{\delta}_{0m}$						+0.264					+0.264	+0.736	
Case B	F_m/P	Axle (1)	Eqs. 4.11 &					+1.000						
		Axle (2)	4.12 or	0	-0.001	+0.003	-0.010	+0.037	-0.138	+0.740	+0.453	-0.105		
		Axle (3)	Chart 5c	-0.026	+0.113	+0.185	-0.035	+0.009	-0.002	+0.001	0	0		
		Total F_m/P		-0.026	+0.112	+0.188	-0.045	+1.046	-0.140	+0.741	+0.453	-0.105		
	$(F_m/P)\bar{\delta}_{0m}$		0	+0.006	+0.024	-0.010	+0.276	-0.030	+0.093	+0.023	-0.001	+0.381	+0.665	

† Case A consists of axle (1) only.

Loading h in adjoining lane,

$$\Delta M_{RC} = (0.800)(5.86)(12)(0.149)(0.314) = 2.64 \text{ k-ft}$$

The definitions of the loading cases used are given in Charts 20 and 23.

The total bending moment increments per rib at the midspan of ribs, computed under the assumption of all floor beams uniform, are obtained by equation (5.10)

Loadings a + h,

$$\Delta M_{RC} = 1.97 + 2.64 = 4.61 \text{ k-ft}$$

Loadings a₁ + h,

$$\Delta M_{RC} = 1.30 + 2.64 = 3.94 \text{ k-ft}$$

(b) Negative moment reduction

In a system with uniform rigidity of all floor beams, a reduction of the negative rib moments over the floor beams due to floor beam flexibility is expected. If the

negative moment in the rib in the rigid system (Section 11.2.2.1.3) is already smaller than the positive moment, the moment reduction, ΔM_{RS} , does not have to be considered.

However, in this case, the moment reduction ΔM_{RS} is computed for the purposes of superposition with the moment increment over the support of ribs, $\bar{\Delta} M_{RS}$, over the heavy floor beams, see Section 11.2.2.3.1b.

The value of ΔM_{RS} , obtained for loading d in a similar manner as ΔM_{RC} , above, is

$$\Delta M_{RS} = 2.30 \text{ k-ft}$$

11.2.2.2.2 Bending Moment Relief in Floor Beams

The bending moment relief in the floor beams is computed for the critical case of 3 lanes loaded (see Section 11.2.2.1.4).

TABLE 11.2.2.3.1a
EFFECT OF HEAVY FLOOR BEAMS ON MOMENTS IN RIBS. COMPUTATION OF \bar{F}_0/P AND \bar{F}_4/P

Loading (Figs. 11.4a & 11.6, Table 11.2.2.2.1)	Value computed	Reference											F_0/P	F_4/P
			(Eq. 5.13)											
Support, m			3'	2'	1'	0	1	2	3	4	5	6		
	$\bar{\delta}_{0m}$	Chart 19	+0.052	+0.125	+0.212	+0.264	+0.212	+0.125	+0.052	+0.010	-0.009	-0.013		
	$\bar{\delta}_{4m}$		-0.009	-0.013	-0.009	+0.010	+0.052	+0.125	+0.212	+0.264	+0.212	+0.125		
Case a†	Total F_m/P	Table 11.2.2.2.1	+0.002	-0.009	+0.034	-0.127	+0.601	+0.601	-0.127	+0.034	-0.009	+0.002		
	Floor Beam 0 (F_m/P) $\bar{\delta}_{0m}$		0	-0.001	+0.007	-0.034	+0.127	+0.075	-0.006	0	0	0	+0.168	
	Floor Beam 4 (F_m/P) $\bar{\delta}_{4m}$		0	0	0	-0.001	+0.031	+0.075	-0.027	+0.009	-0.002	0		+0.085
Case a ₁ with front axle	Total F_m/P	Table 11.2.2.2.1	+0.009	-0.033	+0.360	-0.096	+0.607	+0.545	+0.151	+1.075	+0.065	-0.016		
	Floor Beam 0 (F_m/P) $\bar{\delta}_{0m}$		0	-0.004	+0.076	-0.025	+0.129	+0.068	+0.008	+0.011	-0.001	0	+0.262	
	Floor Beam 4 (F_m/P) $\bar{\delta}_{4m}$		0	0	-0.003	-0.001	+0.032	+0.068	+0.032	+0.284	+0.014	-0.002		+0.424
Case a ₁ without front axle	Total F_m/P	Table 11.2.2.2.1	+0.002	-0.009	+0.035	-0.131	+0.616	+0.543	+0.152	+1.075	+0.065	-0.016		
	Floor Beam 0 (F_m/P) $\bar{\delta}_{0m}$		0	-0.001	+0.008	-0.035	+0.130	+0.068	+0.008	+0.011	-0.001	0	+0.188	
	Floor Beam 4 (F_m/P) $\bar{\delta}_{4m}$		0	0	0	-0.001	+0.032	+0.068	+0.032	+0.284	+0.014	-0.002		+0.427

† See note, Table 11.2.2.2.1.

The values needed in the evaluation of equation (5.14) are computed as follows:

With the impact factor of 0.286 used in the design of the floor beams, the value of Q_0 for a 16-kip wheel load is

$$Q_0 = \frac{P}{2g} = \frac{(16)(1.286)}{26} = 0.792 \text{ k/in.}, \text{ or } 9.5 \text{ k/ft}$$

The value of Q_{1x}/Q_0 , computed by equation (3.30) at location $x = 29 \text{ ft}$ (Fig. 11.5b), is

$$\frac{Q_{1x}}{Q_0} = \frac{8}{\pi} \cos \frac{3\pi}{50} \sin \frac{13\pi}{(12)(50)} \times \left[\sin \frac{18\pi}{50} + \sin \frac{32\pi}{50} + \sin \frac{45\pi}{50} \right] \sin \frac{29\pi}{50} = 0.349$$

Computation of the expression \bar{F}_0/P by equation (5.13) for loading cases **A** and **B** (Fig. 11.5a) is shown in Table 11.2.2.2.2.

The values of F_m/P are obtained by Chart 5c or equations (4.11) and (4.12). The influence ordinates, $\bar{\delta}_{0m}$, for reaction at floor beam 0 are obtained from Chart 19.

The bending moment relief, ΔM_F , in the floor beams

is computed by equation (5.14), with consideration of the AASHO reduction factor of 0.90 for three lanes loaded, as follows:

Loading **A**,

$$\Delta M_F = (9.5) \left(\frac{50}{\pi} \right)^2 (0.349)(0.736)(0.90) = 557 \text{ k-ft}$$

Loading **B**,

$$\Delta M_F = (9.5) \left(\frac{50}{\pi} \right)^2 (0.349)(0.665)(0.90) = 503 \text{ k-ft}$$

It is seen, by comparison with the bending moments in a rigid system, Section 11.2.2.1.4, that in this case the bending moment relief in the floor beams due to their flexibility is considerable.

11.2.2.3 Effects of Heavy Floor Beams

11.2.2.3.1 Adjustment of the Live Load Bending Moments in Ribs

(a) *Positive moment increment*

The maximum additional positive bending moment due to the effects of heavy floor beams will occur at the midspan of the rib panels 1-2 or 2-3 (see sketch, Table 11.2.2.3.1a).

The effects of heavy floor beams on the rib moments are computed for the same loading cases **a**, **a₁**, and **h** as used in Section 11.2.2.2.1.

In order to obtain the bending moment increment $\bar{\Delta}M_{RC}$ at the midspan of the panel 1-2, the effects of the heavy floor beams, $m = 0$ and $m = 4$, are computed and superimposed.

Equations (5.28) with (5.24) and (5.13) are used in the computations.

Reactions, \bar{F}_0 and \bar{F}_4 , at supports $m = 0$ and $m = 4$ of a beam on elastic supports with all supports of uniform rigidity, are computed by equation (5.13) in Table 11.2.2.3.1a.

The additional redundant reactions, X_0 and X_4 , of the heavy floor beams are computed by equation (5.24). With $\beta = 3.01$ and $\bar{v}_{00} = \bar{v}_{44} = 0.264$ (from Chart 19, with $\gamma = 3.2$)

$$\frac{X_0}{P} = \frac{\bar{F}_{0P}}{P} \left(\frac{1}{0.264 + 1/(3.01 - 1)} \right) = 1.313 \frac{\bar{F}_{0P}}{P}$$

Similarly

$$\frac{X_4}{P} = 1.313 \frac{\bar{F}_{4P}}{P}$$

The expression $Q_{0sa}(Q_{1x}/Q_0)$ in equation (5.28) is computed with the values used in Section 11.2.2.2.1.

The computation of the bending moment increments $\bar{\Delta}M_{RC}$ by equation (5.28) is shown in Table 11.2.2.3.1b.

Another method of obtaining the values of \bar{F}_{0P}/P and \bar{F}_{4P}/P is shown in Section 11.2.3.3.

(b) *Negative moment increment*

Over the heavy floor beams, $m = 0, 4 \dots$ etc., the negative bending moments in the ribs are larger than those in a system with uniform floor beam rigidity.

The bending moment increment, $\bar{\Delta}M_{RS}$, over the heavy floor beams is obtained for loading case **d** in a similar manner as the positive moment increment, $\bar{\Delta}M_{RC}$, and is equal to

$$\bar{\Delta}M_{RS} = -1.83 \text{ k-ft}$$

Thus, the total negative bending moment per rib over the heavy floor beams near the midspan of floor beams is (see Sections 11.2.2.1.3 and 11.2.2.2.1)

$$M_{RS} = -6.66 + 2.30 - 1.83 = -6.19 \text{ k-ft}$$

It is seen that this moment is smaller than the negative moment $M_{RS} = -6.66$ k-ft in the ribs near the main girders.

11.2.2.3.2 Adjustment of the Live Load Bending Moments in Floor Beams

(a) *Moment increase in heavy floor beams*

The bending moment increment in the heavy floor beam, $m = 0$ is computed for loading cases **A** and **B**, three lanes loaded, by equation (5.29) with equations (5.24) and (5.13). The effect of the adjoining heavy floor beams, $m = 4$ and $4'$ (see sketch, Table 11.2.2.3.2a), are small and may be disregarded.

The values of \bar{F}_0/P are computed in Table 11.2.2.2.2. The computation of the bending moment increment $\bar{\Delta}M_{P0}$ is shown in Table 11.2.2.3.2b.

It is seen that loading **B** is critical.

(b) *Moment reduction in intermediate floor beams*

The bending moment reduction in floor beam $m = 2$ is computed by equation (5.30) with equations (5.24) and (5.13). The effect of both heavy floor beams, $m = 0$ and $m = 4$, is considered.

TABLE 11.2.2.3.1b

MOMENT INCREMENTS $\bar{\Delta}M_{RC}$ AT MIDSPAN OF RIB PANEL 1-2 DUE TO HEAVY FLOOR BEAMS

(1)	(2)	(3)	(4)	(5)	(6)	(7)	(8)
Loading	Due to Heavy Floor Beam No.	$\frac{F}{P}$	$\frac{X}{P}$	$Q_{0sa} \frac{Q_{1x}}{Q_0}$	$\frac{\bar{\eta}_{cm}}{s}$	$\bar{\Delta}M_{RC} = -(4)(5)(6)$	Total $\bar{\Delta}M_{RC}$
Reference		Table 11.2.2.3.1a	Eq. 5.24	Section 11.2.2.2.1	Chart 17	Eq. 5.28	
Case a	0	0.168	0.221	6.29	+0.004	-0.006	+0.06 k-ft/rib
	4	0.085	0.112	6.29	-0.088	+0.062	
Case a₁ †	0	0.188	0.247	6.29	+0.004	-0.006	+0.30
	4	0.427	0.561	6.29	-0.088	+0.311	
Case h	0	0.168	0.221	8.39	+0.004	-0.007	+0.08
	4	0.085	0.112	8.39	-0.088	+0.083	

† Without front axle.

TABLE 11.2.2.3.2a
EFFECT OF HEAVY FLOOR BEAMS. COMPUTATION OF \bar{F}_0/P AND \bar{F}_4/P FOR LOADING SHOWN

Support, m	2'	1'	0	1	2	3	4	5	6	\bar{F}_0/P and \bar{F}_4/P (Eq. 5.13)
$\bar{\delta}_{0m}$	+0.125	+0.212	+0.264	+0.212	+0.125	+0.052	+0.010	-0.009	-0.013	
$\bar{\delta}_{4m}$	-0.013	-0.009	+0.010	+0.052	+0.125	+0.212	+0.264	+0.212	+0.125	
\bar{F}_m/P	-0.026	+0.112	+0.188	-0.045	+1.046	-0.140	+0.741	+0.453	-0.105	
$(\bar{F}_m/P) \bar{\delta}_{0m}$	-0.003	+0.024	+0.050	-0.010	+0.131	-0.007	+0.007	-0.004	+0.001	+0.189
$(\bar{F}_m/P) \bar{\delta}_{4m}$	0	-0.001	+0.002	-0.002	+0.131	-0.030	+0.196	+0.096	-0.013	+0.379

The computation is made for both cases **A** and **B**. The results are shown for case **B** only, three lanes loaded, in Tables 11.2.2.3.2a and b.

The bending moment relief in the intermediate floor beams $m = 1$ and 3 , next to the heavy floor beams is larger than in floor beams $m = 2$. Thus, proportioning floor beams $m = 1$ and 3 for the bending moments in floor beam $m = 2$ is conservative.

11.2.2.3.3 Adjustment of the Dead Load Moments Due to Superimposed Loads

Similarly as the live load, the superimposed dead load may be represented by its first Fourier component load (see Section 5.3.1).

The first Fourier component load, Q_{1x} , for a uniformly distributed dead load is obtained from equation (3.22) by setting $n = 1$, $b = l$ and $g = l/2$

$$Q_{1x} = \frac{4Q_0}{\pi} \sin \frac{\pi x}{l}$$

In the above equation Q_0 designates the uniformly distributed dead load per unit width of the deck. With the value of $Q_0 = 0.147$ k/ft (see Section 11.2.2.1.5),

$$Q_{1x} = \frac{(4)(0.147)}{\pi} \sin \frac{\pi x}{l} = 0.187 \sin \frac{\pi x}{l}$$

To this must be added the first Fourier component load due to the additional weight of the 4-ft wide center mall, which is $0.352 - 0.147 = 0.205$ k/ft (see Section 11.2.2.1.5). From equation (3.22), with

$Q_0 = 0.205$ k/ft, $l = 50$ ft and $2g =$ width of mall $= 4$ ft,

$$Q_{1x} = \frac{(4)(0.205)}{\pi} \sin \frac{2\pi}{50} \sin \frac{\pi x}{l} = 0.033 \sin \frac{\pi x}{l}$$

Thus, for the entire superimposed dead load, consisting of the wearing surface and the center mall, the value of the first Fourier component load is

$$Q_{1x} = (0.187 + 0.033) \sin \frac{\pi x}{l} = 0.220 \sin \frac{\pi x}{l} \quad (\text{k/ft})$$

Since the above load is applied to each floor beam, the reactions, \bar{F} , of the elastic floor beams of uniform

TABLE 11.2.2.3.2b
EFFECT OF HEAVY FLOOR BEAMS. BENDING MOMENT CHANGES IN FLOOR BEAMS $m = 0$ AND 2

(1)	(2)	(3)	(4)	(5)	(6)	(7)	(8)	(9)	(10)
	Loading Case	Effect of Floor Beam No.	$\frac{\bar{F}_0}{P}$ or $\frac{\bar{F}_4}{P}$	$\frac{X_0}{P}$	$Q_0 \frac{Q_{1x}}{Q_0} \left(\frac{l}{\pi}\right)^2$	$1 - \bar{\delta}_{00}$ or $1 - \bar{\delta}_{44}$	$\bar{\delta}_{m0}$ or $\bar{\delta}_{m4}$	$\bar{\Delta}M =$ (5) (6) (7) or -(5) (6) (8)	$0.90 \sum \bar{\Delta}M$ (k-ft)
Reference			Table 11.2.2.2.2 11.2.2.3.2a	Eq. (5.24)		Chart 19	Chart 19	Eq. (5.29) or (5.30)	AASHTO Sect. 1.2.9
Floor Beam m	A	0	0.264	0.347	840	0.736		+214	+193
	B	0	0.381	0.500	840	0.736		+309	+278
0	B	0	0.189	0.248	840		0.125	-26	-70
		4	0.379	0.498	840		0.125	-52	

rigidity are equal to the load, or, designating the total load per floor beam as P ,

$$\frac{F_m}{P} = 1$$

The ratio of the redundant additional reaction at the heavy floor beam to the load per floor beam, X_0/P , is computed by equation (5.24) with the coefficient computed in Section 11.2.2.3.1a, as

$$\frac{X_0}{P} = (1)(1.313)$$

The additional bending moment at the midspan of the heavy floor beams, $x = l/2$, due to the superimposed dead load is computed by equation (5.29), with $\bar{v}_{00} = 0.264$, as

$$\Delta M_{F_0} = (0.220) \left(\frac{50}{\pi} \right)^2 (1.313)(1 - 0.264) = 54 \text{ k-ft}$$

The bending moment relief at the midspan of the intermediate floor beams, $m = 2$, due to the superimposed dead load, is computed by equation (5.30), with the value of $\bar{v}_{20} = 0.125$ obtained from Chart 19, as

$$\Delta M_{F_2} = 0.220 \left(\frac{50}{\pi} \right)^2 (1.313)(0.125)(2) = 18 \text{ k-ft}$$

The factor of 2 in the above equation is due to the superposition of the effects of the two heavy floor beams, $m = 0$ and $m = 4$, between which the intermediate floor beam $m = 2$ is located.

The bending moment increment in the ribs over the heavy floor beams due to the superimposed dead load is disregarded.

11.2.2.4 Summary of Moments and Stresses

11.2.2.4.1 Ribs

The comparison of the bending moments at the midspan of ribs due to loading cases **a** and **a₁** (Fig. 11.4a) in the critical lane and loading **h** in the adjoining lane (Fig. 11.6) is given below:

Case	Bending Moments (k-ft)		
	Loading a + h	Loading a₁ + h	Section
1. Rigid system	8.46	8.66	11.2.2.1.2
2. Effects of floor beam flexibility	4.61	3.94	11.2.2.2.1
3. Effects of heavy floor beams	0.14	0.38	11.2.2.3.1
Total L.L. Moment	13.21	12.98	

It is seen that loading case **a + h** is critical.

A summary of the maximum moments and stresses in the ribs is given in Table 11.2.2.4.1.

TABLE 11.2.2.4.1
MAXIMUM BENDING MOMENTS AND STRESSES IN RIBS

Location		Loading	Bending Moment (k-ft)	Section Modulus (in. ³)		Stress (ksi)	
				Top	Bottom	Top	Bottom
Point A (Fig. 11.1)	(1)	L.L., rigid system	8.46	34.9	10.8	-2.9	9.4
	(2)	L.L., effect of floor beam flexibility	4.61				
	(3)	L.L., effect of heavy floor beams	0.14				
	(4)	D.L., erection	0.82				
	(5)	D.L., superimposed	0.04				
	(6)	Total, lines (2) to (5)	5.61	31.5	10.7	-2.1	6.3
	(7)	Total, System II stress				-5.0	15.7
	(8)	Max. System I stress				12.5	11.3
	(9)	Total stress				7.5	27.0
Point B (Fig. 11.1)	(10)	L.L., rigid system	-6.66	34.9	10.8	2.3	-7.4
	(11)	D.L., erection	-1.64				
	(12)	D.L., superimposed	-0.07				
	(13)	Total, lines (11) and (12)	-1.71	31.5	10.7	0.6	-1.9
	(14)	Total, System II stress				2.9	-9.3
	(15)	Max. System I stress				-11.2	-9.5
	(16)	Total stress				-8.3	-18.8

TABLE 11.2.2.4.2
MAXIMUM BENDING MOMENTS AND STRESSES IN FLOOR BEAMS

Loading	Intermediate Floor Beams Fig. 11.3c			Heavy Floor Beams Fig. 11.3d			
	Moment (k-ft)	Stress (ksi)		Moment (k-ft)	Stress (ksi)		
		Top	Bottom		Top Pt. ①	Pt. ②	Bottom Pt. ③
D.L., erection				274		-12.3	12.3
D.L., superimposed, rigid floor beams	43			43	-0.9	0.2	1.9
D.L., superimposed, effect of floor beam flexibility	-18			54			
Total D.L. effect	25	-0.3	1.1	371	-0.9	-12.1	14.2
L.L., rigid floor beams	810			810			
L.L., effect of flexibility, uniform floor beams	-503			-503			
L.L., effect of heavy floor beams	-70			278			
Total L.L. effect	237	-3.1	10.3	585	-5.1	1.4	11.5
Total	262	-3.4	11.4	956	-6.0	-10.7	25.7

11.2.2.4.2 Floor Beams

Comparison of the bending moments due to loadings **A** and **B** (Fig. 11.5a) indicates that the maximum total live load moments in floor beams are obtained with loading **B**, three lanes loaded.

A summary of the maximum moments and stresses in the floor beams is given in Table 11.2.2.4.2.

In the computation of the stresses, section moduli of the floor beams computed in Section 11.2.1.3.2 are used.

11.2.3 Design by Charts for AASHO Loads

The section properties and the relative rigidity coefficients are computed as shown in Section 11.2.1.

11.2.3.1 Bending Moments in a System with Rigid Floor Beams

11.2.3.1.1 Live Load Moments in Ribs

The loading and the load positions used are given in Section 11.2.2.1.1a.

(a) Moment at midspan

From Chart 6, for $s = 5.86$ ft, the total moment is obtained as

for loading **a**, $M_c = 13.7$ k-ft
for loading **a**₁, $M_c = 14.1$ k-ft

The moment per rib is computed with the coefficient $R_0/P = 0.615$, obtained from Chart 3a for the 12-kip wheel, as

for loading **a**, $M_{RC} = 0.615 (13.7) = 8.4$ k-ft
for loading **a**₁, $M_{RC} = 0.615 (14.1) = 8.7$ k-ft

(b) Moment at support

The moment at support is obtained for loading **d** from Charts 7 and 3a as

$$M_{RS} = (0.615) (-10.9) = -6.7 \text{ k-ft}$$

11.2.3.1.2 Live Load Moment in Floor Beams

The loading used is given in Section 11.2.2.1.1b. From Chart 15, the reaction of one loaded lane on a floor beam is

	Loading A	Loading B
$\frac{F_0}{P}$	1.00	1.05

From Chart 16 the moment coefficient is obtained for $l = 50$ ft, lane width of 13 ft, 3 lanes loaded, as

$$\frac{M}{F_0 l} = 0.378$$

The maximum bending moments are then computed as follows:

$$M = Pl \left(\frac{F_0}{P} \right) \left(\frac{M}{F_0 l} \right)$$

$= (41.1)(50)(1.0)(0.378) = 775$ k-ft (loading **A**)
 $= (41.1)(50)(1.05)(0.378) = 815$ k-ft (loading **B**)

11.2.3.1.3 Dead Load Moments

Computation of the dead load moments is shown in Section 11.2.2.1.5.

11.2.3.2 Effects of Floor Beam Flexibility, All Floor Beams Uniform

11.2.3.2.1 Additional Bending Moments in Ribs

(a) Positive moment increment

The loadings and their positions are shown in Figures 11.4a and 11.6.

From Charts 20 and 23, for $\gamma = 3.2$, as computed in Section 11.2.1.4.1, and $s = 5.86$ ft.

	Loading a	Loading a₁	Loading h
$\sum \frac{F}{P} \frac{\bar{\eta}_c}{s} =$	0.315	0.210	0.315

From Chart 28, for the "critical" lane loaded, for $l = 50$ ft and $2g = 22$ in., on a four-lane bridge,

$$\frac{Q_{1r}}{Q_0} = 0.126$$

From Chart 29, for one adjoining lane loaded, for $l = 50$ ft

$$\frac{Q_{1z}}{Q_0} = 0.148$$

The values of $Q_0 = P/2g$ are 0.709 k/in. and 0.800 k/in., for the 12-kip and the 16-kip wheel, respectively, as computed in Section 11.2.2.2.1.

With the above values, the additional bending moments per rib, ΔM_{RC} , are computed by equation (5.9) as follows

Loading **a** in critical lane,

$$\Delta M_{RC} = (0.709)(5.86)(12)(0.126)(0.315) = 2.0 \text{ k-ft}$$

Loading **a₁** in critical lane, the 4-kip front wheel not included,

$$\Delta M_{RC} = (0.709)(5.86)(12)(0.126)(0.210) = 1.3 \text{ k-ft}$$

Loading **h** in adjoining lane,

$$\Delta M_{RC} = (0.800)(5.86)(12)(0.148)(0.315) = 2.6 \text{ k-ft}$$

The total bending moment increments per rib are obtained by equation (5.10) as follows:

Loadings **a + h**,

$$\Delta M_{RC} = 2.0 + 2.6 = 4.6 \text{ k-ft}$$

Loadings **a₁ + h**,

$$\Delta M_{RC} = 1.3 + 2.6 = 3.9 \text{ k-ft}$$

(b) Negative moment reduction

The reduction of the negative bending moment, ΔM_{RS} , over the floor beams at the midspan of the floor beams is computed for loading **d** (see Section 11.2.2.2.1 for comments).

From Chart 24, for $\gamma = 3.2$ and $s = 5.86$ ft.,

$$\sum \frac{F}{P} \frac{\bar{\eta}_s}{s} = 0.54$$

With the values of

$$Q_0 = \frac{P}{2g} = \frac{8(1.3)}{22} = 0.473 \text{ k/in.}$$

and $Q_{1r}/Q_0 = 0.126$, as computed in Section 11.2.3.2.1a,

the negative moment reduction is obtained from equation (5.9) as

$$\Delta M_{RS} = (0.473)(5.86)(12)(0.126)(0.54) = 2.3 \text{ k-ft}$$

11.2.3.2.2 Bending Moment Relief in Floor Beams

From Chart 30, for $\gamma = 3.2$, $s = 5.86$, loading **B**,

$$\frac{F_0}{P} - \sum \frac{F_m}{P} \bar{\vartheta}_{0m} = 0.66$$

and from Chart 32, for three lanes loaded, with $l = 50$ ft and the lane width of 13 ft

$$\frac{Q_{1r}}{Q_0} = 0.314$$

With the value of $Q_0 = 9.5$ k/ft, as computed in Section 11.2.2.2.2, the bending moment relief is computed by equation (5.14) as

$$\Delta M_F = 9.5 \left(\frac{50}{\pi} \right)^2 (0.314)(0.66) = 499 \text{ k-ft}$$

11.2.3.3 Effects of Heavy Floor Beams

11.2.3.3.1 Change of the Bending Moments in Ribs

The bending moment increment $\bar{\Delta} M_{RC}$ at the midspan of the deck panels 1-2 or 2-3 (see sketch, Table 11.2.2.3.1) is computed by equation (5.28), similarly as in Section 11.2.2.3.1.

The reactions \bar{F}_0 and \bar{F}_4 of a beam on elastic supports with all supports of uniform rigidity may be obtained from influence lines $\bar{\vartheta}_0 = F_0/P$ and $\bar{\vartheta}_4 = F_4/P$, Figure 11.7. These influence lines are obtained by connecting with a smooth curve the ordinates $\bar{\vartheta}_0$ from Chart 19, for $\gamma = 3.2$.

For the critical loading case **a₁**, without the front 4-kip wheels, with the 12-kip wheel designated as **P** (see Table 11.2.2.3.1a), the following values are obtained from influence lines, Figure 11.7.

$$\bar{F}_0/P = 0.19 \quad \bar{F}_4/P = 0.43$$

Similarly, for loading **h** in the adjoining lane

$$\bar{F}_0/P = 0.17 \quad \bar{F}_4/P = 0.086$$

With the above values the bending moment increments, $\bar{\Delta}M_{RC}$, are obtained as shown in Section 11.2.2.3.1.

The results are:

Due to loading **a**₁, $\bar{\Delta}M_{RC} = +0.31$ k-ft/rib

Due to loading **h**, $\bar{\Delta}M_{RC} = +0.08$ k-ft/rib

11.2.3.3.2 Adjustment of the Bending Moments in Floor Beams

The bending moment corrections $\bar{\Delta}M_F$ are computed, with the values of \bar{F}_0/P and \bar{F}_4/P determined from Figure 11.7, in accordance with the procedure given in Sections 11.2.2.3.2 and 3.

11.2.3.4 Summary of Moments and Stresses

The summaries of the moments obtained by means of charts are similar to those given in Sections 11.2.4.1.2.

11.3 DECK WITH CLOSED RIBS

11.3.1 General

11.3.1.1 Dimensions and Details

The general layout of the deck is shown in Figure 11.8. The bridge cross section with typical details is shown in Figure 11.9. The ribs are spaced at 2 ft-0 in. o.c., except for the ribs adjoining the main girders, where closer spacing is used.

The 9½ in. deep trapezoidal ribs are designed to be air-tight after erection, to preclude corrosion of the

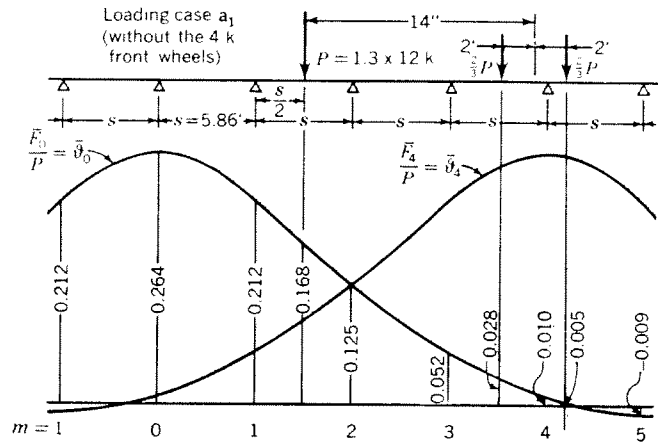


Fig. 11.7. Influence lines for reactions \bar{F}_0 and \bar{F}_4 of a beam on elastic supports, with all supports of uniform rigidity. $\gamma = 3.2$

inside of the ribs. This justifies the use of a ¼ in. thick plate for the ribs, which is common practice in the decks with closed ribs.

The deck plate thickness of ⅜ in. is determined by considerations similar to those in Section 11.2.1.2.

The floor beams, spaced 15 ft-0 in. o.c. are all of the same type. The lower portions of the floor beams serve, in this design, as erection supports for the deck panels.

All material is low-alloy structural steel.

11.3.1.2 Section Properties

11.3.1.2.1 Longitudinal Ribs

The section properties are computed with the effective widths of deck plate given in Lines 3 and 5, respectively, Table 3.3.2.2.

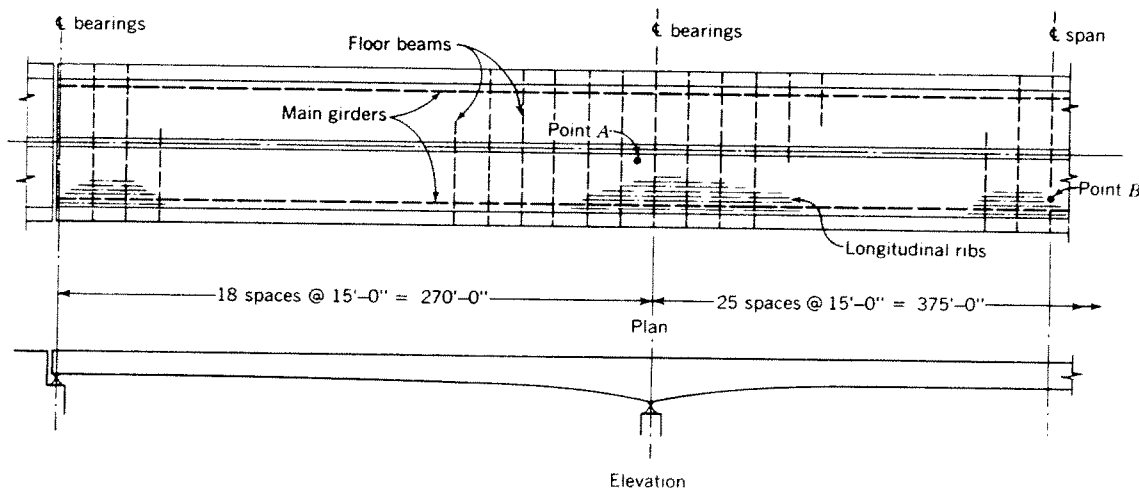


Fig. 11.8. Deck with closed ribs — general layout

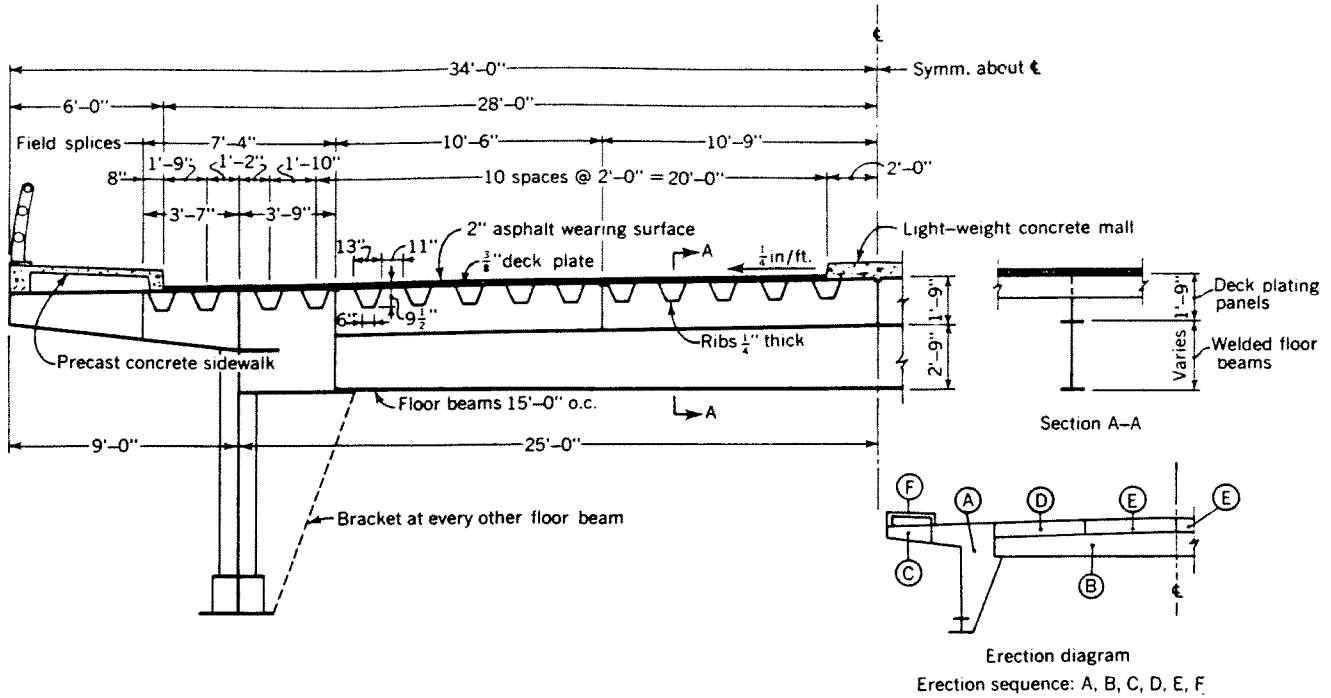


Fig. 11.9. Deck with closed ribs — typical cross section

(a) Values of I_R and S_R used in the computation of the moments and stresses in the ribs on rigid supports

In accordance with Line 3, Table 3.3.2.2,

$$s_1 = 0.7s = (0.7)(180) = 126 \text{ in.}$$

$$\frac{a}{s_1} = \frac{13}{126} = 0.103 \quad \frac{e}{s_1} = \frac{11}{126} = 0.087$$

With the above values, the effective width ratios are obtained from Chart 1 as

$$\frac{a_0}{a} = 1.07 \quad \frac{e_0}{e} = 1.08$$

The effective width of deck plate acting with one rib is then computed by equation (3.6) as

$$a_0 + e_0 = (1.07)(13) + (1.08)(11) = 25.8 \text{ in.}$$

The section properties of the rib (Fig. 11.10a) are:

$$I_R = 197 \text{ in.}^4 \quad S_{RT} = 76.9 \text{ in.}^3 \quad S_{RB} = 26.9 \text{ in.}^3$$

(b) Values of I_R and S_R for computation of the effects of floor beam flexibility

In accordance with Line 5, Table 3.3.2.2,

$$a_0 + e_0 = 1.1(a + e) = (1.1)(13 + 11) = 26.4 \text{ in.}$$

The section properties (Fig. 11.10b) are:

$$I_R = 198 \text{ in.}^4 \quad S_{RT} = 78.5 \text{ in.}^3 \quad S_{RB} = 26.9 \text{ in.}^3$$

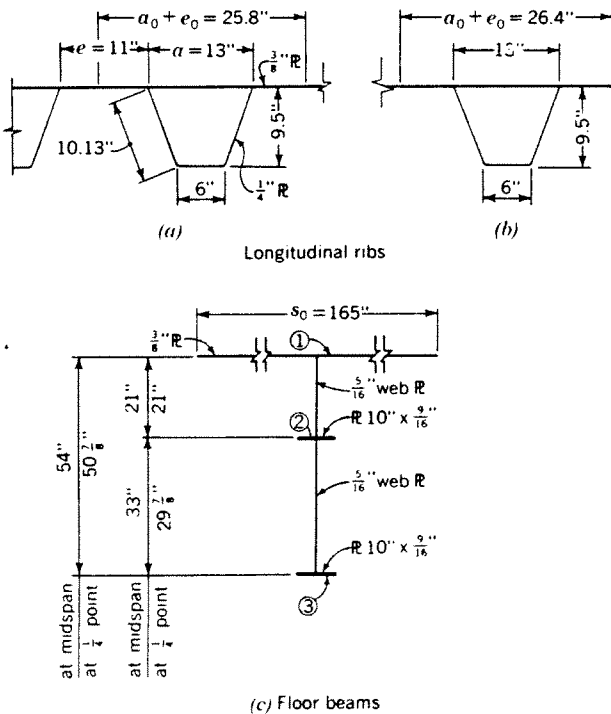


Fig. 11.10. Cross sections of structural elements of the deck with closed ribs

(c) *Torsional rigidity*

The value of GK is computed by equation (3.14) as

$$GK = G \frac{4A^2}{(u/t_R) + (a/t_P)}$$

$$= 11.2 \times 10^3 \left[\frac{4 \left[\left(\frac{13+6}{2} \right) (9.5) \right]^2}{\frac{6+2(10.13)}{0.25} + \frac{13}{0.375}} \right]$$

$$= 2.62 \times 10^6 \text{ k-in.}^2$$

Further, the following coefficients are computed in accordance with formulas given in Section 3.3.3.2:

$$EI_P = 29 \times 10^3 \frac{(0.375)^2}{10.92} = 140 \text{ k-in.}^2/\text{in.}$$

$$\rho = \left(\frac{0.25}{0.375} \right)^3 = 0.296$$

$$s_2 = (0.81)(180) = 145.8 \text{ in.}$$

From equation (3.15a)

$$\lambda = \frac{[2(13+6)(13+11)(6)(10.13) - (0.296)(13)^3(11-6)]}{(13+6)[2(10.13) \times [13^2 + (13)(6) + 6^2] + 6^3 + (0.296)(13)^3]} = 0.347$$

$$c_1 = \frac{0.347}{2} \left(\frac{6}{13} \right) = 0.0801$$

$$c_2 = \frac{0.347}{2} \left(\frac{13-6}{13} \right) - \left(\frac{13+11}{13+6} \right) \left(\frac{6}{2(13)} \right) = -0.1980$$

From equation (3.15)

$$\frac{1}{\mu} = 1 + \frac{2.62 \times 10^6}{140} \left(\frac{13^3}{12(13+11)^2} \right) \left(\frac{\pi}{145.8} \right)^2 \times$$

$$\left[\left(\frac{11}{13} \right)^3 + \left(\frac{11-6}{13+6} + 0.347 \right)^2 + \frac{(0.347)^2 \left(\frac{6}{13} \right)^3}{0.296} + \frac{24}{0.296} \left(\frac{10.13}{13} \right) \left(0.0801^2 - (0.0801)(0.1980) + \frac{0.1980^2}{3} \right) \right]$$

$$= 4.44$$

The effective torsional rigidity, H , of the deck is computed by equation (3.13) as

$$H = \frac{2.62 \times 10^6}{2(4.44)(24)} = 12,280 \text{ k-in.}^2/\text{in.}$$

11.3.1.2.2 **Floor Beams**

In accordance with Line 6, Table 3.3.2.2,

$$s^* = s = 180 \text{ in.} \quad \frac{s^*}{l} = \frac{180}{600} = 0.30$$

The effective width of deck plate acting with one floor beam is obtained from Chart 1 as

$$s_0 = (0.915)(180) = 165 \text{ in.}$$

With this width of plate as the top flange (Fig. 11.10c), the following section properties are computed:

At midspan:

$$I_F = 26,040 \text{ in.}^4,$$

$$S_{F1} = 2660 \text{ in.}^3 \quad S_{F2} = 2320 \text{ in.}^3 \quad S_{F3} = 589 \text{ in.}^3$$

At quarter-points:

$$I_F = 22,770 \text{ in.}^4$$

Average value:

$$I_F = \frac{26,040 + 22,770}{2} = 24,405 \text{ in.}^4$$

For the lower portion of the floor beam, carrying the erection dead load, the section properties at the midspan are obtained as:

$$I_F = 3800 \text{ in.}^4 \quad S_{FT} = S_{FB} = 230 \text{ in.}^3$$

11.3.1.3 **Relative Rigidity Coefficients**

11.3.1.3.1 **Ratio H/D_y**

The deck rigidity in the longitudinal direction, D_y , is computed by equation (3.7) as

$$D_y = \frac{(29 \times 10^3)(197)}{13+11} = 238,000 \text{ k-in.}^2/\text{in.}$$

and the relative rigidity ratio, H/D_y , is

$$\frac{H}{D_y} = \frac{12,280}{238,000} = 0.051$$

11.3.1.3.2 **Relative Rigidity Coefficient**

The relative rigidity coefficient is computed with the average value of the moment of inertia of the floor beams by equation (5.7a) as

$$\gamma = \frac{(600)^4(198)}{(13+11)(180)^3(\pi)^4(24,405)} = 0.077$$

11.3.2 Design by General Formulas

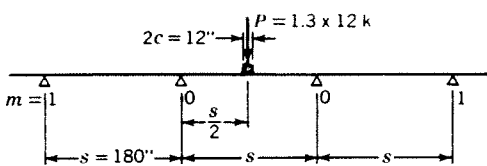
11.3.2.1 Bending Moments in a System with Rigid Floor Beams

11.3.2.1.1 Loading

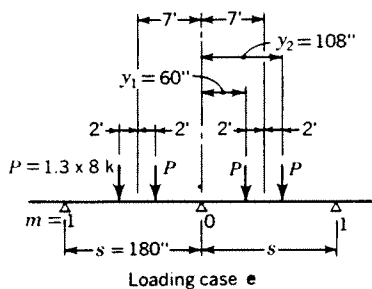
(a) Ribs

In the design of the ribs the 12-kip and 8-kip wheel loads are used (see Section 3.4.2.1).

The load positions are shown in Figure 11.11. In the computation of the bending moment at the midspan loading **a** rather than loading **a**₁ (Fig. 11.4a) is used, since, in this case, the total bending moment, obtained by superposition of the moment in the rigid system and the effects of floor beam flexibility is greater for loading **a**, as determined by preliminary computations.



(a) Loading for maximum moment at support of ribs



(b) Loading for maximum moment at midspan of ribs

Fig. 11.11. Loadings used in the design of the closed ribs in a system with rigid floor beams

In the system with rigid floor beams the additional wheels 6 ft and 4 ft away in the transverse direction of the bridge would cause an increase of the bending moments by approximately 1% and 3.5%, respectively (see Table 4.3.6.2). Considering that the values of the bending moments computed by formulas given in this Manual for the relatively long rib spans of 15 ft are conservative (see Section 4.3.6.2), the effect of the wheels located on the adjacent ribs on the bending moments in a system with rigid floor beams is disregarded in this computation.

A 30% impact factor is used.

The values of Q_0 are:

For 8-kip wheel load

$$Q_0 = \frac{P}{2g} = \frac{8 \times 1.3}{22} = 0.473 \text{ k/in.}$$

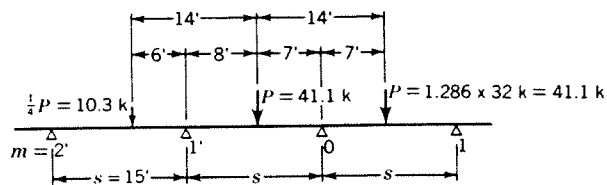
For 12-kip wheel load

$$Q_0 = \frac{12 \times 1.3}{22} = 0.709 \text{ k/in.}$$

(b) Floor beams

The critical loading case (one or three truck axles) and the number of lanes loaded producing the maximum moment in the floor beams is determined by inspection of Charts 5c and 19 and preliminary computations using appropriate values of the Q_{1x}/Q_0 coefficients, with consideration of the AASHO load intensity reduction for multiple lane loading. It is found that loading case **B** (3 truck axles), 3 lanes loaded, governs the design.

The critical position of the axles, determined by inspection of influence line, Chart 5c, is shown in Figure 11.12.



Loading case B

Fig. 11.12. Loading used in the design of the floor beams

The position of trucks in the transverse direction of the bridge is the same as used in the design of the deck with open ribs, Figure 11.5b.

The impact factor is 1.286, as determined in Section 11.2.2.1.1.

11.3.2.1.2 Choice of the Substitute Span, b , in the x -Direction

As discussed in Section 10.3.3.1.2, a reduced rather than the full deck width is used in the computations.

In accordance with the criteria given in Section 10.3.3.1.2, the value of b is chosen as 154 in., or $14g$. This results in 7 terms in each half-wave of the bending moment computation (see Fig. 10.3).

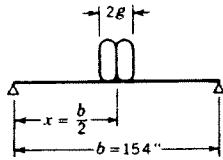
11.3.2.1.3 Fourier Analysis of Loading

In this example the bending moments are computed by equation (4.35) at the midspan ($x = b/2$) of the substitute span, b (Fig. 3.15). For this purpose the values

of the sinusoidal component loads, Q_{nx} , are needed at $x = b/2$.

The computation of the values Q_{nx}/Q_0 by equation (3.23) is shown in Table 11.3.2.1.3.

TABLE 11.3.2.1.3
COMPUTATION OF THE FOURIER COEFFICIENTS
 Q_{nx}/Q_0 AT THE LOCATION $x = b/2$



(1) <i>n</i>	(2) $n\pi g/b$	(3) $\sin(n\pi g/b)$	(4) Q_{nx}/Q_0
1	0.22440	+0.22252	+0.28332
3	0.67320	+0.62349	+0.26462
5	1.12200	+0.90097	+0.22943
7	1.57080	+1.00000	+0.18189
9	2.01960	+0.90097	+0.12746
11	2.46839	+0.62349	+0.07217
13	2.91719	+0.22252	+0.02179
15		-0.22252	-0.01889
17		-0.62349	-0.04670
19		-0.90097	-0.06038
21		-1.00000	-0.06063
23		-0.90097	-0.04988
25		-0.62349	-0.03175
27		-0.22252	-0.01049
29		+0.22252	+0.00977
31		+0.62349	+0.02561
33		+0.90097	+0.03476
35		+1.00000	+0.03638

11.3.2.1.4 Computation of Constants

The constant α_n is computed by equation (4.23) as

$$\alpha_n = \frac{n\pi}{154} \sqrt{2(0.051)} = 0.00651n$$

The values of hyperbolic functions and constants needed in the computation of the positive and the negative moments in the ribs are computed in accordance with Section 10.3.3.1.4, as shown in Tables 11.3.2.1.4a and b.

Dimensions and load ordinates used in the computations are shown in Figure 11.11.

Tables 11.3.2.1.4a and b are filled only as needed in the computations of the bending moments in Sections 11.3.2.1.5 and 6.

11.3.2.1.5 Live Load Moment at Midspan of Ribs

The bending moment M_C at the midspan of ribs is computed for a single wheel load, $P = 1.3$ kip, Figure 11.11 (see Section 11.3.2.1.1).

Hyperbolic functions and constants computed in Table 11.3.2.1.4a are used.

The moment M_C is computed by equation (4.46) as shown in Table 11.3.2.1.5. The evaluation of the series $\sum(Q_{nx}/Q_0)(M_{Cn}/Q_s)$ is done by multiplying the values of Q_{nx}/Q_0 (Table 11.3.2.1.3) by M_{Cn}/Q_s computed by equations (4.47) or (4.56) and (4.57) for each value of n , and summing up the terms. The summation is stopped after the middle term, $n = 35$, of the third half-wave, as discussed in Section 10.3.3.1.2 and illustrated graphically in Figure 10.3.

The result of the summation is, as computed in Table 11.3.2.1.5,

$$\sum_{n=1}^{35} \frac{Q_{nx}}{Q_0} \left(\frac{M_{Cn}}{Q_s} \right) = 0.10199$$

The bending moment per inch width of deck at the location of the centerline of the critical rib is, by equation (4.46),

$$M_C = (0.709)(180)(0.10199) = 13.02 \text{ k-in./in.}$$

The bending moment per rib is obtained by equation (4.35a) as

$$M_{RC} = (13.02)(13 + 11) = 312 \text{ k-in./rib}$$

11.3.2.1.6 Live Load Moment at Support of Ribs

The loading used in the computation of the bending moment M_S at the support of ribs is shown in Figure 11.11 (see Section 11.3.2.1.1).

Hyperbolic functions and constants used in the computation are given in Table 11.3.2.1.4b.

The moments M_S are computed in Table 11.3.2.1.6 separately for the loads, P , located at $y_1 = 60$ in. and $y_2 = 108$ in., in panel 0-1 (Fig. 11.11b). Equations (4.38) with (4.39) and (4.40) are used. For large values of α_s and α_y the shortcut formulas (4.51) and (4.52) are used as noted in Table 11.3.2.1.6.

The total bending moment at support is computed by equation (4.35) as

$$M_S = 2(0.473)(180)(-0.06343 - 0.04501) = -18.47 \text{ k-in./in.}$$

The factor 2 in the above equation is introduced because of the symmetrical loading in panel 0-1', not included in the computations in Table 11.3.2.1.6.

TABLE 11.3.2.1.4a
HYPERBOLIC FUNCTIONS AND CONSTANTS NEEDED IN COMPUTATION OF POSITIVE MOMENT IN RIBS

(1)	(5)	(6)	(7)	(8)	(9)	(10)	(11)	(12)	(13)	(14)	(15)	(16)	(17)	(18)
n	αs	$\sinh \alpha s$	$\cosh \alpha s$	$\coth \alpha s$	$\alpha \frac{s}{2}$	$\cosh \alpha \frac{s}{2}$	αc	$\sinh \alpha c$	$\alpha \left(\frac{s}{2} - c \right)$	$\frac{\cosh}{\alpha \left(\frac{s}{2} - c \right)}$	$e^{-\alpha c}$	α^* Note 1	k Note 2	κ Note 3
1	1.1727	1.46059	1.77012	1.21192	0.5864	1.17692	0.0391	0.03911	0.5473	1.15354		0.19711 ^(a)	2.1372 ^(a)	-0.2484 ^(a)
3	3.5182	16.84701	16.87666	1.00176	1.7591	2.98970	0.1173	0.11757	1.6418	2.67903		0.79117	3.1907	-0.1608
5	5.8637	176.01066	176.01350	1.00002	2.9318	9.40734	0.1955	0.19675	2.7364	7.74807		0.96669	5.0313	-0.1004
7	8.2092	1837.30	1837.30	1.00000	4.1046	30.3175	0.2736	0.27702	3.8309	23.0629		0.99553	7.2416 ^(b)	-0.0694
9	10.5547	19178.6	19178.6		5.2773	97.9227	0.3518	0.35910	4.9255	68.8827	0.70342	0.99945	9.5600	-0.0524
11	12.9001	200176.	200176.		6.4502	316.384	0.4300	0.44337			0.65051	0.99994	11.9008	-0.0421
13	15.2456				7.6228	1022.14	0.5082	0.53036			0.60158	1.00000 ^(b)	14.2456 ^(c)	-0.0351
15	17.5911				8.7955	3302.23	0.5864				0.55630		16.5911	-0.0301 ^(b)
17	19.9366						0.6645				0.51453		18.9366	-0.0264
19	22.2820						0.7427				0.47582		21.2820	-0.0235
21	24.6275						0.8209				0.44004		23.6275	-0.0212
23	26.9730						0.8991				0.40694		25.9730	-0.0193
25	29.3185						0.9773				0.37633		28.3185	-0.0177
27	31.6640						1.0555				0.34802		30.6640	-0.0163
29	34.0094						1.1336				0.32187		33.0094	-0.0151
31	36.3549						1.2118				0.29766		35.3549	-0.0141
33	38.7004						1.2900				0.27527		37.7004	-0.0133
35	41.0459						1.3682				0.25656		40.0459	-0.0125

NOTES:

- 1. (a) eq. (4.27) 2. (a) eq. (4.26) 3. (a) eq. (4.29)
- (b) eq. (4.48) for $n > 13$ (b) eq. (4.49) for $n > 5$ (b) eq. (4.50) for $n > 13$
- (c) eq. (4.49a) for $n > 11$

TABLE 11.3.2.1.4b
HYPERBOLIC FUNCTIONS AND CONSTANTS NEEDED IN COMPUTATION OF NEGATIVE MOMENTS IN RIBS

(1)	(19)	(20)	(21)	(22)	(23)	(24)	(25)	(26)	(27)	(28)	(29)	(30)	(31)	(32)	33	(34)
n	αy_1	$\sinh \alpha y_1$	$\cosh \alpha y_1$	$e^{-\alpha s}$	$\kappa - e^{-\alpha s}$	$e^{-\alpha y_1}$	$\alpha(s - y_1)$	$e^{-\alpha(s - y_1)}$	(23) (26)	αy_2	$\sinh \alpha y_2$	$\cosh \alpha y_2$	$e^{-\alpha s_2}$	$\alpha(s - y_2)$	$e^{-\alpha(s - y_2)}$	(23) (33)
1	0.3909	0.40093	1.07738							0.7036	0.76311	1.25791				
3	1.1727	1.46059	1.77012							2.1109	4.06727	4.18840				
5	1.9546	3.45974	3.60136	0.0028	-0.1032 ^(a)					3.5182	16.84701	16.87666	0.02965	2.3455	0.09580	-0.00989
7	2.7364	7.68481	7.74961	0.0008	-0.0697	0.06482	5.4728	0.00420	-0.00029	4.9255	68.87546	68.88272	0.00726	3.2837	0.03749	-0.00261
9	3.5182	16.84701	16.87666	0.00003	-0.0524	0.02965	7.0365	0.00088	-0.00005	6.3328			0.00178	4.2219	0.01467	-0.00077
11	4.3001			0	-0.0421	0.01357	8.6001	0.00018	-0.00001	7.7401			0.00044	5.1601	0.00574	-0.00024
13	5.0819			0	-0.0351	0.00621	10.1638	0.00004	0	9.1474			0.00011	6.0983	0.00225	-0.00008
15	5.8637			0	-0.0301	0.00284			0	10.5547			0.00003	7.0365	0.00088	-0.00003
17	6.6455			0	-0.0264	0.00130			0	11.9620			0.00001	7.9746	0.00034	-0.00001
19	7.4274			0	-0.0235	0.00059			0	13.3693			0	8.9128	0.00013	0
21	8.2092			0	-0.0212	0.00027			0				0			0
23	8.9910			0	-0.0193	0.00012			0				0			0
25	9.7729			0	-0.0177	0.00006			0				0			0
27	10.5547			0	-0.0163	0.00003			0				0			0
29	11.3365			0	-0.0151	0.00001			0				0			0
31	12.1183			0	-0.0141	0			0				0			0
33				0	-0.0133	0			0				0			0
35				0	-0.0125	0			0				0			0

NOTE: (a) Values of κ from column (18), Table 11.3.2.1.4a.

TABLE 11.3.2.1.5
COMPUTATION OF THE BENDING MOMENT M_c AT MIDSPAN OF RIBS

(1)	(35)	(36)	(37)	(38)	(39)	(40)
n	$\frac{M_0^*}{s}$ eq. (4.43)	$\frac{\cosh \alpha[(s/2) - c]}{\cosh(\alpha s/2)}$ Note 1	A Note 2	B Note 3	$M_{c_n}/Q_s = A + B$ eq. (4.47)	$(4) \times (39)$ eq. (4.46)
1	-0.42883	0.98013	0.21667	-0.06437	0.15230	+0.043150
3	-0.02928	0.89609	0.12590	-0.01946	0.10644	+0.028166
5	-0.00502	0.82362	0.07693	-0.00448	0.07245	+0.016622
7	-0.00108	0.76071	0.05327	-0.00104	0.05223	+0.009500
9	-0.00025	0.70344	0.03993	-0.00025	0.03968	+0.005058
11	-0.00006	0.65051	0.03150	-0.00006	0.03144	+0.002269
13	-0.00002	0.60158	0.02571	-0.00002	0.02569	+0.000560
15	0	0.55630	0.02151	0	0.02151	-0.000406
17	0	0.51453	0.01832	0	0.01832	-0.000856
19	0	0.47582	0.01584	0	0.01584	-0.000956
21	0	0.44004	0.01385	0	0.01385	-0.000840
23	0	0.40694	0.01223	0	0.01223	-0.000610
25	0	0.37633	0.01088	0	0.01088	-0.000345
27	0	0.34802	0.00975	0	0.00975	-0.000102
29	0	0.32187	0.00879	0	0.00879	+0.000086
31	0	0.27966	0.00797	0	0.00797	+0.000204
33	0	0.27527	0.00726	0	0.00726	+0.000252
35	0	0.25656	0.00662	0	0.00662	+0.000241
$\frac{M_c}{Q_0 s} = \sum_{n=1}^{35} \frac{Q_{nz}}{Q_0} \frac{M_{c_n}}{Q_s} =$					+0.101993	

NOTES: 1. For $n > 11$ $\frac{\cosh \alpha[(s/2) - c]}{\cosh(\alpha s/2)} = e^{-\alpha c}$, see eq. (4.56).

2. $A = \frac{1}{2\alpha s \alpha c} \left(1 - \frac{\cosh \alpha[(s/2) - c]}{\cosh(\alpha s/2)} \right)$; for $n > 11$ see eq. (4.56).

3. $B = \frac{M_0^*}{s} \left(1 - \frac{1}{\alpha c} \frac{\sinh \alpha c}{\cosh(\alpha s/2)} \right)$; for $n > 11$ see eq. (4.57).

The bending moment per rib is obtained by equation (4.35a) as

$$M_{RS} = (-18.47)(13 + 11) = -444 \text{ k-in./rib}$$

11.3.2.1.7 Live Load Moments in Floor Beams

The reaction of one truck on floor beam $m = 0$ (Fig. 11.12) is computed by equations (4.11) and (4.12) as

$$F_0 = 2 (41.1) \left[1 - 2.1962 \left(\frac{7}{15} \right)^2 + 1.1962 \left(\frac{7}{15} \right)^3 \right] + 10.3 \left[-0.8038 \left(\frac{6}{15} \right) + 1.3923 \left(\frac{6}{15} \right)^2 - 0.5885 \left(\frac{6}{15} \right)^3 \right]$$

= 51.6 kips per lane

The maximum design moment occurs under the wheel at $x = 29$ ft (Fig. 11.5b) and is, with consideration of the 10% reduction for three lanes loaded (AASHO specifications),

$$M_F = (0.90)(51.6) \left[\frac{18}{50} (29) + \frac{5}{50} (29) + \frac{18}{50} (21) \right] = 971 \text{ k-ft}$$

11.3.2.1.8 Dead Load Moments

The dead loads are as follows:

Ribs: steel weight	27 lbs per sq ft
wearing surface	25 lbs per sq ft
Total	52 lbs per sq ft
Floor beams: erection dead load	490 lbs per ft
superimposed dead load	375 lbs per ft
superimposed	
mall load at center	2090 lbs

TABLE 11.3.2.1.6
COMPUTATION OF THE BENDING MOMENT M_S AT SUPPORT OF RIBS

(1)	(41)	(42)	(43)	(44)	(45)	(46)	(47)	(48)	(49)	(50)	(51)	(52)	(53)	(54)	(55)
n	$\kappa^n \frac{M_0^*}{s}$	C_1	C_2	C_3	C_4	$y_1 = 60 \text{ in.}$				$y_2 = 108 \text{ in.}$					
						$C_1 \sinh \alpha y_1$	$C_1 \sinh \alpha y_1 + C_2 \cosh \alpha y_1$	$C_2 y_1 / s$	η'	$\frac{Q_{nx} M_0^*}{Q_0 s} \eta'$	$C_1 \sinh \alpha y_2$	$C_1 \sinh \alpha y_2 + C_2 \cosh \alpha y_2$	$C_2 y_2 / s$	η'	$\frac{Q_{nx} M_0^*}{Q_0 s} \eta'$
	Eq. (4.40) Note 1	Eq. (4.39)				Note 2		Note 3	Eqs. (4.38) & (4.35)		Note 4		Note 3	Eqs. (4.38) & (4.35)	
1	-1.34296	1.31898	-1.0	-1.2484	1.0	0.55408	-0.52330	-0.41613	0.06057	-0.023046	1.05460	-0.20331	-0.74903	0.04766	-0.018135
3	-0.20864	1.01130		-1.1608		1.44709	-0.29303	-0.38693	0.32004	-0.017669	4.11323	-0.07517	-0.69648	0.22835	-0.012606
5	-0.10492	1.00059		-1.1004		3.46178	-0.13958	-0.36680	0.49362	-0.011882	16.85695	-0.01976 ⁽¹⁾	-0.66024	0.32000	-0.007702
7	-0.07005	1.00004		-1.0694		7.68512	-0.06449	-0.35647	0.57904	-0.007377	68.87822	-0.00462	-0.64164	0.35374	-0.004507
9	-0.05257	1.00000		-1.0524		16.84701	-0.02960 ⁽²⁾	-0.35080	0.61960	-0.004151		-0.00101	-0.63144	0.36755	-0.002463
11	-0.04218			-1.0421			-0.01356	-0.34737	0.63907	-0.001946		-0.00020	-0.62526	0.37454	-0.001140
13	-0.03514			-1.0351			-0.00621	-0.34503	0.64876	-0.000497		-0.00003	-0.62106	0.37891	-0.000290
15	-0.0301 ⁽³⁾			-1.0302			-0.00284	-0.34340	0.65376	+0.000373		0	-0.61812	0.38188	+0.000218
17	-0.0264			-1.0264			-0.00130	-0.34213	0.65657	+0.000810		0	-0.61584	0.38416	+0.000474
19	-0.0235			-1.0235			-0.00059	-0.34117	0.65824	+0.000935		0	-0.61410	0.38590	+0.000548
21	-0.0212			-1.0212			-0.00027	-0.34040	0.65933	+0.000848		0	-0.61272	0.38728	+0.000498
23	-0.0193			-1.0193			-0.00012	-0.33977	0.66011	+0.000636		0	-0.61158	0.38842	+0.000374
25	-0.0177			-1.0177			-0.00006	-0.33923	0.66071	+0.000371		0	-0.61062	0.38938	+0.000219
27	-0.0163			-1.0163			-0.00003	-0.33877	0.66120	+0.000113		0	-0.60978	0.39022	+0.000067
29	-0.0151			-1.0151			-0.00001	-0.33837	0.66162	-0.000098		0	-0.60906	0.39094	-0.000058
31	-0.0141			-1.0141			0	-0.33803	0.66197	-0.000239		0	-0.60846	0.39154	-0.000142
33	-0.0133			-1.0133			0	-0.33777	0.66223	-0.000306		0	-0.60798	0.39202	-0.000181
35	-0.0125			-1.0125			0	-0.33750	0.66250	-0.000301		0	-0.60750	0.39250	-0.000179

NOTES: (1) for $n > 13$ eq. (4.52).
 (2) for $n \geq 9$ eq. (4.51).
 (3) $\eta' = C_1 \sinh \alpha y + C_2 \cosh \alpha y + C_3 y / s + C_4$.
 (4) for $n \geq 5$ eq. (4.51).

The dead load moments in ribs are:

$$M_{RS} = - \frac{(0.052)(15)^2}{12} (2)(12) = -24 \text{ k-in./rib}$$

$$M_{RC} = \frac{(0.052)(15)^2}{24} (2)(12) = 12 \text{ k-in./rib}$$

The moments in floor beams at the main girders due to sidewalk dead load are:

Due to erection loads, $M_{FS} = -9.0 \text{ k-ft}$

Due to superimposed loads, $M_{FS} = -34.0 \text{ k-ft}$

The dead load moments at the midspan of floor beams are:

Due to erection loads,

$$M_{FC} = \frac{(0.490)(50)^2}{8} - 9.0 = 144 \text{ k-ft}$$

Due to superimposed loads,

$$M_{FC} = \frac{(0.375)(50)^2}{8} + \frac{(2.09)(50)}{4} - 34.0 = 109 \text{ k-ft}$$

11.3.2.2 Effects of Floor Beam Flexibility

11.3.2.2.1 Additional Moment at Midspan of Ribs

The loading used in the computation of the bending moment increment, ΔM_{RC} , due to floor beam flexibility is shown in Figure 11.13. The loading in the "critical lane" corresponds to that used in Section 11.3.2.1.5, with the second wheel added. In the adjoining lane two 32-kip truck axles are placed to cause maximum deflection of the floor beams $m = 0$ and $0'$. The front 8-kip axle, having a relieving effect, is omitted. No loads are placed in the outside bridge lanes, since their effects, in this case, would be offset by the load intensity reduction coefficients for multiple lane loading, in accordance with the AASHO specifications.

The values of Q_0 and Q_{1x}/Q_0 needed in the computation of the bending moment increments, ΔM_{RC} , are the same as used in the computations of the deck with open ribs (see Section 11.2.2.2.1).

The values of F_m/P for loading **a** in the critical lane, needed in the evaluation of equation (5.9a), are given in Table 11.2.2.2.1. The values of F_m/P for the loading in the adjoining lane are computed in a similar manner

by equations (4.11) and (4.12) and given in Table 11.3.2.2.1.

The values of $\sum(F_m/P)(\bar{\eta}_{cm}/s)$ are computed in Table 11.3.2.2.1. The ordinates $\bar{\eta}_{cm}/s$ are obtained from Chart 17. Because of the loading symmetry the computation is made for the supports on one side only and the results are used in equation (5.9a) with a factor of 2.

The bending moment increments, ΔM_{RC} , are obtained by equation (5.9a) as follows:

Load in critical lane,

$$\Delta M_{RC} = (0.709)(180)(13 + 11)(0.126)(0.0262)(2) = 20.2 \text{ k-in./rib}$$

Load in additional lane,

$$\Delta M_{RC} = (0.800)(180)(13 + 11)(0.149)(0.0391)(2) = 40.3 \text{ k-in./rib}$$

The total additional moment at midspan of ribs is, by equation (5.10),

$$\Delta M_{RC} = 20.2 + 40.3 = 60.5 \text{ k-in./rib}$$

The bending moment relief at support of ribs, ΔM_{RS} , is not computed.

11.3.2.2.2 Moment Relief in Floor Beams

The loading used in the computation of the bending moment relief ΔM_F is the same as used in the computation of the bending moments in the system with rigid floor beams, Section 11.3.2.1.1b (see Figs. 11.12 and 11.5b).

The values of F_0/P are computed by equations (4.11) and (4.12) and given in Table 11.3.2.2.2. The values of $\bar{\delta}_{0m}$ are obtained for $\gamma = 0.077$ from Chart 19. The computation of the value of $\sum(F_m/P)\bar{\delta}_{0m}$ is given in Table 11.3.2.2.2.

The values of Q_0 and Q_{lx}/Q_0 for three lanes loaded (Fig. 11.5b) are the same as used in Section 11.2.2.2.2.

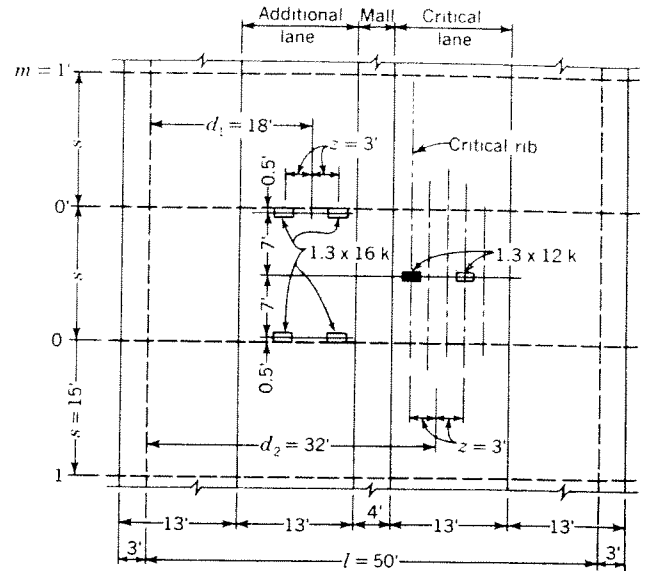


Fig. 11.13. Loading used in the computation of the maximum bending moments at midspan of closed ribs with consideration of floor beam flexibility

The bending moment relief in the floor beam at the location $x = 29$ ft is, by equation (5.14),

$$\Delta M_F = (9.5)\left(\frac{50}{\pi}\right)^2 (0.349)(1.252 - 1.040)(0.90) = 160 \text{ k-ft}$$

The factor of 0.90 is the reduction coefficient for three lanes loaded of the AASHO specifications.

11.3.2.3 Summary of Moments and Stresses

The summary of the bending moments in the ribs and the floor beams is given in Tables 11.3.2.3.1 and 2. The flexural stresses are determined by using the section moduli computed in Sections 11.3.1.2.1 and 2.

TABLE 11.3.2.2.1
ADDITIONAL MOMENT AT MIDSPAN OF RIBS, COMPUTATION OF $\sum(F_m/P)(\bar{\eta}_{cm}/s)$

Loading Case (Fig. 11.13)	Values computed	Reference	$m = 0$	1	2	3	4	$\sum \frac{F_m \bar{\eta}_{cm}}{P s}$
	$\bar{\eta}_{cm}/s$	Chart 17	+0.037	-0.033	-0.006	-0.002	+0.001	
Critical lane loaded	F_m/P	Table 11.2.2.2.1 Case a	+0.601	-0.127	+0.034	-0.009	+0.002	
	$(F_m/P)(\bar{\eta}_{cm}/s)$		+0.0222	+0.0042	-0.0002	0	0	+0.0262
Additional lane loaded	F_m/P	Eqs. 4.11-4.12	+1.028	-0.035	+0.009	-0.003	+0.001	
	$(F_m/P)(\bar{\eta}_{cm}/s)$		+0.0380	+0.0012	-0.0001	0	0	+0.0391

TABLE 11.3.2.2.2
MOMENT RELIEF IN FLOOR BEAMS, COMPUTATION OF $(F_0/P) - (\bar{F}_0/P)$

Values computed	Reference	$m = 3'$	2'	1'	0	1	2	3	\bar{F}_0/P (Eq. 5.13)	$(F_0/P) - (\bar{F}_0/P)$
F_m/P	Eqs. 4.11-4.12	-0.004	+0.029	+0.605	+1.252	+0.437	-0.090	+0.024		
$\bar{\delta}_{0m}$	Chart 19	-0.018	-0.019	+0.215	+0.650	+0.215	-0.019	-0.018		
$(F_m/P)\bar{\delta}_{0m}$		0	-0.001	+0.130	+0.815	+0.094	+0.002	0	1.040	0.212

TABLE 11.3.2.3.1
MAXIMUM BENDING MOMENTS AND STRESSES IN RIBS

Location	Loading	Bending Moment (k-in.)	Stress (ksi)	
			Top	Bottom
Midspan, Point A (Fig. 11.8)	Dead load	12		
	L.L., rigid system	312		
	L.L., effect of floor beam flexibility	61		
	Total, System II System I stress	385	-5.0 12.5	14.3 11.3
	Total stress		7.5	25.6
Support, Point B	Dead load	-24		
	L.L., rigid system	-444		
	Total, System II System I stress	-468	6.1 -11.2	-17.4 -9.5
	Total stress		-5.1	-26.9

TABLE 11.3.2.3.2
MAXIMUM BENDING MOMENTS AND STRESSES IN FLOOR BEAMS

Location	Loading	Bending Moment (k-ft)	Stress (ksi)		
			Top Pt. ①	Pt. ②	Bottom Pt. ③
Lower portion of floor beam	D.L., erection	144	---	-7.5	7.5
Entire section of floor beam	D.L., superimposed	109			
	L.L., rigid floor beam	971			
	L.L., effect of flexibility	-160			
	Total	920	-4.1	4.8	18.8
Total stress			-4.1	-2.7	26.3

11.3.3 Design by Charts for AASHO Loads

The section properties and the relative rigidity coefficients are computed as shown in Section 11.3.1.

The loads used in the design are given in Sections 11.3.2.1.1 and 11.3.2.2.1 and 2.

11.3.3.1 Bending Moments in a System with Rigid Floor Beams

11.3.3.1.1 Live Load Moments in Ribs

(a) *Moment at midspan*

For loading **a** the moment is obtained from Chart 9, with $s = 15$ ft, $H/D_y = 0.051$, as

$$M_C = 13.0 \text{ k-in./in.}$$

The moment per rib, by equation (4.35a), is

$$M_{RC} = (13.0)(13 + 11) = 312 \text{ k-in./rib}$$

For loading **a₁** the moment obtained from Chart 11 is

$$M_C = 13.5 \text{ k-in./in.}$$

$$M_{RC} = (13.5)(13 + 11) = 324 \text{ k-in./rib}$$

(b) *Moment at support*

From Chart 13, for $s = 15$, $H/D_y = 0.051$, loading **e**, the moment at support is obtained as

$$M_S = -18.6 \text{ k-in./in.}$$

$$M_{RS} = -(18.6)(13 + 11) = -446 \text{ k-in./rib}$$

11.3.3.1.2 Live Load Moments in Floor Beams

From Chart 15, for $s = 15$ ft, loading case **B**,

$$\frac{F_0}{P} = 1.25$$

From Chart 16, for $l = 50$ ft, lane width $W = 13$ ft, for 3 lanes loaded,

$$\frac{M}{F_0 l} = 0.378$$

for 2 lanes loaded

$$\frac{M}{F_0 l} = 0.360$$

The above values include the AASHO load reduction coefficient for multiple lanes loaded.

The impact factor is computed, in accordance with the AASHO formula, as:

$$I = \frac{50}{L + 125} = \frac{50}{50 + 125} = 0.286$$

Thus, the axle load, P , including impact is:

$$P = (1.286)(32) = 41.1 \text{ kips}$$

The maximum floor beam moment is then, with 3 lanes loaded,

$$M_F = \frac{M}{F_0 l} \frac{F_0}{P} Pl = (0.378)(1.25)(41.1)(50) = 973 \text{ k-ft}$$

and with 2 lanes loaded

$$M_F = (0.360)(1.25)(41.1)(50) = 925 \text{ k-ft}$$

11.3.3.1.3 Dead Load Moments

The dead load moments are computed as shown in Section 11.3.2.1.8.

11.3.3.2 Effects of Floor Beam Flexibility

11.3.3.2.1 Additional Moment at Midspan of Ribs

In order to compute the additional moments at the midspan of ribs by equation (5.9a) the values of Q_0 , Q_{1z}/Q_0 , and $\sum(F_m/P)(\bar{\eta}_{cm}/s)$ are needed.

The values of Q_0 are computed as shown in Section 11.3.2.1.1.

The values of Q_{1z}/Q_0 are obtained from Charts 28 and 29.

For the critical lane loaded (Fig. 11.13), for $l = 50$ ft, $W = 13$ ft and $2g = 22$ in., the loading coefficient is obtained from Chart 28 as

$$\frac{Q_{1z}}{Q_0} = 0.126$$

For one additional lane loaded (Fig. 11.13), the loading coefficient is, from Chart 29,

$$\frac{Q_{1z}}{Q_0} = 0.149$$

Loading of more than two lanes is not considered because of the AASHO load intensity reduction (see Section 11.3.2.2.1).

The values of $\sum(F_m/P)(\bar{\eta}_{cm}/s)$ or the critical lane are taken from Chart 20.

For $\gamma = 0.077$, loading **a**

$$\sum \frac{F_m}{P} \frac{\bar{\eta}_{cm}}{s} = 0.0526$$

For loading **a₁**

$$\sum \frac{F_m}{P} \frac{\bar{\eta}_{cm}}{s} = 0.0132$$

For the additional lane loaded, loading **h₁**, the value is obtained from Chart 23 as

$$\sum \frac{F_m}{P} \frac{\bar{\eta}_{cm}}{s} = 0.0770$$

The additional moments at midspan of ribs are computed by equation (5.9a) as follows:

Load in critical lane,

loading **a** :

$$\Delta M_{RC} = (0.709)(180)(24)(0.126)(0.0526) = 20.3 \text{ k-in./rib}$$

loading **a**₁ :

$$\Delta M_{RC} = (0.709)(180)(24)(0.126)(0.0132) = 5.1 \text{ k-in./rib}$$

Load in additional lane,

loading **h**₁ :

$$\Delta M_{RC} = (0.800)(180)(24)(0.149)(0.0770) = 39.6 \text{ k-in./rib}$$

11.3.3.2 Moment Relief in Floor Beams

The value of Q_0 for the 16-kip wheels is computed in Section 11.2.2.2.2.

The value of $(F_0/P) - \sum (F_m/P) \bar{\vartheta}_{0m}$, needed in the evaluation of equation (5.14), is obtained from Chart 31, for $\gamma = 0.077$, $s = 15$ ft, Case **B**,

$$\frac{F_0}{P} - \sum \frac{F_m}{P} \bar{\vartheta}_{0m} = 0.21$$

The values of Q_{1x}/Q_0 are obtained from Chart 32, for $l = 50$ ft, $W = 13$ ft.

For 3 lanes loaded

$$\frac{Q_{1x}}{Q_0} = 0.315$$

The above value includes the 10% load reduction in accordance with the AASHO specifications for 3 lanes loaded.

For 2 lanes loaded,

$$\frac{Q_{1x}}{Q_0} = 0.298$$

By equation (5.14) the relieving moments in the floor beams are:

3 lanes loaded,

$$\Delta M_F = (9.5) \left(\frac{50}{\pi} \right)^2 (0.315)(0.21) = 159 \text{ k-ft}$$

2 lanes loaded,

$$\Delta M_F = (9.5) \left(\frac{50}{\pi} \right)^2 (0.298)(0.21) = 151 \text{ k-ft}$$

11.3.3.3 Summary of Moments and Stresses

The governing loading cases are determined as follows:

(a) *Live load moment at midspan of ribs*

Loading **a** + **h**₁:

$$M_{RC} + \Delta M_{RC} = 312 + 20 + 40 = 372 \text{ k-in./rib}$$

Loading **a**₁ + **h**₁:

$$M_{RC} + \Delta M_{RC} = 324 + 5 + 40 = 369 \text{ k-in./rib}$$

It is seen that loading **a** + **h**₁ governs

(b) *Live load moment at support of ribs*

Loading **e**:

$$M_{RS} = -446 \text{ k-in./rib}$$

(c) *Live load moment in floor beams*

3 lanes loaded,

$$M_F + \Delta M_F = 973 - 159 = 814 \text{ k-ft}$$

2 lanes loaded,

$$M_F + \Delta M_F = 925 - 151 = 774 \text{ k-ft}$$

Loading of 3 lanes produces the critical moment.

Summary of the maximum bending moments and stresses is similar to that given in Section 11.3.2.3.

References

A. General, Theory

1. American Association of State Highway Officials: Standard Specifications for Highway Bridges, Eighth Edition, 1961.
2. American Institute of Steel Construction: The Battledock Floor for Highway Bridges, 1938.
3. American Society of Civil Engineers: Deflection Limitation of Bridges. Progress Report of the Committee on Deflection Limitations of Bridges of the Structural Division. A.S.C.E. Proceedings, May 1958, pg. 1633-1.
4. BECKER, G. F. and VAN ORSTRAND, C. E.: Smithsonian Mathematical Tables, Hyperbolic Functions. The Smithsonian Institution, Washington, 1909.
5. BLEICH, F.: Buckling Strength of Metal Structures. McGraw-Hill, New York, 1952.
6. Bureau of Public Roads, U.S. Dept. of Commerce: Policy and Procedure Memorandum 20-4, Aug. 10, 1956.
7. CHWALLA, E.: Die Formeln zur Berechnung der "voll mittragenden Breite" dünner Gurt- und Rippenplatten. Der Stahlbau, vol. 9 (1936), pg. 73.
8. Column Research Council, Engineering Foundation: Guide to Design Criteria for Metal Compression Members, 1960.
9. CORNELIUS, W.: Der wirtschaftliche Entwurf der Stahlplattenfahrbahn (Orthotrope Platte). Die Neue Köln-Mülheimer Brücke, pg. 85. Herausgegeben von der Stadt Köln, 1951.
10. CORNELIUS, W.: Die Berechnung der ebenen Flächentragwerke mit Hilfe der Theorie der orthogonal-anisotropen Platten. Der Stahlbau, vol. 21 (1952), pgs. 21, 43, 60.
11. DIECKMANN, D.: Über Einwirkungen mechanischer Schwingungen bis 100 Hertz auf den Menschen. Verein Deutscher Ingenieure, Berichte, vol. 24 (1957), pg. 117.
12. FARAGO, B. and CHAN, W.: The Analysis of Steel Decks with Special Reference to the Highway Bridges at Amara and Kut in Iraq. Proceedings of the Institution of Civil Engineers, London, vol. 16 (May 1960), pg. 1.
13. FISCHER, G.: Die Berechnung der Stahlfahrbahn-tafel der Bürgermeister-Smidt-Brücke in Brehmen. Der Stahlbau, vol. 21 (1952), pgs. 213, 237.
14. GIENCKE, E.: Die Grundgleichungen für die orthotrope Platte mit exzentrischen Steifen. Der Stahlbau, vol. 24 (1955), pg. 128.
15. GIENCKE, E.: Die Berechnung von durchlaufenden Fahrbahnplatten. Der Stahlbau, vol. 27 (1958), pgs. 229, 291, 315.
16. GIENCKE, E.: Die Berechnung von Hohlrippen-platten. Der Stahlbau, vol. 29 (1960), pgs. 1, 47.
17. GIENCKE, E.: Zur optimalen Auslegung von Fahrbahnplatten. Der Stahlbau, vol. 29 (1960), pg. 179.
18. GIENCKE, E.: Einfluss der Schubweichheit der Längsrippen und Querträger auf die Momente in einer orthotropen Platte. Der Stahlbau, vol. 29 (1960), pg. 351.
19. GIRKMANN, K. and BEER, B.: Anwendung der verschärften Plattentheorie nach Eric Reissner auf orthotrope Platten. Österreichisches Ingenieur-Archiv, vol. 12 (1958), pg. 101.
20. GIRKMANN, K.: Flächentragwerke, Fifth Edition. Springer Verlag, Wien, 1959.
21. GUYON, Y.: Calcul des Ponts Larges à Poutres Multiples Solidarisées par des Entretoises. Annales des Ponts et Chaussées, vol. 116 (1946), pg. 553.
22. HARDENBERG, G.: Economies of Orthotropic Plate Deck Design. Canadian Consulting Engineer, September 1960, pg. 50.
23. HAWRANEK, A. and STEINHARDT, O.: Theorie und Berechnung der Stahlbrücken. Springer Verlag, Berlin, 1958.
24. HAYASHI, K.: Fünfstellige Tafeln der Kreis- und Hyperbelfunktionen sowie der Funktionen e^x und e^{-x} . Walter de Gruyter & Co., Berlin, 1944.
25. HOMBERG, H.: Kreuzwerke. Springer Verlag, Berlin, 1951.
26. HOMBERG, H. and WEINMEISTER, J.: Einflussflächen für Kreuzwerke. Springer Verlag, Berlin, 1956.

27. HUBER, M. T.: Die Grundlagen einer rationellen Berechnung der kreuzweise bewehrten Eisenbetonplatten. Zeitschrift des Österreichischen Ingenieur- und Architekten-Vereines, vol. 66 (1914), pg. 557.
 28. HUBER, M. T.: Die Theorie der kreuzweise bewehrten Eisenbetonplatten. Der Bauingenieur, vol. 4 (1923), pgs. 354, 392.
 29. KLÖPPEL, K.: Zur orthotropen Platte aus Stahl. Die Neue Köln-Mülheimer Brücke, pg. 78. Herausgegeben von der Stadt Köln, 1951.
 30. KLÖPPEL, K.: Über zulässige Spannungen im Stahlbau. Stahlbau-Tagung Baden-Baden, 1954. Stahlbau Verlag, Köln, 1958.
 31. KLÖPPEL, K. and ROOS, E.: Statische Versuche und Dauerversuche zur Frage der Bemessung von Flachblechen in orthotropen Platten. Der Stahlbau, vol. 29 (1960), pg. 361.
 32. KOLLBRUNNER, K. and HERRMANN, G.: Theoretische Beuluntersuchungen der T.K.V.S.B. im Jahre 1947. Schweizerische Bauzeitung, vol. 66 (1948), pg. 146.
 33. KRUG, S. and STEIN, P.: Influence Surfaces of Orthogonal Anisotropic Plates. Springer Verlag, Berlin, 1961 (in German and English).
 34. LYSE, I. and MADSEN, I. E.: Structural Behavior of Battledeck Floor Systems. A.S.C.E. Proceedings, January 1938.
 35. MADER, F. W.: Berechnung orthotroper Platten unter Flächenlasten, Randmomenten und Randdurchbiegungen. Der Stahlbau, vol. 26 (1957), pg. 131.
 36. MADER, F. W.: Die Berücksichtigung der Diskontinuität bei der Berechnung orthotroper Platten. Der Stahlbau, vol. 26 (1957), pg. 283.
 37. MASSONET, C.: Méthode de Calcul des Ponts à Poutres Multiples Tenant Compte de leur Résistance à la Torsion. International Association of Bridge and Structural Engineering Publications, vol. 10 (1950), pg. 147.
 38. MORICE, P. B. and LITTLE, G.: Load Distribution in Prestressed Concrete Bridge Systems. The Structural Engineer, vol. 32 (1954), pg. 83.
 39. MÜLLER-BRESLAU, H.: Die Graphische Statik der Baukonstruktionen, vol. II. A. Kröner Verlag, Leipzig, 1925.
 40. NARUOKA, M. and YONEZAWA, H.: A Study of the Period of Free Lateral Vibration of the Beam Bridge by the Theory of Orthotropic Rectangular Plate. Ingenieur-Archiv, vol. 26 (1958), pg. 20.
 41. OLSEN, H. and REINITZHUBER, F.: Die zweiseitig gelagerte Platte. W. Ernst u. Sohn, Berlin, 1950-51.
 42. PELIKAN, W. and ESSLINGER, M.: Die Stahl-fahrbahn, Berechnung und Konstruktion. M.A.N. Forschungsheft No. 7, 1957.
 43. PELIKAN, W.: Leichtfahrbahnen. Deutscher Ausschuss für Stahlbau, 1908-58. Stahlbau Verlag, Köln, 1958.
 44. PELIKAN, W.: Die Orthotrope Platte der Stahl-fahrbahn. Stahlbau-Tagung Heidelberg, 1958. Stahlbau Verlag, Köln, 1958.
 45. PELIKAN, W.: Neues Bauelement im Stahlbrückenbau. Handbuch des Bauwesens.
 46. PFLÜGER, A.: Die orthotrope Platte mit Hohlsteifen. Österreichisches Ingenieur-Archiv, vol. 9 (1955), pg. 199.
 47. POSTLETHWAITE, F.: Human Susceptibility to Vibration. Engineering, vol. 157 (1944), pg. 61.
 48. RENNER, W. A.: The Bending of Orthogonally Non-Isotropic Slabs. Master's Degree Thesis, University of Illinois, 1939.
 49. SCHLEICHER, F.: Stahlbau. Taschenbuch für Bauingenieure, vol. I, pg. 565, Springer Verlag, Berlin, 1955.
 50. SCHUMANN, H.: Zur Berechnung orthogonal-anisotroper Rechtecksplatten unter Berücksichtigung der diskontinuierlichen Anordnung der Rippen. Der Stahlbau, vol. 29 (1960), pg. 302.
 51. Strüssi, F.: Vorlesungen über Baustatik, Vol. II. Verlag Birkhäuser, Basel/Stuttgart, 1954.
 52. Strüssi, F.: Grundlagen des Stahlbaues, pg. 443 ff. Springer Verlag, Berlin, 1958.
 53. THÜRLIMANN, B.: Tables of Influence Values for Moments in Orthotropic Plates. Fritz Laboratory Report No. 264.6, Lehigh University, 1960.
 54. TIMOSHENKO, S. and WOINOWSKY-KRIEGER, S.: Theory of Plates and Shells, Second Edition, Chapter 11—Bending of Anisotropic Plates. McGraw-Hill, New York, 1959.
 55. TRENKS, K.: Beitrag zur Berechnung orthogonal-anisotroper Rechtecksplatten. Der Bauingenieur, vol. 29 (1954), pgs. 372, 440.
 56. WOLCHUK, R.: Orthotropic Plate Design for Steel Bridges. Civil Engineering, February 1959, pg. 38.
- B. Descriptions of Bridges with Steel Plate Decks*
57. BALBACHEVSKY, G.: Study Tour of the A.F.P.C. Acier-Stahl-Steel, vol. 25 (1960), pg. 457.
 58. BEER, H.: Die Europabrücke über dem Silltal in Tirol. Der Bauingenieur, vol. 36 (1961), pg. 1.
 59. BEYER, E., GRASSL, H., WINTERGERST, L.: Nordbrücke Düsseldorf. Der Stahlbau, vol. 27 (1958), pgs. 1, 184.

60. DÖRNEN, A.: Stahlüberbau der Weserbrücke Porta. *Der Stahlbau*, vol. 24 (1955), pg. 97.
 61. DÖRNEN, A. and TRITTLER, G.: Kombinierte Eisenbahn-und Strassenbrücke über den Lippe-Seiten-Kanal. *Der Stahlbau*, vol. 27 (1958), pg. 7.
 62. *Engineering News-Record*: Novel Deck Saves Steel and Weight. June 16, 1960, pg. 43.
 63. FISCHER, G.: The Severin Bridge at Cologne (Germany). *Acier-Stahl-Steel*, vol. 25 (1960), pg. 97.
 64. GELSON, W. and PLANK, G.: The New Highway Bridges across the Tigris at Amara and Kut in Iraq. *Proceedings of the Institution of Civil Engineers*, London, vol. 16 (May 1960), pg. 33.
 65. GÖRTZ, W.: The Rhine Bridge between Duisburg-Ruhrort and Homberg. Reprinted from *DEMAG News*, No. 144, 1955.
 66. GUT, J.: Die Klappbrücke Krakerøy. *Der Bauingenieur*, vol. 34 (1959), pg. 91.
 67. GUYER, R.: Die St. Alban-Brücke über den Rhein in Basel. II. *Der Stahlüberbau*. *Schweizerische Bauzeitung*, vol. 75 (1957), pg. 453.
 68. HARHOFF, E.: Die Neue Strombrücke. *Denkschrift zum Wiederaufbau der Rheinbrücke Düsseldorf-Neuss, 1950-1951*, pg. 37. Herausgegeben von der Stadt Düsseldorf, 1951.
 69. HESS, H.: Die Severinsbrücke Köln. *Der Stahlbau*, vol. 29 (1960), pg. 225.
 70. HOTCHKISS, J. G.: New Ways to Cut Bridge Weight Lead to Record Spans, *Eng. News-Record*, Nov. 7, 1957.
 71. KLINGENBERG, W.: Brückenbauten an Bundesfernstrassen. *Der Bauingenieur*, vol. 32 (1957), pg. 245.
 72. KLINGENBERG, W.: *Stählerne Strassenbrücken*. Sonderdruck aus *Stahlbautagung Berlin, 1960*. Stahlbau, Verlag, Köln, 1960.
 73. LANGE, K.: Die Strombrücke. Nordbrücke Düsseldorf. Herausgegeben von der Landeshauptstadt Düsseldorf, 1958.
 74. LEONHARDT, F. and PELIKAN, W.: Grundsätzliches zum Entwurf und zur baulichen Durchbildung. Die Neue Köln-Mülheimer Brücke, pg. 16. Herausgegeben von der Stadt Köln, 1951.
 75. MAYER, R.: Die Kurpfalzbrücke über den Neckar in Mannheim. *Der Stahlbau*, vol. 27 (1952), pgs. 85, 117, 146.
 76. RADOJKOVIC, M.: Die neue Strassenbrücke über die Save in Belgrad, *Der Stahlbau*, vol. 27 (1958), pgs. 29, 70.
 77. ROLOFF, W.: Die Strassenbrücke über den Rhein zwischen Mannheim und Ludwigshafen. *Der Stahlbau*, vol. 29 (1960), pg. 333.
 78. SCHAECHTERLE, K. and WINTERGERSI, L.: Wiederaufbau der Rheinbrücke Düsseldorf-Neuss. *Der Bauingenieur*, vol. 27 (1952), pg. 1.
 79. SCHÖTTGEN, J.: Stählerner Überbau der Rheinbrücke Speyer. *Der Stahlbau*, vol. 26 (1957), pg. 29.
 80. SCHÜSSLER, K. and PELIKAN, W.: Die Neue Rheinbrücke Köln-Mülheim. *Der Stahlbau*, vol. 20 (1951), pg. 141.
 81. SIEVERS, H. and GORTZ, W.: Der Wiederaufbau der Strassenbrücke über den Rhein zwischen Duisburg-Ruhrort und Homberg. *Der Stahlbau*, vol. 25 (1956), pg. 81.
 82. VOGEL, G.: Die Montage des Stahlüberbaues der Severinsbrücke Köln. *Der Stahlbau*, vol. 29 (1960), pg. 269.
 83. ZUCKER, O.: Bau der Eisenbahnbrücke über die Autobahn in Wuppertal-Ost. *Der Stahlbau*, vol. 29 (1960), pg. 344.
- C. *Wearing Surfaces, Corrosion Protection*
84. The Asphalt Institute: *The Asphalt Handbook*. College Park, Maryland, 1960.
 85. Dow Chemical Company: *Technical Bulletins on Dow-Latex Concrete*.
 86. Forschungsgesellschaft für das Strassenwesen e. V.: *Vorläufiges Merkblatt für bituminöse Fahrbahn-Beläge auf Leichtfahrbahnen im Stahlbrückenbau*. Köln, 1961.
 87. GOLDBERGER, H. W.: The Use of Epoxy Resins on the New Jersey Turnpike. *Public Works*, March 1960, pg. 98.
 88. Johns-Manville Co.: *Technical Bulletins on Asphalt Planks*.
 89. KAMPMANN, G.: Messung und Beurteilung von Reibungsbeiwerten auf Bituminösen Decken, insbesondere auf Rauhbelägen. *Bitumen*, vol. 17 (1955), pg. 86.
 90. KIRSCHMER, O.: Versuche mit Belägen aus Gussasphalt auf Stahlfahrbahnen. *Bitumen*, vol. 14 (1952), pg. 201.
 91. KIRSCHMER, O.: *Fahrbahnbeläge für Orthotrope Platten und deren Prüfung*. M. A. N. Forschungsheft, 1954.
 92. KIRSCHMER, O.: Neuere Erkenntnisse bei Brückenbelägen. *Der Stahlbau*, vol. 27 (1958), pg. 16.
 93. M. A. N.: *Test Reports on Asphalt Wearing Surfaces on Steel Decks, 1950, 1951*.
 94. McCAY, W. J., McNUTT, D. J., LAMAR, C. E., LYMAN, H. E., TILLMAN, H. E.: *Steel Pipe Coating Symposium*. *Civil Engineering*, November 1960, pg. 68.

95. MERSCH, K.: Betrachtungen zum "Vorläufigen Merkblatt für bituminöse Fahrbahnbeläge auf Leichtfahrbahnen im Stahlbrückenbau." Bau und Bauindustrie, No. 9, 1961, pg. 354.
96. Philip Carey Mfg. Co.: Technical Bulletins on Asphalt Planks.
97. Protex-a-Coat, Inc.: Technical Bulletins on Epoxy-Synthetic Asphalt Concrete Pavement.
98. Reliance Steel Products Co.: Technical Bulletins and Publications on Relcote Applications.
99. SEILS, A. and KRANITZKY, W.: Sind Stahlbauwerke, bei denen allseits geschlossene Hohlkörper verwendet werden, durch Wasseransammlung oder Innenkorrosion gefährdet? Der Stahlbau, vol. 22 (1953), pgs. 80, 113.
100. SEILS, A.: Erläuterungen zu den "Technischen Vorschriften für den Rostschutz von Stahlbauwerken" (RoSt) der Deutschen Bundesbahn, Der Stahlbau, vol. 17 (1958), pgs. 126, 165.
101. SEILS, A. and KRANITZKY, W.: Der Korrosionsschutz im Innern geschlossener Hohlkästen. Der Stahlbau, vol. 28 (1959), pg. 46.
102. Sika Chemical Corporation: Technical Bulletins on epoxy compounds. Test Report on Guardkote Concrete of March 9, 1959 (unpublished).
103. TROTT, J. J. and WILSON, D. S.: The Development of Asphalt Surfacing for Steel Bridge Decks. Preliminary Publication, Sixth Congress of the International Association for Bridge and Structural Engineering, Stockholm, 1960, pg. 889.
104. UHLIG, H.: The Corrosion Handbook. John Wiley & Sons, New York, 1948.
105. WOODS, K. B.: Highway Engineering Handbook. McGraw-Hill, New York, 1960.

PHOTO CREDITS

- Fig. 1.5: Deutscher Stahlbauverband, Cologne
- Fig. 1.9: M.A.N., Gustavsburg
- Fig. 1.11: Gutehoffnungshütte, Sterkrade
- Fig. 1.13: Phoenix-Rheinrohr A.G.
- Fig. 1.16: Goertz-Bauer, Düsseldorf
- Fig. 1.18: Gutehoffnungshütte, Sterkrade
- Fig. 1.19: Gutehoffnungshütte, Sterkrade
- Fig. 1.20: Gutehoffnungshütte, Sterkrade
- Fig. 1.22: Deutscher Stahlbauverband, Cologne
- Fig. 1.25: C.B.A. Engineering Ltd., Vancouver
- Fig. 1.35: M.A.N., Gustavsburg
- Fig. 6.11: Verlag W. Ernst und Sohn, Berlin
- Fig. 7.9: M.A.N., Gustavsburg
- Fig. 7.12: DEMAG, Duisburg
- Fig. 7.21: DEMAG, Duisburg
- Fig. 8.3: M.A.N., Gustavsburg
- Fig. 8.4: M.A.N., Gustavsburg
- Fig. 8.7: Building Dept., City of Düsseldorf
- Fig. 8.9: Prof. Dr. O. Kirschmer, Darmstadt
- Fig. 8.10: Philip Carey Mfg. Co.
- Fig. 8.11: Shell Chemical Co.
- Fig. 8.12: Reliance Steel Products Co.

APPENDIX

Appendix I — Design Charts

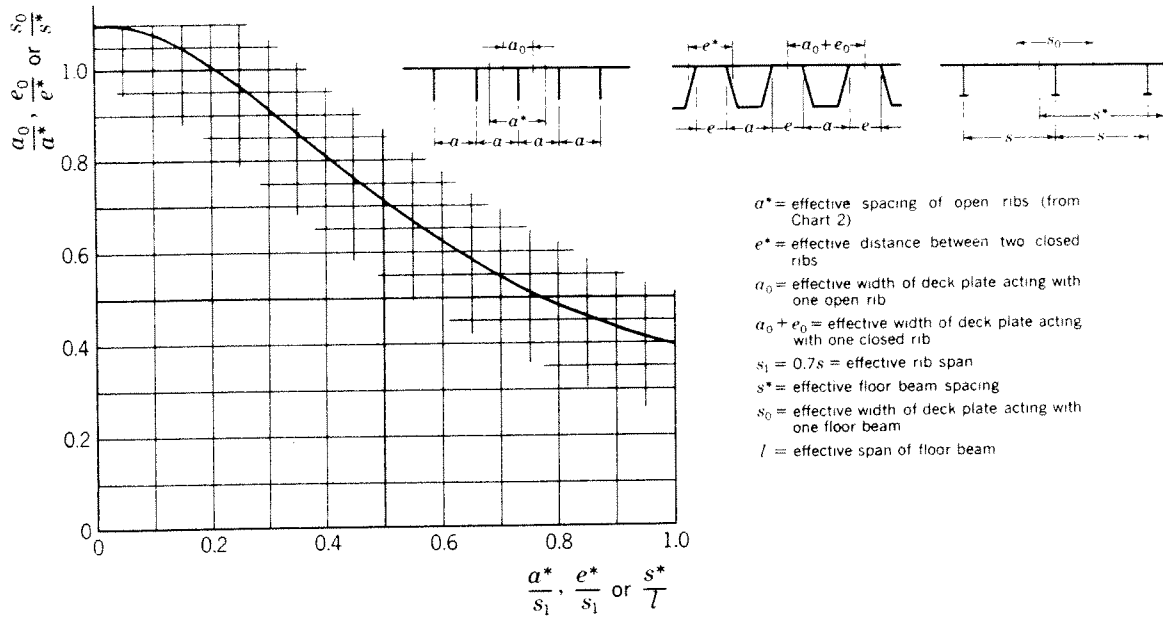


Chart 1. Effective width of deck plate acting with one rib or floor beam

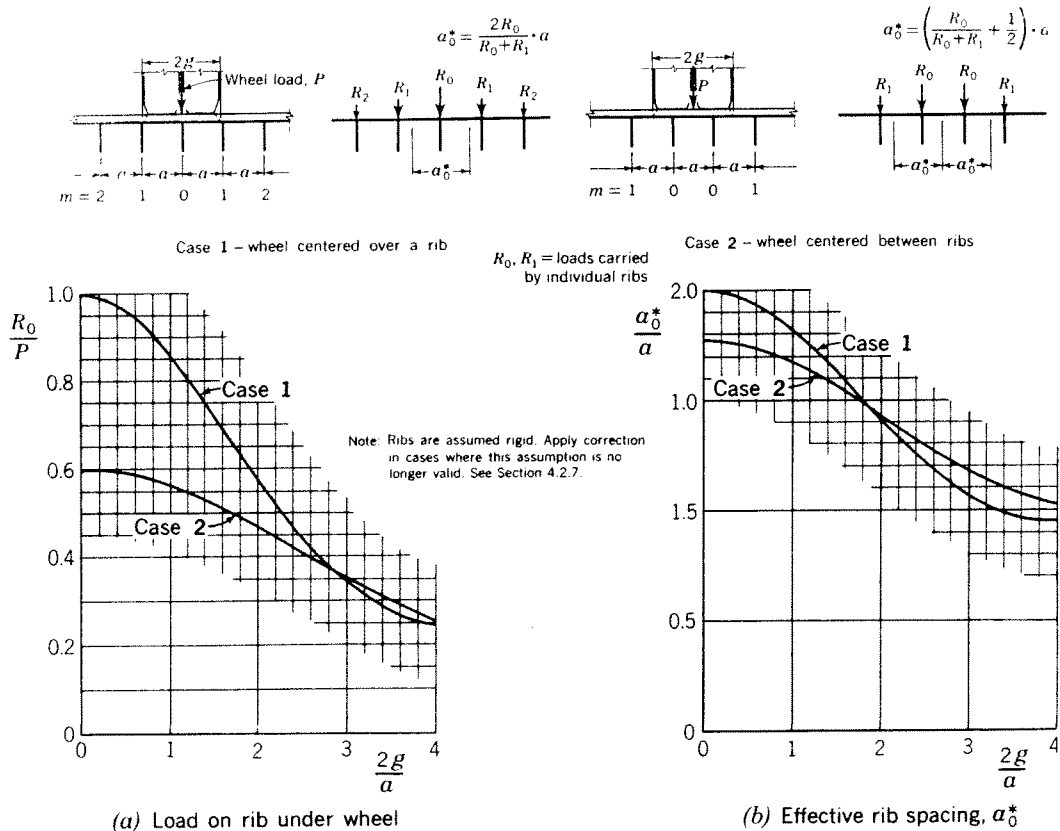


Chart 2. Load on rib under wheel and effective spacing of open ribs, general case

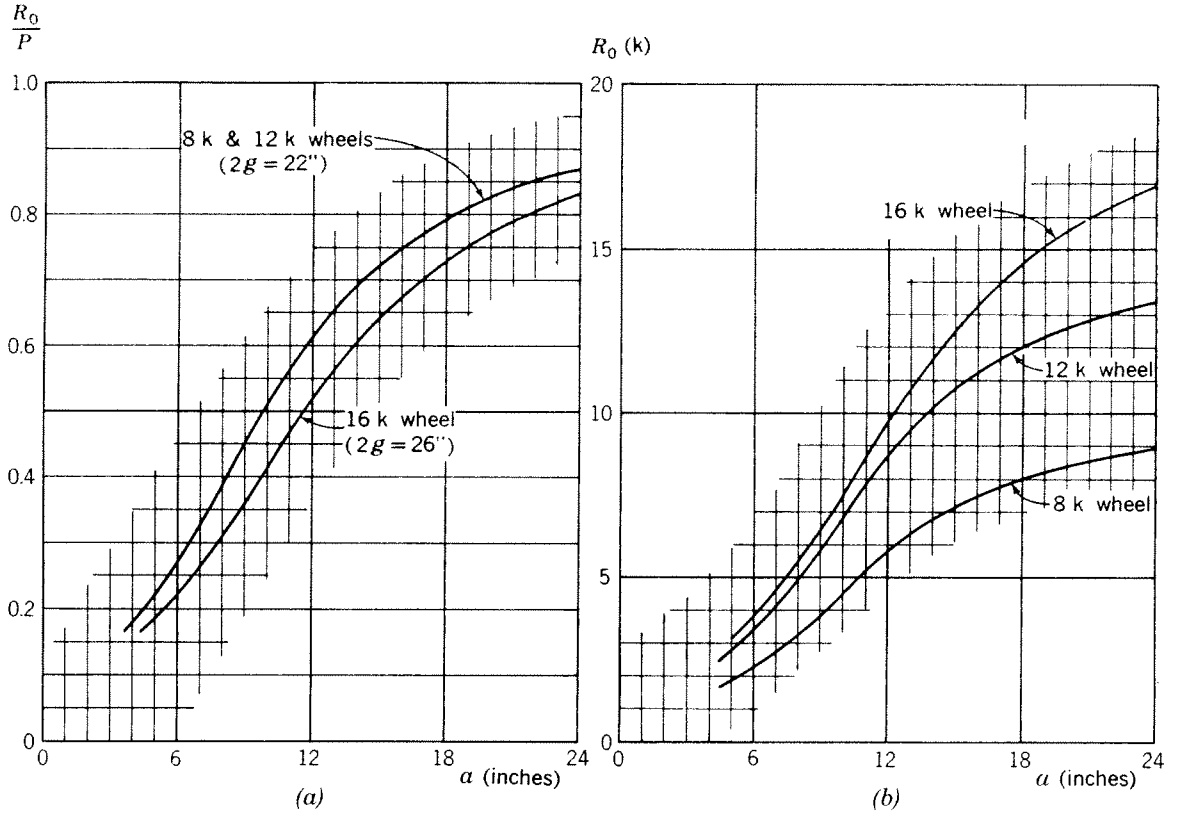
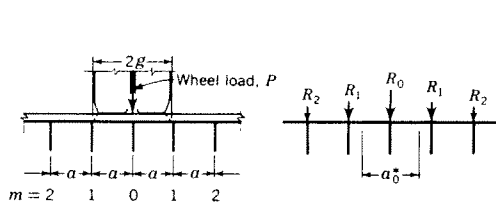


Chart 3. Load on open rib under wheel, AASHO loading



Notes: (1) Curves on Chart 3 include 30% impact.
 (2) Ribs are assumed rigid. Apply correction in cases where this assumption is no longer valid. See Section 4.2.7.

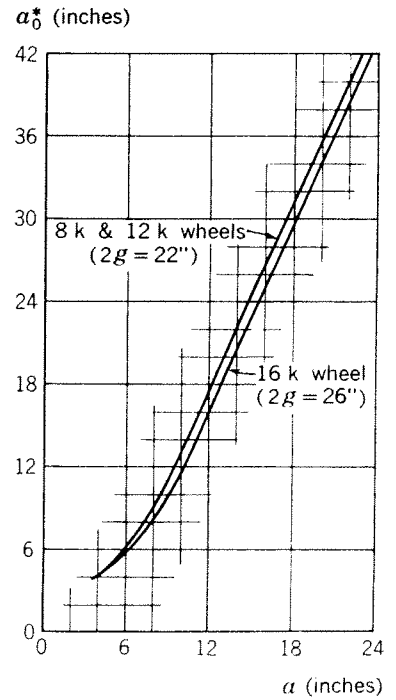


Chart 4. Effective spacing of open ribs, AASHO loading

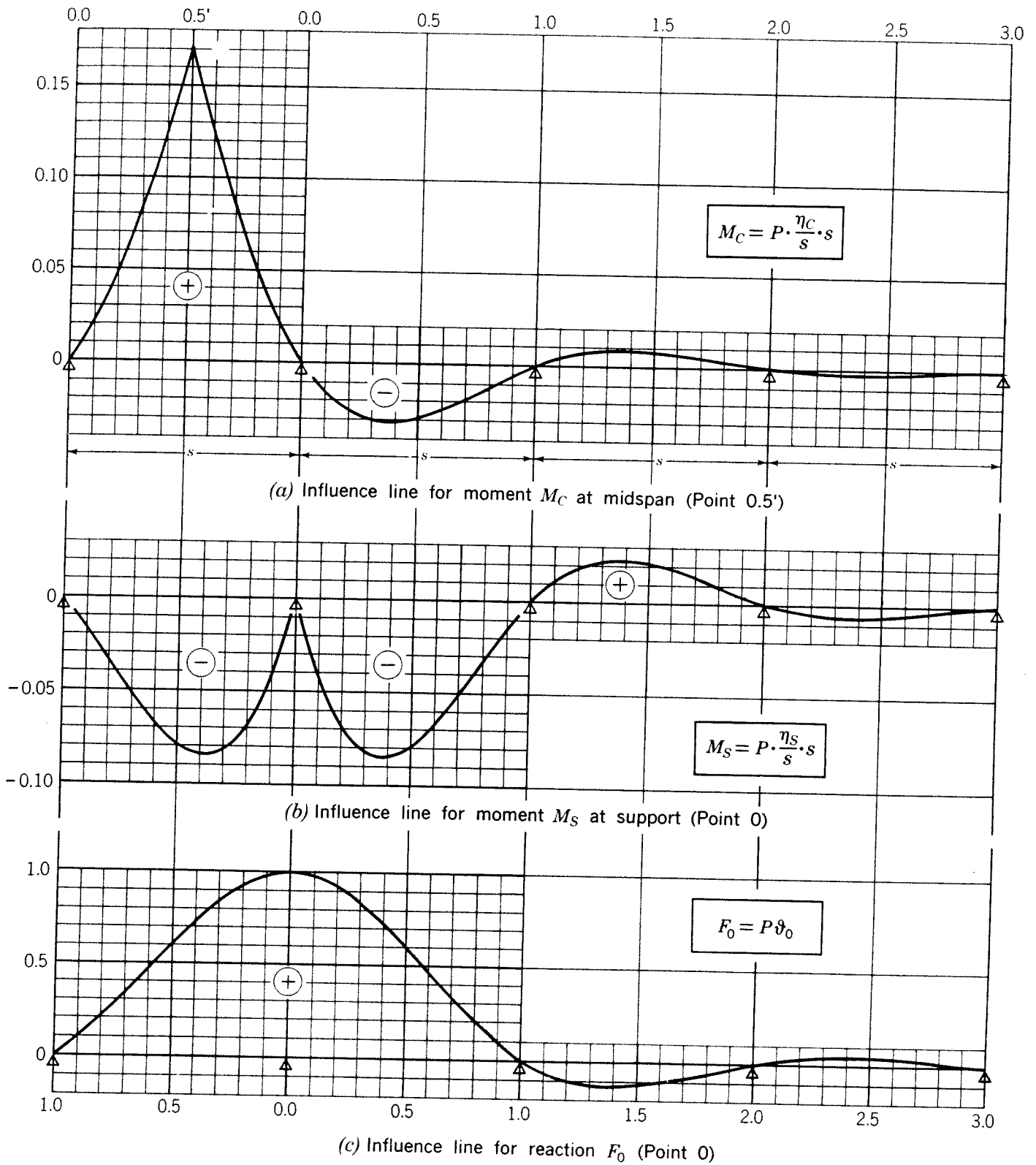


Chart 5. Influence lines of a beam on an infinite number of rigid supports

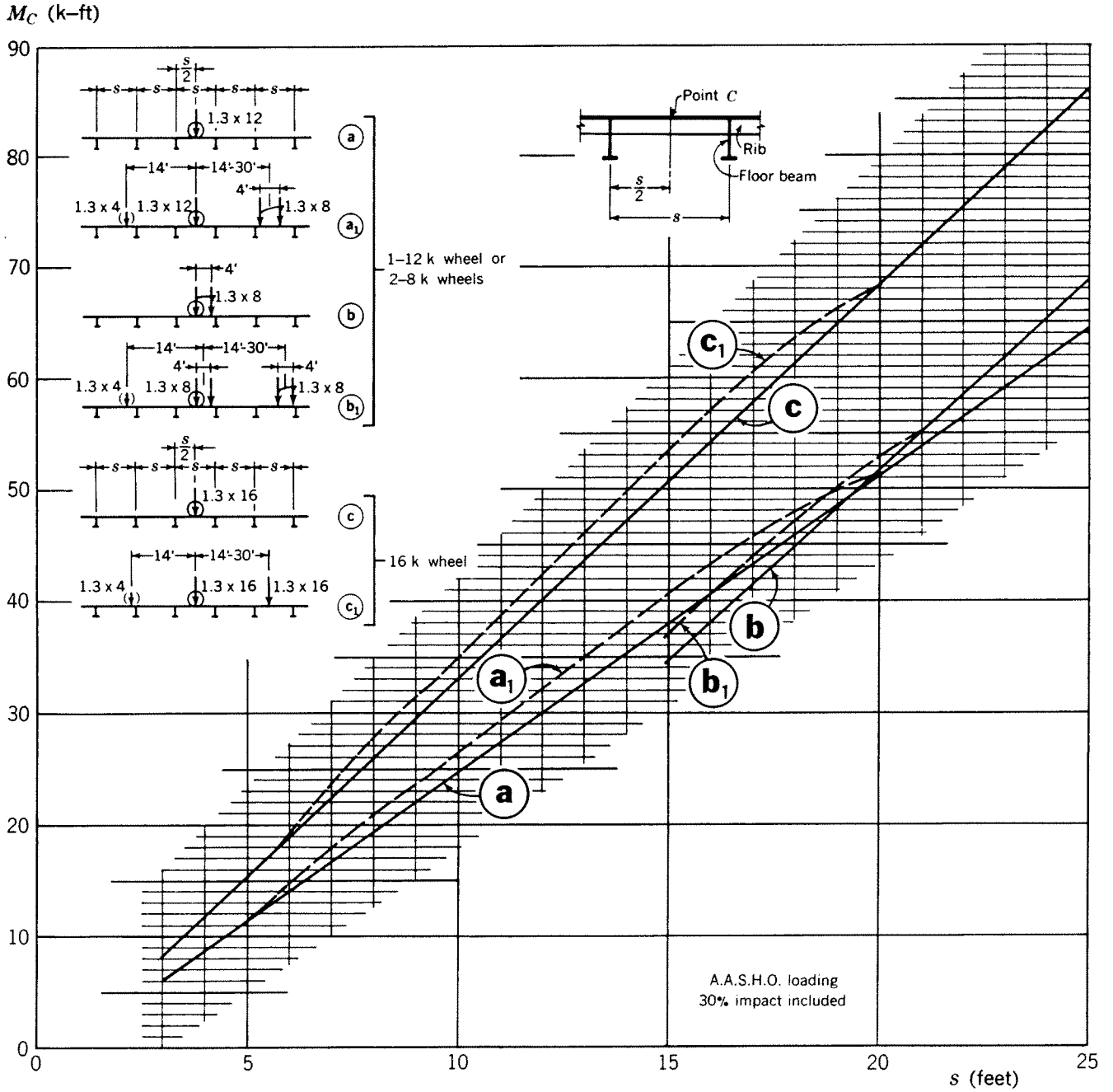


Chart 6. Total maximum moment at midspan of ribs on rigid supports

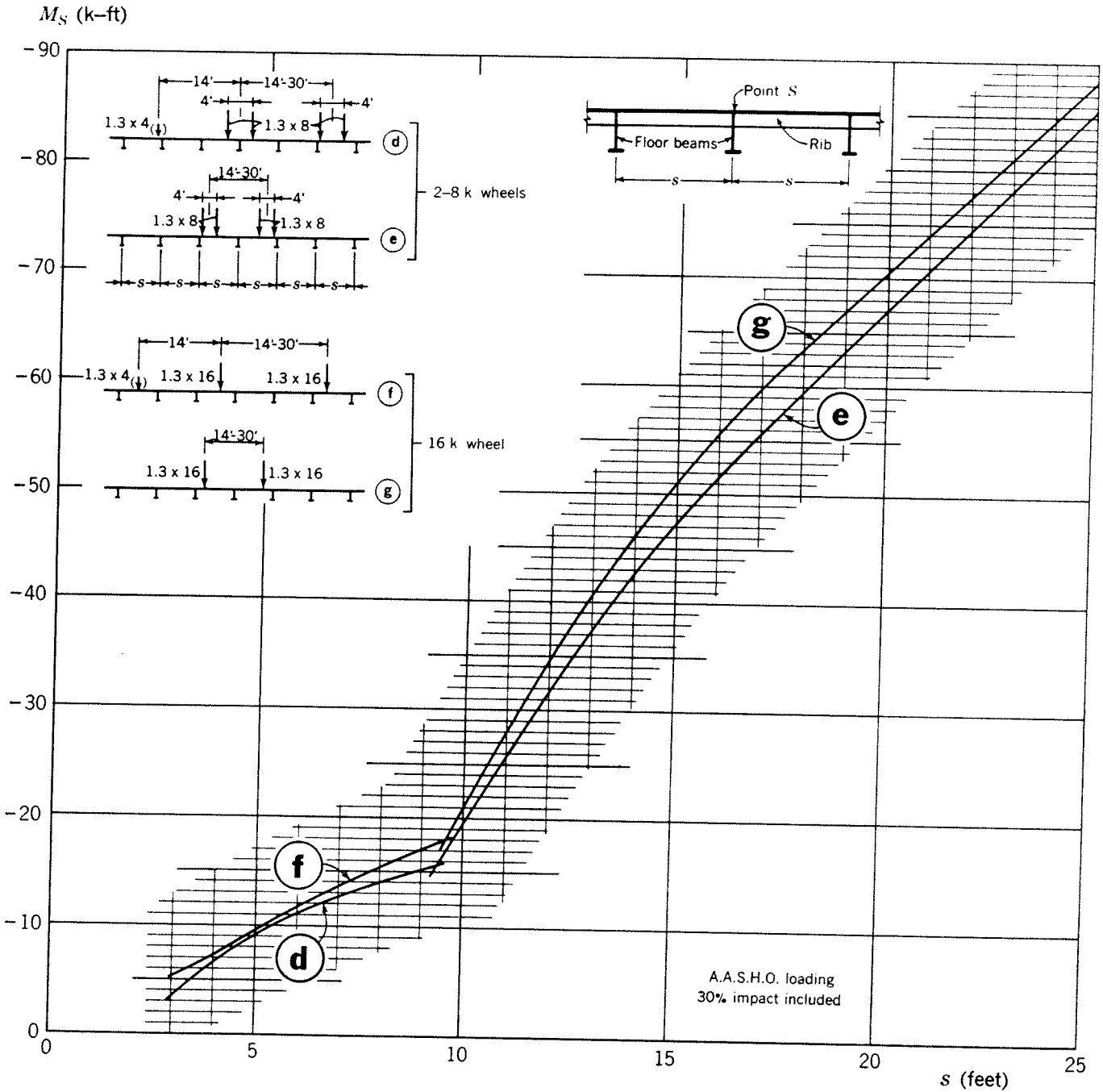
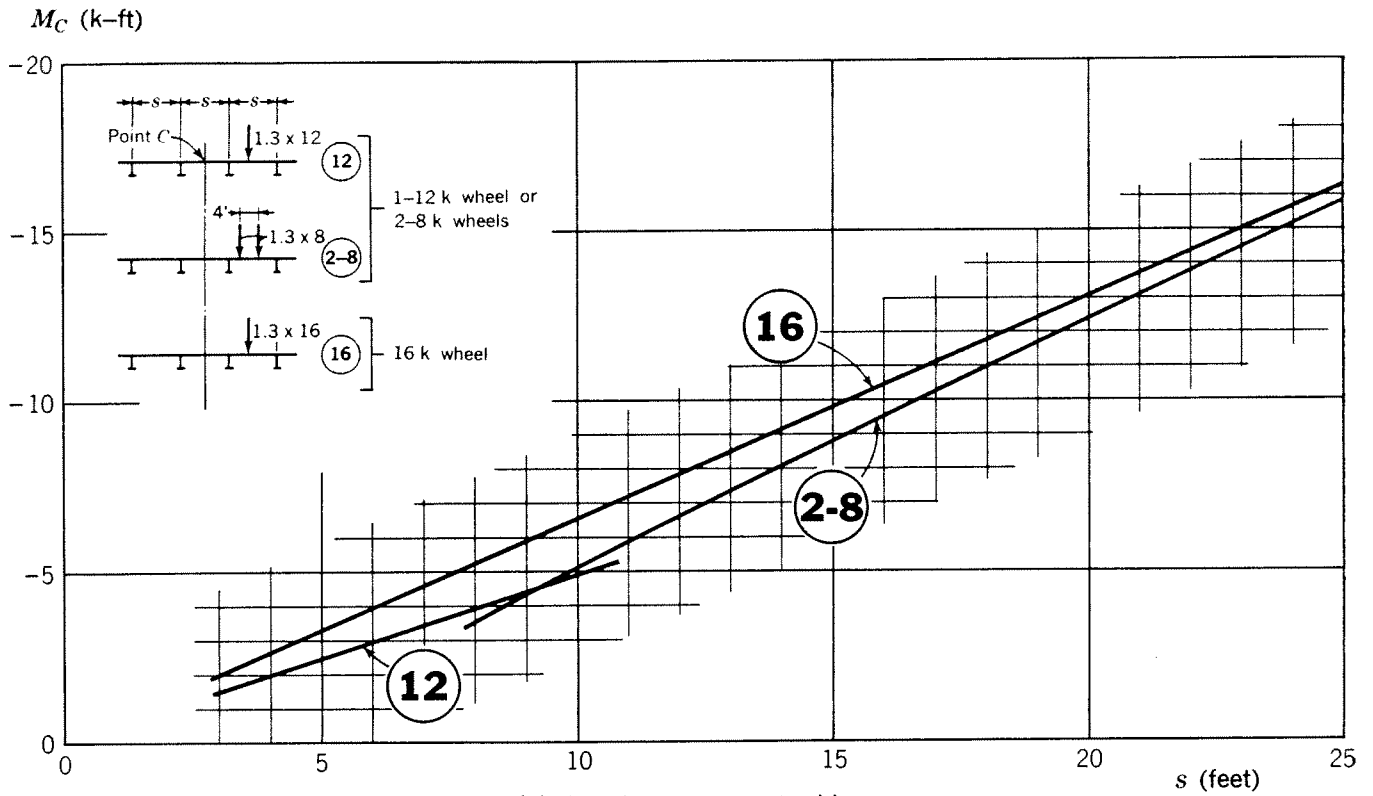
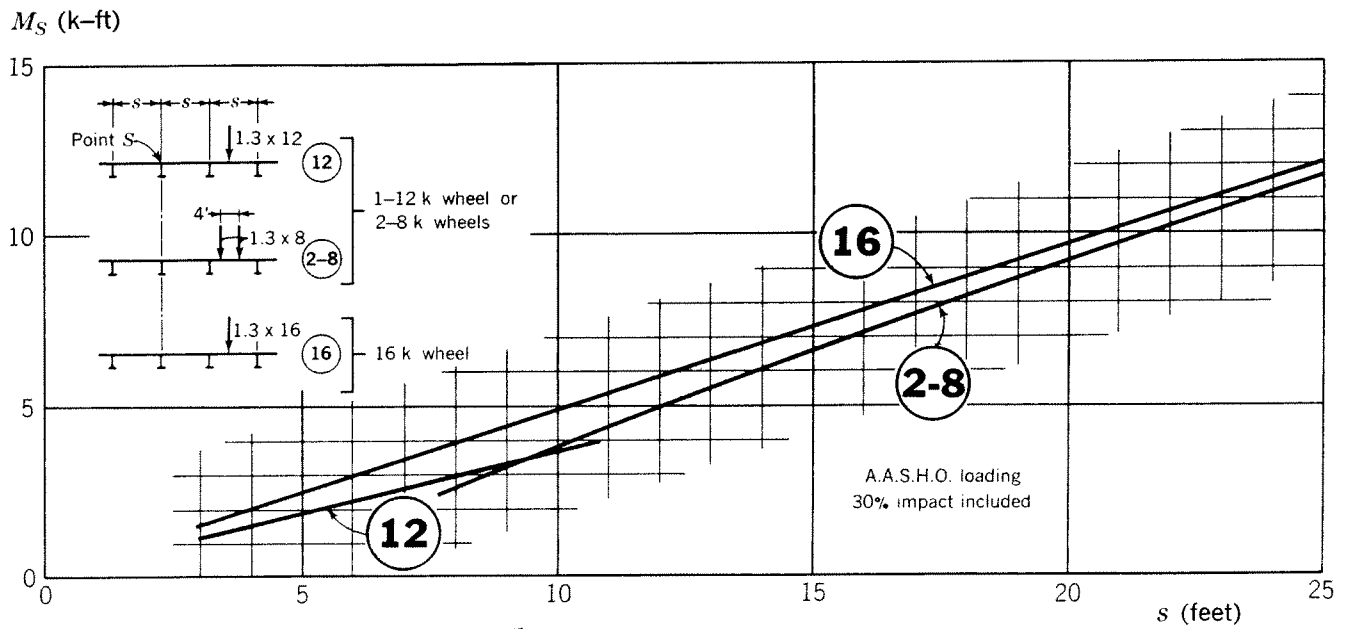


Chart 7. Total maximum moment at support of ribs on rigid supports



(a) Negative moment at midspan



(b) Positive moment at support

Chart 8. Total maximum moments for computing alternating stresses in ribs on rigid supports

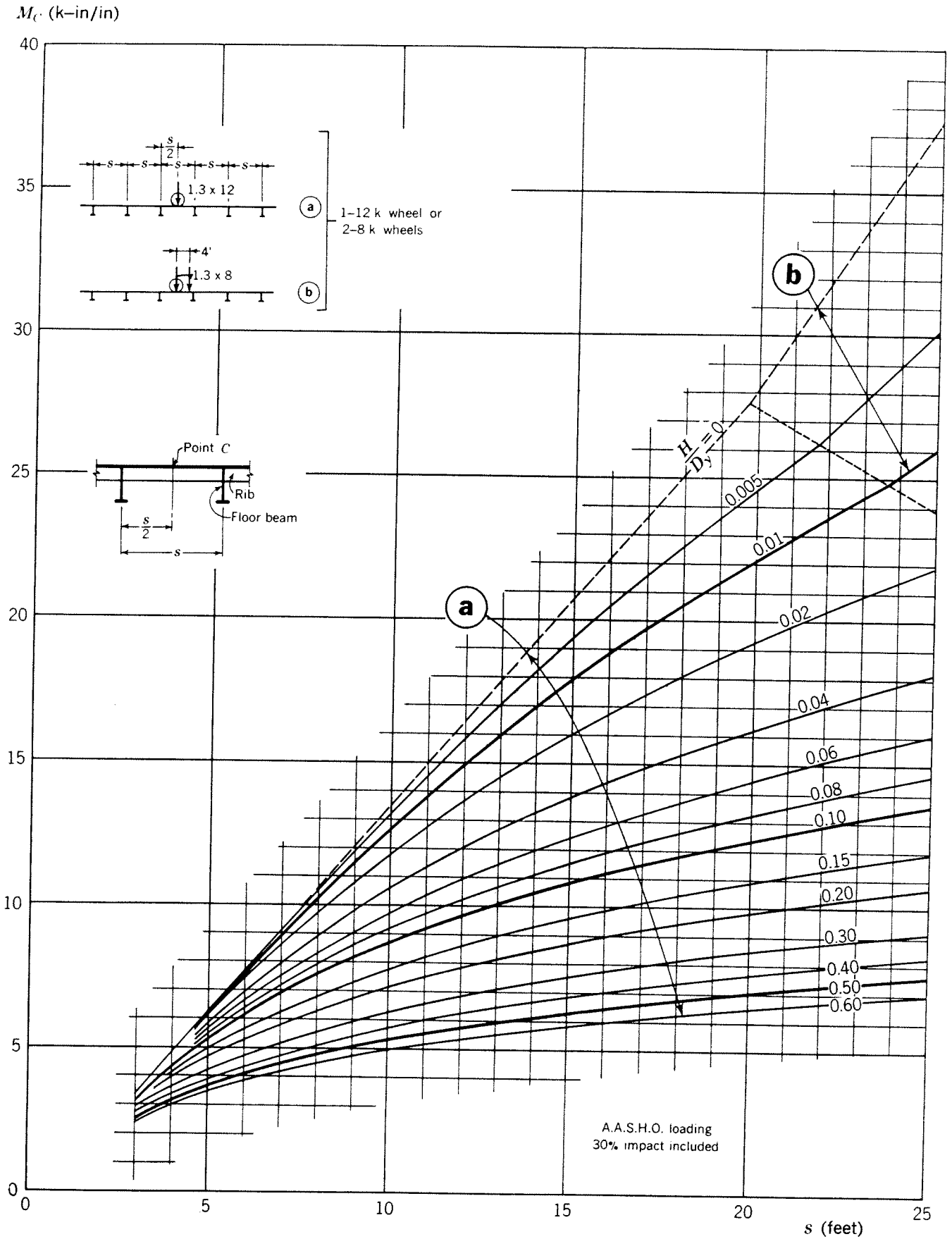


Chart 9. Maximum moment at midspan of the deck with closed ribs on rigid supports, loading a and b

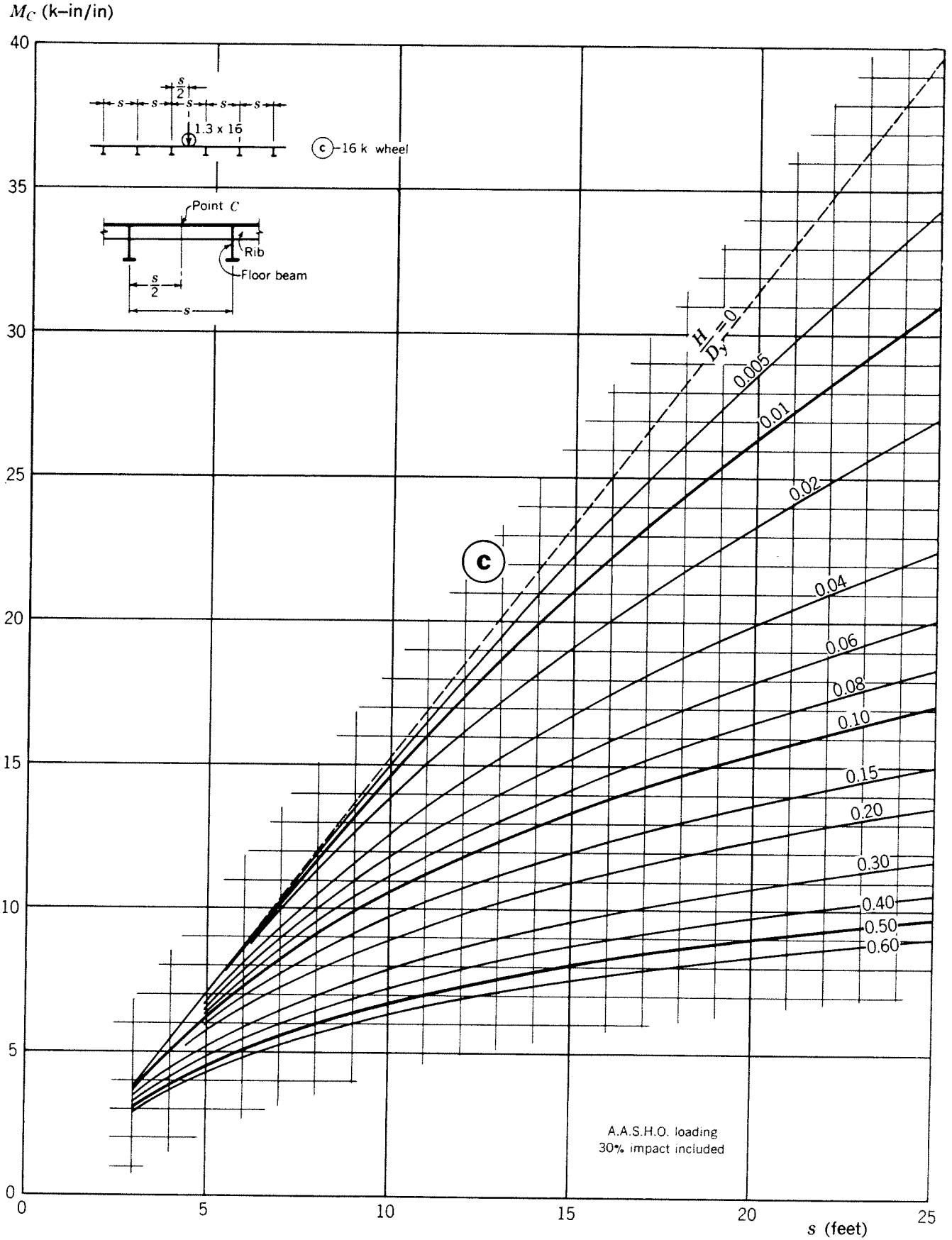


Chart 10. Maximum moment at midspan of the deck with closed ribs on rigid supports, loading c

M_c (k-in/in)

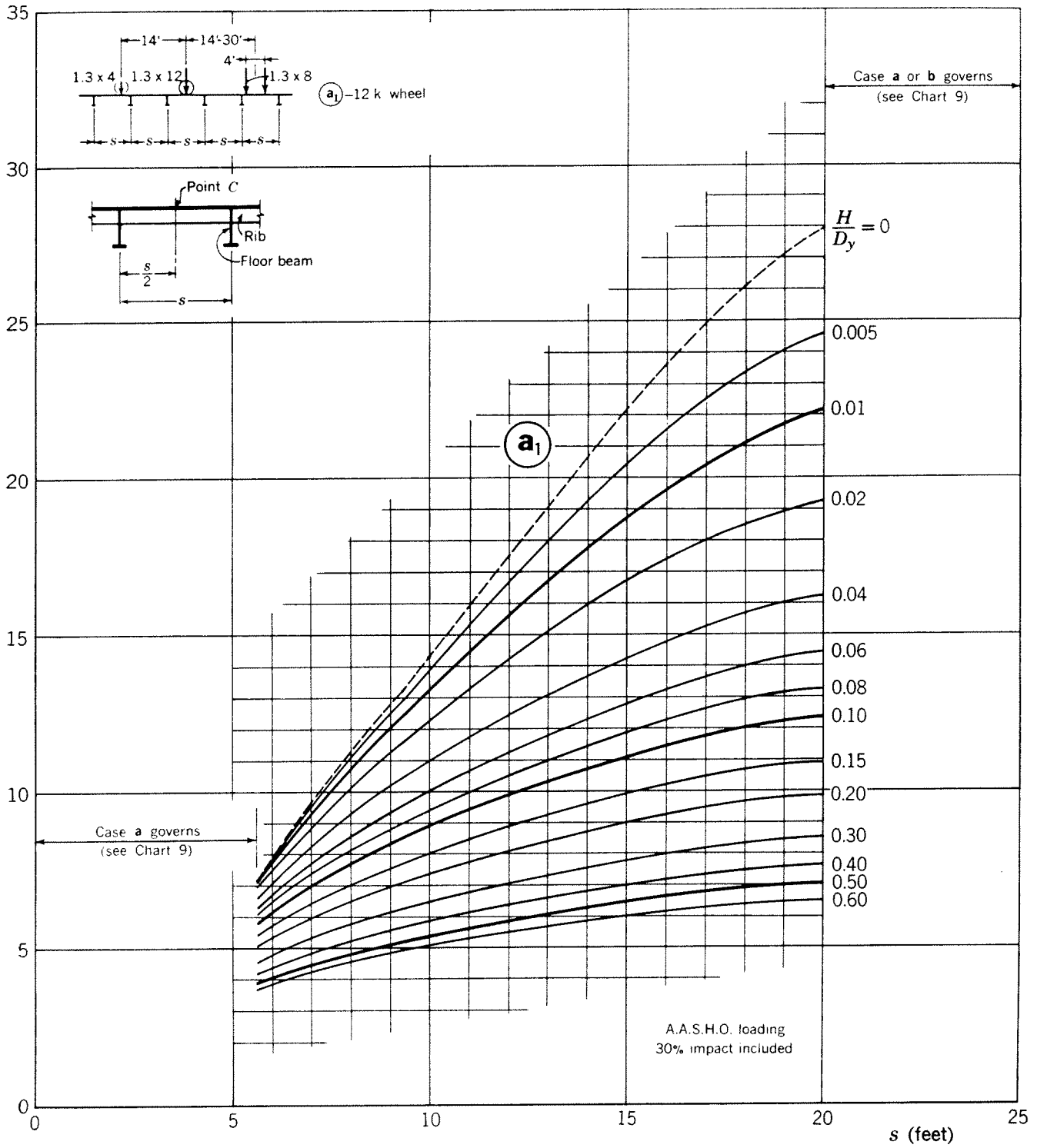


Chart 11. Maximum moment at midspan of the deck with closed ribs on rigid supports, loading a_1

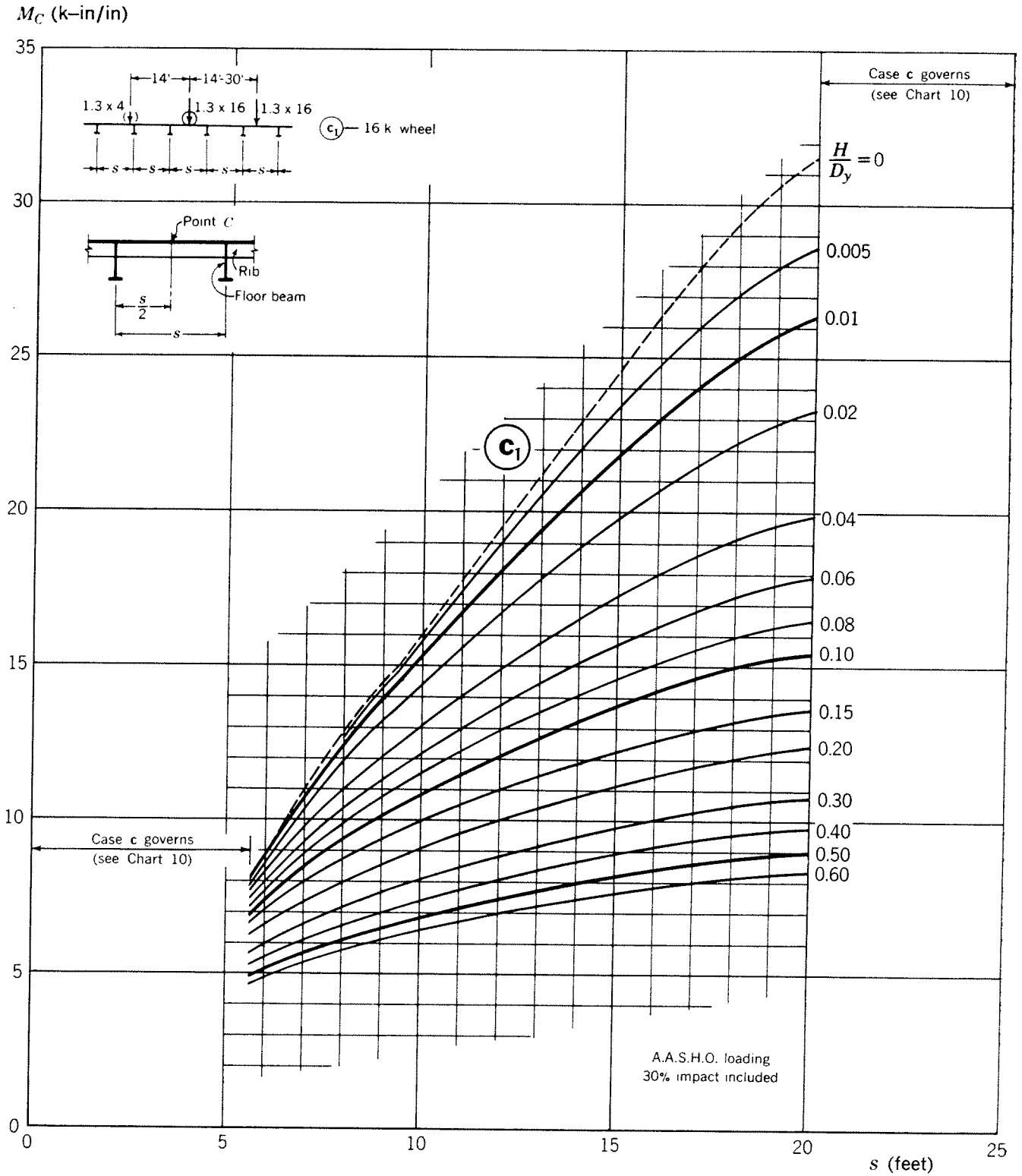


Chart 12. Maximum moment at midspan of the deck with closed ribs on rigid supports, loading c_1

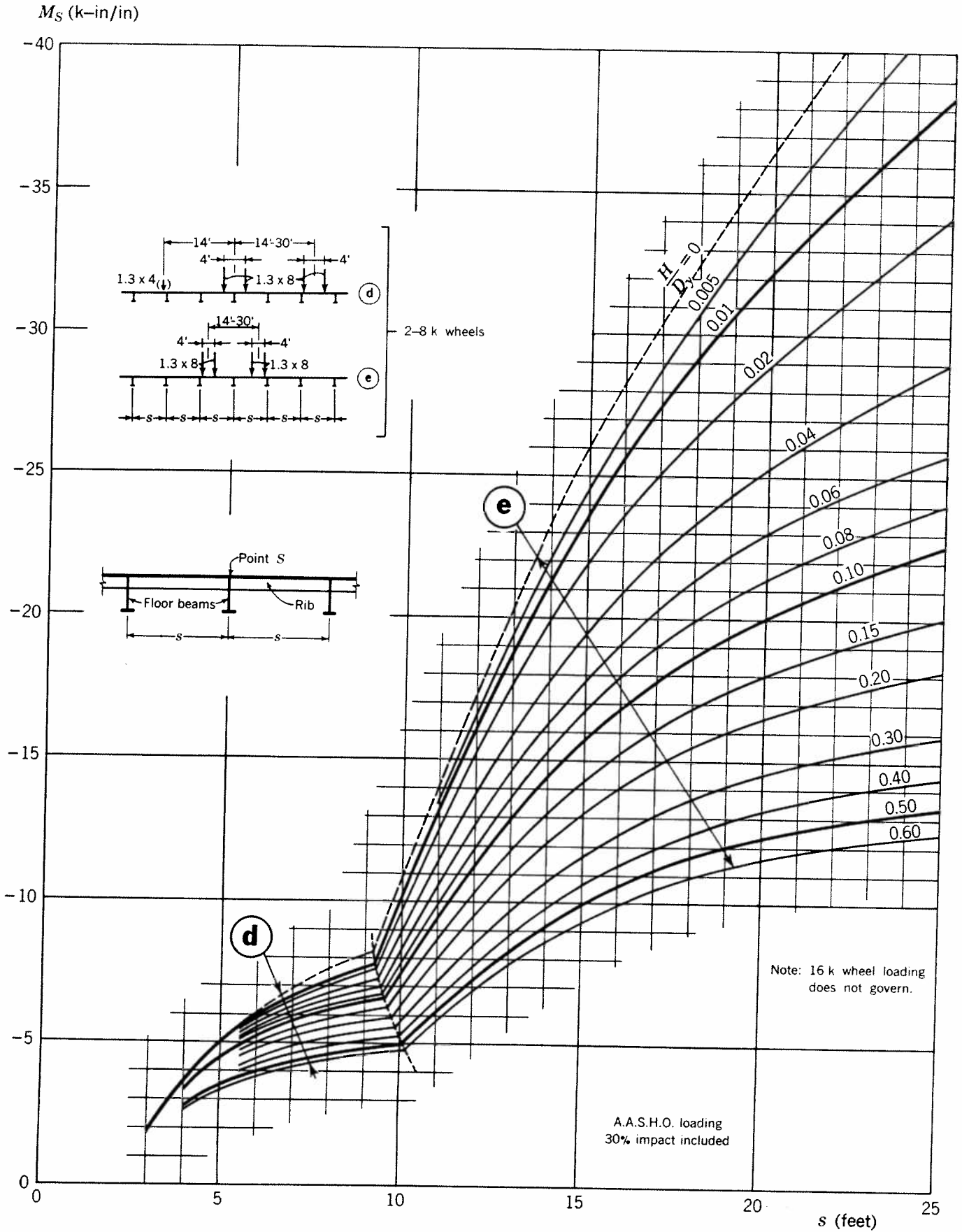
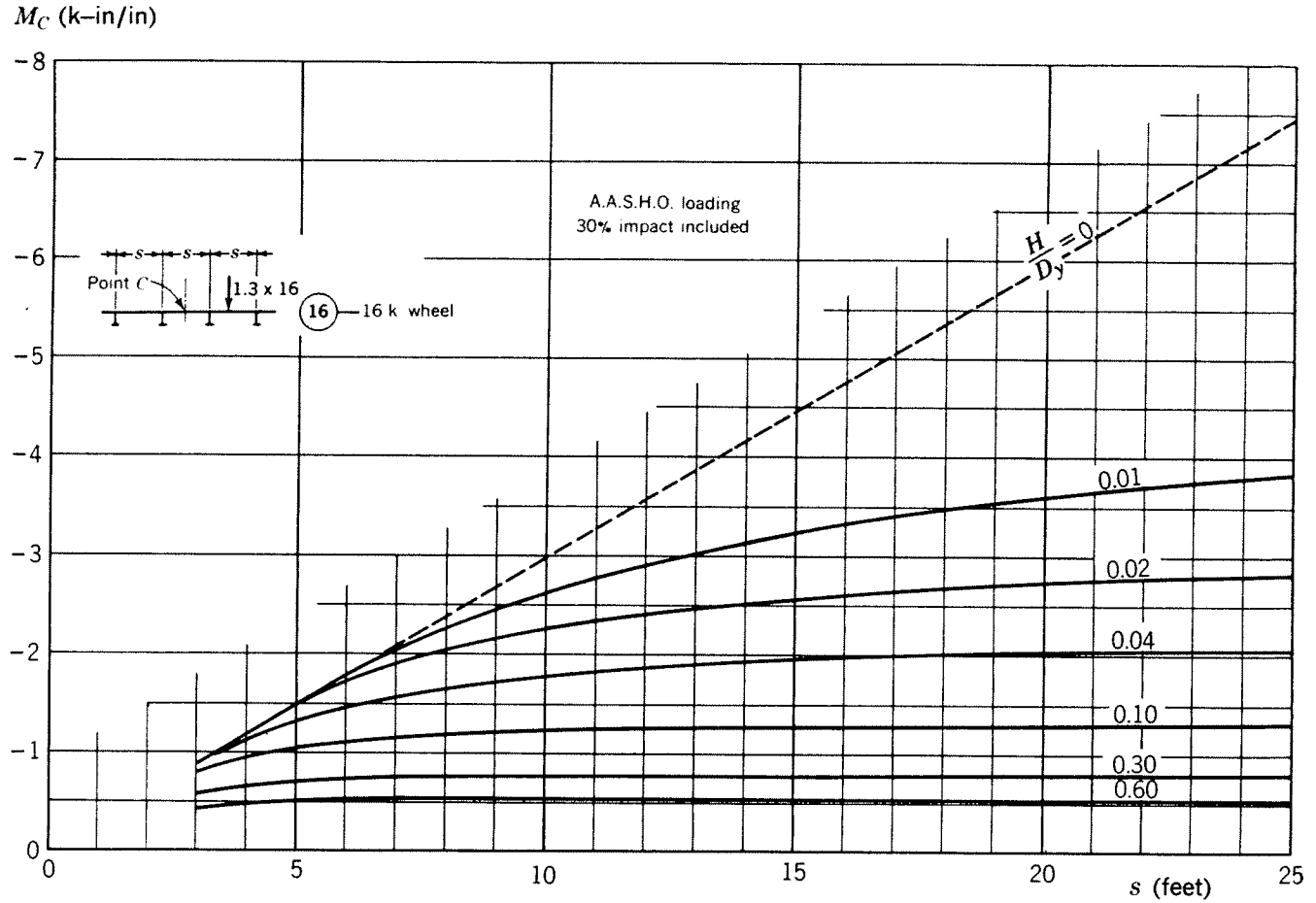
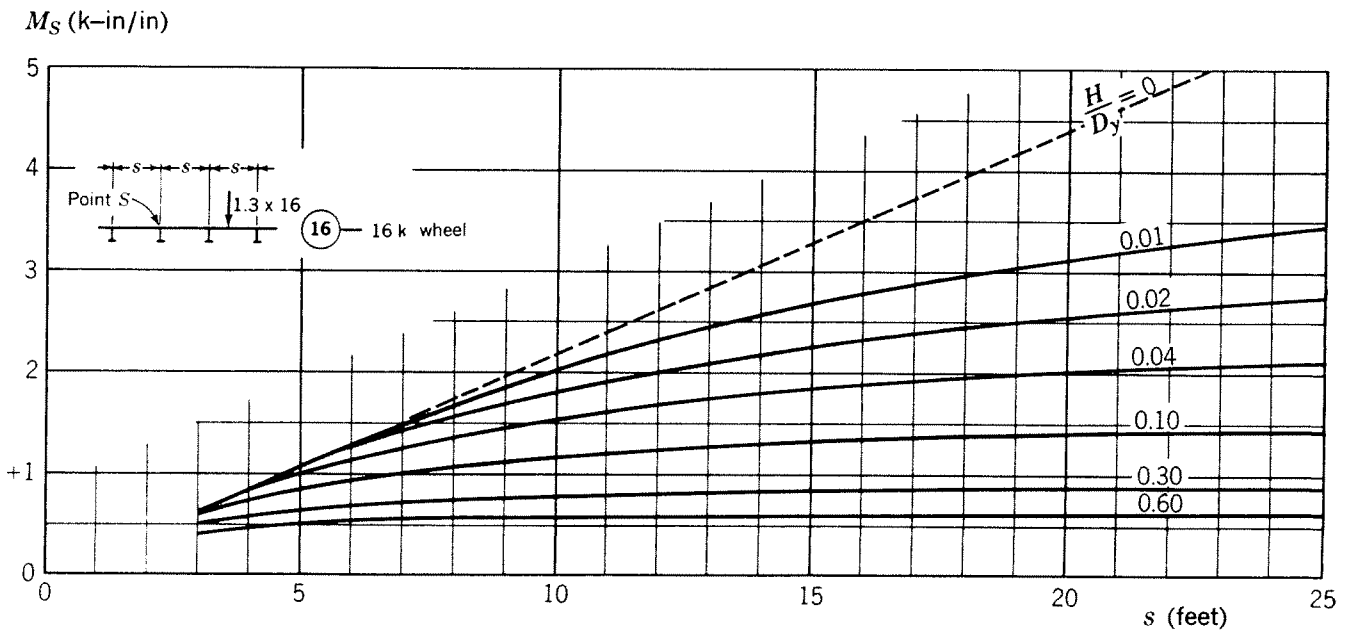


Chart 13. Maximum moment at support of the deck with closed ribs on rigid supports



(a) Negative moment at midspan



(b) Positive moment at support

Chart 14. Maximum moments for computing alternating stresses in the deck with closed ribs

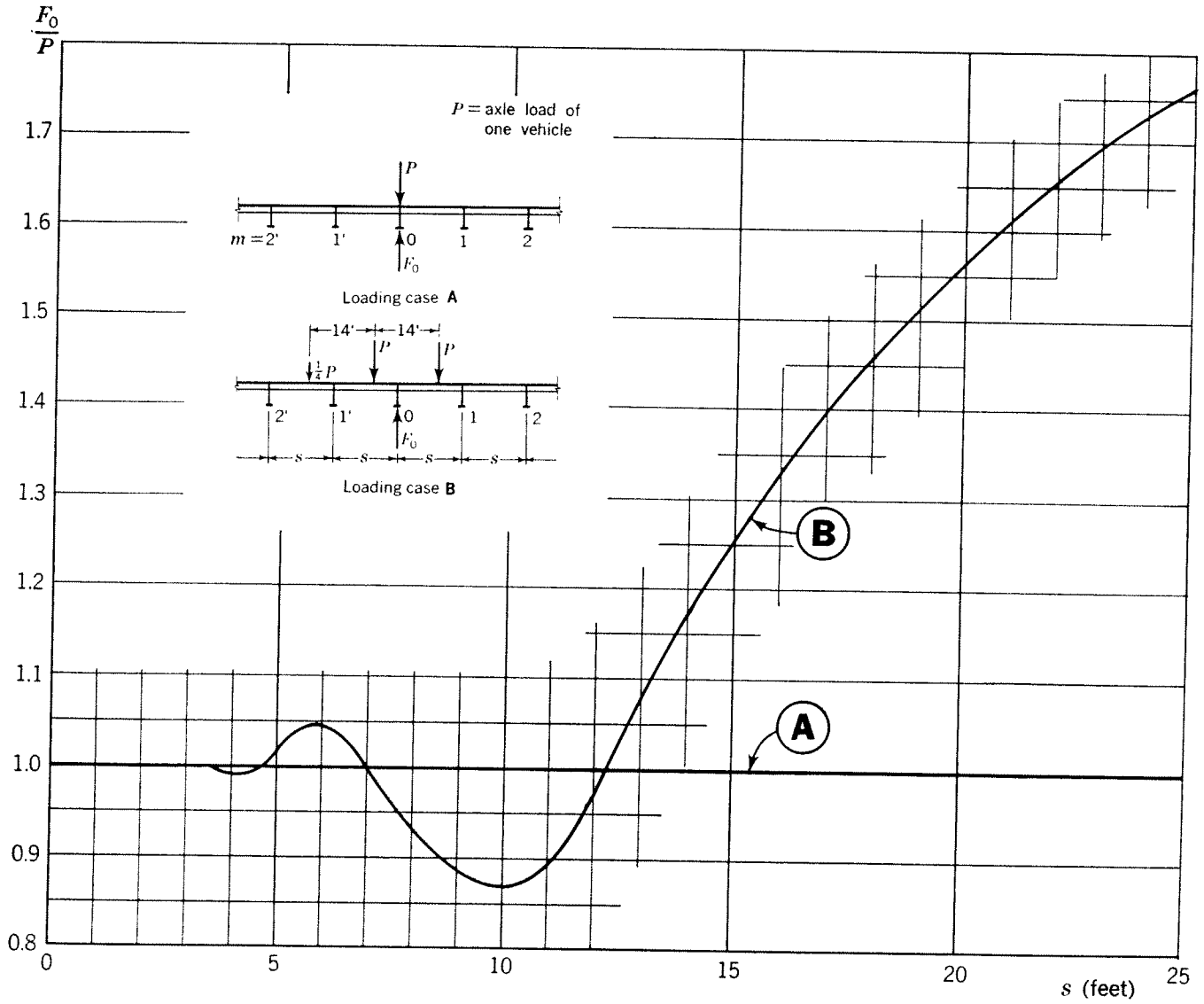


Chart 15. Maximum load, F_0 , on a rigid floor beam due to one AASHO vehicle

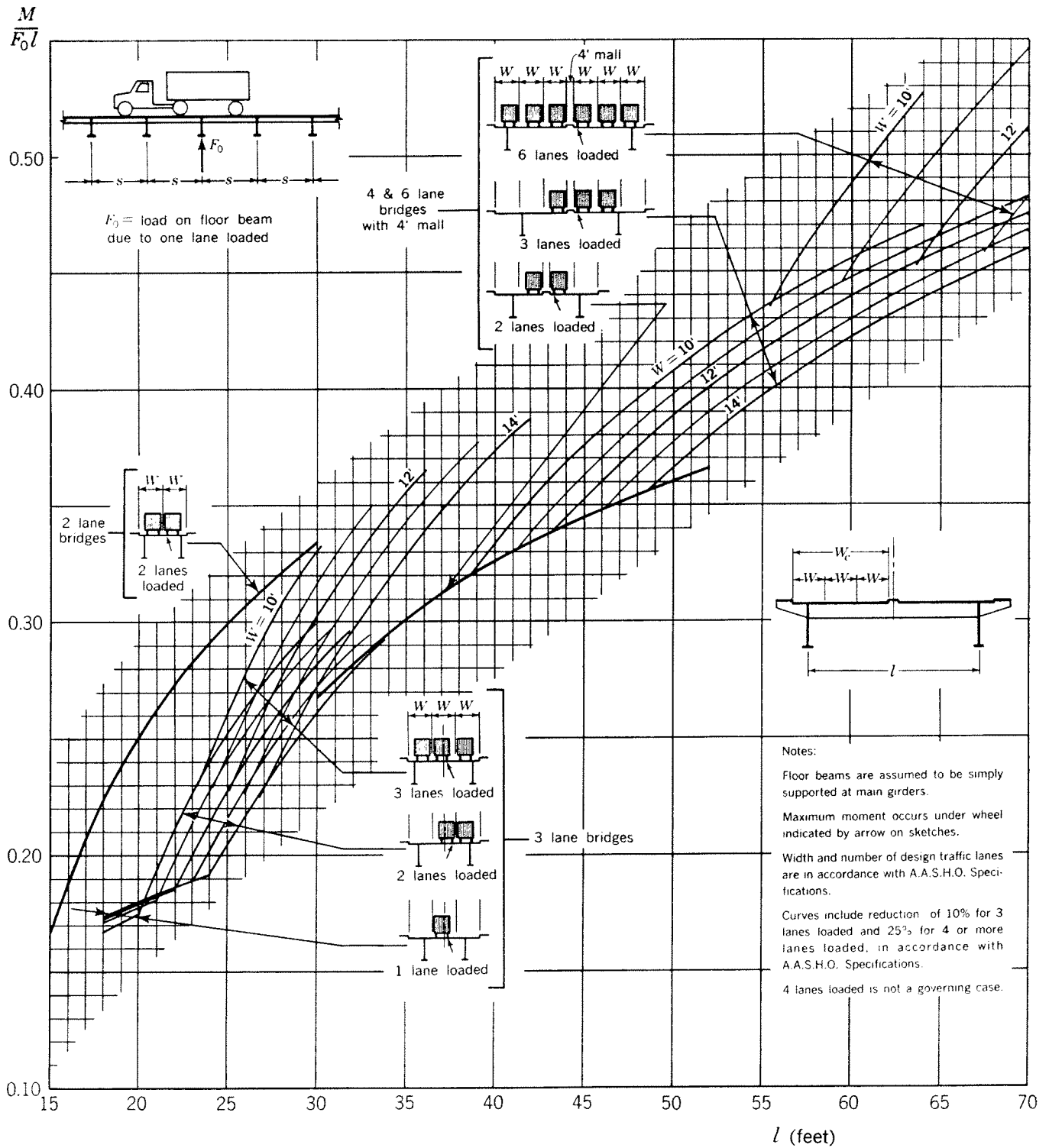


Chart 16. Maximum live load moment in a rigid floor beam

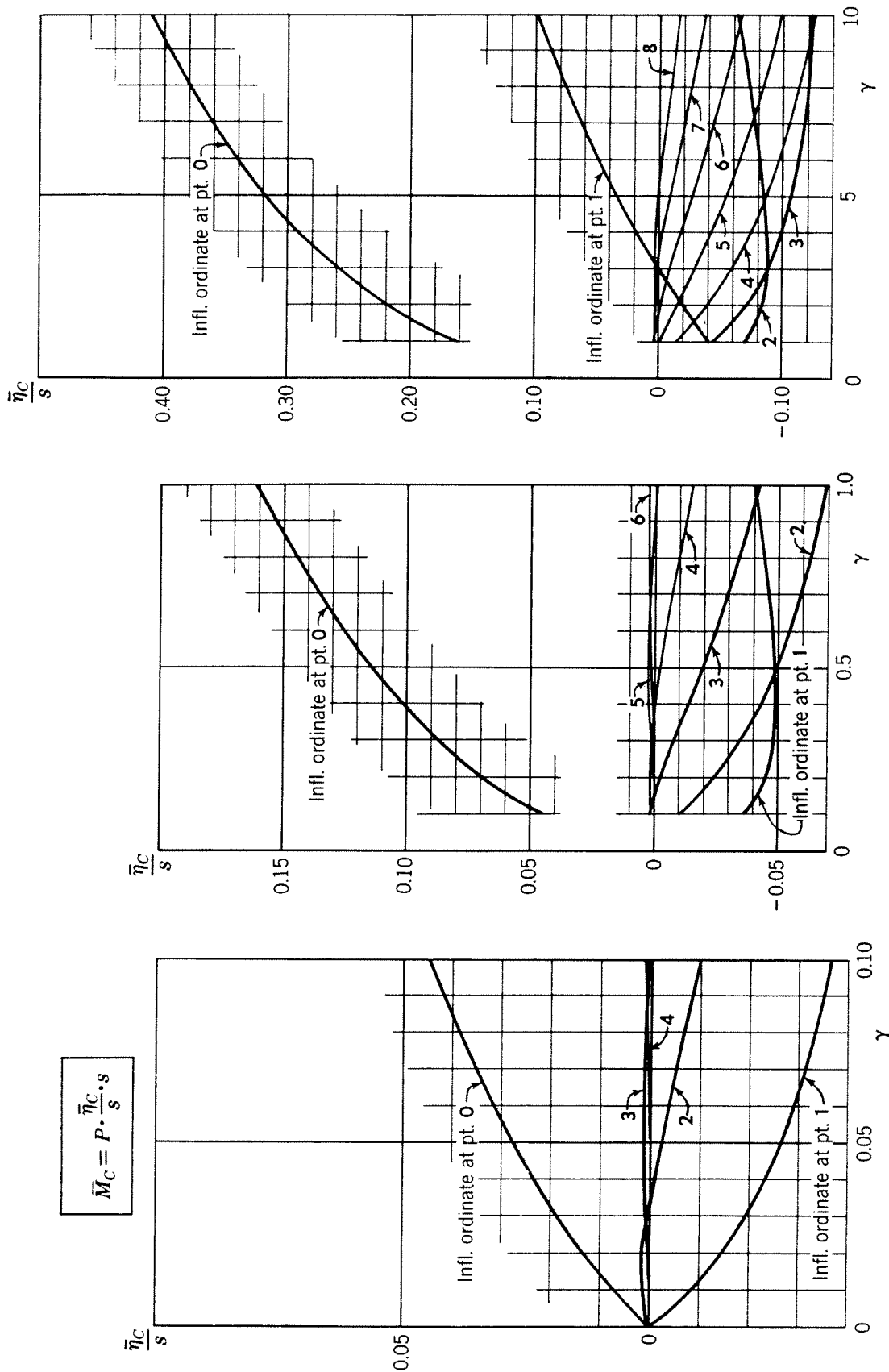


Chart 17. Influence ordinates for moment at midspan of a continuous beam on elastic supports

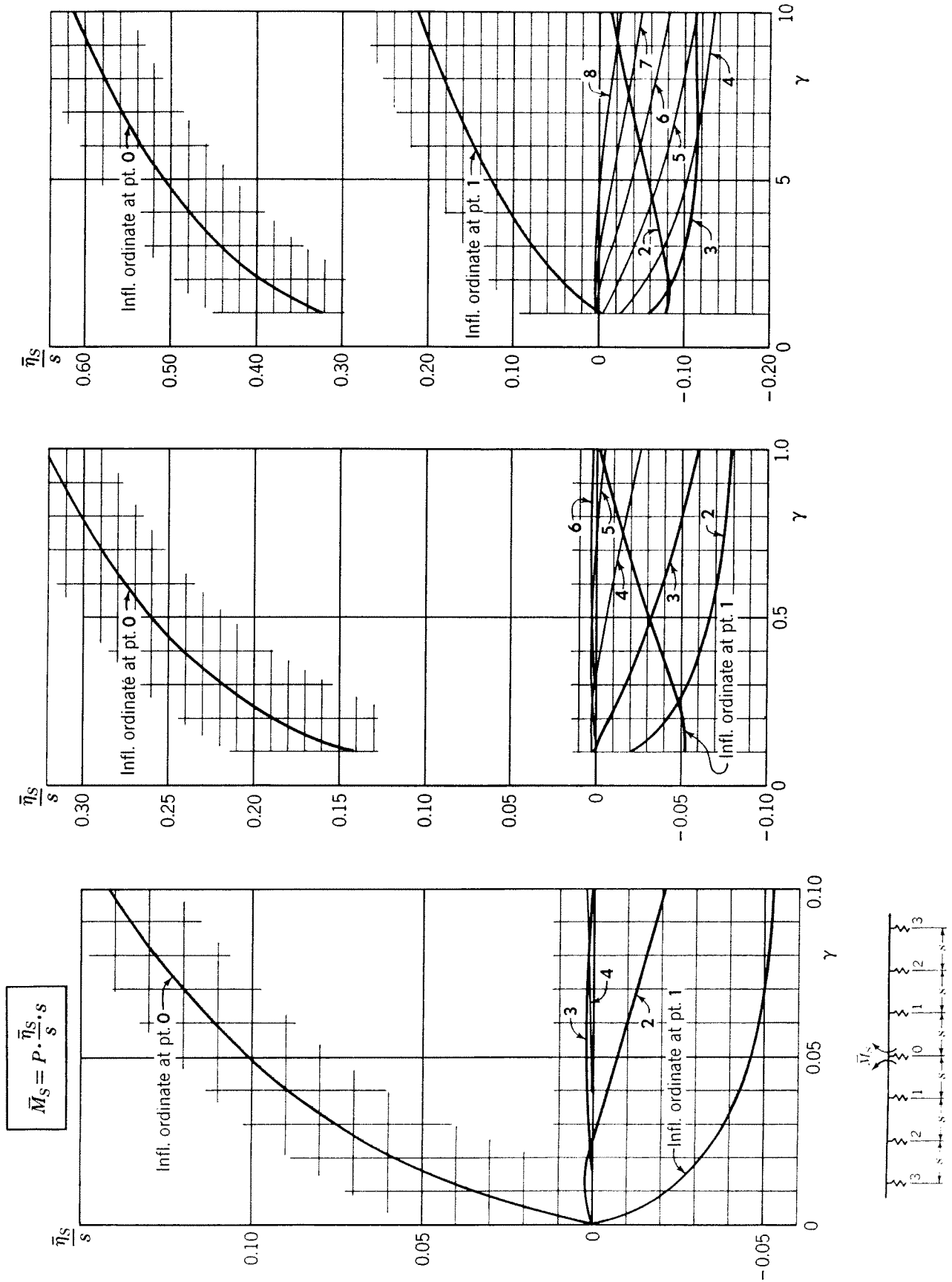


Chart 18. Influence ordinates for moment at support of a continuous beam on elastic supports

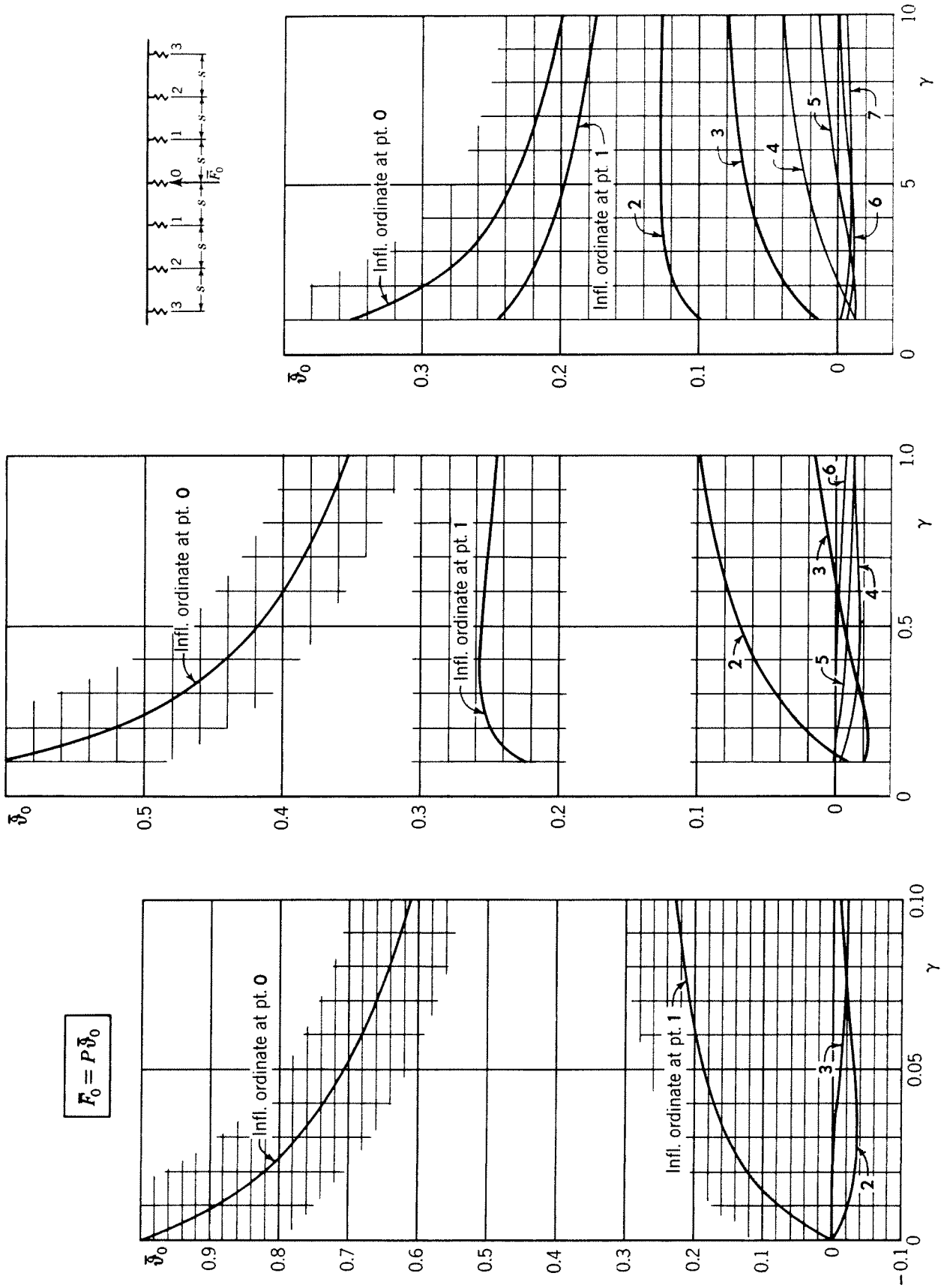


Chart 19. Influence ordinates for reaction at point 0 of a continuous beam on elastic supports

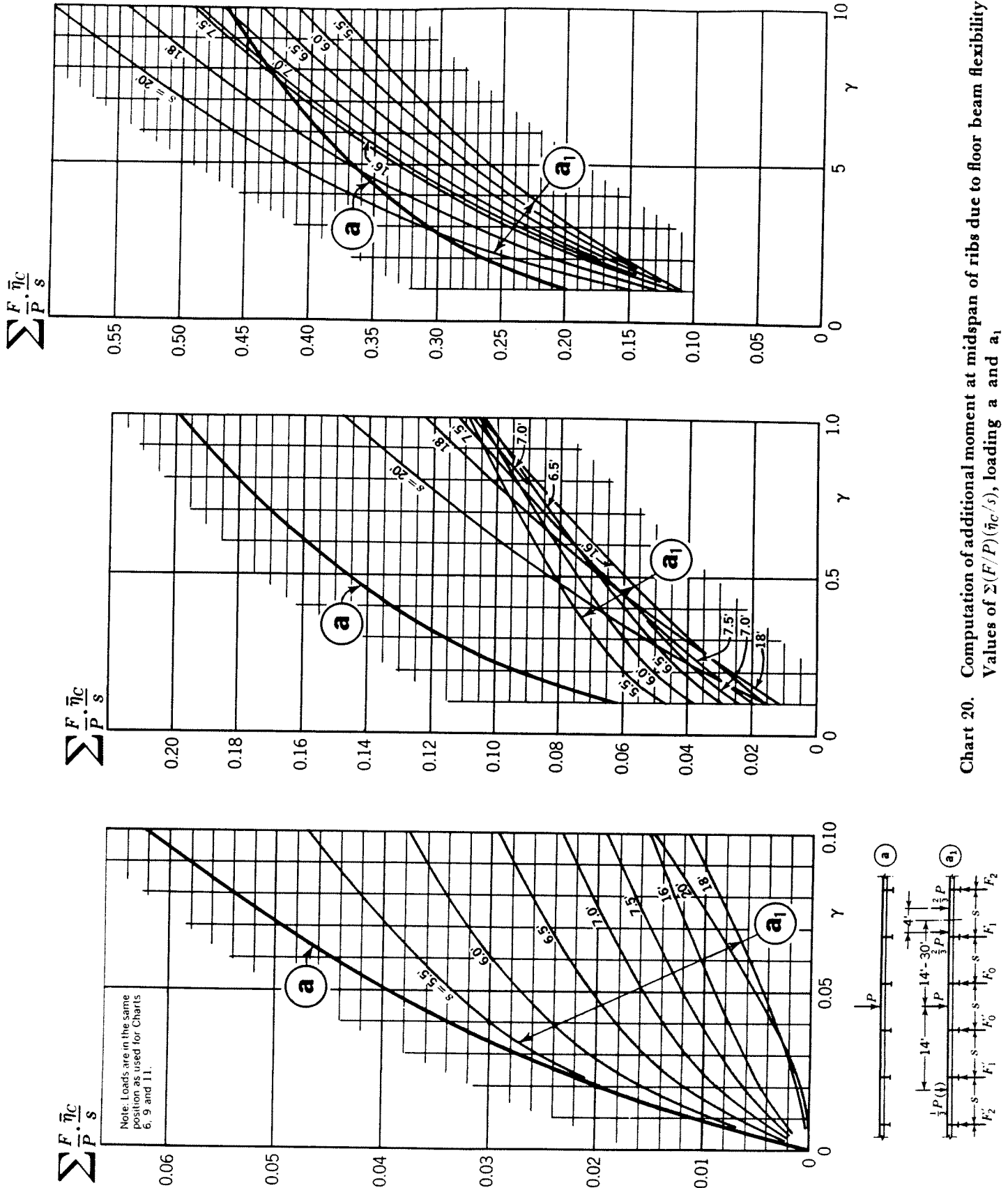


Chart 20. Computation of additional moment at midspan of ribs due to floor beam flexibility. Values of $\Sigma(F/P)(\eta_c/s)$, loading a and a_1

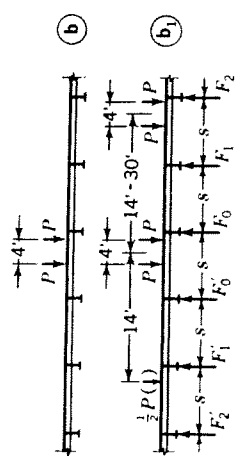
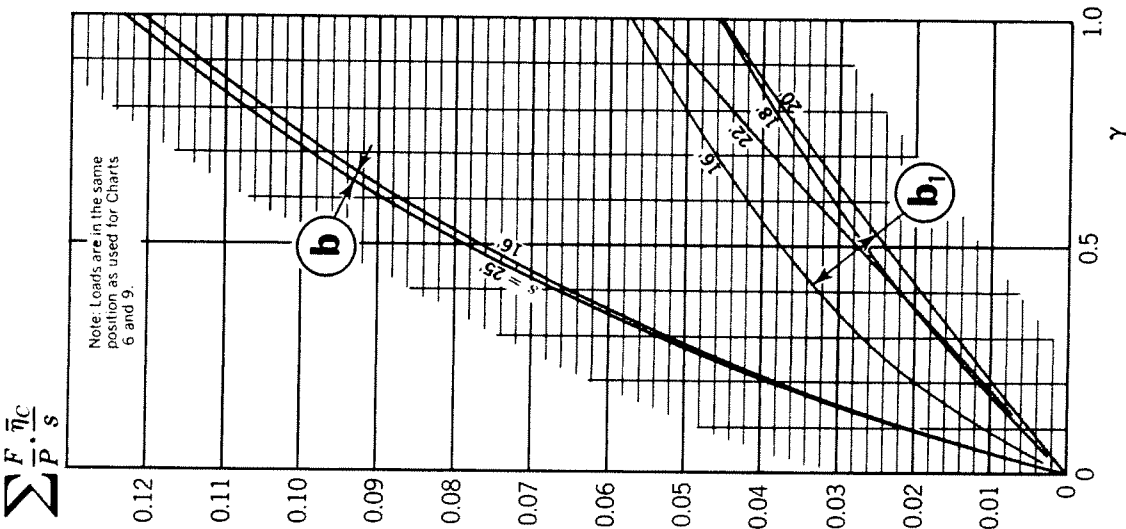
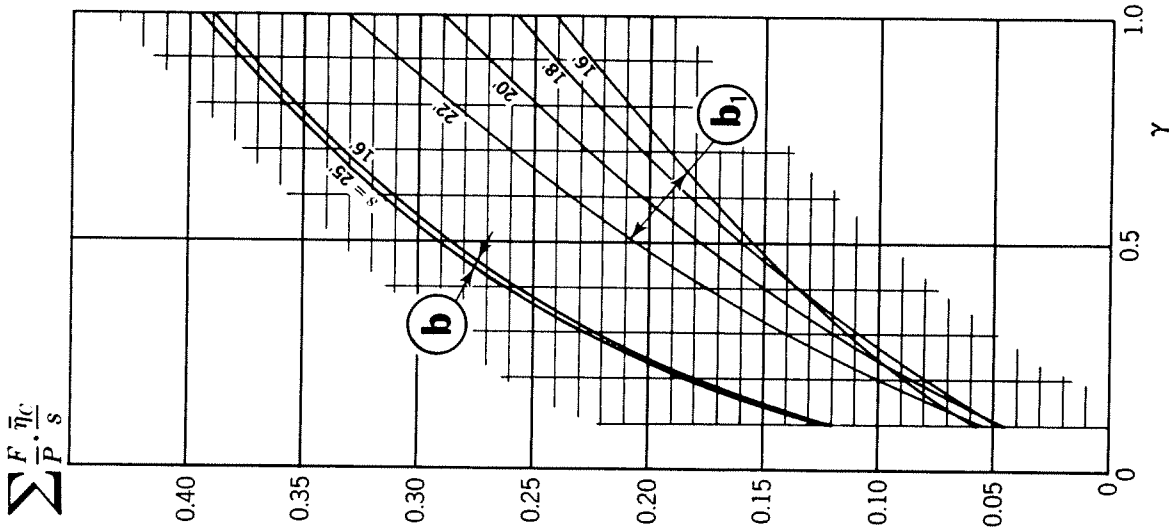
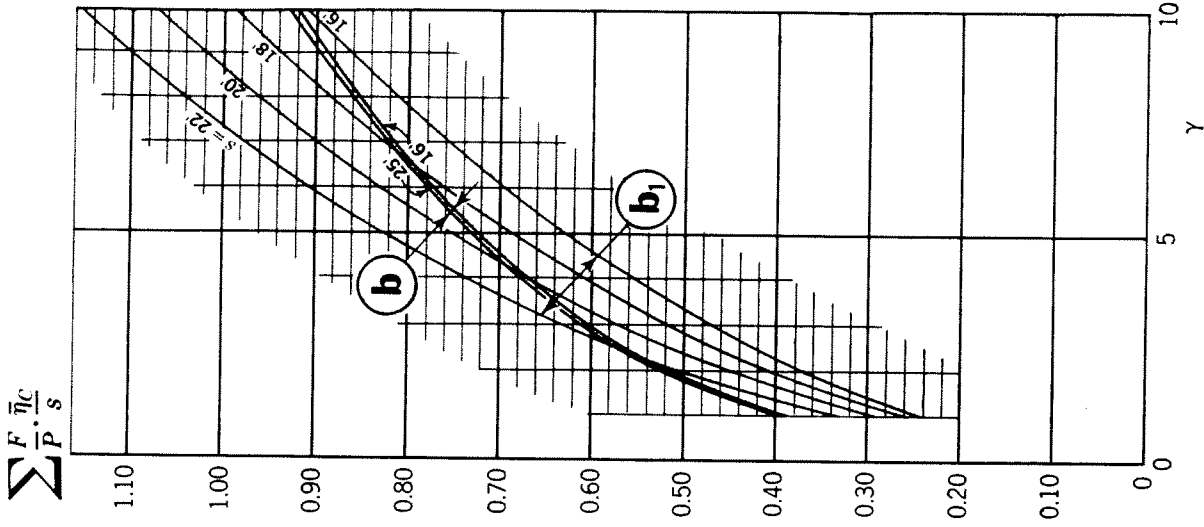


Chart 21. Computation of additional moment at midspan of ribs due to floor beam flexibility. Values of $\Sigma(F/P)(\bar{\eta}_c/s)$, loading b and b_1

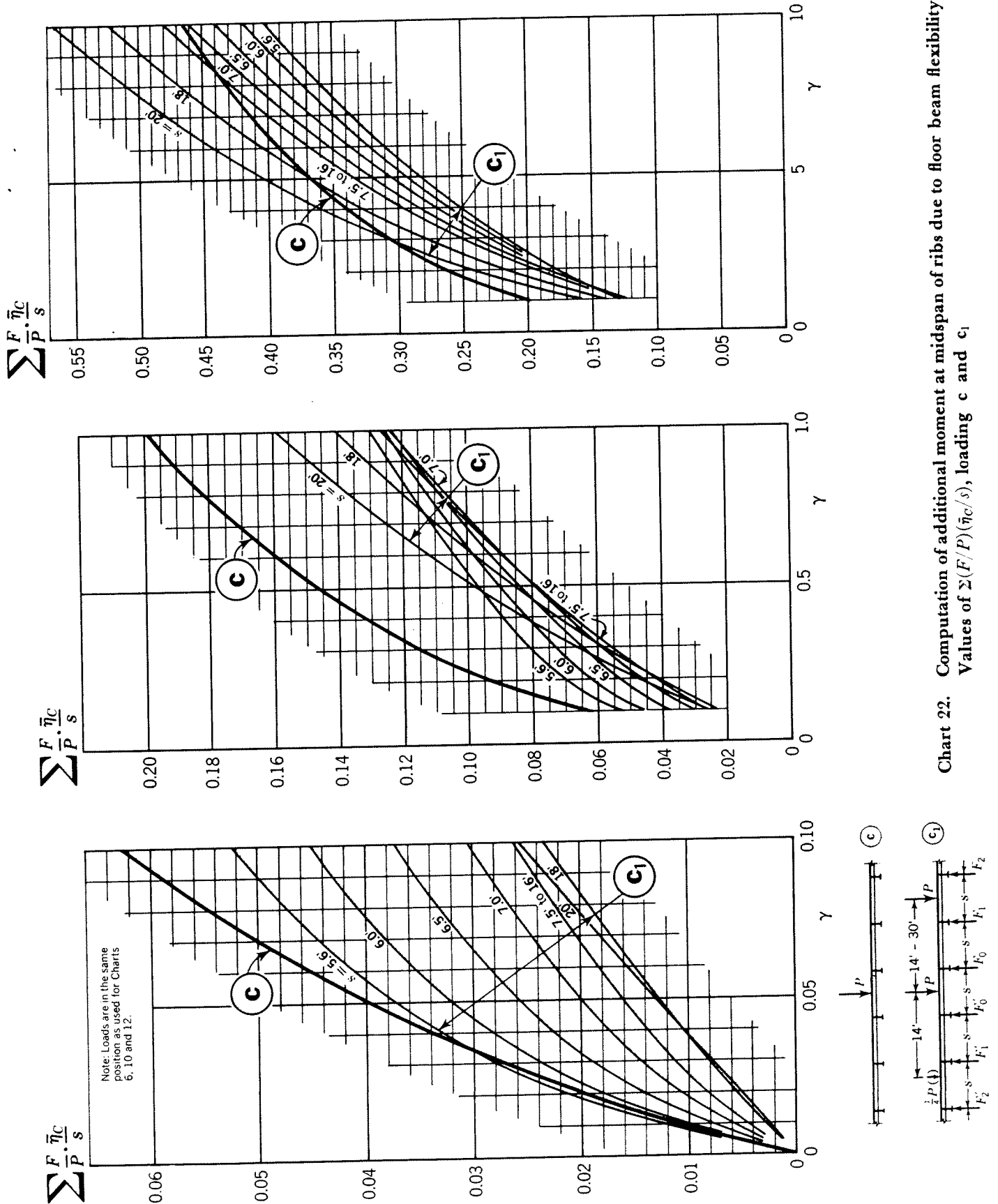


Chart 22. Computation of additional moment at midspan of ribs due to floor beam flexibility. Values of $\Sigma(F/P)(\pi c/s)$, loading **c** and **c1**

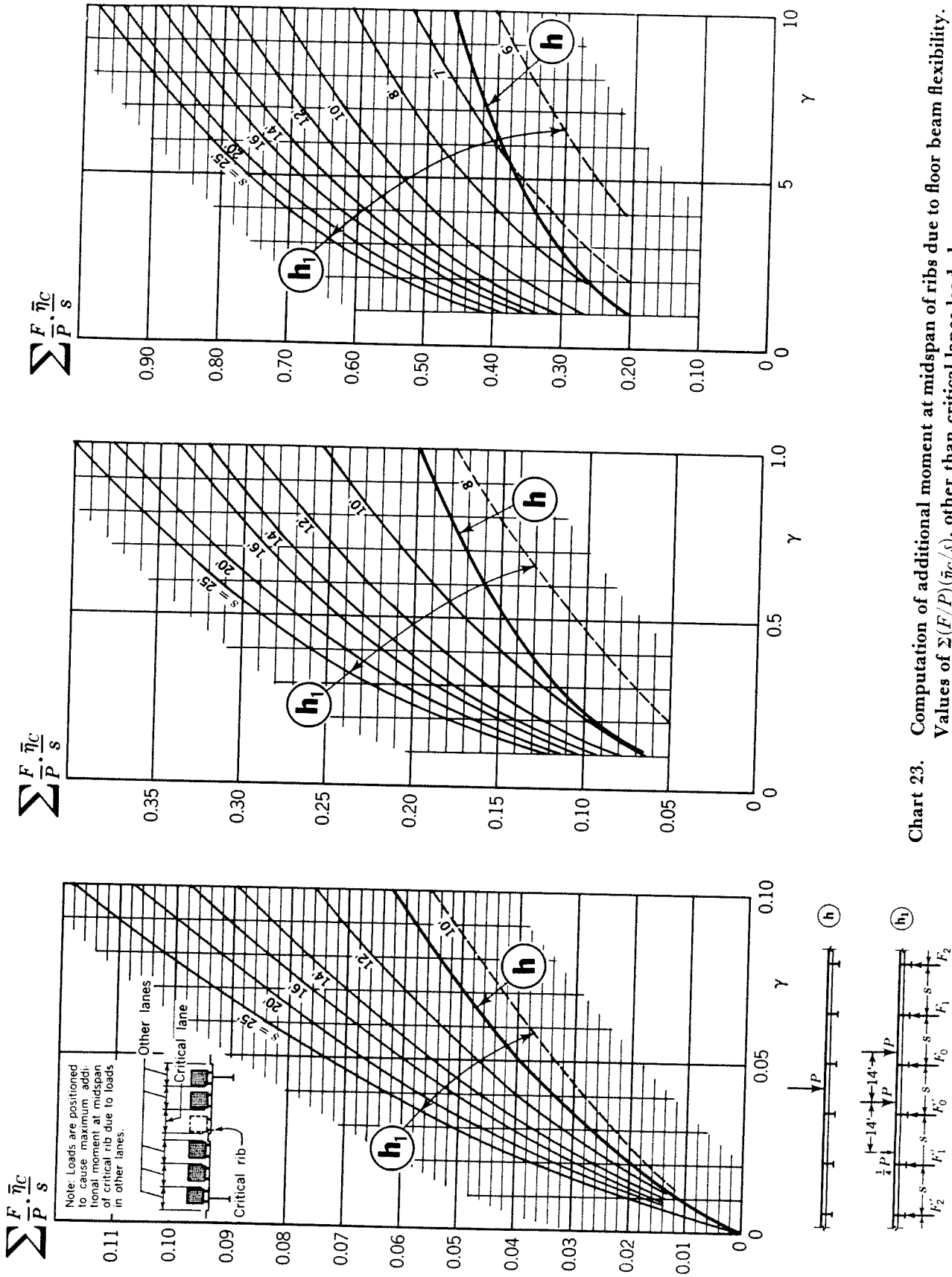


Chart 23. Computation of additional moment at midspan of ribs due to floor beam flexibility. Values of $\Sigma(F/P)(\bar{\pi}c/s)$, other than critical lanes loaded

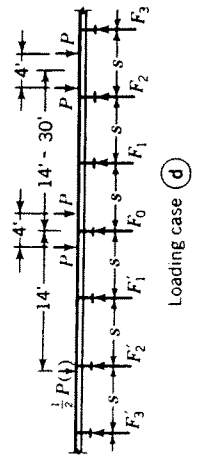
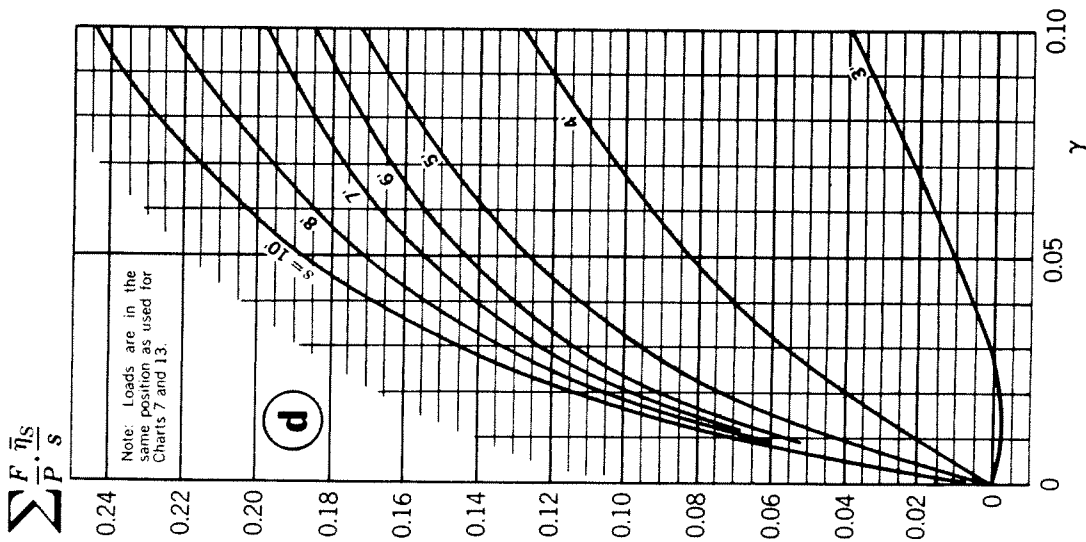
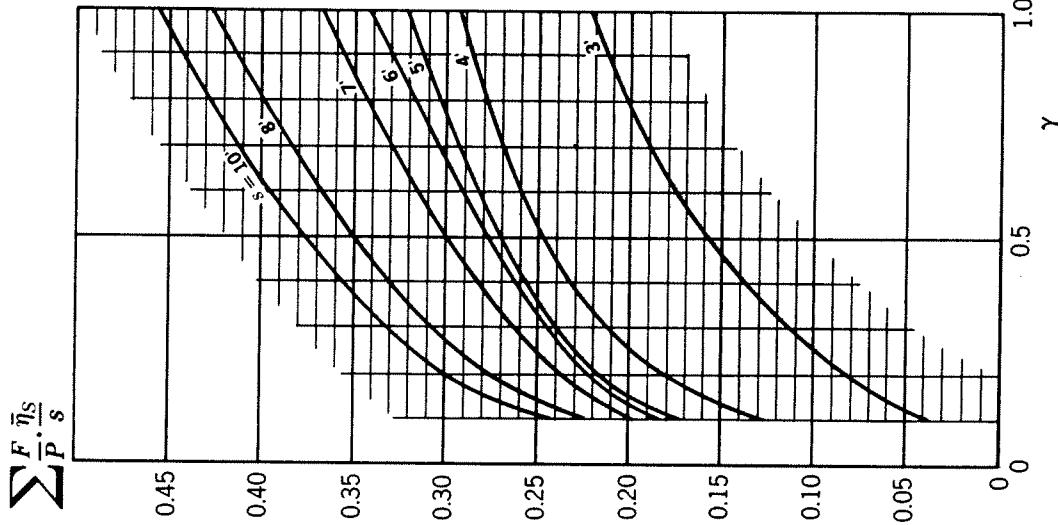
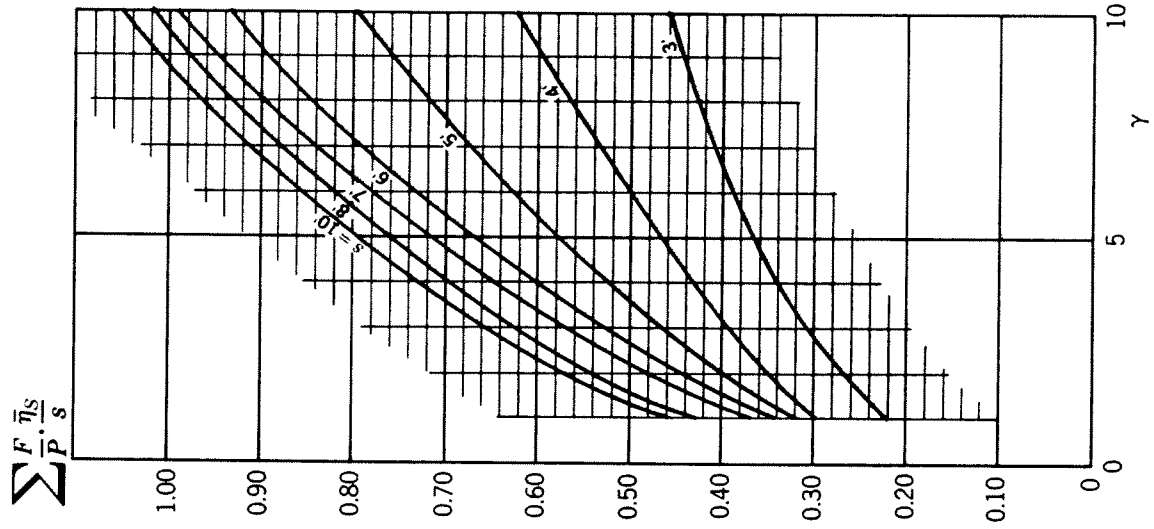


Chart 24. Computation of moment relief at the support of ribs due to floor beam flexibility. Values of $\Sigma(F/P)(\bar{\eta}_s/s)$, loading d

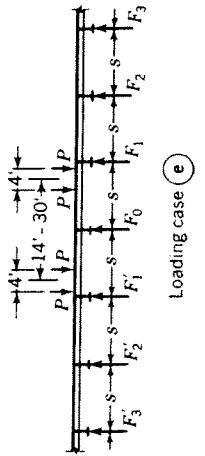
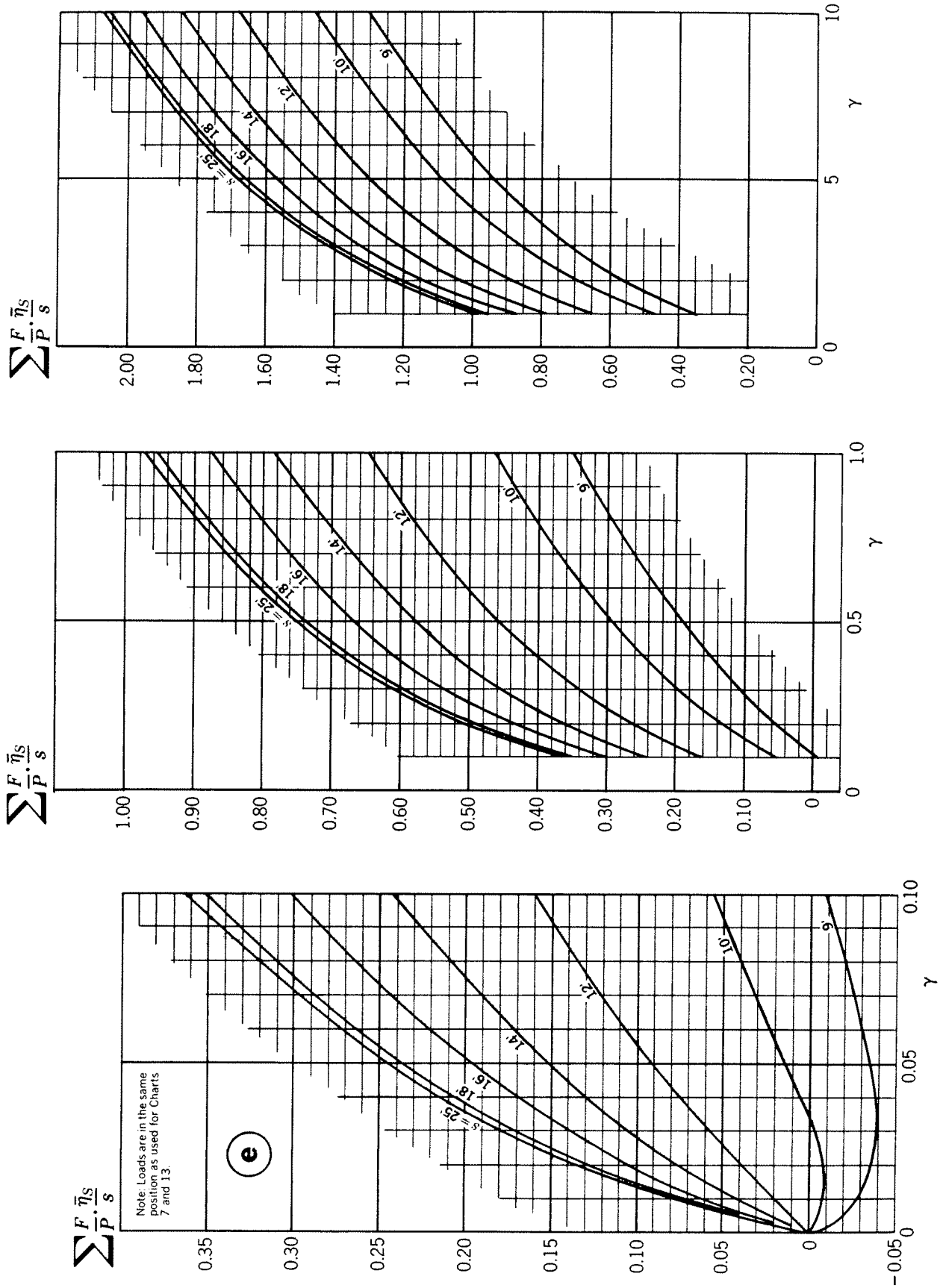


Chart 25. Computation of moment relief at the support of ribs due to floor beam flexibility. Values of $\sum(F/P)(\eta_s/s)$, loading e

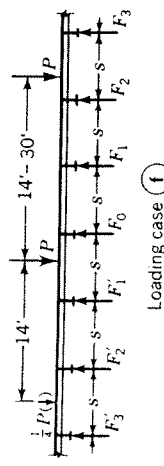
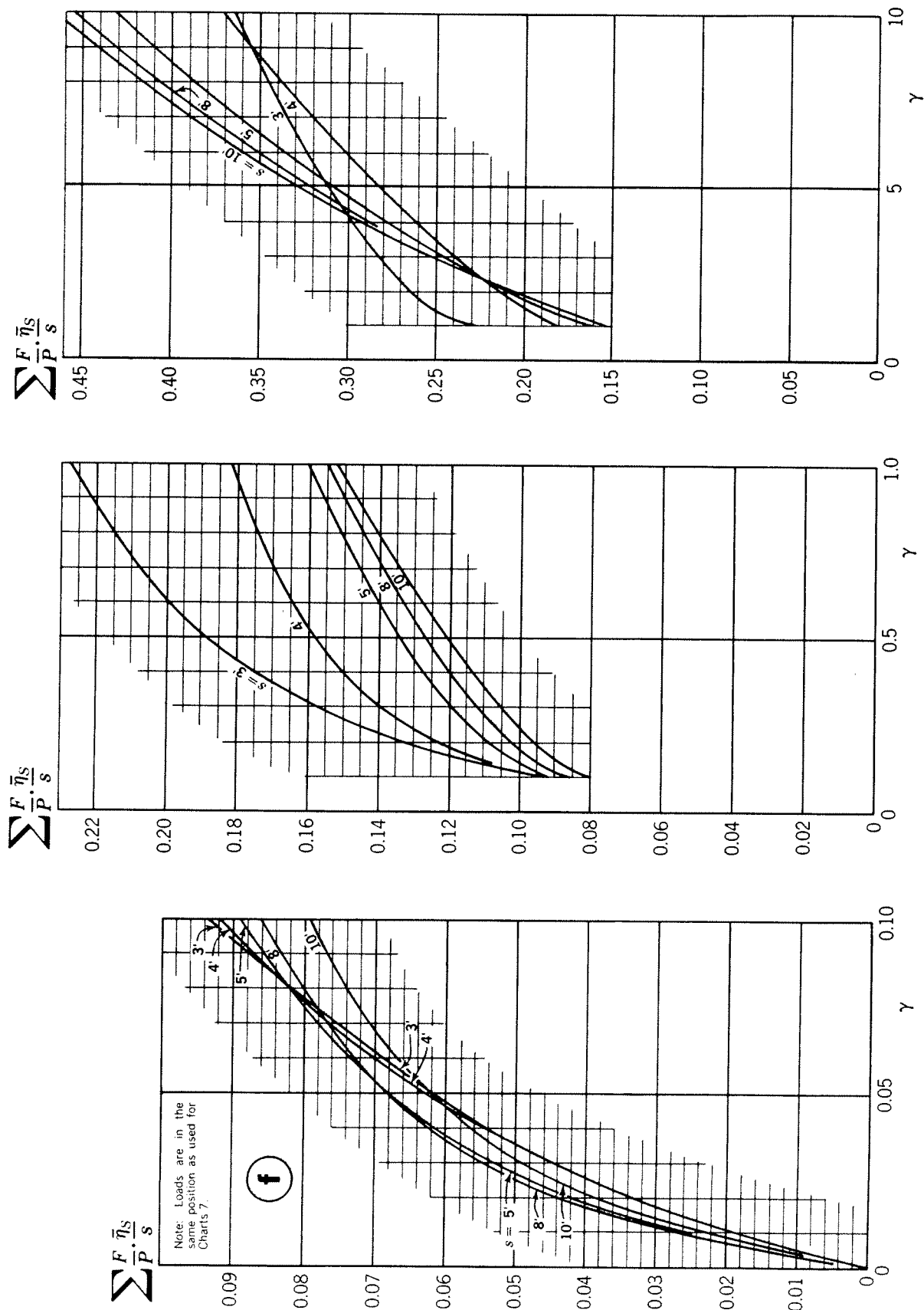


Chart 26. Computation of moment relief at the support of ribs due to floor beam flexibility. Values of $\Sigma(F/P)(\bar{\eta}_s/s)$, loading **f**

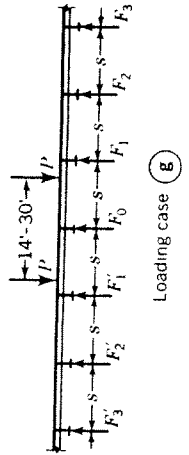
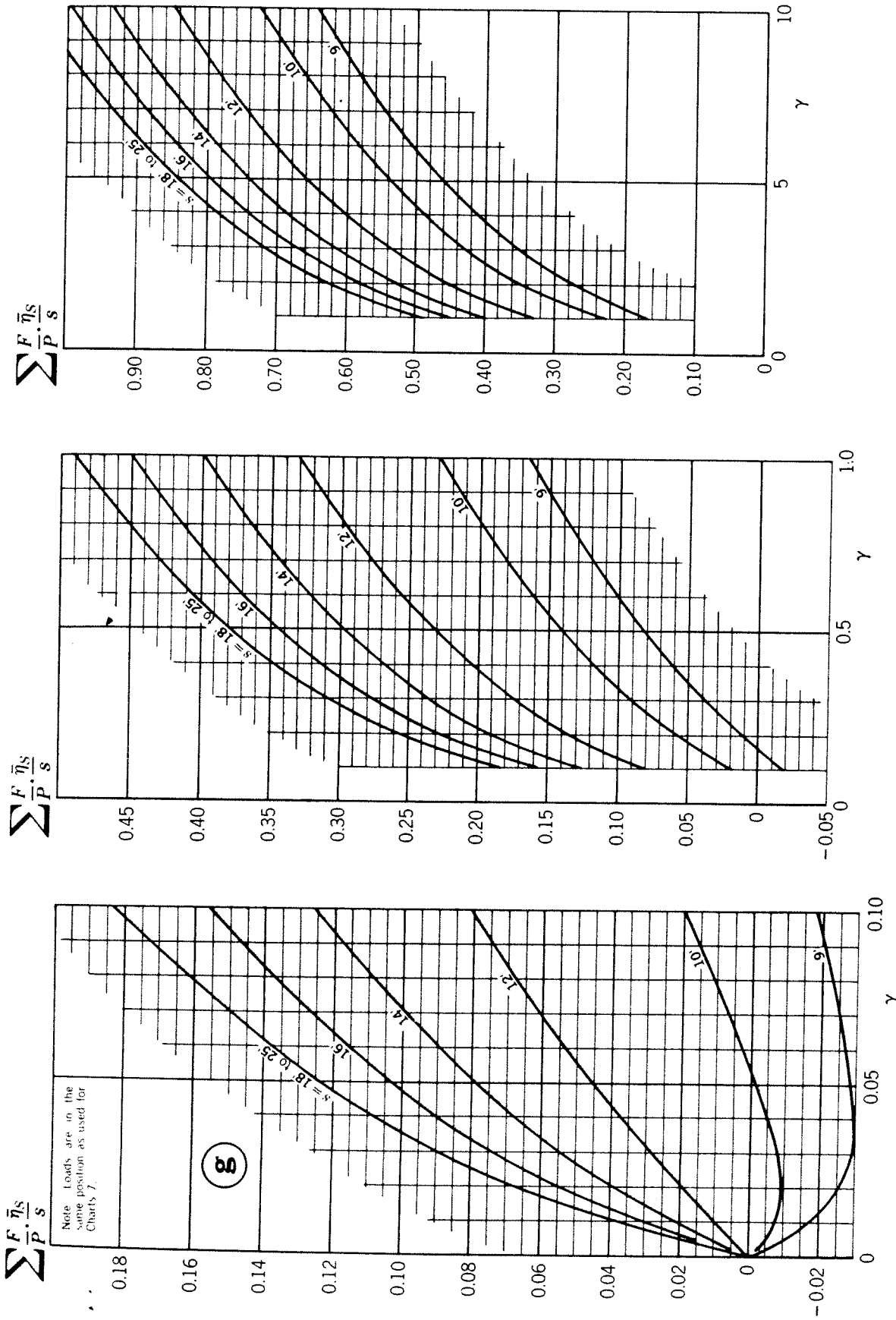


Chart 27. Computation of moment relief at the support of ribs due to floor beam flexibility. Values of $\sum(F_i/P)(\eta_i/s)$, loading g

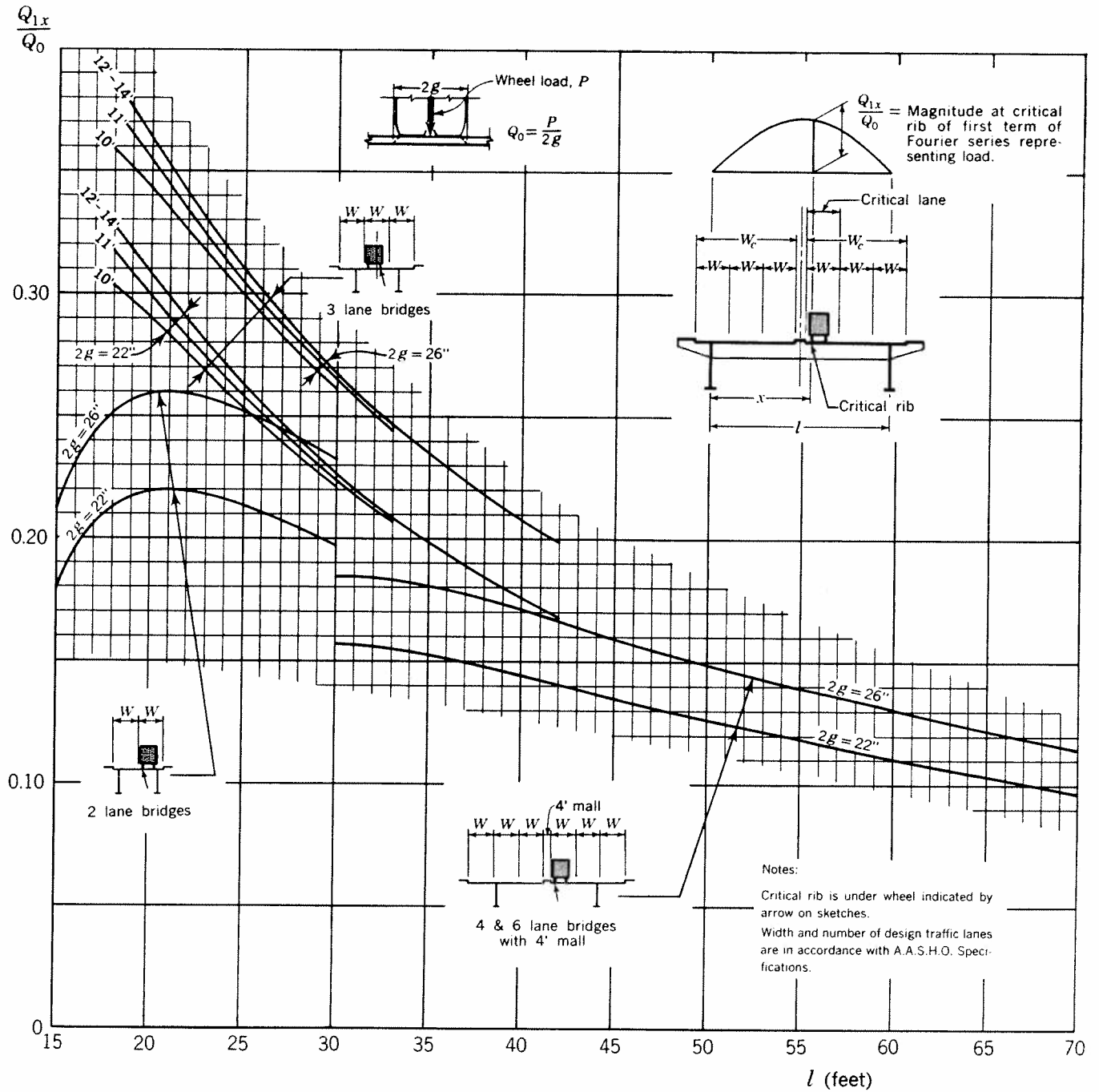


Chart 28. Computation of additional moment in ribs due to floor beam flexibility. Values of Q_{1x}/Q_0 at critical rib, lane over critical rib loaded

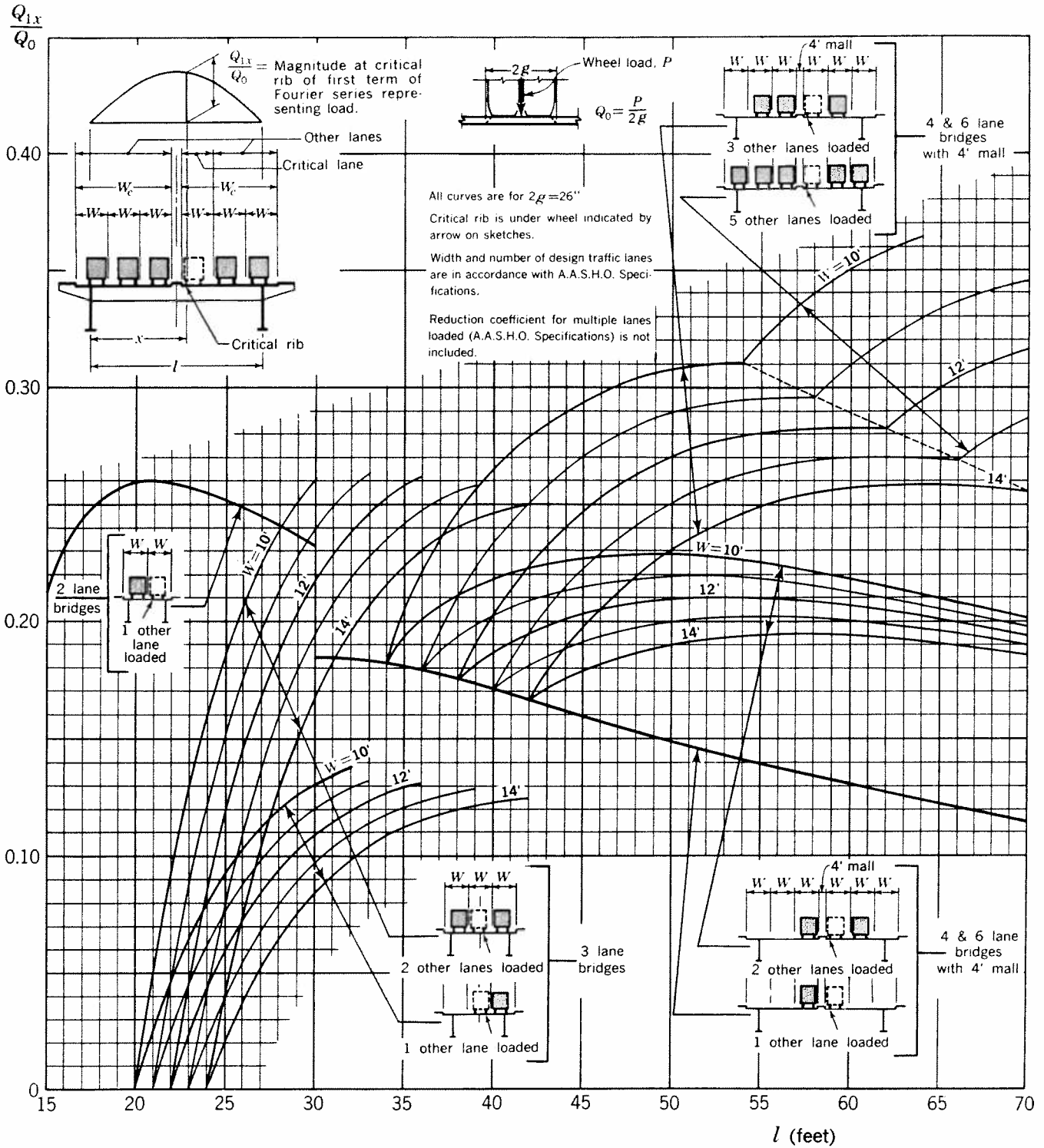


Chart 29. Computation of additional moment in ribs due to floor beam flexibility. Values of Q_{1x}/Q_0 at critical rib, lane over critical rib loaded

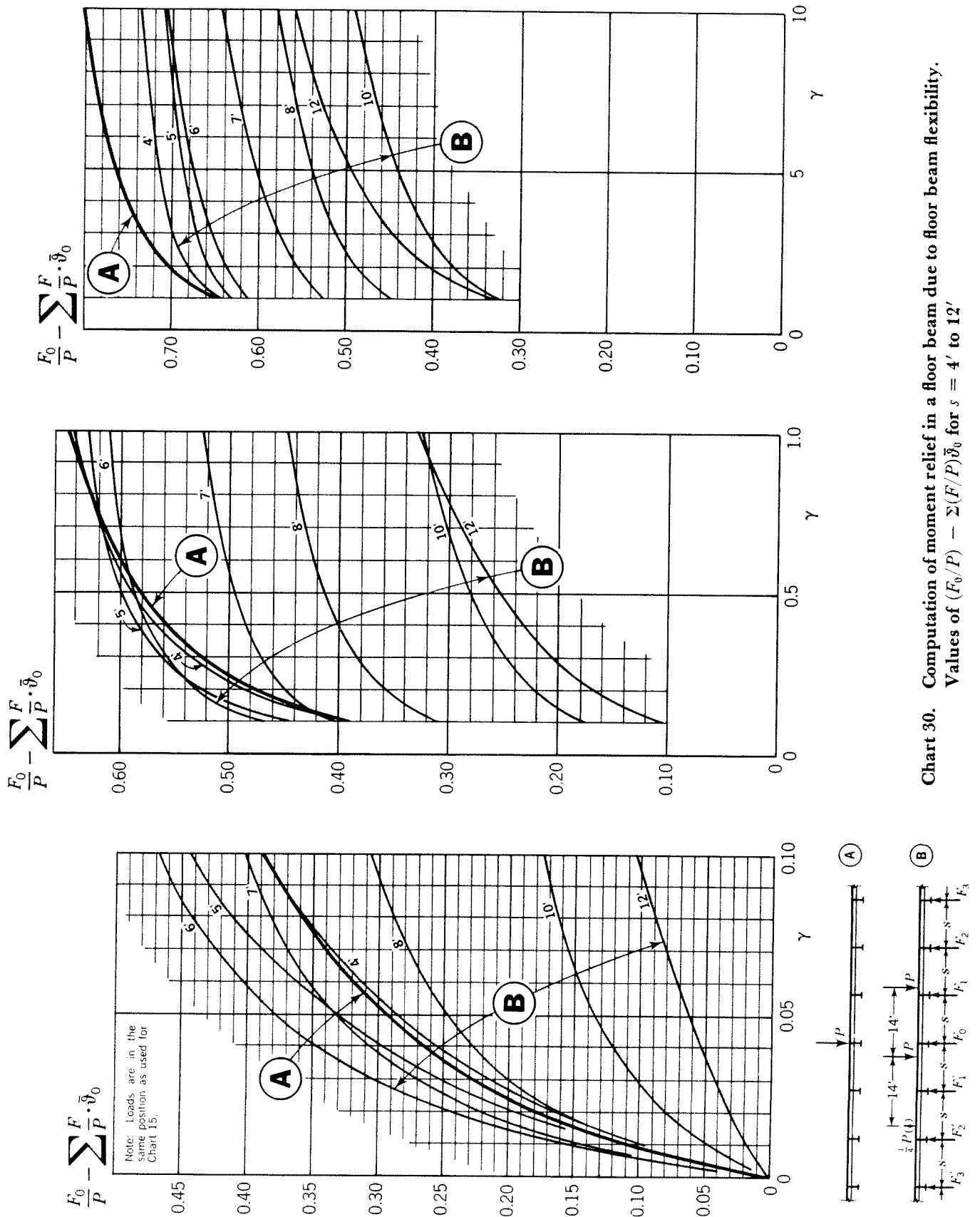
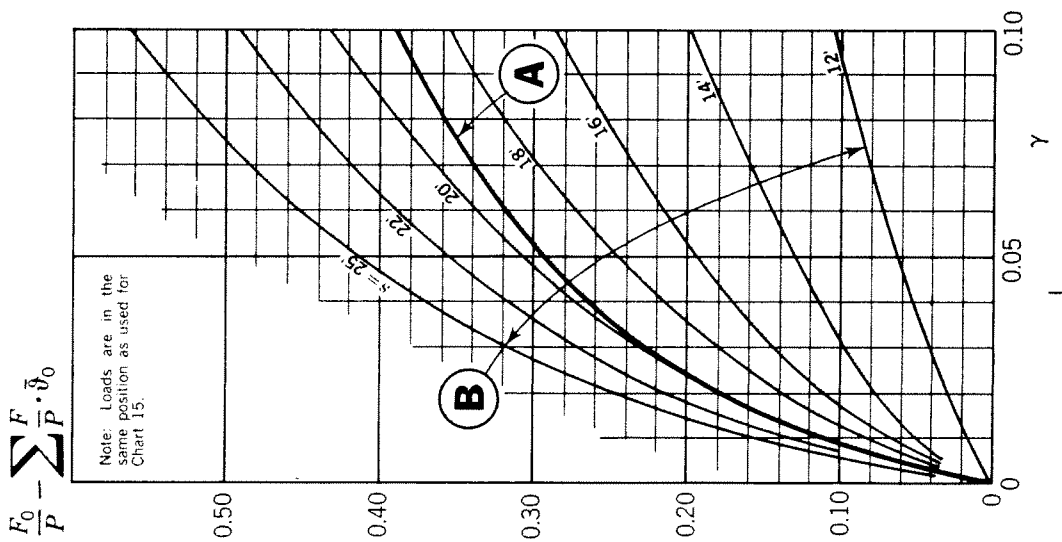
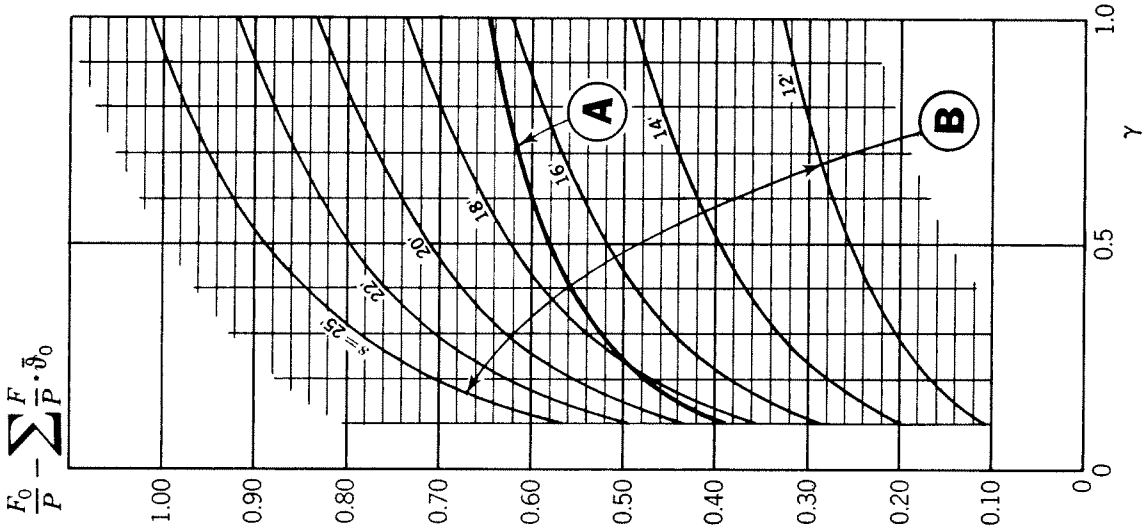
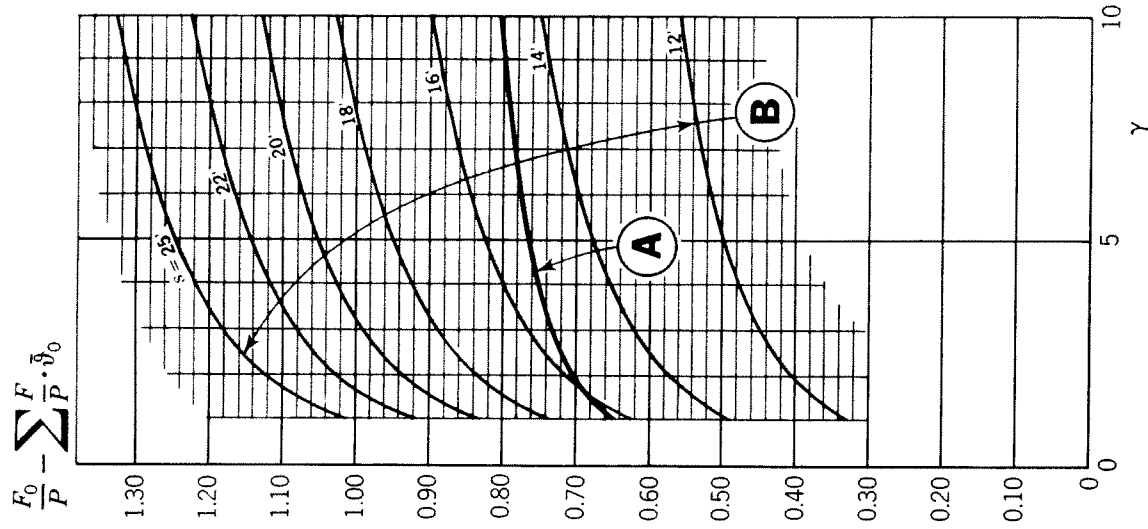


Chart 30. Computation of moment relief in a floor beam due to floor beam flexibility. Values of $(F_0/P) - \sum(F/P)\delta_0$ for $s = 4'$ to $12'$



Note: Loads are in the same position as used for Chart 15.

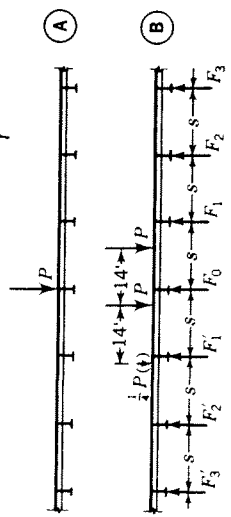


Chart 31. Computation of moment relief in a floor beam due to floor beam flexibility. Values of $(F_0/P) - \sum(F/P)\delta_0$ for $s = 12'$ to $25'$

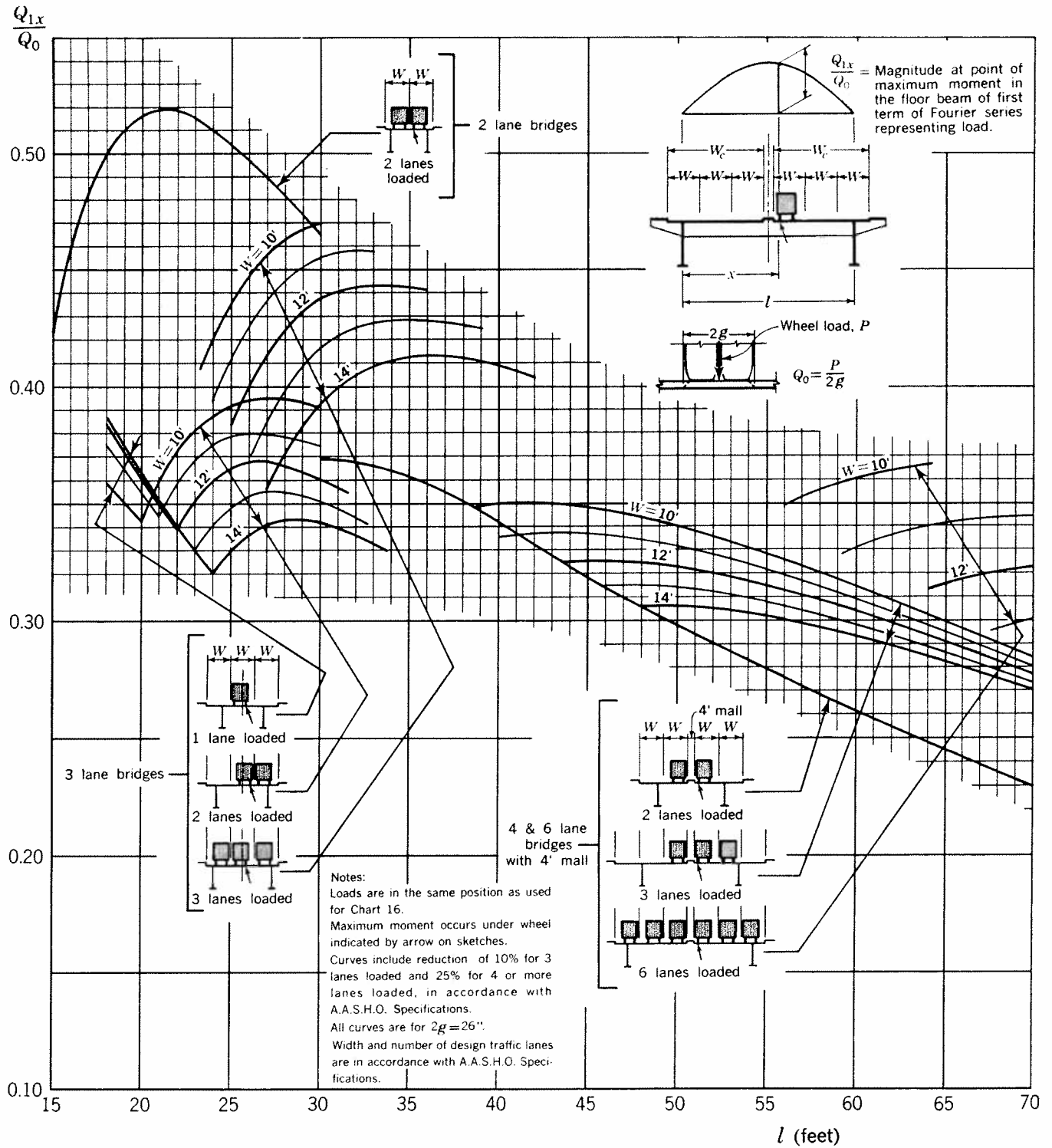


Chart 32. Computation of moment relief in a floor beam due to floor beam flexibility. Values of Q_{1x}/Q_0 at critical point of a floor beam

Appendix II—Buckling Formulas for Steel Decks

II.1 LOCAL BUCKLING OF RIB PLATE

II.1.1 Elastic Buckling

The ideal buckling stress, f_i , for a plate loaded as shown in Figure II.1a, with edge conditions shown in Figure II.1c is, for an elastic material with constant modulus of elasticity, given by the following equation [32]:

$$f_i = k \frac{\pi^2 E}{12(1 - \nu^2)} \left(\frac{t}{h}\right)^2 \quad (\text{II.1})$$

where

- E = modulus of elasticity of the material
- ν = Poisson's ratio
- t = plate thickness
- h = plate width
- k = constant, depending on the loading and the edge conditions. Various values for k for long plates are given in Table II.1

TABLE II.1

VALUES OF k IN EQUATION (II.1) FOR LOADING AND EDGE CONDITIONS SHOWN IN FIGURE II.1a AND II.1c [32]

Loading	Edge Condition				
	(1)	(2)	(3)	(4)	(5)
A	6.97	5.40	4.00	1.28	0.43
B	13.56	12.16	7.81	6.26	1.71
C	13.56	9.89	7.81	1.64	0.57

The values of k given in Table II.1 are valid for plates with a length-to-width ratio, s/h , greater than 1.5 (see Fig. II.1). This condition is always satisfied with the ribs of steel plate decks, with a possible exception in the case of flexural (System II) stresses in short ribs, where the length of the rib subjected to compression (portions of the rib near the supports at floor beams) may be shorter than $1.5h$. Therefore the values of the buckling stresses in the ribs subjected to local flexure, computed with the k -values from Table II.1 may be conservative. See also comments in Section II.1.3.2.

With the values of $E = 29,000$ ksi and $\nu = 0.3$, equation (II.1) becomes

$$f_i = 26,200k \left(\frac{t}{h}\right)^2 \quad \text{k/in.}^2 \quad (\text{II.1a})$$

II.1.2 Inelastic Buckling

The ideal buckling stress, f_i , given by equation (II.1) is the critical buckling stress, f_{cr} , of the plate if its value does not exceed the proportional limit, f_p , of the material. When the stress given by equation (II.1) exceeds the proportional limit, the critical buckling stress, f_{cr} , will be smaller than the ideal buckling stress, f_i .

The inelastic buckling theory of plates is rather complex; Bleich [5] shows that the critical buckling stress of plates may be computed by the formula:

$$f_{cr} = k \frac{\pi^2 E \sqrt{\tau}}{12(1 - \nu^2)} \left(\frac{t}{h}\right)^2 = f_i \sqrt{\tau} \quad (\text{II.2})$$

where

- $\tau = E_T/E$
- E_T = tangent modulus = slope of the stress-strain diagram of the material at the stress f_{cr}

Note that when $f_{cr} < f_p$, $\tau = 1$, and equation (II.2) is identical with equation (II.1).

The value of τ may be approximated with sufficient accuracy by the following equation [5]:

$$\tau = \frac{(f_y - f_{cr})f_{cr}}{(f_y - f_p)f_p} \quad (\text{II.3})$$

where f_y is the yield stress of the material.

Introducing equation (II.3) into equation (II.2) and solving for f_{cr}/f_y , the following relationship is obtained:

$$\frac{f_{cr}}{f_y} = \frac{1}{1 + \frac{f_p}{f_y} \left(1 - \frac{f_p}{f_y}\right) \left(\frac{f_y}{f_i}\right)^2} \quad (\text{II.4})$$

For a steel plate, an average value of $f_p/f_y = 0.75$ may be used, resulting in

$$\frac{f_{cr}}{f_y} = \frac{1}{1 + 0.1875 \left(\frac{f_y}{f_i}\right)^2} \quad (\text{II.4a})$$

The values of f_{cr}/f_y computed by equation (II.4a) are shown as Curve 1 in Figure II.2.

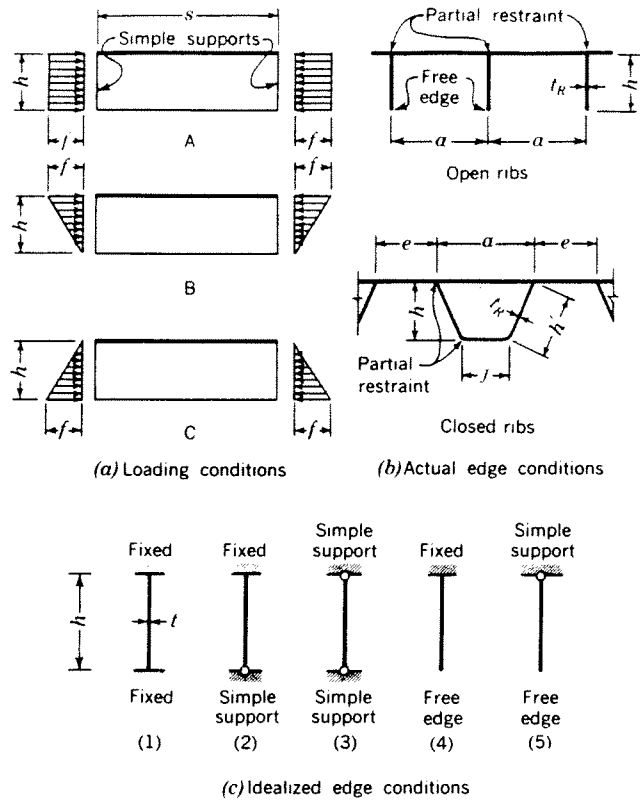


Fig. II.1. Elastic stability of the ribs. Loading and edge conditions

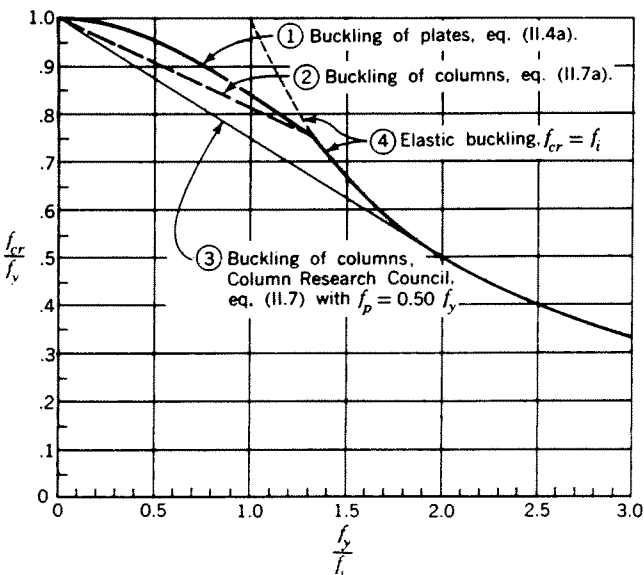


Fig. II.2. Buckling curves for plates and columns

II.1.3 Computation of Critical Buckling Stress

II.1.3.1 Choice of k

II.1.3.1.1 Open Ribs

The edge conditions of the open ribs are not accurately defined by any of the cases in Figure II.1c, but lie somewhere between cases (4) and (5). Based on a method given in [5], the following values of k are proper for the usual rib and deck plate proportions.

(a) System I stresses

The case of System I compressive stresses (nearly uniform compression over the cross section of the ribs) corresponds to loading case A of Figure II.1. The value of k for the ribs is found to be between 0.6 and 1.0. The k -values will be at the lower end of the range for short, thick widely spaced ribs and thin deck plates and at the upper end of the range for deep, slender closely spaced ribs and thick deck plates. As a guide in choosing k , the appropriate value of k for the $8\frac{1}{2}$ -in. \times $1\frac{1}{2}$ -in. ribs spaced 12 in. o.c. and $\frac{3}{8}$ -in. thick deck plate of the numerical example, Section 11.2, may be taken as 0.7.

(b) System II stresses

The flexural compressive stresses in the ribs in the negative bending moment areas near the floor beams most nearly resemble the loading case C of Figure II.1. Since, as noted in Sections II.1.1 and II.1.3.2, the assumptions used in the investigation of the local buckling due to System II stresses are conservative, larger values of k , ranging between 1.0 and 1.4, seem to be appropriate in this case.

(c) System I + II stresses

In this case the values of k may be chosen between 0.8 and 1.2.

II.1.3.1.2 Closed Ribs

For the closed ribs the following assumptions are sufficiently accurate:

(a) *Sides of rib*: assume rib fixed at the deck plate and simply supported at the bottom (edge condition (2), Fig. II.1c), $k = 5.4$ to 9.9 depending on loading (see Table II.1). Note that h' must be substituted for h in equation (II.1a).

(b) *Bottom of rib*: assume both sides simply supported (edge condition (3), Fig. II.1c), $k = 4.0$. The buckling stress in the bottom of the rib will not be critical except when $j > 0.86h'$ for loading case A, or $j > 0.64h'$ for loading case C. Note that j must be substituted for h in equation (II.1a).

II.1.3.2 Determination of f_{cr}

With the value of k determined, the ideal buckling stress, f_t , is computed by equation (II.1a). Using this stress, the value of f_{cr} is determined from Curve 1, Figure II.2.

When the value of f_t is less than $0.75f_y$, Figure II.2 need not be used, since, in such case, $f_{cr} = f_t$.

It should be noted that for thick ribs (small values of h/t) the value of k has little effect on f_{cr} , which, in such cases, is near the yield stress.

Regarding local buckling due to System II or System I + II compressive stresses in the ribs, it should be noted that these stresses reach their maximum near the floor beams and fall off rapidly in the direction toward the midspan of the ribs, and, therefore, the value of f_{cr} determined by this method will be conservative. Local buckling deformation due to System II stresses is unlikely, since before any measurable deformations could occur due to local buckling of the loaded rib, the load would be redistributed through membrane stresses to the adjacent ribs.

Because of the geometric conditions of steel plate decks of usual proportions the local buckling strength of the deck plate is always greater than that of the ribs and need not be investigated.

II.2 OVERALL BUCKLING OF THE DECK

II.2.1 Elastic Buckling

The floor beams of steel bridge decks of usual dimensions are sufficiently rigid to act as transverse stiffeners of the deck, which will buckle as an edge-loaded plate with simply supported edges at the floor beams. Buckling of the individual longitudinal ribs of the deck is impossible, because of the elastic restraint provided by the deck plate and the adjoining ribs.

In the investigation of buckling of the bridge deck subjected to a uniform compression as the flange of the main girders it is permissible to consider buckling in the vertical direction of one rib only as a part of the deck.

Writing Euler's buckling formula in the nomenclature used in this Manual, the ideal buckling stress is obtained as

$$f_t = \frac{\pi^2 E}{\left(\frac{s}{r}\right)^2} \quad (\text{II.5})$$

or, for steel,

$$f_t = \frac{286,000}{\left(\frac{s}{r}\right)^2} \quad \text{k/in.}^2 \quad (\text{II.5a})$$

where r is the radius of gyration of a rib computed from the moment of inertia, I_R , of one rib as defined in Section 3.3.2.2 and the cross-sectional area of the corresponding section.

II.2.2 Inelastic Buckling

When the ideal buckling stress, f_t , exceeds the proportional limit of the material, the critical buckling stress, f_{cr} , will be smaller than f_t . The critical buckling stress is given by the tangent modulus formula [5], which can be expressed as

$$f_{cr} = f_t \tau \quad (\text{II.6})$$

where $\tau = E_T/E$ as before.

With Bleich's approximation for τ as given in equation (II.3), solving equation (II.6) for f_{cr}/f_y results in

$$\frac{f_{cr}}{f_y} = 1 - \frac{f_p}{f_y} \left(1 - \frac{f_p}{f_y}\right) \frac{f_y}{f_t} \quad (\text{II.7})$$

Using the value $f_p/f_y = 0.75$ as before, the ratio f_{cr}/f_y is obtained as

$$\frac{f_{cr}}{f_y} = 1 - 0.1875 \frac{f_y}{f_t} \quad (\text{II.7a})$$

The values of f_{cr}/f_y computed by equation (II.7a) are given by Curve 2 in Figure II.2.

Curve 3, given for comparison, is based on the f_p/f_y ratio of 0.5, and is recommended by the Column Research Council for the design of rolled columns [8]. This choice of the proportional limit reflects the effect of the residual stresses in rolled sections of structural carbon steel.

In steel plate decks of low-alloy steel the relative magnitudes of the residual stresses are likely to be smaller than those in the rolled sections. Therefore the use of Curve 2, based on the f_p/f_y ratio of 0.75, is recommended in the design of the ribs.